ISSN

VOL. 536 NOS. 1 + 2 JANUARY
COMPLETE IN ONE ISSUE

14th International Symposium on Column Liquid Chromatography Boston, MA, May 20–25, 1990 Part II

JOURNAL OF CHROMATOGRAPHY

INCLUDING ELECTROPHORESIS AND OTHER SEPARATION METHODS

SYMPOSIUM VOLUMES

ELSEVIER

JOURNAL OF CHROMATOGRAPHY

Scope. The *Journal of Chromatography* publishes papers on all aspects of chromatography, electrophoresis and related methods. Contributions consist mainly of research papers dealing with chromatographic theory, instrumental development and their applications. The section *Biomedical Applications*, which is under separate editorship, deals with the following aspects: developments in and applications of chromatographic and electrophoretic techniques related to clinical diagnosis or alterations during medical treatment; screening and profiling of body fluids or tissues with special reference to metabolic disorders; results from basic medical research with direct consequences in clinical practice; drug level monitoring and pharmacokinetic studies; clinical toxicology; analytical studies in occupational medicine.

Submission of Papers. Manuscripts (in English; *four* copies are required) should be submitted to: Editorial Office of *Journal of Chromatography*, P.O. Box 681, 1000 AR Amsterdam, The Netherlands, Telefax (+31-20) 5862 304, or to: The Editor of *Journal of Chromatography, Biomedical Applications*, P.O. Box 681, 1000 AR Amsterdam, The Netherlands. Review articles are invited or proposed by letter to the Editors. An outline of the proposed review should first be forwarded to the Editors for preliminary discussion prior to preparation. Submission of an article is understood to imply that the article is original and unpublished and is not being considered for publication elsewhere. For copyright regulations, see below.

Subscription Orders. Subscription orders should be sent to: Elsevier Science Publishers B.V., P.O. Box 211, 1000 AE Amsterdam, The Netherlands, Tel. (+31-20) 5803 911, Telex 18582 ESPA NL, Telefax (+31-20) 5803 598. The *Journal of Chromatography* and the *Biomedical Applications* section can be subscribed to separately.

Publication. The *Journal of Chromatography* (incl. *Biomedical Applications*) has 38 volumes in 1991. The subscription prices for 1991 are:

J. Chromatogr. (incl. *Cum. Indexes, Vols. 501–550*) + *Biomed. Appl.* (Vols. 535–572):
Dfl. 7220.00 plus Dfl. 1140.00 (p.p.h.) (total *ca.* US$ 4696.50)

J. Chromatogr. (incl. *Cum. Indexes, Vols. 501–550*) only (Vols. 535–561):
Dfl. 5859.00 plus Dfl. 810.00 (p.p.h.) (total *ca.* US$ 3746.50)

Biomed. Appl. only (Vols. 562–572):
Dfl. 2387.00 plus Dfl. 330.00 (p.p.h.) (total *ca.* US$ 1526.50).

Our p.p.h. (postage, package and handling) charge includes surface delivery of all issues, except to subscribers in Argentina, Australia, Brasil, Canada, China, Hong Kong, India, Israel, Malaysia, Mexico, New Zealand, Pakistan, Singapore, South Africa, South Korea, Taiwan, Thailand and the U.S.A. who receive all issues by air delivery (S.A.L. — Surface Air Lifted) at no extra cost. For Japan, air delivery requires 50% additional charge; for all other countries airmail and S.A.L. charges are available upon request. Back volumes of the *Journal of Chromatography* (Vols. 1–534) are available at Dfl. 195.00 (plus postage). Claims for missing issues will be honoured, free of charge, within three months after publication of the issue. Customers in the U.S.A. and Canada wishing information on this and other Elsevier journals, please contact Journal Information Center, Elsevier Science Publishing Co. Inc., 655 Avenue of the Americas, New York, NY 10010, U.S.A., Tel. (+1-212) 633 3750, Telefax (+1-212) 633 3990.

Abstracts/Contents Lists published in Analytical Abstracts, Biochemical Abstracts, Biological Abstracts, Chemical Abstracts, Chemical Titles, Chromatography Abstracts, Clinical Chemistry Lookout, Current Contents/Life Sciences, Current Contents/Physical, Chemical & Earth Sciences, Deep-Sea Research/Part B: Oceanographic Literature Review, Excerpta Medica, Index Medicus, Mass Spectrometry Bulletin, PASCAL-CNRS, Pharmaceutical Abstracts, Referativnyi Zhurnal, Research Alert, Science Citation Index and Trends in Biotechnology.

See inside back cover for Publication Schedule, Information for Authors and information on Advertisements.

0021-9673/91/$03.50

This issue is printed on acid-free paper.

Printed in The Netherlands

JOURNAL OF CHROMATOGRAPHY

VOL. 536 (1991)

JOURNAL of CHROMATOGRAPHY

INCLUDING ELECTROPHORESIS AND OTHER SEPARATION METHODS

SYMPOSIUM VOLUMES

ELSEVIER
AMSTERDAM — OXFORD — NEW YORK — TOKYO

J. Chromatogr., Vol. 536 (1991)

0021-9673/91/$03.50

Printed in The Netherlands

SYMPOSIUM VOLUME

FOURTEENTH INTERNATIONAL SYMPOSIUM ON COLUMN LIQUID CHROMATOGRAPHY

PART II

Boston, MA (U.S.A.), May 20–25, 1990

Guest Editor

B. L. KARGER

(Boston, MA)

The proceedings of the *Fourteenth International Symposium on Column Liquid Chromatography, Boston, MA, May 20–25, 1990*, are published in two consecutive volumes of the *Journal of Chromatography*: Vols. 535 (1990) and 536 (1991). The Foreword to the proceedings and information on the Science Advisory and Organizing Committees only appear in Vol. 535. A combined Author Index to both Vols. 535 and 536 only appears in Vol. 536.

VOL. 536, NOS. 1+2 JOURNAL OF CHROMATOGRAPHY JANUARY 4, 1991

CONTENTS

14TH INTERNATIONAL SYMPOSIUM ON COLUMN LIQUID CHROMATOGRAPHY, BOSTON, MA, MAY 20–25, 1990, PART II

Journal of Chromatography, 536 (1991) 1–15
Elsevier Science Publishers B.V., Amsterdam

CHROMSYMP. 2043

Metal ligand-induced alterations in the surface structures of lactoferrin and transferrin probed by interaction with immobilized copper(II) ions

T. WILLIAM HUTCHENS* and TAI-TUNG YIP
USDA/ARS Children's Nutrition Research Center, Department of Pediatrics, Baylor College of Medicine, 1100 Bates, Houston, TX 77030, and Texas Children's Hospital, Houston, TX 77030 (U.S.A.)

ABSTRACT

We have evaluated immobilized Cu(II) ions as a potential site-directed molecular probe to monitor ligand-induced alterations in protein surface structures. Metal ion-induced alterations in the surface structures of different lactoferrins (human and porcine), transferrins (human and rabbit), and ovotransferrin (chicken) were examined. Although these 78 000-dalton glycoproteins are related gene products with similar overall structure and function, they differ greatly in the number and distribution of surface-exposed electron-donor groups thought to interact with Cu(II) ions. Each of these proteins interacted with immobilized Cu(II) ions through sites which are distinct from the two specific high affinity metal binding sites identified for iron. In both the presence and absence of bound iron, transferrins interacted more strongly with the immobilized Cu(II) ions than did lactoferrins; ovotransferrin interacted only weakly. Although iron binding *increased* the affinities of lactoferrins for immobilized Cu(II), iron binding *decreased* the affinities of transferrins and ovotransferrin for immobilized Cu(II) ions. Iron-saturated and iron-free lactoferrins were resolved by pH gradient elution, but only in the presence of 3 *M* urea; they were not resolved by imidazole affinity elution. Conversely, the iron-saturated and iron-free forms of transferrin were only separated by imidazole affinity elution. Urea did not influence the resolution of apo and holo ovotransferrins by imidazole . The differential effects of urea and imidazole suggest the participation of different types of surface electron-donor groups. The progressive site-specific modification of surface-exposed histidyl residues by carboxyethylation revealed several lactoferrin forms of intermediate affinity for immobilized iminodiacetate–Cu(II) ions. In summary, independent of species, the affinity for immobilized Cu(II) ions increased as follows: iron-saturated ovotransferrin < metal-free ovotransferrin < apolactoferrin < hololactoferrin < < diferric or holotransferrin < monoferric transferrin < apotransferrin. We have demonstrated the use of immobilized Cu(II) ions to distinguish and to monitor ligand-induced alterations in protein surface structure. The results are discussed in relation to protein surface-exposed areas of electron-donor groups.

INTRODUCTION

Stationary phase-immobilized transition metal ions have been evaluated for their potential for peptide and protein purification [1–10]. These evaluations have resulted from the expectation that immobilized metal ions may interact with proteins and peptides in a site-specific manner [1,11]. A select group of model peptides and proteins have been used to demonstrate such interactions [3,4,9,12,13]. Little effort,

0021-9673/91/$03.50

however, has been focused on variations in the mobile phase that may modify the relative affinities (*i.e.*, specificity) with which immobilized metal ions interact with various solvent-exposed electron-donor groups on the surface of a protein [2,6,7,10]. We have found that variations in the concentration and type of salt [12] and the use of urea [6,7,10,14] or ethylene glycol can dramatically alter immobilized metal ion retention of peptides and proteins. We report here that such experimental approaches can greatly facilitate the use of high-performance stationary phases of immobilized metal ions to monitor ligand-induced alterations in protein surface structure.

Lactoferrins and transferrins were chosen for these investigations for several reasons. High-resolution structural data for rabbit serum holotransferrin and human lactoferrin (apo and holo forms) are now available [15–18]. Each of these proteins has a large number and variety of solvent-exposed electron-donor groups on its surface, so the ability to detect minor alterations is challenged. There is spectroscopic evidence to suggest that conformational changes are associated with occupancy of the two high-affinity metal-binding sites [19–21]. For lactoferrin, *in vitro* generation of the iron-free form by incubation at low pH has been shown to result in irreversible structural damage [19,21]. Because the apo and holo forms of lactoferrin have each been associated with a wide spectrum of different biological activities [21–29], separation of the apo and holo forms of lactoferrin is important. Except for a recent report from our laboratory [29], the resolution of apo and holo lactoferrins has not been reported previously by any means other than analytical-scale electrophoresis [30].

In this report, we demonstrate that (1) immobilized copper ions on high-performance stationary phases can be a sensitive probe of metal ligand-induced alterations in the surface structures of ovotransferrin, transferrins and lactoferrins, (2) these three subclasses of transferrin gene family products can be distinguished by their differential affinity for immobilized Cu(II) ions, (3) these proteins interact with immobilized Cu(II) ions through sites which are clearly distinct from the two specific high affinity metal binding sites identified for iron, (4) species-dependent variations in the amino acid sequence or bound carbohydrate moiety of these glycoproteins do not influence these findings, and (5) mobile phase constituents (*e.g.*, counter ions) and modifying reagents such as urea and imidazole differentially affect the resolution of the apo and holo forms of these proteins.

MATERIALS AND METHODS

Ultra-pure urea was obtained from Bethesda Research Labs. (Gaithersburg, MD, U.S.A.). It was used immediately after it had passed through a mixed-function deionizing resin AG501-X8(D) from Bio-Rad (Richmond, CA, U.S.A.). Imidazole was obtained from Sigma (St. Louis, MO, U.S.A.) and used after treatment with Norit A charcoal to reduce ultraviolet (280 nm) absorption. Human and porcine lactoferrins were purified to homogeneity from colostrum by affinity chromatography on immobilized single-stranded DNA [29]. Metal ions were removed from the lactoferrins by prolonged incubation (4 h at 37°C) and dialysis (18 h at 4°C) against a low pH buffer (0.1 *M* sodium phosphate at pH 4.0–4.2 with 1 mg/ml ascorbic acid) containing 1 mg/ml deferoxamine mesylate (Sigma) as the iron chelator. Rabbit and human serum transferrins, and chicken ovotransferrin (substantially iron-free) were obtained from Sigma. To iron-saturate the lactoferrins, transferrins, or ovotransferrin, sodium

bicarbonate was added to a concentration of 0.1 *M*, followed by the addition of ferrous sulfate in 0.01 *M* HCl and incubation at 37°C for a minimum of 15 min. ^{59}Fe (DuPont NEN, Boston, MA, U.S.A.) was added, as indicated, to monitor iron dissociation and hololactoferrin or holotransferrin elution properties. Copper-saturated lactoferrins and transferrins were prepared by the addition of copper(II) sulfate in the presence of 0.1 *M* sodium bicarbonate. Excess metal ions were removed by dialysis. Metal ion saturation, loss of metal ions and/or metal ion transfer were monitored by spectral analysis at 465/280 nm for the iron-saturated form and at 430/280 nm for the copper-saturated (iron-free) form. The protein-bound metal ion contents were also analyzed by energy-dispersive X-ray fluorescence spectroscopy using a Kevex 0600 XRF spectrometer.

The TSK chelate 5PW (10 μm, 750 × 7.5 mm) columns, prepared with iminodiacetate functional groups [31], were a gift from Dr. Kato of Tosoh Manufacturing Co., Yamaguchi, Japan. The Beckman System Gold high-performance liquid chromatograph (Fullerton, CA, U.S.A.) was used with a Beckman Model 166 or 167 flow-through ultraviolet spectrophotometer. A Sensorex (Stanton, CT, U.S.A.) flow cell and a Corning (Ithaca, NY, U.S.A.) pH meter were used for continuous monitoring of the column effluent pH. After the metal-chelating stationary phase [immobilized iminodiacetate (IDA)] was washed with water, 50 m*M* copper sulfate in water was passed through the column. Excess metal ions were washed away with 0.1 *M* sodium acetate buffer at pH 3.5 containing 0.5 *M* NaCl (1 ml/min). Three different column equilibration and elution buffer systems were used. The immobilized Cu(II) columns were equilibrated with (i) 20 m*M* sodium phosphate (pH 7.0) containing 3 *M* urea and 0.5 *M* NaCl, (ii) 100 m*M* sodium acetate (pH 5.5 to 5.0) containing 0.5 *M* NaCl and 3 *M* urea (as indicated), or (iii) 20 m*M* sodium phosphate or 4-(2-hydroxyethyl)-1-piperazineethanesulfonic acid (HEPES) (pH 7.0) containing 0.5 *M* NaCl, 1 m*M* imidazole and 3 *M* urea (as indicated). A specific sample was loaded onto the column, which was then developed (1 ml/min) with a linear gradient of either (i) 0.1 *M* sodium phosphate, 0.5 *M* NaCl and 3 *M* urea from pH 7.0 to pH 3.6, or (ii) 0.1 *M* sodium acetate, 0.5 *M* NaCl and 3 *M* urea from pH 5.5 or 5.0 to pH 3.5, or (iii) 20 m*M* sodium phosphate or HEPES (pH 7.0) containing from 1 to 20 m*M* imidazole ($\pm$ 3 *M* urea). The absorbance at 280 nm and pH were measured continuously. Imidazole gradient slopes were verified separately by monitoring absorbance at 230 nm. Where indicated, fractions of 1 min each were collected.

Diethylpyrocarbonate (Sigma) stock solution was prepared in anhydrous ethanol, and the concentration was determined immediately before use by adding an aliquot of the stock to a solution of known concentration of imidazole and measuring the absorbance at 240 nm on a Beckman DU-70 spectrophotometer. Aliquots of this stock solution of diethylpyrocarbonate were added to a known concentration of iron-saturated human lactoferrin at room temperature such that the final molar ratio of diethylpyrocarbonate to lactoferrin was equal to the values given in Fig. 5. No further alterations in lactoferrin retention times were observed after incubation for 30 to 40 min with the stated concentration of diethylpyrocarbonate.

Lactoferrin and transferrin protein structures were evaluated using the program FRODO [32] (version 6.6 by James W. Pflugrath, John S. Sack and Mark A. Saper in the laboratory of Florante A. Quiocho at the Department of Biochemistry, Rice University, Houston, TX, U.S.A.) and the program ACCESS [33] (version 2.0 by B.

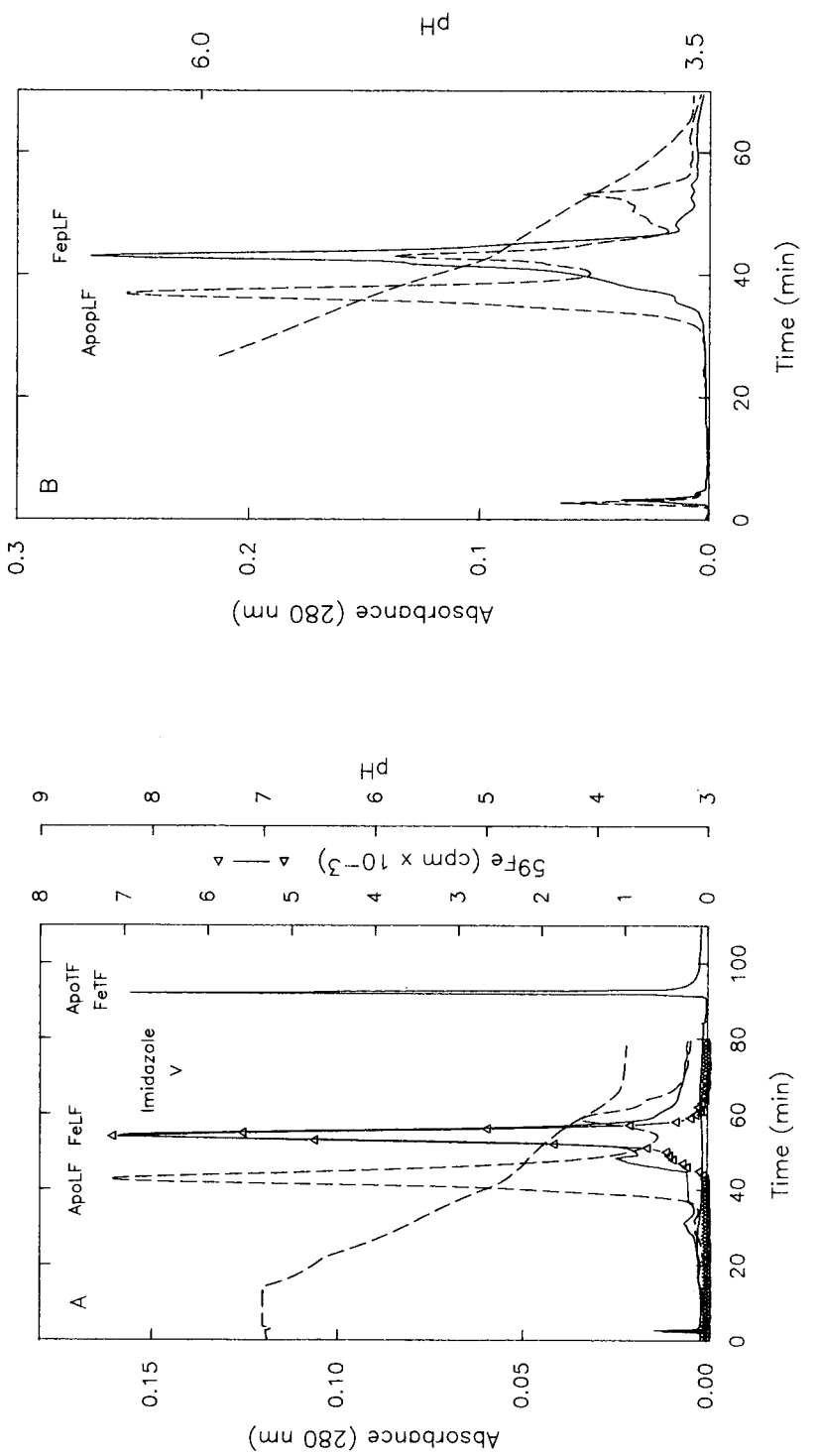

Fig. 1. Separation of apolactoferrin (dashed line) and iron-saturated human (A) and porcine (B) lactoferrins (solid line) on IDA–Cu(II) columns with a phosphate-buffered gradient of decreasing pH in the presence of 3 *M* urea. Both apotransferrin and iron-saturated transferrin were eluted only upon introduction of 20 m*M* imidazole (imidazole-labeled arrow). UV absorbance was monitored at 280 nm. The elution of iron-saturated human lactoferrin was determined by measuring protein-bound ^{59}Fe radioactivity (open triangles). LF = lactoferrin; TF = transferrin.

Lee, F. M. Richards, T. J. Richmond, and M. D. Handschumacher, Yale University, New Haven, CT, U.S.A.) on a VAX 8810 computer equipped with an Evans and Sutherland PS390 molecular graphics terminal. The refined coordinates for human lactoferrin [15–17] were generously provided by Dr. Edward N. Baker and colleagues at Massey University, New Zealand. The coordinates for diferric rabbit serum transferrin [18] were kindly provided by Dr. Peter Lindley at Birbeck College, University of London, U.K.

RESULTS

The metal-free forms of ovotransferrin, transferrins, and lactoferrins were found to vary in the strength of their interaction with immobilized Cu(II) ions. Furthermore, the alteration(s) in protein surface structure that occurs upon free metal ion (iron) occupation of the two specific high affinity metal binding sites was apparent with IDA–Cu(II) affinity chromatography. The iron-saturated form of lactoferrin interacted with the immobilized Cu(II) ions with an affinity even higher than that of the iron-free form. Fig. 1A demonstrates the resolution of the metal-free and iron-saturated forms of human lactoferrin. We found that this resolution was only possible with high-performance IDA–Cu(II) columns eluted with a decreasing pH gradient in the presence of 3 *M* urea. Regardless of buffer type (*e.g.*, phosphate or acetate), urea was necessary to achieve the resolution of apo and hololactoferrins. Fig. 1A also illustrates the greatly increased affinity of human transferrin for IDA–Cu(II) relative to human lactoferrin.

Apotransferrin and iron-saturated transferrin, although tightly bound to IDA–Cu(II), were neither eluted nor resolved under conditions which permitted the resolution of apolactoferrin from hololactoferrin (Fig. 1A). The iron-free and iron-saturated forms of transferrin were eluted together by displacement with imidazole, after completion of the descending pH gradient.

The metal ligand (iron)-induced increase in the affinity of lactoferrin for immobilized Cu(II) ions was independent of species; similar results were obtained for human and porcine lactoferrins. Fig. 1B shows that the affinity (elution position) of iron-free porcine lactoferrin was less than that of iron-saturated porcine lactoferrin. Approximately 25–30% of the isolated (neat) porcine colostral whey lactoferrin was found to be iron-saturated upon spectroscopic analysis. The presence of this iron-saturated lactoferrin fraction in our purified porcine lactoferrin preparation was indicated by its co-elution with porcine lactoferrin which had been fully saturated with hiron *in vitro* before chromatography (Fig. 1B; solid line). The degree of bound iron in all fractions was routinely verified by spectroscopic analyses as described in Materials and Methods.

Fig. 2 demonstrates that human lactoferrin and human transferrin could also be separated on the IDA–Cu(II) affinity column using an acetate-buffered pH gradient. Again, however, the metal-free and iron-saturated forms of human lactoferrin could only be resolved using the acetate pH gradient protocol if 3 *M* urea was present (Fig. 2B). In the presence of 3 *M* urea, the lactoferrins and transferrins were resolved *within* the acetate pH gradient; the apo and holo forms of human transferrin, however, were still not separated. At the pH required for transferrin elution (pH 4), iron is readily released from transferrin [21]. This effect was confirmed by spectral analyses of the

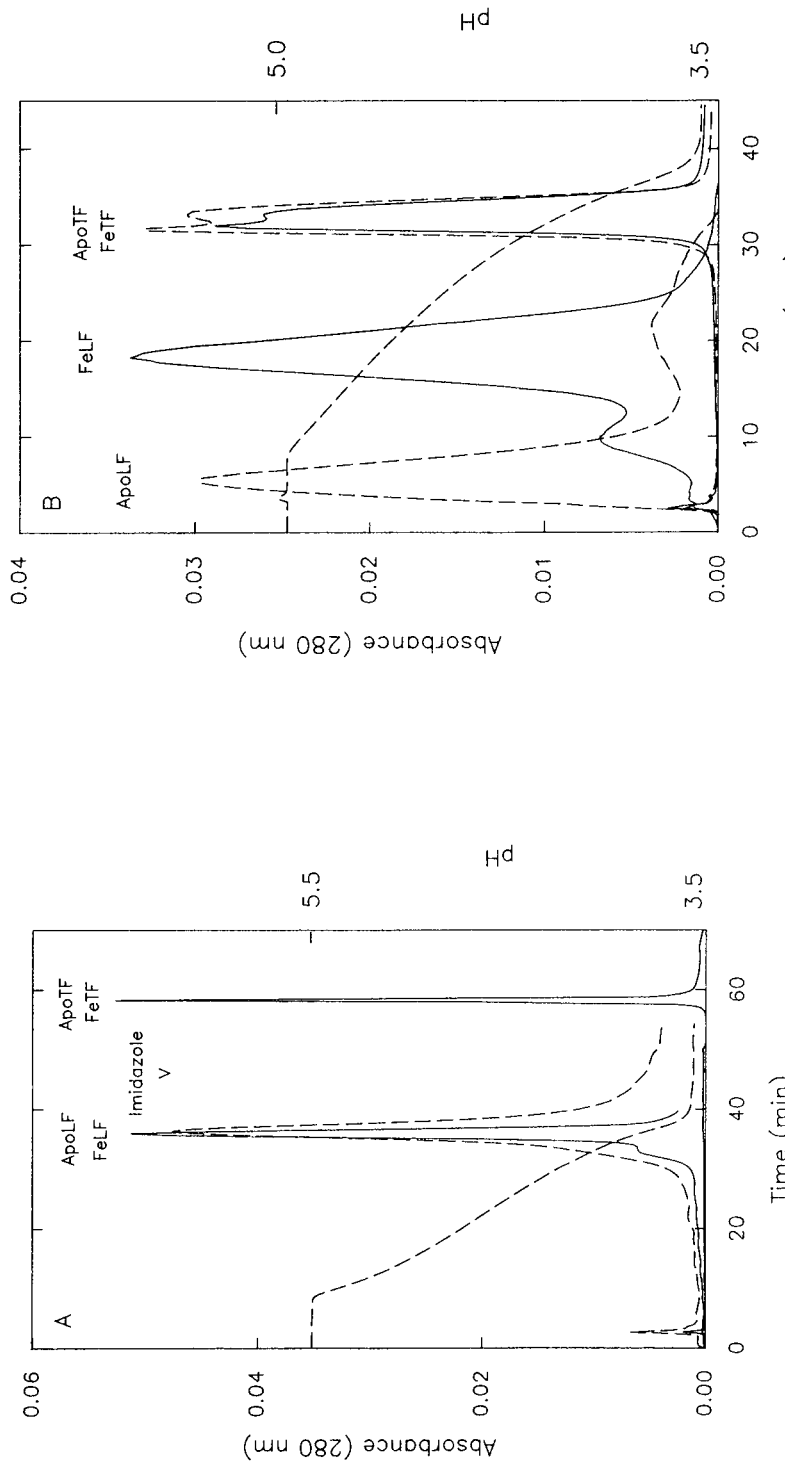

Fig. 2. Separation of the iron-free (dashed line) and iron-saturated (solid line) forms of human lactoferrin and human transferrin on IDA–Cu(II) affinity columns using an acetate buffer pH gradient elution protocol in the absence (A) and presence (B) of 3 *M* urea. In the absence of urea, both apotransferrin and iron-saturated transferrin were eluted only upon introduction of 20 m*M* imidazole (imidazole-labeled arrow).

transferrin peak after pH gradient elution from the immobilized Cu(II) affinity column. Thus, it was not possible to resolve the apo and holo forms of transferrin by pH gradient elution under any of the conditions evaluated.

The elution profiles illustrated in Fig. 3A show that an increasing concentration gradient of imidazole (1–10 m*M*) was able to resolve the iron-free and iron-saturated forms of human transferrin at neutral pH (to preserve bound iron in the case of holotransferrin). The copper-saturated transferrin was not completely resolved from the iron-free (apo) form. In contrast, the metal-free, copper-saturated, and iron-saturated forms of human lactoferrin were not separated by the imidazole gradient elution protocol. Even in the presence of 3 *M* urea, only the apo form was slightly resolved from the metal-saturated forms (Fig. 3B). These results made it apparent that iron binding had opposite effects on the affinities of human lactoferrin and human transferrin for the immobilized Cu(II) ions: it *increased* lactoferrin affinity, but *decreased* transferrin affinity. Regardless of the elution protocol used, however, each form of transferrin (*i.e.*, apo and holo) demonstrated a higher affinity for immobilized Cu(II) ions than did any form of lactoferrin. To evaluate the species specificity of this observation, the effects of bound iron on human transferrin affinity for immobilized Cu(II) ions were confirmed with rabbit serum transferrin. Fig. 3C compares the elution properties of human and rabbit serum transferrins before and after saturation with iron.

Fig. 4 demonstrates that chicken ovotransferrin has a much weaker, but detectable, affinity for immobilized Cu(II) ions. Nevertheless, metal ligand (iron)-dependent alterations in ovotransferrin affinity for IDA–Cu(II) ions were clearly evident. Like the iron-saturated forms of human and rabbit transferrins, iron-saturated ovotransferrin showed a decreased affinity for immobilized Cu(II) ions. The metal ligand-dependent decrease in affinity for IDA–Cu(II) ions was observed in both the absence (Fig. 4A) and presence (Fig. 4B) of 3 *M* urea. In fact, the weak affinity of iron-free ovotransferrin for immobilized Cu(II) ions was unaffeced by the inclusion of urea.

To investigate the specific surface residues responsible for these observations, a relatively site-specific chemical modifying reagent was examined. The human lactoferrin elution profiles shown in Fig. 5 demonstrate the progressive alteration in hololactoferrin affinity for IDA–Cu(II) ions after carboxyethylation with increasing molar ratios of diethylpyrocarbonate. Multiple intermediate and low affinity interactions remained evident even after modification with a 10-fold molar excess of diethylpyrocarbonate. If the concentration of diethylpyrocarbonate was increased another 10-fold, lactoferrin interaction with the immobilized Cu(II) was eliminated.

Despite their similarity in size (78 000 dalton) and overall tertiary structure, an examination of the surface structures of rabbit serum holotransferrin and human lactoferrin (both apo and holo forms) revealed widely different local concentrations and distributions of amino acid residues, including electron-donor groups capable of interaction with immobilized transition metal ions. The program ACCESS [33] was used to calculate the degree to which specific residues were solvent-accessible, that is, able to achieve contact with a spherical probe the diameter of a water molecule (1.4 Å). We evaluated closely those residues already known or proposed to interact with immobilized transition metal ions (*i.e.*, His, Cys and Trp) [1,11–13]. Although several surface-exposed sulfur atoms were evident, neither protein contains reduced sulf-

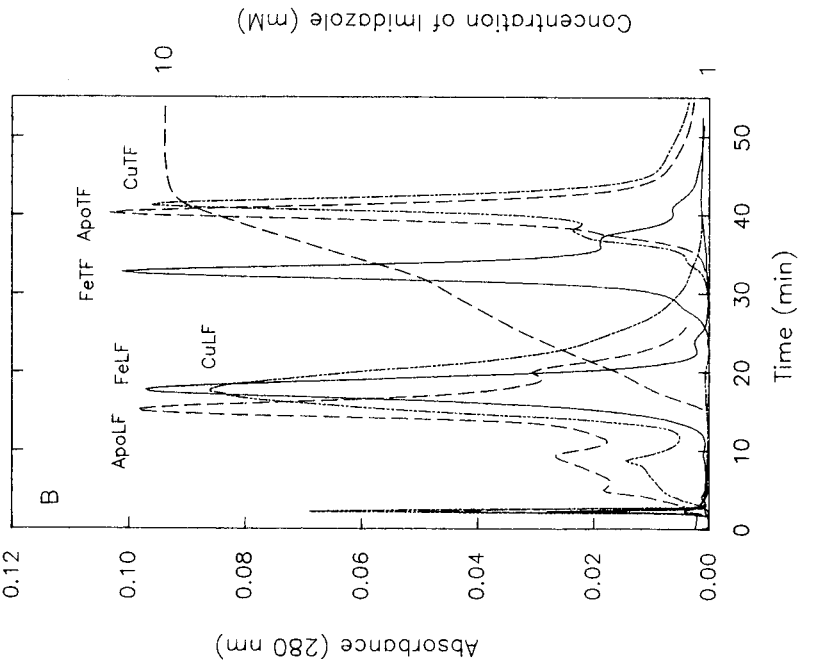
B
ApoLF
FeLF
CuLF
FeTF
ApoTF
CuTF
Absorbance (280 nm)
0.12
0.10
0.08
0.06
0.04
0.02
0.00
0
10
20
30
40
50
Time (min)
1
10
Concentration of Imidazole (mM)

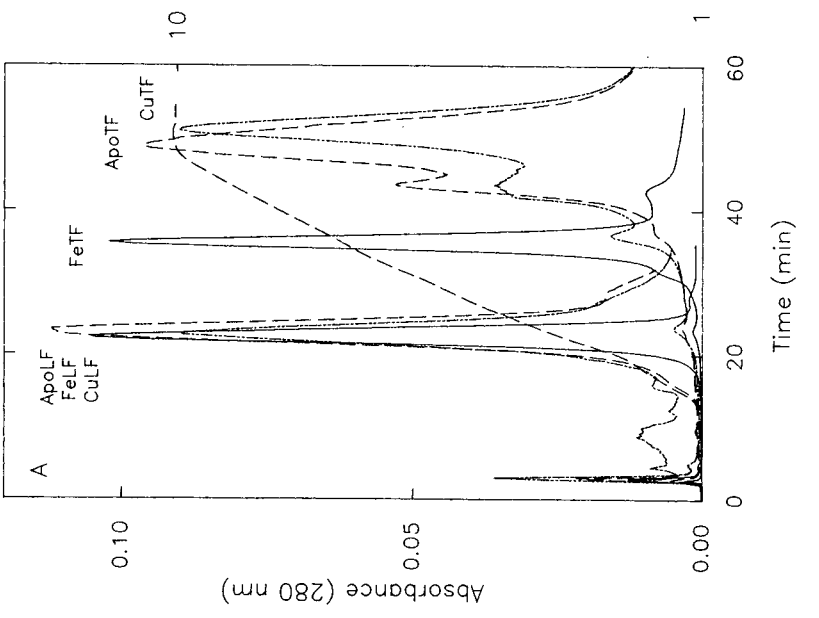
A
ApoLF
FeLF
CuLF
FeTF
ApoTF
CuTF
Absorbance (280 nm)
0.10
0.05
0.00
0
20
40
60
Time (min)
1
10
Concentration of Imidazole (mM)

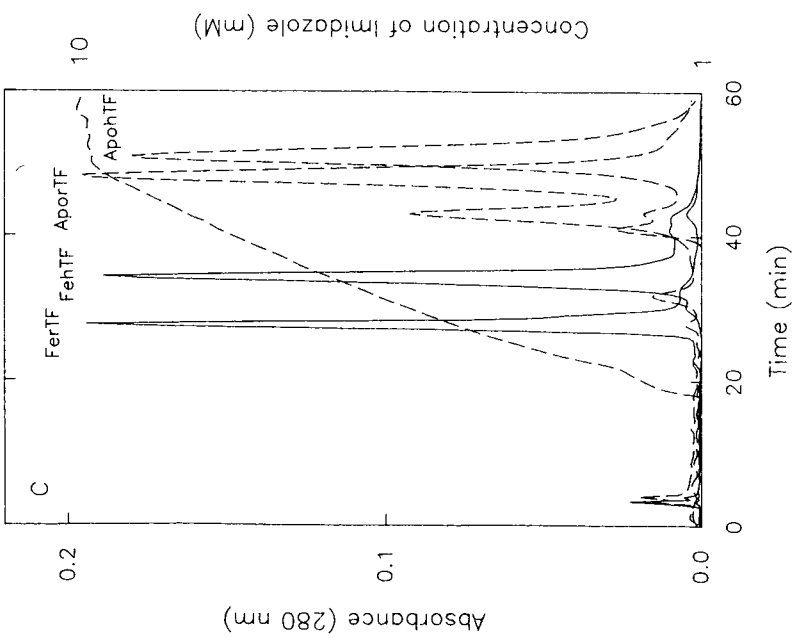

Fig. 3. Separation of iron-free (dashed line), iron-saturated (solid line), and copper-saturated (dashed/dotted line) lactoferrins and transferrins on an IDA–Cu(II) affinity column using an imidazole elution gradient in the absence (A and C) and presence (B) of 3 *M* urea. (A) and (B) illustrate results obtained with human lactoferrin (LF) and human transferrin (TF). (C) shows a comparison of results obtained with human serum transferrin (hTF) and rabbit serum transferrin (rTF). The Fe and Apo prefix to these abbreviations designates iron-saturated and metal-free transferrins, respectively.

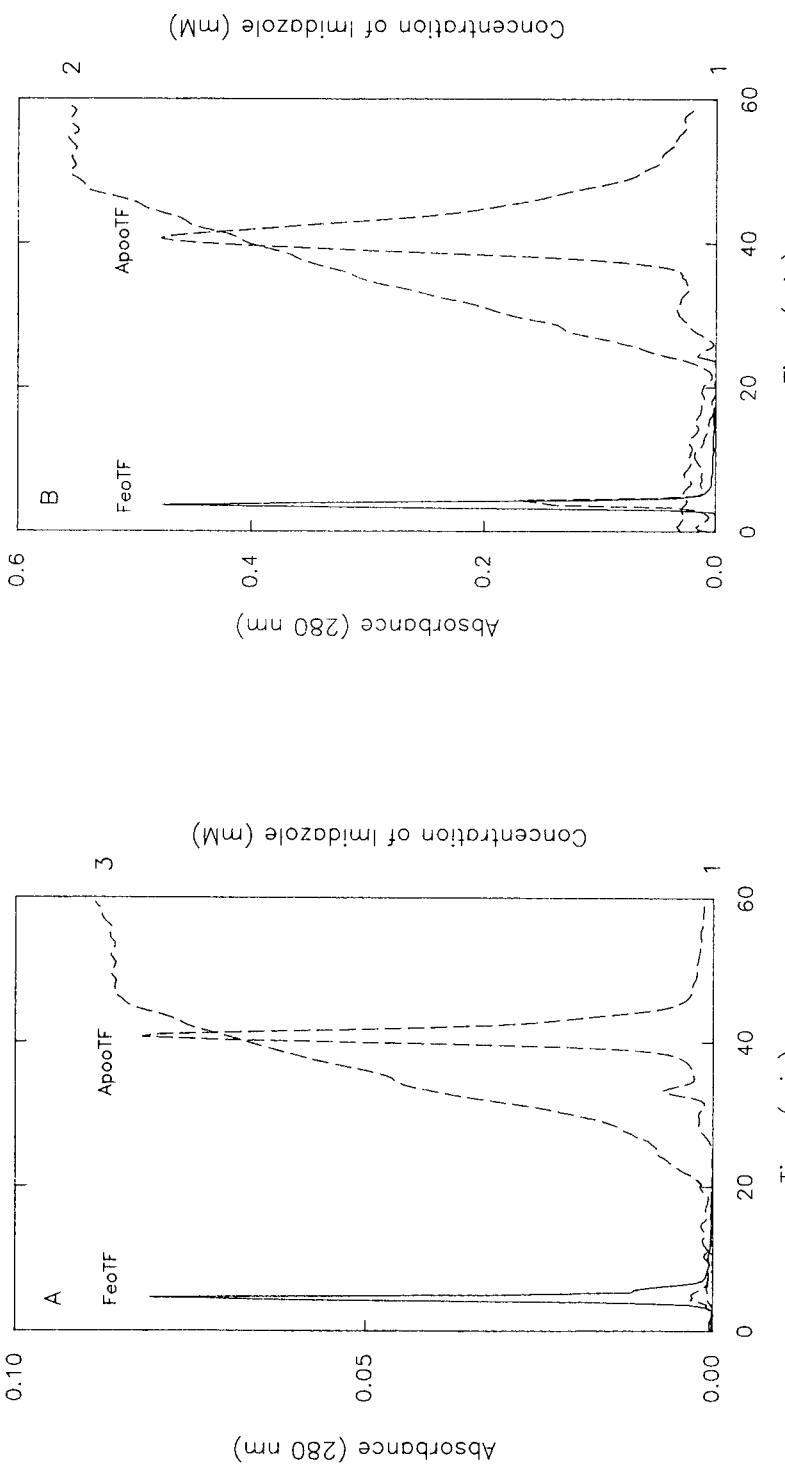

Fig. 4. Resolution of metal-free (Apo; dashed line) and Fe(II)-saturated (Fe; solid line) chicken ovotransferrins (oTF) on columns of IDA–Cu(II) using a shallow imidazole elution gradient (dashed line) in the absence (A) and presence (B) of 3 *M* urea.

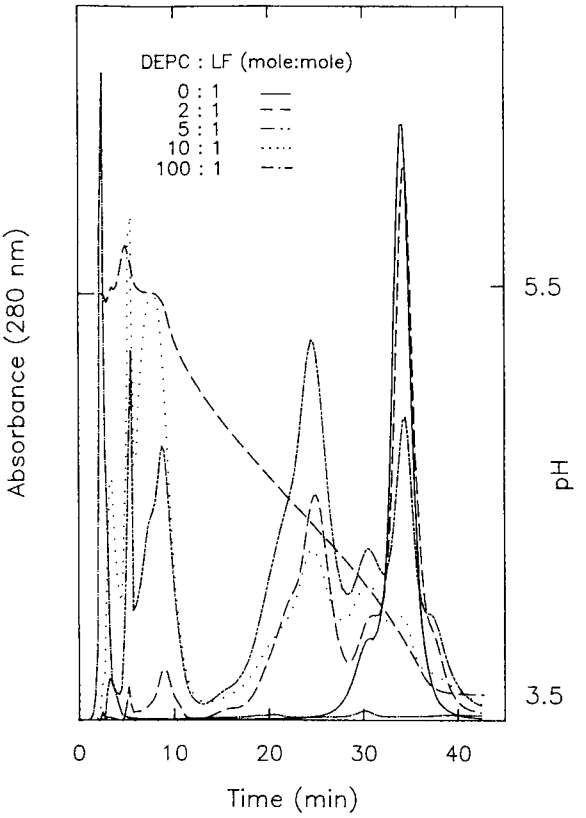

Fig. 5. Interaction of human hololactoferrin (LF) with immobilized Cu(II) ions after carboxyethylaton with increasing molar ratios of diethylpyrocarbonate (DEPC). The pH gradient elution protocol was as described in Fig. 2A.

hydryl groups. Lactoferrin and transferrin each contain two specific groups of metal binding residues within (approximately 1.0 nm from the molecular surface) the "iron-binding" clefts of their N-lobes and C-lobes. The specific metal-binding residues in the N-lobe of lactoferrin (Asp 60, Tyr, 92, Tyr 192 and His 253) and the C-lobe of lactoferrin (Asp 395, Tyr 435, Tyr 528 and His 597) are similar to those in the N-lobe of transferrin (Asp 63, Tyr 95, Tyr 188 and His 249) and the C-lobe of transferrin (Asp 392, Tyr 426, Tyr 517 and His 585) [15,16]. One can infer from the data presented here, however, that the amino acid residues in the two "specific" metal-binding clefts did not participate in the interaction of lactoferrin or transferrin with immobilized Cu(II) ions. Therefore, other more exposed electron-donor groups were evaluated. The total surface area of several types of electron-donor groups on the surface of rabbit holotransferrin was significantly greater than that of the human hololactoferrin. The relative differences between hololactoferrin and holotransferrin in total exposed surface areas of Trp residues (129 *versus* 163 $Å^2$), Phe residues (585 *versus* 833 $Å^2$) and Tyr residues (313 *versus* 433 $Å^2$) are small compared to the difference in exposed His residues (328 *versus* 1011 $Å^2$). The effects of specific near-neighbor relationships, although likely to be important, have not yet been considered.

DISCUSSION

This investigation addresses the general problem of identifying specific experimental probes to monitor ligand-induced alterations in the surface structure of proteins. A primary concern was to identify probes that could also be used to achieve actual separation of such protein conformers. Stationary phase immobilized ligands specific for individual residues or domains are likely candidates for these purposes. Immobilized transition metal ions have already received considerable attention in this regard [1–4]. Surface-exposed histidine, cysteine, and tryptophan residues have been the primary focus of attention as the electron-donor groups likely to be responsible for protein and peptide interactions with immobilized transition metal ions [1,3,9,12]. However, the use of immobilized metal ions to monitor and exploit ligand-induced alterations in protein surface structures has not yet been examined.

In the case of lactoferrin, iron-binding is thought to initiate (or stabilize) a 53° inward domain rotation toward a more compact state [17]. It seemed likely that this ligand-induced alteration in surface structure might result in decreased interactions with immobilized metal ions. Thus, the results with lactoferrin were surprising. We have found that both Cu(II)-saturated lactoferrin and Fe(II)-saturated lactoferrin were bound to immobilized Cu(II) ions even more tightly than the metal-free or so-called apolactoferrin. We must conclude from these data that the interaction of lactoferrin with either Cu(II) or Fe(II) ions increases either the surface exposure or reactivity of residues responsible for the interaction with immobilized Cu(II) ions. We can conclude further that the two specific metal ligand binding sites are *not* contributing to the interaction of the metal ion-saturated lactoferrin forms with immobilized Cu(II) ions. The fact that apolactoferrin collected from the IDA–Cu(II) column could also be specifically labeled with two atoms each of either iron or copper ions provides additional evidence for our conclusion.

The effects of iron binding on transferrin and ovotransferrin affinity for immobilized Cu(II) ions were quite opposite the effects of bound iron on lactoferrin affinity for IDA–Cu(II). Iron binding decreased significantly the affinity of transferrin and ovotransferrin for immobilized Cu(II) ions. Iron-saturated transferrins were, however, still bound to IDA–Cu(II) with considerable affinity (higher affinity than any from of lactoferrin). Transferrin saturated with Cu(II) ions actually appeared to have an increased affinity for immobilized Cu(II) ions. Therefore, in contrast to recent conclusions presented elsewhere [34], the specific metal-binding ligands in the N- and C-lobes that are responsible for high affinity iron binding are *not* those involved in transferrin interaction with immobilized Cu(II) ions. Overall, the affinities of the ovotransferrin, lactoferrin, and transferrin for immobilized Cu(II) ions were found to increase as follows: iron-saturated (holo) ovotransferrin < metal-free (apo) ovotransferrin < apolactoferrin < hololactoferrin << iron-saturated transferrin < monoferric transferrin < metal-free or apotransferrin. These findings were predicted in part by the large differences in surface-exposed areas of electron-donor groups (transferrins > lactoferrins).

Through an inspection of the high-resolution structure of human apolactoferrin [17], two points can be made regarding lactoferrin affinity for immobilized metal ions. The quantity of solvent-exposed electron-donor groups previously thought to interact with immobilized metal ions (specifically His residues) on the surface of lactoferrin is

either unaffected or is actually *decreased* in the presence of bound iron, because bound iron stabilizes the closed (more compact) N-lobe and C-lobe configurations. Yet, we found that iron binding *increased* lactoferrin affinity for immobilized Cu(II) ions. If the number and area of surface-exposed immobilized metal ion binding sites is not changed, perhaps internal near-neighbor effects, altered by iron binding, act to increase the affinity of exposed groups for immobilized Cu(II) ions. In the case of transferrin, our data predict the opposite since iron binding decreases transferrin affinity for immobilized Cu(II) ions. These predictions await confirmation by structural solutions to the apo form of transferrin.

There were species-dependent deviations in lactoferrin and transferrin affinity for immobilized Cu(II) ions. Yet, the differences in the amino acid sequence and carbohydrate moieties for the two different transferrins (human and rabbit) and lactoferrins (human and porcine) evaluated did not influence the observed positive effects (for each lactoferrin) and negative effects (for each transferrin) of bound ligand (iron) on affinity for immobilized Cu(II) ions. The effects of altered carbohydrate composition (*e.g.*, recombinant lactoferrins) or carbohydrate removal (*e.g.*, deglycosylation) have not yet been evaluated in detail.

When the electron-donor groups on a protein surface are sufficiently solvent-exposed, mobile phase constituents (including buffer components and free metal ions) may influence their affinity or capacity to interact with immobilized metal ions. The use of mobile phase modifying reagents to promote selective protein recognition of immobilized ligands has been discussed (*e.g.*, ref. 35). The *differential* effects of urea and imidazole on the resolution of lactoferrin and transferrin in their apo and holo forms were clearly evident and suggest the participation of different types of surface electron-donor groups. In contrast to relatively simpler "one-site" protein models (*e.g.*, lysozyme), multiple types (affinities) of interactions exist between lactoferrin and IDA-immobilized Cu(II) ions [36]. Analyses of equilibrium binding data, performed as described previously [36,37], confirmed the contrasting influence of urea and imidazole on the interaction of these proteins with immobilized Cu(II) ions (data not shown). Much more work is needed to clarify the role of solvent on protein interactions with immobilized metal ions.

The site-specific carboxyethylation of lactoferrin with diethylpyrocarbonate did not abolish completely its affinity for immobilized Cu(II) ions until the molar ratio of diethylpyrocarbonate to surface-exposed histidyl residues was greater than 14:1. While histidine modification is most likely under these conditions, the actual number and type of surface residues modified has not been verified. We have also found that N-hydroxysuccinimide esters, known to react with primary amines (*e.g.*, lysine residues or amino terminus), can be used to eliminate the affinity of transferin for immobilized transition metal ions (unpublished observation). Thus, the mechanism(s) by which urea and imidazole differentially influence the reaction of specific residues with the immobilized metal ions remains unknown.

The effects of excess free metal ions in the mobile phase were negligible. Previous investigations [36] have shown that the presence of added free Cu(II) ions did not affect the chromatographic behavior of iron-saturated lactoferrin on affinity columns of immobilized Cu(II). Equilibrium binding experiments confirmed the absence of detectable alterations in lactoferrin affinity for immobilized Cu(II) ions even in the presence of 100 μM Cu(II) [36]. These data demonstrate that protein surface binding

sites for free Cu(II) ions and IDA-immobilized Cu(II) ions are functionally distinct, that is, individual metal ion ligand binding sites on the surface of these proteins are not necessarily those that determine stable interactions with immobilized metal ions.

The unusually high affinity of transferrin (and lactoferrin) for immobilized Cu(II) ions must result from very effective and (or) very extensive protein surface–stationary phase interactions. Because of their distribution over the protein surface, and in the absence of extensive protein denaturation at the immobilized Cu(II) ion stationary phase, it seems unlikely that all of the electron-donor residues (*e.g.*, His residues) on the surface of lactoferrin or transferrin are participating in the immobilization event. Nevertheless, relatively distant attachment (*i.e.*, metal-binding) sites on a protein surface may interact with separate immobilized metal ions to create a macromolecular chelation (macrochelation) event (see Fig. 1 of ref. 37). This multi-point macrochelation mechanism results in a high affinity interaction event, even though the separate contribution by each individual residue may be relatively weak. This view is separate and distinct from the possibility of high affinity microchelation events which may occur when localized (vicinal) clusters of two or more surface-exposed residues participate in the interaction (microchelation) with a single immobilized metal ion.

Our results may have broader implications. Intracellular metal ions are associated with protein surfaces. These interactions remain largely uncharacterized. Protein surface-immobilized metal ions may influence macromolecular recognition events. The potential sensitivity of surface immobilized Cu(II) ions to distinguish and monitor ligand-induced alterations in protein surface structure has now been demonstrated *in vitro*. These findings suggest potential control mechanisms which may be operational *in vivo*. Given what we expect may be a general role for metal ions in the regulation or facilitation of biopolymer interactions [38], stationary phase immobilized metal ions present a useful model system for the further investigation of surface-immobilized metal ions in macromolecular recognition events.

ACKNOWLEDGEMENTS

We are most grateful to Dr. Edward N. Baker and his colleagues at Massey University in New Zealand for helpful discussions, and for making available their refined structural coordinates for human lactoferrin as well as preprints of manuscripts in press. We thank Dr. Peter Lindley at Birbeck College, University of London for providing the coordinates for diferric rabbit serum transferrin. We thank Dr. John S. Sack at Baylor College of Medicine for providing us with version 6.6 of PS300 FRODO. We thank Dr. F. M. Richards at Yale University for sending us ACCESS (version 2) and VOLUME. We would like to thank Ms. E. Roseland Klein and Mr. Jerry D. Eastman from our Publications Department for their editorial assistance during the preparation of this manuscript.

This project has been funded, in part, with federal funds from the U.S. Department of Agriculture, Agricultural Research Service under Cooperative Agreement number 58-7MN1-6-100. The contents of this publication do not necessarily reflect the views or polices of the U.S. Department of Agriculture, nor does mention of trade names, commercial products or organizations imply endorsement by the U.S. Government.

REFERENCES

1 J. Porath, J. Carlsson, I. Olsson and G. Belfrage, *Nature (London)*, 258 (1975) 598.
2 J. Porath and B. Olin, *Biochemistry*, 22 (1983) 1621.
3 E. Sulkowski, *Trends Biotechnol.*, 3 (1985) 1.
4 G. Muszynska, Y.-J. Zhao and J. Porath, *J. Inorg. Biochem.*, 26 (1986) 127.
5 A. Figueroa, C. Corradini, B. Feibush and B. L. Karger, *J. Chromatogr.*, 371 (1986) 335.
6 C. M. Li and T. W. Hutchens, *Biol. Chem. Hoppe-Seyler*, 368 (1987) 758.
7 T. W. Hutchens and C. M. Li, *J. Mol. Recog.*, 1 (1988) 80.
8 T.-T. Yip and T. W. Hutchens, in T. W. Hutchens (Editor), *Protein Recognition of Immobilized Ligands*, Alan R. Liss, New York, 1989, p. 45.
9 E. S. Hemdan, Y.-J. Zhao, E. Sulkowski and J. Porath, *Proc. Natl. Acad. Sci. U.S.A.*, 86 (1989) 1811.
10 T. W. Hutchens, C. M. Li, Y. Sato and T.-T. Yip, *J. Biol. Chem.*, 264 (1989) 17206.
11 F. R. N. Gurd and P. E. Wilcox, *Adv. Protein Chem.*, 11 (1956) 311.
12 T.-T. Yip, Y. Nakagawa and J. Porath, *Anal. Biochem.*, 183 (1989) 159.
13 Y. Nakagawa, T.-T. Yip, M. Belew and J. Porath, *Anal. Chem.*, 168 (1988) 75.
14 T.-T. Yip and T. W. Hutchens, *J. Cell. Biol.*, 107 (1988) 543a.
15 B. F. Anderson, H. M. Baker, E. J. Dodson, G. E. Norris, S. V. Rumball, J. M. Waters, E. N. Baker, *Proc. Natl. Acad. Sci. U.S.A.*, 84 (1987) 1769.
16 B. F. Anderson, H. M. Baker, D. W. Rice and E. N. Baker, *J. Mol. Biol.*, 209 (1989) 711.
17 B. F. Anderson, H. M. Baker, G. E. Norris, S. V. Rumball and E. N. Baker, *Nature (London)*, 344 (1990) 784.
18 S. Bailey, R. W. Evans, R. C. Garratt, B. Gorinsky, S. Hasnain, C. Horsburgh, H. Jhoti, P. F. Lindley, A. Mydin, R. Sarra and J. L. Watson, *Biochemistry*, 27 (1988) 5804.
19 E. W. Ainscough, A. M. Brodie, J. E. Plowman, S. J. Bloor, J. S. Lœhr and T. M. Loehr, *Biochemistry*, 19 (1980) 4072.
20 E. W. Ainscough, A. M. Brodie, S. J. McLachlan and V. S. Ritchie, *J. Inorg. Biochem.*, 18 (1983) 103.
21 J. H. Brock, in P. Harrison, (Editor), *Topics in Molecular and Structural Biology*, Verlag Chemie, Basel, 1985, p. 183.
22 B. L. Nichols, K. S. McKee, J. F. Henry and M. Putman, *Pediatr. Res.*, 21 (1987) 563.
23 G. C. Bagby, Jr. V. D. Rigas, R. M. Bennett and A. A. Vandenbark, *J. Clin. Invest.*, 68 (1981) 56.
24 R. M. Bennett, M. M. Merritt and G. Gabor, *Br. J. Haematol.*, 63 (1986) 105.
25 R. M. Bennett, J. Davis, S. Campbell and S. Portnoff, *J. Clin. Invest.*, 71 (1987) 611.
26 H. S. Birgens, L. Ostergaard Kristensen, N. Borregaard, H. Karle and N. E. Hansen, *Aur. J. Haematol.*, 41 (1988) 52.
27 B. Lonnerdal, *Am. J. Clin. Nutr.*, 42 (1985) 1299.
28 T. W. Hutchens, J. F. Henry and T.-T. Yip, *Clin. Chem.*, 35 (1989) 1928.
29 T. W. Hutchens, J. S. Magnuson and T.-T. Yip, *Pediatr. Res.*, 26 (1989) 618.
30 S. Kunar and K. L. Bhatia, *J. Chromatogr.*, 434 (1988) 228.
31 Y. Kato, K. Nakamura and T. Hashimoto, *J. Chromatogr.*, 354 (1986) 511.
32 T. A. Jones, in D. Sayre (Editor), *Computational Crystallography*, Clarendon Press, Oxford, 1982, p. 303.
33 B. Lee and F. M. Richards, *J. Mol. Biol.*, 55 (1971) 379.
34 E. Sulkowski, in S. K. Sikdar, M. Bier and P. Todd (Editors), *Frontiers in Bioprocessing*, CRC Press, Boca Raton, FL, 1990, p. 343.
35 T. W. Hutchens and J. Porath, *Clin. Chem.*, 33 (1987) 1502.
36 T. W. Hutchens and T.-T. Yip, *J. Chromatogr.*, 500 (1990) 531.
37 T. W. Hutchens, T.-T. Yip and J. Porath, *Anal. Biochem.*, 170 (1988) 168.
38 E. Eisenstein, D. W. Markby and H. K. Schachman, *Proc. Natl. Acad. Sci. U.S.A.*, 86 (1989) 3094.

Journal of Chromatography, 536 (1991) 17–30
Elsevier Science Publishers B.V., Amsterdam

CHROMSYMP. 2060

Effect of metal ions on the unfolding kinetics of α-lactalbumin on weakly hydrophobic surfaces

SHIWEN LIN, PETER OROSZLAN and BARRY L. KARGER*
Barnett Institute, Northeastern University, Boston, MA 02115 (U.S.A.)

ABSTRACT

The effect of metal ion [Ca^{2+} and $Zn(NH_3)_4^{2+}$] on the unfolding kinetics of bovine-α-lactalbumin (α-LACT) on a weakly hydrophobic chromatographic surface (ethyl polyether phase bonded on porous silica, C_2 ether) has been studied using surface intrinsic fluorescence spectroscopy and liquid chromatography. Chromatographic results on the C_2 ether phase revealed two peaks for α-LACT, the first being the folded and the second an unfolded conformation, as determined by fluorescence spectroscopy. The retention time for the second peak was found to depend on the specific metal additive in the mobile phase. Fluorescence studies showed a slow change in emission maximum from *ca.* 330 nm to 350 nm and a 5-fold increase in emission intensity for the adsorbed protein in the unfolded state. By following the fluorescence emission intensity at a given wavelength during the unfolding process, biphasic kinetics were observed with the kinetic constants depending on the specific metal-ion additive. In addition, solution refolding rates of the desorbed, unfolded species were measured and found to be consistent with literature refolding rate constants.

INTRODUCTION

The adsorption of proteins to liquid–solid interfaces is a subject of broad interest, including the design of biocompatible materials, bioanalytical sensors and the chromatographic separation of biomolecules [1,2]. From the separation point of view, an understanding of the protein adsorption process can aid in the optimization of conditions for selectivity, resolution and the minimization of the loss of biological activity of the protein [3]. One of the most important aspects of this adsorption process is the degree of alteration of the three-dimensional protein structure associated with solute contact with the chromatographic surface. The particular protein structure which interacts with the solid support can significantly influence retention. In addition, asymmetrically broadened or multiple peaks have been observed, depending on the rate and extent of structural alteration during adsorption and desorption [4–8].

To date, most studies of protein structural alteration upon adsorption have focused on the protein in solution after desorption [8,9]. Obviously, more detailed information can be obtained by exploring the protein while in contact with the surface of the adsorbent. Methods to study proteins on surfaces include antibody binding [10], ellipsometry [11], Raman [12], circular dichroism [13], Fourier-transform infrared

0021-9673/91/$03.50

(FT–IR) [14], total internal reflectance fluorescence (TIRF) [15,16] and intrinsic fluorescence spectroscopy [17].

Recently, this laboratory has developed a direct intrinsic fluorescence spectroscopic method combined with gradient elution chromatography for the study of adsorbed proteins on chromatographic surfaces [3,18–20]. Our studies have demonstrated that conformational changes of proteins on typical chromatographic surfaces used in reversed-phase liquid chromatography (RPLC) and hydrophobic interaction chromatography (HIC) can be followed by an examination of the fluorescence changes as a function of contact time of the protein with the surface. This approach has been shown to provide significant insight into the real-time, on-column structural change of proteins in contact with the surface. In a previous paper, detailed methodologies have been defined to elucidate kinetic processes of change of α-LACT on two HIC adsorbents [19].

Subsequent to the discovery that α-LACT was a calcium metalloprotein [21], extensive studies have been made on the binding properties and induced conformational changes caused by a variety of metal ions [22]. In contrast to calcium binding, which stabilizes the native conformation, Zn^{2+}, on binding to apo α-LACT, appears to stabilize the so-called *A* conformation, *i.e.*, a conformation closely resembling that of the acid-denatured α-LACT, which possesses a flexible molten globule structure [23] and exposed hydrophobic patches [24]. These metal binding characteristics and induced conformational changes of α-LACT have been utilized in low-pressure HIC to affect separation. Lindahl and Vogel [25] reported that Ca^{2+} eluted adsorbed α-LACT from Phenyl-Sepharose by inducing a less hydrophobic conformation, whereas elution could not be achieved by addition of Zn^{2+}. In high-performance liquid chromatography (HPLC), addition of Ca^{2+} has also been used to manipulate the retention and maintain biological activity of other calcium-binding proteins [26]. Salt addition to the mobile phase would appear to be a general approach for the manipulation of selectivity in the chromatographic separation of proteins [27,28].

Previous chromatographic work in this laboratory has demonstrated [8,19] that calcium-depleted α-LACT eluted as two well separated peaks from an ethyl polyether column (C_2 ether). The kinetics of conversion of the first peak to the second peak were observed by varying the time and temperature while the protein was in contact with the surface [7]. It was found that the second peak of α-LACT, identified as the unfolded species by on-line second-derivative UV spectroscopy, could undergo refolding in solution [8]. Conformational alteration of α-LACT has also been shown to occur on other commercially available HIC columns, *i.e.*, poly(alkyl) aspartamide columns [29]. Our chromatographic results further indicated that addition of a small concentration of calcium to the mobile phase caused a different HIC elution profile of α-LACT [8]. This paper examines further the effect of metal ions on the structural changes of adsorbed α-LACT using on-column intrinsic fluorescence.

EXPERIMENTAL

Equipment

The instrumental components for the on-column fluorescence measurements have been previously described in detail [19]. Briefly, a Suprasil quartz spectroscopic flow cell (35 μl, 11 × 2 mm I.D.) was utilized as both a cell for the surface fluorescence

studies using an SPF-500 spectrofluorometer (SLM-Aminco, Urbana, IL, U.S.A.) and as a microcolumn attached to a Series 410 BIO LC liquid chromatographic pump (Perkin-Elmer, Norwalk, CT, U.S.A.). The outlet of the flow-cell column was connected to a 1046A fluorescence LC detector (Hewlett-Packard, Palo Alto, CA, U.S.A.) *via* an empty Suprasil quartz spectroscopic flow cell. The sample compartment, injector and tubing (PTFE, 1.5 mm O.D. × 0.3 mm I.D.) attached to the column were thermostated at 5.8 ± 0.2°C by an Exacal and FTC Model 350A flow-through cooler system (Neslab, Newington, NH, U.S.A.), controlled by a thermocouple (Omega, Stanford, CT, U.S.A.). The chromatographic and spectroscopic data were processed with a data acquisition system (Nelson Analytical, Cupertino, CA, U.S.A.) and Spectrum Processor software (SLM Instruments, Urbana, IL, U.S.A.).

The packing in the flow cell (cell I) was made from Vydac silica gel (particle size 6 μm, pore diameter 300 Å, specific surface area 90 m^2/g) (Separations Group, Hesperia, CA, U.S.A.) bonded with an ethyl polyether phase (C_2 ether) and prepared as described elsewhere [30]. The surface coverage was 4.0 $\mu mol/m^2$ as determined by elemental analysis (assuming a binding stoichiometry to the silica of 2 ethoxy groups per silane molecule). The packing of the silica gel into the flow cell was carefully performed by hand to obtain a homogeneous distribution of the support in the column. Column conditioning was accomplished by injecting 10 μl aliquots of a 5.0-mg/ml protein solution 20 times, followed each time by elution under HIC-gradient conditions. The reproducibility of the gradient retention time for independent injections was 0.3% coefficient of variation (C.V.) ($n = 5$) from run to run, and was 0.5% C.V. ($n = 3$) from column to column.

Chemicals

Calcium-depleted bovine-milk α-LACT was purchased from Sigma (St. Louis, MO, U.S.A.). The purity of the protein was found to be sufficient for the chromatographic and fluorescence experiments [19]. High-purity-grade ammonium sulfate (treated to reduce the content of heavy metals) was the product of Sigma. HPLC-grade water and reagent-grade ammonium acetate were purchased from J. T. Baker (Philipsburg, NJ, U.S.A.).

The protein samples (5.0 mg/ml) were freshly prepared in 1 *M* ammonium sulfate–0.5 *M* ammonium acetate, pH 6.3. For the metal additive experiments, 1 m*M* $CaCl_2$ or $ZnCl_2$ was added to the same sample buffer.

Procedures

Mobile phase solutions of 3 *M* ammonium sulfate–0.5 *M* ammonium acetate (mobile phase A) and 0.5 *M* ammonium acetate (mobile phase B) were prepared by dissolving the correct weight of salt in degassed HPLC water and adjusting the pH to 6.3. Metal-ion-containing mobile phases were prepared by pipeting the correct volume of 0.5 *M* $CaCl_2$ or $ZnCl_2$ into the non-metal-containing mobile-phase solutions. These solutions were filtered by passing through an 0.45-μm membrane filter and then degassed under vacuum before use.

A 10-μl injected volume of a 5.0-mg/ml sample (50 μg) of α-LACT was determined as a convenient amount, and 0.3 ml/min a convenient flow-rate for the surface fluorescence and chromatographic measurements; the surface kinetics were independent of injected protein concentration (0.5–5.0 mg/ml) and mobile-phase

flow-rate (0.1–0.5 ml/min) [19]. Upon injection, the incubation solvent (mobile phase A) transported the sample in a 10-μl loop into the flow-cell column (cell I). The time of solute travel from the injector (including the sample loop) to the column was 12 s, at a flow-rate of 0.3 ml/min. Thus, 12 s after injection was defined as the initial contact time of the protein to the surface, *i.e.*, zero time. A 10-min linear gradient from 100% mobile phase A to 100% mobile phase B was used to elute the protein from the flow-cell column after a given period of incubation. For the solution-refolding experiments, the second empty flow cell (cell II) was switched into the light path, and the fluorescence was monitored in this cell. The time from cell I to cell II was determined to be 6 s and to the chromatographic fluorescence detector to be 34 s, at a flow-rate of 0.3 ml/min. The reproducibility of maximum emission intensity at fixed sampling time for independent injections of the same protein solution on the column was 0.5% C.V. (n = 5). The procedure for the fluorescence data acquisition and manipulation have been detailed in the previous paper [19].

RESULTS AND DISCUSSION

It is important to note that at high concentrations of NH_4^+ and nearly neutral pH, significant amounts of NH_3 can be present in the mobile phase. Based on an extrapolated formation constant of $2 \cdot 10^{10}$ for $Zn(NH_3)_4^{2+}$ at 5.8°C [31], 98, 58 and 0.2% of added $ZnCl_2$ (1 mM) will be in the complex form of $Zn(NH_3)_4^{2+}$, if the solution conditions are 3.0, 1.0 and 0 M ammonium sulfate plus 0.5 M ammonium acetate, pH 6.3, respectively. Thus, in the incubation mobile phase (mobile phase A, 3 M ammonium sulfate and 0.5 M ammonium acetate, pH 6.3), the added 1 mM $ZnCl_2$ will exist predominately as $Zn(NH_3)_4^{2+}$. In mobile phase B (0.5 M ammonium acetate, pH 6.3), almost all the added $ZnCl_2$ will be in the free ionic form Zn^{2+}. Note that in the HIC gradient from 3 M to 0 M $(NH_4)_2SO_4$, the surface tension of the solution not only decreases, but also $Zn(NH_3)_4^{2+}$ is converted to Zn^{2+}.

Hydrophobic interaction chromatography

Fig. 1 presents the HIC chromatograms for α-LACT on the C_2 ether phase in the packed flow cell (cell I) under gradient-elution conditions from 3 M to 0 M ammonium sulfate. The chromatograms are a function of incubation time of the adsorbed protein with an isocratic hold of mobile phase A. In agreement with previous results [8,9], two peaks are observed, the second peak increasing with the incubation time at the expense of the first. By following the decrease in area of the first peak as a function of incubation time, the apparent first-order rate constant was determined to be $6.9 \cdot 10^{-2}$ min^{-1} (r^2 = 0.998). It should be noted that this value was larger than that reported in the earlier paper [19], *i.e.*, $7.4 \cdot 10^{-3}$ min^{-1}; however, two different C_2 ether bonded phases were used in these two studies. The synthesized adsorbent in the present work had a larger surface area (90 *vs.* 72 m^2/g) and a higher absolute carbon loading than that of the previous study. The overall higher hydrophobicity of the surface was thus presumably a significant factor in the faster unfolding kinetics of the protein on the surface. In addition, the slightly higher column temperature used in this work (5.8 *vs.* 4.0°C) also contributed to the faster kinetics. Nevertheless, the ten-fold difference in the rate of unfolding demonstrates that this parameter can be a sensitive function of surface characteristics and thus could be useful in the characterization of chromato-

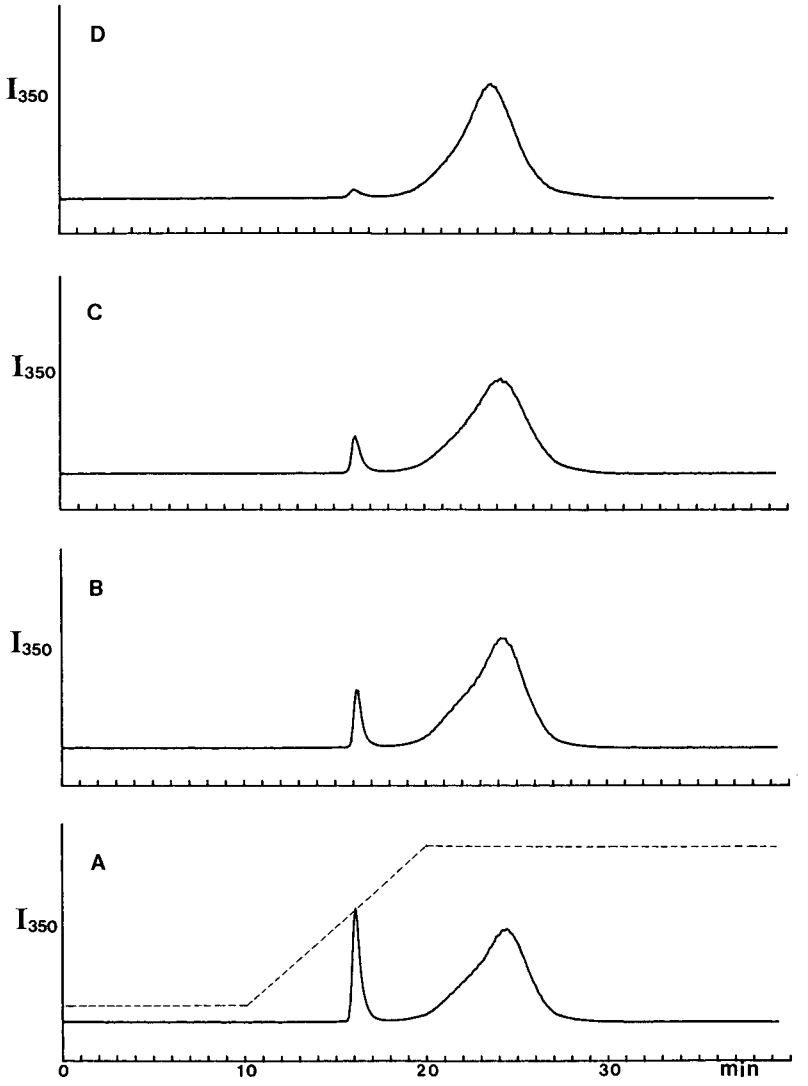

Fig. 1. Gradient-elution chromatograms of α-LACT as a function of incubation time (10 min gradient delay time not included) with mobile phase A. (A) 0 min; (B) 10 min; (C) 20 min; (D) 50 min. Conditions: 10-min gradient from 100% mobile phase A (3 *M* ammonium sulfate–0.5 *M* ammonium acetate, pH 6.3) to 100% mobile phase B (0.5 *M* ammonium acetate, pH 6.3). Sample: calcium-depleted bovine α-LACT, 5.0 mg/ml in 33% A, 67% B, 10-μl injection. Fluorescence detection wavelength: 350 nm, flow-rate 0.3 ml/min, temperature 5.8°C.

graphic adsorbents. The broad and asymmetric second peak in Fig. 1 will be considered shortly.

The influence of added metal ion on the elution profile is shown in Fig. 2. In all three cases, *i.e.*, no metal-ion additive, 1 m*M* Ca^{2+} and 1 m*M* $Zn(NH_3)_4^{2+}$ in the

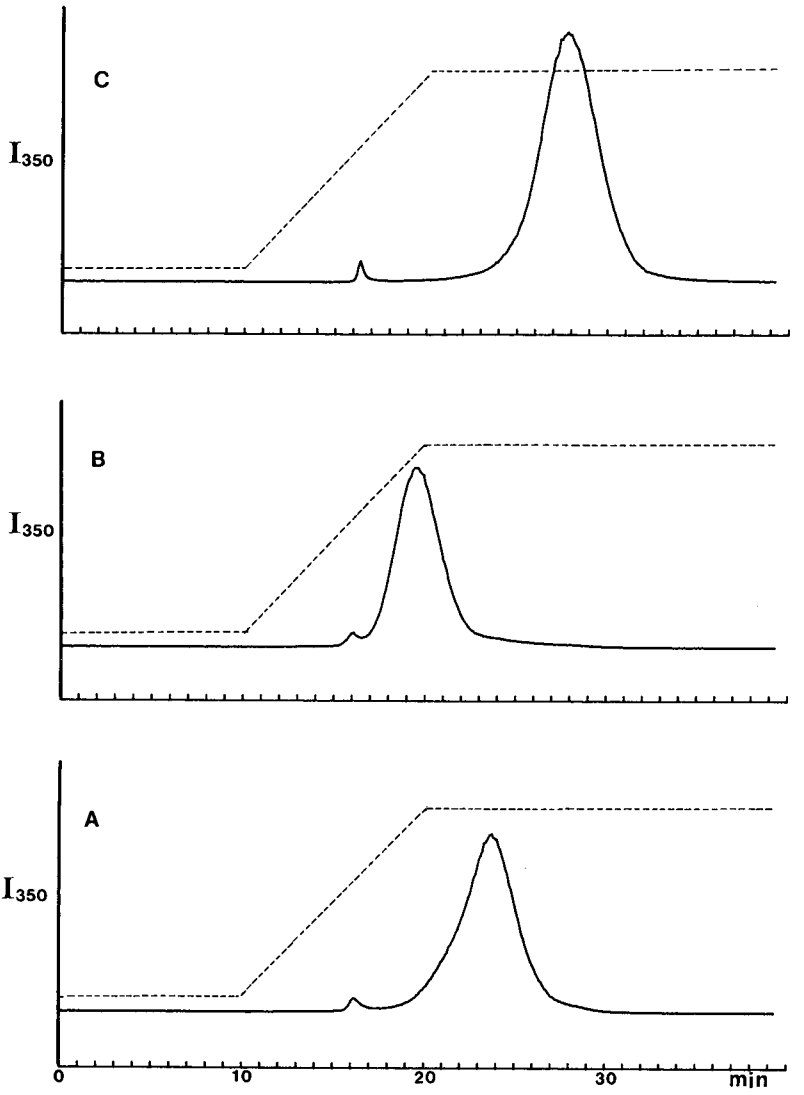

Fig. 2. Gradient-elution chromatograms of α-LACT as a function of metal-ion additives in the mobile phase. (A) no metal-ion additive, incubation 50 min; (B) 1 m*M* $CaCl_2$ added in both mobile phases A and B as well as the sample solution, incubation 80 min; (C) 1 m*M* $ZnCl_2$ added in both mobile phases and the sample solution, incubation 80 min. Other conditions are the same as in Fig. 1.

mobile phase, two peaks were observed, with the first peak in all cases eluting at the same position of the gradient (1.26 *M* ammonium sulfate) while the second peak eluted at different gradient positions. With the Ca^{2+}-containing mobile phase, the second peak was eluted at the end of the gradient whereas without metal ion and with the zinc-added mobile phase, the second peak was eluted 4 min and 8 min after the end of the gradient, respectively. As will be shown later, the differences in the retention time of

the second peak for the various mobile phases are a consequence of the differences in the refolding rates of the desorbed species under the second peak.

Fig. 2 further shows that a slower conversion of the first peak into the second was observed in the presence of Ca^{2+} (80 min incubation time), relative to that of the metal-ion-free condition (50 min incubation time). Small amounts of the first peak were still seen after 80 min incubation with the calcium-containing mobile phase, while a shorter incubation time (50 min) had to be used in order to maintain roughly the same amount of the first peak in the absence of Ca^{2+}. Interestingly, with $Zn(NH_3)_4^{2+}$ in the mobile phase, conversion of the first peak to the second was also slower than the non-metal-ion-additive case.

Since the chromatographic method can only probe the gross unfolding kinetics, we next explored the surface unfolding of the adsorbed protein for a more detailed kinetic picture. This examination was accomplished by *in situ* intrinsic fluorescence of the protein on the chromatographic surface.

Kinetic analysis of the surface-unfolding of α-LACT

Fig. 3 shows the emission spectra of α-LACT on the C_2 ether phase as a function of incubation time with and without metal-ion additive. In order to minimize photodecomposition, a discrete method of data collection was employed [19]. The fluorescence emission spectra were collected by scanning for 10 s intervals from 325 to 355 nm at 30, 60 and 300 s after injection. Two major features of the three mobile phases in this figure are: (1) the general increase in emission intensity with incubation time and (2) the 16-nm red shift in the emission maximum (from 333 nm in the first minute of surface contact to 349 nm after 60 min) in the absence and presence of Ca^{2+} or $Zn(NH_3)_4^{2+}$. Similar to the fluorescence behavior of α-LACT in solution reported by others [32], the increase in emission intensity and the red shift in the emission maximum strongly suggest unfolding of the adsorbed protein.

The surface kinetics of structure change of the adsorbed protein can be derived from the plot of fluorescence intensity *vs.* incubation time at a given wavelength. Fig. 4 presents the on-column fluorescence emission intensity at 350 nm as a function of incubation time of the adsorbed α-LACT with and without 1 m*M* Ca^{2+} or 1 m*M* $Zn(NH_3)_4^{2+}$ in the mobile phase. As can be seen, the fluorescence intensity of α-LACT in the presence of Ca^{2+} increased at a slower rate compared to the metal-ion-free mobile phase, in agreement with the chromatographic results of Fig. 2. Interestingly, in the presence of 1 m*M* $Zn(NH_3)_4^{2+}$ in the incubation mobile phase, the rate of increase in fluorescence intensity was reduced even further.

Curve fitting of the plots in Fig. 4 revealed that in all three cases the unfolding process could be fitted to a biphasic kinetics model (Fig. 3). The macroscopic rate constants were derived from curve fitting according to the equation [19]

$$I(t) = I_\infty - I_1^* e^{-\lambda_1 t} - I_2^* e^{-\lambda_2 t} \quad (1)$$

and the results are shown in Table I. As can be seen, the macroscopic rate constants for the slow kinetic phase (λ_2) are of the same magnitude as the rate constants derived from chromatography, while the fast kinetic phase (λ_1) can be monitored only by on-column fluorescence. Addition of Ca^{2+} in the incubation mobile phase reduced the macroscopic rate constants of unfolding of α-LACT by 30 and 40% for the fast and

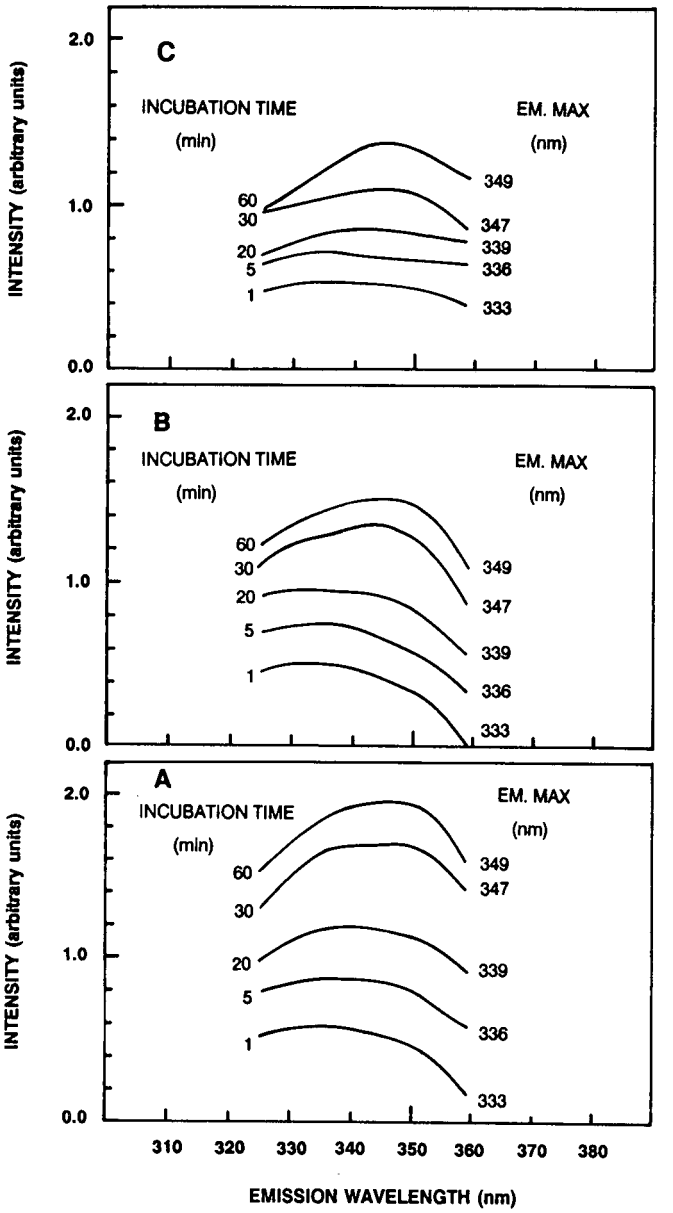

Fig. 3. Fluorescence spectra of α-LACT on the C_2 ether phase as a function of incubation time (see Fig. 1 for other conditions). (A) No metal-ion additive; (B) 1 m*M* $CaCl_2$; (C) 1 m*M* $ZnCl_2$ added in the incubation solvent. Excitation wavelength: 295 nm; emission scan: 2 nm/s; resolution: 0.5 nm; incubation solvent: mobile phase A (3 *M* ammonium sulfate–0.5 *M* ammonium acetate, pH 6.3); temperature 5.8°C.

slow kinetic phases, respectively. In the presence of $Zn(NH_3)_4^{2+}$, the rate constants for the two kinetic phases were even smaller, both by a factor 3, relative to the non-metal-ion case.

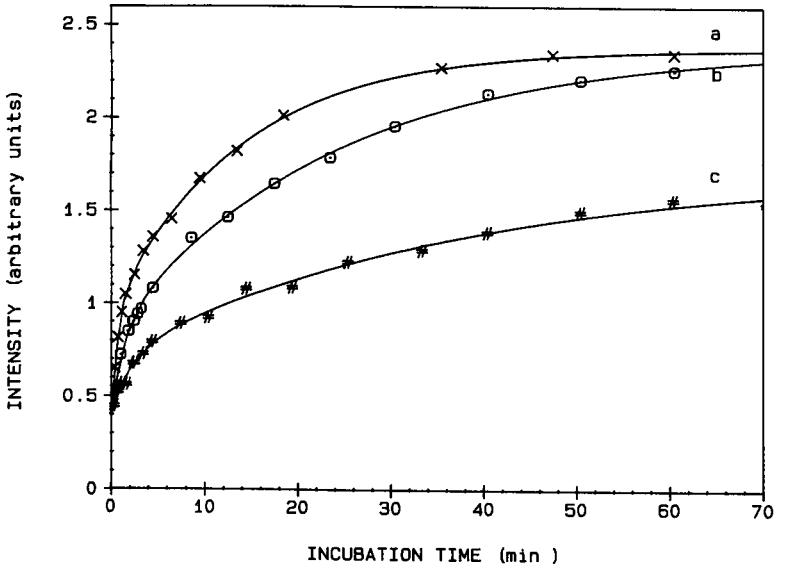

Fig. 4. Fluorescence emission intensity (at 350 nm) of α-LACT adsorbed on the C_2 ether phase as a function of incubation time. Conditions are the same as in Fig. 3. Lines are fitted to a biphasic equation (eqn. 1 in the text). Curves: (a) no metal ion additive, (b) 1 m*M* $CaCl_2$, (c) 1 m*M* $ZnCl_2$ added in the incubation solvent.

Kinetic analysis of the microscopic unfolding process was performed using a kinetic model of

$$F \underset{k_2}{\overset{k_1}{\rightleftarrows}} X \xrightarrow{k_3} U \tag{2}$$

where *F* denotes the initial folded state, *U* the final unfolded state and *X* a kinetic intermediate [19]. The validity of this model is seen in that neither parabolic

TABLE I

BIPHASIC KINETIC PARAMETERS FOR THE UNFOLDING OF α-LACT ON THE C_2 ETHER PHASE

Experimental conditions are the same as in Fig. 3. I_1^* and I_2^* are the dimensionless amplitudes for the two exponential phases. $I(0)$ is the intercept corresponding to the $I(t)$ value at $t=0$. See Fig. 4 and eqn. 1.

Additive		$I(0)$	I_1^*	I_2^*	I_∞	λ_1 (min^{-1})	λ_2 (min^{-1})
None		0.40	0.68	1.71	2.83	1.25	0.073
	$\pm\sigma$	0.04	0.03	0.01	0.20	0.03	0.003
1 m*M* Ca^{2+}		0.38	0.44	1.50	2.32	0.81	0.043
	$\pm\sigma$	0.03	0.02	0.03	0.10	0.02	0.001
1 m*M* $Zn(NH_3)_4^{2+}$		0.42	0.21	0.97	1.60	0.44	0.028
	$\pm\sigma$	0.04	0.08	0.03	0.20	0.06	0.001

TABLE II

MICROSCOPIC RATE CONSTANTS FOR THE UNFOLDING OF α-LACT ON THE C_2 ETHER PHASE; $F \underset{k_2}{\overset{k_1}{\rightleftarrows}} X \overset{k_3}{\rightarrow} U$

Experimental conditions are the same as in Fig. 3.

Additive	k_1 (min^{-1})	k_2 (min^{-1})	$K_e = k_1/k_2$	k_3 (min^{-1})
None	0.97 ± 0.04	0.13 ± 0.04	7.6 ± 0.3	0.22 ± 0.02
1 m*M* Ca^{2+}	0.42 ± 0.02	0.27 ± 0.04	1.5 ± 0.1	0.16 ± 0.02
1 m*M* $Zn(NH_3)_4^{2+}$	0.12 ± 0.03	0.23 ± 0.04	0.52 ± 0.1	0.12 ± 0.01

($F \rightarrow X \rightarrow U$) nor sigmoidal ($F \rightarrow X \rightleftarrows U$) curves of fluorescence intensity I *vs.* time t were observed. The microscopic rate constants, k_1, k_2 and k_3 were derived from the macroscopic parameters in Table I and are tabulated in Table II.

The microscopic parameters reveal that the rate constant of the early unfolding stage, $F \rightarrow X$, decreased when Ca^{2+} was added to the system, whereas the surface refolding process, $X \rightarrow F$, was accelerated by the presence of Ca^{2+}. Microscopic reversibility permitted the calculation of the constant, K_e, for the process $F \rightleftarrows X$. A value of $K_e = 7.6$ was obtained for the case of the non-metal-ion mobile phase (Table II). A K_e value of 1.5 in the presence of Ca^{2+} showed that the formation of the kinetic intermediate was thermodynamically less favorable with added Ca^{2+}, in agreement with literature reports that in solution calcium binding stabilized the folded state F [21]. In the presence of $Zn(NH_3)_4^{2+}$, a K_e value of 0.5 was obtained, indicating that the formation of the intermediate was unfavorable under these conditions.

The relative amounts of each species, F, X and U, as a function of time can be obtained from the microscopic rate constants using the integrated rate law for each component. The results of this calculation for the three mobile phases are shown in Fig. 5. As can be seen, the decay of the folded species F in the presence of Ca^{2+} was slower relative to the non-metal-ion case, while in the presence of $Zn(NH_3)_4^{2+}$, the decay of the folded state F was even slower, with a smaller accumulation of the intermediate X.

It is well known that Zn^{2+} binding to α-LACT favors a more flexible conformation in solution [24], whereas our results have shown that $Zn(NH_3)_4^{2+}$ appeared to stabilize the folded state on the surface. Since a significant difference in the ionic radius, charge density and coordination exists between the two forms of zinc in solution, it is not surprising that $Zn(NH_3)_4^{2+}$ may interact with α-LACT in a different way than Zn^{2+}. The effect of $Zn(NH_3)_4^{2+}$ appears to be consistent with the known cation stabilization of α-LACT in solution [22]; in the case of Zn^{2+}, specific binding is known to occur to cause destabilization [24]. (The inaccessibility of the zinc binding site on the adsorbed protein to components of the solution may also play a role.) It is further interesting to note that $Zn(NH_3)_4^{2+}$ slowed the surface-induced unfolding of α-LACT to an even greater extent than Ca^{2+}.

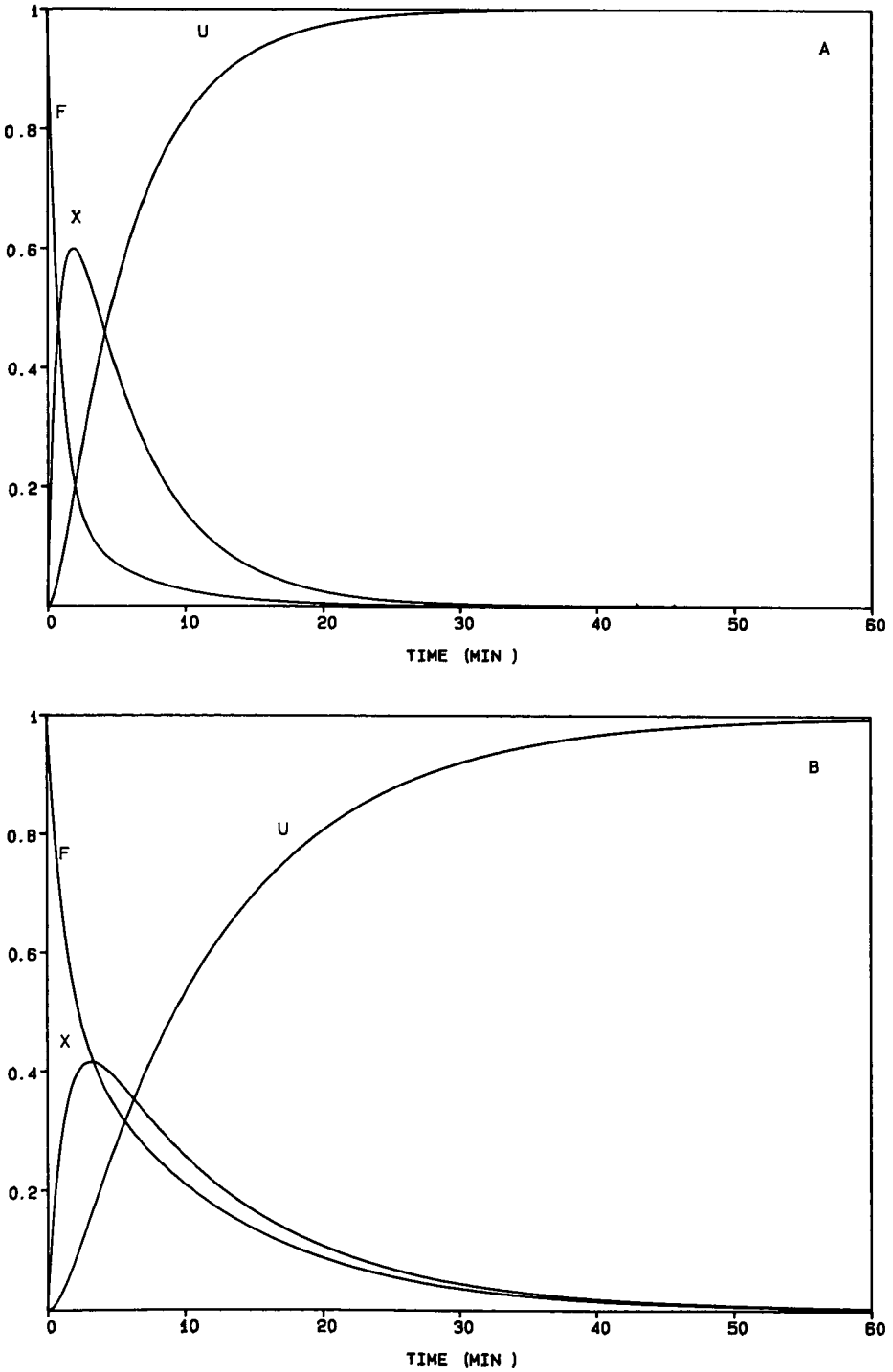

Fig. 5

(Continued on p. 28)

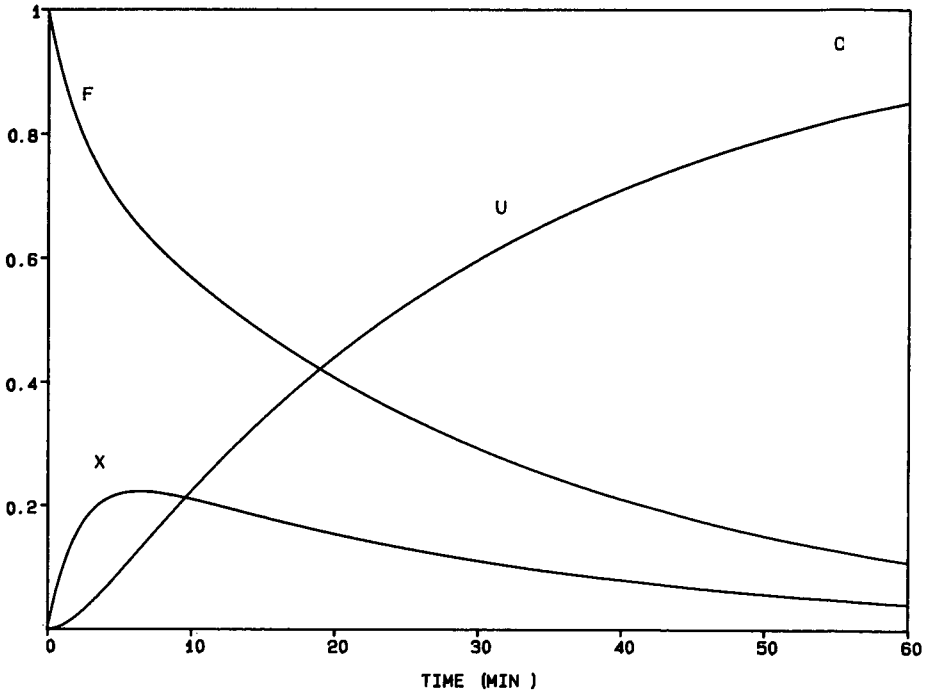

Fig. 5. Relative amounts of F (folded), X (kinetic intermediate) and U (unfolded) states as a function of time for α-LACT, adsorbed on C_2 ether phase at 5.8°C in the absence (A) and presence of 1 mM Ca^{2+} (B) and 1 mM $Zn(NH_3)_4^{2+}$ (C). Conditions as in Fig. 3. The model is based on biphasic kinetics.

Solution refolding upon desorption

In the previous work [19], the solution-refolding kinetics of α-LACT of the second peak was measured by following the change in intrinsic fluorescence of the desorbed species in a second empty flow cell (Cell II) connected in series. We again measured the solution-refolding rate constants in the absence and presence of Ca^{2+} or Zn^{2+}. The mobile-phase flow was stopped when the second eluted peak reached the empty flow cell, and the fluorescence emission spectra were collected.

The plots of natural logarithm of the fluorescence intensity at 350 nm (background corrected) *vs.* time were linear ($r^2 = 0.995$) with first-order rate constants of refolding of 0.83 min^{-1} ($t_{\frac{1}{2}} = 50$ s) and 0.48 min^{-1} ($t_{\frac{1}{2}} = 86$ s), for the metal-ion-free mobile-phase condition and in the presence of 1 mM Zn^{2+}, respectively. The refolding process in the presence of Ca^{2+} was too fast to be followed by the present method. This is reasonable since the half life for refolding at 4.5°C in the presence of Ca^{2+} as measured by circular dichroism [33], was $t_{\frac{1}{2}} = 0.25$ s, whereas the time needed to transport the eluted peak to flow cell II was 6 s. The fast refolding with Ca^{2+} is expected since this metal ion stabilizes the folded conformation in solution. The refolding rate constant for α-LACT in the metal-free case is in agreement with the value reported by others [18,33], as can be seen from Table III. On the other hand,

TABLE III

REFOLDING RATE CONSTANTS AND HALF LIVES FOR α-LACT

Additive	This work[a]		Lit. [33][b]	
	k_r (min^{-1})	$t_{\frac{1}{2}}$ (s)	k_r (min^{-1})	$t_{\frac{1}{2}}$ (s)
None	0.83 ± 0.04	50 ± 1	0.78	55
1 m*M* Ca^{2+}	≫20	≪6	162	0.25
1 m*M* Zn^{2+}	0.48 ± 0.02	86 ± 3	–	–

[a] 5.8°C, pH 6.3, 0.5 *M* ammonium acetate; fluorescence emission.
[b] 4.5°C, pH 7.0, 0.05 *M* sodium cacodylate; CD decay.

Zn^{2+} is destabilizing [22], and thus, the surface-unfolded species after desorption can only refold more slowly than in the case of no metal-ion additive.

The retention of α-LACT (see Fig. 2) in the absence and presence of the metal ion additives can be interpreted in terms of the different refolding rates. With the Ca^{2+}-containing mobile phase, once the unfolded protein desorbed, it rapidly refolded in solution. Since the folded form was unretained under the elution condition of the second peak, the migration of the second peak was accelerated. In the absence of metal ion in the mobile phase, the half life for the refolding of the desorbed species was comparable to the unretained time (t_0 = 39 s) of the system, yielding a peak in the isocratic region. In the presence of Zn^{2+} in mobile phase B, the refolding of the desorbed species was even slower and the peak eluted later in the isocratic region.

CONCLUSIONS

This work has extended previous studies on the on-column conformational changes of α-LACT in HIC. The crucial role of spectroscopic measurements in elucidating detailed chromatographic behavior of proteins has been further shown. The interesting effects of metal-ion additives on the surface-unfolding and solution-refolding rate constants have been characterized. Because of different solution-refolding kinetics, the retention of the unfolded species varied with the specific additive. Moreover, one metal ion, zinc, was found to be stabilizing in 3 *M* $(NH_4)_2SO_4$ and destabilizing in buffer alone (0.5 *M* NH_4OAC, pH 6.3).

The results also demonstrate the danger in generalizing retention patterns of proteins from the retention models of small molecules. In the case of proteins, complications can arise from the fact that biopolymers can readily adopt different conformations with different strengths of interaction to the adsorbent surface. At the same time this flexibility of proteins can provide great potential for manipulating separation. For example, as already noted the addition of Ca^{2+} to α-LACT adsorbed to an HIC support caused elution, after a great deal of background matrix material was first removed without Ca^{2+} in the mobile phase [25]. In addition, isocratic separation of two variants of growth hormone was possible by determining a specific elution condition under which the conformational stability of the two species differed from one another [20]. These examples point to the need to understand protein-HPLC retention as fully as possible.

ACKNOWLEDGEMENTS

The authors greatly acknowledge NIH GM 15847 for support of this work. Contribution No. 422 from the Barnett Institute.

REFERENCES

1 J. L. Brash and T. L. Horbett (Editors), *Proteins at Interfaces: Physical and Biochemical Studies (ACS Symposium Series*, No. 343), American Chemical Society, Washington, DC, 1987.
2 J. D. Andrade (Editor), *Surface and Interfacial Aspects of Biomedical Polymers*, Vol. 2, Plenum, New York, 1985.
3 B. L. Karger and R. Blanco, in T. W. Hutchens (Editor), *Protein Recognition of Immobilized Ligands*, Alan R. Liss, New York, 1989, p. 141.
4 K. Benedek, S. Dong and B. L. Karger, *J. Chromatogr.*, 317 (1984) 227.
5 R. H. Ingraham, S. Y. M. Lau, A. K. Taneja and R. S. Hodges, *J. Chromatogr.*, 327 (1985) 77.
6 M. T. W. Hearn, A. N. Hodder and M. I. Aguilar, *J. Chromatogr.*, 327 (1985) 47.
7 X.-M. Lu, K. Benedek and B. L. Karger, *J. Chromatogr.*, 159 (1986) 19.
8 S.-L. Wu, K. Benedek and B. L. Karger, *J. Chromatogr.*, 371 (1986) 3.
9 M. E. Soderquist and A. G. Walton, *J. Colloid Interface Sci.*, 75 (1980) 389.
10 B. Furie, R A. Blanchard, D. J. Robinson, M. M. Tai and B. C. Furie, *Methods Enzymol.*, 125 (1982) 60.
11 B. M. Morrisey, L. E. Smith, R. R. Stromberg and C. A. Fenstermaker, *J. Colloid Interface Sci.*, 56 (1976) 557.
12 R. M. Gendreau, S. Winters, R. I. Leininger, D. Fink and C. R. Hassler, *Appl. Spectrosc.*, 35 (1981) 353.
13 A. Aurengo, M. Masson and E. Dupeyrat, *Appl. Opt.*, 22 (1982) 602.
14 G. R. McMillin and A. G. Walton, *J. Colloid Interface Sci.*, 48 (1974) 345.
15 V. Hlady, R. A. van Wagenen and J. D. Andrade, in J. D Andrade (Editor), *Surface and Interfacial Aspects of Biomedical Polymers*, Vol. 2, Plenum, New York, 1985, p. 81.
16 C. F. Schmidt, R. M. Zimmermann and H. E. Gaub, *Biophys. J.*, 57 (1990) 577.
17 C. H. Lochmuller and S. S. Saavedra, *Langmuir*, 3 (1987) 433.
18 X.-M. Lu, A. Figueroa and B. L. Karger, *J. Am. Chem. Soc.*, 110 (1988) 1978.
19 P. Oroszlan, R. Blanco, X.-M. Lu, D. Yarmush and B. L. Karger, *J. Chromatogr.*, 500 (1990) 481.
20 P. Orozlan, G. Teshima, S.-L Wu, W. S. Hancock and B. L. Karger, to be submitted.
21 Y. Hiraoka, T. Segawa, K. Kuwajima, S. Sugai and N. Murai, *Biochem. Biophys. Res. Commun.*, 95 (1980) 1098.
22 M. J. Kronman, *Crit. Rev. Biochem. Mol. Biol.*, 24 (1989) 565.
23 K. Gast, D. Zirwer, H. Welfle, V. E. Bychkova and O. B. Ptitsyn, *Int. J. Biol. Macromol.*, 8 (1986) 231.
24 G. Musci, and L. J. Berliner, *Biochemistry*, 24 (1985) 6945.
25 L. Lindahl and H. J. Vogel, *Anal. Biochem.*, 140 (1984) 394.
26 M. W. Berchtold, C. W. Heizmann and K. J. Wilson, *Anal. Biochem.*, 129 (1983) 120.
27 R. M. Chicz and F. E. Regnier, *J. Chromatogr.*, 443 (1988) 193.
28 J. L. Fausnaugh and F. E. Regnier, *J. Chromatogr.*, 359 (1986) 31.
29 K. Benedek, *J. Chromatogr.*, 458 (1988) 93.
30 N. T. Miller, B. Feibush and B. L. Karger, *J. Chromatogr.*, 316 (1985) 519.
31 R. M. Smith and A. E. Martell, *Critical Stability Constants*, Plenum, New York, Vol. 4, 1978, p. 41.
32 A. V. Ostrovsky, L. P. Kalinichenko, V. I. Emelyanenko, A. V. Klimanov and E. A. Permyakov, *Biophys. Chem.*, 30 (1988) 105.
33 Y. Harushima, K. Kuwajima and S. Sugai, *Biopolymers*, 27 (1988) 629.

Journal of Chromatography, 536 (1991) 31–42
Elsevier Science Publishers B.V., Amsterdam

CHROMSYMP. 2049

Capillary zone electrophoresis of α_1-acid glycoprotein fragments from trypsin and endoglycosidase digestions

WASSIM NASHABEH and ZIAD EL RASSI*
Department of Chemistry, Oklahoma State University, Stillwater, OK 74078-0447 (U.S.A.)

ABSTRACT

Capillary zone electrophoresis with fused-silica tubes having hydrophilic coating on the inner walls was evaluated in the separation of peptide and glycopeptide fragments from trypsin digestion of α_1-acid glycoprotein. Submapping of glycosylated and nonglycosylated tryptic fragments of the glycoprotein by capillary electrophoresis was facilitated by selective isolation of the glycopeptides on concanavalin A silica-based stationary phases prior to the electrophoretic run. In addition, the electrophoretic map and submaps of the whole tryptic digest and its concanavalin A fractions, respectively, allowed the elucidation of the microheterogeneity of the glycoprotein. Also, capillary zone electrophoresis proved suitable for the mapping of the oligosaccharide chains cleaved from the glycoproteins by endoglycosidase digestion. The oligosaccharides cleaved from human and bovine α_1-acid glycoprotein were analyzed after derivatization with 2-aminopyridine, which allowed their sensitive detection by on column UV absorption. The separation was best achieved when 0.1 *M* phosphate solution, pH 5.0, containing 50 m*M* tetrabutylammonium bromide was used as the running electrolyte. The effect of the organic salt on separation was attributed to ion-pair formation and/or hydrophobic interaction.

INTRODUCTION

High-performance capillary electrophoresis (HPCE) is rapidly developing and becoming an important tool for the separation of a wide variety of biological substances including peptides [1–3], proteins [4–6], nucleic acid fragments [7–9] and recently oligosaccharides [10]. The recent advances in instrumentation and the many sound features of HPCE, *e.g.*, various modes of separation, high resolving power, and small sample requirement, have made it possible for the technique to play this role.

This study is concerned with investigating the potential of capillary zone electrophoresis (CZE) in the separation and characterization of glycoprotein fragments, *i.e.*, peptides, glycopeptides and oligosaccharide chains. In this regard, we have selected human α_1-acid glycoprotein (AGP) as a model protein for the evaluation of CZE in analytical glycoprotein chemistry and analytical biotechnology. Besides being one of the best physicochemically characterized glycoproteins [11], human AGP is an attractive model because of its relatively high content of carbohydrates. Indeed, this single polypeptide chain of 181 amino acids has five glycosylation sites at asparagine residues in positions 15, 38, 54, 75 and 85 in the N-terminal of the molecule [12]. The N-linked oligosaccharide chains, which are of complex types at different degree of

0021-9673/91/$03.50

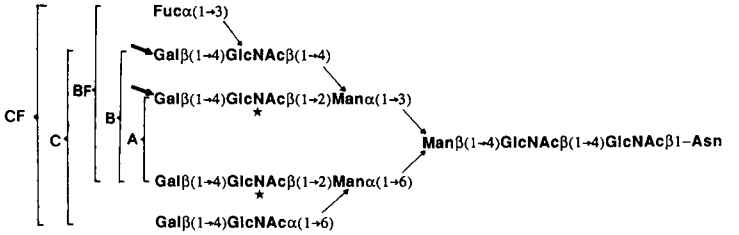

Fig. 1. Primary structures of the five carbohydrate classes as elucidated by Schmid *et al.* [12]. Classes A, B and C are the bi-, tri- and tetraantennary complex N-linked glycans, respectively, whereas BF and CF are the fucosylated B and C structures. Two additional glycans having the tetraantennary basic structure like class C were also reported [24]. One has two additional fucose each linked to the outer chain at the GlcNAc residues marked with a star, while the second one has an outer chain prolonged by Galβ(1-4) GlcNAc at either of the Gal residues marked with an arrow.

branching and sialylation (see Fig. 1), make up 45% of the total weight of the protein [11] (approx. mol.wt. = 41 000).

As will be shown in this report, CZE with its high resolving power and unique selectivity is well suited for the separation and characterization of peptide and glycopeptide fragments from the tryptic digest of human AGP, especially when combined with lectin affinity chromatography. For the selective isolation of glycopeptides prior to CZE analysis we have used concanavalin A silica-based stationary phases. This arrangement allowed CZE tryptic mapping of the whole digest as well as CZE submapping of glycosylated and non-glycosylated fragments. In addition, the usefulness of the technique in mapping the carbohydrate units of the protein liberated by endoglycosidase digestion is also demonstrated. The CZE methodology that generated the fingerprint for an endoglycosidase digest of human AGP, was also applied to the glycans of bovine AGP. In both cases the oligosaccharides were derivatized with 2-aminopyridine (2-AP), which provides the carbohydrates with a positive charge and a UV-absorbing (also fluorescent) tag [13].

EXPERIMENTAL

HPCE instrument

The instrument for capillary electrophoresis used in this study resemble that reported earlier [10]. It was constructed from a Glassman High Voltage (Whitehouse Station, NJ, U.S.A.) Model EH30P3 high-voltage power supply of positive polarity and a Linear (Reno, NV, U.S.A.) Model 200 UV–VIS variable-wavelength detector equipped with a cell for on-column capillary detection. In all experiments, sample injection was made by electromigration at a voltage and for a duration that varied from one mixture to another, and are indicated in the figure legends. The detection wavelength was set at 200 nm or 240 nm for sensing the polypeptides or derivatized oligosaccharides, respectively. The electropherograms were recorded with a Shimadzu computing integrator (Columbia, MD, U.S.A.) equipped with a floppy disk drive and a CRT monitor.

Capillary columns

Fused-silica capillary columns of 50-μm I.D. and 365-μm O.D. having polyimide-cladding were obtained from Polymicro Technology (Phoenix, AZ, U.S.A.). All capillaries (except where indicated) used in this study were modified in house with a hydrophilic coating on the inner walls. The inert coating, which consisted essentially of hydroxypolyether will be evaluated in CZE of proteins in an upcoming article [14]. It was prepared by allowing the capillary to react first with γ-glycidoxypropyltrimethoxysilane and then with a mixture of polyethylene glycol (mol.wt. 2000) and polyethylene glycol diglycidyl ether (mol.wt. 600) [14]. The running electrolyte was renewed after 5–6 runs and the capillary column was flushed successively with fresh buffer, water, methanol, water, and again running buffer before each injection in order to ensure reproducible separations.

High-performance liquid chromatography (HPLC) instrumentation and columns

The chromatograph was assembled from an LDC/Milton Roy (Riviera Beach, FL, U.S.A.) Model CM4000 solvent delivery pump with dual-beam variable-wavelength detector Model Spectro Monitor 3100. A Rheodyne (Cotati, CA, U.S.A.) Model 7125 sampling valve with a 100-μl sample loop was used for injection. Chromatograms were recorded with a Shimadzu (Columbia, MD, U.S.A.) Model C-R5A integrator.

A home made concanavalin A (Con A)–silica column (100 × 4.6 mm I.D.) was prepared by attaching Con A to Zorbax silica gel (DuPont, Willmington, DE, U.S.A.) using a procedure similar to that described by Larsson *et al.* [15]. Zorbax is a spherical silica with 300-Å and 7-μm pore and particle diameters, respectively. A bakerbond wide-pore octadecyl-silica column (250 × 4.6 mm I.D.) having mean particle and pore diameters of 5 μm and 300 Å, respectively, was a gift from J. T. Baker (Phillipsburg, NJ, U.S.A.).

Reagents and materials

Human and bovine AGPs, L-1-tosylamide-2-phenylethyl chloromethyl ketone (TPCK)-treated trypsin, mannose (Man), galactose (Gal), N-acetylglucosamine (GlcNAc), N-acetylgalactosamine (GalNAc), N-acetylneuraminic acid (NeuNAc), methyl-α-D-mannopyranoside, 2-AP, Brij 35 and Tris were obtained from Sigma (St. Louis, MO, U.S.A.). Peptide-N-glycosidase F (PNGase F) from *Flavobacterium meningosepticum* was obtained from Boehringer Mannheim (Indianapolis, IN, U.S.A.). Reagent-grade sodium phosphate monobasic and dibasic, boric acid, phosphoric acid, hydrochloric acid, acetic acid, sodium hydroxide and HPLC-grade methanol and acetonitrile were obtained from Fisher Scientific (Pittsburgh, PA, U.S.A.). Mercaptoethanol, sodium cyanoborohydride, polyethylene glycol and γ-glycidoxypropyltrimethoxysilane and tetrabutylammonium bromide were from Aldrich (Milwaukee, WI, U.S.A.). Distilled water was used to prepare the running electrolyte as well as the solutions used in column cleaning and pretreatment. All solutions were filtered with 0.2-μm UniPrep syringeless filters obtained from Genex (Gaithersburg, MD, U.S.A.) to avoid column plugging.

Tryptic digest

The digestion of AGP with TPCK-treated trypsin was carried out in a 10 m*M*

Tris buffer containing 100 m*M* ammonium acetate and 0.1 m*M* calcium chloride, pH 8.3, at a trypsin substrate ratio of 1:100 and a temperature of 37°C [16]. Trypsin was added again after 2 h and the digestion was stopped after a total of 4 h by addition of 10% (v/v) phosphoric acid. Thereafter, the whole digest was desalted by passing it on a Bakerbond wide-pore octadecyl-silica column (250 × 4.6 mm I.D.) equilibrated with water at 0.05% (v/v) trifluoroacetic acid (TFA). The bound fragments were eluted stepwise with acetonitrile–water (80:20, v/v) at 0.05% TFA (v/v). In this desalting process, single amino acids in the tryptic digest are lost but no major peak showed in the dead volume of the column. The pooled fraction was evaporated to dryness using a SpeedVac Concentrator (from Savant, Farmingdale, NY, U.S.A.). The dried materials were dissolved in the appropriate buffer used in the subsequent experiments.

Part of the dried materials was used for the CZE tryptic mapping, another part was fractionated on Con A–silica column into groups of peptide and glycopeptide fragments which were employed to produce CZE submaps of glycosylated and non-glycosylated peptides, and a third part was incubated with PNGase F to generate the oligosaccharides.

Cleavage of oligosaccharides

The whole digest, which was desalted on the reversed-phase chromatographic (RPC) column as described above was then dissolved in 20 m*M* phosphate buffer containing 2 m*M* EDTA, 1% (v/v) mercaptoethanol, and 0.1% (w/v) Brij 35, pH 7.5. To this solution 3 units of peptide-N-glycosidase F were added, and the incubation was maintained at 37°C for 24 h [17]. Thereafter, the mixture was evaporated to dryness with a Savant SpeedVac Concentrator. The dried materials containing the cleaved oligosaccharides, the peptide fragments, and other reagents employed in the incubation step was used as is without a sample clean up prior to the derivatization of its oligosaccharide components.

Derivatization of mono- and oligosaccharides

Commercially available standard monosaccharides such as Man, Gal, GalNAc, GlcNAc and NeuNAc, which are the constituents of the carbohydrate chains of glycoproteins as well as the oligosaccharides cleaved from the glycoprotein were tagged with 2-aminopyridine (2-AP) at their reducing termini as described by Hase *et al.* [13]. The mixtures containing the pyridylamino (PA) derivatives of the various sugars were first evaporated to dryness using SpeedVac Concentrator. Subsequently, the dried materials were dissolved in water and then applied to capillary electrophoresis without any sample clean up from excess derivatizing agent and other components of the reaction mixture.

RESULTS AND DISCUSSION

CZE tryptic mapping and submapping

All CZE tryptic mapping and submapping of human AGP were performed on a capillary with hydrophilic coating on the inner walls, and using 0.1 *M* phosphate solution, pH 5.0, as the running electrolyte. The hydrophilic coating minimized solute-wall interactions and also permitted the electrophoresis of basic proteins in the pH range 2.0 to 7.0 with high separation efficiencies [14]. Furthermore, with the coated

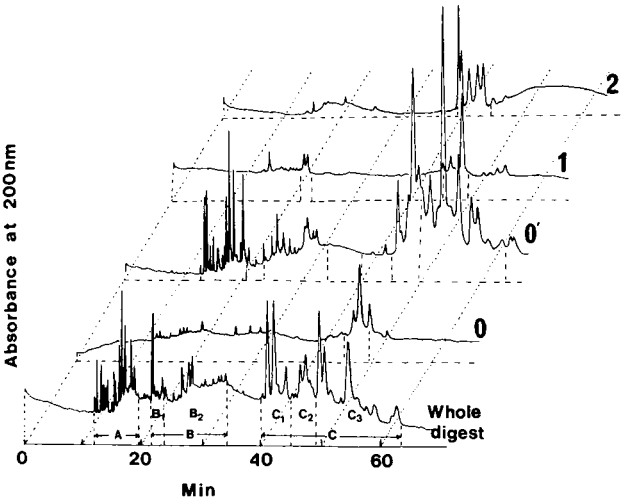

Fig. 2. CZE tryptic mapping and submapping of human AGP. Capillary, fused-silica tube with hydrophilic coating on the inner walls, 45 cm (to the detection point), 80 cm total length × 50 μm I.D.; electrolyte, 0.1 *M* phosphate solution, pH 5.0; running voltage, 22.5 kV; current was *ca.* 55 μA; injection by electromigration for 4 s at 22.5 kV. Fractions: 0 = Con A non-reactive (excluded from the column); 0′ = Con A non-reactive (unretained by the column); 1 = Con A slightly reactive (eluted with buffer); 2 = Con A strongly reactive (eluted with the haptenic sugar).

capillaries, the electroosmotic flow decreased by a factor of *ca.* 3.5 on the average when compared with the uncoated capillary.

Fig. 2 illustrates the CZE mapping and submapping of peptide fragments from the tryptic digest of human AGP. The electropherogram of the whole digest has an elution pattern characteristic of a mixture whose peptide fragments are widely different in size and net charge. Three areas, with different peak capacity, denoted by A, B and C can be distinguished on the electropherogram of the whole digest. They are separated by two quasi peakless areas (see whole digest, Fig. 2). Obviously, small and positively charged peptide fragments are likely to be present in area A, slightly neutral peptides may be located in area B, and large and negatively charged tryptic fragments may be seggregated in area C. The values of the nominal "overall mobility", $\bar{\mu}_{\text{overall}}$, for areas A, B and C are $2.94 \cdot 10^{-4}$, $1.7 \cdot 10^{-4}$ and $0.88 \cdot 10^{-4}$ cm^2/V · s, respectively. The nominal overall mobility refers to the mobility at the center of each area. The overall mobility, which is the sum of electrophoretic mobility and electroosmotic mobility, was calculated by the equation, $\bar{\mu}_{\text{overall}} = Ll/Vt$, where L, l, V and t are the total length of the capillary, the distance from the injection point to the detection point, the applied voltage and the time for the solute to migrate the length l, respectively.

As seen in Fig. 2, the map for the whole tryptic digest of human AGP demonstrates the high resolving power of CZE and reveals the microheterogeneities of the glycoprotein as manifested by the excessive number of peaks for a protein of 181 amino acid residues with 20 trypsin cleavage sites (8 lysine and 12 arginine residues) [11,18]. In fact, by neglecting all sources of heterogeneity in the protein, the tryptic digest should result only into 12 peptide and 5 glycopeptide fragments, and three single amino acids (two lysine and one arginine). However, more than any other serum

glycoproteins, AGP is a highly heterogeneous protein [11,18,19]. One of the unique aspects of the primary structure of polypeptide chain of pooled human AGP is its peculiar structural polymorphism [11]. Substitutions were found at 21 of the 181 amino acids in the single polypeptide chain, which is responsible in part for multiple peptide and glycopeptide fragments in the tryptic digest. More details concerning the primary structure of the protein can be found in refs. 11 and 18. Another source of multiple fragments in the tryptic digest is the microheterogeneities of the oligosaccharide chains attached [11,19,20]. Indeed, the variation in the terminal sialic acid causes charge heterogeneity in the glycopeptide fragments cleaved at the same location by trypsin, the differences in the extent of glycosylation among a population of the protein molecules lead to fragments having the same peptide backbone but with or without carbohydrate chains, and the variation in the nature of the oligosaccharide chains at each location yields several glycopeptides that have the same peptide backbone, but different in their oligosaccharide structures.

To further elucidate the microheterogeneity of the glycoprotein and to generate CZE submaps for the tryptic digest, *i.e.*, maps of groups of peptide or glycopeptide fragments, we have combined high performance lectin affinity chromatography and capillary electrophoresis. Fig. 3 shows affinity chromatography group separation of the peptide fragments from human AGP performed on silica-bound Con A column. The pooled fractions labelled 0 and 0′ contain the Con A non-reactive species, whereas those labelled 1 and 2 have the Con A slightly and strongly reactive fragments, respectively. Whereas the components of fraction 1 were slightly retained by Con A and eluted from the column with the equilibrating buffer (binding buffer), the components of fraction 2 interacted strongly with Con A and eluted from the column with the haptenic sugar, methyl-α-D-mannopyranoside.

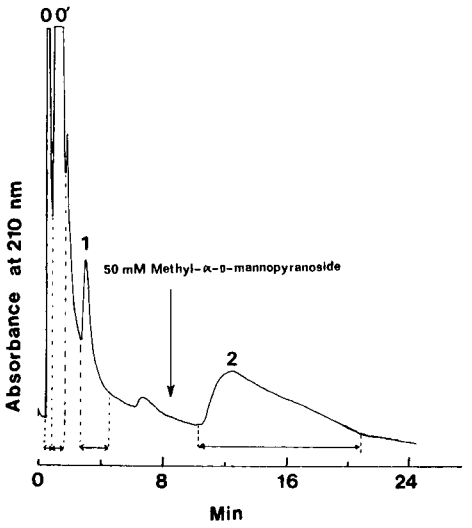

Fig. 3. High-performance lectin affinity chromatography of human AGP tryptic digest. Column, silica-bound Con A, 100 × 4.6 mm I.D.; flow-rate, 1 ml/min; temperature, 25°C. Binding buffer, 20 m*M* phosphate, pH 6.5, containing 0.1 *M* NaCl; debinding buffer, 50 m*M* methyl-α-D-mannopyranoside in the binding buffer.

The different Con A fractions were first desugared and/or desalted on an RPC column (see Experimental) and then analyzed by CZE. The results are depicted in Fig. 2, and are refered to as submaps denoted by 0, 0′, 1 and 2. The tryptic fragments of fraction 0 were excluded from the Con A column, may be due to electrostatic repulsion between the peptides of the fraction and the Con A surface of same charge at pH 6.5 (p*I* value of Con A is *ca.* 4.5–5.5 [21]). Indeed, the CZE submap 0 exhibited peaks eluting late from the capillary, and corresponding to area C_2 on the whole map, which is mainly populated by negatively charged peptide fragments as reflected from the value of its nominal overall mobility ($\bar{\mu}_{overall} = 1.0 \cdot 10^{-4}$ cm^2/V · s). Fraction 0′, the peptide fragments of which did not interact with the Con A and eluted in the column void volume, yielded the CZE submap 0′ containing most peaks that are in the map of the whole digest except those in areas B_1 and C_1. The two submaps 0 and 0′ are mostly populated by non-glycosylated fragments, since their components are repulsed from or not retained by the Con A column.

Con A fraction 1 produced a CZE submap containing glycopeptide fragments with tri- and tetraantennary glycans that are known to interact weakly with Con A [22]. The submap 1 has some of the fragments that are missing in submap 0′ (area B_1), but has fragments from area C_2 and minor peaks from area C_3 on the whole map. Fraction 2 produced a CZE submap with peaks corresponding to area C_1 on the whole map that are missing from submaps 0, 0′ and 1. They are believed to be the glycopeptides with biantennary glycans that strongly bind to a Con A affinity column [22,23]. An area on the whole map worth mentioning is area C_2 whose components are found in submaps 0, 0′ and 1. The components of this area on submaps 0, 0′ and 1 are likely to be different from each others but overlap in the whole digest due to insufficient selectivity.

The approach tested and developed here is capable of elucidating the micro-heterogeneity of the protein, and is convenient for CZE submapping of tryptic fragments of interest, *e.g.*, glycopeptides. This methodology is expected to work also with other glycoproteins, and the CZE submapping of all the glycosylated tryptic fragments with different type of glycans may require the use of more than one lectin column in the prefractionation step.

CZE mapping of oligosaccharide chains from AGP

Human AGP oligosaccharides were cleaved from the glycopeptide fragments of the tryptic digest using PNGase F, an endoglycosidase that cleaves all types of N-linked oligosaccharide chains between the asparagine and the carbohydrate units [17]. The CZE mapping of the PA derivatives of these oligosaccharides is portrayed in Fig. 4a. It was performed on a coated capillary using 0.1 *M* phosphate solution, pH 5.0, containing 50 m*M* tetrabutylammonium bromide as the running electrolyte. As can be seen in Fig. 4a, the electropherogram shows six well defined peaks and a few minor peaks, eluting after the excess 2-AP and some spikes. The glycans of AGP (see Fig. 1) are known for their microheterogeneities caused mainly by variation in their terminal sialic acid. This may explain the presence of several peaks in the CZE map. The spikes indicated the presence of undissolved matters in the sample, since they were more numerous when applying the mixture to CZE without centrifugation.

Based on the above results, CZE can play an important role in the field of glycan separation and characterization. In addition, it holds promise for rapidly monitoring

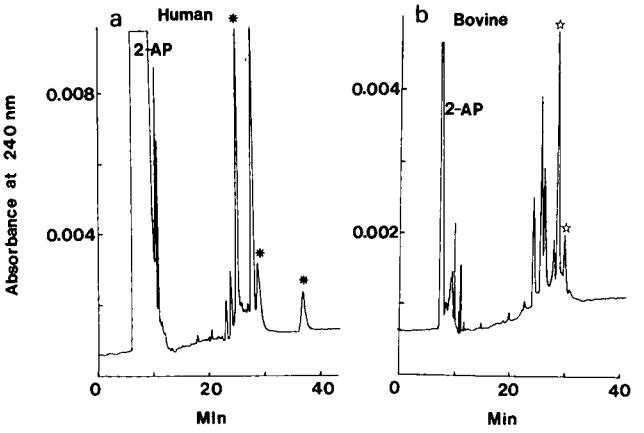

Fig. 4. CZE mapping of pyridylamino derivatives of human (a) and bovine (b) AGP oligosaccharides. Capillary, fused-silica tube with hydrophilic coating on the inner walls, 45 cm (to the detection point), 80 cm total length × 50 μm I.D.; electrolyte, 0.1 *M* phosphate solution, pH 5.0, containing 50 m*M* tetrabutylammonium bromide; running voltage, 18 kV; current, 80 μA; injection by electromigration for 2 s at 18 kV. For stars and asterisks, see text.

the extent of deglycosylation. Indeed, in another set of experiments, the oligosaccharides were cleaved directly from the glycoprotein using the same amount of protein starting materials as in the preceding experiment and keeping other conditions identical, *i.e.*, pH, temperature, number of PNGase F units and the time of digestion. The extent of deglycosylation from the whole protein decreased when compared to that from the glycopeptide fragments. This was ascertained from the disappearance of three major peaks from the CZE map (indicated by asterisks in Fig. 4a). This can be explained by the better accessibility of the endoglycosidase to the cleaving site in the glycopeptides than in the intact glycoprotein.

To evaluate the potential of CZE in elucidating the difference in glycan structures, the oligosaccharides from bovine AGP were cleaved from the glycopeptides and derivatized with 2-AP as in the case of human glycoprotein. Subsequently, the derivatized bovine AGP oligosaccharides were analyzed by CZE using the same electrophoretic conditions as in Fig. 4a, and their corresponding CZE map is depicted in Fig. 4b. The map shows an elution pattern different from that of the oligosaccharides derived from the human glycoprotein. Both human and bovine AGPs have been found to have the same sialic acid, galactose and mannose content [25]. The major differences are such that 50% of the sialic acid in bovine AGP are N-glycolylneuraminic acid and the fucose content is very low [25]. These differences are accentuated by CZE mapping of both types of glycans; compare Fig. 4a and b.

In a recent report from our laboratory [10], we have demonstrated the capability of CZE in the separation of the PA derivatives of maltooligosaccharides. This study has shown the effectiveness of tetrabutylammonium bromide in affecting full separation of the oligomers. The organic salt was also useful in the separation of glycans. The comparison of Fig. 5a and b demonstrates the high selectivity and high resolution attained upon adding tetrabutylammonium bromide to the running

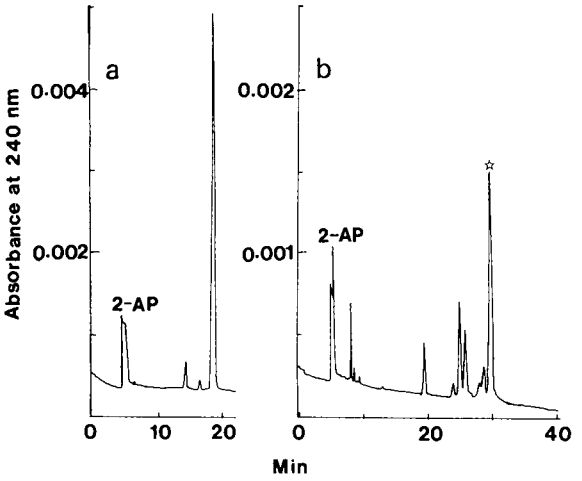

Fig. 5. CZE mapping of pyridylamino derivatives of bovine AGP oligosaccharides without (a) or with (b) 50 m*M* tetrabutylammonium bromide in the running electrolyte. Capillary, fused-silica tube with hydrophilic coating on the inner walls, 35 cm (to the detection point), 70 cm total length × 50 μm I.D.; electrolyte, 0.1 *M* phosphate solution, pH 5.0; running voltage, 15 kV; currents were *ca.* 55 μA in (a) and 90 μA in (b); injection by electromigration for 8 s at 15 kV. For star, see text.

electrolyte. Indeed, in the absence of the organic salt (Fig. 5a), the glycans were separated as two minor peaks and one large peak, whereas upon adding tetrabutylammonium bromide to the running electrolyte several additional peaks appeared in the map (Fig. 5b). The improvement in selectivity upon adding the organic salt to the running electrolyte can be explained by ion pair formation between the quarternary ammonium salt and the sialic acid of the carbohydrate chains and/or by hydrophobic interaction between the alkyl chains of the organic cation and the PA-oligosaccharides. On the other hand, the addition of tetrabutylammonium bromide increased the ionic strength of the running electrolyte, and as expected the residence time of the separated glycans increased. This is due to the reduction in electroosmotic flow [6], as a consequence of a decrease in both the thickness of the double layer and the ζ potential of the capillary wall [26]. The decrease in the rate of the flow is more reflected on the late eluting zones than 2-AP. The migration time of 2-AP increased slightly by a factor of 1.08.

The comparison of electropherograms in Figs. 4b and 5b reveals the influence of the effective capillary length, *i.e.*, the distance from the injection end to the detection point, on the separation of glycans at approximately the same field strength. The difference between these two electropherograms is such that the former was performed on a capillary of 80 cm total length and 45 cm effective length whereas the latter was obtained with a capillary of 70 cm total length and 35 cm separation distance. Although a better selectivity was obtained in Fig. 5b, especially for the fast migrating zones, the peaks of the electropherogram in Fig. 4b are sharper and concomitantly complete resolution was obtained for the last two peaks (indicated by stars in Figs. 4b and 5b).

As pointed out in the Experimental section, the derivatization of the oligo-

saccharides was carried out in the presence of the protein or the peptide fragments without an isolation step of the cleaved oligosaccharides. Also the mixture containing the derivatized oligosaccharides, excess derivatizing agent and other components of the reaction mixture (see Experimental) was applied directly to CZE. Since the remaining protein, peptides and other components of the reaction mixture do not form an interference at the wavelength of detection (240 nm) and the excess 2-AP elute first in the electrophoretic run, solid phase extraction or other isolation procedures were not needed prior to CZE analysis. This represents an advantage for the method established here in terms of reduced time and labor. In addition, since no extraction step is involved, the approach used here eliminates sample loss.

The results of the above study demonstrate the effectiveness of the technique in the area of glycoconjugate research. In addition, since CZE uses nanoliter quantities for several runs, the small sample size most often encountered in the domain of glycans is not a limiting factor and the technique can be explored further in the separation and analysis of carbohydrate chains of glycoproteins provided that authentic standards are available.

CZE analysis of monosaccharide constituents of glycoproteins

The above electrophoretic systems were also employed in the separation of the constituents of carbohydrate chains of glycoproteins using coated capillaries. The standards Gal, Man, GlcNAc, GalNAc and NeuNAc were first derivatized with 2-AP. Following, the PA-sugars were electrophoresed on a coated capillary, using 0.1 *M* phosphate solution, pH 5.0, with or without tetrabutylammonium bromide. In the

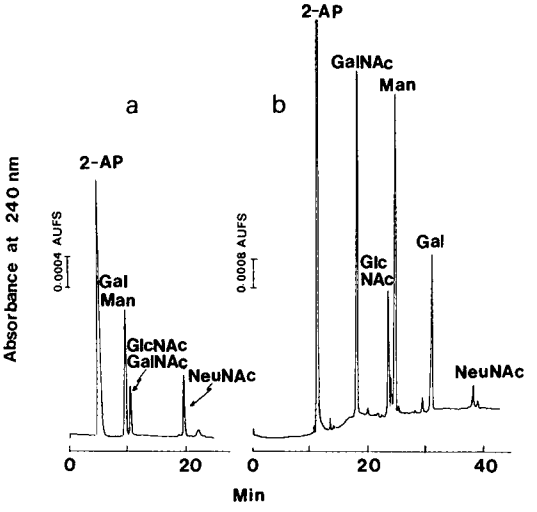

Fig. 6. CZE of pyridylamino derivatives of standard monosaccharides. (a) Capillary, fused-silica tube with hydrophilic coating on the inner wall, 35 cm (to the detection point), 70 cm total length × 50 μm I.D.; electrolyte, 0.1 *M* sodium phosphate solution, pH 5.0, containing 50 m*M* tetrabutylammonium bromide; running voltage, 15 kV; current was *ca.* 90 μA; injection by electromigration for 8 s at 15 kV. (b) Capillary, uncoated fused-silica tube, 50 cm (to the detection point), 80 cm total length × 50 μm I.D.; electrolyte, 0.2 *M* sodium borate, pH 10.5; running voltage, 18 kV; current was 75 μA; injection by electromigration for 1 s at 10 kV.

presence of 50 m*M* tetrabutylammonium bromide in the running electrolyte (see Fig. 6a), the PA derivatives of the monosaccharides were only separated into groups whereby, Man and Gal separated from GalNAc and GlcNAc and the PA derivative of NeuNAc being a zwitterion at pH 5.0 migrated at slower paste. In the absence of tetrabutylammonium bromide in the running electrolyte the acetylated (GlcNAc and GalNAc) and nonacetylated (Man and Gal) monosaccharides coeluted. The migration modulus, η, which is the ratio of the migration times in the presence to that in the absence of tetrabutylammonium bromide were 1.13 for Gal and Man, 1.16 for GlcNAc and GalNAc and 1.04 for NeuNAc. Although, only group separation can be obtained when tetrabutylammonium bromide is added to the running electrolyte, the method established here may prove useful in the analysis of sugar residues of glycans cleaved by sequential exoglycosidases.

The full resolution of the PA derivatives of the standard monosaccharides was brought about by using uncoated capillary and borate-sugar complexes at high pH (see Fig. 6b), an electrophoretic system exploited earlier by Honda *et al.* [27] for a series of monosaccharides and by Wallingford and Ewing [28] for catecholamines. The anionic borate-sugar complexes created the charge for electrophoretic separation, as shown in Fig. 6b. It is well known that compounds containing *cis*-oriented hydroxyl groups form stronger complexes with borate than those having *trans*-oriented diols [29]. Mannose has *trans*-diols at C-3/C-4 position, and therefore migrated faster than galactose which has *cis*-diols at the same location. This trend does not follow for GalNAc and GlcNAc, may be due to the presence of N-acetyl group which may affect the binding of borate. NeuNAc is a negatively charged species at high pH and the binding of borate to this molecule slows even further its migration.

ACKNOWLEDGEMENTS

The financial supports from the University Center for Water Research at Oklahoma State University (OSU), from the College of Arts and Sciences, Dean Incentive Grant Program at OSU, and from the Oklahoma Center for the Advancement of Science and Technology (Oklahoma Health Research Program, grant No. HN9-004) are gratefully acknowledged.

REFERENCES

1 P. D. Grossman, J. C. Colburn, H. H. Lauer, R. G. Nielsen, R. M. Riggin, G. S. Sittampalam and R. C. Rickard, *Anal. Chem.*, 61 (1989) 1186.
2 Z. Deyl, V. Rohlicek and M. Adam, *J. Chromatogr.*, 480 (1989) 371.
3 J. Frenz, S.-L. Wu and W. S. Hancock, *J. Chromatogr.*, 480 (1989) 379.
4 H. H. Lauer and D. McManigill, *Anal. Chem.*, 58 (1986) 166.
5 R. M. McCormick, *Anal. Chem.*, 60 (1988) 2322.
6 M. Bushey and J. J. Jorgenson, *J. Chromatogr.*, 480 (1989) 301.
7 A. S. Cohen, D. Najarian, J. A. Smith and B. L. Karger, *J. Chromatogr.*, 458 (1988) 323.
8 A. Cohen, D. Najarian, A. Paulus, A. Guttman, J. Smith and B. L. Karger, *Proc. Natl. Acad. Sci. U.S.A.*, 85 (1988) 9660.
9 H. Drossman, J. A. Luckey, A. J. Kostichka, J. D'Cunha and L. M. Smith, *Anal. Chem.*, 62 (1990) 900.
10 W. Nashabeh and Z. El Rassi, *J. Chromatogr.*, 514 (1990) 57.
11 K. Schmid, in F. W. Putnam (Editor), *The Plasma Proteins*, Vol. 1, Academic Press, New York, 2nd ed., 1975. pp. 183–228.

12 K. Schmid, J. P. Binette, L. Dorland, F. G. Vliegenhart, B. Fourmet and J. Montreuil, *Biochim. Biophys. Acta*, 581 (1979) 356.
13 S. Hase, S. Hara and Y. Matsushima, *J. Biochem.*, 85 (1979) 217.
14 W. Nashabeh and Z. El Rassi, in preparation.
15 P. O. Larsson, M. Glad, L. Hansson, M.-D. Hansson, S. Ohlson and K. Mosbach, *Adv. Chromatogr.*, 21 (1982) 41.
16 C. B. Kasper, in S. B. Needleman (Editor), *Protein Sequence Determination*, Springer-Verlag, Berlin, New York, 1975, p. 114.
17 A. L. Tarentino, C. M. Gomez and T. H. Plummer, *Biochemistry*, 24 (1985) 4665.
18 W. C. Baker and F. W. Putnam, in F. W. Putnam (Editor), *The Plasma Proteins*, Vol. 4, Academic Press, New York, 2nd ed., 1984, p. 394.
19 F. W. Putnam, in F. W. Putnam (Editor), *The Plasma Proteins*, Vol. 4, Academic Press, New York, 2nd ed., 1984, pp. 74–76.
20 E. Chandrasekaran, M. Davila, D. Dixon and J. Mendicino, *Cancer Res.*, 44 (1984) 1557.
21 D. Malamud and J. W. Drysdale, *Anal. Biochem.*, 86 (1978) 620.
22 I. Nicollet, J. Lebreton, M. Fontaine and M. Hiron, *Biochim. Biophys. Acta*, 668 (1981) 235.
23 J. Montreuil, S. Bouquelet, H. Debray, B. Fournet, G. Spik and G. Strecker, in M. F. Chaplin and J. F. Kennedy (Editors) *Carbohydrate Analysis, a Practical Approach*, IRL Press, Oxford, 1986, p. 161.
24 H. Yoshima, A. Matsumoto, T. Mizuochi, T. Kawasaki and A. Kobata, *J. Biol. Chem.*, 256 (1981) 8476.
25 R. Got, R. Bourrillon and P. Cornillot, *Biochim. Biophys. Acta*, 58 (1962) 126.
26 C. J. Van Oss, *Sep. Purif. Methods*, 8 (1979) 119.
27 S. Honda, S. Iwase, A. Makino and S. Fujiwara, *Anal. Biochem.*, 176 (1989) 72.
28 R. A. Wallingford and A. G. Ewing, *J. Chromatogr.*, 441 (1988) 299.
29 H. L. Weith, J. L. Wiebers and P. T. Gilham, *Biochemistry*, 9 (1970) 4396.

Journal of Chromatography, 536 (1991) 43–55
Elsevier Science Publishers B.V., Amsterdam

CHROMSYMP. 2044

Non-ideal behaviour of silica-based stationary phases in trifluoroacetic acid–acetonitrile-based reversed-phase high-performance liquid chromatographic separations of insulins and proinsulins

S. LINDE* and B. S. WELINDER
Hagedorn Research Laboratory, 6 Niels Steensens Vej, DK-2820 Gentofte (Denmark)

ABSTRACT

Several C_{18} stationary phases were found to behave non-ideally when insulins and proinsulins were eluted with shallow acetonitrile gradients in 0.1% trifluoroacetic acid, resulting in poor peak shapes or no elution at all. With triethylammonium phosphate or ammonium sulphate as buffer components, the insulins and proinsulins were eluted with excellent peak shapes, presumably owing to better masking of residual silanol groups on the stationary phases. Similar use of trifluoroacetic acid–acetonitrile gradients on the less hydrophobic C_4 or C_3 stationary phases resulted in excellent peak shapes. The difficult separation of rat proinsulin I and II, which are important for the study of rat insulin biosynthesis, was only achieved with two different stationary–mobile phase combinations.

INTRODUCTION

Reversed-phase high-performance liquid chromatography (RP-HPLC) has become the most widely used separation mode for polypeptides owing to its high resolution capacity. For insulin and insulin-related compounds, the most popular mobile phases have been trifluoroacetic acid (TFA), alkylammonium phosphates or neutral salts in combination with acetonitrile (ACN) (see ref. 1 for a review).

Rats and mice are unusual among mammals in producing two different non-allelic proinsulins (I and II) in the islets of Langerhans, which subsequently are processed to insulin I and II and also C-peptide I and II. We recently described the successful RP-HPLC separation of rat proinsulin I and II (both containing 86 amino acids with four amino acid differences), a more difficult separation than that of the two insulins (51 amino acids, two differences) and the two C-peptides (31 amino acids, two differences). The separation was achieved using a LiChrosorb RP-18 column, eluted with a very shallow TFA–acetonitrile (ACN) gradient (0.1%/min) [2].

During this work we observed certain disturbing column-to-column variations, which could sometimes be overcome by "preconditioning" the columns with alkylammonium phosphate. However, from columns obtained during the last 12–

0021-9673/91/$03.50

18 months, rat insulins and proinsulins and also human insulin and proinsulin could not be eluted at all with TFA–ACN.

The aim of this study was to evaluate the usability of shallow TFA–ACN gradients on several silica-based C_{18}, C_8, C_4 and C_3 reversed-phase columns for the separation of rat and human insulins and proinsulins.

EXPERIMENTAL

Reagents

Trifluoroacetic acid (peptide synthesis grade) was obtained from Applied Biosystems, phosphoric acid (analytical-reagent grade) from Merck, ammonium sulphate (Aristar) from BDH, triethylamine (99%) from Janssen Chimica and acetonitrile (HPLC grade S) from Rathburn Chemicals. All other chemicals were of analytical-reagent grade. Distilled water was obtained from a Millipore Milli-Q plant, and all buffers were filtered (0.45 μm, Millipore) and vacuum/ultrasound degassed before use.

HPLC equipment

The HPLC system consisted of two Waters Assoc. Model M 6000A pumps, a WISP 710A autosampler, a Model 660 solvent programmer, a Model 730 data module and a Pye Unicam LC–UV detector.

Columns

LiChrosorb RP-18 (5 μm), LiChrospher 100 RP-18 (5 μm) and LiChrosorb RP-8 (5 μm) columns (250 × 4.0 mm I.D.) were obtained from Merck, Nucleosil 100-5C_{18}, 120-5C_{18}, 300-5C_{18} and 300-5C_4, all 5 μm, columns (250 × 4.0 mm I.D.) from Machery-Nagel & Co., an Ultrasphere-ODS (5 μm) column (250 × 4.6 mm I.D.) from Beckman, a Zorbax Bio Series Protein Plus (6 μm) column (250 × 4.6 mm I.D.) from DuPont and a Bakerbond Wide-Pore Butyl (5 μm) column (250 × 4.6 mm I.D.) from J. T. Baker.

Mobile phases and gradients

The columns were eluted with linear acetonitrile gradients (5 or 6% during 30 or 60 min) in 0.1% TFA, 0.125 *M* triethylammonium phosphate (TEAP) (pH 4.0) or 0.125 *M* ammonium sulphate (AS) (pH 3.0 or 4.0). The flow-rate was 1.0 ml/min and experiments were performed at room temperature (*ca.* 22°C) or 45°C. Detailed descriptions are given in the legends to the figures.

Samples

Human insulin (HI) and proinsulin (HPI) were obtained from Novo Nordisk A/S. Medium from cultured newborn rat islet cells was used as a source of rat insulins. This medium contained 44 μg/ml insulin I and II (determined by radioimmunoassay [3]) and equimolar amounts of C-peptide I and II. Biosynthetically labelled rat islet polypeptides, including rat proinsulin I and II (10–20 ng per 50 islets) were prepared by incubation of rat islets with [^{3}H]leucine and [^{35}S]methionine as described previously [2].

Registration and counting

The column eluate was monitored at 210 nm. In experiments with labelled polypeptides, the eluate was collected in 0.5-min fractions (Pharmacia FRAC 300 fraction collector) and counted in a Packard Tri-Carb liquid scintillation counter (Model 460 C) after addition of 4 ml of Optiphase HiSafe (LKB).

RESULTS

The separation of rat insulin I and II, C-peptide I and II and proinsulin I and II (all present in rat islets) on a LiChrosorb RP-18 column is shown in Fig. 1. The UV profile in the upper panel represents the stored polypeptides and the lower panel shows the distribution of radioactivity in the newly synthesized polypeptides. It can be seen that the amounts of stored proinsulins compared with insulins are very small (1–2%), and only small amounts of newly synthesized proinsulins during this 60-min labelling period are converted to insulins and C-peptides. The fact that methionine is present only in proinsulin II and insulin II facilitates the peak identification.

Some batches of LiChrosorb RP-18 columns did not perform satisfactorily (non-ideal, tailing insulin peaks) when new columns were eluted initially with the TFA–ACN gradient (Fig. 2, top panel). We observed that repeated (4–6) chromato-

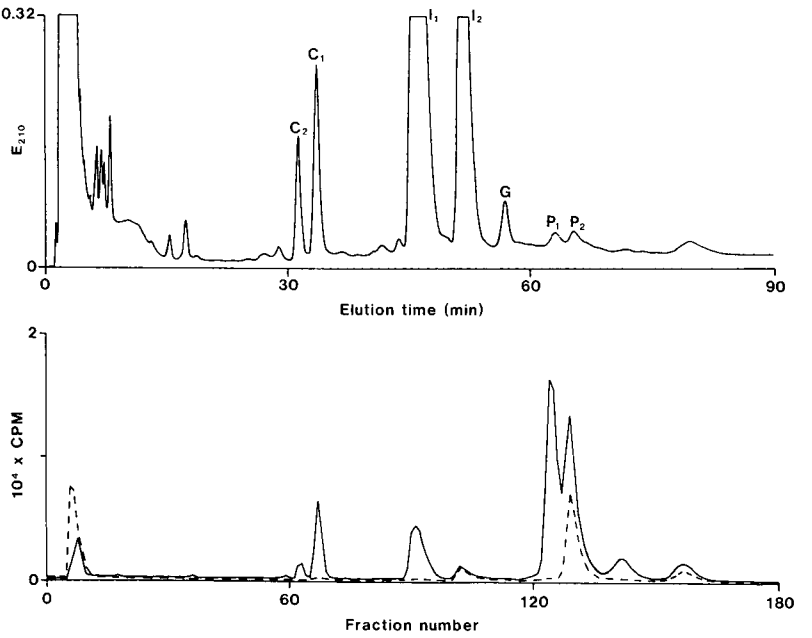

Fig. 1. RP-HPLC separation of a 3-*M* acetic acid extract of 9500 rat islets, labelled for 60 min with 0.5 mCi of [^{3}H]leucine and 0.5 mCi of [^{35}S]methionine (this amino acid being present only in insulin II and proinsulin II), using a LiChrosorb RP-18 column eluted at 1.0 ml/min with a linear ACN gradient (30–36%) in 0.1% TFA during 60 min. Peaks: C_1 = C-peptide I; C_2 = C-peptide II; I_1 = insulin I; I_2 = insulin II; G = glucagon; P_1 = proinsulin I; P_2 = proinsulin II. The absorbance at 210 nm (upper panel) represents the stored islet polypeptides and the radioactivity in the collected fractions (solid line, [^{3}H]leucine; dashed line, [^{35}S]methionine) (lower panel) represents the newly synthesized islet polypeptides.

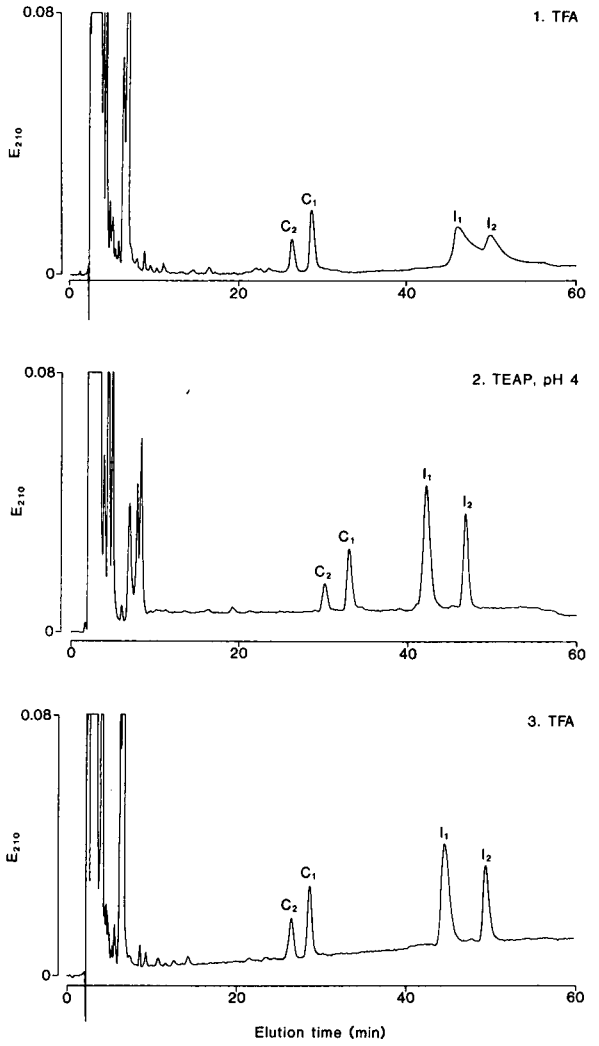

Fig. 2. RP-HPLC separation of 50 μl of rat islet cell culture medium containing 2.2 μg of insulin I + II plus equimolar amounts of C-peptides I and II. Peaks as in Fig. 1. The same LiChrosorb RP-18 column was eluted at 1.0 ml/min with a linear ACN gradient during 60 min in 0.1% TFA (30–36%, top panel), in 0.125 *M* TEAP (pH 4.0) (25–30%, middle panel) and again in 0.1% TFA (bottom panel).

grams of acidified culture medium containing rat insulins and C-peptides could precondition the columns to a better performance, *i.e.*, similar to the separation shown in Fig. 2, bottom panel. We further noticed that the LiChrosorb columns performed well (ideal peak shapes) when eluted with a TEAP–ACN gradient (Fig. 2, middle panel) and, thereafter, that elution with the TFA–ACN gradient resulted in excellent peak shapes (Fig. 2, bottom panel).

However, recent batches of LiChrosorb columns could not be "preconditioned" to elute the rat insulins, whereas the peak shapes of the C-peptides were excellent

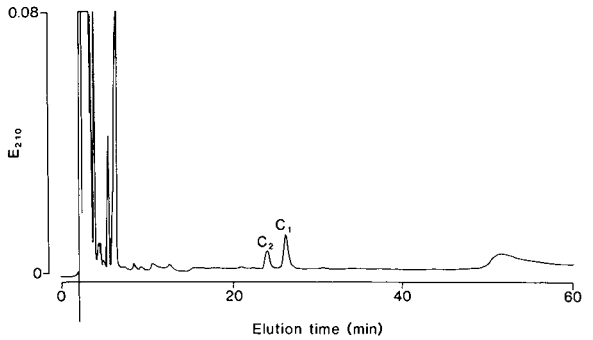

Fig. 3. RP-HPLC separation of 50 μl of rat islet cell culture medium in 0.1% TFA–ACN as in Fig. 2, but on a more recent batch of LiChrosorb RP-18. C_1 and C_2 are the C-peptides; the insulins were not satisfactorily eluted (irreversible binding).

(Fig. 3). Neither human insulin nor proinsulin could be eluted at all from these columns (data not shown), indicating irreversible binding to the stationary phase.

In order to obtain a satisfactory elution of insulins and proinsulins in the preferred TFA–ACN mobile phase, several different stationary phases were examined. The characteristics of the individual stationary phases are summarized in Table I and the results are given in Table II. Although some of these columns initially separated the insulins and proinsulins with excellent peak shapes, insulins and proinsulins gradually become irreversibly bound to the C_{18} stationary phases. No irreversible binding of the C-peptides was ever observed.

An example of the increasing irreversible binding of the insulins and proinsulins is shown in Fig. 4. Human insulin (HI) and proinsulin (HPI) were initially eluted as

TABLE I

CHARACTERISTICS OF THE STATIONARY PHASES

Bonded phase	Stationary phase	Particle shape	Particle size (μm)	Pore size (Å)	Carbon load (%)	End-capped
C_{18}	LiChrosorb RP-18	Irregular	5	100	16.0	No
	LiChrospher 100 RP-18	Spherical	5	100	12.5	No
	Ultrasphere-ODS	Spherical	5	80	10–11	Yes
	Nucleosil 100-5C_{18}	Spherical	5	100	14	HMDS[a]
	Nucleosil 120-5C_{18}	Spherical	5	120	11	HMDS
	Nucleosil 300-5C_{18}	Spherical	5	300	6	HMDS
C_8	LiChrosorb RP-8	Irregular	5	100	9.5	No
C_4	Nucleosil 300-5C_4	Spherical	5	300	1	HMDS
	Bakerbond WP Butyl	Spherical	5	300	n.a.[b]	n.a.
C_3	Zorbax Protein Plus	Spherical	6	300	n.a.	n.a.

[a] HMDS = hexamethyldisilazane.
[b] n.a. = Not available.

TABLE II

BINDING PHENOMENA OF POLYPEPTIDES FROM PANCREATIC ISLETS TO REVERSED-PHASE STATIONARY PHASES

Mobile phase, 0.1% TFA in acetonitrile; gradient, 0.1%/min; room temperature (22°C).

Bonded phase	Stationary phase	C-peptides	Insulins and proinsulins	Comments	Fig. No.
C_{18}	LiChrosorb RP-18	No irreversible binding	Sometimes irreversible binding	In some instances preconditioning was possible	1, 2, 3
	LiChrospher 100 RP-18	No irreversible binding	Irreversible binding		
	Ultrasphere-ODS	No irreversible binding	Increasing to irreversible binding	Initially excellent peak shapes	
	Nucleosil 100-5C_{18}	No irreversible binding	Increasing to irreversible binding	Initially excellent peak shapes	
	Nucleosil 120-5C_{18}	No irreversible binding	Increasing to irreversible binding	Initially tailing peaks	4
	Nucleosil 300-5C_{18}	No irreversible binding	Increasing to irreversible binding	Initially tailing peaks	
C_8	LiChrosorb RP-8	No irreversible binding	Some non-specific binding	Non-ideal peak shapes	
C_4	Nucleosil 300-5C_4	No irreversible binding	No irreversible binding	Excellent peak shapes[a]	5
	Bakerbond WP Butyl	No irreversible binding	No irreversible binding	Excellent peak shapes[a]	
C_3	Zorbax Protein Plus	No irreversible binding	No irreversible binding	Excellent peak shapes[a]	5

[a] None of these stationary phases was able to separate rat proinsulin I and II.

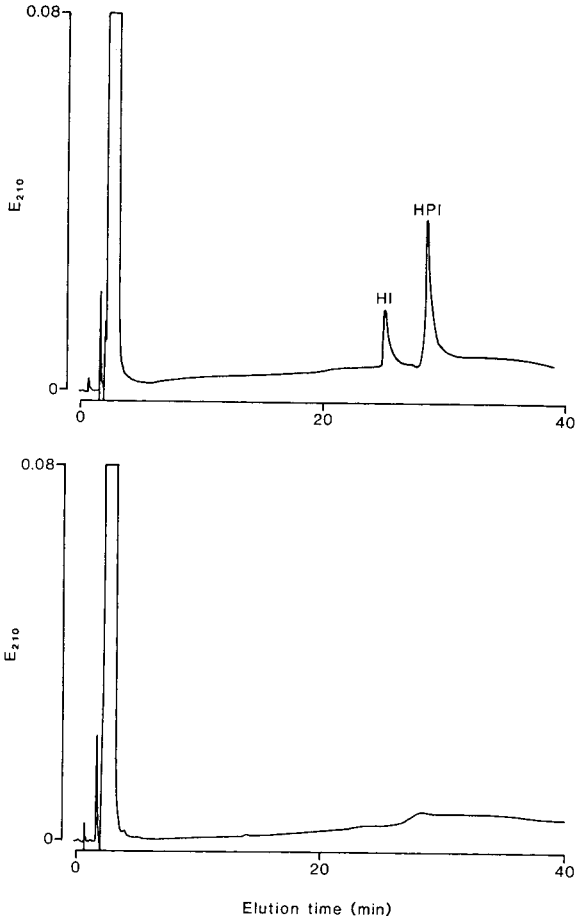

Fig. 4. RP-HPLC separation of *ca.* 1 μg of human insulin (HI) and *ca.* 3 μg of human proinsulin (HPI) on a Nucleosil 120-5C_{18} column eluted at 1.0 ml/min with a linear ACN gradient (30–36%) in 0.1% TFA during 30 min. Upper panel, first injection; lower panel, fourth injection.

tailing peaks (upper panel), but in later experiments these polypeptides were bound to the stationary phase, Nucleosil 120-5C_{18} (lower panel).

A C_8 stationary phase (LiChrosorb RP-8) also showed non-ideal insulin and proinsulin peak shapes and partial binding (data not shown), whereas insulins and proinsulins were eluted with excellent peak shapes from C_4 and C_3 stationary phases (Table II), exemplified for HI and HPI on Zorbax Protein Plus and Nucleosil 300-5C_4 (Fig. 5). However, none of these columns was able to separate rat proinsulin I and II.

It should be mentioned that excellent insulin and proinsulin peak shapes were obtained from all stationary phases after elution with TEAP (pH 4.0)–ACN (data not shown). Unfortunately, the rat proinsulins were not separated, except partly after chromatography on the Ultrasphere-ODS columns [2].

Fig. 6 shows the separations with TFA–ACN on Nucleosil 300-5C_4 eluted at

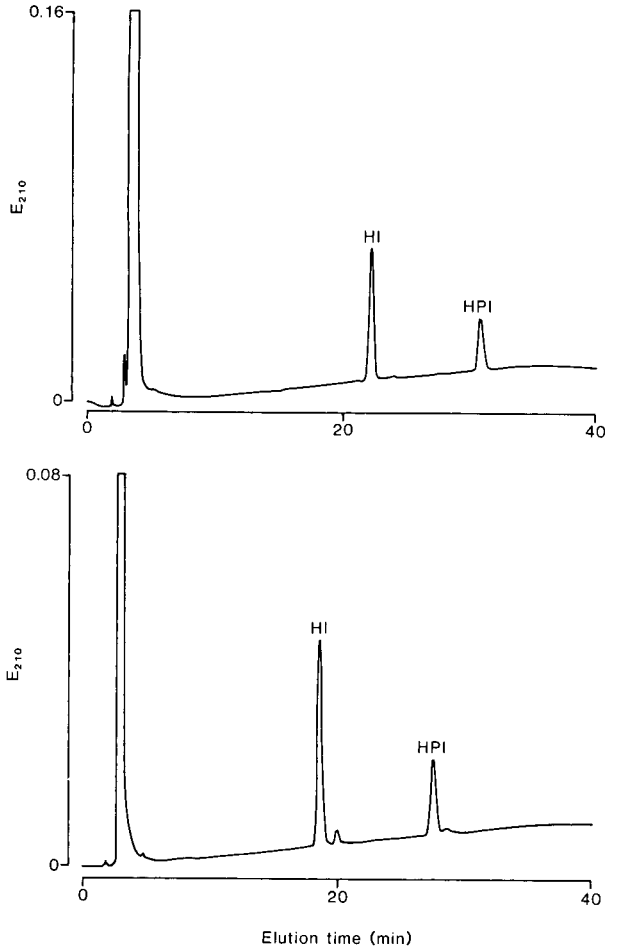

Fig. 5. RP-HPLC separation of *ca.* 1 μg of HI and *ca.* 1 μg of HPI on a Zorbax Protein Plus column (upper panel) and a Nucleosil 300-5C_4 column (lower panel), both eluted at 1.0 ml/min with a linear ACN gradient (26–32%) in 0.1% TFA during 30 min.

room temperature (upper panel) and at 45°C (lower panel); the higher separation temperature resulted in baseline separation of the two rat proinsulins.

The optimization of the separation of the labelled rat islet polypeptides on LiChrosorb RP-18 eluted with AS–ACN is shown in Fig. 7. Initial separation of the rat proinsulins was achieved by changing the pH from 4.0 to 3.0 (top and middle panels), whereas increasing the temperature to 45°C resulted in an almost baseline separation of the proinsulins (bottom panel). This beneficial effect of temperature was not observed when LiChrosorb with TFA–ACN was used (data not shown).

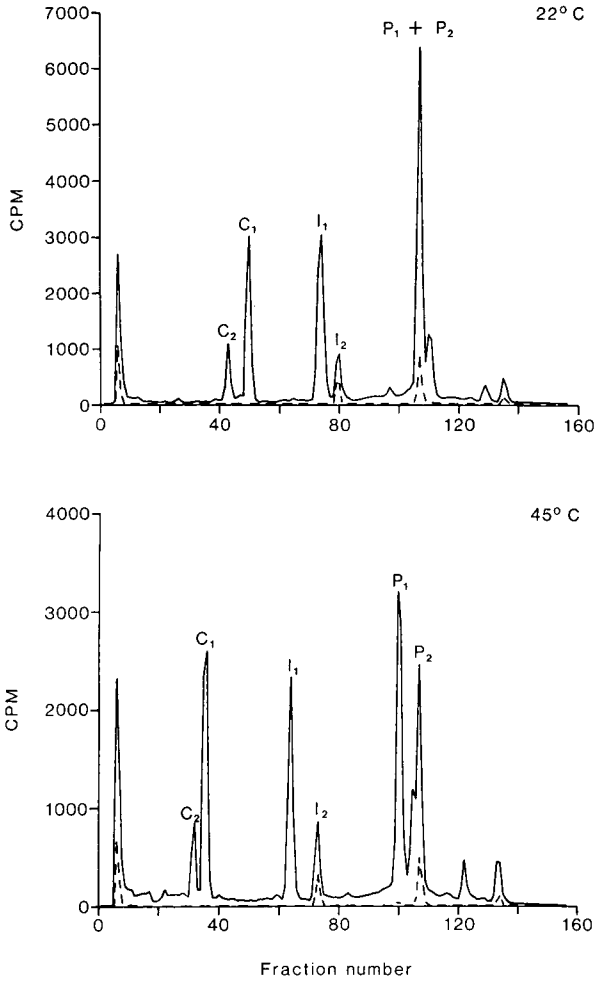

Fig. 6. RP-HPLC separation of a 3-*M* acetic acid extract of 50 rat islets (labelled as described in Fig. 1) using a Nucleosil 300-5C_4 column eluted at 1.0 ml/min with a linear ACN gradient (26–32%) in 0.1% TFA during 60 min. The separation shown in the upper panel was performed at room temperature (*ca.* 22°C) and that in the lower panel at 45°C. The solid lines represent ^{3}H radioactivity and the dashed lines ^{35}S radioactivity. Peaks as in Fig. 1.

DISCUSSION

For the study of the rat insulin biosynthesis, a method capable of separating and determining all the conversion products (*i.e.*, insulins and C-peptides), in addition to proinsulin I and II, is required. RP-HPLC methods giving partial separations of some of these polypeptides (coelution of proinsulins, no detection of C-peptides) have been published [4,5], whereas the successful separation of all the polypeptides involved (including the two rat proinsulins) could be achieved with the LiChrosorb RP-18 system with TFA–ACN [2]. A similar separation was obtained using an Ultrasphere

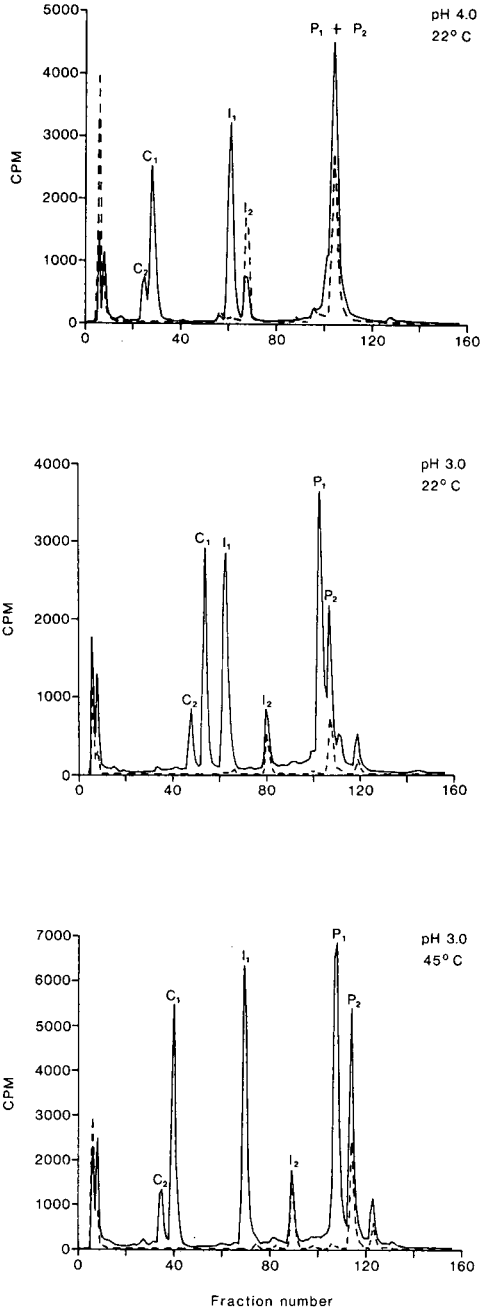

Fig. 7. RP-HPLC separation of a 3-*M* acetic acid extract of 50 rat islets (labelled as described in Fig. 1) using a LiChrosorb RP-18 column eluted at 1.0 ml/min with a linear ACN gradient in 0.125 *M* ammonium sulphate during 60 min. Top panel, 22°C, pH 4.0, 24–29% ACN; middle panel, 22°C, pH 3.0, 25–30% ACN; bottom panel, 45°C, pH 3.0, 26–31% ACN. The solid lines represent ^{3}H radioactivity and the dashed lines ^{35}S radioactivity. Peaks as in Fig. 1.

system with TEAP (pH 4.0)–ACN [2], but a volatile mobile phase would be preferable for these analyses.

As our latest batches of LiChrosorb RP-18 either separated the insulins and proinsulins with unacceptable peak shapes, or the binding to the stationary phase was so strong that elution with TFA–ACN was impossible, we examined the behaviour of other RP columns in this mobile phase. The instantaneously or gradually increasing irreversible binding of insulins and proinsulins in shallow TFA–ACN gradients was found to be general for the all C_{18} stationary phases examined and also for a LiChrosorb C_8 column (Table II) independent of pore size (80–300 Å), carbon load (6–14%) or end-capping. In contrast, a 330-Å C_{18} Vydac column has been reported to separate several different insulin species with shallow TFA–ACN gradients without such problems [6]. In some instances, petreatment of new LiChrosorb RP-18 columns with TEAP–ACN allowed their use in TFA–ACN gradients, but even after this preconditioning recent batches of this column type could not be used with shallow gradients (Fig. 3).

After elution of RP columns with shorter alkyl chains (C_3 or C_4) with TFA–ACN, excellent peak shapes for insulins and proinsulins were obtained (Fig. 5), but the selectivity in these systems was too low to separate the two rat proinsulins (three different C_3/C_4 columns, Table II). Interestingly, the selectivity could be improved if the separation temperature was increased from 22 to 45°C (Fig. 6, lower panel), resulting in the separation of both proinsulins and insulins and C-peptides, although the effect of temperature on polypeptide retention times has been reported to be minimal [7].

A similar improvement in the efficiency following an increase in separation temperature was observed with a LiChrosorb RP-18 column eluted with AS–ACN (Fig. 7), whereas the results obtained on the same column eluted with TFA–ACN were comparable (*i.e.*, irreversible binding of insulins and proinsulins) at 22 and 45°C (data not shown).

Although RP-HPLC of peptides and proteins has been performed for more than a decade, the underlying mechanisms are far from well understood. Most experience was gained after the introduction of TFA [8], phosphoric acid [9] and alkylammonium salts [10] as mobile phase additives. The primary function of these substances is the (hopefully total) elimination of non-specific binding of peptides and proteins to the stationary phase in general and to free silanol groups in particular by ion pairing to charged groups in the sample molecules and to the free silanol groups [7,11].

The deleterious influence of these groups on the chromatographic process may vary from reduced recovery and non-ideal peak shapes to total loss of the injected peptide or protein sample [11–18]. This sample loss, which is directly related to an increasing molecular weight of the sample [19], is most pronounced for nanogram amounts [20,21], but losses also occur on the microgram scale [19]. It is most common after the use of C_{18} columns [7], which are more hydrophobic, but also better resolving, than C_4 or C_8 columns [11].

Free silanol groups are present in various amounts in all silica-based RP-HPLC columns (including the so-called "end-capped" columns), and additional groups are constantly created during chromatography owing to chemical instability of silica-based stationary phases in the commonly used highly acidic mobile phases [7,11,12,22]. Shielding of these groups is therefore of the greatest importance. Alkylammonium

salts (and especially TEAP) are very effective agents, whereas TFA is less suitable for this protection [7,11,18,23].

Blocking these very active sites on the stationary phase with smaller or larger amounts of the sample before the actual analysis has been reported [17,24], but the possibly beneficial effect seems to depend on the actual protein sample.

Our findings in this study that TEAP in some instances could "mask" the irreversible binding sites on the LiChrosorb columns (thereby allowing their successive use in TFA–ACN), and that the use of TEAP invariably resulted in excellent peak shapes, support some of the above-mentioned literature reports.

Further, a rapidly occurring stripping of ligands from C_{18} columns (perhaps a result of a poor binding procedure) has been reported to occur very rapidly with new columns [25]. The introduction of several sites with strong non-specific polypeptide binding combined with the poor ion-pairing capacity of dilute TFA and the very hydrophobic C_{18} ligand might explain most of our observations, but also the type of silica gel used may be important [15,26]. Since the irreversible binding to the C_{18} columns was only observed for the insulins and proinsulins (MW 6 and 9 kilodaltons, respectively) and not for the less hydrophobic C-peptides (MW 3 kilodaltons) it can be concluded that most C_{18} columns eluted with shallow TFA–ACN gradients are not suitable for the separation of polypeptides with molecular weights and hydrophobicities equal to or higher than those of insulins and proinsulins.

Finally, it should be emphasized that column reproducibility, recently reported to be a problem in many laboratories in the U.S.A. and Europe [27], is a phenomenon which must be taken very serious.

ACKNOWLEDGEMENT

The excellent technical assistance of Ragna Jørgensen is greatly appreciated.

REFERENCES

1 B. S. Welinder, H. H. Sørensen and B. Hansen, *J. Chromatogr.*, 361 (1986) 357.
2 S. Linde, J. H. Nielsen, B. Hansen and B. S. Welinder, *J. Chromatogr.*, 462 (1989) 243.
3 L. G. Heding, *Diabetologia*, 8 (1972) 260.
4 P. A. Halban, C. J. Rhodes and S. E. Shoelson, *Diabetologia*, 29 (1986) 893.
5 M. L. Gishizky and G. M. Grodsky, *FEBS Lett.*, 2 (1987) 227.
6 J. Rivier and R. McClintock, *J. Chromatogr.*, 268 (1983) 112.
7 F. Lottspeich and A. Henschen, in A. Henschen, K.-P. Hupe, F. Lottspeich and W. Voelter (Editors), *High Performance Liquid Chromatography in Biochemistry*, VCH, Weinheim, 1985, p. 139.
8 H. P. J. Bennet, H. M. Hudson, C. McMartin and G. E. Purdon, *Biochem. J.*, 168 (1977) 9.
9 W. S. Hancock, C. A. Bishop, S. O. Prestidge and M. T. W. Hearn, *Anal. Biochem.*, 89 (1978) 203.
10 J. Rivier, *J. Liq. Chromatogr.*, 1 (1978) 343.
11 J. Rivier and F. McClintock, in A. R. Kerlavage (Editor), *The Use of HPLC in Receptor Biochemistry*, Alan R. Liss, New York, 1989, p. 77.
12 C. T. Wehr, R. L. Lundgard and K. D. Nugent, *LC · GC Int.*, 2 (1989) 25.
13 W. S. Hancock and D. R. K. Harding, in W. S. Hancock (Editor), *Handbook of HPLC for the Separation of Amino Acids, Peptides and Proteins*, Vol. II, CRC Press, Boca Raton, FL, 1984, p. 3.
14 H. Engelhardt, H. Müller and U. Schön, in A. Henschen, K.-P. Hupe, F. Lottspeich and W. Voelter (Editors), *High Performance Liquid Chromatography in Biochemistry*, VCH, Weinheim, 1985, p. 15.
15 J. Nawrocky and B. Buszewski, *J. Chromatogr.*, 449 (1988) 1.
16 R. E. Majors, *LC · GC Int.*, 3 (1989) 12.

17 P. S. Sadek, P. W. Carr, L. D. Bowers and L. C. Haddad, *Anal. Biochem.*, 153 (1986) 359.
18 M. Andre, *J. Chromatogr.*, 351 (1986) 341.
19 M. T. W. Hearn, in Cs. Horváth (Editor), *High Performance Liquid Chromatography*, Vol. 3, Academic Press, New York, 1983, p. 87.
20 C. T. Wehr, L. Correia and S. R. Abott, *J. Chromatogr. Sci.*, 20 (1982) 114.
21 D. M. Desiderio, S. Yamada, F. S. Tanzer, J. Horton and J. Trimble, *J. Chromatogr.*, 217 (1981) 437.
22 J. F. Kennedy, Z. S. Rivera and C. A. White, *J. Biotechnol.*, 9 (1989) 83.
23 M. E. F. Biemond, W. A. Sipman and J. Olivié, *J. Liq. Chromatogr.*, 2 (1979) 1407.
24 R. S. Blanquet, K. H. Bui and D. W. Armstrong, *J. Liq. Chromatogr.*, 9 (1986) 1933.
25 J. L. Glajch, J. J. Kirkland and J. Köhler, *J. Chromatogr.*, 384 (1987) 81.
26 J. D. Pearson, N. T. Lin and F. E. Regnier, *Anal. Biochem.*, 124 (1982) 217.
27 R. E. Majors, *LC · GC*, 7 (1989) 10.

Journal of Chromatography, 536 (1991) 57–73
Elsevier Science Publishers B.V., Amsterdam

CHROMSYMP. 2016

Optimization of experimental conditions in preparative liquid chromatography

Trade-offs between recovery yield and production rate

SADRODDIN GOLSHAN-SHIRAZI and GEORGES GUIOCHON*

* *Department of Chemistry, University of Tennessee, Knoxville, TN 37996-1600 and Division of Analytical Chemistry, Oak Ridge National Laboratory, Oak Ridge, TN 37831-6120 (U.S.A.)*

ABSTRACT

The optimization of the experimental conditions in preparative chromatography under constraints of recovery yield, product purity and maximum available pressure is discussed. It is shown that there are optimum values of the loading factor and the column limit efficiency which permit the achievement of the maximum production rate under specified constraints of recovery yield and product purity. The optimum loading factor is given by a simple equation. The optimum column efficiency is calculated from numerical solutions of the semi-ideal model. The optimum column length for a given packing material and particle size and the optimum mobile phase velocity are then derived. These optimum values depend on the maximum available pressure, and the production rate increases rapidly with increasing pressure. If a given column is available and it is shorter than the optimum length, it should be operated at the optimum loading factor and at the optimum column efficiency. The mobile phase velocity, and hence the production rate, are less than those for the column of optimum length. If the column is longer than the optimum and cannot be cut, it should be operated at the maximum available pressure, at a mobile phase velocity lower than the optimum and with a loading factor larger than the optimum.

INTRODUCTION

The optimization of experimental conditions in preparative chromatography is a topic of great current interest. This process of separation or purification is expensive. Colin [1] has shown that the main contributions to that cost are, in order of decreasing importance, (i) the mobile-phase components (solvent, additives), including solvent losses and solvent regeneration; (ii) the amortization of the instrument; (iii) the periodic replacement of the stationary phase; (iv) labor; (v) other items, including energy, instrument maintenance and site preparation. Hence, it is important to maximize the production rate of a given instrument–column combination. Obviously, this requires the operation of the process at high concentrations, under non-linear conditions. When the column is "overloaded", bands interfere and overlap. However,

0021-9673/91/$03.50

because the displacement effect [2–6] enhances the separation between adjacent bands, high production rates of highly pure fractions may be achieved under these "overlapping band" conditions. The inconvenience of this mode of operation is similar to one of the major difficulties encountered in displacement chromatography, where the recovery yield becomes significantly smaller than unity.

This may be of limited concern for the isolation or purification of low- or medium-molecular-weight chemicals whose conformers exchange rapidly, as opposed to biopolymers. The recovery yield for given injection of the feed of such products may be moderate as long as this permits a significant increase in production rate (or rather a decrease in production costs) over "touching band" conditions. The intermediate fractions can be recycled, and the final recovery yield can be extremely high. The operation is profitable as long as the additional processing costs are offset by the revenue brought by the increase in the production rate. On the other hand, some peculiarities of the specific problem considered may be important and prevent or drastically limit this mode of operation. For proteins, the risk of a change in conformation, and hence in biological activity, is considered so serious that regulatory agencies require batch certification for the fractions which would have to be reprocessed. Given the cost and inconvenience of this procedure, intermediate fractions are better wasted. This results in the formulation of an additional constraint in the optimization development, a recovery yield constraint, which is added to the purity constraints.

Knox and Pyper [7] were the first to discuss the optimization of experimental conditions in preparative liquid chomatography. They addressed the touching-band case for a two-component mixture which they discussed thoroughly, making two critical assumptions, however. First, they ignored the competition between the two components for interaction with the stationary phase and considered the behavior of the two bands to be independent. Second, they assumed that the band profiles are right triangles, which is equivalent to replacing the equilibrium isotherms by their first two-term expansion (parabolic isotherm). This assumption has been rightly criticized by Snyder *et al.* [8], who nevertheless used it implicitly in their reformulation of the Knox and Pyper calculations [9]. Within the framework of their assumptions, Knox and Pyper [7] were able to calculate the sample size needed to achieve touching-band conditions and from there to derive the optimum values of the experimental parameters. They predicted that the optimum column should give a resolution of 1.7 between the peaks of the two components under linear conditions (sample size corresponding to a very small value of the loading factor). They also predicted an optimum value for the ratio d_p^2/L, where d_p is the average particle diameter and L the column length.

Recently, we published a theoretical analysis of the optimization problem for a binary mixture in the overlapping-band case (no yield constraint) [10,11] and in the touching-band case [12]. The practical consequences of this work have been explained in detail in several publications [13–17]. The procedures for the determination of the experimental conditions have been described and illustrated [10–12].

These analyses take into account the competition between the two components by assuming competitive Langmuir isotherms. We know that this isotherm does not account exactly for the competitive interaction between the components of a mixture, but that it predicts properly the trends and gives at least a good semi-quantitative

estimate of the individual band profiles and hence of the production rate[a] and recovery yield[a] [6,18,19]. In the case of touching bands [12], we have shown that the influence of the competitive interaction between the two components changes slightly the optimum column characteristics (optimum length or particle size) or the optimum mobile-phase flow velocity. On the other hand, the optimum loading factor, and hence the maximum production rate, are considerably different from the values predicted by Knox and Pyper [7]. Depending on the feed composition, they may be dramatically increased or decreased. In the case of overlapping bands, an equation was derived between the optimum sample size and the required purity [10]. The optimum operating conditions were related to the characteristics of the separation problem studied [11]. It was shown that allowing the collection of slightly impure (*e.g.*, 99% pure) fractions permits a large increase in the production rate when the second-eluted component is in excess [10,11].

Our previous work, however, considered only two extreme cases, 100% recovery yield (touching-band case) and maximum possible production rate, which results in a low recovery yield (*ca.* 60%). In this paper, we discuss the influence of a recovery yield constraint on the optimization of these experimental conditions.

THEORY

Summary of previous results

Consider first a two-component mixture, within the framework of the ideal model[b] [10]. The production rate increases in proportion to the sample size until, beyond the touching-band condition, a chromatogram is obtained such that a cut at the retention time of the second component shock (which gives a 100% yield) gives a fraction having exactly the required degree of purity, Pu_2. If we continue to increase the amount of feed injected at each cycle, the production rate remains constant and the recovery yield decreases. The optimum sample size for which this maximum production rate is achieved is such that the corresponding value of the loading factor for the second component, $L^*_{f,2}$, is given by the following equation [10]:

$$L^*_{f,2} = \frac{\left[\dfrac{\alpha-1}{\alpha(1-x)}\right]^2}{(1+b_1r_1/b_2)} \tag{1}$$

where α is the relative retention of the two compounds ($\alpha = a_2/a_1 = k'_{0,2}/k'_{0,1}$), the coeficient a_i being the first coefficient of the equilibrium isotherm of component i and $k'_{0,i}$ is its retention factor, b_i is the second coefficient of the single-component Langmuir isotherm of component i and x is given by

---

[a] The production rate is the amount of the corresponding component in the purified fraction at the required degree of purity which is produced per unit time. The recovery yield is the ratio between the amount of the component of interest that is collected in the product fraction and the amount injected in the column with the feed.

[b] The ideal model assumes that the column efficiency is infinite. In practice, although real columns have a finite efficiency, many results of the ideal model can be applied directly or with only minor corrections.

$$x = \sqrt{\frac{1 - Pu_2}{Pu_2 \alpha r_1}} \tag{2}$$

For touching bands, the purity of the collected fraction is 100%, so $x = 0$ in eqn. 1. Finally, r_1 is the root of the characteristic equation of the problem [20], which has been shown to be practically equal to C_1^0/C_2^0 [3], where C_i^0 is the concentration of component i in the feed.

Thus, eqn. 1 can be rewritten as

$$L_{f,2}^* = \frac{\left[\frac{\alpha - 1}{\alpha(1-x)}\right]^2}{1 + \frac{q_{s,2} C_{0,1}}{\alpha q_{s,1} C_{0,2}}} \tag{3}$$

where $q_{s,i} = a_i/b_i$ is the adsorbent saturation capacity for component i. The sample size, n, is given by

$$n = L_{f,2}^*(1 + C_1^0/C_2^0)(1 - \varepsilon)SLq_{s,2} \tag{4}$$

where ε is the packing porosity, S is the column geometrical cross-sectional area and L is the column length. The sample size given by eqns. 3 and 4 gives the maximum production rate and a total recovery yield in the ideal model.

We have shown that for real columns whose efficiency is finite, the optimum sample size for maximum production rate is still given by eqns. 3 and 4 [11]. However, the recovery yield achieved with this optimum sample size, which was total with an ideal column, is now less than 100%. It depends on the column efficiency, increasing with the column limit efficiency (*i.e.*, the efficiency measured at very small loading factors) and tending towards unity when the efficiency becomes infinite. The column efficiency, in turn, depends on the mobile phase velocity, u, which turns out to control both the cycle time (proportional to $1/u$) and the recovery yield. Accordingly, there will be an optimum value of the mobile phase flow velocity at which the production rate is maximum. It turns out that this mobile phase velocity corresponds to a very high value of the reduced velocity (unless the separation is extremely difficult, with α values below 1.05) and that the corresponding recovery yield is around 60% in about all instances [11].

As suggested by Knox and Pyper [7], there is an optimum value for the ratio d_p^2/L the value of which depends on the recovery yield [11]. However, the demonstration of this result [7,11] assumes a simplified column plate height equation ($h = Cv$). For a general plate height equation (*e.g.*, the Knox equation), this result remains valid as a first approximation at high velocities, *i.e.*, for all but the most difficult separations (*e.g.*, with $\alpha \ll 1.1$, and when small particles are used). Thus, if we introduce a recovery yield constraint, as we are going to do here, the optimum column will change with the recovery yield constraint chosen. The fact that there is an optimum value for the ratio d_p^2/L but no separate optimum value of the particle size and the column length means that we can chose arbitrarily one of these parameters and adjust the other. For example, if the optimum value of d_p^2/L is 10 (d_p in μm, L in cm), we can take a 10-cm

long column packed with 10-μm particles or a 40-cm long column packed with 20-μm particles. With the latter column, both the cycle time and the sample size will be four times larger than with the former, so the production rate will remain the same. However, from the point of view of production rate optimization, we could as well chose a 0.9-cm long column packed with 3-μm particles or a 250-cm long column packed with 50-μm particles. Neither of these columns would be very practical.

As in our previous work, we have neglected here the extra-column effects which may modify the band shape and the separation. The interaction between these sources of band broadening and the band profile in non-linear chromatography has been discussed recently [21]. It is easier in preparative than in analytical chromatography to design injection systems, connecting tubes and detectors with a volume that is small compared with that of the column. However, the feed volume injected is always large. The influence of the feed volume on the band profile has also been discussed [22]. It has been found to be small compared with that of the non-linear effects (displacement and tag-along effects).

Statement of the optimization problem

The primary aim of this work was the determination of the optimum experimental conditions for the maximum production rate of the second-eluted component of a binary mixture, at a given degree of purity, with a certain recovery yield. The second aim was an investigation of the trade-offs between production rate and recovery yield.

In this discussion, we assume that the chromatographic system has already been selected. Thus, the retention factors, k'_i, of the two components are constant, in addition to the relative retention, α, and the column saturation capacities, $q_{s,i}$, for the two components, their molecular diffusion coefficients and the coefficients of the Knox plate height equation [23]. Finally, we assume that the chromatograph used cannot be operated above a certain inlet pressure, ΔP.

In previous papers we have already discussed the influence on the production rate of the relative retention [17] and of the maximum available inlet pressure [11,16] and shown that the maximum production rate always increases rapidly with increasing values of these two parameters.

General equations used

For the equilibrium isotherms, we used the classical competitive Langmuir equation [24]:

$$q_i = \frac{a_i C_i}{1 + b_1 C_1 + b_2 C_2} \tag{5}$$

where q_i and C_i are the concentrations of component i in the stationary and the mobile phases (both in mol/l) at equilibrium and a_i and b_i are numerical coefficients. All of the calculations presented here were performed for binary mixtures of variable compositions of two components and a maximum available pressure of 100 bar, except for a study of the influence of the operating pressure. In most instances, the relative retention, α, is 1.20.

For the plate height equation, we used the classical Knox equation [23]:

$$h = \frac{B}{v} + Av^{1/3} + Cv \tag{6}$$

where $h = H/d_p$ is the reduced plate height, *i.e.*, the ratio of the actual column plate height to the average particle size, and $v = ud_p/D_m$ is the reduced mobile phase velocity or Peclet number for the particle size. In the calculations the results of which are reported here, the coefficients A, B and C are 1, 2 and 0.1 respectively.

To calculate the relationship between the mobile phase flow velocity, the inlet pressure and the column characteristics, we use the classical Darcy equation and its well known relatives:

$$u = \frac{d_p^2 \Delta P}{\phi \eta L} \tag{7a}$$

$$v = \frac{\Delta P d_p^3}{\phi \eta D_m L} \tag{7b}$$

where η is the mobile phase velocity, D_m is the component diffusivity in the mobile phase and ϕ is the column hydrodynamic resistance factor (*ca.* 1000).

Optimization strategies

The recovery yield depends on the degree of band overlap, determined by both the loading factor (which controls the degree of column overloading) and the column efficiency (which controls the thickness of the shock layers and increases the band width beyond the value predicted by the ideal model). The production rate for the second component is [10]

$$\frac{Pr_2}{(1 - \varepsilon)S} = \frac{uL_{f,2}R_2q_{s,2}}{k'_{0,2}} \tag{8}$$

In this equation, we assume that the cycle time is $t_c = k'_{0,2}t_0$, the time spent by the last-eluted fraction of the second component in the stationary phase. If another value of the cycle time is used, eqn. 8 should be multiplied by $(t_{R,0,2} - t_0)/t_c$. R_2 is the recovery yield for the second component and ε is the packing porosity. Note that the production rate is proportional to the loading factor and independent of the column length, because with a constant column cross-sectional area, the loading factor corresponding to a given sample size is inversely proportional to the column length. The values of the production rate (Pr_2) and the recovery yield (R_2) are related to the experimental conditions.

Many combinations of mobile phase flow velocity and loading factor may result in the same value of the recovery yield, and we need to find out rapidly which combination gives the highest production rate. It is impossible to find out rapidly the exact combination of parameter values giving the maximum production rate for a given fraction purity and a given recovery yield. However, it is possible to derive rapidly approximate values which are close enough to the optimum values for practical purposes. We present here four different methods, which are all simple, compare them and choose the most effective among them. With the first two methods, we start from the experimental conditions giving the maximum possible production rate and a recovery yield of *ca.* 60%, and we vary one of the operational parameters, the sample size or the mobile phase velocity.

Optimization strategy I. We can keep the sample size constant, at the value given by eqns. 3 and 4, and decrease the mobile phase velocity to increase the column efficiency and the recovery yield until the constraint is met. In so doing, we decrease the production rate, because R_2 will increase much more slowly than the cycle time, *i.e.*, $1/u$.

Eqns. 7 and 8 in ref. 11, which give the recovery yield and the production rate, are valid as long as the sample size is given by eqns. 3 and 4. Thus, in this approach, we can use them to calculate Pr_2 and R_2 (Note: in these equations there is an unfortunate typographical error [11;25]; the correct equations are given in ref. 25 and are used here). Accordingly, the constraint on the recovery yield introduces a relationship between the parameters of the separation, and the required limit column efficiency is obtained by solving the combination of eqn. 5 and the correct eqn. 7 in ref. 11 [25]:

$$N_0 = \frac{16(1 + k'_{0,2})^2}{k'^2_{0,2} w^2_{2,\text{th}}} \left(\left\{ \frac{\alpha - 1}{\alpha(1 - x)} (1 - \sqrt{R_2}) \left[2 - \frac{\alpha - 1}{\alpha(1 - x)} (1 + \right. \right. \right.$$

$$\left. \left. \left. + \sqrt{R_2}) \right] \frac{\gamma}{w_{2,\text{th}}} + 1 \right\}^2 - 1 \right)^{-1} \qquad (9)$$

where R_2 is the required recovery yield and $w_{2,\text{th}}$ and γ are given by the following relationships:

$$w_{2,\text{th}} = \frac{(\alpha - 1)\,[1 + \alpha + 2q_{s,2}C_{0,1}/(q_{s,1}C_{0,2})]}{\alpha^2[1 + q_{s,2}C_{0,1}/(\alpha q_{s,1}C_{0,2})]^2} \qquad (10a)$$

and

$$\gamma = \frac{1 + q_{s,2}C_{0,1}/(q_{s,1}C_{0,2})}{1 + q_{s,2}C_{0,1}/(\alpha q_{s,1}C_{0,2})} \qquad (10b)$$

The calculation of N_0 requires only the knowledge of the single-component isotherm coefficients readily obtained by the retention time method[a] [26,27]. We have shown that the production rate always increases with increasing inlet pressure [11,12,16]. Hence the column must be operated at the maximum pressure available, and its efficiency must be N_0. Thus the optimum column length at fixed particle size (or, conversely, the optimum d_p for a given L) is derived from eqns. 6 and 7b. The optimum column length (or particle size) depends on the recovery yield required (see eqn. 9).

Eqn. 9 shows that, for any required value of the recovery yield, there is an optimum limit column efficiency, N_0, which depends also on the required purity of the fractions, the relative composition of the feed and the isotherm parameters (α, $q_{s,i}$ and $k'_{0,2}$). The existence of an optimum value of N_0 is a general result, although eqn. 9 has been derived for a loading factor given by eqn. 3. If another loading factor must be

[a] The retention time method uses the analytical equation of the single-component band profile in the case of a Langmuir isotherm to determine the parameters of this isotherm.

used, there is still an optimum column efficiency for any required yield. However, this efficiency must be calculated by using the solution of the semi-ideal model.

Optimization strategy II. We can keep the mobile phase flow velocity constant, and hence the rate constant of the mass transfer kinetics and the column limit efficiency, and reduce the sample size until the recovery yield constraint is met. This approach will give the lowest production rate that can be achieved while maintaining a certain value of the recovery yield.

The column efficiency, and hence the column length and reduced flow velocity, are kept constant and equal to those giving the maximum possible production rate. These values are those calculated for the maximum possible production rate (no yield constraint) and are given by eqns. 5, 7 and 8 in ref. 11. The sample size must be reduced from the value given by eqns. 3 and 4 until the required yield is achieved. A series of successive individual profile computations permits the rapid calculation of the loading factor for which the yield is equal to the stated value of the constraint.

Optimization strategy III. Obviously, neither of the above two approaches will give the maximum possible production rate at the requested recovery yield. To achieve this result, both the parameters $L_{f,2}$ and u must be adjusted. We may attempt to keep constant the product $R_2 L_{f,2}$ in eqn. 8. Since the recovery yield at the maximum possible production rate (no yield constraint) is *ca.* 60%, we may reduce the loading factor by the ratio $0.6/R_2$, where R_2 is the requested value of the yield. Thus, the loading factor is given by

$$L_{f,2} = L^*_{f,2} \cdot \frac{0.6}{R_2} \tag{11}$$

where $L^*_{f,2}$ is given by eqn. 3. We then adjust the column efficiency to achieve the desired recovery yield. This procedure provides an adjustment of both parameters. Although not rigorous, the method is reasonable, as it is in agreement with the results of a simplex study which showed a quasi-linear relationship between the recovery yield and both $L_{f,2}$ and u [28]. The required efficiency is obtained by calculating series of chromatograms corresponding to the loading factor given in eqn. 11 and different values of the column efficiency and determining the value of the efficiency for which the recovery yield is equal to the required value. The optimum column length and mobile phase velocity are calculated as described in the first strategy.

Optimization strategy IV. Starting from the optimum values predicted by the third approach, the loading factor is slightly increased, while the mobile phase velocity is decreased (the efficiency is increased) in order to achieve the desired recovery yield. The procedure is repeated until the maximum production rate is observed. The determination of the optimum values of the loading factor, $L_{f,2}$, and the column efficiency is made by calculation of series of chromatograms.

Optima in chromatography are usually rather flat. Hence the third approach will most often give an excellent approximation of the optimum conditions, while the fourth approach will converge rapidly towards the true optimum.

RESULTS AND DISCUSSION

We first compare the results obtained with the different approaches outlined in the previous section. We show that one of these methods performs better than the others. Then, we use the results obtained with this preferred method to investigate the trade-offs between recovery yield and production rate.

Table I compares the production rates obtained with the four different strategies. The calculations were performed for a 1:9 binary mixture with a relative retention, α, of 1.20 and for 10-μm particles. The other experimental conditions (Table I) are typical of current practice in preparative liquid chromatography. For this mixture, the maximum possible production rate, with a 60% recovery yield, is 0.46 mol m^{-2} s^{-1} (see Table II). Note that, in agreement with eqn. 8, the values of the production rate are proportional to the loading factor and the recovery yield.

The different strategies can be ranked in order of the performance allowed. The second strategy is obviously the worst. The first strategy gives twice as large a production rate, but is still less than two thirds of the production rate predicted by the third strategy. The fourth strategy gives only a marginal increase in production rate, about 3% at best, which is hardly significant. On the other hand, strategy IV is more complex and requires more computation time. Accordingly, in the remainder of this paper, we shall use exclusively the third strategy.

The maximum production rate of the second component that can be achieved with 1:9 mixture, while achieving a 95% recovery yield, is two thirds of the maximum possible production rate, which would bring a recovery yield of only 60%. In economical terms, it means that by reducing the throughput by a factor of 2.3, we reduce the production rate by only 1.5. The savings on the throughput and on the amount of feed to be recycled or wasted due to the large increase in yield are certainly significant. Probably the least costly production rate would be achieved for a throughput corresponding to a value of the recovery yield between 60 and 95%.

TABLE I

OPTIMUM EXPERIMENTAL CONDITIONS FOR A SPECIFIC VALUE OF THE RECOVERY YIELD WITH VARIOUS OPTIMIZATION STRATEGIES

Recovery yield constraint: 95%. Experimental conditions: $\alpha = 1{,}2$, $k'_{0,1} = 3$; column saturation capacity, $q_{s,1} = q_{s,2} = 5$; phase ratio, $F = 0.25$; maximum available pressure, $\Delta P = 100$ bar; solute molecular diffusion coefficients, $D_m = 1 \cdot 10^{-9}$ m^2/s; mobile phase viscosity, $\eta = 1$ cP ($1 \cdot 10^{-3}$ Pa s); packing particle average diameter, $d_p = 10$ μm; degree of purity of the collected fractions, 99%; cycle time, $t_c = t_{R,02} - t_0$; plate height equation, $h = 2/\nu + \nu^{0.33} + 0.1\nu$; composition of the binary mixture, 1:9 (10% of the first component).

Strategy used	N_0	L (m)	ν	Loading factor (%)	Production rate, $Pr_2/(1-\varepsilon)S$ (mol m^{-2} s^{-1})
I	5100	0.32	31.0	4.82	0.198
II	550	0.0884	113.2	0.7	0.104
III	1050	0.127	78.7	3.04	0.316
IVa	1250	0.14	71.2	3.4	0.319
IVb	1400	0.15	66.7	3.7	0.327

Trade-offs between production rate and recovery yield

Using the same binary mixture as for the calculation of the data in Table I, Table II compares the production rates predicted by the third optimization strategy for different values of the required recovery yield, from 60% (in practice the maximum possible production rate without yield constraint) to near 100% (corresponding to the touching-band case). The production rate decreases slowly at first with increasing required recovery yield, the loss of production rate being 10% for an 80% yield and 22% for a required yield of 90%. Beyond 90%, the loss increases rapidly and becomes precipitous above 99%. For the touching-band condition, the production rate is 15% of the maximum production rate possible and still only 22% of the production rate possible with the excellent recovery yield of 95%. Allowing a recovery yield of 99.9%, which is equivalent to total recovery for all practical purposes, still gives a 2.5 times larger production rate than the touching-band case. However, the reason for this remarkable increase in the production rate is that we have accepted to produce 99% pure fractions, not that we have accepted a decrease in yield of 0.1%. Touching bands permit, at least in theory, both a total recovery yield and the production of totally pure products. When the concentration of the less retained component in the feed is much less than the concentration of the more retained component, allowing a small amount of impurity in the product permits a large increase in production rate [10]. This is no longer true at higher concentrations of the less retained component.

The data in the Table II show also that the required efficiency increases rapidly with increasing recovery yield, as well as the column length, while the reduced velocity and the loading factor decreases steadily. Although the throughput decreases, allowing important savings on solvent costs, the column required is longer and the amount of packing material needed per unit amount of feed purified increases.

TABLE II

TRADE-OFFS BETWEEN PRODUCTION RATE AND RECOVERY YIELD; OPTIMUM EXPERIMENTAL CONDITIONS FOR MAXIMUM PRODUCTION RATE AT VARIOUS SPECIFIED VALUES OF THE RECOVERY YIELD

Same experimental conditons as in Table I, except for the recovery yield constraint. R_s is the resolution observed between the two component bands at very low value of the loading factor (linear conditions).

Yield (%)	N_0	R_s	L (m)	v	Loading factor (%)	Production rate, $Pr_2/(1-\varepsilon)S$ (mol m^{-2} s^{-1})
60[a]	550	0.76	0.084	113	4.82	0.46
80[b]	650	0.83	0.097	103	3.60	0.413
90[b]	825	0.94	0.111	90	3.20	0.361
95[b]	1050	1.05	0.127	78.7	3.04	0.316
99[b]	1800	1.38	0.173	57.7	2.92	0.232
99.9[b]	3000	1.79	0.234	42.9	2.9	0.172
Touching band[c]	3230	1.85	0.244	41	1.24	0.0705

[a] Values calculated using eqns. 5, 7 and 8 in ref. 11 (maximum possible production rate, with no yield constraint).

[b] Values calculated using strategy III, as explained in the text.

[c] Values calculated using the procedure described in ref. 12.

TABLE III

TRADE-OFFS BETWEEN PRODUCTION RATE AND RECOVERY YIELD: OPTIMUM EXPERIMENTAL CONDITIONS FOR MAXIMUM PRODUCTION RATE AT VARIOUS SPECIFIED VALUES OF THE RECOVERY YIELD AND INFLUENCE OF THE PARTICLE SIZE

Same experimental conditions as in Table II, except average particle size, $d_p = 20$ μm.

Yield (%)	N_0	R_s	L (m)	v	Loading factor (%)	Production rate, $Pr_2/(1-\varepsilon)S$ (mol m^{-2} s^{-1})
60	500	0.73	0.315	253	4.82	0.505
80	650	0.83	0.363	220	3.6	0.449
90	850	0.95	0.42	190	3.2	0.381
95	1100	1.08	0.483	166	3.04	0.358
99	1800	1.38	0.633	126	2.92	0.254
99.9	3000	1.78	0.841	95	2.90	0.191
Touching band [12]	3380	1.90	0.90	89	1.27	0.0785

Table III shows data similar to those in Table II, but corresponding to packing material with an average particle size of 20 μm. The optimum column length is approximately four times longer than that found with 10-μm particles (see Table II), and the maximum production rates for each stated recovery yield are very nearly the same. The difference between the production rates is *ca.* 10% at both ends (yields of 60 and 99.9%) and 14% for a required yield of 95%. This results confirms the observation by Knox and Pyper [7] and our general demonstration [12] that, when columns are operated at high velocities, there is a near-optimum value of d_p^2/L, but no separate optima of the particle size and the column length.

Table IV shows data corresponding to a binary mixture of the same two components, but with a very different composition, 3:1 instead of 1:9 used for Tables

TABLE IV

TRADE-OFFS BETWEEN PRODUCTION RATE AND RECOVERY YIELD: OPTIMUM EXPERIMENTAL CONDITIONS FOR MAXIMUM PRODUCTION RATE AT VARIOUS SPECIFIED VALUES OF THE RECOVERY YIELD AND INFLUENCE OF THE MIXTURE COMPOSITION

Same experimental conditions as in Table II, except composition of the feed, 3:1 binary mixture (25% of the second component).

Yield (%)	N_0	R_s	L (m)	v	Loading factor (%)	Production rate, $Pr_2/(1-\varepsilon)S$ (mol m^{-2} s^{-1})
60[a]	1500	1.26	0.156	64	0.875	0.0473
80[b]	1800	1.38	0.173	57.7	0.656	0.0422
90[b]	2200	1.50	0.195	51.4	0.584	0.0377
95[b]	2700	1.70	0.22	45.6	0.553	0.0333
99[b]	4000	2.06	0.277	36.0	0.53	0.0263

[a] Values calculated from eqns. 5, 7 and 8 in ref. 11.
[b] Values calculated from strategy III, as explained in the text.

I–III. The concentration of the second component decreases from 90 to 25%, *i.e.*, 3.6 times. In the former instance, the displacement effect predominates, and we know how favorable this effect is to the separation chemist. It enhances the production rate for both the second and the first component. In the present instance (Table IV), the tag-along effect predominates and spreads the second-component band over a wide range of retention times. If we compare Tables II and IV, we observe that the production rate for the second component decreases nearly 10-fold, corresponding to a total throughput (amount of feed processed by the column per unit time) decrease by a factor of *ca.* 2.6. When a compound is eluted second, its purification (Table II) is much easier and less costly than its extraction (Table IV). Compared with the optimum conditions for the 1:9 mixture, the column required for the extraction of the second component from the 3:1 mixture is nearly twice as long, the optimum mobile phase velocity is nearly two thirds as large and the loading factor is about six times smaller.

The only possibility of increasing the production rate would be the use of a combination of two chromatographic separations, the mixture collected with the mixed zone during the first stage being reprocessed. This raises new and interesting problems of optimization, which are beyond the scope of this work.

Table V illustrates the influence of the feed composition on the production rate for the second component, with a required recovery yield of 95% (and a product purity of 99%, as in the remainder of this work). The loading factor is calculated from eqn. 11. The production rate increases dramatically with increasing concentration of the second component, from 5 to 95%. At the same time, the optimum column efficiency decreases more than four-fold and the column length about two-fold, while the loading factor increases 43-fold and the optimum mobile-phase velocity more than two-fold. All these effects combined provide for a production rate increase by a factor of 100 and a more than five-fold increase in the total feed throughput. The relative ease with which the second component can be purified from small proportions of the first component, compared with the difficulty in extracting small amounts of this second component from an excess of the first, illustrates the importance of the displacement effect in

TABLE V

TRADE-OFFS BETWEEN PRODUCTION RATE AND RECOVERY YIELD: OPTIMUM EXPERIMENTAL CONDITIONS FOR MAXIMUM PRODUCTION RATE FOR VARIOUS FEED COMPOSITIONS

Same experimental conditions as in Table II, except variable feed composition. Recovery yield, 95%. Results calculated using strategy III, as explained in the text.

Feed composition	N_0	R_s	L (m)	v	Loading factor (%)	Production rate, $Pr_2/(1-\varepsilon)S$ (mol m^{-2} s^{-1})
5:95	950	1.0	0.120	83.3	4.62	0.509
10:90	1050	1.05	0.127	78.7	3.04	0.316
25:75	1300	1.18	0.144	69.6	1.93	0.177
50:50	1720	1.35	0.169	59.3	1.15	0.090
75:25	2700	1.70	0.220	45.6	0.553	0.033
90:10	3000	1.78	0.233	43.0	0.217	0.0123
95:5	4100	2.08	0.281	35.5	0.107	0.0050

TABLE VI

TRADE-OFFS BETWEEN PRODUCTION RATE AND RECOVERY YIELD: OPTIMUM EXPERIMENTAL CONDITIONS FOR MAXIMUM PRODUCTION RATE AT VARIOUS VALUES OF THE SELECTIVITY

Same experimental conditions as in Table II, except various values of selectivity and average particle size d_p = 20 μm. Recovery yield, 95%. Results calculated using strategy III, as explained in the text.

Selectivity, α	N_0	R_s	L (m)	v	Loading factor (%)	Production rate, $Pr_2/(1-\varepsilon)S$ (mol m^{-2} s^{-1})
1.1	3400	1.04	0.903	88.6	0.93	0.0594
1.2	1100	1.08	0.483	166	3.04	0.358
1.3	620	1.12	0.354	226	5.68	0.783
1.5	330	1.18	0.253	317	11.37	1.91
1.7	225	1.20	0.206	388	16.8	3.05

preparative chromatography [4,5]. It also emphasizes the need to select, as far as possible, the order of elution of the feed components.

Table VI describes the influence of the relative retention of the two components on the maximum production rate of 99% pure fractions of the second component, with a recovery yield of 95%. The optimum loading factor is calculated from eqn. 11. The optimum column efficiency decreases rapidly with increasing relative retention and so does the optimum column length. At the same time, the optimum mobile phase velocity increases rapidly, in addition to the optimum loading factor. The maximum production rate increases nearly as $[(\alpha-1)/\alpha]^3$ [17]. The same dependence has been predicted in both the touching-band case (100% yield) and the overlapping case (maximum possible production rate, no yield constraint) [12,17].

Finally, Table VII illustrates the influence of the operating pressure[a] on the

TABLE VII

TRADE-OFFS BETWEEN PRODUCTION RATE AND RECOVERY YIELD: OPTIMUM EXPERIMENTAL CONDITIONS FOR MAXIMUM PRODUCTION RATE AT VARIOUS VALUES OF THE OPERATING PRESSURE

Same experimental conditions as in Table II, except various values of inlet pressure. Recovery yield, 95%. Results calculated using strategy III, as explained in the text.

Operating pressure, ΔP (bar)	N_0	R_s	L (m)	v	Loading factor (%)	Production rate, $Pr_2/(1-\varepsilon)S$ (mol m^{-2} s^{-1})
20	1050	1.05	0.065	30.6	3.04	0.121
50	1050	1.05	0.095	52.6	3.04	0.21
100	1050	1.05	0.127	78.7	3.04	0.316
200	1050	1.05	0.172	116	3.04	0.462

[a] The operating pressure is the highest pressure at which the equipment can be operated safely on a routine basis.

maximum production rate of 99% pure product, with a 95% recovery yield. The optimum loading factor and the optimum column efficiency are both independent of the pressure. Both the optimum velocity and the optimum column length (at a given value of d_p) increase nearly in proportion to the square root of the operating pressure, so the cycle time remains constant. Thus, the production rate increases with increasing sample size; at a constant loading factor, the latter, in turn, increases in proportion to the increasing column length. The production rate is nearly proportional to the square root of the operating pressure [12].

Optimization of a given column

In this instance, the column length and particle size are determined and cannot be adjusted. Only the sample size and the mobile phase flow velocity can be optimized. The value of the ratio d_p^2/L can be either larger or smaller than the optimum value for the separation considered.

If d_p^2/L is larger than the optimum (*i.e.*, the column is too short for the packing material used), it cannot be operated at the maximum available pressure, because the efficiency would be insufficient. We must operate it at the optimum efficiency, with the optimum loading factor calculated above (eqn. 11). Hence we must use a lower flow velocity than with a column of optimum length to achieve the optimum efficiency, and the production rate is lower than that possible with the column of optimum length. The data in Table VIII (last three lines) illustrate this situation. If we compare these with the similar data in Table II, we see that the column length in Table VIII (10 cm) is shorter than the optimum length for production with a recovery yield in excess of about 82%.

TABLE VIII

TRADE-OFFS BETWEEN PRODUCTION RATE AND RECOVERY YIELD FOR A GIVEN COLUMN: OPTIMUM EXPERIMENTAL CONDITIONS FOR MAXIMUM PRODUCTION RATE AT VARIOUS SPECIFIED VALUES OF THE RECOVERY YIELD

Same experimental conditions as in Table II, except fixed column length (0.10 m).

Yield (%)	N_0	R_s	L (m)	v	Loading factor (%)	Production rate, $Pr_2/(1-\varepsilon)S$ (mol m^{-2} s^{-1})
60[a]	685	0.85	0.10	100	5.4	0.45
80[a]	685	0.85	0.10	100	3.60	0.408
90[b]	825	0.94	0.10	78	3.20	0.313
95[b]	1050	1.05	0.10	57	3.04	0.228
99[b]	1800	1.38	0.10	5.6	2.92	0.103

[a] In this case, the column is longer than the optimum (see Table II) and cannot be operated at the optimum velocity (the inlet pressure would exceed the maximum available pressure). The column efficiency being higher than the optimum (*cf.*, Table II), we must inject a sample larger than that corresponding to the optimum loading factor in order to achieve the required yield. This does not compensate for the decreased flow velocity, and the production rate is lower that would be possible with the column of optimum length.

[b] In this case, the column is shorter than the optimum. We must operate it at the velocity giving the optimum efficiency and use the optimum loading factor given in Table II. Compared with the optimum conditions (Table II), the mobile phase velocity will be lower and the production rate smaller. The production rate decreases rapidly with increasing required yield.

Under such conditions, the column must be operated at the flow velocity that gives the same efficiency as the optimum column (compare the second columns in Table II and VIII), and with the same loading factor as for the optimum column (compare the sixth columns in Tables II and VIII). The production rate is decreased by 15% for a recovery yield of 90% and by more than 50% for a recovery yield of 99%.

For each column, there is a optimum flow velocity for the maximum production rate. This optimum velocity is such that the column has the optimum efficiency (see Table II). Accordingly, there is an optimum value of the inlet pressure [11,16]. If the column is too short, this optimum pressure is lower than the maximum available pressure.

If d_p^2/L is smaller than the optimum (*i.e.*, the column is too long for the packing material used), the optimum pressure is higher than the maximum available pressure, and we cannot operate it at a high enough velocity to achieve the optimum column efficiency (see the first two lines in Table VIII and corresponding data in Table II). The column is operated at the maximum available pressure, at the flow velocity given by eqn. 7b, and it has the efficiency derived from eqn. 6. However, this column efficiency exceeds the optimum efficiency for the maximum production rate. In order to achieve the required recovery yield, we must use this excessive efficiency and overload the column more. The loading factor is increased, but the production rate is lower than is possible with the optimum column, although in the example chosen here the loss is almost negligible (1–2%).

Finally, Table IX compares the performances of various columns packed with the same stationary phase but having different lengths and used to separate the same binary mixture as used for Table I (1:9 mixture), with the same recovery yield of 95%. The loss in production rate that accompanies the use of a column of improper length can be very important. It is especially costly if the column is too long.

TABLE IX

OPTIMUM EXPERIMENTAL CONDITIONS FOR MAXIMUM PRODUCTION RATE WITH A GIVEN COLUMN AT A SPECIFIED YIELD

Same experimental conditions as in Table II, except fixed column length, as indicated. In all instances the required recovery yield is 95% and the required degree of purity of the products is 99%.

L (m)	N_0	v	Loading factor (%)	Production rate, $Pr_2/(1-\varepsilon)S$ (mol m^{-2} s^{-1})
0.10[a]	1050	57	3.04	0.228
0.127[b]	1050	78.7	3.04	0.316
0.20[c]	2300	50	4.4	0.29
0.30[c]	4560	33.3	4.7	0.208
0.40[c]	7300	25.0	4.82	0.162

[a] The column length is shorter than the optimum. In this case, the maximum production rate is obtained at the column efficiency and loading factor of the optimum column (see Table II). However, the linear velocity is smaller than the optimum, and so is the production rate.

[b] Optimum column length (see Tabel II).

[c] The column length is longer than the optimum. The column is operated at the maximum available pressure. Compared with the optimum, the mobile phase velocity is lower, the loading factor higher and the production rate smaller.

CONCLUSION

The theory of optimization presented here is based entirely on the theory of non-linear chromatography and as such is as rigorous as possible. It avoids the pitfalls of uncontrolled empiricism more or less hidden in previous attempts and the use of adjustable parameters [8,9,29]. Nevertheless, the optimum conditions are simple to derive in most cases. However, this approach suffers from two serious limitations.

First, it deals only with binary mixtures. The two-component problem is the simplest separation case; it is relevant for the separation of closely related isomers produced by chemical synthesis (*e.g.*, separation of enantiomers). In practice, a number of impurities may have to be eliminated or the component of interest must be extracted from a complex mixture. In this case, as in the optimization of the experimental conditions for minimum analysis time, the cycle time depends on the retention time of the last-eluted impurity. We may want to operate the column at a higher mobile-phase velocity than the optimum value obtained by considering the binary mixture made of the main compound of interest in the feed and the most closely eluted impurity to be eliminated. This would permit a reduction of the cycle time, although a smaller sample size will have to be used.

Second, the present approach is based on the assumption that the competitive Langmuir isotherm accounts satisfactorily for the interaction behavior of the two main components of the feed. This is not true except, to some extent, for enantiomers [18]. The more rigorous ideal adsorbed solution model [30] gives slightly better results, but it cannot take into account two important effects, the variation of the activity coefficients of solutes with their concentrations and the molecular interactions between the feed components in the stationary phase [31]. Accounting properly for these effects is the last hurdle in the full understanding of the mechanism of preparative chromatography, but a major one.

ACKNOWLEDGEMENTS

This work was supported in part by Grant CHE-8901382 of the National Science Foundation and by the cooperative agreement between the University of Tennessee and the Oak Ridge National Laboratory. We acknowledge the support of our computational efforts by the University of Tennessee Computing Center.

REFERENCES

1 H. Colin, *6th Symposium on Preparative Chromatography, Washington, DC, May 1989*, Discussions.
2 G. Guiochon and S. Ghodbane, *J. Phys. Chem.*, 92 (1988) 3682.
3 S. Golshan-Shirazi and G. Guiochon, *Anal. Chem.*, 62 (1990) 217.
4 J. Newburger, L. Liebes, H. Colin and G. Guiochon, *Sep. Sci.*, 22 (1987) 1933.
5 J. Newburger and G. Guiochon, *J. Chromatogr.*, 484 (1989) 153.
6 A. M. Katti and G. Guiochon, *J. Chromatogr.*, 499 (1990) 25.
7 J. H. Knox and H M. Pyper, *J. Chromatogr.*, 363 (1986) 1.
8 L. R. Snyder, G. B. Cox and P. E. Antle, *Chromatographia*, 24 (1987) 82.
9 L. R. Snyder and G. B. Cox, *J. Chromatogr.*, 483 (1989) 85.
10 S. Golshan-Shirazi and G. Guiochon, *Anal. Chem.*, 61 (1989) 1276.
11 S. Golshan-Shirazi and G. Guiochon, *Anal. Chem.*, 61 (1989) 1368.
12 S. Golshan-Shirazi and G. Guiochon, *J. Chromatogr.*, 517 (1990) 229.

13 S. Golshan-Shirazi and G. Guiochon, *Am. Biotechnol. Lab.*, 8, No. 2 (1990) 24.
14 S. Golshan-Shirazi and G. Guiochon, *Am. Biotechnol. Lab.*, 8, No. 8 (1990) 26.
15 S. Golshan-Shirazi and G. Guiochon, *Ind. Chromatogr. News*, 2 (1990) 8.
16 S. Golshan-Shirazi and G. Guiochon, *J. Chromatogr.*, 511 (1990) 402.
17 S. Golshan-Shirazi and G. Guiochon, *J. Chromatogr.*, 523 (1990) in press.
18 S. Jacobson, S. Golshan-Shirazi and G. Guiochon, *J. Am. Chem. Soc.*, 112 (1990) 6492.
19 A. M. Katti, Z. Ma and G. Guiochon, *AIChE J.*, in press.
20 S. Golshan-Shirazi and G. Guiochon, *J. Phys. Chem.*, 93 (1989) 4143.
21 E. V. Dose and G. Guiochon, *Anal. Chem.*, 62 (1990) 1723.
22 A. M. Katti and G. Guiochon, *Anal. Chem.*, 61 (1989) 982.
23 J. H. Knox, *J. Chromatogr. Sci.*, 15 (1977) 352.
24 G. M. Schwab, *Ergebnisse der Exacten Naturwissenschaften*, Vol. 7, Springer, Berlin, 1928, p. 276.
25 S. Golshan-Shirazi and G. Guiochon, *Anal. Chem.*, 61 (1989) 2464.
26 S. Golshan-Shirazi and G. Guiochon, *Anal. Chem.*, 60 (1988) 2364.
27 S. Golshan-Shirazi and G. Guiochon, *Anal. Chem.*, 61 (1989) 462.
28 G. Guiochon and S. Ghodbane, *Chromatographia*, 26 (1989) 53.
29 L. R. Snyder, J. W. Dolan and G. B. Cox, *J. Chromatogr.*, 483 (1989) 63.
30 M. D. LeVan and T. Vermeulen, *J. Phys. Chem.*, 85 (1981) 3247.
31 S. Goldshan-Shirazi and G. Guiochon, *J. Chromatogr.*, submitted for publication.

Journal of Chromatography, 536 (1991) 75–84
Elsevier Science Publishers B.V., Amsterdam

CHROMSYMP. 2017

Applications of preparative high-performance liquid chromatography in oleochemical research

ANDREAS BRUNS
Henkel Research Corporation, 2330 Circadian Way, Santa Rosa, CA 95407 (U.S.A.)

ABSTRACT

The application of preparative high-performance liquid chromatography to oleochemical and related products is discussed with examples that cover the field of glycerol and fatty acid derivatives, fatty alcohol ethoxylates, tocopherols, guanidines and glucose telomers. Columns of 21.5 to 100 mm I.D. and 250 to 400 mm length are used for reversed-phase and normal-phase chromatography. Semi-preparative separations with 100-mg column loads are presented as well as technical-scale applications with 15-g raw material injections per separation cycle.

INTRODUCTION

Products that are based on natural raw materials often show quite complex compositions. This is especially true for oleochemical products. Nevertheless, "pure" substances are required for many research or analytical applications and, therefore, powerful separation and purification techniques, like preparative high-performance liquid chromatography (Prep-HPLC), are of high interest in this field. The preparative application of HPLC is relatively young and that is why its use as a routine technique is still rapidly growing [1,2]. The amount of purified material that is required for a certain purpose specifies the scale of Prep-HPLC that has to be used [1].

Instead of discussing the more theoretical aspects of Prep-HPLC, such as the calculation of column loadabilities [3–5], this paper outlines the broad applicability of Prep-HPLC to oleochemical products by presenting a variety of different separation and purification examples.

EXPERIMENTAL

Four different chromatography systems were used for these Prep-LC applications: (1) Labomatic MD 80/100 medium pressure pump, Labochrom MP 20 pulse dampner, Labochrom pressure controller, Labochrom injection valve, Labochrom PGC columns, Jobin Yvon "Iota" refractive index (RI) detector with preparative cell and Isco "Foxy" fraction collector. (2) Waters 600 pump, Wisp 710 autosampler, Jobin Yvon "Iota" RI detector with preparative cell and Isco "Foxy" fraction collector. (3) Waters LC 3000 pump, sample injection via the pump through one of the four

0021-9673/91/$03.50

solvent lines, Waters 481 UV detector with semi-preparative cell, Gilson 201 fraction collector. (4) Merck Prepbar 100, fully explosion proof preparative/technical scale chromatography system.

All solvents were HPLC grade from Prochrom (Wesel, F.R.G.) or Merck (Darmstadt, F.R.G.). The organic solvents were evaporated with Büchi rotary evaporaters, a Christ freeze drying system was used for the evaporation of water.

All the preparative chromatographic conditions were directly scaled up from in house developed analytical conditons, for detailed Prep-HPLC conditions refer to figure captions.

RESULTS AND DISCUSSION

Glycerol derivatives

Glycerol derivatives are important oleochemical products with a broad application field. Glycerol fatty acid esters are for instance commonly used emulsifiers, whereas oligoglycerols can be used as polyols for polymer chemical applications.

The chromatograms in Figs. 1 and 2 show the purification of glycerol diacetate and glycerol diacetate monopropionate. These compounds were needed as standards in gas chromatography (GC). Both raw material contained less then 50% of the products of interest. Normal-phase chromatography on unmodified silica as the stationary phase resulted in purities $\geqslant 95\%$, as determined by GC. The two examples

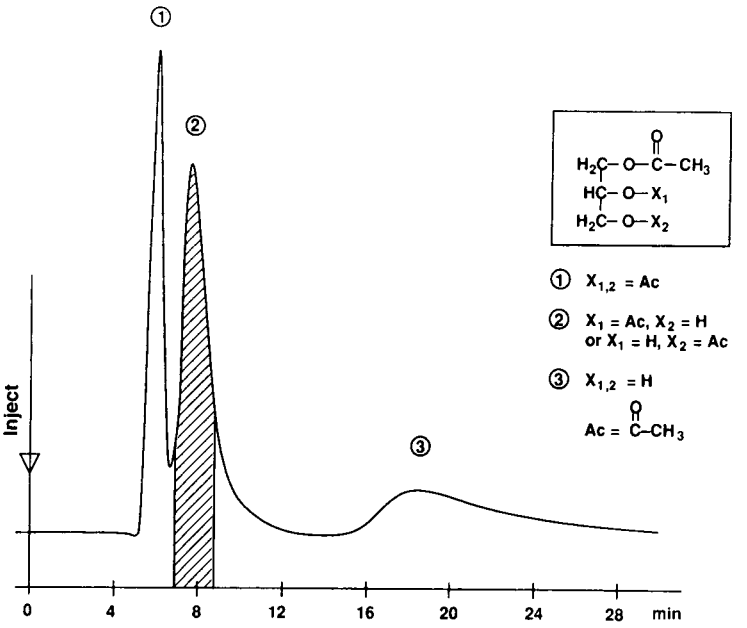

Fig. 1. Preparative chromatogram and structure for glycerol diacetate, shaded peak represents main product fraction. System: Labomatic MPLC; column: LiChroprep Si 100, 40–63 μm, 480 × 37 mm I.D., self packed; eluent: *n*-hexane–ethylacetate (20:80, v/v); flow: 35 ml/min; injection concentration and volume: 1.5 ml sample in 10 ml eluent; detection: RI

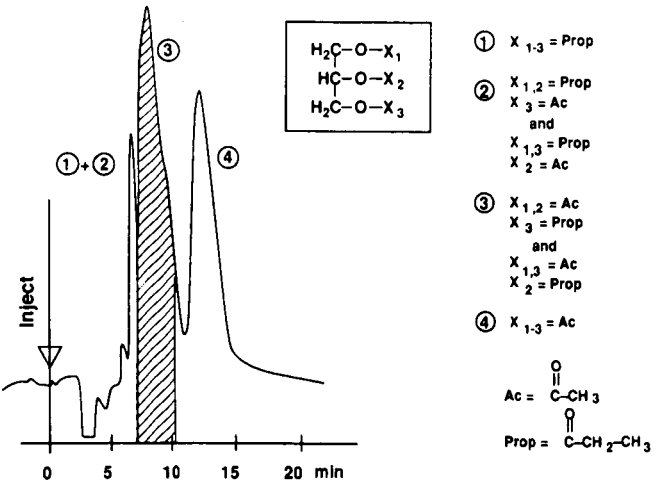

Fig. 2. Preparative chromatogram and structure for glycerol diacetate monopropionate, shaded peak represents main product fraction. System: Labomatic MPLC; column: LiChroprep Si 100, 40–63 μm, 480 × 37 mm I.D., self packed; eluent: *n*-hexane–*tert.*-butyl methyl ether (80:20, v/v); flow: 62 ml/min; injection concentration and volume: 1 ml sample in 10 ml eluent; detection: RI.

demonstrate that for simple separation problems even medium-pressure equipment with large-particle-size column packing material can result in sufficient purity.

Glycerol monohydroxystearate was purified on a 50-mm I.D. cyano column in the normal-phase mode (Fig. 3). A technical-scale high-performance system was used and 97% purity (HPLC) were achieved from a 57% pure raw material. The purified product was used as GC-standard.

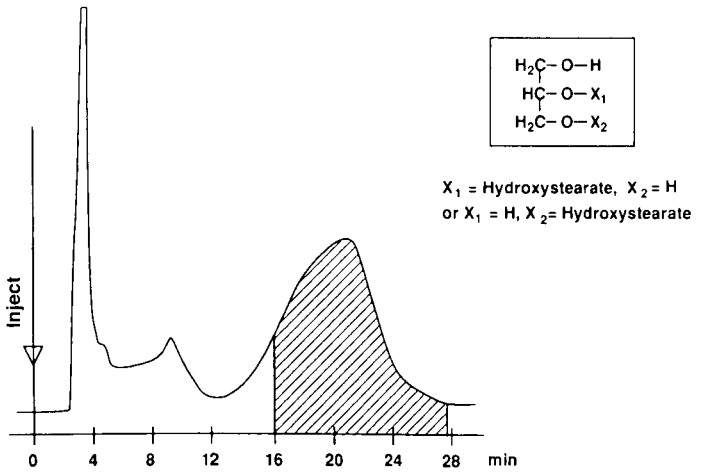

Fig. 3. Preparative chromatogram and structure for glycerol monohydroxystearate, shaded peak represents main product fraction. System: Merck Prepbar 100; column: LiChroprep CN, 25-40 μm, 250 × 50 mm I.D., LiChroprep CN guard column; eluent: *n*-hexane–2-propanol (95:5, v/v); flow: 120 ml/min, injection concentration and volume: 3.4% in 15 ml heptane–2-propanol (67:33, v/v); detection: UV 230 nm.

In the analytical HPLC chromatogram of an oligoglycerol sample the first four peaks could be assigned to the oligomers with $n = 1$–4 by retention time comparison with commercially available standards (Deutsche Solvay-Werke, Solingen, F.R.G.). The identities of two later-eluted components were questionable. Fig. 4 shows the preparative chromatogram of this oligoglycerol sample, where the unidentified peaks are marked with $n = ?$. Fractionation on a 22.5 mm I.D. diol-modified silica column and identification by GC–mass spectrometry (MS) (after silylation) showed that they corresponded to the higher oligomers with $n = 5$ and $n = 6$.

Fatty acid derivatives

Dicarboxylic acids are for instance used for polymer production. Purification to $\geqslant 95\%$ for the use as a GC-standard was the goal for a C_{16}-dicarboxylic acid. In addition the byproducts should be isolated and identified spectroscopically. The methyl ester derivative of this sample was used for Prep-HPLC (Fig. 5). The main compound, a C16:1 dimethylester with the double bond in position 3, was isolated in $>98\%$ purity (NMR). The structures were assigned with the aid of GC–MS (after OsO_4-silylation [6]) and showed that all components were C_{16}-diacid methyl esters with zero, one or two double bonds in different positions (see structure assignments in Fig. 5).

High purity oleic acid is a valuable raw material for further synthetic applications. Liquid chromatography was tested as an alternative or additional technique to purification of this material by distillation. Whereas in the above example 100-mg amounts of the sample were injected into a 22.5-mm I.D. silica column, we used column loads of 10 g raw material on a 100-mm I.D. reversed-phase column for the purification of oleic acid (Fig. 6). For a raw material that contained 85% oleic acid,

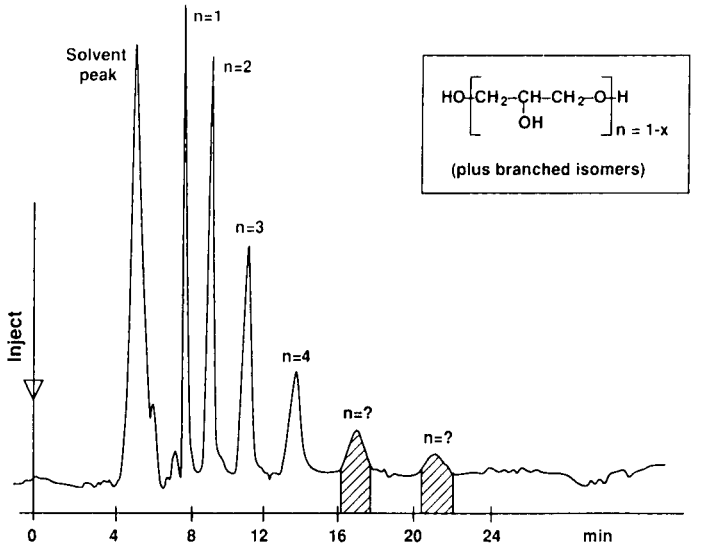

Fig. 4. Preparative chromatogram and structure for oligoglycerols, shaded peaks represent fraction cuts. System: Waters 600; column: LiChrosorb Diol, 7 μm, 250 × 22.5 mm I.D.; eluent: acetonitrile–water (85:15, v/v); flow: 20 ml/min; injection concentration and volume: 7% in 0.9 ml eluent; detection: RI.

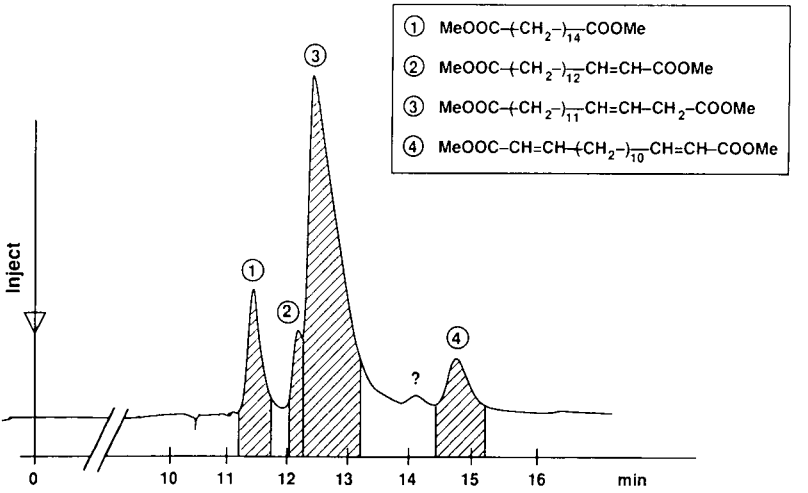

Fig. 5. Preparative chromatogram and structures for C_{16}-dicarboxylic acid methylesters, shaded peaks represent fraction cuts. System: Waters 600; column: LiChrosorb Si 60, 7 μm, 250 × 22.5 mm I.D.; eluent: *n*-hexane–ethylacetate (90:10, v/v); flow: 20 ml/min; injection concentration and volume 20% in 0.5 ml eluent; detection: RI. Me = Methyl.

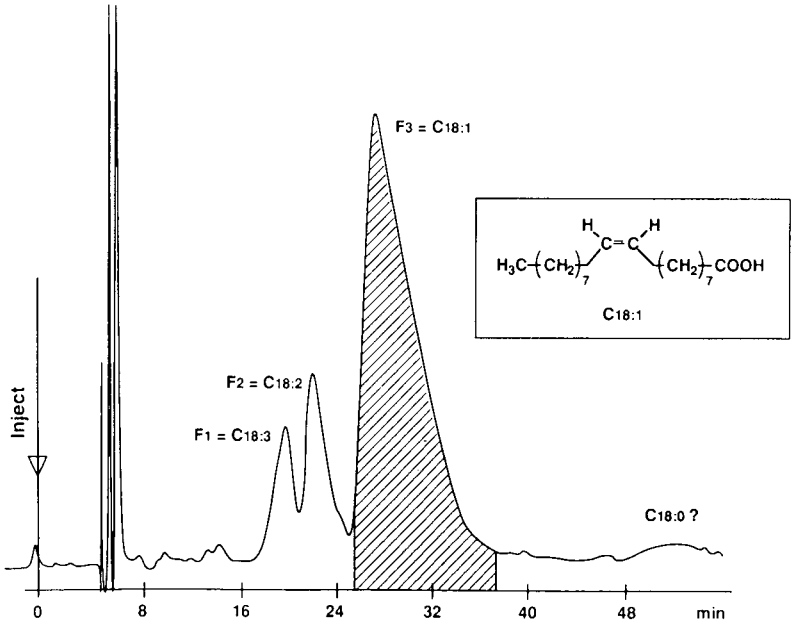

Fig. 6. Preparative chromatogram and structure for oleic acid purification, shaded peak represents main product fraction. System: Merck Prepbar 100; column: LiChroprep RP 18, 5–20 μm, 400 × 100 mm I.D.; eluent: methanol–water–acetic acid (90:9.9:0.1, v/v/v); flow: 400 ml/min; injection concentration and volume: 10 g raw material in 50 ml methanol; detection: RI.

this approach resulted in oleic acid with 95% purity (GC) and 4% palmitic acid as a byproduct, which could be separated by distillation. Until now, the purity of technical-grade oleic acid was limited by the inability of distillation processes to separate fatty acids that differ only in the number of double bonds. As this application demonstrates, the combination of distillation and chromatographic purification allows purification of oleic acid to $\geqslant 98\%$.

Fatty alcohol ethoxylates

Fatty alcohols are direct derivatives of fatty acids and are used as raw material for ethoxylation processes, resulting in non-ionic surfactants. These products show a broad distribution of ethoxylate oligomers. Pure C_{12}-fatty alcohol-based ethoxylate oligomers with $n > 8$ were needed as reference materials for physical tests (the oligomers with $n \leqslant 8$ are commercially available from Nikko Chemicals, Tokyo, Japan).

Fig. 7 demonstrates the preparative chromatogram. The separation conditions were scaled up from thin-layer chromatography by using unmodified silica as the stationary phase and butanone with a significant percentage of water as the eluent. These unusual conditions served the purpose for the preparative separation and enabled the production of 200 to 500-mg amounts of the $n = 9$–15 ethoxylate oligomers in 90–99% purity (HPLC).

Tocopherols

Natural vitamine E is derived from vegetable oils and is comprised of a mixture of D-α-, -β-, -γ- and -δ-tocopherols (Fig. 8). Considerable quantities of the D-γ-to-

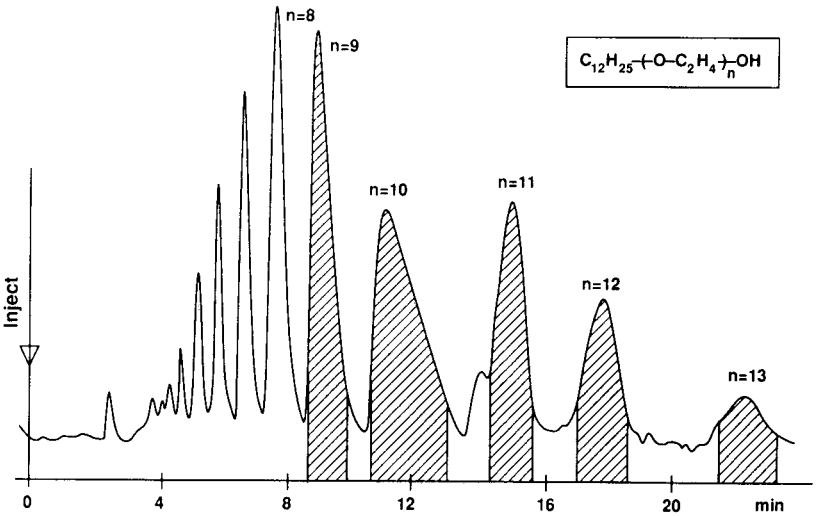

Fig. 7. Preparative chromatogram and structure for C_{12}-fatty alcohol ethoxylates, shaded peaks represent fraction cuts. System: Waters 600; column: LiChrosorb Si 60, 7 μm, 250 × 22.5 mm I.D.; eluent: butanone–water (92:8, v/v); flow: 18 ml/min; injection concentration and volume: 40% in 0.5 ml eluent; detection: RI.

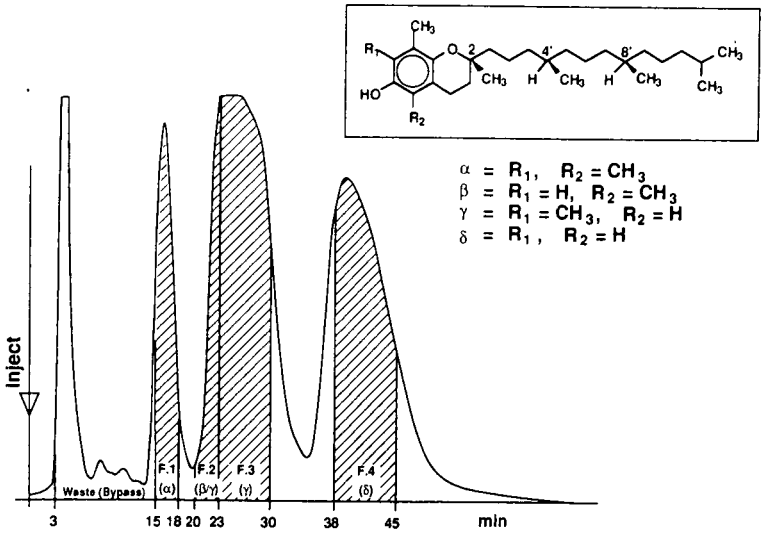

Fig. 8. Preparative chromatogram and structure for tocopherols, shaded peaks represent fraction cuts. System: Merck Prepbar 100; column: LiChroprep Si 60, 25–40 μm, 400 × 100 mm I.D.; eluent: *n*-hexane–*tert.*-butyl methyl ether (97:3, v/v); flow: 450 ml/min; injection concentration and volume: 15 g raw material in 50 ml eluent; detection: UV 205 nm.

copherol had to be isolated in a purity > 90% for application tests. The raw material contained only 70% tocopherols, 60% of which was the D-γ-analogue.

For the purification a technical-scale separation with a 100-mm I.D. column and unmodified silica as the stationary phase [7] was used (Fig. 8). The analytical HPLC data showed the D-γ-fraction to have a purity of 95%.

Guanidines

Products that have interesting metal extraction properties by an ion-pair extraction mechanism [8,9] can be synthesized from oleochemical feedstocks. Bis(2-ethyl-hexyl)guanidine (for structure see Fig. 9) was used as a model compound to study the metal loading behavior of these products.

This guanidine was purified on a 21.5-mm I.D. column in the reversed-phase mode, using a polymer-based stationary phase. This was because of the low pH that had to be used in order to control the peak tailing of the basic compounds. The use of sulfuric acid for pH control originated from the analytical conditions, in which an ion-pairing system was applied to control tailing. A buffer–ion-pairing system did not appear to be very convenient for preparative-scale chromatography and that was how sulfuric acid was found to work well for the purpose. The peak area ratios of the main product (shaded peak in chromatogram, Fig. 9) and the byproducts (trialkyl guanidines and bisguanidines according to NMR and MS) do not reflect the real weight percent ratios. This is due to detector overload, which causes a non-linear response.

Bis(2-ethyl-hexyl)guanide (25 g) was isolated in >98% purity (purity assignments according to NMR mole percent). This shows that even with small-scale Prep-HPLC equipment it is possible to purify significant amounts of products conveniently, as long as the instruments are fully automated.

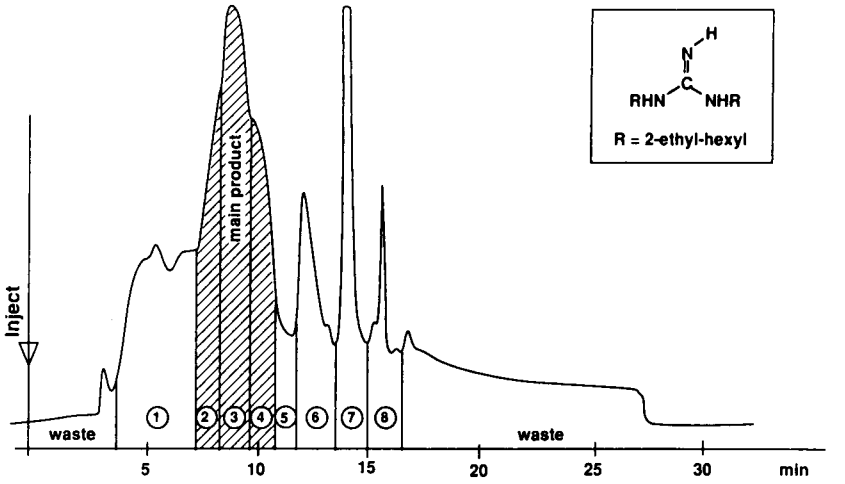

Fig. 9. Preparative chromatogram and structure for bis(2-ethyl-hexyl)guanidine, numbers represent fraction cuts, shaded peak represents main product fraction. System: Waters LC 3000; column: Hamilton PRP-1, 10 μm, 250 × 21.5 mm I.D.; eluents: A = methanol–water–sulfuric acid (75:24.95:0.05, v/v/v), B = methanol–sulfuric acid (99.95:0.05, v/v); gradient: hold 100% A 5 min, then go to 100% B in 10 min, hold 100% B for 10 min, reequilibrate 5 min; flow: 20 ml/min; injection concentration and volume: 20% in 2.5 ml solvent B; detection: UV 214 nm.

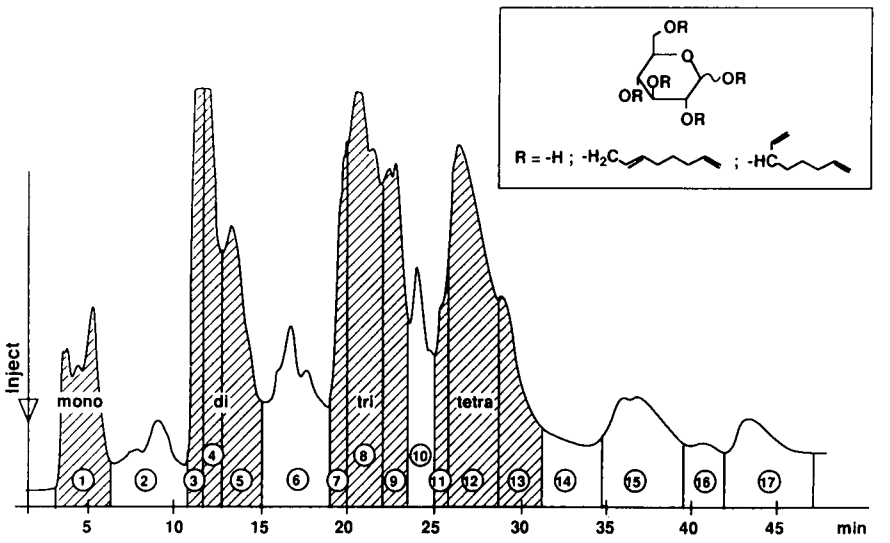

Fig. 10. Preparative chromatogram and structure for glucose telomers, numbers represent fraction cuts, shaded peaks represent main components. System: Waters LC 3000; column: LiChrosorb RP 18, 10 μm, 250 × 22.5 mm I.D.; eluents: A = acetonitrile–water (40:60, v/v), B = acetonitile; gradient: 100% A to 100% B in 20 min, hold 100% B for 30 min, reequilibrate 5 min; flow: 20 ml/min; injection concentration and volume: 20% in 3.0 ml solvent B; detection: UV 210 nm.

Glucose telomers

In addition to fats and oils carbohydrates are attractive natural raw materials, for instance for glucose based surfactants such as alkyl glucosides [10,11] or for the so-called glucose telomers, a new group of products synthesized from glucose and butadiene according to the telomerization mechanism [12,13].

To characterize these glucose telomers in further detail and establish analytical standards for quantitative HPLC analysis, the compounds with different degrees of substitution were separated (for structures see Fig. 10). For preparative chromatography a reversed-phase system with a 22.5-mm I.D. C_{18}-column was used. The chromatogram (Fig. 10) shows the separation of the different groups that represent the different degrees of substitution. The various isomers within each of these groups were not separated. Quantities of 4–9 g of the mono- to tetra-octadienyl-substituted glucose telomers were isolated in purities >90% (according to GC, GC–MS and HPLC). The amount of penta-substituted material (fractions 15 and 17) was very low according to the spectroscopic results.

CONCLUSION

In a broad field of applications it has been demonstrated that preparative high-performance liquid chromatography is a very versatile separation and purification tool for oleochemical products. Depending on the separation problem, there is a wide variety of chromatographic separation techniques available. In principle, any analytical HPLC procedure can be scaled up to the preparative or even technical scale. Obviously, preparative and especially technical-scale HPLC is not a low-budget technology, but it does offer very high separation efficiencies and therefore it is certainly a very helpful addition to the conventional purification techniques, like extraction, crystallization, or distillation.

ACKNOWLEDGEMENTS

Dr. W. Winkle and Dr. A. Werner-Busse are thanked for contributing analytical HPLC conditions that have been used for scale-up. The assistance of Dr. V. Puchta and Dr. D. Berg is gratefully appreciated. Special thanks are due to the members of the chromatography and spectroscopy laboratories in Düsseldorf and Santa Rosa for their skillful support.

REFERENCES

1 M. Verzele and C. Dewaele, *Preparative High Performance Liquid Chromatography*, TEC, Gent, 1986, pp. 10–26.
2 P. D. McDonald and B. A. Bidlingmeyer in B. A. Bidlingmeyer (Editor), *Preparative Liquid Chromatography (Journal of Chromatography Library*, Vol. 38), Elsevier, Amsterdam, 1987, pp. 1–95.
3 K. P. Hupe and H. H. Lauer, *J. Chromatogr.*, 203 (1981) 41.
4 G. Cretier and J. L. Rocca, *Chromatographia*, 21 (1986) 143.
5 S. Ghodbane and G. Guiochon, *J. Chromatogr.*, 450 (1988) 27.
6 H. Budzikiewicz, *Analytiker Taschenbuch*, Vol. 5, Springer, Heidelberg, 1984, pp. 135–138.
7 A. Bruns, D. Berg and A. Werner-Busse, *J. Chromatogr.*, 450 (1988) 111.
8 Y. Marcus and A. S. Kertes, *Ion Exchange and Solvent Extraction of Metal Complexes*, Wiley-Interscience, New York, 1969.

9 W. Lin, P. Mattison and M. Virnig, *U.S. Pat.*, (1985) 4 814 007.
10 W. Koenigs, E. Knorr, *Chem. Ber.*, 34 (1901) 957.
11 A. Bruns, W. Waldhoff and W. Winkle, *Chromatographia*, 27 (1989) 340.
12 A. Behr, in R. Ugo (Editor), *Aspects of Homogeneous Catalysis*, Vol. 5, Reidel, Dordrecht, Boston, Lancaster, 1984, pp. 5–48.
13 L. I. Zakharkin, V. V. Guseva, D. D. Sulaimankulova and G. NM. Korneva, *Zh. Org. Khim.*, 24 (1988) 119.

Journal of Chromatography, 536 (1991) 85–93
Elsevier Science Publishers B.V., Amsterdam

CHROMSYMP. 2028

Large-scale purification of haptenated oligonucleotides using high-performance liquid chromatography

RONALD L. MORGAN and JOSEPH E. CELEBUSKI*
Research and Development, Abbott Laboratories, Abbott Park, IL 60064 (U.S.A.)

ABSTRACT

We report methodology for the succesful separation of unreacted oligonucleotide from end labeled material (fluorescein or biotin) on an milligram scale using high-performance liquid chromatography (HPLC). The oligonucleotides (19–24-mers) were synthesized on an automated instrument using cyanoethylphosphoramidite chemistry. These oligonucleotides possessed a primary amino group at either the 5′-end or the 3′-end. After trityl-on HPLC purification and detritylation, the amine-terminated oligonucleotides were treated with either fluorescein isothiocyanate or biotin-(aminocaproyl)$_2$-N-hydroxysuccinimide active ester to give the haptenated materials. After removal of excess labeling reagent, the labeled oligonucleotides were purified by reversed-phase HPLC using a polystyrene-based column, with C_{18} groups on the phenyl part of the polystyrene backbone. The terminally labeled oligonucleotides hybridized to their complementary sequences, as observed by size-exclusion chromatography.

INTRODUCTION

In connection with a program designed to commercialize non-radioactive DNA probe technology [1], we investigated the covalent labeling of oligonucleotides with non-radioactive reporter groups. Several technologies exist to accomplish this objective. Keller and coworkers [2,3] have introduced haptens onto bulk DNA using both nucleophilic attack and photochemistry. Another technique for introduction of haptens onto DNA is to synthesize terminally [4] and internally [5] aminated oligonucleotides which can then be specifically labeled with an appropriate hapten. Tous *et al.* [6] and Smith *et al.* [7] have obtained fluoresceinated, terminally labeled oligonucleotides in this fashion. Telser *et al.* [8] have prepared oligonucleotides which were internally labeled with biotin, fluorescein and pyrène, and studied their thermodynamic characteristics. Others have chemically labeled oligonucleotides with biotin [9–11]. While the synthetic chemistry of labeling DNA with small molecules has been dealt with in detail, the chromatographic techniques for adequate separation of starting oligonucleotide from product, especially on a milligram scale, are less well investigated. The aforementioned references use polyacrylamide gel electrophoresis (PAGE) or reversed-phase high-performance liquid chromatography (HPLC) columns for their oligonucleotide separations. However, PAGE suffers from a low loading capacity, while reversed-phase HPLC will give coelution of fluorescein isothiocyanate (FITC) labeled oligonucleotide with non-labeled oligonucleotide. Biotinylated

0021-9673/91/$03.50

oligonucleotides show no separation at all on reversed-phase HPLC. In this paper we describe the results of a comparative study of several separation conditions for haptenated oligonucleotides.

EXPERIMENTAL

Materials

Fluorescein isothiocyanate was purchased from Eastman Kodak (Rochester, NY, U.S.A.). Biotin-(aminocaproyl)$_2$-*N*-hydroxysuccinimide ester and Aminomodifier II were obtained from Clontech (Palo Alto, CA, U.S.A.). Triethylamine was supplied by Aldrich (Milwaukee, WI, U.S.A.); glacial acetic acid by J. T. Baker (Phillipsburg, NJ, U.S.A.); ethanol by Aaper Alcohol and Chemical (Shelbyville, KY, U.S.A.); concentrated ammonium hydroxide by Mallinckrodt (Paris, KY, U.S.A.); HPLC-grade water and acetonitrile by Fisher (Fair Lawn, NJ, U.S.A.), acrylamide-N,N′-methylenebisacrylamide (Bis), tetramethylethylenediamine (TEMED), ammonium persulfate, xylene cyanol and Bromophenol Blue by Bio-Rad (Richmond, CA, U.S.A.); urea by Boehringer Mannheim (Indianapolis, IN, U.S.A.). NAP-5 Sephadex columns were obtained from Pharmacia (Piscataway, NJ, U.S.A.). Amino-controlled pore glass was purchased from Glen Research (Herndon, VA, U.S.A.).

Equipment

A Waters Assoc. (Milford, MA, U.S.A.) HPLC system was used for all HPLC separations. This consisted of a 600E system controller, U6K injector, 745B data module or NEC Powermate 386/20 and a 484 detector or a 991 photodiode array detector. The columns used were Waters μBondapak C_{18}, 30 × 0.39 cm, Hamilton (Reno, NV, U.S.A.) PRP-1, 25 × 0.41 cm, and EM Science (Cherry Hill, NJ, U.S.A.) Polyspher RP-18, 15 × 0.46 cm. Oligonucleotides were synthesized on Applied Biosystems (Foster City, CA, U.S.A.) 380A or 380B DNA Synthesizers using β-cyanoethylphosphoramidite chemistry with the SYN 11 program, for both the 5′-aminated (Clontech) and 3′-aminated (Glen Research) oligonucleotides. Deprotection of the oligonucleotides was performed at 55°C for 6 h in concentrated ammonium hydroxide. Gel electrophoresis was performed on a Bio-Rad Sequi-Gen apparatus, with an E-C apparatus (St. Petersburg, FL, U.S.A.) EC 650 power supply. All HPLC separations were performed at ambient temperature. A Beckman (San Ramon, CA, U.S.A.) DU-70 spectrophotometer was used for measuring ultraviolet (UV) absorption spectra. A Savant SpeedVac (Farmingdale, NY, U.S.A.) was used for concentration of samples and a Jouan (Saint Herblain, France) centrifuge was used for centrifugation.

HPLC purification of trityl-on oligonucleotides

The aqueous mobile phase (A) for the trityl-on HPLC purification was 0.1 *M* triethylammonium acetate (pH 7.0). The organic mobile phase (B) was acetonitrile. The following linear gradient was used: 10 to 40% B in 15 min, hold at 40% B for 10 min, then linear to 10% B in 5 min. A Waters μBondapak C_{18} at 1.5 ml/min was used for the trityl-on chromatography. The purified product is collected at approximately 14 min and concentrated to a residue on a SpeedVac.

Manual detritylation of oligonucleotides

The trityl-on purified oligonucleotides were taken up into 1.0 ml of acetic acid–water (80:20, v/v) and were left to stand at room temperature for 1 h. The solvent was removed on a SpeedVac and the residue was taken up into 100 μl of 0.3 *M* sodium acetate. Precipitation of the oligonucleotide was initiated by addition of 1.0 ml of −20°C ethanol and was effected by immersion of the suspension in a −78°C (dry ice–isopropanol) bath. Centrifugation of the suspension (−10°C, 12 560 *g*, 15 min) gave a pellet which was used for the haptenation reactions.

Synthesis of haptenated oligonucleotides

Fluoresceinated oligonucleotides. To a solution of 1 μmol of detritylated, terminally aminated 24-mer oligonucleotide (determined by UV absorption) in 250 μl sodium borate buffer (pH 9.0) 8 mg (20 μmol) fluorescein isothiocyanate dissolved in 250 μl of dimethylformamide (DMF) was added. The reaction was left to proceed in the dark at room temperature for 16 h. The reaction mixture was loaded onto a NAP-5 column which had been equilibrated with 10 ml water. The column was eluted with 1.0 ml water and the eluate was collected and concentrated on the SpeedVac.

Biotinylated oligonucleotides. To a solution of 1 μmol detritylated, terminally aminated 24-mer oligonucleotide in 250 μl sodium phosphate buffer (pH 7.2) 11 mg (20 μmol) of biotin-(aminocaproyl)$_2$-N-hydroxysuccinimide ester in 250 μl of DMF was added. The reaction was left to stand in the dark at room temperature for 17 h. The reaction was worked up as in the fluorescein case to give the concentrate, ready for HPLC or gel separation.

Polyacrylamide gel electrophoresis of haptenated oligonucleotides

A 150 ml solution of 12% acrylamide–Bis/8 *M* urea/89 m*M* Tris/89 m*M* sodium borate/2 m*M* EDTA, pH 8.0 was left to polymerize for 4 h in a 21 × 40 × 0.2 cm Bio-Rad Sequi-Gen apparatus, after addition of ammonium persulfate and TEMED. After pre-electrophoresis of the cell (1 h, 20 W), the oligonecleotides were loaded onto the gel. Generally, no more than 1 μmol of oligonucleotide in 150 μl of formamide could be applied at once. After 4–5 h at 40 W, the bromophenol blue dye had eluted off the gel, signaling the end of the run. At this point, the gel was overlaid on a silica gel plate and the DNA bands were visualized by UV shadowing. The product (slowest moving major) bands were excised and extracted with 1.0 *M* triethylammonium bicarbonate overnight. The extracts were concentrated, taken up into 0.5 ml of water and desalted on a NAP-5 column. The eluate was checked for DNA concentration by UV absorbance.

Reversed-phase HPLC purification of haptenated oligonucleotides (Hamilton PRP-1 procedure)

The aqueous mobile phase (A) for the purification of haptenated oligonucleotides was 0.1 *M* sodium phosphate (pH 8.9). The organic mobile phase (B) was 50% aqueous acetonitrile. The following linear gradient was used: 10 to 30% B in 23 min, then 30 to 10% B in 10 min. The flow-rate was 1 ml/min and the injection volume was 150 μl. The detector was adjusted to 290 nm and 2.0 a.u.f.s.

Reversed-phase HPLC purification of haptenated oligonucleotides (Polyspher RP-18, EM Science procedure)

The aqueous mobile phase (A) for the purification of haptenated oligonucleotides was 0.1 *M* sodium phosphate (pH 8.8). The organic mobile phase (B) was 50% aqueous acetonitrile. The following linear gradient was used: 20 to 50% B in 36 min, then 50 to 20% B in 14 min. The flow-rate was 0.6 ml/min and the injection volume was 150 μl. The detector was adjusted to 290 nm and 2.0 a.u.f.s.

Hybridization determination by size-exclusion HPLC

The ability of haptenated complementary single stranded oligonucleotides to hybridize was demonstrated by size-exclusion HPLC using a Bio-Rad Bio-Sil SEC-125 as follows: the mobile phase was 0.1 *M* sodium phosphate (pH 7.0), the flow-rate was 1 ml/min at 280 p.s.i. and the detector was adjusted to 260 nm and 0.5 a.u.f.s. An aqueous solution of each oligonucleotide, concentration approximately 1 μg per 40 μl, was injected individually and each retention time determined for the single stranded oligonucleotides. Equivalent amounts of complementary single stranded oligonucleotides were mixed at room temperature and injected under the previous conditions. Typical retention times for single stranded 24-mers were 7.7–7.9 min and changed to 7 min when hybridized.

RESULTS AND DISCUSSION

We have found that a 2-mm thick, 21 × 40 cm polyacrylamide gel will separate labeled from non-labeled material quite well on a 0.5–1.0 μmol scale upon electrophoresis. In all cases observed, labeled material migrates more slowly than non-labeled. However, efficiency of separation falls off drastically at higher oligonucleotide loadings. Our investigations of separation technology for large-scale work then shifted from gel electrophoresis to suitable HPLC columns and conditions. We first examined the separation afforded by a Waters μBondapak C_{18} HPLC column (30 × 0.39 cm). On an analytical scale (0.1 μmol), a C_{18} ODS column did not separate biotinylated oligonucleotide from the starting oligonucleotide. We then attempted a separation of FITC-labeled oligonucleotide from starting, amine-terminated oligonucleotide. Due to fluorescein's lipophilicity, one would expect good separation of labeled from non-labeled material for fluoresceinated oligonucleotide. In fact, separation was seen between fluoresceinated and non-fluoresceinated oligonucleotide (Fig. 1). However, upon further investigation of the fractions by denaturing gel electrophoresis, it was determined that peak 1, from Fig. 1, was starting oligonucleotide, while peak 2 was a mixture of starting material and product. Under the non-denaturing chromatographic conditions, it is possible that intercalation of the fluorescein label into a neighboring oligonucleotide is occurring. This supposition prompted us to investigate the HPLC of oligonucleotides under denaturing conditions.

One chromatographic support which is well suited for the large-scale separation of oligonucleotides under denaturing conditions is polystyrene reversed-phase (PRP) material, with divinylbenzene crosslinks. Several studies [12–14] have shown that PRP columns possess outstanding loading capacities and will function under extremes of pH (2–13), as well as at high salt concentration. As shown in Fig. 2, the Hamilton PRP-1 column (25 × 0.41 cm) will fractionate oligonucleotides. Unfortu-

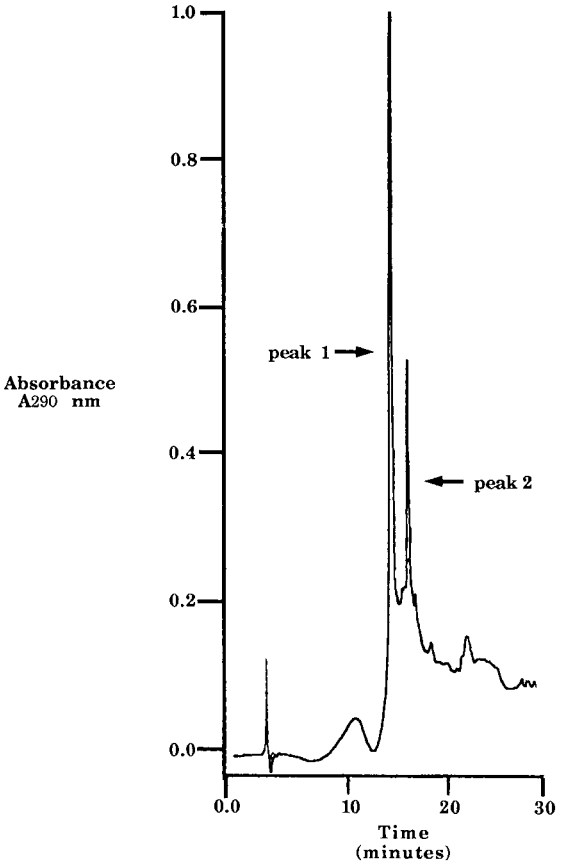

Fig. 1. Injection of 2.4 μg of a 23-mer, 5'-end labeled with FITC. Peak 1, eluting at 16.3 min, is starting 23-mer. Peak 2, eluting at 17.98 min, is a mixture of starting and fluoresceinated oligonucleotide. Column is Waters μBondapak C_{18}, flow-rate 1 ml/min. Gradient table: initial, 5% B, 95% A; 5 min, 20% B, 80% A; 35 min, 50% B 50% A. Solvent A is 0.1 *M* triethylammonium acetate, solvent B is acetonitrile.

nately, "ghosting" frequently occurs. Ghosting is a phenomenon in which some injected oligonucleotide is retained on the column during a sample run. The retained oligonucleotide is eluted in a subsequent run, when the gradient conditions that eluted the major part of the initial charge are attained. Ghosting was detected when, after thoroughly washing the HPLC injector port and syringe, the ghost peak still eluted in a blank injection. This even occurs after repeated column washes. Ghosting is seen in trityl-on as well as trityl-off HPLC and so is not limited to the case of haptenated oligonucleotides. The phenomenon is largely restricted to injections of 1 μmol and larger. This phenomenon is not a problem if the column is used for only one oligonucleotide. If the intended use for the column is for multiple oligonucleotide separations, the probability of contamination is unacceptably high. From the above experiences, the criteria for a suitable HPLC support were determined to be high loading capacity, good resolution, stability to extremes of pH and salt concentration and no ghosting. As the PRP-1 column fulfilled all of the criteria save the last one, it seemed a

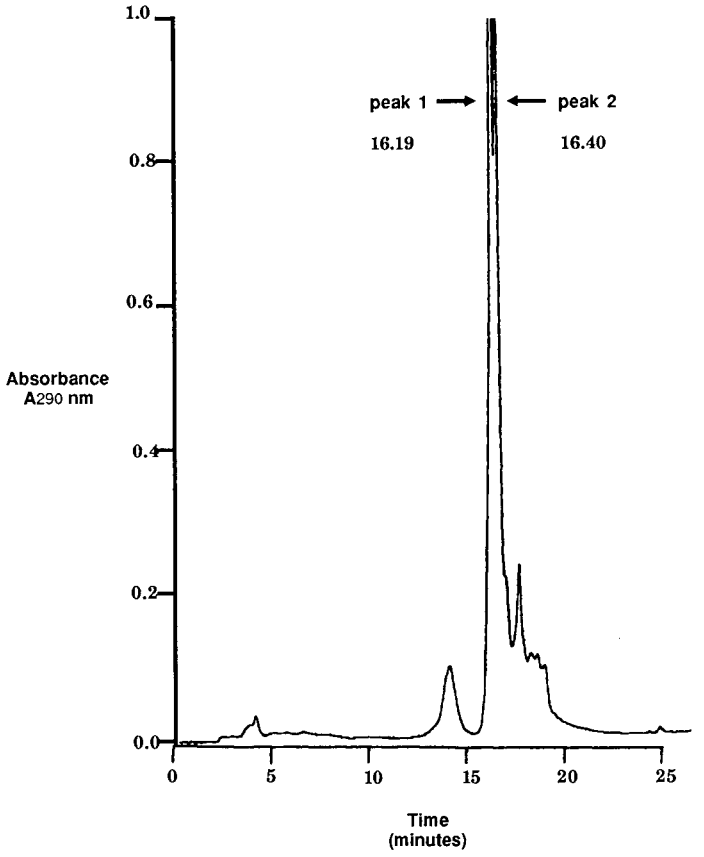

Fig. 2. Injection of 200 μg of a 25-mer, 5'-end labeled with FITC. Column is Hamilton PRP-1. Peak 1, eluting at 16.19 min, is unreacted starting material, while peak 2, eluting at 16.4 min, is haptenated oligonucleotide.

worthwhile exercise to examine other polystyrene-based supports which were covalently modified. The EM Science Polyspher RP-18 column (15 × 0.46 cm) is a 3-C_{18} styrene/3-C_{18}-1,4-divinylbenzene cross-linked polymeric support which is generally used in situations requiring ODS column resolution under unusual salt or pH conditions. We have found that this support is admirably suited to the task of resolving haptenated from non-haptenated oligonucleotide, as well as removal of excess haptenation reagent. The separation time between starting material and product ranges between 9 and 11 min, with a flow-rate of 0.6 ml/min on the analytical column. Fig. 3 shows the resolution seen for a typical preparation of a fluoresceinated, end-labeled oligonucleotide, while Fig. 4 depicts the separation between terminally biotinylated oligonucleotide from terminally aminated starting oligonucleotide. We have obtained 1.5 mg of purified 25-mer from the analytical EM column in a single crude injection of 2.2 mg, with recovery of unreacted starting material. Importantly, no ghosting is observed when blanks are injected onto an RP-18 column after a sample run. Best separation results are obtained on the RP-18 when the pH of the load matches of the pH of the eluent.

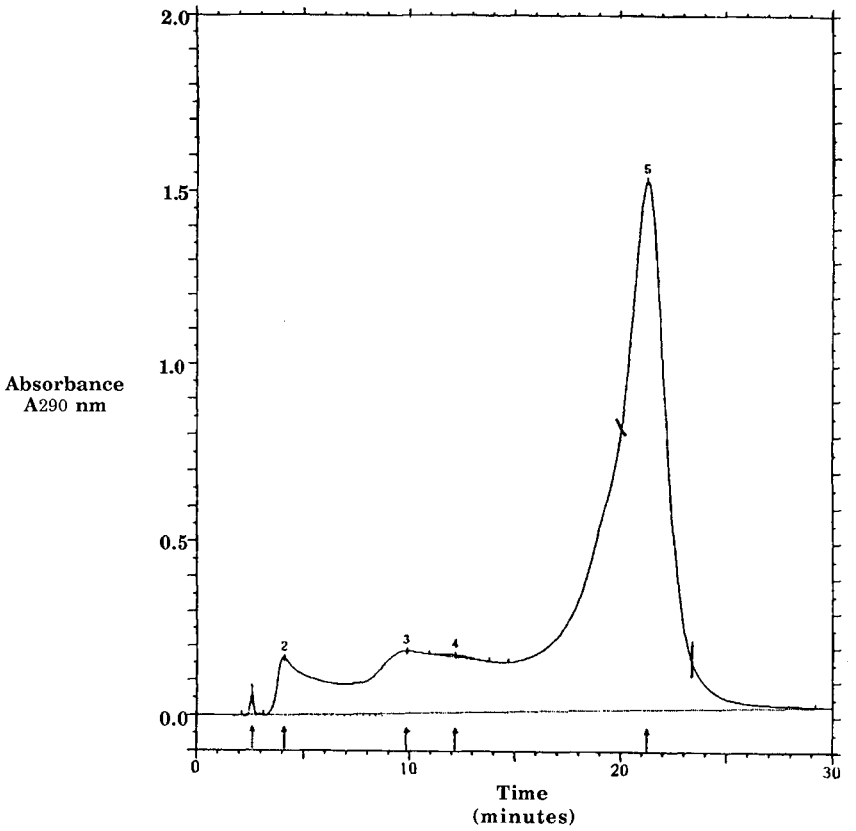

Fig. 3. HPLC trace of 249 μg loading of a 24-mer, 5'-end labeled with FITC. Column is EM Science Polyspher RP-18. Peaks 3 and 4, eluting at 9.9 and 12.3 min, are starting oligonucleotide. Peak 5, eluting at 21.3 min, is FITC-labeled material.

Finally, hybridization of the haptenated oligonucleotides to their complementary sequences has been examined qualitatively by hyperchromicity measurements and quantitatively by size-exclusion chromatography on a high-performance liquid chromatograph (Fig. 5). In all cases, the terminally haptenated oligonucleotides were able to hybridize to their complementary strands.

CONCLUSION

We have found that C_{18} column HPLC will not adequately separate fluoresceinated from non-fluoresceinated oligonucleotide, as checked by polyacrylamide gel electrophoresis. PAGE itself has the problem of low loading capacity. Unmodified polystyrene reversed-phase columns have high loading capacity and afford some separation of haptenated from non-haptenated oligonucleotide, but have "ghosting" as a setback. Taking all of these limitations into account, we now employ the RP-18 HPLC column from EM Science to separate haptenated from non-haptenated oligonucleotide. It has the characteristics of high loading capacity, good resolution, and no "ghosting" in its favor.

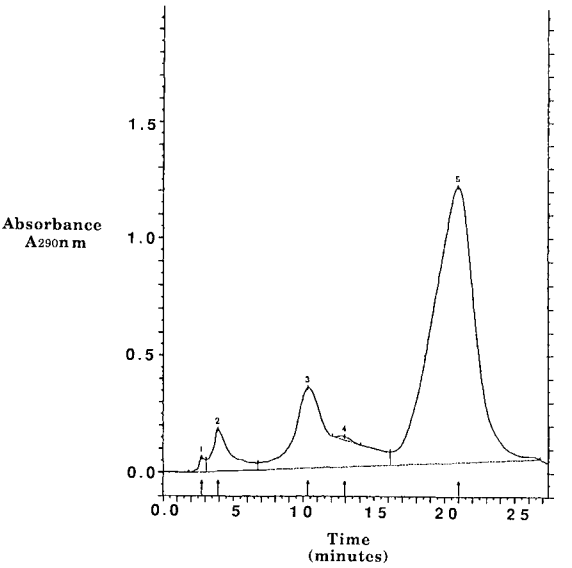

Fig. 4. Injection of 345 μg of a 25-mer, 3′-end labeled with biotin-(aminocaproyl)2-N-hydroxysuccinimide ester. Column is EM Science Polyspher RP-18. Peaks 3 and 4, eluting at 10.4 and 13 min, are starting oligonucleotide, while peak 5, eluting at 21 min, is biotinylated material.

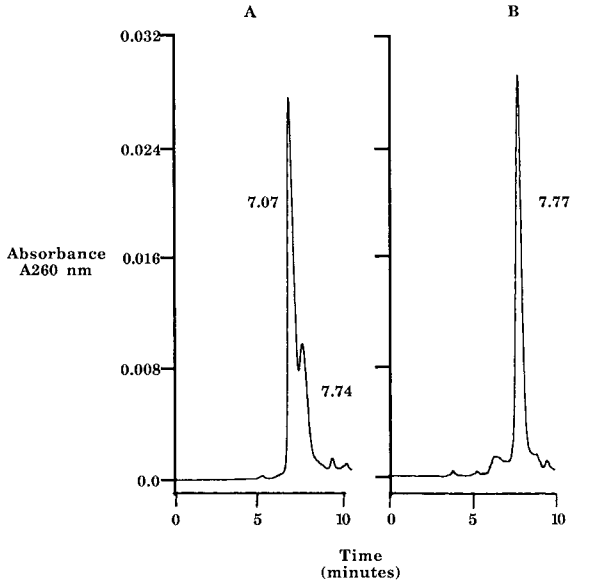

Fig. 5. (A) Injection of 24-mer, 5′-end labeled with FITC and hybridized to complementary strand, 7.07 min peak; (B) 24-mer by itself, 7.77 min retention time. Note the residual peak at 7.74 min from unhybridized material in (A). This disappears upon further admixture with complementary DNA. Column is Bio-Sil SEC-125.

ACKNOWLEDGEMENTS

We thank Cliff Chan for the oligonucleotide synthesis work and Julie Johanson for some of the purifications. We thank Abbott Laboratories for allowing the publication of this manuscript. Finally, we thank a reviewer for calling ref. 7 to our attention.

REFERENCES

1 A. M. Maxam and W. Gilbert, *Proc. Natl. Acad. Sci. U.S.A.*, 74 (1977) 560–564.
2 G. H. Keller, C. U. Cumming, C.-P. Huang, M. M. Manak and R. Ting, *Anal. Biochem.*, 170 (1988) 441–450.
3 G. H. Keller, D.-P. Huang and M. M. Manak, *Anal. Biochem.*, 177 (1989) 392–395.
4 P. S. Nelson, R. Sherman-Gold and R. Leon, *Nucleic Acids Res.*, 17 (1989) 7179–7186.
5 G. B. Dreyer and P. B. Dervan, *Proc. Natl. Acad. Sci. U.S.A.*, 82 (1985) 968–972.
6 G. Tous, J. Fausnaugh, P. Vieira and S. Stein, *J. Chromatogr.*, 444 (1988) 67–77.
7 L. M. Smith, S. Fung, M. W. Hunkapiller, T. J. Hunkapiller and L. E. Hood *Nucleic Acids Res.*, 13 (1985) 2399–2412.
8 J. Telser, K. A. Cruickshank, L. E. Morrison and T. L. Netzel, *J. Am. Chem. Soc.*, 111 (1989) 6966–6976.
9 A. C. Forster, J. L. McInnis, D. C. Skingle and R. H. Symons, *Nucleic Acids Res.*, 13 (1985) 745–761.
10 R. P. Viscidi, C. J. Connelly and R. H. Yolken, *J. Clin. Microbiol.*, 23 (1986) 311–317.
11 A.Reisfeld, J. M. Rothenberg, E. A. Bayer and M. Wilchek, *Biochem. Biophys. Res. Commun.*, 142 (1987) 519–526.
12 M. W. Germann, R. T. Pon and J. H. van de Sande, *Anal. Biochem.*, 165 (1987) 399–405.
13 S. Ikuta, R. Chattopadhyaya and R. E. Dickerson, *Anal. Chem.*, 56 (1984) 2253–2257.
14 *User Bulletin, No. 50*, Applied Biosystems, Foster City, CA, 1988.

Journal of Chromatography, 536 (1991) 95–106
Elsevier Science Publishers B.V., Amsterdam

CHROMSYMP. 2026

Purification of proteins on an epoxy-activated support by high-performance affinity chromatography

DOROTHY J. PHILLIPS*, BONNIE BELL-ALDEN, MARK CAVA[a], EDWARD R. GROVER and W. HARRY MANDEVILLE
Waters Division of Millipore, 34 Maple Street, Milford, MA 01757 (U.S.A.)
ROBERT MASTICO
University of Leeds, Leeds (U.K.)
WAYNE SAWLIVICH and GEORGE VELLA
Waters Division of Millipore, 34 Maple Street, Milford, MA 01757 (U.S.A.)
and
ANDREA WESTON
University of Rhode Island, Kingston, RI 02881 (U.S.A.)

ABSTRACT

The use of a rigid silica-based packing material with large particle and pore size, 37–55 μm and 500 Å pore, for affinity chromatography makes it possible to combine high selectivity with short analysis times. Both large and small molecules have been covalently bonded to the Protein-Pak™ Affinity Epoxy-Activated bulk packing for purification of glycoproteins, immunoglobulins, enzymes, lectins and other proteins. Recombinant protein A, GammaBind™ G, heparin, Cibacron Blue F3G-A, sulfanilamide, N-acetyl-D-glucosamine, concanavalin A and aminophenylboronic acid were covalently attached to the affinity packing for selective purification of proteins.

INTRODUCTION

Conventional chromatography of proteins relies on small differences in surface hydrophobicity (hydrophobic interaction and reversed-phase), surface charge (ion-exchange), and molecular size and shape (size exclusion) to separate target molecules that may be, at most, 0.1% of the dry weight of the starting material. However, these same proteins often have the characteristic ability to bind reversibly to other molecules as specific stable complexes. This ability has been utilized in affinity chromatography to purify proteins several thousand fold from complex mixtures in a single step [1].

Affinity chromatography was first used with cyanogen bromide activation on agarose supports [2]. This support is still widely used, but has disadvantages: ligand leakage, non-specific adsorption, matrix compressibility, and microbial attack.

[a] Present address: Zymark Corp., Hopkinton, MA 01448, U.S.A.

0021-9673/91/$03.50

Agarose is a soft gel and requires low flow-rates which result in long separation times, especially for large-scale purifications. Analysis times can be decreased by the use of rigid and non-adsorptive diol-bonded silicas adapted from size-exclusion chromatography [3]. Silica has certain advantages not possible with agarose: mechanical strength, well-defined and accessible pore volume, and resistance to microbial attack. These characteristics of silica along with the selectivity of covalently bound ligand result in a specific interaction and together have been combined to produce high-performance affinity chromatography (HPAC).

For the development of HPAC, the characteristics of the silica for purification of biopolymers were first defined. Silica used in high-performance liquid chromatography (HPLC) range in pore size from 60 to 4000 Å. Below 150 Å the performance of an HPAC column suffers because of poor solute diffusion and unavailability of the surface. Above 1000 Å the capacity is too low and the silica becomes friable. Therefore, pore sizes between 500 and 1000 Å are most commonly used. In conventional HPLC, small (<10 μm) particle sizes have been used to minimize band spreading and maximize resolution [4]. In HPAC, resolution depends on selectivity, not efficiency (plate count); thus, there are few advantages to high plate counts or small particle sizes in HPAC.

Immobilization reactions that form covalent bonds between the support and the ligand are required. A number of chemical reactions have been used including cyanogen bromide, active ester (N-hydroxysuccinimide), epoxide, tresyl chloride, carbonyldiimidazole, thiol and diazonium salts. Epoxy-activated packings have been developed because of the mild coupling conditions, simplicity of the reaction, the versatility of the epoxy functionality (immobilizes ligands by amino, thiol and hydroxyl groups), and the stability of the covalent bond with the ligand. The concentration of active groups is normally $\leqslant 5$ μmol/m^2 (about 300 μmol/g). For large proteins a monolayer is about 0.01 μmol/m^2. This coverage could lead to immobilization of a larger ligand by 100 bonds/molecule. While this would be a stable layer, the activity of the immobilized ligand may be low due to potential distortion of the three-dimensional structure required for activity. Turková *et al.* [5] reported that the affinity chromatographic efficiency of a specific adsorbent for porcine pepsin depended strongly on the concentration of the immobilized inhibitor. At low concentration (0.85 μmol of aminocaproyl-L-Phe-D-Phe-OCH_3/g dry gel), pepsin was eluted from the column as a sharp peak, whereas at high inhibitor concentration (155 μmol/g dry gel) several peaks of pepsin were noted in the chromatogram exhibiting the same proteolytic activity. The authors attributed the results to additional unspecific multipoint ligand–enzyme interactions with increasing ligand density on the support surface.

Each activation reaction has been used with a variety of lengths and types of spacer arms to assure that the immobilized ligand can be reached by the substance to be purified. Hydrophilic spacer arms (polyethylene glycol, for instance) are most favored. Lengths of spacer arms have varied from as few as 4 to as many as 50 atoms. Increasing the length of the spacer arm can reduce the capacity of the support. Therefore, the length and concentration of the spacer arm should be optimized for maximum activity.

A variety of immobilized ligands may be used in this technique. These molecules can be divided into general and specific ligands. General ligands include lectins such as concanavalin A, immunoglobulin-binding proteins, like Proteins A and G, and

triazine dyes, such as Cibacron Blue F3G-A. Specific ligands normally include antibodies directed against a particular antigen, and enzyme inhibitors or substrates. The most important characteristic of the immobilized ligand must be the ability to bind strongly to its specific biological compound but not so strongly that the conditions needed to release the protein also denature it.

The most common elution conditions involve introduction of a competing ligand, general conditions such as lowering the pH to less than 3, increasing the ionic strength of the buffer, or using a chaotropic buffer. Any of these methods may suffice depending on the hardiness of the immobilized ligand and the specific complex formed. HPAC, when used with the correct ligand and chromatography conditions, can result in the purest and, in some cases, most biologically active product of any method available.

A new silica-based affinity packing has been produced with the characteristics described above for use with biocompatible medium- and high-pressure LC instrumentation. The rigid silica-base has an average pore size of 500 Å and a particle size range of 37–55 μm. The Protein-Pak™ affinity epoxy-activated packing is manufactured by a polymerization process that encapsulates the silica matrix with a hydrophilic bonding layer containing the epoxide functionalities. The bonds formed between the silane with the epoxide functionalities and the silica are as stable as, if not more stable than, most other silica–silane interactions, minimizing any concern about epoxide leaching. Active sites of the silica are blocked by the hydrophilic bonding layer to produce low non-specific binding properties.

The ligands used to evaluate the performance of this new activated packing are listed in Table I. This report discusses the immobilization and affinity chromatography for N-acetyl-glucosamine, sulfanilamide, heparin and recombinant Protein A (rProtein A).

MATERIALS

Hemoglobin, carbonic anhydrase, antithrombin III, lysozyme, nitrophenyl acetate, glycine, wheat germ agglutinin, heparin, and sulfanilamide were purchased from Sigma (St. Louis, MO, U.S.A.). rProtein A was purchased from Repligen (Cambridge, MA, U.S.A.). Wheat germ meal was purchased from Hodgson (Gaines-

TABLE I

PROTEIN-PAK AFFINITY EPOXY-ACTIVATED PACKING COUPLINGS

Immobilized ligands	Applications
GammaBind™ G	Human immunoglobulin G (IgG)
rProtein A	Mouse IgG in serum
Sulfanilamide	Carbonic anhydrase
N-Acetyl-D-glucosamine	Wheat germ lectin
Heparin	Lysozyme, antithrombin III
Concanavalin A	Ribonuclease B, Horseradish peroxidase
Cibacron Blue	Bovine serum albumin
Aminophenylboronic acid	Uridine, adenosine, sorbitol

ville, MO, U.S.A.). The affinity packings used were the Waters Protein-Pak affinity epoxy-activated packing, epoxy-activated Sepharose from Pharmacia (Piscataway, NJ, U.S.A.) and BakerBond™ Prepscale™ glycidoxypropyl affinity matrix from J. T. Baker (Phillipsburg, NJ, U.S.A.). The Microcolumns and the advanced purification (AP) glass columns were from Waters, a Division of Millipore (Milford, MA, U.S.A.). Two HPLC systems were used. The Model 650 advanced protein purification system with the Model 484 tunable absorbance detector and the 745 data module was used. The second system was the Model 600E solvent delivery system with the 440 detector or 490 programmable multiwavelength detector. The HPLC systems were connected to a Foxy fraction collector and Waters Model 712 or 710 WISP autosampler. The Model 600E system was interfaced to the Waters 840 data and control station.

IMMOBILIZATION METHODS AND AFFINITY CHROMATOGRAPHY

Lectin isolation of N-acetylglucosamine affinity column

N-Acetylglucosamine coupling to epoxy-activated packing. Epoxy-activated silica (3 g, 154 μmol/g) was washed with water on glass filter followed by 0.1 *M* sodium hydroxide (20 ml each). N-Acetylglucosamine (200 mg) dissolved in 0.1 *M* sodium hydroxide was added to the silica. The mixture was heated at 45°C on a shaker for 18 h. The reaction mixture was centrifuged and the supernatant was discarded. The pellet was washed with water (2 ×), 0.05 *M* Tris chloride (pH 8) (2 ×), and 0.5 *M* sodium chloride (1 ×). The pellet was resuspended in 0.07 *M* sodium phosphate (pH 7.0) 0.15 *M* sodium chloride and poured into an AP1 (100 × 10 mm) glass column. The column was equilibrated with the same buffer.

Wheat germ preparation. Wheat germ meal (50 g) was stirred in hexane (150 ml) for 2 h. The mixture was filtered and the residue was air dried overnight. The residue was suspended in 0.05 *M* sodium acetate (pH 4.5) (250 ml). The protein was precipitated from solution by addition of solid ammonium sulfate to 40% saturation. The precipitate was collected by centrifugation and resuspended in acetate buffer. The solution was dialyzed against the same buffer overnight. The extract was centrifuged and the supernatant was applied to the N-acetyl-D-glucosamine (GlcNAc) column.

Sample application and elution. Wheat germ agglutinin (WGA) standard (10 μl, 5 mg/ml) in 0.07 *M* sodium phosphate (pH 7.0) with 0.15 *M* sodium chloride (buffer A) was injected at a flow-rate of 1 ml/min. At 7 min the eluent was switched to buffer B (buffer A + GlcNAc, 10 mg/ml) to elute bound protein. Crude wheat germ preparation (1.0 ml of 6.8 mg/ml) was applied and WGA was purified. WGA (1.2 mg/ml) was recovered with elution buffer.

Carbonic anhydrase isolation on the sulfanilamide column

Conditions for coupling sulfanilamide to epoxy-activated packing. Epoxy-activated packing (5 g, 155 μmol/g) was washed with water and methanol; the supernatants were decanted. Sulfanilamide (266 mg) dissolved in 3.6 ml of methanol was added to the washed silica in a capped glass test tube. The coupling was carried out on a rotating wheel for 24 h at 45°C. The supernatant was removed on a coarse-porosity sintered-glass funnel, and the packing was washed with 20 ml each of methanol (3 ×), methanol–water (1:1, v/v) (1 ×), water (1 ×), and 1 *M* sodium chloride (1 ×). All supernatants were saved for quantitation of sulfanilamide remaining in

solution by HPLC (amount bound determined by the difference between amount applied and amount in solution). The material was slurry-packed into an AP1 glass column and deactivated by recycling 100 ml of 1 *M* ethanolamine (pH 10) through the column at room temperature for 24 h.

Bovine hemolysate preparation. Bovine whole blood was centrifuged at 7700 *g* for 20 min to remove the red blood cells. The pellet (erythrocytes) was washed with cold 0.9% sodium chloride (3 ×) and centrifuged at 3000 *g* for 10 min after each wash. The pellet was washed with cold water (1:1, v/v) to lyse the cells and centrifuged at 3000 *g*. The supernatant (hemolysate) was used for chromatography and the pellet was discarded.

Sample application and elution. The hemolyzate (200 μl) was applied to the AP1-sulfanilamide affinity column. The column was washed with buffer C [100 m*M* Tris (pH 8.7) with 200 m*M* sodium sulphate] until the absorbance at 280 nm returned to baseline; the retained material was eluted with buffer D [50 m*M* Tris (pH 6.5) with 200 m*M* potassium thiocyanate]. The enzyme activity of the retained material (the peak fractions), carbonic anhydrase, was measured by esterase activity for conversion of nitrophenyl acetate to nitrophenol, and monitored by the increase in absorbance at 400 nm.

Other ligand couplings

Similar conditions were used for immobilizing heparin and rProtein A. The Protein-Pak affinity epoxy-activated packing was slurried in coupling buffer [buffer–packing, 3:1 (v/v)], allowed to settle and then the buffer was decanted. Heparin or rProtein A (3 mg/ml packing) were dissolved in the coupling buffer, 0.1 *M* sodium borate with 0.15 *M* sodium chloride at pH 8.5–9. After the ligand was added to the packing the coupling was carried out for three days at room temperature. Following coupling the packing was blocked with 1 *M* ethanolamine in 0.1 *M* sodium borate (pH 9.0) for 24 h. Excess ligand and blocking solution were removed by using 6 ml of solution per gram of packing for each wash: coupling buffer (1 ×); 1 *M* sodium chloride (4 ×), and 10 m*M* sodium phosphate (pH 7.4) with 150 m*M* sodium chloride (2 ×).

Determination of human IgG capacity

The coupling of epoxy-activated Sepharose 6B from Pharmacia and BakerBond Prepscale glycidoxypropyl affinity matrix (silica-based) were carried out in the Waters Microcolumn. The performance of the Waters Protein-Pak affinity epoxy-activated Microcolumn was compared to the other two packings. The volume of each packing used in the study was kept constant (silica: 1 g = 2 ml; agarose, 1 g = 3 ml). rProtein A (3 mg/ml) was immobilized on the three epoxy-activated packings at room temperature for 72 h in 0.1 *M* sodium borate (pH 8.3) with 0.15 *M* sodium chloride. The packings were then blocked with 1 *M* ethanolamine in the sodium borate buffer for 24 h. The amount of rProtein A coupled was determined by its extinction coefficient at 228 nm and/or by size exclusion chromatography on a Waters Protein-Pak 200SW column.

The human IgG (5–10 mg/ml) was applied to the rProtein A affinity packings after they were equilibrated in the binding buffer, 100 m*M* potassium phosphate (pH 7.4) with 0.15 *M* sodium chloride. After washing three times with the binding

buffer to remove unretained IgG, the bound IgG was eluted with 0.15 *M* sodium citrate (pH 2.2) with 0.15 *M* sodium chloride. The amount of human IgG was determined by its extinction coefficient, 1.4 A.U./(mg/ml), at 280 nm.

RESULTS AND DISCUSSION

Fig. 1 presents the chromatography for rProtein A coupled to the Protein-Pak affinity epoxy-activated packing in an analytical column (75 × 3.9 mm I.D.). Native Protein A is a 42 000 dalton polypeptide from *Staphylococcus aureus* and has five homologous sites for binding immunoglobulins through their Fc regions [6]. The rProtein A is used extensively for purification of immunoglobulins. Fig. 1 shows that human IgG was retained on the rProtein A affinity packing. When an IgG sample containing 2.6 mg in 100 μl was applied to the column, a small unretained breakthrough peak was observed, indicating that the column bound about 90% of the immunoglobulin.

Heparin is an acid mucopolysaccharide from animal tissue which prevents blood clotting. It contains an equal amount of D-glucosamine and D-glucuronic acid with O-

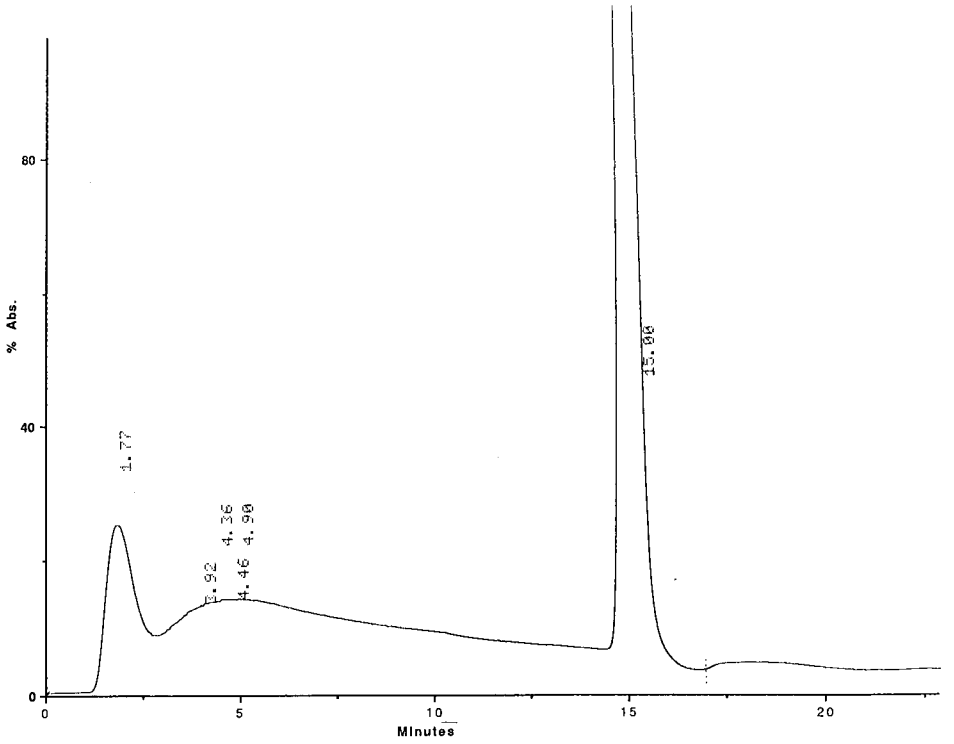

Fig. 1. Immobilized Protein A on Protein-Pak affinity epoxy-activated bulk packing for IgG isolation. Analytical column, 75 × 3.9 mm I.D.; buffer A, 10 m*M* sodium phosphate buffer (pH 7.4) with 150 m*M* sodium chloride; buffer B, 2% citric acid (pH 2.5) 150 m*M* sodium chloride; gradient and flow-rates, 0 to 10 min at 0.5 ml/min in buffer A, 10 to 14 min at 1 ml/min in buffer B and 14 to 22 min in buffer A at 1.5 ml/min for equilibration; detector, 280 nm. The sample was 2.6 mg human IgG (100-μl injection).

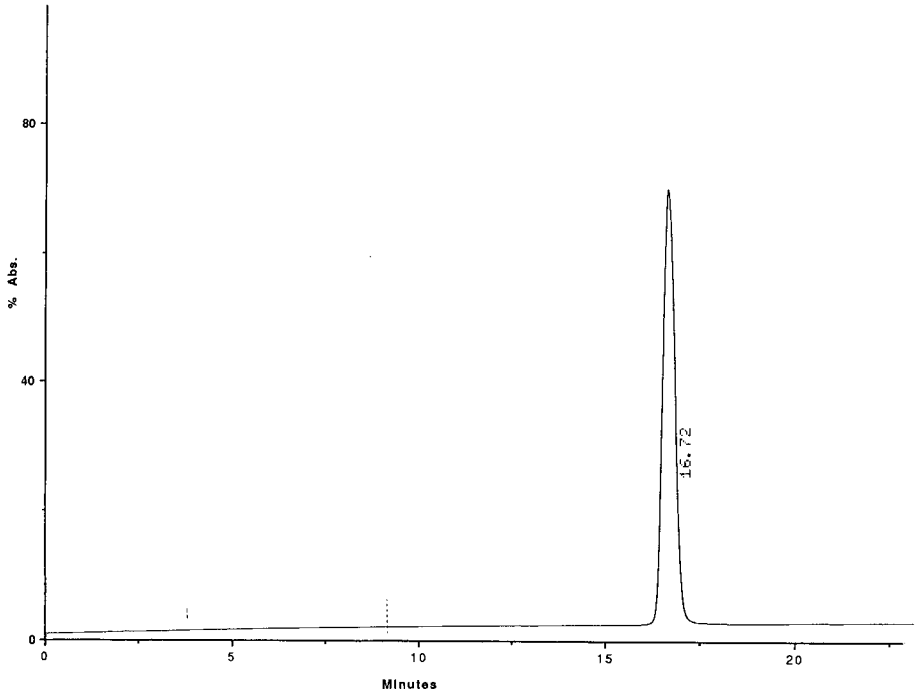

Fig. 2. Immobilized heparin for lysozyme isolation. Analytical column, 75 × 3.9 mm I.D.; buffer A, 10 m*M* Tris chloride (pH 7.5) with 10 m*M* sodium chloride; buffer B, 10 m*M* Tris chloride (pH 7.5) with 0.3 *M* sodium chloride; gradient and flow-rate, 0 to 10 min at 0.5 ml/min, 10 to 14 min at 1 ml/min in buffer B, 14 to 22 min in buffer A at 1.5 ml/min for equilibration; detector, 280 nm. The sample was a 10-μl injection of lysozyme, 200 μg.

and N-sulphate residues [7]. The heparin ligand is frequently used for the purification of antithrombin III, an inhibitor of thrombin [8]. The heparin affinity column bound lysozyme and antithrombin III as noted in Figs. 2 and 3, respectively. The heparin column had a capacity of about 2 mg lysozyme/ml based on protein breakthrough. Antithrombin III was retained on the column and is the third peak in Fig. 3. The peak at 14.96 min (peak 2) in Fig. 3 may be antithrombin II, which also binds to heparin but with less affinity than antithrombin III. Due to the significantly stronger affinity of heparin for antithrombin III than for lysozyme, a 10-fold higher salt concentration (3 *M versus* 0.3 *M* sodium chloride) was required to elute the antithrombin III.

Two applications involved the use of affinity chromatography to purify a selected material from a crude mixture. Carbonic anhydrase, a widely occurring zinc-containing enzyme, plays an important role in respiration, carbon dioxide transport, and other physiological processes [7]. Carbonic anhydrase is found in several places in the body including the red blood cells or erythrocytes [9]. Sulfanilamide, an inhibitor of carbonic anhydrase, was coupled to the packing at almost equal molar amount to the epoxy-activation level (155 μeq./g). In order to determine that the affinity column was functioning as expected, a mixture of hemoglobin and carbonic anhydrase standards was applied to the column; the earlier protein was unretained, whereas the enzyme was

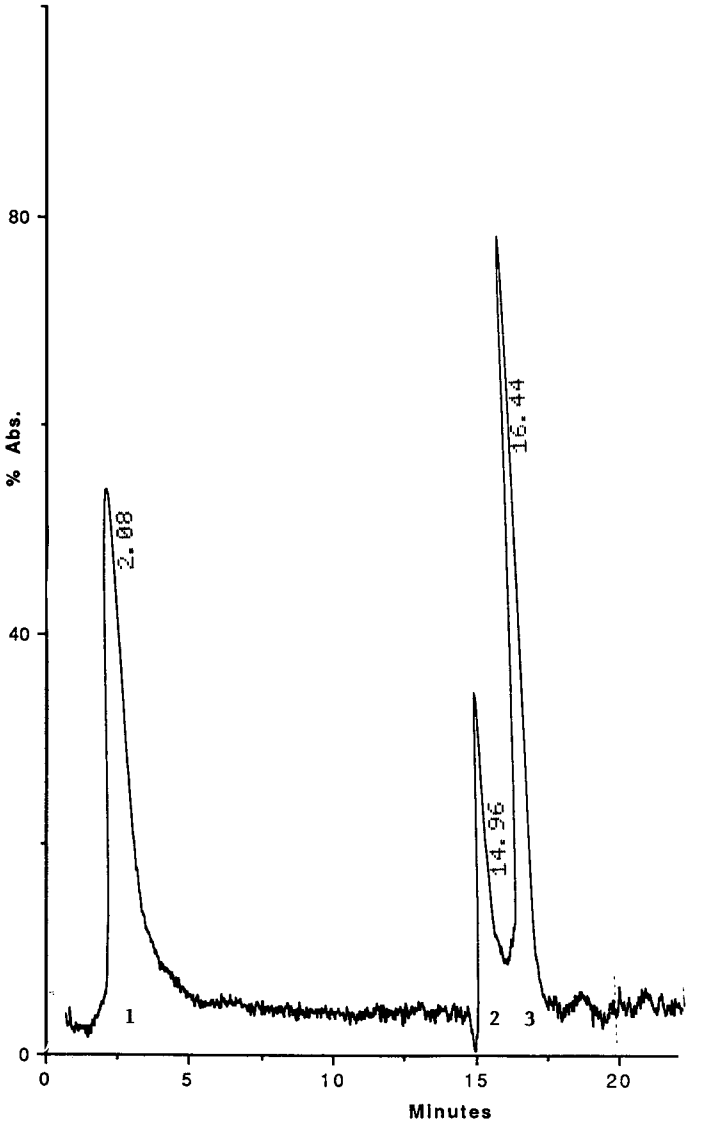

Fig. 3. Heparin coupled to Protein-Pak affinity epoxy-activated bulk packing for antithrombin III isolation. Analytical column, 75 × 3.9 mm I.D.; buffer A, 10 m*M* Tris chloride (pH 7.5) with 10 m*M* sodium chloride; buffer B, 10 m*M* Tris chloride (pH 7.5) with 3 *M* sodium chloride; gradient and flow-rates were 0 to 10 min at 0.5 ml/min, 10 to 14 min at 1 ml/min in buffer B, 14 to 22 min in buffer A at 1.5 ml/min for equilibration; detector, 280 nm. The sample was a 100-μl injection of antithrombin III, 29 μg. Peaks 1 and 3 are antithrombin III; peak 2 is unknown.

bound and released by a chaotropic agent, with 100% recovery, as shown in Fig. 4. The bovine hemolyzate was prepared and 200 μl of the preparation was applied to the column; the chromatogram is presented in Fig. 5. The second peak contained the esterase for conversion of nitrophenyl acetate to nitrophenol. Table II shows that of

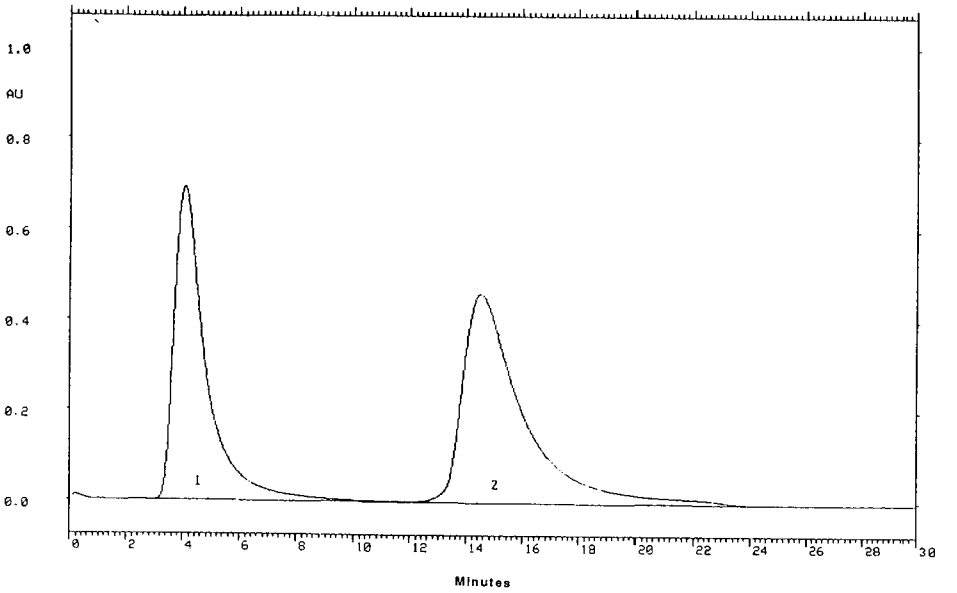

Fig. 4. Carbonic anhydrase isolation on sulfanilamide-coupled Protein-Pak affinity epoxy-activated bulk packing. AP1 glass column, 100 × 10 mm I.D.; buffer A, 100 m*M* Tris sulphate with 200 m*M* sodium sulphate (pH 8.7); buffer B, 200 m*M* potassium thiocyanate in 50 m*M* Tris sulphate (pH 6.5). Initial flow-rate, 1 ml/min; from 2 to 40 min, 2 ml/min. The chromatography was isocratic in buffer A for 7 min, followed by a step to 100% buffer B for 10 min; at 17 min the column was equilibrated in buffer A. The sample contained hemoglobin (1.5 mg, peak 1) and carbonic anhydrase (1.5 mg, peak 2). The recovered carbonic anhydrase had a specific activity of 13 units/mg for esterase activity for converting nitrophenyl acetate to nitrophenol.

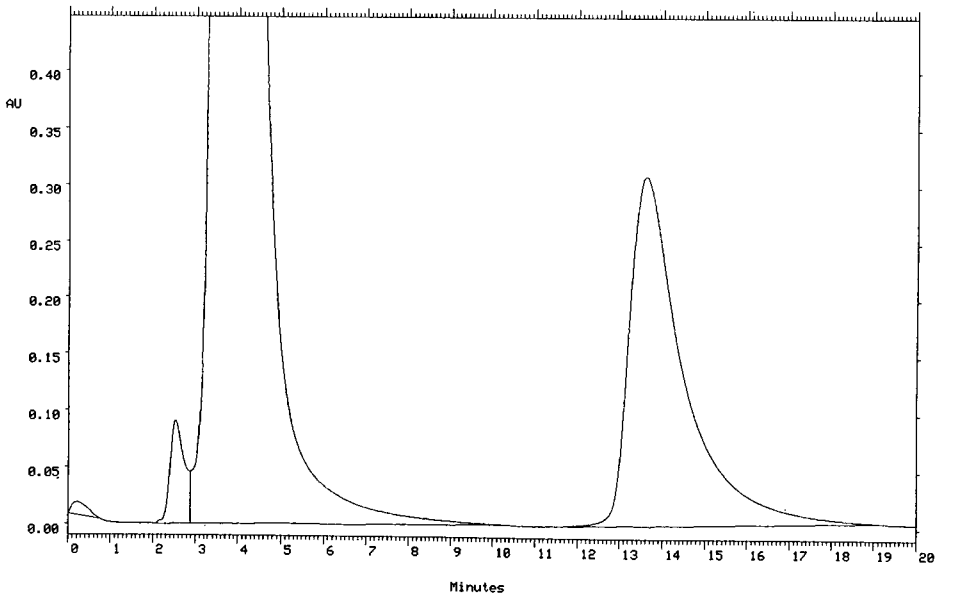

Fig. 5. Carbonic anhydrase purification from bovine hemolysate using sulfanilamide-coupled Protein-Pak affinity epoxy-activated bulk packing. The same as Fig. 4 except the sample was 200 μl hemolyzate from bovine erythrocytes. Peak 1 contains mostly hemoglobin (major component, 4.2 mg). Carbonic anhydrase (0.59 mg) is in peak 2 and was identified by its biological activity.

TABLE II

PURIFICATION OF CARBONIC ANHYDRASE FROM BOVINE HEMOLYZATE

The 200 μl of bovine hemolyzate (24 mg protein/ml) applied to the sulfanilamide-affinity column gave a retained peak (peak 2) with carbonic anhydrase activity. Peak 2 contained 12% of the protein applied and had a purification factor of 8.

	Protein concentration (mg/ml)	Total volume (ml)	Total protein (mg)	Total biological activity[a] (units)	Specific activity (units/mg)	Purification factor	% Recovery of biological activity
Crude	23.8	1.0	23.8	8.75	0.37	1	100
Affinity purified (peak 2)	0.06	10	0.59	1.75	2.96	8	100

[a] Carbonic anhydrase activity of the peak fractions was measured by converting nitrophenyl acetate to nitrophenol at pH 7.5.

the 4.8 mg applied, 0.59 mg was carbonic anhydrase and that there was an 8-fold purification of the enzyme.

The epoxy packing was able to bind covalently N-acetyl-D-glucosamine at pH 11, as had been reported for the epoxy-activated Sepharose 6B [10]. The mode of attachment of the ligand to the support is through one of the hydroxyl groups on the sugar; C-6 hydroxyl is unrestricted and kinetically favored over the C-4 and C-3

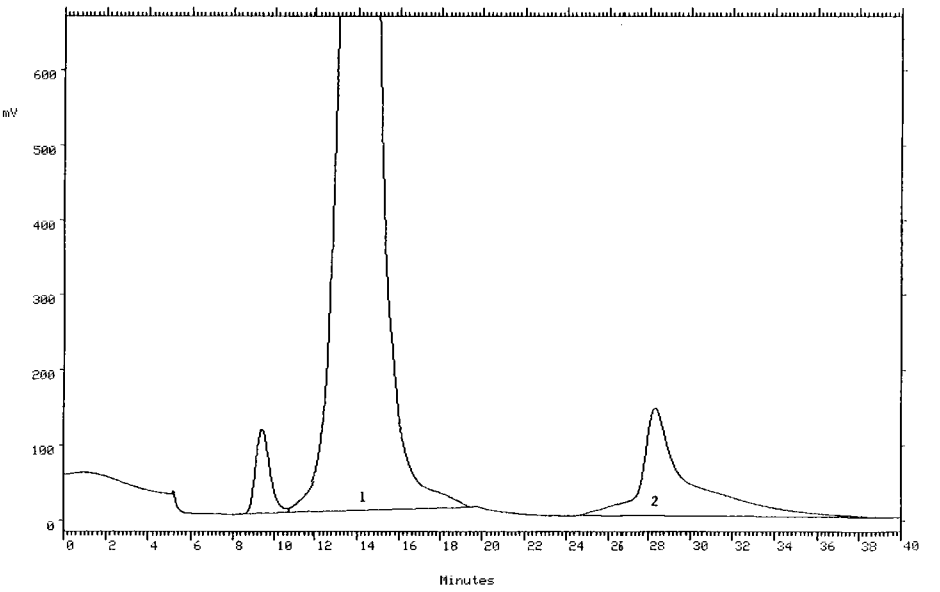

Fig. 6. Wheat germ lectin isolation using N-acetyl-D-glucosamine as ligand. AP1 glass column, 100 × 10 mm I.D.; buffer A, 70 m*M* sodium phosphate (pH 7.0) with 150 m*M* sodium chloride; buffer B, buffer A with N-acetyl-D-glucosamine (10 mg/ml); gradient, 0 to 7 min at 1.0 ml/min in buffer A and a step at 7 min to buffer B (1 ml/min); detector, 280 nm. The sample was 1 ml of crude wheat germ preparation; 1.2 mg/ml of the lectin was eluted.

TABLE III

HUMAN IgG CAPACITY ON EPOXY-ACTIVATED PACKINGS WITH rPROTEIN A LIGAND

Recombinant Protein A was immobilized at 25°C for 72 h in 0.1 *M* sodium borate (pH 8.5) with 0.15 *M* sodium chloride. Human IgG binding buffer, 10 m*M* sodium phosphate (pH 7.4) with 0.15 *M* sodium chloride; and elution buffer, 0.1 *M* sodium citrate (pH 2.2) with 0.15 *M* sodium chloride.

	Capacity mg IgG/ml packing	% Recovery bound IgG	Ratio mg IgG/mg rProtein A ligand
Waters Protein-Pak Affinity Epoxy-Activated Microcolumn	17	86	8
Pharmacia epoxy-activated Sepharose 6B	11	63	5.5
Bakerbond Prepscale glycidoxypropyl affinity matrix	13	73	6.5

hydroxyl groups. The C-2 hydroxyl group is blocked and cannot react. Wheat germ lectin specifically binds N-acetyl-D-glucosamine and its polymers. The affinity packing in the AP1 glass column retained the wheat germ agglutinin standard, which was eluted by competitive binding of the free N-acetyl-D-glucosamine in the mobile phase at a concentration of 10 mg/ml. Elution by the free sugar has been found to be a more gentle method than the more common technique of using dilute acetic acid [10]. Wheat germ agglutinin was purified from the wheat germ meal preparation on the N-acetyl-D-glucosamine column, as presented in Fig. 6. An amount of 50 g of wheat germ meal yielded a crude preparation with 6.8 mg/ml of total protein. When the crude sample was applied to the affinity column, 1.2 mg/ml of wheat germ agglutinin was recovered with the elution buffer.

A study was conducted to compare the performance of the Protein-Pak affinity epoxy-activated packing with that of two other epoxy-activated materials, epoxy-activated Sepharose and Bakerbond Prepscale glycidoxypropyl affinity packings. The three packings coupled about the same amount of rProtein A, 0.7 mg/ml. The Protein-Pak affinity epoxy-activated Microcolumn showed a slightly higher human IgG capacity and % mass recovery than the Pharmacia and Baker columns, 17 mg human IgG/ml with 86% recovery *versus* 11 mg/ml with 63% and 13 mg/ml with 73% recovery, respectively. The data are summarized in Table III. rProtein A on the Waters affinity packing also performed better than a protein A column on the epoxy-activated silica from Alltech which had a human IgG capacity of 7 mg/g or 14 mg/ml [11].

CONCLUSIONS

Since affinity chromatography is the only chromatographic method in which specific molecules are isolated on the basis of their selective interaction with an immobilized ligand, there is increasing demand for immobilization of ligands via a variety of functional groups. Activated affinity packings such as Protein-Pak affinity epoxy-activated packing, which can covalently bond molecules with amino, hydroxyl or sulfhydryl groups, have broad applications for purification of proteins.

The applications shown here demonstrated that this epoxy-activated packing can bind small and large molecules through amines or hydroxyl groups. It was possible

to recover the proteins retained on the immobilized ligands with maintenance of biological activity. The rProtein A ligand performed better for human IgG isolation when immobilized on the Protein-Pak epoxy-activated Microcolumn than on either the Pharmacia or Baker affinity packing.

This more rigid packing material can withstand greater backpressures, thus allowing higher flow-rates and significantly shorter analysis times for large scale preparative chromatography. Most purifications were carried out on the derivatized Protein-Pak affinity epoxy-activated packing in less than 1 h. The results of these studies show the potential for preparative-scale separations that can be performed at high flow-rates, keeping analysis times significantly shorter than those for soft gels (for which the slower linear velocities must be used).

REFERENCES

1 P. Mohr and K. Pommerening, *Affinity Chromatography, Practical and Theoretical Aspects* (*Chromatographic Science Series*, Vol. 33), Marcel Dekker, New York, 1985.
2 P. Cuatrecasas, M. Wilcheck and C. B. Anfinsen, *Proc. Natl. Acad. Sci. U.S.A.*, 61 (1968) 636.
3 S. Ohlson, L. Hansson, P. O. Larsson and K. Mosbach, *FEBS Lett.*, 93 (1978) 5.
4 L. R. Snyder and J. J. Kirkland, *Introduction to Modern Liquid Chromatography*, Wiley, New York, 1979.
5 J. Turková, K. Bláha and K. Adamová, *J. Chromatogr.*, 236 (1982) 375.
6 J. J. Langone, *J. Immunol. Methods*, 55 (1982) 277.
7 T. Scott and M. Brewer (Editors), *Concise Encyclopedia of Biochemistry*, Walter de Gruyter, New York, 1983.
8 R. E. Jordan, T. Zuffi and D. D. Schroeder, in T. C. J. Gribnau, J. Visser and R. J. F. Nivard (Editors), *Affinity Chromatography and Related Techniques*, Elsevier, Amsterdam, 1982, p. 275.
9 J. E. A. McIntosh, *Biochem. J.*, 114 (1969) 463.
10 P. Vretblad, *Biochim. Biophys. Acta*, 434 (1976) 169.
11 L. R. Massom, C. Ulbright, P. Snodgrass and H. W. Jarrett, *BioChromatography*, 4 (1989) 144.

Journal of Chromatography, 536 (1991) 107–111
Elsevier Science Publishers B.V., Amsterdam

CHROMSYMP. 2018

High-performance liquid chromatography for the assessment of glucoamylase, immobilized on metallic membranes

H. J. WANG* and R. L. THOMAS
223 Poole Agricultural Center, Department of Food Science, Clemson University, Clemson, SC 29634-0371 (U.S.A.)

ABSTRACT

High-performance size-exclusion chromatography was used to quantitate the amount of glucoamylase (GA) immobilized on various membrane materials. The amount of GA immobilized ranged from 0.39 to 1.90 g/ft^2 of membrane. A Dextro-Pak C_{18} plastic cartridge in a radial compression module was used to evaluate the reaction products of the immobilized GA, using 1.0% dextrin as a substrate. The low-molecular-weight oligo-saccharides (degree of polymerization 1–10) in 24.0 and 1.0% dextrin and in the membrane permeates were identified and quantitated in 25 min. High-performance liquid chromatography analyses were demonstrated to be easier and more sensitive than conventional protein assays and colorimetric sugar analyses.

INTRODUCTION

Immobilization techniques have been introduced into the enzyme industries to increase product quality and reduce cost [1,2]. Various protein assays were used to estimate the amount of enzyme adsorbed on the carriers. The Lowry method [3] was used to determine the amount of glucoamylase (GA) immobilized on silanized aluminium oxide [4] and on polyvinylpyrrolidone gel [5] for the saccharification of starch and the digestion of cassava solution. Bio-Rad protein assay [6] was used by McKamy [7] for the determination of GA adsorbed on a metallic membrane for the hydrolysis of dextrin. However, these protein assays could only approximate the amount of enzyme actually immobilized. Therefore, high-performance size-exclusion chromatography (HPSEC) was used for the determination of the specific amount of GA immobilized on a metallic membrane with simultaneous estimation of the molecular weight of GA.

In addition, due to the increasing interest regarding the individual sugar level of starch hydrolyzates, high-performance liquid chromatography (HPLC) techniques have also become essential methods for the determination of sugar concentrations instead of conventional colorimetric assays, which can only measure total carbohydrate. A radially compressed C_{18} cartridge, having the capability of resolving oligomers up to a degree of polymerization (DP) of 14, was used for the investigation of partially hydrolyzed starch [8]. Recently, a Waters Dextro-Pak plastic C_{18} cartridge

0021-9673/91/$03.50

was used to analyze oligosaccharides of DP 1–10 in hydrolyzed starch [9], corn syrup solids [10], and maltodextrins [10,11]. Separation of the saccharides was based on the chain length [12].

EXPERIMENTAL

Materials

Glucoamylase from Rhizopus mold (mixture of *exo*-1,4-D-glucosidase, EC 3.2.1.3) with an activity of 12 000 units/g was purchased from Sigma (St. Louis, MO, U.S.A.). Type I dextrin was also purchased from Sigma. Maltose, maltotriose, and β-D-glucose were obtained from Fisher Scientific (Dallas, TX, U.S.A.).

The metallic membrane system, the membrane coating materials {designated WD1, WD2, WD1 + WD2, F1, ZOSS (hydrous zirconium oxide) and ZOPA [hydrous zirconium oxide poly(acrylic acid)]} and the membrane-coating techniques were provided by DuPont Separation Systems (Seneca, SC, U.S.A.). WD1, WD2, WD1 + WD2 and F1 were coated on porous, stainless-steel tubes 5 ft. × 1.25 in. I.D. (152 cm × 3.18 cm I.D.). The composition of these membrane materials is proprietary for test materials of DuPont Separation Systems [11]. ZOSS and ZOPA were coated on 2 ft. × 0.625 in. I.D. (61 cm × 1.59 cm I.D.) porous, stainless-steel tubes. Each stainless-steel tube was installed in a sintered, stainless-steel shell [13]. The ZOPA membrane was selected for dextrin hydrolysis by immobilized GA.

Methods

The immobilization of GA was carried out according to the procedures of McKamy [7]. A 10-l volume of 0.1% (w/v) GA in 0.05 *M* sodium acetate buffer at pH 5.0 was recirculated through each membrane material which had been coated on a porous, stainless-steel tube. The maximum GA immobilization on the membrane was achieved after 20 min at room temperature. The amount of GA immobilized on the membrane was determined from the decrease of its concentration in the buffer solution by the HPSEC method. A 10-l volume of distilled water, adjusted to pH 5.0 was recirculated through the membrane to remove not-immobilized GA. Finally, a 10-l volume of 1.0% dextrin in distilled water, adjusted to pH 5.0, was recirculated through the ZOPA membrane to the feed tank at 300 p.s.i. pressure. The permeates (dextrin hydrolyzates) were collected at various times.

The GA concentration was determined with a Beckman TSK 3000SW column (300 × 7.5 mm), connected to a TSK precolumn (75 × 7.5 mm). The mobile phase was a 0.1 *M* potassium phosphate buffer (pH 6.0), which had been filtered through a 0.45-μm filter and degassed under vacuum. GA standard was prepared by dissolving GA in the phosphate buffer to yield a 1.0 mg/ml solution. Each GA sample was passed through a 0.45-μm filter before HPSEC analysis. A 20-μl sample of GA solution was eluted at a flow-rate of 0.5 ml/min and detected with a Waters Model 440 absorbance detector at 280 nm. The GA concentration was calculated with reference to peak-height standard curves, which were integrated with a Waters Model 740 data module, attenuated at 128×. The GA concentration was also determined by the Bio-Rad protein assay [6] using GA as a standard.

Low-molecular-weight (DP 1–10) oligosaccharides were resolved by HPLC using a 10 cm × 8 mm I.D. C_{18} cartridge installed in a rubber sleeve wihtin a RCM-100

radial compression module which was described by Fallick and Rausch [14]. The rubber sleeve is surrounded by a hydraulic fluid (glycerine), pressure is generated by moving three lever-driven pistons into the glycerine. The pressure is transmitted through the flexible sleeve to the wall of the cartridge, as well as to the particles of the packed bed. A modified inlet connector was used to fit the Guard-Pak precolumn inserts directly into the Radial-Pak C_{18} cartridge (Waters Assoc., Milford, MA, U.S.A.). HPLC-grade water as the mobile phase was filtered through a 0.22-μm filter and degassed under vacuum. Sugar standards for DP 1, 2 and 3 were prepared from 1.0 mg/ml glucose, maltose and maltotriose, respectively. Standard solutions were used to determine the retention time and concentration. The sugars were passed through a 0.45-μm filter prior to injection. The concentration of each saccharide (DP 4–10) was determined relative to a glucose standard [9]. A 15-ml volume of the dextrin hydrolyzate was eluted with water at a flow-rate of 1.0 ml/min and detected with a Waters Model 410 differential refractive index detector.

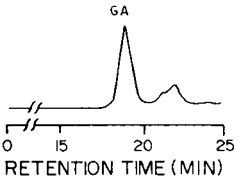

Fig. 1. Chromatogram of 1.0 ml/mg GA solution.

RESULTS AND DISCUSSION

A chromatogram for the analysis of GA is shown in Fig. 1. The first peak is ascribed to GA and the other peaks represents protein contaminants in the enzyme preparation. These contaminants can be detected by conventional colorimetric protein assays. Therefore, separation and quantitation of GA by HPSEC allowed the quantitation of GA alone.

The amount of GA immobilized on various membrane materials is shown in Table I. The variations among membrane materials were no doubt caused by the

TABLE I

QUANTITATION OF GA IMMOBILIZED ON VARIOUS MEMBRANE MATERIALS BY MEANS OF HPSEC AND BIO-RAD PROTEIN ASSAY

Membrane materials	Glucoamylase (g/ft.^{2} of membrane)	
	HPSEC	Bio-Rad
WD1	1.90	6.97
WD2	1.74	6.23
ZOSS	1.29	4.84
Bare tube	1.21	4.23
ZOPA	1.19	4.11
F1	0.76	3.10
WD1 + WD2	0.39	1.36

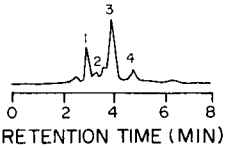

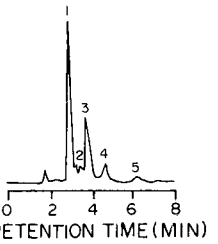

Fig. 2. Chromatogram of low-molecular-weight oligosaccharides present in membrane permeate without GA treatment (MPWOG). 1 = Glucose; 2 = maltose; 3 = maltotriose; 4 = DP 4.

Fig. 3. Chromatogram of low-molecular-weight oligosaccharides present in membrane permeate with immobilized GA treatment (MPWG). 1 = Glucose; 2 = maltose; 3 = maltotriose; 4 = DP 4; 5 = DP 5.

characteristics of the membranes. Comparisons were made between the HPSEC method and the Bio-Rad protein assay. The amount of GA determined by Bio-Rad protein assay was about 2.5 times higher than that from HPSEC. This may be expected because of the variations in binding ability of the dye to different proteins and the detection of all of the proteins in the enzyme preparation. Also, the contaminant protein may be bound more than GA. This indicates an advantage of using HPSEC for the specific quantitation of GA.

A 1.0% dextrin solution was used for the comparisons of low-molecular-weight oligosaccharides in the membrane permeates with and without immobilized GA treatment (MPWG and MPWOG, respectively). Figs. 2 and 3 illustrate the differences of the oligomers between MPWOG and MPWG, respectively, after a 10-min membrane operation. Table II shows the HPLC analyses of the low-molecular-weight oligosaccharides in various dextrin samples. The content of low-molecular-weight oligosaccharides in MPWOG was significantly ($p < 0.05$) lower than that in the 1.0% dextrin feed, indicating that the ZOPA membrane rejected a significant ($p < 0.05$) amount of low-molecular-weight oligosaccharides from a dextrin solution. The

TABLE II

COMPOSITION (mg/ml) OF DEXTRIN SAMPLES AND MEMBRANE PERMEATES DETERMINED BY HPLC

	24.0% Dextrin	1.0% Dextrin	MPWOG[d]	MPWG[e]
Glucose	1.019	0.0520[a]	0.0254[b]	0.0936[c]
Maltose	0.744	0.0393[b]	0.0100[a]	0.0123[a]
Maltotriose	4.110	0.1687[b]	0.0925[a]	0.0855[a]
DP 4	0.711	0.0022[b]	0.0005[a]	0.0005[a]
DP 5	0.332	0.0095	–	–
DP 6	0.201	0.0005	–	–
DP 7	0.170	0.0003	–	–
DP 8	0.120	–	–	–
DP 9	0.097	–	–	–
DP 10	0.084	–	–	–

[a,b,c] For each constituent, values with the same letter are not significantly ($p > 0.05$) different.
[d] MPWOG = Membrane permeate without GA treatment.
[e] MPWG = Membrane permeate with immobilized GA treatment.

glucose content in MPWG was signficantly higher ($p < 0.05$) than that in MPWOG and in 1.0% dextrin solution. This demonstrates the technical feasibility of immobilizing GA on a ZOPA membrane. This may be of benefit in continuous production of glucose syrups of higher purity, since many of the low-molecular-weight oligosaccharides are unable to pass through the membrane.

REFERENCES

1 M. Cheryan, *Ultrafiltration Handbook*, Technomic Publ., Lancaster, Basel, 1986, p. 297.
2 H. H. Weetall and W. H. Pitcher, *Science (Washington, D.C.)*, 232 (1986) 1396.
3 O. H. Lowry, N. J. Rosebrough, A. L. Farr and R. J. Randall, *J. Biol. Chem.*, 193 (1951) 265.
4 W. Krakowiak and H. S. Łódź, *Starch/Stärke*, 36 (1984) 60.
5 H. Maeda, S. Kajiwara and N. Q. Araujo, *Eur. J. Appl. Microbiol. Biotechnol.*, 16 (1982) 92.
6 M. M. Bradford, *Anal. Biochem.*, 72 (1976) 248.
7 D. L. McKamy, *Thesis*, Clemson University, Clemson, SC, 1988, p. 22.
8 N. W. H. Cheetham, P. Sirimanne and W. R. Day, *J. Chromatogr.*, 207 (1981) 439.
9 J. R. Brooks and V. K. Griffin, *Cereal Chem.*, 64 (1987) 253.
10 J. R. Brooks and V. K. Griffin, *J. Food Sci.*, 52 (1987) 712.
11 V. K. Griffin and J. R. Brooks, *J. Food Sci.*, 54 (1989) 190.
12 J. J. Warthesen, *Cereal Chem.*, 61 (1984) 194.
13 R. L. Thomas, P. H. Westfall, Z. A. Louvieri and N. D. Ellis, *J. Food Sci.*, 51 (1986) 559.
14 G. J. Fallick and C. W. Rausch, *Am. Lab.*, 11 (1979) 87.

Journal of Chromatography, 536 (1991) 113–121
Elsevier Science Publishers B.V., Amsterdam

CHROMSYMP. 2004

Analysis of protein denaturation by high-performance continuous differential viscometry

P. K. DUTTA*, K. HAMMONS, B. WILLIBEY and M. A. HANEY
Viscotek Corp., 1032 Russell Drive, Porter, TX 77365 (U.S.A.)

ABSTRACT

The intrinsic viscosity of protein solutions changes when denaturation occurs. Therefore, viscosity measurement using traditional glass capillary viscometers has been a key method to study the process of protein denaturation. Such measurements are laborious, time consuming and need at least 10 ml of sample. The Viscotek differential viscometer can be used as an on-line detector for high-performance liquid chromatography to monitor the viscosity of column effluent. In this study, samples were injected using an autosampler onto a "delay" column containing glass beads in place of the high-performance liquid chromatography columns. Results indicate guanidine hydrochloride, heat and pH act as denaturing agents and changes the intrinsic viscosities of serum albumin, turkey egg albumin, and ovalbumin solutions. The differential viscometer is sensitive and provides accurate measurements of minor changes in viscosities of very dilute protein solutions undergoing denaturation. The advantage of using the differential viscometer instead of conventional glass capillary viscometer is the increased sensitivity, precision, speed and operational ease that permits measurements of solution viscosity of low sample concentrations up to 1.2 μg of pure proteins.

INTRODUCTION

Most proteins, globular and fibrous in their native states, are folded into well-defined, essentially rigid, three-dimensional structures [1,2]. The macromolecular nature of these proteins is best understood when they are in a denatured or unfolded state [3]. Denaturation is a non-proteolytic modification of a native protein that leads to definite changes in chemical, physical and biological properties [4]. There are many physical and chemical properties that change during denaturation [5]. These physicochemical changes that occur can be monitored by viscometry, optical rotatory dispersion, circular dichroism, nuclear magnetic resonance and electron spin resonance. The gross conformational changes generally result in the modification of the rheological behavior of proteins in solution. Therefore, viscosity measurement has been a key method in many denaturation studies [3–7]. Viscometry is a useful tool because of its extreme sensitivity and technical simplicity. Since the intrinsic viscosity provides information on the overall size and shape of the molecule, it is a sensitive and simple indicator of denaturation. The intrinsic viscosity of proteins in solution increases when denaturation occurs. Such an increase may correspond to an aggregation of the denatured molecules, a change in the shape of hydrated protein

0021-9673/91/$03.50

molecules, unfolding of the polypeptide chains or anisotropic swelling of the particles. The increase in viscosity is often due to several of these processes which may occur almost simultaneously in a protein solution undergoing denaturation. Thus, it has been found that the globular proteins have very low values of intrinsic viscosity, little more than predicted for a nonsolvated sphere and they increase markedly upon denaturation [7].

Despite its great utility, the solution viscosity method of studying protein denaturation has declined in popularity in recent years. Until very recently, viscometric methods have not kept pace with the rapid evolution of most analytical methods towards sophisticated instrumentation capable of greater sensitivity, speed and ease of operation. Traditional viscometers such as the glass capillary tubes of Ostwald or Ubbelohde [8] are still the most widely used viscometers for solution viscosity measurement today. However, these viscometers require high solute concentrations and lack the speed and sensitivity to meet the needs of viscosity measurements of dilute protein solutions.

In this paper, we have used the Viscotek differential viscometer (DV) [9–12] detector on-line with an isocratic high-performance liquid chromatography (HPLC) setup for measuring viscosity of dilute protein solutions undergoing denaturation. The solutions are dilute enough that a single-point determination of intrinsic viscosity can be made, without the need to exrapolate the viscosities of several sample concentrations. We show that the DV yields a solution viscosity measurement of unmatched sensitivity, precision, speed and operational ease using microlitre injection volumes of very low sample concentration.

EXPERIMENTAL

Chemicals and reagents

Proteins such as bovine serum albumin, chicken egg albumin (ovalbumin), turkey egg albumin, β-lactoglobulin, lysozyme and hemoglobin were obtained from Sigma (St. Louis, MO, U.S.A.). All proteins were used as received, without further purification. Water was HPLC Omnisolv grade from EM Science (Cherry Hill, NJ, U.S.A.) and monobasic sodium phosphate was from Mallinckrodt (Paris, KY, U.S.A.). All other chemicals obtained from commercial sources were used without purification.

The buffer used in the mobile phase was adjusted to the appropriate pH by addition of potassium hydroxide. The mobile phase was filtered through a 0.45-μm membrane (Micro Filtration Systems, Dublin, CA, U.S.A.) and vacuum-degassed.

Sample preparation

Protein solutions were prepared in 5 m*M* NaH_2PO_4 at pH 7.0. Concentrations ranged from 1.5–2.8 mg/ml. The proteins were first dissolved in 5 m*M* NaH_2PO_4 (pH 7.0) and allowed to stand for 30 min. The proteins at this stage show their native state. The protein solutions were heated in a 60°C water-bath in the presence and absence of 0.1 *M* 2-mercaptoethanol for 30 min for the thermal denaturation experiment. In the experiment showing denaturation by guanidine hydrochloride (GuHCl), the proteins were dissolved directly in 4 *M* GuHCl and 0.1 *M* 2-mercaptoethanol to obtain randomly coiled polypeptide chains. For denaturation by changing pH, proteins were dissolved directly in 5 m*M* NaH_2PO_4 having different pH values.

Equipment and condition

The HPLC–DV system was modular in design and consisted of a Micromeritics (Norcross, GA, U.S.A.) Model 728 autosampler, Valco (Houston, TX, U.S.A.) Model EQ60 remote switching valve fitted with a 50-μl loop, Scientific System (State College, PA, U.S.A.) Model 222B HPLC pump and Viscotek (Porter, TX, U.S.A.) Model 110-02 (range adjusted at 4) viscometer detector. Experiments were performed on a "delay" column that was packed with DMCS-treated glass beads (100–200 mesh) in 450 mm × 3 mm I.D. stainless-steel tube (Alltech, Deerfield, IL, U.SA.) in place of usual HPLC packing. The purpose of the delay column is to provide the dispersion effect needed to generate an easily detectable elution profile at finite time. No retentive separation of protein samples was intended. The elution buffer consisted of 5 m*M* NaH_2PO_4 (pH 7.0) with flow-rate maintained at 0.5 ml/min. The protein solutions were analyzed by duplicate injections on the DV while measuring both the inlet pressure and the differential pressure.

A schematic of the DV detector [11,12] is shown in Fig. 1. The pneumatic pulse dampener shown is a PTFE tube (304 mm × 2.5 mm I.D.). Briefly, the protein solution from the delay column flows continuously through the balanced bridge network, which consists of four capillaries (R1–R4). Res 1 is located out of the flowstream and act as a compensate volume reservoir so that any flow-rate fluctuations cause equal pressure changes on each side of the differential pressure transducer. The other reservoir (Res 2) holds up the protein solution and prevents it from entering capillary R4. For any time slice in the elution profile, protein solution will be in capillaries R1, R2 and R3 but the elution buffer will be in capillary R4. Res 1 and Res 2 are large (30

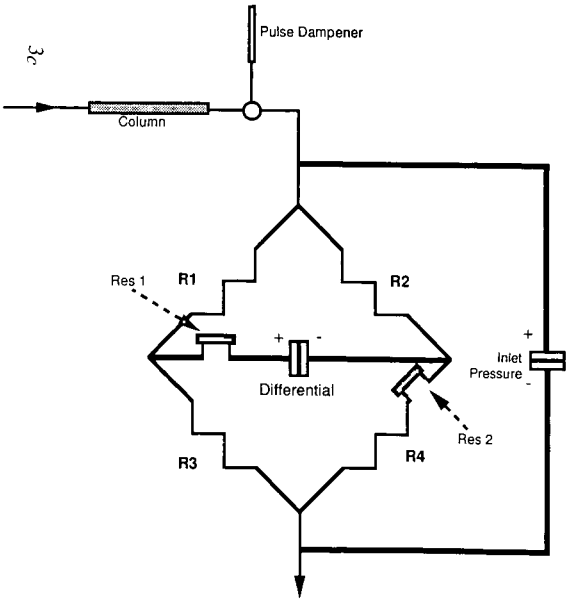

Fig. 1. Simplified schematic diagram of the differential viscometer. See text.

ml) reservoirs so that the 5 m*M* NaH_2PO_4 (pH 7.0) elution buffer is not entirely displaced until after the chromatographic peak is completely eluted. Two pressure measurements are normally made by use of transducers. The differential pressure, ΔP, is due to the difference in the viscosity of the protein solution in capillary R3 and viscosity of the elution buffer in capillary R4. Protein solution viscosities in R1 and R2 cancel each other. Another transducer measures P_i, the inlet pressure into the bridge. The DV detector nulls the solvent pressure as desired yielding a differential (ΔP) signal proportional to the specific viscosity of the protein solution. The DV being highly sensitive, can measure the specific viscosity near zero concentration, thereby obtaining the intrinsic viscosity from a single measurement. The following expression relates the specific viscosity (η_{sp}) to these two pressure measurements [10].

$$\eta_{sp} = 4\Delta P/(P_i - 2\Delta P)$$

The intrinsic viscosity [η], is defined as,

$$[\eta] = (\eta_{sp}/c)_{c \to 0}$$

where c is the concentration of the protein solution in g/dl. In the present experiments, the concentrations and specific viscosities are low enough that the extrapolation implied in the above equation can be neglected.

Calculation

Intrinsic viscosity was calculated [10–12] from data collected using the above equations on an IBM compatible personal computer system with Viscotek's UNICAL software.

RESULTS AND DISCUSSION

In the first experiment, the intrinsic viscosity determinations were made on native proteins. The high sensitivity of the balanced bridge design is illustrated in Fig. 2. The integrated area under the elution peak was used to calculate intrinsic viscosity. In its native state, β-lactoglobulin had higher intrinsic viscosity than other native proteins (Table I). The total time required for analysis of a sample was about 3 minutes, from injection to final computer report. The negative dips (Fig. 2) in the baseline before the peaks seems anomalous and is difficult to explain. This behaviour is not normally observed in size-exclusion chromatography peaks with the viscometer detector. In the present case, with no chromatographic columns to disperse the injected sample, the negative dip may be a result of a very sharp concentration gradient in the viscometer bridge. It is likely that for the very sharp peaks observed in these experiments, a bridge with shorter capillaries would be required. More experiments are presently being conducted to confirm this. However, the intrinsic viscosity values (Table I) reported of the various native proteins are very close to values reported elsewhere [3–5]. The small difference between the observed values reflects the difference in the type of salt concentration and temperature at which the intrinsic viscosity was measured. The precision of the DV technique for determining intrinsic

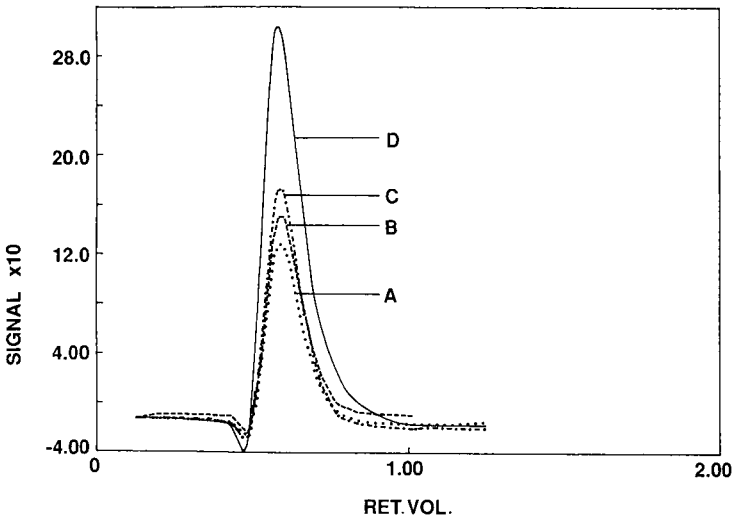

Fig. 2. Elution profile of native proteins dissolved in 5 m*M* NaH_2PO_4 (pH 7). A = Hemoglobin; B = ovalbumin; C = serum albumin; D = β-lactoglobulin. RET. VOL. = Retention volume in ml; signal in mV.

viscosity was excellent. It had a standard deviation of less than 0.002 for duplicate injections. In a separate experiment, we made dilutions of the native protein solutions. It was seen that the differential viscometer was sensitive and precise enough to measure intrinsic viscosity of 1.2 μg of protein samples. There was no direct correlation [13] between molecular weight and intrinsic viscosity (Table I).

Next, we explored the use of the DV as a tool for investigation of the denaturation process. For any protein, the value of intrinsic viscosity after denaturation largely depends on the denaturing agent. Therefore, we investigated the effect of some well known denaturing agents. As illustrated in Figs. 3 and 4, there is an appreciable increase in intrinsic viscosity of both ovalbumin and serum albumin solutions at both acidic and basic pH conditions. The results clearly demonstrate that

TABLE I

INTRINSIC VISCOSITIES OF PROTEINS IN NATIVE STATE AND 4 *M* GUANIDINE HYDROCHLORIDE

Protein[a]	Mol. wt.	Native state, $[\eta]$ (dl/g)[b]	Denatured state, $[\eta]$ (dl/g)[b]
Hemoglobin (A)[a]	64 500	0.017	0.069
Ovalbumin (B)[a]	45 000	0.020	0.163
Serum albumin (C)[a]	66 000	0.022	0.361
β-Lactoglobulin (D)[a]	36 800	0.037	0.113
Turkey egg albumin	45 000	0.020	0.389

[a] This designation corresponds to elution profiles shown in Fig. 2.
[b] Mean of three samples, each injected twice.

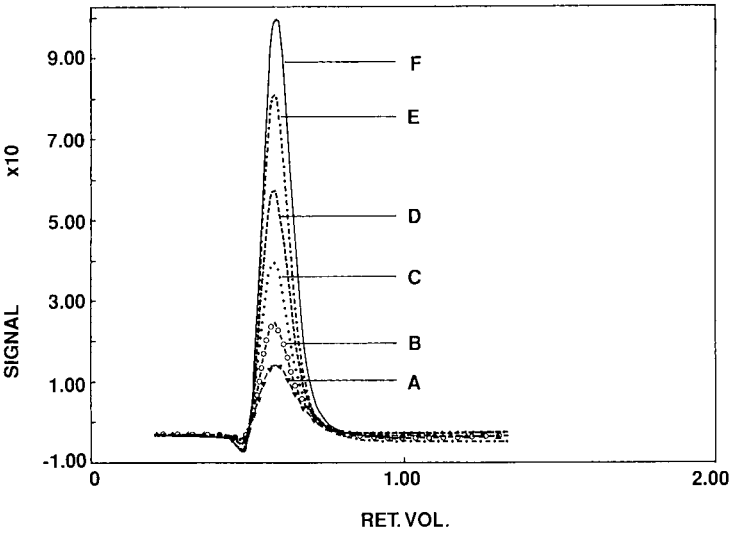

Fig. 3. Elution profile of ovalbumin when exposed to varying pH conditions. A = pH 7; B = pH 2.5; C = pH 4.5; D = pH 6.0; E = pH 8.0; F = pH 12.0. RET. VOL. = Retention volume in ml; signal in mV.

both ovalbumin and serum albumin were subject to structural changes as the pH of these solutions were altered. Increasing acidity possibly caused expansion of the molecules [14] that resulted in the increase of intrinsic viscosity. In the alkaline state, there is a huge increase in intrinsic viscosity because intermolecular disulfide bonds are readily formed, which result in aggregation, gelation or precipitation. Several other reactions leading to irreversible products are also possible [4]. Thus, it is evident that viscosity of protein solutions is complicated by the electrostatically interacting anionic and cationic protein side chains and by their action on water molecules. The viscosity

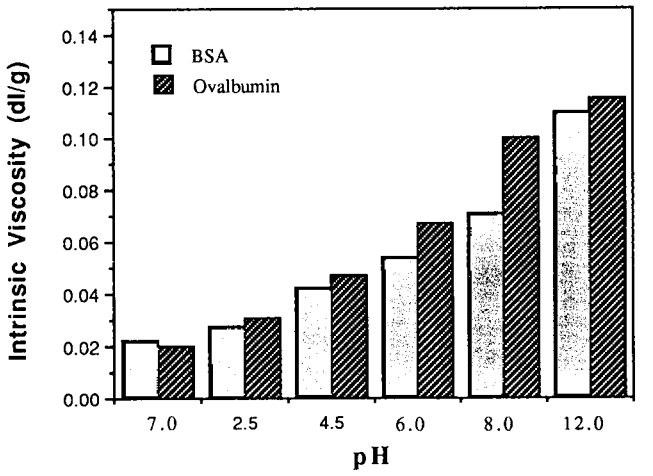

Fig. 4. Effect of varying pH conditions on bovine serum albumin (BSA) and ovalbumin.

of a protein solution therefore depends on the pH of the solution. The rate of denaturation is low at the isoelectric point of the protein and increases in acid or alkaline solutions [4].

The acid denaturation of the serum albumin is interesting. The intrinsic viscosity, which is 0.020 dl/g for the native serum albumin (Fig. 4) rises to only 0.031 dl/g when pH is lowered to 2.5. It proves that only limited expansion of the molecule occurs, which leaves the major globular regions of the molecule intact [15,16].

The effect of temperature on serum albumin, ovalbumin and turkey egg albumin was also investigated (Fig. 5, Table II). There was an increase of intrinsic viscosity upon heating the ovalbumin solution (Fig. 5A). This may be due to aggregation. However, it also immediately suggests a positive enthalpy effect associated with the previously postulated expansion equilibrium [17]. This thermal effect is reversible. When solutions were cooled after brief exposure to 60°C, they regained their original room temperature viscosity values. However, when turkey egg albumin (Fig. 5B) and serum albumin were heated, the intrinsic viscosity value decreased. This is probably due in part to the hydrolysis of the protein [17]. However, when heating was done in the presence of 0.1 m*M* 2-mercaptoethanol, which reduces disulfide bonds, the intrinsic viscosity increased in oval albumin, serum albumin and turkey egg albumin (Fig. 5).

Organic solutes such as GuHCl are powerful denaturating agents for proteins [18]. The action of 4 *M* GuHCl in the presence of 0.1 m*M* 2-mercaptoethanol to reduce disulfide bonds on some native globular proteins was monitored. In all cases (Fig. 5, Table I) the intrinsic viscosity increased [19]. Results obtained here and from optical rotatory measurement [4] clearly demonstrate that proteins in concentrated GuHCl solutions are randomly coiled without their disulfide bonds. The effect of GuHCl on protein conformation can be explained on the basis of free energy effects localized at hydrophobic interactions and peptide groups [18].

The differential viscometry technology can be also very useful in the determination of size [14,18], shape and solvation of proteins together with detection of chemical modification [20] by combination with other techniques. Work on these application areas is presently being performed in our laboratory. Research is also being conducted in our laboratory to develop a HPLC/size-exclusion chromato-

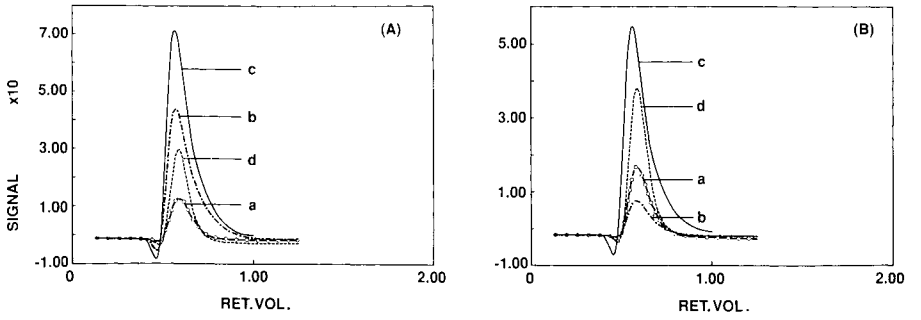

Fig. 5. Elution profile of (A) ovalbumin and (B) turkey egg albumin when exposed to varying denaturating conditions. a = Native protein; b = protein solution heated at 60°C for 30 min; c = protein solution heated at 60°C for 30 min in presence of 2-mercaptoethanol; d = native proteins dissolved in 4 *M* guanidine hydrochloride. RET. VOL. = Retention volume in ml; signal in mV.

TABLE II

EFFECT OF TEMPERATURE ON INTRINSIC VISCOSITIES OF NATIVE PROTEINS

Protein	Intrinsic viscosity (dl/g)[a]		
	Native state	Denatured state	
		Heat[b]	Heat with 2-mercaptoethanol[c]
Ovalbumin	0.020	0.056	0.449
Turkey egg albumin	0.020	0.012	0.360
Serum albumin	0.022	0.010	0.296

[a] Mean of three samples, each injected twice.
[b] Heated in water bath at 60°C for 30 min without any 2-mercaptoethanol.
[c] Heated in water bath at 60°C for 30 min in the presence of 0.1 m*M* 2-mercaptoethanol.

graphy–DV approach that would provide specific information about proteins undergoing the process of denaturation.

The following general statements are made regarding intrinsic viscosity measurement by high-performance continuous differential viscometry technology. (1) The balanced bridge design of the differential viscometer allows measurement of solution viscosity in a routine manner. The precison of the 2 min per sample analysis run time is much superior to that of the Ubbelohde tube for solution viscosity measurement. (2) Intrinsic viscosity measurements on proteins are particularly useful in showing changes in molecular configuration due to denaturation. (3) When globular proteins "denature" by the action of either GuHCl, heat or changing pH, the intrinsic viscosity normally increases. (4) It is possible to use only 1.2 μg of protein for measuring intrinsic viscosities.

ACKNOWLEDGEMENT

We are grateful to Dr. W. W. Yau of E. I. du Pont de Nemours & Co., Inc., Central Research and Development Department, Wilmington, DE, U.S.A., for helpful discussion and critical comments on the manuscript.

REFERENCES

1 M. Levitt and C. Chothia, *Nature (London)*, 261 (1976) 552.
2 J. S. Richardson, *Adv. Protein Chem.*, 34 (1981) 167.
3 C. Tanford, *Adv. Protein Chem.*, 24 (1970) 1.
4 C. Tanford, *Adv. Protein Chem.*, 23 (1968) 121.
5 S. Lapanje, *Physicochemical Aspects of Protein Denaturation*, Wiley, New York, 1978.
6 M. Joly, *A Physico-Chemical Approach to the Denaturation of Proteins*, Academic Press, New York, 1965.
7 J. H. Bradbury, in P. Alexander and R. J. Block (Editors), *A Laboratory Manual of Analytical Methods of Protein Chemistry*, Vol. 3, Pergamon, New York, 1961, Ch. 11, p. 99.
8 L. Ubbelohde, *Ind. Eng. Chem. Ed.*, 9 (1937) 85.
9 M. A. Haney, *J. Appl. Polym. Sci.*, 30 (1985) 3023.

10 M. A. Haney, *J. Appl. Polym. Sci.*, 30 (1985) 3037.
11 M. A. Haney, *Am. Lab.*, 17 (1985) 41.
12 M. A. Haney, *Am. Lab.*, 17 (1985) 116.
13 J. T. Yang, *Adv. Protein Chem.*, 16 (1961) 323.
14 J. T. Yang and J. F. Foster, *J. Am. Chem. Soc.*, 77 (1955) 2374.
15 J. F. Foster, in F. W. Putnam (Editor), *The Plasma Proteins*, Vol. 1, Academic, New York, 1960, p. 179.
16 T. T. Herskovits and M. Laskowski, Jr., *J. Biol. Chem.*, 237 (1962) 2481.
17 J. F. Foster and J. T. Yang, *J. Am. Chem. Soc.*, 77 (1955) 3895.
18 C. Ghelis and J. Yon, *Protein Folding, Academic*, New York, 1982, Ch. 5, p. 223.
19 C. Tanford, K. Kawahara and S. Lapanje, *J. Amer. Chem. Soc.*, 89 (1967) 729.
20 A. Holtzer and S. Lowey, *Biopolymers*, 1 (1963) 497.

Journal of Chromatography, 536 (1991) 123–129
Elsevier Science Publishers B.V., Amsterdam

CHROMSYMP. 2003

Cation-exchange high-performance liquid chromatography of synthetic salmon calcitonin

MARIA E. MUNERA*, FRED R. BORGER, EVERETT FLANIGAN and DILIP K. PARIKH
Armour Division, Rhone-Poulenc-Rorer Pharmaceutical Corporation, Kankakee, IL 60901 (U.S.A.)

ABSTRACT

Several species of calcitonin, namely, porcine, human, and salmon, are of clinical importance. Previous studies have shown that reversed-phase high-performance liquid chromatography (HPLC) can be used for the analysis of synthetic calcitonin. To confirm the homogeneity of synthetic HPLC purified salmon calcitonin, an analytical method, based on cation-exchange HPLC with a linear sodium chloride gradient in phosphate buffer was developed. The method is capable of selectively analyzing salmon calcitonin in complex synthetic matrices, separating it from synthetic by-products and degradation products, and provides a rapid and precise chemical assay for determining calcitonin content and quality.

INTRODUCTION

Salmon calcitonin (SCT) is a single-chain polypeptide, consisting of 32 amino acid residues. It contains a disulfide bridge at the amino terminus, resulting in a seven-residue cyclic structure. The peptide has a carboxyl-terminal proline. Calcitonin is produced by parafollicular cells, wich are located in the thyroid in mammals but are associated with the ultimobranchial body in lower animals, such as the salmon. The major action of calcitonin is to inhibit osteoclast-mediated bone resorption. The hormone is used in the treatment of Paget's disease of the bone, post-menopausal osteoporosis, and in the treatment of hypercalcemia.

Synthetic SCT is prepared by the Merrifield solid-phase peptide synthesis technology [1] with modifications, and purified by ion-exchange, reversed-phase and gel chromatography.

Peptides manufactured by chemial synthesis require exacting definition of their identity. It is necessary to show that the end product of the synthesis has the intended structure and that undesirable synthetic by-products, if detected, are removed from the target peptide, or at least, that quantities of by-products are limited. Finally, it is necessary to show that the characteristics of successive production lots are consistent.

In recent years, reversed-phase high-performance liquid chromatography (RP-HPLC) has become the method of choice for the separation and analysis of a wide variety of peptides and proteins [2–8]. The ability of RP-HPLC to separate deletion analogues and derivatives of SCT has been described [3]. Porcine (PCT), human (HCT), and SCT are resolved easily. The ability to resolve calcitonins from various

0021-9673/91/$03.50

species has been noted by Corran and Zanelli [9] and justifies the use of RP-HPLC, not only for identification, but also for determining the level of impurities.

The impurities generated in the synthetic salmon calcitonin production process may differ from the parent molecule in either size, charge, or hydrophobicity.

RP-HPLC is used to demonstrate the homogeneity of SCT preparations. This technique separates SCT from peptide impurities based on relative hydrophobicity. Since RP-HPLC purification is employed as part of the manufacturing process for SCT, another method employing a different separation principle than RP-HPLC is needed. Experiments that have led to the development of cation-exchange chromatography are described.

EXPERIMENTAL

Materials

PCT and SCT were obtained from the Manufacturing Laboratories of Armour Pharmaceutical Company. HCT was obtained from Sigma (St. Louis, MO, U.S.A.). UV-grade acetonitrile (Burdick & Jackson, Muskegon, MI, U.S.A.), analytical-grade reagents, and distilled, deionized Mill-Q water (Millipore, Bedford, MA, U.S.A.) were used.

Method

Cation-exchange HPLC. Cation-exchange HPLC of SCT was performed on a Bio-Gel TSK, SP-5PW (75 × 7.5 mm I.D.) column (Bio-Rad, Richmond, CA, U.S.A.). The flow-rate was 1.0 ml/min. The mobile phases consisted of 20 m*M* potassium phosphate buffer (pH 6.8), containing 5% (v/v) acetonitrile and 20 m*M* potassium phosphate buffer, 500 m*M* NaCl (pH 6.8), containing 5% (v/v) acetonitrile. A linear gradient from 0–100% B in 20 min was employed. The injection volume was 200 μl and the peptides were detected at 220 nm and 0.1 a.u.f.s.

Instrumentation. A Beckman Model 322 liquid chromatograph, equipped with 112M pumps, and a Hewlett-Packard Model 1000F series computer, equipped with a Beckman computer automated laboratory system was used. The pumps were connected to a SP8500 dynamic mixer prior to a WISP (710B) autosampler. A Kratos Spectroflow 773 provided UV detection at 220 nm.

RESULTS

Comparison between RP-HPLC and cation-exchange HPLC

A comparison of the cation-exchange chromatograms (Fig. 1) and the reversed-phase chromatogram (Fig. 2) for lot D520-148A, shows that the cation-exchange method is capable of separating SCT from peptide impurities with a resolution very similar to RP-HPLC.

The resolving power of cation-exchange HPLC is further emphasized by Fig. 3, which shows the separation of three deletion peptides from SCT. The delection analogues, des(Asp-3)SCT, des(Leu-16)SCT, and (22–32)SCT fragment are easily separated from each other and from SCT.

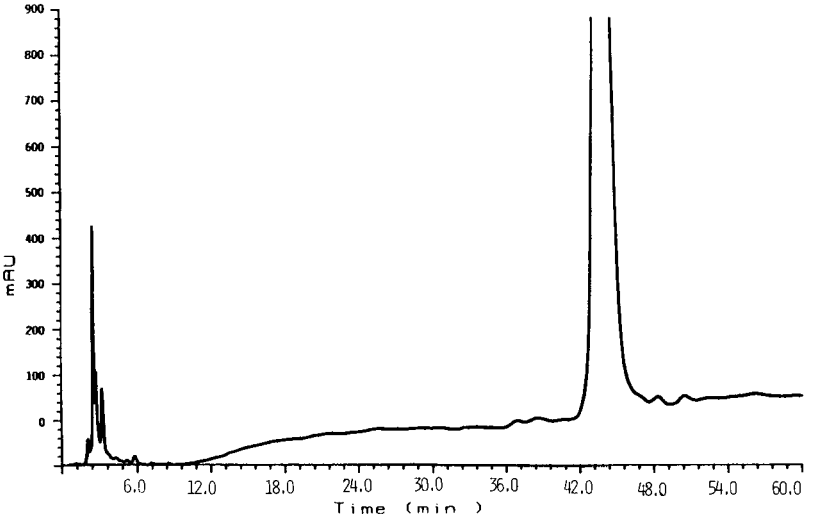

Fig. 1. RP-HPLC of SCT. Column, B&J OD5 C_{18} (250 × 4.6 mm I.D.). Linear AB gradient (1% B/min), where solvent A is 0.054 *M* KH_2PO_4 in water–acetonitrile–methanol (75:20–5, v/v/v) (pH 2.86) and solvent B is acetonitrile–methanol (80:20, v/v), flow-rate, 1 ml/min; injection volume 200 μl, concentration 0.2 mg/ml. Detection at 220 nm.

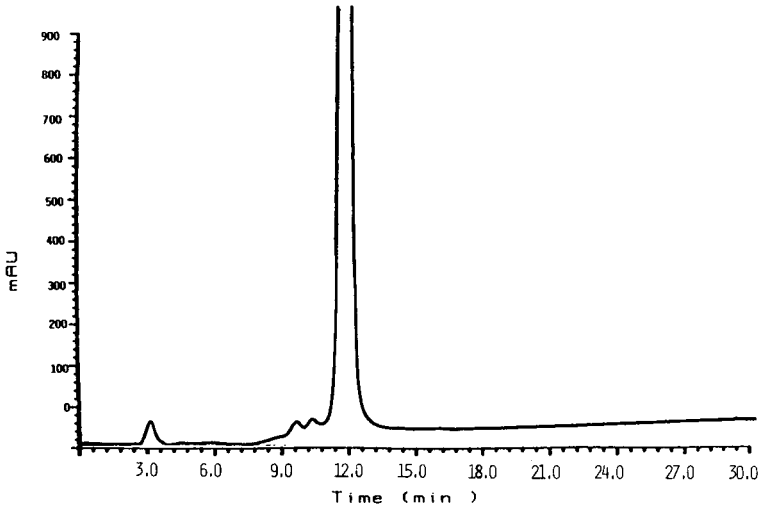

Fig. 2. Cation-exchange HPLC of SCT. Column Bio-Rad Bio-Gel TSK, SP-5PW (75 × 7.5 mm I.D.). Linear AB gradient (5% B/min), where solvent A consisted of 20 m*M* potassium phosphate buffer (pH 6.8), containing 5% (v/v) acetonitrile and solvent B is 20 m*M* potassium phosphate buffer, 500 m*M* sodium chloride (pH 6.8), containing 5% (v/v) acetonitrile. Injection volume 200 μl, concentration 0.2 mg/ml. Detection at 220 nm.

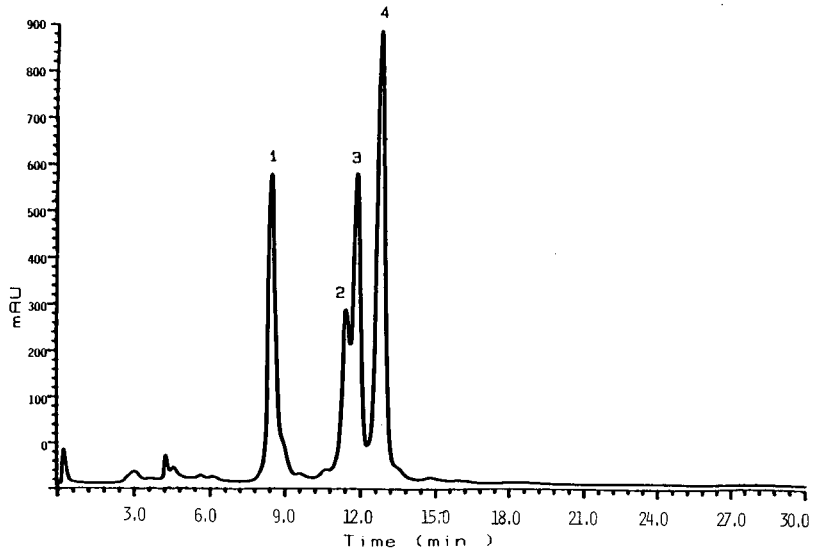

Fig. 3. Cation-exchange HPLC of a mixture of SCT analogues. Peaks: 1 = des(Asp^3)SCT; 2 = des-(Leu^{16})SCT; 3 = SCT; 4 = fragment (32–22)SCT. Conditions as in Fig. 2.

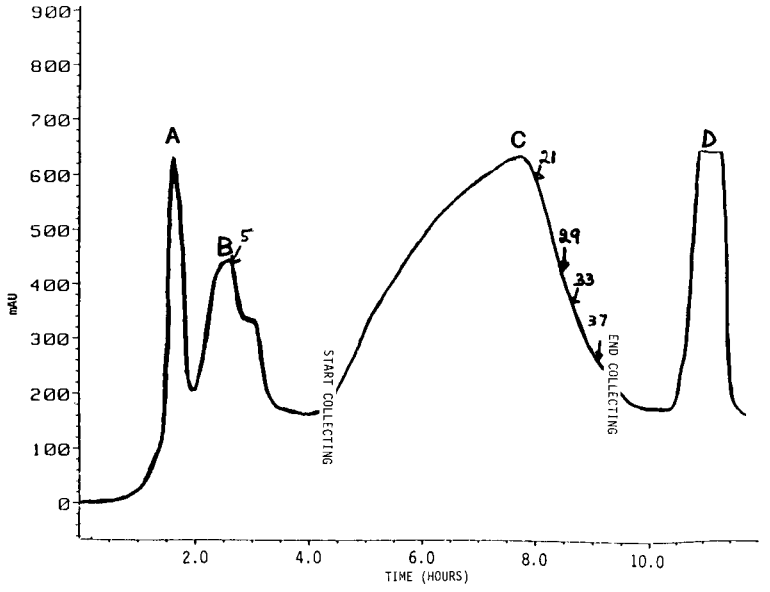

Fig. 4. Production ion exchange (column 3) chromatography of crude calcitonin solution. Fractions between 4.5 and 9.0 h are normally saved for further purification by RP-HPLC. Detection at 220 nm.

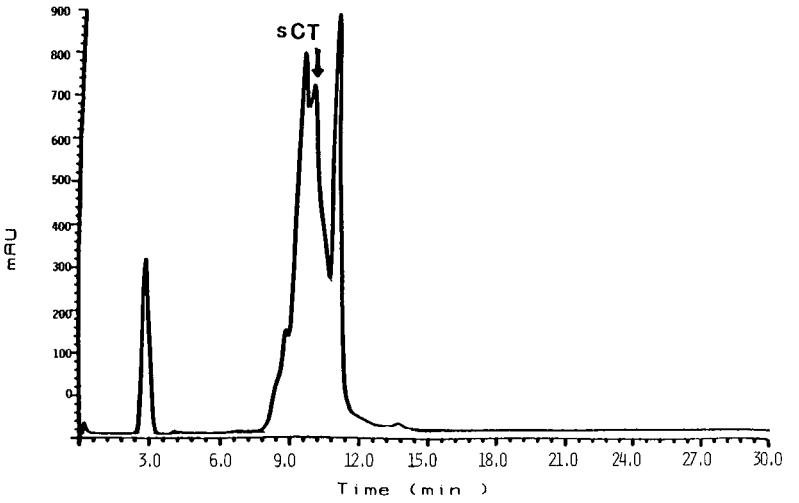

Fig. 5. Cation-exchange HPLC of a mixture of peptides from position B-5 of process ion-exchange column 3. Fraction retention time = 2.7 h. Column, gradient and detection as in Fig. 2. Injection volume 20.0 μl. Concentration (1–1000) of process ion-exchange column 3 eluent.

Resolution and selectivity

The ability of cation-exhange HPLC to separate SCT from by-products of the manufacturing process was investigated by chromatographic analysis of in-process samples obtained during the purification steps (*e.g.*, the eluent from a production in-exchange column). The elution profile of this column monitored at 220 nm shows four peaks, A, B, C, and D as identified in Fig. 4. Figs. 5–7 show the cation-exchange

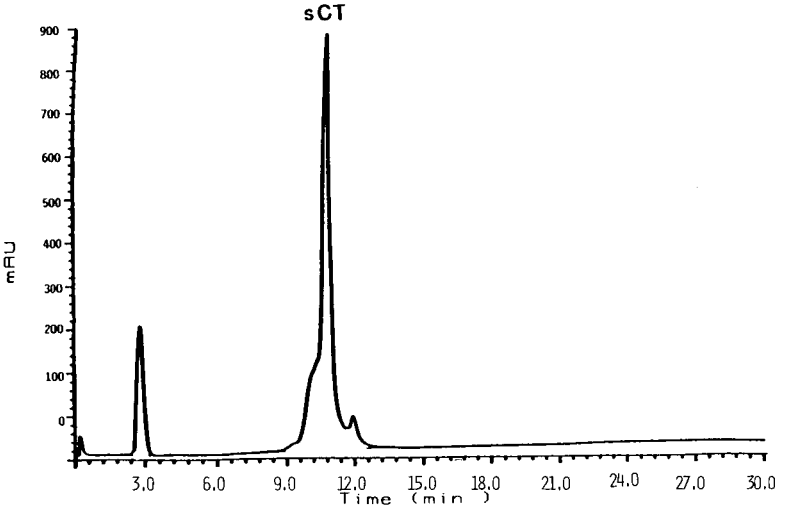

Fig. 6. Cation-exchange HPLC of peptides from position C-21 of process ion-exchange column 3. Fraction retention time = 8.2 h. Column, gradient and detection as in Fig. 2. Injection volume 20.0 μl.

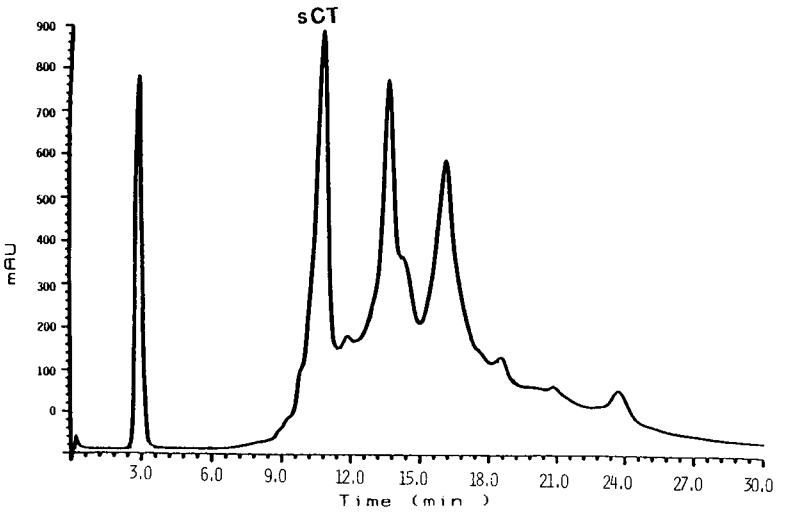

Fig. 7. Cation-exchange HPLC of peptides, polymers, dimers, and trimers from peak D of process ion-exchange column 3. Fraction retention time = 11.0 h. Conditions as in Fig. 2. Concentration (1–1000) of process ion-exchange column 3 eluent.

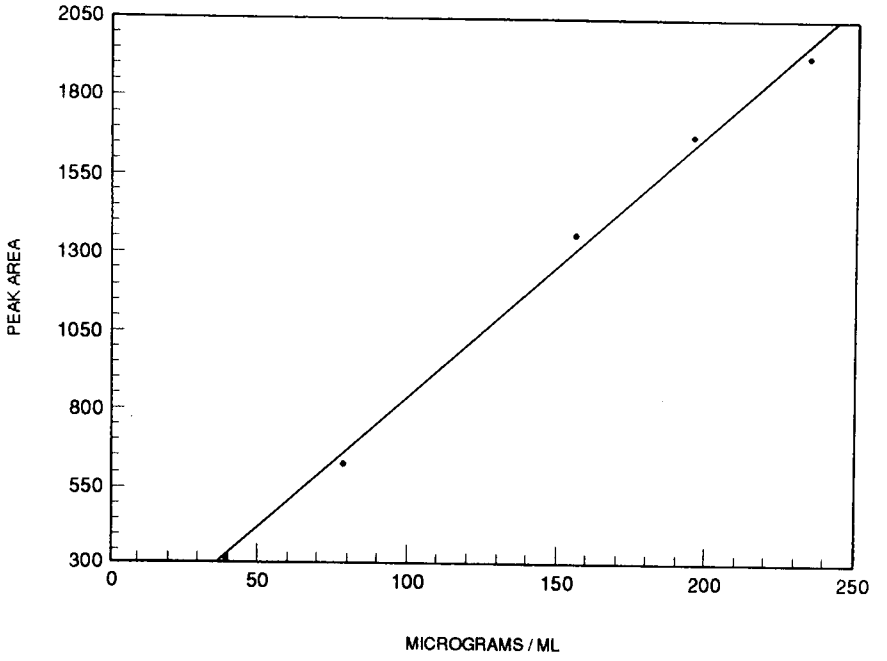

Fig. 8. Calibration plot for SCT. Peak area percent is used to correct for actual concentration of SCT peptide in the samples. Correlation coefficient = 0.999. x-intercept = 0.85 mg/ml, y-intercept = −0.156 area counts.

chromatograms for the analysis of several fractions taken from peaks B, C, and D of the eluent from the production column of the purification process. These chromatograms show that cation-exchange HPLC has the sufficient resolving power to separate SCT from a complex synthetic matrix, which contains fragments, deletion, and chemically modified sequences of SCT.

Calibration plot

The linearity of response has been investigated from 50–150% of the operating range of the assay. The pertinent statistical parameters as calculated for the peak response and the calibration plot are shown in Fig. 8. In general, the data exhibit excellent linearity over the specified range regardless of whether quantification is performed by peak area (correlation coefficient greater than 0.998) or peak height (data not shown).

DISCUSSION

Our studies show that cation-exchange HPLC is capable of separating and selectively analyzing HPLC-purified salmon calcitonin from its process by-products, impurities, and related peptides with resolution similar to that obtained by RP-HPLC [3,10].

These studies with cation-exchange HPLC further confirm the homogeneity of HPLC-purified salmon calcitonin. As shown, cation-exchange HPLC easily identifies SCT analogues which are similar in molecular weight, but have different molecular charges. Variation of the acetonitrile content and buffer salt concentration suggests that the cation-exchange HPLC system separates the peptides mainly by the net charge of the peptides.

REFERENCES

1 R. B. Merrifield, *Adv. Enzymol.*, 23 (1969) 221–296.
2 G. S. Fullmer and R. H. Wasserman, *J. Biol. Chem.*, 254 (1979) 7208.
3 M. L. Heinitz, E. Flanigan, R. C. Orlowski and F. E. Regnier, *J. Chromatogr.*, 443 (1988) 229–245.
4 F. E. Regnier, *Science (Washington, D.C.)*, 238 (1987) 319–323.
5 J. L. Meek, *Proc. Natl. Acad. Sci.*, 77 (1980) 1632–1637.
6 J. L. Meek and Z. L. Rossetti, *J. Chromatogr.*, 211 (1981) 15–19.
7 J. M. R. Parker, D. Gno and R. S. Hodges, *Biochemistry*, 25 (1986) 5424–5429.
8 M. Kunitai, D. Johnson and C. R. Snyder, *J. Chromatogr.*, 371 (1986) 319–323.
9 P. H. Corran and J. M. Zanelli, in W. S. Hancock, (Editor), *Handbook of HPLC for Separation of Amino Acids, Peptides and Proteins*, Vol. II, CRC Press, Boca Raton, FL, 1984, pp. 445–459.
10 W. J. Mayer, D. K. Parikh and D. A. Long, *J. Chromatogr.*, 536 (1991) in press.

Journal of Chromatography, 536 (1991) 131–135
Elsevier Science Publishers B.V., Amsterdam

CHROMSYMP. 2047

Phosphate-gradient high-performance liquid chromatographic method for the analysis of synthetic salmon calcitonin

WILLIAM J. MAYER*,[a], DAVID A. LONG and DILIP K. PARIKH
Armour Division, Rhône-Poulenc Rorer, P.O. Box 511, Kankakee, IL 60911 (U.S.A.)

ABSTRACT

A gradient reversed-phase high-performance liquid chromatographic method was developed for the quantitative analysis of salmon calcitonin. A 0.054-*M* potassium monobasic phosphate buffer was modified with an acetonitrile–methanol (4:1) mixture as the mobile phase. Several gradient slopes are used during the separation and analysis so that potential peptidal component impurities in salmon calcitonin samples can be separated without wasting analysis time. The method is applicable to the determination of salmon calcitonin in the peptide portion of the sample as well as in the total sample. The analytical results are expressed as percent chromatographic purity instead of activitiy units.

INTRODUCTION

Salmon calcitonin (sCT) is a synthetic 32 amino acid peptide (Fig. 1) that is used primarily for the treatment of post-menopausal osteoporosis and Paget's disease. Other indications include general osteoporosis, osteogenesis imperfecta, and as an analgesic.

Isocratic high-performance liquid chromatographic (HPLC) separations of sCT were reported previously [1–3] but without any details about the chromatographic efficiency. The Merrifield synthesis process, while very efficient at synthesizing the 32 amino acid peptide chain, also produces a significant number of impurity peptidal components which are similar to salmon calcitonin. While most of these components are removed by chromatographic purification steps [1], it was necessary to develop an analytical gradient HPLC system capable of a separation based on very slight differences in component polarities. At the same time, it was desirable to save time. It was decided to concentrate our efforts on separating the peptidal components which have

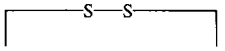

Cys-Ser-Asn-Leu-Ser-Thr-Cys-Val-Leu-Gly-Lys-
Leu-Ser-Gln-Glu-Leu-His-Lys-Leu-Gln-Thr-Tyr-
Pro-Ary-Thr-Asn-Thr-Gly-Ser-Gly-Thr-Pro-NH2

Fig. 1. Structure of salmon calcitonin

[a] Present address: Rhône-Poulenc Rorer, 500 Virginia Drive, Ft. Washington, PA 19034, U.S.A.

0021-9673/91/$03.50

similar polarity —and therefore similar HPLC retention times— as sCT. The remaining components, mostly non-peptidal, would be eluted at the beginning of the chromatogram, while retained peptide-like components would be eluted at the end of the gradient. By modifying the initial mobile phase conditions and employing fast and shallow gradient profiles [4], it was possible to effect nearly complete separation of sCT from the other peptidal components of the sample within a reasonable time, *i.e.*, < 1 h.

EXPERIMENTAL

A modular HPLC system was used for the analysis. It consisted of a Spectra-Physics Model 8700 gradient pumping system with a dynamic mixer (San Jose, CA, U.S.A.) and a Beckman Model 501 Automatic sample injector (Fullerton, CA, U.S.A.). An LDC Spectromonitor III variable-wavelength UV detector (Rivera Beach, FL, U.S.A.) was used to monitor the column effluent. Samples were separated on a B&J OD5 (octadecylsilane, 5 μm) 25 cm $\times$ 4.6 mm I.D. column, obtained from American Scientific Products (McGaw Park, IL, U.S.A.). Data were collected on a Hewlett-Packard HP 1000 minicomputer with CALS software from CIS-Beckman (Waldwick, NJ, U.S.A.).

Doubly distilled water was obtained from an in-house distillation system. Chrompure HPLC-grade acetonitrile and methanol as well as the potassium monobasic phosphate were obtained from Burdick & Jackson (McGaw Park, IL, U.S.A.). sCT standards and samples were obtained from the peptide synthesis department at Armour Division.

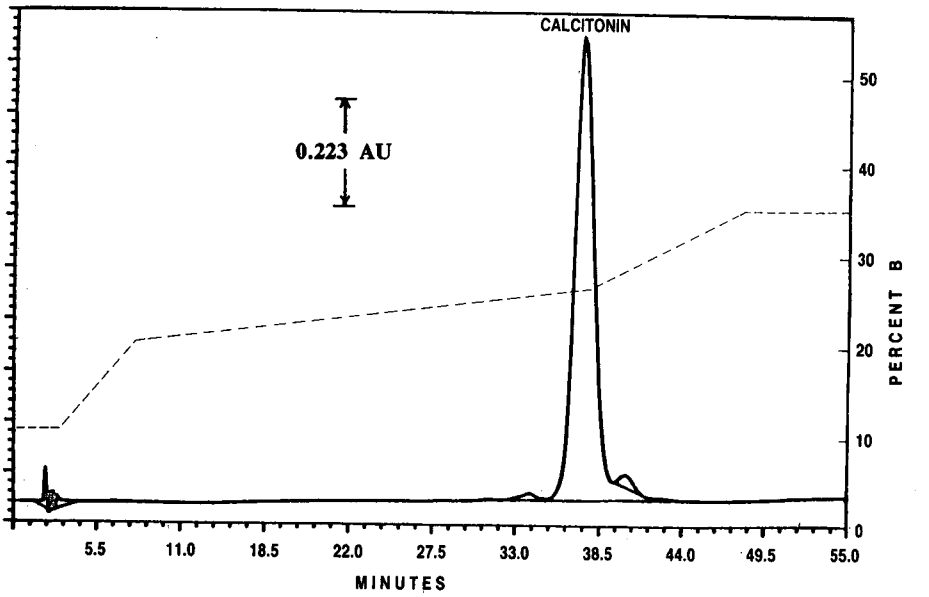

Fig. 2. Typical separation of salmon calcitonin as described in text. CALS integration system factors set to perform tangent skim of peaks immediately following the salmon calcitonin peak.

Phosphate buffer

Potassium monobasic phosphate solution (0.054 *M*) was adjusted to a pH of 2.86 with 85% phosphoric acid. After filtration through a 0.45-μm PTFE filter (Alltech, Deerfield, IL, U.S.A.), three volumes of the buffer were mixed with one volume of the organic phase to make mobile phase A.

Organic phase

Acetonitrile–methanol (4:1). A portion of organic phase was mixed with the phosphate buffer to make mobile phase A and the rest was used as mobile phase B.

Gradient elution

The gradient controller on the Spectra-Physics 8700 pumping system was used to make the gradient profile as shown in Fig. 2. The flow-rate was kept constant at 1.0 ml/min. After a 15-min equilibration time, a blank gradient was run in order to equilibrate the system, and to ascertain that no unexpected peaks (primarily from the aqueous buffer source) would be eluted during the gradient separation.

Approximately 2 mg of each of the sCT samples and standards were dissolved in enough buffer–organic (64:36) mixture to make 10 ml of solution; 100-μl sample injections were made into the HPLC system.

RESULTS AND DISCUSSION

A typical separation of a sCT sample is shown in Fig. 2. With this gradient system sCT has a retention time of *ca.* 38 min. During the critical part of the separation, the amount of the organic component could vary by only 0.1875% per

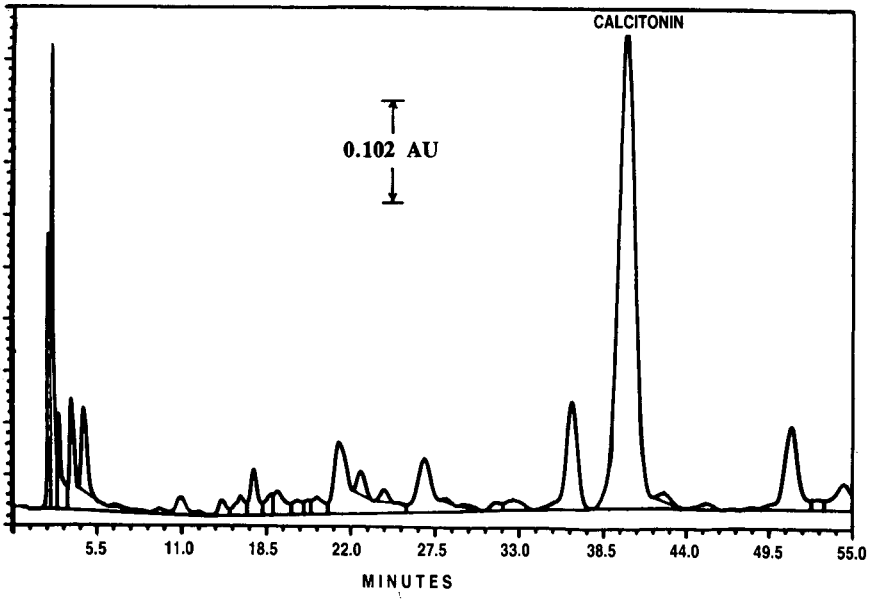

Fig. 3. Separation of a crude extract of sCT. (For conditions, see text.)

minute (0.25% per minute of mobile phase B). This is on the same order as that recommended for the gradient elution of peptide digests [5]. A tangent skim of the peaks immediately following on the tail of the sCT peak produces the most accurate area of the sCT peak as well as better peak symmetry than either a perpendicular drop or forcing a baseline at the valley points.

The peak area calibration plot gave a linear regression with a correlation coefficient of 0.9983 with x and y intercepts of -0.25 (μg/ml) and 0.123 (area counts), respectively.

As the tangent skimming peak integration process always brings into question the reproducibility of the system, a series of ten standard sCT injections were monitored during an extended analytical run of 20 sCT samples. The standard peak areas were reproducible with relative standard deviation of 0.64%. There were no problems with the ability of the CALS software to reproducibly determine when the detector signal returned to the prescribed baseline. The small peak on the tailing side of the sCT peak also was reproducibly "skimmed" from the sCT peak without any difficulty. With a relative standard deviation (R.S.D.) of only slightly less than 1%, it is also likely that we are at the limit of the ability of the Beckman 501 autosampler to inject 100 μl of sample reproducibly after flushing the sample loop and connecting tubing.

The retention time of the sCT peak has a tendency to change slightly from day-to-day and run-to-run. We have noticed that two factors in particular are responsible for this variance, *i.e.*, freshness of the mobile phase and the column condition. Over a 13 h analytical run, the retention time of sCT would increase by 1 min. The lengthening of the retention time for sCT during the assay is likely the result of the preferential evaporation of the organic components from mobile phase A during the continuous helium sparging as refilling the mobile phase reservoirs with fresh mixtures reduces the retention time to that obtained originally. The retention times of sCT on three different B&J OD5 columns ranged from 35.5 to 39.8 min. As these columns had various histories prior to their use for the separation of sCT, the variation observed was not considered significant.

The effects of the pH and the organic content of the initial mobile phase conditions on the retention times was investigated. Of primary concern was any effect on the retention time of sCT. While the procedure is quite specific about the pH of the phosphate buffer prior to mixing, it was found that varying the pH of the buffer from 2.80 to 2.90 while holding the organic content constant resulted in very little change of the sCT retention time. However, modifying the organic content of mobile phase A from 24.5 to 25.5% produces a considerable change in the retention time. A difference of 0.5% in the organic solvent concentration can produce as much as a 5.7% change in the retention time. This is not entirely unexpected, as the gradient slope is sufficiently shallow during the major part of the separation that the difference in retention times is roughly equivalent to the time it would take for the gradient to catch up to the mobile phase composition at the time of the sCT elution during a normal assay. sCT will be eluted only when the mobile phase composition is within a narrow range as the retention times of molecules with higher molecular weight are much more sensitive to slight changes in organic composition than are lower molecular-weight molecules [6]. However, the separation of sCT from other peptidal components does not deteriorate with this change in retention time.

This procedure is suitable for the determination of sCT as either a percent of the

entire sample or as a percent of only the peptidal portion of the sample. The determination of the peptidal portion of the sample requires the assumption that the peaks near the void volume are non-peptidal and due to salts, solvents, etc., from the synthesis and sample preparation of sCT. Non-peptidal assignments also are based on the chromatographic profile of the excipients expected in the material. A well-characterized primary reference standard is then used to determine the amount of sCT as a percent of the entire sample. For some highly purified sCT samples it was quite easy to determine a peptidal purity of 98.5% as sCT and a total sample analysis of 93.5% as sCT.

The resolving power of this system is demonstrated by Fig. 3, which shows the separation of a crude extract of sCT. The crucial portion of the separation is its ability to resolve impurities following the elution of sCT from the sCT peak. With the CALS software it is possible to perform a tangent skim of the impurities from the sCT peak and thus provide the best approximation to the peak area of sCT. If need be, the integration parameters can be modified to obtain the best fit for the peak area determination of both sCT and the impurities being monitored.

REFERENCES

1 M. L. Heinitz, E. Flanigan, R. C. Orlowski and F. E. Regnier, *J. Chromatogr.*, 443 (1988) 229; and ref. 17 cited therein.
2 P. Rivaille, D. Raulais and G. Milhaud, *J. Chromatogr. Sci.*, 12 (1979) 273.
3 E. C. Nice, M. Capp and M. J. O'Hare, *J. Chromatogr.*, 185 (1979) 413.
4 M. Knip, *Horm. Metabol. Res.*, 16 (1984) 487.
5 M. T. W. Hearn, *J. Liq. Chromatogr.*, 3 (1980) 1255.
6 J. W. Dolan, *LC · GC*, 4 (1986) 1178.

Journal of Chromatography, 536 (1991) 137–142
Elsevier Science Publishers B.V., Amsterdam

CHROMSYMP. 2050

Isocratic high-performance liquid chromatography–photodiode-array detection method for determination of lysine- and arginine-vasopressins and oxytocin in biological samples

PARINAM S. RAO*, GERALD S. WEINSTEIN, DAVID W. WILSON, NISA RUJIKARN and DENIS H. TYRAS

Division of Cardiothoracic Surgery, Long Island Jewish Medical Center, New Hyde Park, NY 11042 (U.S.A.)

ABSTRACT

A simple, isocratic, sensitive (1 ng), and specific high-performance liquid chromatographic (HPLC) method based on photodiode-array detection (PAD) is described for simultaneous quantitation of the bioactive peptides, lysine vasopressin (LVP), arginine vasopressin (AVP) and oxytocin (OXY). Acidified pig plasma and left ventricular (LV) tissue samples were first extracted with Sep-Pak C_{18} columns, and the bioactive peptides were eluted with methanol, then dried at 37°C and reconstituted with HPLC mobile phase. The bioactive peptides were separated by HPLC on a Dynamax 3009-A C_8 column with a mobile phase of 0.1% trichloroacetic acid–50 m*M* heptanesulfonic acid–30m*M* triethylamine–20% acetonitrile in water, pH 2.5 and identified with a Waters 990-PAD system (spectrum index plots in the range 200–400 nm). Standards of LVP, AVP and OXY and their mixtures showed a linear increase in the range 5 to 100 ng and were eluted at 6.1, 6.9 and 4.6 min, respectively. Spectrum analysis showed a distinct absorption peak at 280 nm, corresponding to peptide bonds. The reproducibility of the method coefficient of variation for standards is 6.9, 5.8 and 4.7% for LVP, AVP and OXY, respectively.

In plasma and tissue it is much higher: 12.9% (LV tissue) and 18.6% (plasma) for LVP. Pig plasma contains negligible amounts of AVP and OXY; LVP is much higher (0.28 ± 0.19 ng/ml). In pig tissue, LVP predominates (6.95 ng/g wet weight) compared to AVP (1.45) and OXY (1.50). Spectral analysis is necessary to identify the bioactive peptide peaks among interfering substances and to increase the sensitivity four-fold. The method described here is useful for the simultaneous determination of LVP, AVP and OXY in the nanogram range and can be extended to picogram levels by employing PAD spectral analysis techniques.

INTRODUCTION

The bioactive peptide hormones in this study are important clinical and pharmaceutical substances [1]. Lysine vasopressin (LVP) is an antidiuretic, arginine vasopressin (AVP) has antidiuretic, pressor and neurotransmitter activity [2]. Oxytocin (OXY) is used as a birth-inducing and lactation agent. The hormones are synthesized in the hypothalamus (AVP) and paraventricular nucleus (LVP) of primates [3] and transported to the posterior pituitary for storage and eventual release. Vasopressins

0021-9673/91/$03.50

are released in response to hyperosmolality, hypovolemia, hypotension, emotional stress, posture, temperature and with many pharmacological agents [4]. Vasopressin assays are clinically useful in hyponatremia, diabetes insipidus and in antidiuretic hormone as a neurotransmitter [5]. Radioimmunoassay kits for AVP measurements are available [6], but not for LVP or OXY. Pig plasma predominantly contains only LVP and its measurement is very important for elucidating its role after acute hemorrhage and during prolongation of hypovolemia and hypotension in developing swine.

We describe here a direct isocratic high-performance liquid chromatography (HPLC)–photodiode-array detection method for simultaneous determination of LVP, AVP and OXY in standard mixtures and in biological samples.

EXPERIMENTAL

Materials

HPLC-grade acetonitrile (Fisher, Springfield, NJ, U.S.A.) was used. Analytical grade chemicals were obtained from the following sources: trifluoroacetic acid (Fisher), heptanesulfonic acid (Waters PIC-B7, Milford, MA, U.S.A.), and triethyl amine (Kodak, Rochester, NY, U.S.A.). Water was purified with a Milli-RO and Milli-Q filtration system (Millipore, Bedford, MA, U.S.A.).

The HPLC system consisted of a Waters 510 HPLC pump system, coupled to a Waters 840 Data and Chromatography Control Station with a Waters U6K injector and a Waters 990 photodiode-array system, PAD (Waters Assoc., Milford, MA, U.S.A.). The column used was a Dynamax 300-A C_8, measuring 5 mm by 28 cm (Rainin Instruments, Woburn, MA, U.S.A.). Injections were made with a 25-μl Hamilton syringe (Waters Assoc.).

Methods

The mobile phase consisted of 0.1% trifluoroacetic acid–50 m*M* heptanesulfonic acid–30 m*M* triethyl amine–20% acetonitrile in water (pH adjusted to 2.5 with Na_2HPO_4) filtered through the Duropore filter (0.22 μm) (Waters Assoc.) and degassed on the day of use. The flow-rate was 1 ml/min, and the sample volume injected was 20 μl. The UV absorption spectral index and spectrum analysis were performed with the PAD technique in the range 200–400 nm.

Standards of AVP, LVP and OXY (Calbiochem, La Jolla, CA, U.S.A.) and their mixtures (1–100 ng) were used. Pig EDTA plasma (2 ml) of LV tissue (500 mg homogenized in 6 ml 0.1 *M* Tris, pH 7.4) was acidified with 200 μl of 1 *M* hydrogenchloride (pH 3.0). Extraction of biopeptides from plasma was performed using methanol washed octadecasilyl-silica (ODS-Silica) columns (Waters Assoc.). The peptides were then eluted from the column with 3 ml of methanol over a period of 3 min and with another 2 ml for 1 min. The methanol eluate was evaporated to dryness in a 37°C bath under an air jet. After complete drying, specimens were reconstituted with 200 μl of mobile phase, ready for analysis by HPLC.

RESULTS AND DISCUSSION

The spectrum index and spectrum analysis plots with a standard mixture (10 ng) of AVP, LVP, and OXY are shown in Fig. 1. Oxytocin has a retention time of 4.6

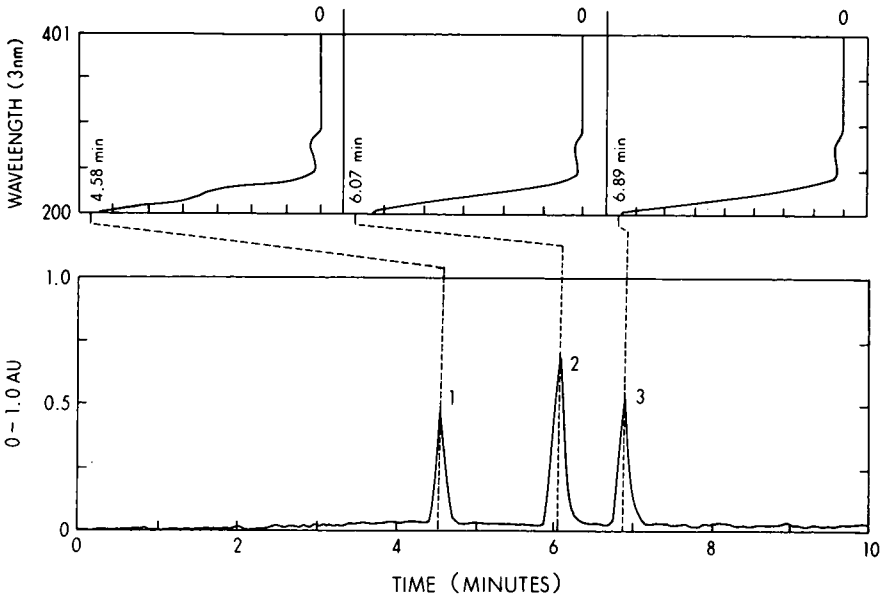

Fig. 1. Spectrum index plot of a standard (10 ng) mixture of (1) OXY (4.58 min), (2) LVP (6.07 min) and (3) AVP (6.89 min). The absorption spectra of the retention time peaks in the range 200–401 nm (inset, top).

TABLE I

PRECISION OF THE METHOD (COEFFICIENT OF VARIATION, C.V.)

Sample	Range (ng)	C.V. (%)		
		Standard (n = 15)	Pig LV tissue[a] (n = 5)	Pig plasma[a] (n = 5)
AVP	10–100	6.9	19.6	24.6
LVP	20–100	5.8	12.9	18.6
OXY	5–100	4.7	15.5	17.8

TABLE II

NORMAL VALUES IN PIG LV TISSUE AND PLASMA

Results are mean values ± S.D. (n = 5)

Sample	AVP	LVP	OXY
Pig LV tissue (ng/g wet weight)	1.45 ± 1.30	6.95 ± 4.75	1.50 ± 0.95
Pig plasma (ng/ml	0.05 ± 0.09	0.28 ± 0.19	0.10 ± 0.11

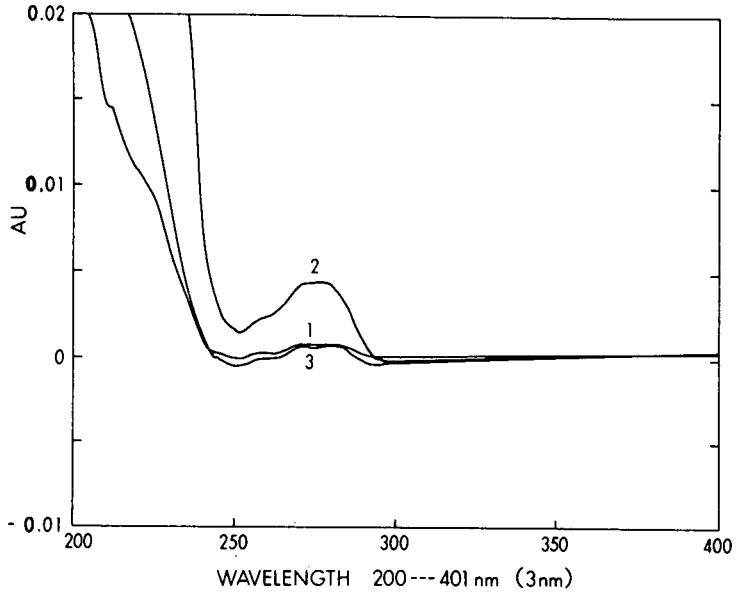

Fig. 2. Spectrum analysis plot of a standard (10 ng) mixture of (1) OXY, (2) LVP and (3) AVP (peak at 280 nm).

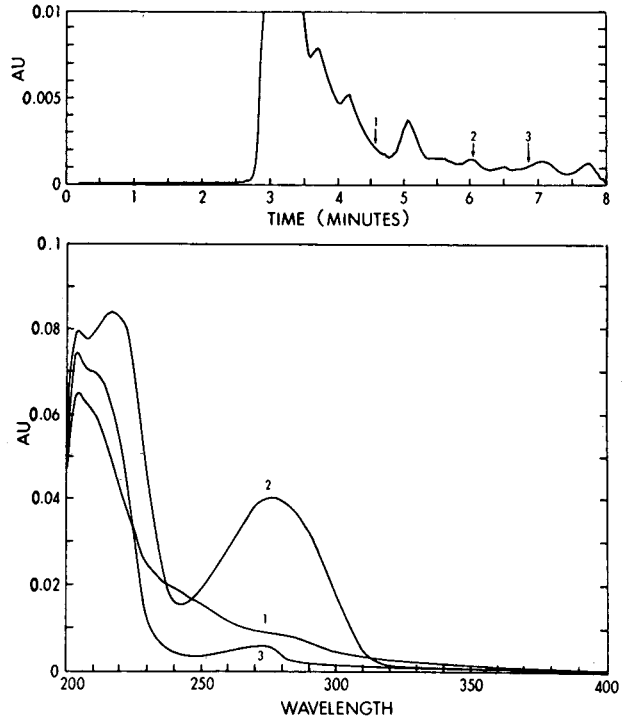

Fig. 3. Spectrum index (top) and spectrum analysis (bottom,) plots of Pig plasma. 1 = OXY (4.58 min); 2 = LVP (6.07 min); 3 = AVP (6.89 min).

min and appeared first, followed by LVP (6.1 min) and then AVP (6.9 min). All three have absorption maxima at 280 nm (top, Fig. 1). A linear increase with each standard in the range 1–100 ng was obtained, validating the method. The reproducibility of the method for duplicates ($n = 15$) is presented in Tables I and II. For standards, the C.V. values were 6.9, 5.8 and 4.7% for LVP, AVP and OXY, respectively. Inclusion of heptanesulfonic acid (ion-pairing agent) and triethyl amine (peak symmetry) and adjustment of pH to 2.5 with phosphate buffer (ion-exchange effect) gave very distinct peaks with good separation within 8 min. In the absence of the above agents (pH *ca.* 1.2), LVP and AVP were eluted at the same retention time (3.8 min) followed by OXY (5.0 min), making quantitation of LVP/AVP impractical.

Spectrum analysis of the standards (Fig. 2) shows characteristic absorption peaks at 275–280 nm for all three peptides. OXY, in addition, has a distinct additional peak at 225 nm, while the others continue to have a peak at about 200 nm.

Photodiode array spectral index analysis of pig plasma (Fig. 3) shows many small indiscrete peaks, probably from other bioactive peptides. The AVP and OXY are negligible (top, Fig. 3) and LVP (6.07 min) shows an absorption peak at 275 nm (absorbance = 0.04), corresponding to 0.26 ng/ml. This value is high compared to the levels (5–10 pg) reported by radioimmunoassay method and most of it may be due to the interfering peak at 6.5 min. Pig. LV tissue spectrum index analysis (Fig. 4) reveals

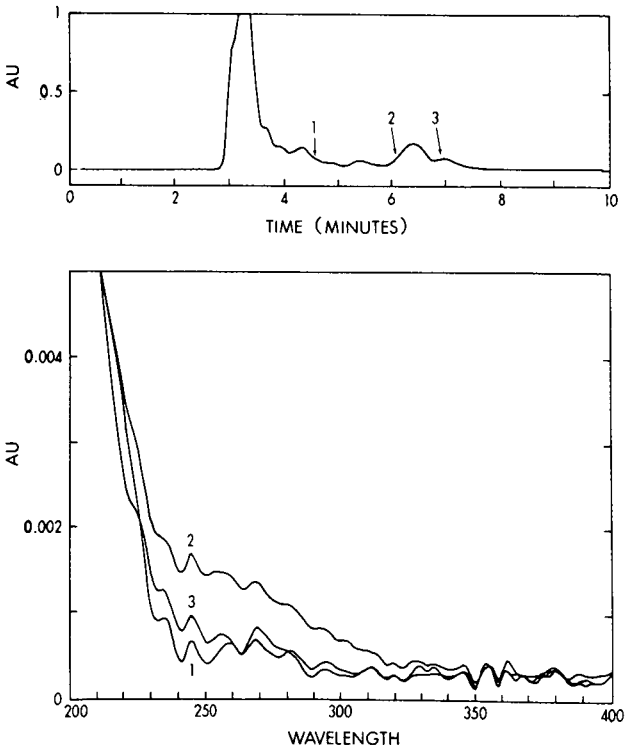

Fig. 4. Spectrum index (top) and spectrum analysis (bottom) of Pig LV tissue. 1 = OXY (4.57 min); 2 = LVP (6.06 min); 3 = AVP (6.88 min).

negligible amounts of AVP and OXY, measurable only by spectrum analysis plot (bottom, Fig. 4). AVP and OXY contents average 1.45 and 1.50 ng/g wet weight, respectively. LVP, on the other hand, is appreciable and measures 6.95 ± 4.75 ng/g wet weight.

HPLC provides a direct, sensitive (1 ng) and reproducible method for simultaneous determination of AVP, LVP, and OXY *in vitro* and in pharmacological samples. In biological samples, spectral analysis of the individual biopeptides is essential to distinguish them from interfering biopeptides and to improve sensitivity four-fold.

REFERENCES

1 K. Krummen and R. W. Frei, *J. Chromatogr.*, 132 (1977) 27.
2 G. I. Clark, P. Wood, L. Merrick and D. W. Lincoln, *Nature, (London)*, 282 (1979) 746.
3 P. T. Pullan, B. H. Clappison and C. I. Johnston, *J. Clin. Endocrinol. Metab.*, 49 (1979) 580.
4 R. Davis, M. L. Forsling and J. D. H. Slater, *J. Clin. Invest.*, 60 (1977) 1438.
5 K. Shimizu and M. Hoshino, *Contrib. Nephrol.*, 9 (1978) 42.
6 C. G. Beardwell, *J. Clin. Endocrinol. Metab.*, 33 (1971) 1024.

Journal of Chromatography, 536 (1991) 143–153
Elsevier Science Publishers B.V., Amsterdam

CHROMSYMP. 2015

High-performance liquid chromatography–time-of-flight mass spectrometry and its application to peptide analyses

RICHARD C. SIMPSON[a]

Department of Chemistry and Biochemistry, University of Maryland Baltimore County Campus, Baltimore, MD 21228 (U.S.A.)

W. BART EMARY, IHOR LYS and ROBERT J. COTTER*

Department of Pharmacology and Molecular Sciences, Johns Hopkins University, School of Medicine, Baltimore, MD 21205 (U.S.A.)

and

CATHERINE C. FENSELAU

Department of Chemistry and Biochemistry, University of Maryland Baltimore County Campus, Baltimore, MD 21228 (U.S.A.)

ABSTRACT

High-performance liquid chromatography (HPLC) has been successfully interfaced on-line with liquid secondary-ion time-of-flight mass spectrometry, utilizing a continuous-flow interface. Time-of-flight mass spectrometry (TOF-MS) is a low-resolution, high-mass-range technique, compatible with extremely rapid data acquisition rates. Thus a TOF-MS system is extremely well suited for coupling with HPLC. This paper describes the interface used to couple the HPLC and TOF-MS as well as the basic operating principles of such a system. Using both standard and packed-capillary reversed-phase HPLC columns, the HPLC–TOF-MS system has been successfully used to separate and detect peptides, providing molecular weight information for the peptide analytes. Experimental data, including chromatograms (UV, reconstructed ion and selected ion) and mass spectra, are presented to demonstrate the ability of the HPLC–liquid secondary-ion TOF-MS system to resolve chromatographically analytes as well as to resolve mass spectrometrically analytes which are unresolved on the chromatographic column.

INTRODUCTION

The past decade has witnessed a vast increase in the number of techniques used to interface high-performance liquid chromatography (HPLC) with mass spectrometry (MS). To date, some of the more common interface techniques have included moving belt [1], thermospray [2], continuous-flow fast-atom bombardment (FAB) [3] and particle beam [4]. In recent years, there has been an increased interest in developing interfaced HPLC–MS techniques which are suited for use with large and somewhat fragile macromolecules of biological interest. HPLC–continuous-flow FAB-MS has proven to be quite amenable to such applications, in large part due to its high-

[a] Present address: Department of Drug Metabolism, SmithKline Beecham Pharmaceuticals, P.O. Box 1539, King of Prussia, PA 19406, U.S.A.

0021-9673/91/$03.50

mass-range capabilities (approximately 10 000 daltons) and the gentle ionization process, which preserves molecular information. Unfortunately, in order to achieve the high-mass capabilities, continuous-flow FAB is typically performed with a magnetic sector mass spectrometer which generally operates at relatively slow scan rates (s/decade) over the mass range being monitored. Such slow scan rates may result in "missing" a chromatographic peak or skewing the mass spectral information obtained within an eluted chromatographic peak. Substitution of a quadrupole mass spectrometer for the magnetic-sector instrument results in vastly improved scan rates (perhaps 1 s/2–3 decades). The use of the electrospray interface with a quadrupole instrument has proven to be very successful in the HPLC–MS analyses of biopolymers [5,6]. Unfortunately, quadrupole instruments have somewhat limited upper mass ranges, typically 2000 to 3000 daltons. The ideal solution to this dilemma would be to utilize a gentle ionization technique such as FAB in conjunction with a mass spectrometer possessing both a high mass range and a rapid scan rate.

One possible means of approaching these goals is to interface a liquid chromatograph with a time-of-flight (TOF) mass spectrometer. A TOF instrument has a mass range at least as large as that of a magnetic sector instrument. Recently, a TOF instrument was used to acquire the mass spectra of proteins with molecular weights in excess of 200 000 daltons [7]. Additionally, a TOF instrument has scanning speeds which easily surpass those obtained on a quadrupole system [8,9].

Our laboratories have been involved in the development and application of techniques which interface liquid chromatography with TOF-MS. The present paper describes the principles and use of HPLC-liquid secondary-ion time-of-flight mass spectrometry (LSI-TOF-MS) and its application to the HPLC–MS analyses of peptide mixtures. Examples in which both standard and capillary HPLC are employed are presented to demonstrate the capabilities of the interfaced system.

EXPERIMENTAL

The LSI-TOF-MS instrument was constructed in-house and has been described previously [8–10]. Briefly, an ion gun provides a pulsed primary ion beam of 5 keV Xe^+, which are directed at the glycerol–analyte target exiting the tip of the continuous-flow probe interface. The pulsed beam of primary ions sputters secondary analyte ions from the glycerol target. The primary ion pulse width is long enough (approximately 10 μs) to produce a high yield of the secondary analyte ions. After a brief delay, these secondary analyte ions are then extracted from the source region by application of voltage pulses to the source backing plate, draw-out and accelerating grids. The delay time and draw-out pulses provide time, energy and spatial focusing of the analyte ions. The analyte ions are then accelerated to 3 keV and enter the field-free drift tube for mass separation prior to striking a dual channelplate detector at the end of the flight tube. The resulting detector signal is then amplified and directed into the analog input of a high-speed data acquisition system. The high-speed data acquisition system, including the associated software package, was also constructed in-house and is controlled by a 80386-based PC system. Operating principles of the data acquisition and processing system have been discussed in detail elsewhere [10] and will not be repeated in the present paper.

The continuous-flow probe which is actually used to interface the liquid

chromatograph to the mass spectrometer is a modified version of a previously reported probe, constructed in our laboratory [11]. The modifications primarily consist of employing a metal solder seal around the fused-silica capillary at the outlet tip of the probe. The use of a metal seal provides better electrical conductivity to reduce charge build-up on the probe tip and better thermal conductivity, which provides more uniform evaporation of liquid from the probe tip, resulting in more stable pressures within the mass spectrometer.

To prevent freezing and associated blockage of the probe tip due to mobile phase evaporation in the high vacuum of the mass spectrometer, heat was applied to the tip of the flow probe. Electrical current was passed through a length of copper wire, wrapped around the probe tip, providing resistive heating of the wire. To monitor the temperature of the probe tip, a thermocouple was placed within the metal solder seal at the probe tip. The current passing through the heating wire was adjusted to maintain a tip temperature in the range of 40 to 60°C, a typical value being 50°C. Variation of the tip temperature over this range did not appear to affect significantly the quality of the mass spectra obtained.

The flow-rate of the liquid actually passing into the mass spectrometer was set at 1 μl/min. When the LSI-TOF-MS system was interfaced to a conventional HPLC system, operating at a mobile phase flow-rate of 1 ml/min, a 1:1000 split of the mobile phase was required after the UV detector and prior to the mass spectrometer. The split was accomplished by placing 1 m of 60 μm I.D. fused-silica capillary (SGE, Austin, TX, U.S.A.) between the UV detector and the flow-probe tip. The inlet end of the capillary was simply inserted (not sealed) into the liquid flow path at the exit of the UV detector. The vacuum of the mass spectrometer drew liquid into the capillary, while the length and I.D. of the capillary provided sufficient flow resistance to regulate the liquid flow into the mass spectrometer to 1 μl/min. The remaining 0.999 ml/min was collected as waste at the outlet of the UV detector.

When interfacing a capillary HPLC system to the LSI-TOF-MS system, the mobile phase flow-rate was fixed at 1 μl/min and the chromatographic system was mechanically connected to the inlet of the flow probe with a 60-μm I.D. fused-silica capillary. The mobile phase was entirely transferred into the mass spectrometer, eliminating the need for a splitter.

The conventional HPLC system was a Beckman 114M binary solvent system (Berkeley, CA, U.S.A.), fitted with a Rheodyne 7125 injection valve with a 50-μl sample loop (Cotati, CA, U.S.A.). The variable-wavelength UV detector was a Kratos Spectraflow 757 (Ramsey, NJ, U.S.A.), set at 280 nm.

The capillary HPLC system was a μLC-500 pump and a μLC-10 UV detector, having a 30-nl flow cell and 1 mm optical path-length (Isco, Lincoln, NE, U.S.A.), fitted with a Model CI4W micro-injection valve with a 200-nl internal sample loop (Valco Instruments, Houston, TX, U.S.A.).

Columns

The conventional HPLC column was a base-deactivated 5 μm C_{18} cartridge column, 83 mm × 4.6 mm (Perkin-Elmer, Norwalk, CT, U.S.A.). The fused-silica capillary column was 20 cm × 200 μm I.D. Fused-silica capillary tubing was obtained from Polymicro Technologies (Phoenix, AZ, U.S.A.) and cut to length. The column blank was prepared as described by Shelly *et al.* [12]. However, EPO-TEK 377 epoxy

(Epoxy Technology, Billerica, MA, U.S.A.) was substituted for the originally described formulation due to its acid resistance in organic solutions. Additionally, 2 μm pore size ultra-high-molecular-weight polyethylene frit material (Upchurch Scientific, Oak Harbor, WA, U.S.A.) was substituted for the porous PTFE frit material originally described. The column blank was slurry-packed in-house with 5-μm base-deactivated C_{18} material (Supelco, Bellefonte, PA, U.S.A.).

Reagents and chemicals

All biochemicals were obtained from Sigma Chemicals (St. Louis, MO, U.S.A.). HPLC grade solvents were obtained from Burdick and Jackson (Muskegon, MI, U.S.A.). All other chemicals were of reagent-grade purity.

Mobile phase

For conventional HPLC separations, the mobile phase was prepared by pre-mixing a solution of acetonitrile–water (25:75, v/v). This solution was then made 5% (v/v) in glycerol and 0.1% (v/v) in trifluoroacetic acid. The mobile phase flow-rate was 1 ml/min.

For capillary HPLC separations, the mobile phase was prepared by pre-mixing a solution of acetonitrile–water (28:72, v/v). This solution was then made 10% (v/v) in glycerol and 0.1% (v/v) in trifluoroacetic acid. The mobile phase flow-rate was set at 1 μl/min.

All mobile phases were degassed by helium sparging prior to use.

RESULTS AND DISCUSSION

TOF-MS

Time-of-flight mass spectrometry involves measuring the time required for an ion to travel from the ion source region of the mass spectrometer to its detector. Ions are produced in "packets", then accelerated out of the source region and into a field-free drift tube, approximately 1 m in length. Our instrument has a 65-cm flight tube. All ions receive equal kinetic energy of approximately 3 keV during acceleration out of the ion source. Therefore, ions will separate into groups according to their velocity (and hence mass) as they travel the length of the flight tube. The mass-to-charge ratio of an ion is determined by its flight time. Since their kinetic energy is equal, the lighter low-mass ions transit the flight tube faster than heavier high-mass ions do. Eqn. 1, which describes the velocity of the ions in the flight tube, shows that the velocity (v) is inversely proportional to the square root of the mass of the ion (m).

$$v = \left[\frac{2zeV}{m}\right]^{1/2} \tag{1}$$

In practice, the velocities of the ions are not measured. Instead, the time required to transit the flight tube, or time of flight (TOF), is what is actually measured. Eqn. 2 shows the TOF as directly proportional to the square root of the mass of the ion (m), where L is the length of the flight tube, z is the charge on the ion, e is the charge of an electron and V is the accelerating potential. The mass spectrometer is calibrated by fitting the TOF for ions of known masses to eqn. 2.

$$\mathrm{TOF} = \left[\frac{m}{2zeV}\right]^{1/2} L \tag{2}$$

The concept of interfacing HPLC with a TOF-MS system is quite attractive, due to several characteristics of a TOF-MS instrument. A TOF-MS system has extremely rapid scan rates (up to 10^8 decade/s) thus enabling many scans to be acquired across even the narrowest of chromatographic peaks. In principle, no mass-dependent voltage or field is scanned in a TOF-MS instrument. Rather, masses are resolved in a time domain and recorded sequentially by a transient recorder. Obtaining such a large number of scans across the chromatographic peak permits signal averaging to be used as a means of improving the signal-to-noise ratio relative to that of a single or very small number of scans. Additionally, the wide mass range capability of a TOF-MS system is very well matched to the detection of macromolecular biomolecules such as peptides and proteins. Another important consideration is the fact that in TOF-MS all ions from each ionization event may be detected. This permits full-scan and selected-ion data to be acquired at the same time. This is in contrast to scanning magnetic-sector or quadrupole instruments, which are essentially mass filters, permitting only ions of a specific mass to reach the detector.

The use of secondary-ion mass spectrometry (SIMS), which might also be thought of as fast-ion bombardment (FIB), as the ionization mode in our instrument produces little fragmentation of labile molecules, resulting in the ability to obtain molecular weight information. The information obtained by SIMS ionization is very similar to that obtained with FAB ionization. Although our instrument utilizes an ion gun for SIMS ionization, an atom gun could, in principle, be substituted to yield FAB spectra utilizing TOF mass resolution.

Conventional HPLC–LSI-TOF-MS

The UV and reconstructed ion chromatograms for a chromatographically resolved two-component peptide mixture are shown in Fig. 1. The excellent match of peak shapes and resolution in the two chromatograms indicates that the flow probe interface does not introduce any substantial band broadening, nor does it exhibit any substantial memory effect. A memory effect, due to the slow ionization and removal of analyte from the probe tip, would result in significant peak tailing and loss of chromatographic resolution. The 5-min time offset between the UV and ion chromatograms is due to the delay volume between the exit of the UV detector and the tip of the flow probe interface. The difference in peak height ratios observed in the two chromatograms indicates that the peptides have different molar absorbtivities at 280 nm, while their ionization efficiency is approximately equal.

The LSI-TOF-MS spectra obtained for each component of this chromatographically resolved mixture are shown in Fig. 2. The spectra in this paper are the raw spectra. They have not been converted into the familiar "stick" spectra. The protonated molecular ion is the predominant species observed in each spectrum, with no evidence of any significant fragmentation of the molecular ion. The ions in the spectra labeled as "G_xH^+" are protonated oligomers of the glycerol matrix, and are commonly observed. These ions may be used for mass calibration of the TOF instrument.

Although the previous example presents the type of data obtainable with the

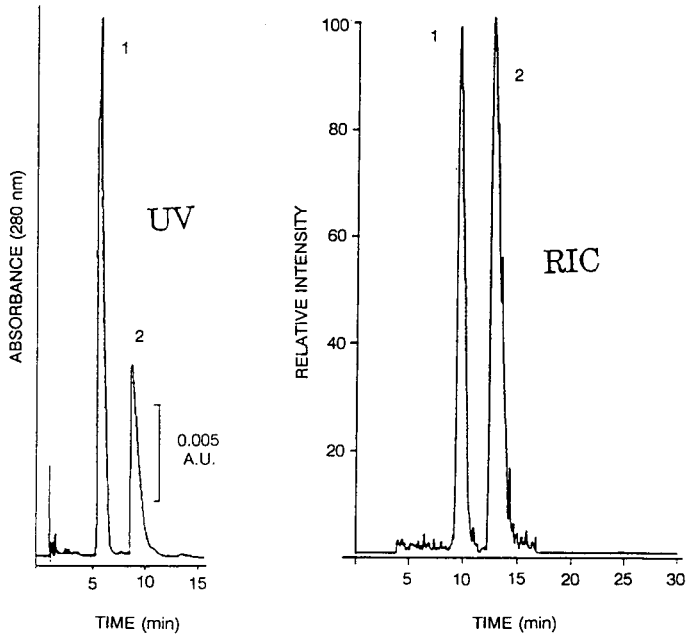

Fig. 1. Chromatograms of a chromatographically resolved two-component peptide mixture obtained by conventional HPLC–LSI-TOF-MS. (Left) UV chromatogram; (right) reconstructed ion chromatogram. 50 nmol of each peptide injected on-column and detected by UV; 50 pmol of each component transferred to the mass spectrometer. Peaks: 1 = Tyr–Gly–Gly–Phe–Met (mol.wt. 574); 2 = Tyr–Met–Gly–Phe–Pro–NH_2 (mol.wt. 613). (Reprinted with permission from ref. 10. © 1990 American Chemical Society.)

HPLC–LSI-TOF-MS instrument, it does not provide an example of some of the more powerful aspects of a combined HPLC–MS system. A more illustrative example of that is given in Fig. 3. This figure shows a chromatogram of a four-component peptide mixture, where components 3 and 4 are not chromatographically resolved. However, by manipulation of the mass spectral data, the selected-ion chromatograms for the protonated molecular ion region for each of the two coeluting peptides may be generated. Thus, even though the two peptides are not chromatographically resolved, they may be mass spectrometrically resolved.

To verify that the two coeluting peptides can be mass-spectrometrically resolved, the mass spectra of the individual components as well as that of the peak containing the coeluting peptides must be examined. In Fig. 4 the LSI-TOF-MS spectrum of pure peptide 3 is presented, as well as the spectrum for the peak containing coeluting peptides 3 and 4. As is clearly demonstrated, the mass spectrometer easily resolves the individual peptides within the merged chromatographic peak. Thus, the selected-ion chromatograms in Fig. 3 are specific for each peptide.

Capillary HPLC–LSI-TOF-MS

The previous examples were for a conventional HPLC instrument interfaced to the LSI-TOF-MS instrument via a 1:1000 flow splitter. Although the performance of the system and quality of the data are satisfactory, one must realize that 99.9% of the

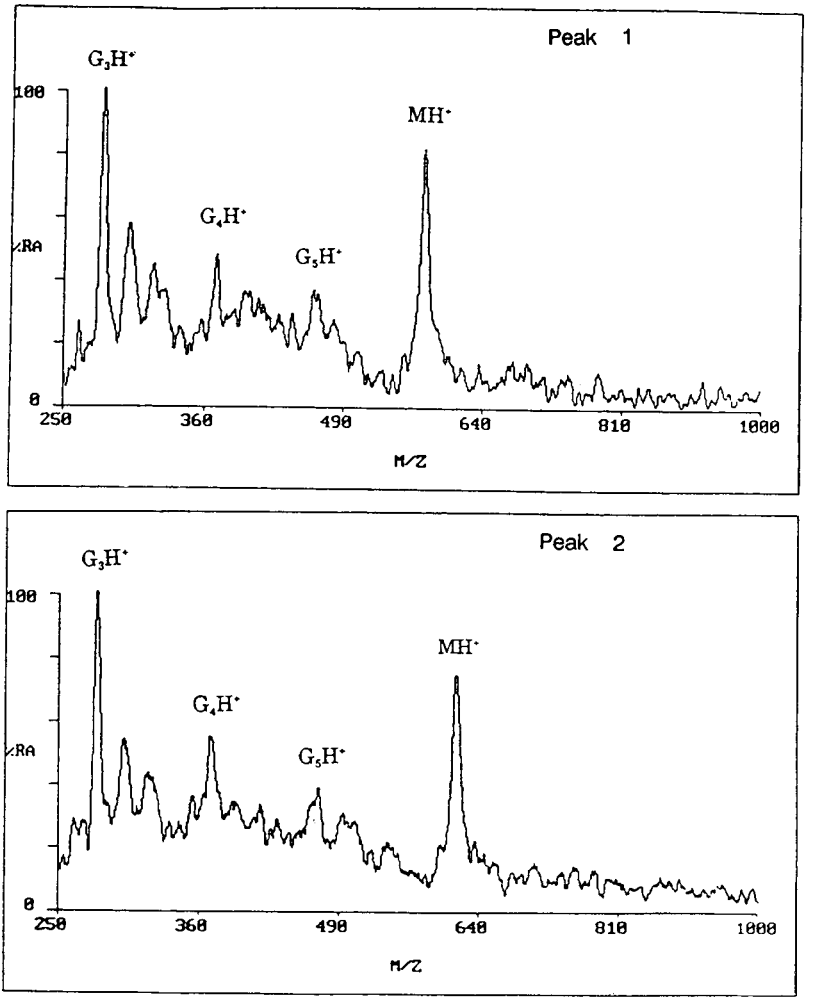

Fig. 2. HPLC–LSI-TOF-MS spectra for each of the peptides chromatographically resolved in Fig. 1.

sample injected into the HPLC column is directed to waste or a fraction collector at the exit of the UV detector. A much better method would be to utilize flow-rates low enough that a splitter is not required and the entire mobile phase and analyte load are transferred directly to the mass spectrometer. The low mobile phase flow-rates used in capillary HPLC is a primary advantage of interfacing a capillary HPLC system with the LSI-TOF-MS instrument.

The capillary HPLC–LSI-TOF-MS UV and reconstructed ion chromatograms for a two-component peptide mixture are presented in Fig. 5. As indicated by Fig. 5, the flow probe appears to be quite compatible with capillary columns, and has no adverse influence on the chromatographic resolution or peak shape.

The use of a capillary HPLC system does not affect the type of mass spectral information acquired. The LSI-TOF-MS spectrum of the first peak in the capillary

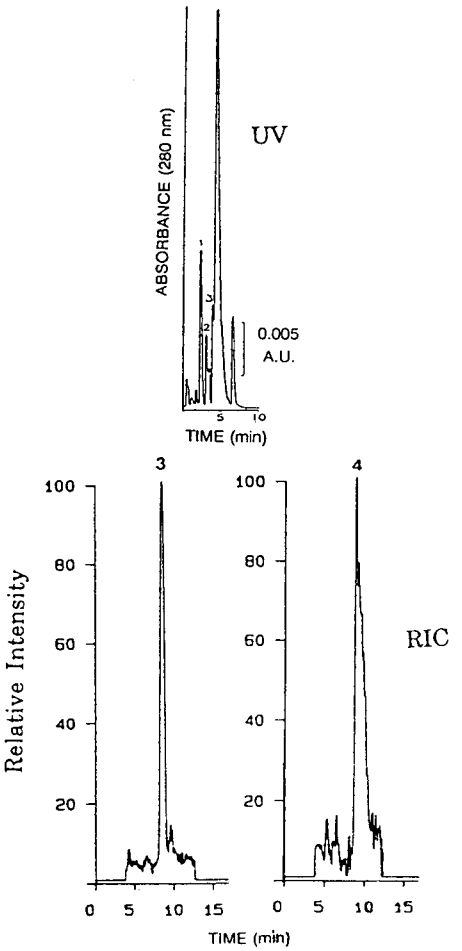

Fig. 3. UV and selected ion chromatograms of a four-component peptide mixture. Components 3 and 4 are not chromatographically resolved. They may be mass spectrometrically resolved by selected-ion chromatograms of the protonated molecular ion region for each peptide. Peaks: 1 = Tyr–Gly–Gly–Phe–Met (mol.wt. 574); 2 = Tyr–Met–Gly–Phe–Pro–NH_2 (mol.wt. 613); 3 = Arg–Tyr–Leu–Gly–Tyr–Leu (mol. wt. 784); 4 = Leu–Trp–Met (mol.wt. 448). (Reprinted with permission from ref. 10. © 1990 American Chemical Society.)

chromatogram of Fig. 5 is shown in Fig. 6. As was observed in the spectra acquired with the conventional HPLC–LSI-TOF-MS system, the capillary system yields spectra in which the predominant species is the protonated molecular ion of the peptide analyte. In addition, the mass spectral data obtained with the capillary system may be subjected to the same types of data manipulation and processing as that used on the conventional HPLC–LSI-TOF-MS system discussed earlier.

There are issues remaining to be resolved which have not been addressed in this paper. One of these is the relatively low mass-spectrometric resolution achieved by a TOF system, typically in the range of 100 to 500. This resolution is substantially less than that which may be achieved with a magnetic sector instrument. However, several

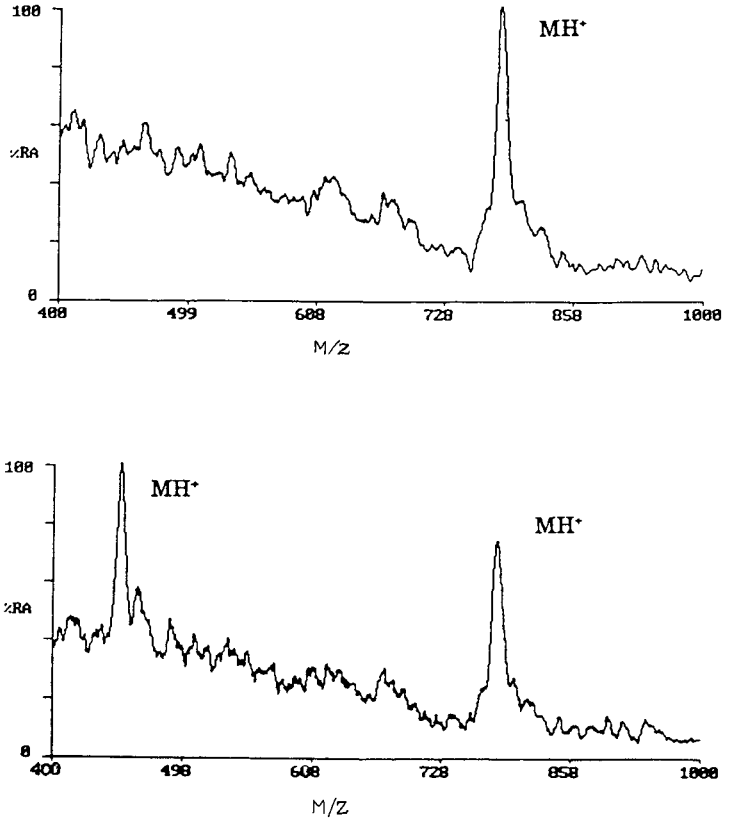

Fig. 4. HPLC–LSI-TOF-MS spectra for pure peptide 3 (top) and of the peak containing a mixture of peptides 3 and 4 (bottom). (See Fig. 3.)

laboratories are developing methods to increase the resolution obtainable with a TOF system to that obtainable with magnetic instruments [13,14].

Also, a system such as that described in the current paper is not yet commercially available. Our sytem is a prototype, built primarily in-house. Thus, many laboratories may not be able to gain immediate access to such a system.

Finally, the very rapid scanning rate over a wide mass range which can be achieved with TOF-MS generates huge amounts of data at extremely rapid rates. Not only must the data system be capable of acquiring data very rapidly, it must also be capable of quickly and efficiently storing the raw data. These requirements are beyond the abilities of most data acquisition systems, thus requiring the use of specialized or custom-built data processing systems.

Although these factors currently represent obstacles which must be overcome, they also represent, in combination with the current achievements, the numerous research opportunities available in the further development and refinement of HPLC–LSI-TOF-MS.

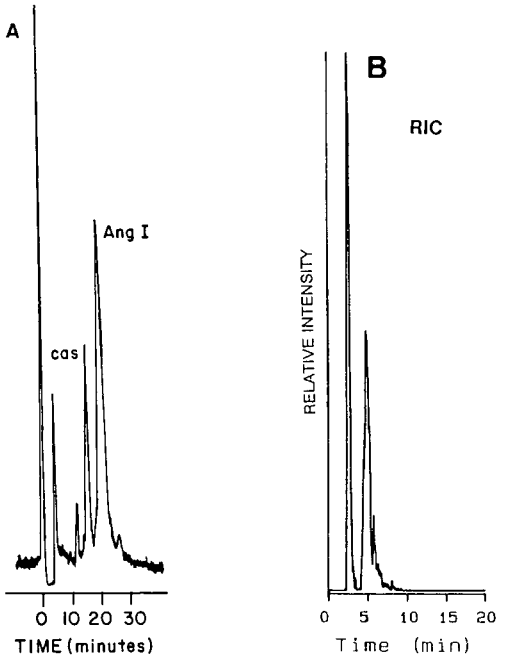

Fig. 5. Capillary HPLC–LSI-TOF-MS (A) UV and (B) reconstructed ion chromatograms of a two-component peptide mixture. 25 pmol α-casein [fragment 90–95] (mol.wt. 784, first peak) and 15 pmol human angiotensin I (mol.wt. 1296, second peak) were injected.

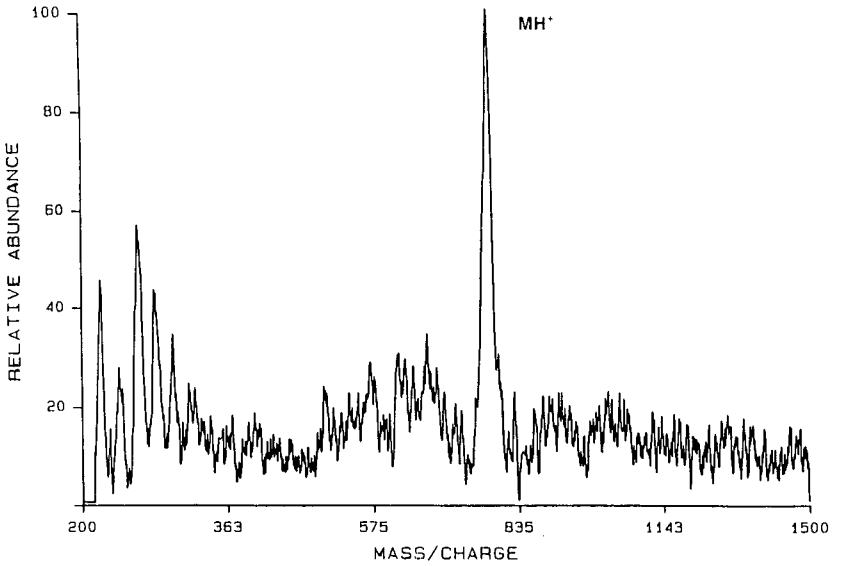

Fig. 6. HPLC–LSI-TOF-MS spectrum of the first peptide peak obtained from capillary HPLC–LSI-TOF-MS separation of a two-component peptide mixture shown in Fig. 5.

CONCLUSIONS

The preliminary data obtained and presented in this paper provide a strong argument for the further development of HPLC–LSI-TOF-MS systems. We have demonstrated that interfacing HPLC to LSI-TOF-MS is possible, and that such a system is quite versatile in that it may utilize either conventional or capillary HPLC. Even under the stringent dead-volume requirements of capillary HPLC, the interfaced system showed no signs of significant deterioration in the quality of the chromatographic separations obtainable. The sensitivity of the HPLC–LSI-TOF-MS instrument is approximately constant, whether operated in the conventional or capillary modes. For the peptides examined in this paper the sensitivity was in the low picomole range. As demonstrated by the examples presented, the HPLC–LSI-TOF-MS system produces spectra which exhibit predominantly protonated molecular ions with little fragmentation. Although the peptides used as examples all have molecular weights under 1000 daltons, the TOF-MS technique is applicable to much larger molecules.

ACKNOWLEDGEMENTS

The authors gratefully acknowledge financial support of this research by NIH grants (GM 33967 to RJC and GM 21248 to CCF). The authors also acknowledge the contributions of A. Hoffman in the design and fabrication of the prototype transient recorder. This work was carried out at the Middle Atlantic Mass Spectrometry Laboratory, an NSF-supported Regional Instrumentation Facility.

REFERENCES

1 M. J. Hayes, E. P. Lankmayer, P. Vorous, B. L. Karger and J. M. McGuire *Anal. Chem.*, 55 (1983) 1745.
2 C. R. Blakely and M. L. Vestal, *Anal. Chem.*, 55 (1983) 750.
3 R. M. Caprioli, T. Fan and J. S. Cottrell, *Anal. Chem.*, 58 (1986) 2949.
4 R. C. Willoughby and R. F. Browner, *Anal. Chem.*, 56 (1984) 2626.
5 J. A. Loo, C. G. Edmonds, R. D. Smith, M. P. Lacey and T. Keough, *Biomed. Environ. Mass Spectrom.*, 19 (1990) 286.
6 R. D. Smith, J. A. Loo, C. G. Edmonds, C. J. Barinaga and H. R. Udseth, *Anal. Chem.*, 62 (1990) 882.
7 M. Karas, A. Ingendoh, U. Bahr and F. Hillenkamp, *Biomed. Environ. Mass Spectrom.*, 18 (1989) 841.
8 J. K. Olthoff, J. P. Honovich and R. J. Cotter, *Anal. Chem.*, 59 (1987) 999.
9 J. K. Olthoff, I. A. Lys and R. J. Cotter, *Rapid Commun. Mass Spectrom.*, 2 (1988) 171.
10 W. B. Emary, I. Lys, R. J. Cotter, R. C. Simpson and A. Hoffman, *Anal. Chem.*, 62 (1990) 1319.
11 K.-H. Chen and R. J. Cotter, *Rapid Commun. Mass Spectrom.*, 2 (1988) 237.
12 D. C. Shelly, J. G. Gluckman and M. Novotny, *Anal. Chem.*, 56 (1984) 2990.
13 J. Grotemeyer and E. W. Schlag, *Org. Mass Spectrom.*, 22 (1987) 758.
14 R. Grix, R. Kutscher, G. Li, U. Gruner and H. Wollnik, *Rapid Commun. Mass Spectrom.*, 2 (1988) 83.

Journal of Chromatography, 536 (1991) 155–164
Elsevier Science Publishers B.V., Amsterdam

CHROMSYMP. 2024

High-performance affinity chromatography of immunoglobulin E on a column of dinitrophenylamino acids covalently bound to a highly cross-linked polymeric micropellicular support

SURAPOTE WONGYAI
Institute of Radiochemistry, University of Innsbruck, A-6020 Innsbruck (Austria)
JANOS M. VARGA
Department of Dermatology, University of Innsbruck, A-6020 Innsbruck (Austria)
and
GÜNTHER K. BONN*
Institute of Radiochemistry, University of Innsbruck, A-6020 Innsbruck (Austria)

ABSTRACT

Coupling of different dinitrophenyl (DNP) amino acids to 2.5-μm highly cross-linked polystyrene–divinylbenzene beads was performed, using carbodiimide as catalyst. The binding capacity of affinity-purified monoclonal anti-DNP mouse immunoglobulin E (IgE) antibody to DNP-lysine-coated beads is *ca.* 4 nmols per mg of beads. The structure of the active coupled functional groups was investigated by X-ray photoelectron spectroscopy. The application of these ligand-carrying beads to the high-performance affinity chromatography of IgE antibody was demonstrated and the purity of IgE was confirmed by sodium dodecyl sulphate–polyacrylamide gel electrophoresis. This method is also suitable for coupling several other carboxyl compounds to a highly cross-linked polystyrene matrix.

INTRODUCTION

One of the technical problems in high-performance affinity chromatography (HPAC) is establishing 'anchoring functions' on the surface of solid supports which are suitable for the covalent attachment of ligands or ligand-binding proteins. With silica-based supports a large number of alternatives are available [1]. However, with organic supports, such as polystyrene (PS), the choices are more limited. Currently, the following approaches are used for the derivatization of PS for covalent immobilization of various molecules: copolymerization of monomers containing functional groups [2], chemical modification of polymerized products [3] and radiochemical modification of polymerized products by graft polymerization [4] or by radio-derivatization [5]. The basic assumption in all these approaches is that PS products consist of chemically pure PS, which is only reactive under relatively harsh conditions, such

0021-9673/91/$03.50

as those necessary for electrophilic substitutions, to obtain the required anchoring functions. We have recently discovered that highly cross-linked PS beads react with carboxyl-containing compounds in the presence of carbodiimides. This suggests that these beads contain nucleophilic groups on their surface in sufficient numbers to serve as 'anchoring functions' for covalent binding of ligands, such as dinitrophenyl (DNP-amino) acids [6].

Immunoglobulin E (IgE) is one of the subclasses of human immunoglobulins and plays an important role in allergies [7,8].

EXPERIMENTAL

Instrument

The equipment consisted of a high-performance liquid chromatographic (HPLC) gradient system (Model 402; Bio-Rad Labs., Richmond, CA, U.S.A.). Injections were made using 20- and 300-μl sample loops. The γ and β liquid scintillation counters were an LKB Wallac CliniGamma 1272 counter and an LKB Wallac 1215 (Pharmacia, Uppsala, Sweden), respectively.

Column

Highly cross-linked polystyrene–divinylbenzene particles having a rugulose exterior and a mean diameter of 2.5 μm were prepared by emulsion polymerization, using a two-step swelling method with 1-chlorododecane as swelling reagent [9]. The starting 0.9-μm styrene emulsion was produced by the emulsifier-free method [10], modified with regard to ionic strength optimization, which was performed with sodium chloride in order to achieve the required homogeneous size distribution. The derivatized beads were suspended in water. The slurry was sonicated and packed into a 30 × 4.6 mm I.D. stainless-steel column. Water was used as the driving solvent at a starting pressure of 300 bar for 10 min and a final pressure of 500 bar for 30 min by using a Haskel Model MP-110 air-driven fluid pump (Ammann-Technik, Kölliken, Switzerland).

Chemicals

Styrene and divinylbenzene were purchased from Riedel- de Haën (Seelze, F.R.G.). The radiochemicals were obtained from the following suppliers: [2-^{3}H]glycine, 5-hydroxy[G-^{3}H]tryptamine, L-[4,5-^{3}H]lysine and [1,4(N)-^{3}H]putrescine from Amersham (Amersham, U.K.); and [^{3}H]acetic acid, L-[3,4-^{3}H]valine, L-[4-^{3}H(N)]proline and L-[^{3}H(G)]serine from Du Pont (New England Nuclear, Vienna, Austria). DNP-[^{3}H]glycine was prepared from 2,4-dinitrofluorobenzene and [2-^{3}H]glycine according to a published method [6]. 1-Ethyl-3-(3-dimethylaminopropyl)carbodiimide (EDC) was purchased from Sigma (St. Louis, MO, U.S.A.) and DNP-amino acids were obtained from Fluka (Buchs, Switzerland). A solution containing 1% bovine serum albumin (BSA), 4% PEG 1000 and 0.05% Tween 20 in phosphate-buffered saline (PBS) at pH 7.2 (abbreviated to PBSAT) was used as a binding buffer in the affinity studies.

Antibody

Affinity-purified monoclonal anti-DNP mouse IgE antibody, IgE(aDNP), clone SPE-7, was obtained from Sigma. Iodination of IgE(aDNP) was carried out by the Enzymobead method (single reaction, Bio-Rad Labs.) following the manufacturer's directions. The iodinated product was purified on a 50 × 10 mm I.D. Sephadex G-25 column, equilibrated with 0.2 *M* phosphate buffer at pH 7.2. Radioactivity of the collected fractions was measured in a gamma counter. The purity of IgE(aDNP) was checked by sodium dodecyl sulphate–polyacrylamide gel electrophoresis (SDS-PAGE) under reducing conditions [11].

Coupling of DNP-[^{3}H]Gly to polystyrene beads

Five different concentrations of DNP-Gly were prepared in a coupling solution (0.1 *M* NaCl, adjusted to pH 3.0 with HCl). An amount of $6 \cdot 10^5$ cpm of DNP-[^{3}H]Gly was added to 250 μl of 10 m*M* DNP-Gly. From this solution, four other standards were prepared by sequential three-fold dilutions. A 10-mg amount of 2.5-μm highly cross-linked polystyrene beads was suspended in 250 μl of the coupling solution and 25 μl (containing 1 mg of beads) were pipetted into two series of ten Eppendorf vials each, one series without EDC ('O') and one with EDC ('E'). From each of the standard solutions, 25 μl were added to both series. A 50-μl volume of coupling solution was added to the 'O' and 50 μl of a 4-mg/ml solution of EDC in the coupling solution to the 'E' series. The suspensions were mixed by vortexing and incubated at room temperature for 1 h on a shaking table. Following centrifugation at 13 000 rpm for 3 min in a microfuge, the beads were first washed five times with 1 ml of 90% ethanol, then once with 1 ml of 0.1 *M* sodium hydrogencarbonate and 1 ml of water, with centrifugation at each step. The tips of the vials were cut off with a red-hot razor blade and counted in the beta counter with 2 ml of Biofluor emulsifier cocktail (New England Nuclear, Boston, MA, U.S.A.). About $5 \cdot 10^6$–$1 \cdot 10^7$ cpm of DNP-[^{3}H]Gly were coupled with 100 mg of the beads, as described above.

The stability of the bond was checked by the following procedure. The DNP-[^{3}H]Gly-coated beads were resuspended in 5 ml of water, and 100-μl aliquots were centrifuged at 13 000 rpm of 3 min. A 50-μl volume of the reagents listed in Table I was added each individual pellet of beads and incubated on the shaking table for 5 h. After adding 1 ml of water and recentrifugation, the beads were washed three times with 0.1 *M* sodium hydrogencarbonate and transferred quantitatively to the counting tubes with 0.5 ml of 0.5% Tween 20. The uptake of radioactivity was compared with the untreated bead.

Coupling of different radiochemicals to the beads

An amount of $1 \cdot 10^6$ cpm per 250 μl of each of the compounds listed in Table II was diluted with water to give 250 μl, then mixed with another 250 μl of 20 m*M* of the corresponding unlabelled standard. A 200-mg amount of the beads was suspended in 10 ml of coupling solution and 100-μl aliquots were used for coupling.

Binding of IgE(aDNP) to beads coated with different DNP-amino acids

A 1-ml volume of 5 m*M* DNP-amino acids listed in Table III was coupled with 10 mg of the beads in Eppendorf vials following the procedure given in the preceding paragraph, then 500 μl of $5 \cdot 10^5$ cpm [^{125}I]IgE(aDNP) were added and the mixture

was incubated at room temperature for 4 h on a shaking table. The beads were washed eight times with 1 ml of PBSAT and the radioactivity was measured in a gamma counter. As DNP-lysine turned out to be the best ligand for IgE, the binding capacity of PS–DNP-lysine was then determined. A $6 \cdot 10^5$ cpm amount of [^{125}I]IgE (aDNP) was mixed with 50 μl of monoclonal anti-DNP mouse IgE (50 μg) and diluted to 300 μl with PBSAT. Again, four other standards were prepared by sequential three-fold dilutions. DNP-lysine was coupled with 12 mg of the beads. The coated pellet was resuspended in 1.2 ml of PBSAT and 100-μl aliquots were used for capacity measurements.

Atomic composition of highly cross-linked micropellicular PS beads

The atomic composition of the highly cross-linked PS beads was determined by X-ray photoelectron spectroscopy (XPS) using the method of Bertoti *et al.* [12]. The spectra were recorded with a Kratos XSAM 800 spectrometer, operated in the fixed retarding ratio mode, using Mg Kα radiation (1253.6 eV). Spectra were referenced to the C 1*s* line of adventitious carbon, fixed at a binding energy of 284.6 eV. The gold decoration method was used to check the applicability of this method. Ion etching was performed with 2.5-keV Ar^+ ions with an ion current density of 3.4 μA cm^{-2}. A detailed description of the experimental conditions can be found elsewhere [13]. Wide-scan spectra in the 50–1250 eV kinetic energy range were recorded for all samples. Detailed spectra of the C 1*s*, O 1*s*, Si 2*p*, Na 2*s*, Al 2*p*, Cl 2*p* and K 2*p* lines were recorded after each etching step. The effective sampling depths for these lines were 2–4 nm. For quantitative analysis the method and experimental cross-section values of Evans *et al.* [14] were applied.

Affinity chromatography of monoclonal anti-DNP mouse IgE

After coupling as outlined above, the PS–DNP-lysine beads were packed into a HPLC column (see above). The column was equilibrated with PBSAT at 0.02 ml/min. A $2 \cdot 10^5$ cpm amount of [^{125}I]IgE was introduced via a 20-μl injection loop. A flow-rate of 0.2 ml/min was maintained for 100 min and then increased to 0.5 ml/min. Fractions of 1 ml were collected until no radioactivity was observed above the background. In order to test the strength of affinity interaction, the bound antibody was eluted with two eluents at 0.5 ml/min, *viz.*, 1 *M* ammonium thiocyanate and 2.5 m*M* DNP-lysine. The purity of each fraction was confirmed by SDS-PAGE. The binding capacity of the column was determined as described above, using $5 \cdot 10^5$ cpm of the labelled IgE and eluting with 2.5 m*M* DNP-lysine. Labelled IgE in the fractions was subjected to SDS-PAGE and using 'cold' (*i.e.*, unlabelled) IgE as the control.

Applications

Crude IgE from two types of cell suspensions were iodinated as above and introduced directly into the column via a 320-μl injection loop, using 1 *M* ammonium thiocyanate first, followed by 2.5 m*M* DNP-lysine. The fractions were also subjected to SDS-PAGE.

RESULTS AND DISCUSSION

In Fig. 1 the amount of DNP-[^{3}H]glycine that is attached to the beads is depicted as a function of ligand concentration. If the coupling procedure is performed without EDC as a catalyst, no significant coupling of DNP occurs. The radioactivity remaining after treatment with acids, oxidizing agents and bases is given in Table I. The bond between the ligand and the support is resistant to detergents such as Tween 20 and to high salt concentrations (2 *M* KCl) at low pH, whereas bases and oxidizing agents break the bond between the ligand and the matrix. The sensitivity towards acids and oxidizing agents may vary according to the reagent used. There is no significant leakage of DNP during incubation with the buffer used as the mobile phase for the antibody-binding studies in this work. These investigations suggest the bond between DNP-[^{3}H]glycine and the polymeric support is covalent in nature. To compare the effect of functional groups on coupling, different radioactively labelled compounds were used at pH 6 and 3. Generally, coupling was superior at pH 6 except with DNP-glycine (which showed optimum coupling at pH 3) (Table II).

The nature of the bond formed between PS and carboxyl compounds is unknown. Carboxyls can react in the presence of carbodiimides with a variety of nucleophiles in addition to amino groups [15]. According to the atomic composition of the beads, obtained by XPS, the polymer contains *ca.* 174 O atoms per 1000 C atoms. This is equivalent to 1.4 O atoms per vinyl monomer. These oxygens, in various forms (aliphatic, aromatic, hydroxyls, peroxides, etc.), may serve as reactive groups on the surface of PS beads. The sensitivity of the bond to bases is indicative of ester-type linkages between DNP-amino acids and PS. The possible nucleophile is the hydroxyl group of poly(vinyl alcohol) (PVA). PVA was used as a stabilizer during the polymerization step and it is known to be incorporated into the surface of micropellicular PS [16]. A recent report demonstrated that the adsorption of PVA at a polystyrene latex surface yields layers of controlled thickness [17], useful as a reactive coating on the polymer surface. The reaction scheme proposed for the coupling mechanism is shown in Fig. 2. The presence of about 0.5% of acetate groups in PVA [17] may make the particles reactive with amino-containing compounds, such as putrescine and histamine, in the presence of carbodiimide (see Table II).

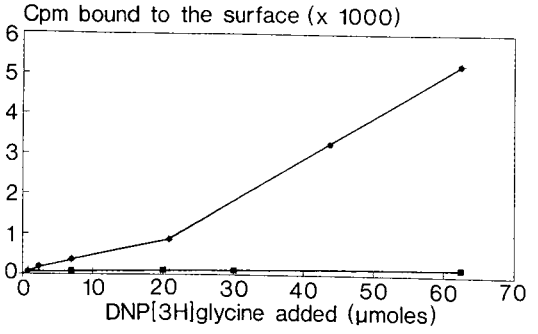

Fig. 1. Coupling of DNP-[^{3}H]glycine to highly cross-linked polystyrene sorbent (●) with and (■) without EDC. The calculated maximum coupling capacity is 780 pmol of DNP-glycine per mg of PS beads.

TABLE I

PERCENTAGE OF DNP-[^{3}H]GLY REMAINING BOUND TO THE BEADS AFTER TREATMENT WITH VARIOUS REAGENTS

Reagent	Bound (%)	Reagent	Bound (%)
Untreated	100	NaOH, 1.00 *M*	15
H_2SO_4, conc.	42	NaOH, 0.10 *M*	27
HCl, conc.	45	NaOH, 0.01 *M*	22
HNO_3, conc.	88	$NaHCO_3$, 0.1 *M*	76
$HClO_4$, 70%	37	$KMnO_4$, 5%	25
CH_3COOH, 100%	78	KCl, 2 *M*–glycine, 0.2 *M* (pH 3)	94
Acetic anhydride	87	Binding buffer (PBSAT)	94

The binding capacities of different DNP-amino acids as affinity ligands for IgE were examined by coupling them to the beads and the uptake of [^{125}I]IgE(aDNP) was compared with that of DNP-glycine (see Table III). DNP-lysine-coupled beads showed the highest capacity for IgE(aDNP). When [^{125}I]IgE(aDNP) was added to the DNP-lysine coupled beads in increasing concentrations, saturation-type binding occurred. The capacity calculated from a double reciprocal plot is *ca.* 4 nmol of IgE(aDNP) per mg of beads.

The PEG present in PBSAT increases the stability of antibody–ligand complexes [18,19] and the BSA minimizes non-specific interactions. Addition of the surfactant (Tween 20) reduces 'non-specific' hydrophobic and van der Waal's interactions [20]. Of the injected IgE, 57% was adsorbed to the stationary phase; this was first eluted with ammonium thiocyanate as a non-specific eluent, followed by DNP-lysine as a competitive eluent [20,21]. Fig. 3 shows the chromatogram of the adsorbed and eluted IgE. Owing to the different tertiary structures possible, two IgE peaks are obtained, which exhibit different binding properties. Fig. 4 shows the SDS-PAGE of the collected fractions. The fractions which were eluted by ammonium thiocyanate and DNP-

TABLE II

COUPLING OF DIFFERENT RADIOCHEMICALS TO THE BEADS AT pH 3.0 AND 6.0

Radiolabelled chemicals	Amount coupled (pmol/mg PS)	
	pH 3.0	pH 6.0
DNP-glycine	21.71	9.74
L-Proline	3.14	6.16
Acetic acid	1.48	3.01
L-Valine	1.86	11.20
L-Serine	0.89	2.06
5-Hydroxytryptamine	2.08	36.21
L-Lysine	2.24	25.10
Putrescine	2.29	73.68
Glycine	1.43	7.38

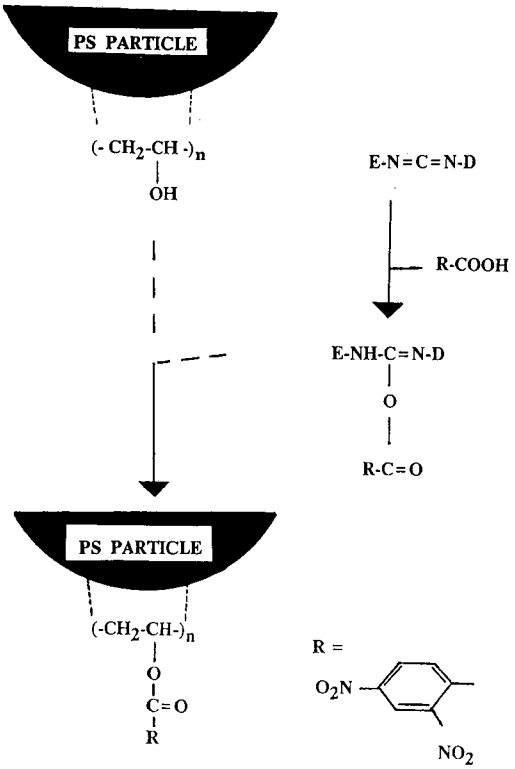

Fig. 2. Proposed reaction scheme. The available nucleophile on the surface of the polystyrene particle is believed to be the hydroxyl group of poly(vinyl alcohol) which is used as a stabilizer in the polymerization step [16].

TABLE III

BINDING EFFICIENCY OF DIFFERENT DNP-AMINO ACID-COUPLED BEADS TO [^{125}I]IgE (aDNP)

DNP-amino acid coupled to the beads	IgE bound at pH 3.0 (% of total IgE added)
Lysine	95.56
Alanine	6.61
Proline	9.87
Ornithine	10.75
Asparagine	12.96
Valine	15.12
Aspartic acid	12.30
Glycine	8.48

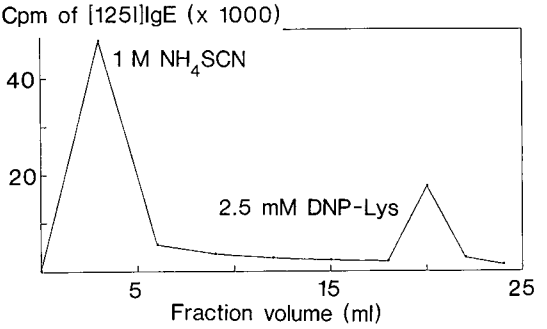

Fig. 3. Chromatogram of [^{125}I]IgE(aDNP) with 1 *M* ammonium thiocyanate and 2.5 m*M* DNP-lysine as eluents.

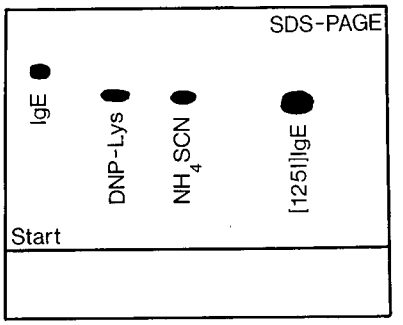

Fig. 4. Electropherogram of IgE from different fractions in Fig. 3.

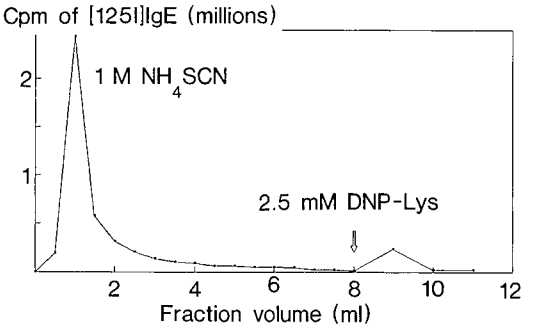

Fig. 5. Chromatogram of immunoglobulin E from crude B 4 cell suspension.

lysine show the same electrophoretic mobilities as the [^{125}I]IgE(aDNP) standard. A chromatogram of iodinated crude IgE from one type of B 4 cell suspension (see Fig. 5) also shows two peaks. Fig. 6 shows an electropherogram of the ammonium thiocyanate fractions of crude IgE from B 4 and B 142 hybridoma cultures, both having the same mobility. PVA-coated polystyrene beads have been shown to be useful for

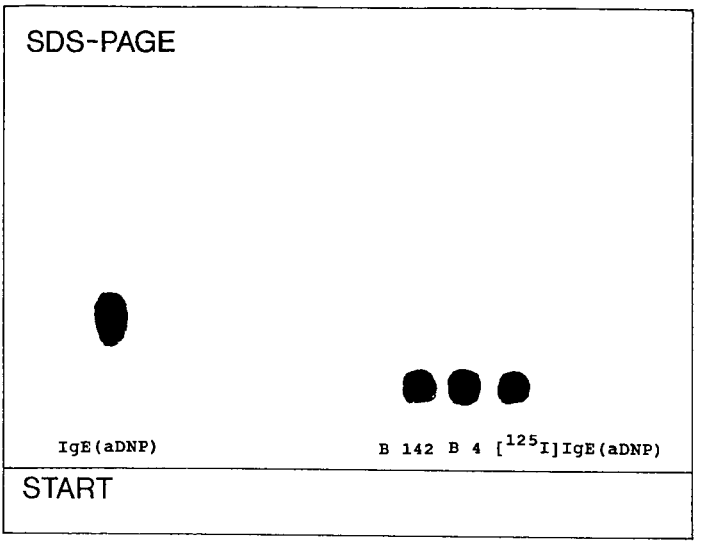

Fig. 6. Electropherogram of labelled IgE (ammonium thiocyanate fraction) from two types of cell suspensions (B 4 and B 142).

various further derivatizations by covalent bonding of affinitiy ligands. Such beads in the DNP-lysine-coated form have been used successfully for resolving immunoglobulins, showing high selectivity and binding capacity. This type of affinity column can readily be employed for the preparative one-step purification of immunoglobulin E from hybridoma culture supernatants.

ACKNOWLEDGEMENTS

This work was supported by the Österreichischen Nationalbank and by the Fonds zur Förderung der wissenschaftlichen Forschung (Vienna). Surapote Wongyai was supported by the Austrian Government (Vienna). We thank Ms. G. Kalchschmid for her help with SDS-PAGE.

REFERENCES

1 K. Ernst-Cabrera and M. Wilchek, *Trends Anal. Chem.*, 7 (1988) 58.
2 W. G. Lloyd and T. E. Durscher, *J. Appl. Polym. Sci.*, 7 (1963) 2025.
3 V. P. Chu and P. J. Tarcha, *J. Appl. Polym. Sci.*, 34 (1987) 1912.
4 P. H. Larsson, S. G. O. Johansson, A. Hult and S. Göthe, *J. Immunol. Methods*, 98 (1987) 129.
5 J. M. Varga and P. Fritsch, *FASEB J.*, 4 (1990) 2671.
6 J. M. Varga, G. Klein and P. Fritsch, *FASEB J.*, 4 (1990) 2678.
7 L. E. Hood, I. L. Weissman, W. B. Wood and J. H. Wilson (Editor), *Immunology*, Bejamin/Cummings, Menlo Park, CA, 2nd ed., 1984.
8 K. Ishizaka and T. Ishizaka, *Clin. Exp. Immunol.*, 6 (1970) 25.
9 J. Ugelstad, P. C. Mork, K. H. Kaggerud, T. Ellingsen and A. Berge, *Adv. Colloid Interface Sci.*, 13 (1980) 101.
10 A. Kotera, K. Furusawa and Y. Takeda, *Kolloid Z. Z. Polym.*, 239 (1970) 677.
11 I. K. Laemmli, *Nature (London)*, 227 (1970) 680.

12 I. Bertoti, M. Mohai, M. Revesz and G. Alexander, *Vacuum,* 37 (1987) 129.
13 A. Toth, I. Bertoti, T. Szekely and M. Mohai, *Surf. Interface Anal.*, 7 (1985) 282.
14 S. Evans, R. G. Pritchard and J. M. Thomas, *J. Electron Spectrosc. Relat. Phenom.*, 14 (1978) 341.
15 M. Bodanszky, *Principles of Peptide Synthesis*, Springer, Berlin, 1984.
16 J. R. Miller, D. G. Smith, W. E. Marr and T. R. E. Kressmann, *J. Chem. Soc.*, (1963) 218.
17 S. Chibowski, *J. Colloid Interface Sci.*, 134 (1990) 174.
18 W. B. Jakoby and M. Wilchek, *Methods Enzymol.* (1974) p. 16.
19 M. Ceska and J. M. Varga, *Eur. J. Immunol.*, 2 (1972) 58.
20 P. D. G. Dean, W. S. Johnson and F. A. Middle (Editor), *Affinity Chromatography — a Practical Approach*, IRL Press Oxford, 1985.
21 A. F. Bergold, A. J. Muller, D. A. Hanggi and P. W. Carr, in Cs. Horváth (Editor), *High-Performance Liquid Chromatography — Advances and Perspectives*, Vol. 5, Academic Press, New York, 1988, pp. 95–209.

Journal of Chromatography, 536 (1991) 165–183
Elsevier Science Publishers B.V., Amsterdam

CHROMSYMP. 2033

High-performance liquid chromatography of amino acids, peptides and proteins

CVII.[a] Analysis of group retention contributions for peptides separated with a range of mobile and stationary phases by reversed-phase high-performance liquid chromatography

M. C. J. WILCE, M. I. AGUILAR and M. T. W. HEARN*
Department of Biochemistry and Centre for Bioprocess and Technology, Monash University, Clayton, Victoria 3168 (Australia)

ABSTRACT

An extensive data base which comprises the retention data of a total of 2106 peptides has been established and used to derive individual amino acid group retention coefficients. A multiple linear regression matrix approach was employed for solving the numerical value of the coefficients from the multivariate structure–retention dependencies. Statistical analysis of the retention data revealed that a minimum of 100 peptides is required to provide consistent values of the amino acid coefficients. Categorisation of all peptides allowed the influence of various chromatographic parameters on the coefficients to be evaluated. In particular, a decrease in the alkyl chain length of the chemically modified *n*-alkylsilica from octadecyl to butyl did not generally coincide with a decrease in the value of the group retention coefficients of individual amino acids. This study has established a detailed computational basis for characterising peptide retention behaviour and provides further insight into the mechanism of the interaction of peptides with immobilised hydrocarbonaceous ligands.

INTRODUCTION

Reversed-phase high-performance liquid chromatography (RP-HPLC) is now the most widely used technique for the analytical, micro-, semi-preparative separation of peptides and proteins. This is due to a number of important reasons including: (i) the excellent resolution that can be achieved for homologous, as well as structurally disparate compounds under a wide range of chromatographic conditions; (ii) the high recovery of solutes (even at ultra microanalytical levels); (iii) the reproducibility of the separation; (iv) the ability to utilize RP-HPLC to evaluate various physicochemical

[a] For Part CVI, see ref. 29.

0021-9673/91/$03.50

parameters associated with peptide and protein surface interactions and folding (conformational) hierarchies.

Despite the ever increasing usage of RP-HPLC for the separation and analysis of peptides and proteins, the molecular processes that control the interaction between the non-polar stationary phase, the mobile phase, and the solute are not yet fully understood. The development of models to describe the mechanisms by which peptides and proteins interact with reversed-phase chromatographic systems would provide the basis for practical optimisation protocols concomitant with the elucidation of peptide and protein binding mechanisms.

No fully developed mechanistic, thermodynamic or extrathermodynamic models are yet available which adequately accommodate all the structural (primary, secondary, tertiary and higher order) properties and kinetic vagaries of peptide or protein retention behaviour with porous, chemically modified *n*-alkylsilicas. Because of this, most investigators have relied upon empirical non-mechanistic models. The most fully evolved and accessible of these models is based on the linear solvent strength (LSS) gradient elution concepts as originally developed by Snyder (see refs. 1–4). This model provides a quantitative basis for the evaluation of peptide and protein retention behaviour under ideal reversed-phase conditions, and allows a more rational selection of chromatographic parameters to achieve a set of optimal chromatographic conditions, particularly for those peptides that do not succumb to sorbent-induced conformational effects.

Several studies have characterised the retention behaviour of closely related structural analogues in terms of the LSS model and have demonstrated that the interaction of peptides with the hydrocarbonaceous stationary phase is intimately dependent on the relative topographic arrangement of primary hydrophobic and hydrophilic amino acid residues [2,4,5] coded within the peptide sequences. While the LSS retention model provides a useful basis for the optimisation of peptide separations, a number of chromatographic experiments are required for the procedure. An alternative experimental approach to the optimisation of peptide separations, based on a more complete understanding of the interaction processes of peptides and proteins in RP-HPLC, is to use chromatographically derived hydrophobicity coefficients to predict and confirm the retention time of peptides of known amino acid composition. Knowledge of reliable sets of amino acid coefficients would also be useful in validating LSS retention predictions with peptides which show regular retention behaviour. Several sets of retention coefficients have been reported which have been derived by a number of different methods [6–17]. A commonly used procedure for the measurement of the influence of individual amino acids residues on peptide retention times involves the use of synthetic peptide analogues in which designated positions are systematically changed [16,17].

We have previously reported an alternative approach for the derivation of hydrophobicity coefficients in which retention coefficients were determined using iterative linear regression analysis of retention data derived from peptides with significantly different amino acid sequences [6]. The results of these and several other studies generally indicate that the hydrophobic contribution of amino acid residues in small peptides results in an essentially additive effect on peptide retention to alkylsilicas [6–17]. These observations are in accordance with the linear free energy relationships and associated predictions of the Martin[64], Hansch[65] and Hammet[66]

equations. With larger peptides, where secondary and tertiary structural features become more important, greater deviations of experimental retention times from those calculated from the summated coefficients have typically been observed. These differences arise as a consequence of the solute interacting with the sorbent through only a proportion of its total molecular surface. In an attempt to allow for the deviations in predicted retention time from experimentally observed retention behaviour of large polypeptides and proteins, Mant *et al.* [18], used a linearisation approach, in which correction factors were introduced to derive the predicted retention time based on the use of the natural logarithm of the length of the particular peptide or protein. This numerical method follows the observation that there is an exponential-like relationship between predicted and observed retention time with an increase in peptide chain length. Although such numerical correction methods give improved correlation between the predicted and experimental retention times for the test set of solutes, they unfortunately shed no light on the mechanism of binding for these larger molecules nor do they represent a *de novo* procedure for the prediction of retention of peptides of similar length and composition but difference sequence.

It is now well established that peptides and proteins interact with the stationary phase surface in an orientation specific manner [19–22]. Thus, their chromatographic retention behaviour is determined by the molecular composition of a specific contact region. For small peptides comprising between *ca.* 3–15 amino acid residues, the contact region may represent a large proportion of the molecular surface. However, for large polypeptides and protein molecules, the chromatographic contact region will be a relatively small portion of the entire solute surface. Because the molecular composition of the contact region largely determines the retention properties of a particular solute, chromatographic retention parameters contain a vast amount of information regarding the interactive segment of the peptidic species.

The present investigation therefore extends our previous studies by deriving coefficients from a database of over 2000 peptides. In particular this study permitted a detailed analysis of the influence of several experimental parameters such as stationary phase and mobile phase composition on the individual coefficients for each amino acid. These data are particularly relevant to further understanding of the mechanistic basis of the interaction of peptides and proteins in RP-HPLC.

MATERIALS AND METHODS

An extensive literature search was carried out to establish the chromatographic data base for this study. The information required included peptide sequence, retention characteristics, and chromatographic conditions. Hydrophobic group retention coefficients were calculated from the literature peptides and their retention data using multiple linear regression analyses.

The multiple linear regression was carried out using a matrix approach for solving sets of simultaneous equations. For the multiple linear regression technique used in this study the group retention contribution of each amino acid is considered as an unknown X_i. The percentage mole fraction of organic modifier present at the time of elution of each peptide, MF_k, and the corresponding amino acid composition are considered as a set of simultaneous equations as follows;

$$a_{11}X_1 + a_{12}X_2 + \ldots a_{1n}X_n = MF_1$$
$$a_{21}X_1 + a_{22}X_2 + \ldots a_{2n}X_n = MF_2$$
$$a_{m1}X_1 + a_{m2}X_2 + \ldots a_{mn}X_n = MF_m$$

which can be rewritten in matrix form,

$$\mathbf{A} = \begin{bmatrix} a_{11} & a_{12} & \ldots & a_{1n} \\ a_{21} & a_{22} & \ldots & a_{2n} \\ \cdot & \cdot & & \cdot \\ a_{m1} & a_{m2} & \ldots & a_{mn} \end{bmatrix}$$

$$\mathbf{X} = \begin{bmatrix} X_1 \\ X_2 \\ \cdot \\ X_n \end{bmatrix} \qquad \mathbf{b} = \begin{bmatrix} MF_1 \\ MF_2 \\ \cdot \\ MF_m \end{bmatrix}$$

The vector **X**, of group retention coefficients, can be solved as $\mathbf{X} = (\mathbf{A}^T\mathbf{b})(\mathbf{A}^T\mathbf{A})^{-1}$. These equations were then solved with partial pivoting. The theoretical *MF* for each peptide was then calculated by addition of the appropriate retention coefficients. Thus, in order to compare the retention data derived from the range of chromatographic conditions listed in Table I, all elution times were converted to *MF* according to the known rate of change of organic solvent concentration. The degree of correlation between the calculated group retention coefficients and the retention data was assessed by the correlation coefficient, R^2.

The multiple linear regression was performed on one of two computers. For small data sets, it was most convenient to use a multiple linear regression program written by the authors in Pascal for the IBM PC/AT or compatible, but for large data sets the group retention coefficients were calculated using the multiple linear regression routine from the SPSS^X package on the Monash University VAX computer. Both programs produced identical results. A simple database program was also written in Pascal by the authors for the IBM PC/AT to store the peptide data and to allow the retrieval of particular peptides and their chromatographic data from criteria specified by the user.

RESULTS AND DISCUSSION

Derivation of amino acid coefficients

Peptidic solutes are retained in RP-HPLC by the expulsion of the solute from the polar mobile phase with concomitant adsorption onto the non-polar stationary phase. The differential retardation of the solute species is dependent upon its intrinsic hydrophobicity, the eluotropicity of the mobile phase and the nature of the hydrocarbonaceous stationary phase.

The basis of the calculations to derive the amino acid group retention coefficients assumes that peptide retention can be described solely in terms of ideal reversed-phase behaviour, and that there is a first order dependency of peptide retention on the mole fraction of organic modifier. Thus in the absence of electrostatic or hydrogen bonding effects, the solute retention will be determined solely by the nature of the solvophobic

solute–ligand interaction and is given in terms of the capacity factor k' according to

$$k'_{\text{hydrophobic}} = \varphi K_{\text{hydrophobic}}$$

where K is the equilibrium association constant and φ is the phase ratio (volume stationary phase/volume mobile phase). The selectivity between two peptides, P_i and P_j separated under a defined set of chromatographic conditions can then be expressed as

$$\ln \alpha_{i,j} = \ln (k'_j/k'_i)$$

If we consider two peptides of similar sequence only differing by one amino acid residue, then the group retention coefficient due to the different amino acid can be defined as

$$\tau = \ln \alpha_{i,j} = \ln (k'_{\text{peptide } i}) - \ln (k'_{\text{peptide } j})$$

The τ contribution is thus a function of the differences in the overall standard unitary free energy changes and can be formally associated with the transfer of peptide solute i from the mobile phase to the stationary phase relative to the transfer of peptide j of identical residue number. According to the solvophobic theory [23] the surface area of the solute molecule which is in contact with the non-polar stationary phase plays a significant role in determining the magnitude of hydrophobic interaction. Since linear free energy relationships are anticipated between bulk phase partition parameters and functional group contributions, linear relationships should also exist between retention behaviour, as expressed by $\ln k'$ values and the surface area of the solute contact region with the stationary phase. Furthermore, as these hydrophobicity coefficients are derived from chromatographic retention data, they are physicochemically related to the binding energy of each amino acid. Derivation of the coefficients in this manner therefore provides a general approach to quantitating the relative propensity of each residue in a particular amino acid sequence to interact with a surface of defined ligand structure and density. As discussed earlier, the optimisation of solute retention can be achieved by varying the organic modifier, or through manipulation of secondary chemical equilibria such as ion-pairing, ionisation and solvation effects, or by selecting different stationary phases [1–4]. This paper considers, through the use of group retention coefficients, changes in the interactive nature of amino acid residues under a range of chromatographic conditions such as changes in the chain length of the stationary phase ligand, and different organic modifiers in the mobile phase.

To derive amino acid group retention coefficients for a large number of peptides from a range of chromatographic conditions, and to explore the effect of varied chromatographic conditions on the group retention coefficients, a database of 2106 peptides was established as described in the Materials and Methods section. A total of 44 different sets of peptides consisting of 1337 peptides and 14 726 amino acids were selected from this database including those from our previous studies. Table I lists the chromatographic conditions which include both the stationary phase and mobile phase characteristics, and the literature reference for each peptide data set. Over the

TABLE I

PARAMETERS AND LITERATURE SOURCES OF CHROMATOGRAPHIC DATA

NR = Not recorded in literature reference; DL = data collected in this laboratory.

Data set number	Stationary phase[a]	Mobile phase[b]	Flow-rate	Column length	Column type	Ref.
1	C18	TA	1.00	250	Ultrasphere ODS	30
2	C18	TA	1.50	300	μBondapak	31
4	C18	TA	1.00	NR	Chromegabond MC-18	32
5	C18	TA	3.00	250	SynChropak RP-P	33
6	C18	TA	0.70	NR	RPC18	33
7	C18	TPA	0.70	NR	SynChropak RP-P	33
8	C4	TA	1.00	250	RP304	34
10	C18	TPA	1.00	NR	Unknown	35
11	C18	TA	3.00	250	RP300	36
12	C18	TA	1.50	250	Vydac TP RP	37
13	C18	TA	0.50	300	TSK LS-410	38
14	C18	TA	0.80	300	TSK-Gel LS-410AK	38
16	C8	TA	1.00	250	Altex Ultrasphere	39
18	C8	TA	1.00	250	Altex Ultrasphere	39
19	C8	TA	1.20	NR	Aquapore RP300	40
20	C18	TA	0.50	250	SynChropak	41
21	C4	TA	0.80	250	Vydac	41
22	C18	TA	1.00	250	Vydac	42
23	C4	TA	1.00	250	NR	43
24	C18	TA	1.00	250	Nucleosil	44
25	C18	TA	1.00	250	Developmental column	DL
26	C4	TA	1.00	250	Bakerbond wide pore	DL
27	C18	TA	1.00	250	Bakerbond wide pore	DL
28	C18	TA	1.00	250	Bakerbond wide pore	DL
31	C18	TA	1.00	300	μBondapak	45
35	C18	TA	2.00	250	Aquapore RP-300	46
37	C18	TA	1.00	150	Cosmosil 5C18-P	47
60	C8	TPA	1.00	250	LiChrosorb RP-8	48
61	C18	TA	0.80	300	Cosmosil 5C18	49
62	C4	TPA	1.00	250	Bakerbond	50
63	C18	TPA	1.00	300	Bakerbond	50
65	C18	TA	1.00	159	NR	51
69	C18	TA	1.20	250	μBondapak	52
70a	C18	TA	1.20	250	μBondapak	53
70b	C18	TA	1.00	250	μBondapak	53
73	C18	TA	1.00	NR	Ultropac TSK ODS-120	54
74	C18	TA	1.00	250	μBondapak	55
75	C18	TA	1.00	250	RP-P SynChropak	56
76	C18	TA	1.00	250	RP-P SynChropak	57
77	C18	TA	1.00	250	Brownlee RP-300	58
79	C18	TA	1.00	150	Cosmosil 5C18	59
81	C18	TA	1.00	NR	Cosmosil 5C18 P	60
83	C18	TA	1.00	NR	TSK Gel 410AK	61
86	C18	TPA	1.00	300	TSK Gel LS 410 A	62
87	C18	TPA	1.00	300	TSK Gel LS 410 A	63

[a] C18 = Reversed-phase octadecyl stationary phase. C8 = reversed-phase octyl stationary phase. C4 = reversed-phase butyl stationary phase.

[b] TA = Trifluoroacetic acid–acetonitrile–water; TPA = trifluoroacetic acid–1-propanol–acetonitrile–water. All peptides were separated with gradient elution between mobile phases composed of 0.1% trifluoroacetic acid–water and 0.1% trifluoroacetic acid–acetonitrile or (1-propanol–acetonitrile)–water mixtures.

range of conditions examined it has been observed that there is a direct linear relationship between retention time and the percentage organic modifier present at the time of elution of a peptidic solute [12].

The group retention coefficients presented here were generated with a multiple linear regression that solves sets of simultaneous equations in a matrix format. An alternative computational approach for the derivation of group retention coefficients is multiple linear analysis with forcing [6], which in some circumstances has been shown to generate comparable results. Although the programming of forcing routines is less complex than the matrix method and also has a much smaller memory overhead, the matrix method is considered to be superior because the group retention coefficients are derived by statistical means. This matrix approach thus provides significantly more information about the individual group retention coefficients. In particular the interrelationship between the variability of the group retention coefficients for a particular amino acid, and the co-correlation of the group retention coefficients between different amino acid residues, allow independent or synergistic effects on solute retention to be explored.

The establishment of a large peptide database allowed the selection of groups of peptides depending on their chromatographic characteristics. Before multiple linear regression analysis of these groups could be examined the influence of various parameters such as sample size and peptide length on the computational results were addressed.

The effect of sample size

The statistical significance of any mathematical procedure is closely dependent on the number of data points available. The availability of several hundred peptides for the derivation of coefficients provided the opportunity for statistical evaluation of the influence of the sample size on the group retention coefficients. Seven different sample sizes were generated which consisted of 25, 30, 50, 70, 100, 200 and 500 peptides. The peptides for the sample size study were all randomly selected from 971 peptides. They were all separated with an octadecylsilica stationary phase with gradient elution between mobile phases of 0.1% trifluoroacetic acid (TFA)–water and 0.1% TFA–acetonitrile (ACN)–water mixtures. The random selection for each sample size was repeated six times to obtain six randomly selected groups of peptides for comparison. Each randomly selected group was then subjected to multiple linear regression to determine the group retention coefficients. Table II lists the six correlation coefficients, (R^2), for the comparison of the observed *MF versus* predicted *MF* within each randomly selected peptide set, the average of these values and the sum of variance for each of the seven sample size groups. The average correlation coefficient, R^2, and the sum of variance for each sample size are plotted in Fig. 1. Examination of the correlation coefficients in Table II indicate that the correlation coefficients increase with decreasing sample sizes, which suggests that sample sizes of less than 30 peptides provide the most accurate group retention coefficients solely for that specific set of peptides. However, the influence of sample size on the final value of each retention coefficient was further assessed through the determination of the sum of variances, listed in Table II and plotted in Fig. 1. The variance of the group retention coefficients for the amino acids between the six data sets within each sample size were calculated according to

$$\text{variance} = \frac{1}{6}\sum_{j=1}^{6}(X_{i,j} - M)^2$$

where M is equal to the mean of the group retention coefficients X_1 to X_6. The variance for each amino acid within each sample size were summed to give the sum of variance, listed in Table II and plotted in Fig. 1. As demonstrated in Fig. 1 both the sum of variances, and R^2 of the group retention coefficients reach an asymptotic plateau when the sample size is greater than 100 peptides. The sum of variances indicates that the small randomly selected peptide data sets produce group retention coefficients that vary considerably for each amino acid between data sets. Thus smaller sample sizes, such as a data set of 10–25 peptides, result in group retention coefficients that are accurate descriptors only for the particular set of peptides from which they were derived. Interestingly, except for a remarkably few exceptions most hydrophobic coefficients have been previously derived using data sets of this sample size and this would account for their lower utility for predicting retention behaviour with unrelated peptides. As is evident from the present study, larger data sets result in lower correlation coefficients but also lower sums of variances and provide amino acid group retention coefficients which are more universally applicable.

This variation between group retention coefficients calculated from small data sets, *i.e.*, less than 100 peptides, may be derived from the fact that the calculated retention coefficient of a particular amino acid in a peptide is not simply a result of its interaction with the chromatographic system, *i.e.*, the non-polar stationary phase and the aquo-organic–ionic modifier elution system. Rather it is a measure of the interaction of a particular amino acid with the chromatographic system in a discrete environment within the peptide. If it is assumed that only those amino acids that are sequentially adjacent have a nearest neighbour effect, or take part in creating a Nearest Neighbour Environment (NNE) for a particular amino acid, then that amino acid can be found in a total of 400 different NNEs. The group retention coefficient of any amino

TABLE II

REPLICATE AND AVERAGE CORRELATION COEFFICIENTS (OBSERVED *MF VERSUS* PREDICTED *MF*), AND THE SUM OF VARIANCE FOR RANDOMLY SELECTED PEPTIDE DATA SETS OF VARIED SAMPLE SIZE

Number of peptides	Replicate number						Average	Sum of variance
	1	2	3	4	5	6		
	Correlation coefficient, R^2							
500	0.49	0.39	0.43	0.40	0.48	0.49	0.46	7.2
200	0.48	0.48	0.47	0.50	0.51	0.49	0.49	16.5
100	0.58	0.52	0.70	0.46	0.47	0.47	0.53	44.7
70	0.65	0.69	0.57	0.47	0.58	0.59	0.59	61.3
50	0.65	0.72	0.60	0.63	0.87	0.66	0.68	157.2
30	0.89	0.85	0.69	0.91	0.63	0.88	0.81	456.2
25	0.97	0.98	0.94	0.92	0.97	0.95	0.96	1504.3

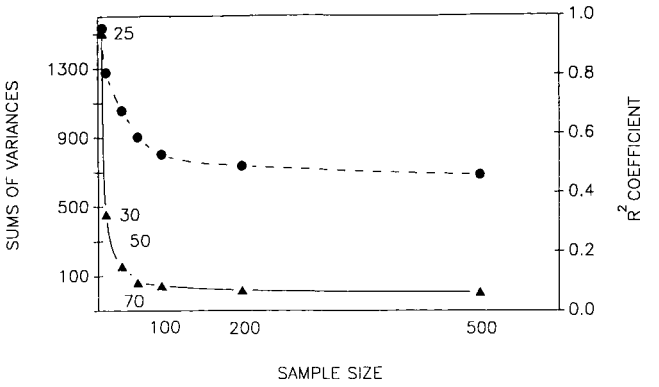

Fig. 1. Dependence of the (▲) sums of variances and (●) correlation coefficient, R^2, for calculated group retention coefficients with varying sample size.

acid will therefore be affected by its NNE. With a small sample size only a very limited number of these NNE will exist for a certain amino acid. As a consequence, it would be anticipated that a smaller variation in the calculated group retention coefficients, *i.e.*, higher correlation coefficient, R^2, would be observed. Conversely, with a large sample, as observed with the 500 peptide sample size data set a particular amino acid will be found in a far greater range of NNE of which the retention coefficient will represent an average. Similar conclusions have been made by Houghten and DeGraw [17] who systematically substituted every residue position of a 13-amino acid peptide with all of the 20 naturally occurring amino acids, thus generating 13 sets of 20 peptides.

Furthermore, if the secondary structure of a peptide is considered, spatially adjacent amino acids will also form part of the NNE. If a particular amino acid has a penchant for specific regions of secondary structure as proposed by Chou and Fasman [24], then the group retention coefficient will include information concerning secondary structure preferences for each amino acid.

The effect of peptide length

As stated earlier, for larger peptides there is generally poorer correlation between the observed retention time and the theoretical retention time based on the summation of the group retention coefficients than for small peptides. From temperature studies on the retention behaviour of a range of peptides we have deduced that these reduced correlations are due to stabilized secondary structures that effectively control the orientation of those amino acid residues that will interact with the stationary phase [19,20]. To study the effect of peptide length on the group retention coefficients, and to establish an optimum length for the generation of hydrophobic retention coefficients, a group of coefficients were calculated from sets of peptides selected from those peptides eluted from an octadecyl stationary phase with a gradient mobile phase of 0.1% TFA–ACN–water. The variation in peptide length ranged from 4–15 residues. In order to generate group retention coefficients which cover a reasonable number of NNEs, each sample size data set comprised more than 100 peptides. Table III lists the maximum peptide length, the number of peptides selected in each group, the

TABLE III

CORRELATION COEFFICIENTS FOR PEPTIDE DATA SETS SELECTED ACCORDING TO PEPTIDE LENGTH

Maximum peptide length	Number of peptides	Correlation coefficient, R^2
15	778	0.60
10	611	0.58
8	478	0.58
5	248	0.66
4	165	0.63

correlation coefficients, R^2, and the sample size. The relative constancy of the correlation coefficients of between 0.58 to 0.66 demonstrates that there is no appreciable effect of peptide length on the group retention coefficients within the range of peptide length considered in this study. From Fig. 2, which shows the frequency distribution of chain length of all the peptides used for this study, it can be seen that by far the greater majority of the peptides are less than 15 residues in length.

Collective grouping of the peptides

As noted in the earlier section, *The effect of sample size*, the minimum size for a set of peptides required to generate consistent group retention coefficients is approximately 100 record entries. In order to satisfy this criterion, the peptide literature data sets were combined according to the nature of either the stationary and/or the mobile phase to produce data sets of greater than 100 peptides. The range of chromatographic conditions was examined (Table I) and 12 groups were chosen as shown in Table IV. The mormalised individual amino acid coefficients for each of the 12 groups are plotted in histograms shown in Fig. 3.

The first 6 groupings in the histograms, MF to MFCTF1C, examine the effect of particular chromatographic parameters on the group retention coefficients. Group 1 represents the group retention coefficients calculated using all the available peptides and their MF. The next 5 groups incorporate a stepwise refinement of the selection criteria, thereby reducing the number of variable parameters. This allows the impact of a particular parameter to be assessed. Group 2 represents the group retention coefficients for all peptides eluted with a gradient of aqueous TFA–ACN as the mobile phase. Group 3 shows the group retention coefficients for peptides eluted from octadecylsilica sorbents. Group 4, designated MFC18TA, corresponds to a chromatographic system incorporating a octadecylsilica column and an aqueous TFA–ACN gradient mobile phase. Group 5 and group 6 represent further refinement of the selection criteria of group 4. Group 5 (MFTF1) contains only data obtained with a flow-rate of 1.0 ml/min, while group 6 (MFTF1C) represents data obtained with a flow-rate of 1.0 ml/min and a column length of 250 nm.

Group 7 and 8, MFTPA and MFC18TPA, contain retention data of peptides eluted with a gradient mobile phase of aqueous 0.1% TFA–1-propanol–ACN (33:77). The group retention coefficients in group 7 are generated from peptides eluted on all stationary phases, while group 8, MFC18TPA, is taken from those peptides eluted

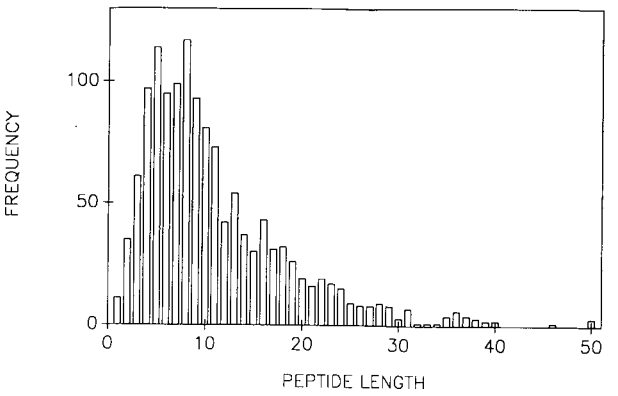

Fig. 2. Frequency distribution histogram of the length of peptides used in this study.

with the same mobile phase but only with octadecylsilica columns. The final four groups, MFC4 to MFC8TA, represent a set of chromatographic conditions in which the nature of the chemically bonded alkyl ligand is changed. Group 9, MFC4, are those group retention coefficients generated from peptides eluted on a *n*-butylsilica bonded stationary phase, and MFC4TA, group 10, those peptides chromatographed on a *n*-butylsilica column and with a gradient mobile phase of 0.1% TFA–ACN–water. The final two groups 11 and 12 contain peptides eluted from an octylsilica column and with 0.1% TFA–ACN–water.

The classification used to generate groups 1–6, MF to MFCTF1C, allows the assessment of the influence of different chromatographic parameters on the group retention coefficients for peptides eluted in a gradient of TFA–ACN–water and with an octadecylsilica column. Table IV shows the correlation coefficients, R^2, for all the

TABLE IV

EXPLANATION OF PEPTIDE RETENTION DATA GROUPINGS

The chromatographic selection criteria are shown in the second column, followed by the number of peptides in each group and the correlation coefficient (observed *versus* expected *MF*).

Database codes	Explanation	Number of peptides	Correlation coefficient, R^2
MF	All peptides	2016	0.29
MFTA	TFA–ACN	1258	0.62
MFC18	RP-C18	1244	0.57
MFC18TA	RP-C18 and TFA–ACN	971	0.66
MFCTF1	RP-C18, TFA–ACN and flow-rate 1.0 ml/min	494	0.69
MFCTF1C	RP-C18, TFA–ACN, flow-rate 1.0 ml/min and column length 250 mm	325	0.69
MFTPA	TFA–propanol–ACN	220	0.69
MFC18TPA	RP-C18 and TFA–propanol–ACN	196	0.69
MFC4	RP-C4	136	0.77
MFC4TA	RP-C4 and TFA–ACN	96	0.80
MFC8	RP-C8	104	0.87
MFC8TA	RP-C8 and TFA–ACN	104	0.87

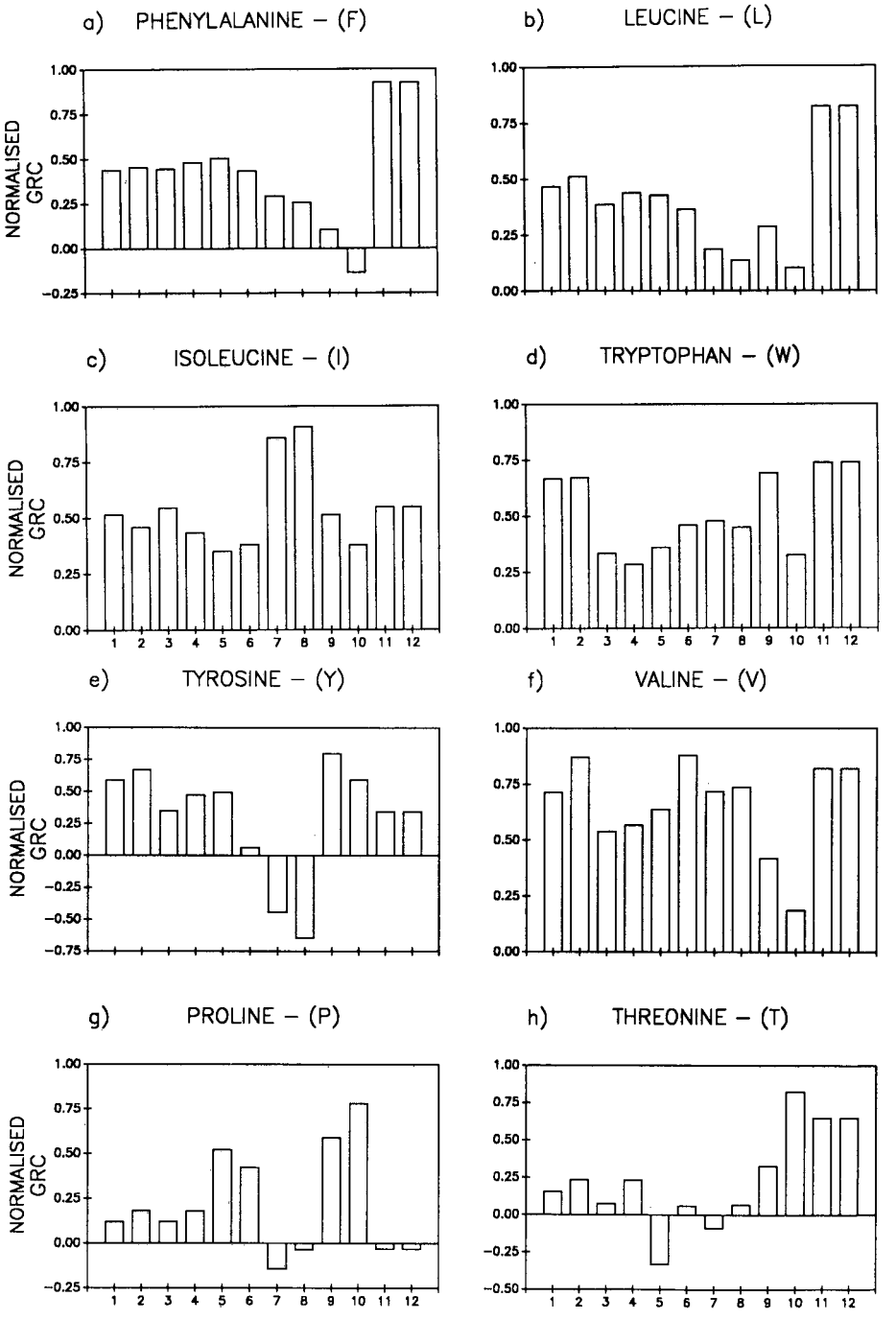
a) PHENYLALANINE – (F)
b) LEUCINE – (L)
c) ISOLEUCINE – (I)
d) TRYPTOPHAN – (W)
e) TYROSINE – (Y)
f) VALINE – (V)
g) PROLINE – (P)
h) THREONINE – (T)
NORMALISED GRC
1.00
0.75
0.50
0.25
0.00
−0.25
−0.50
−0.75
1 2 3 4 5 6 7 8 9 10 11 12

Fig. 3.

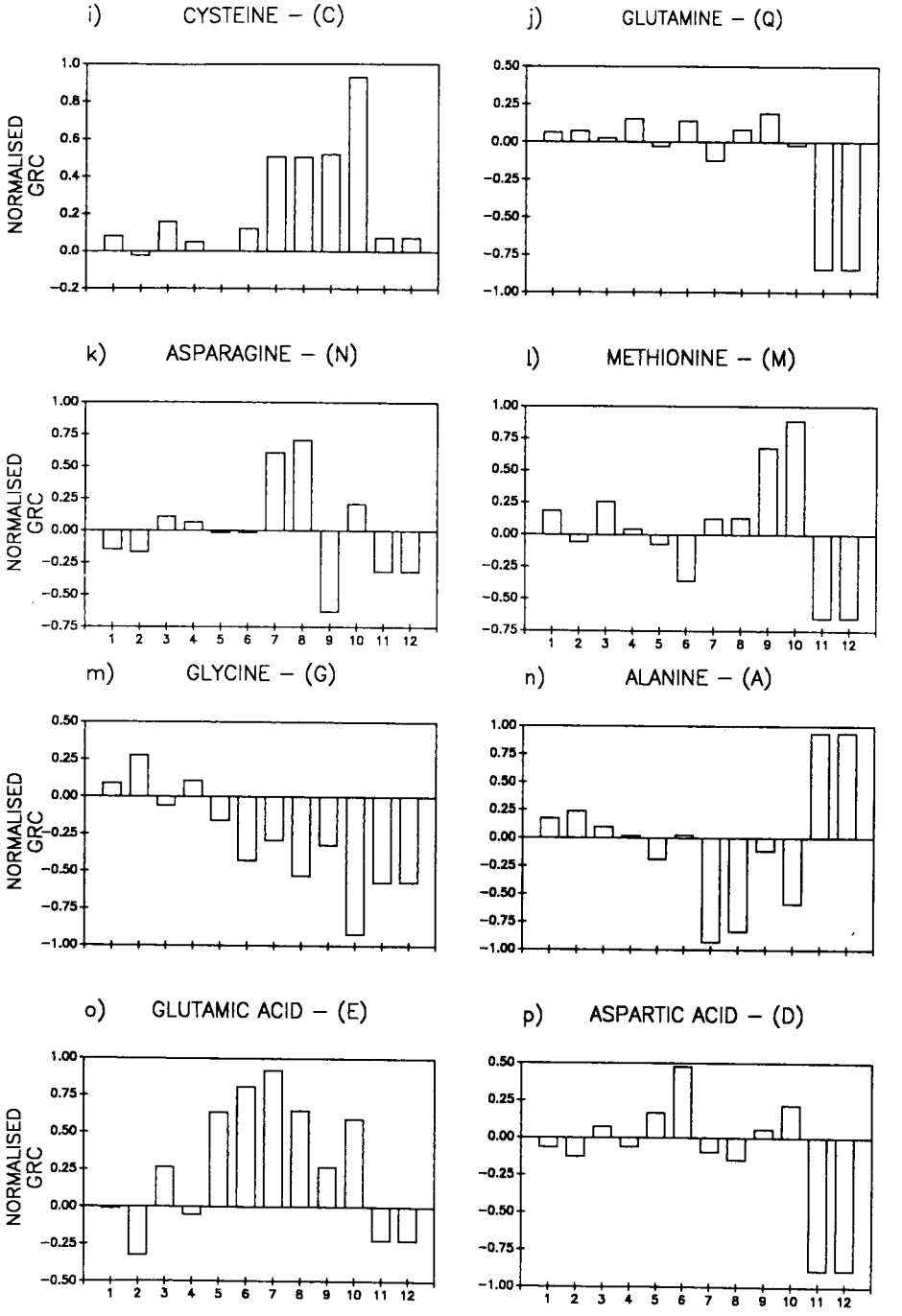

Fig. 3.

(Continued on p. 178)

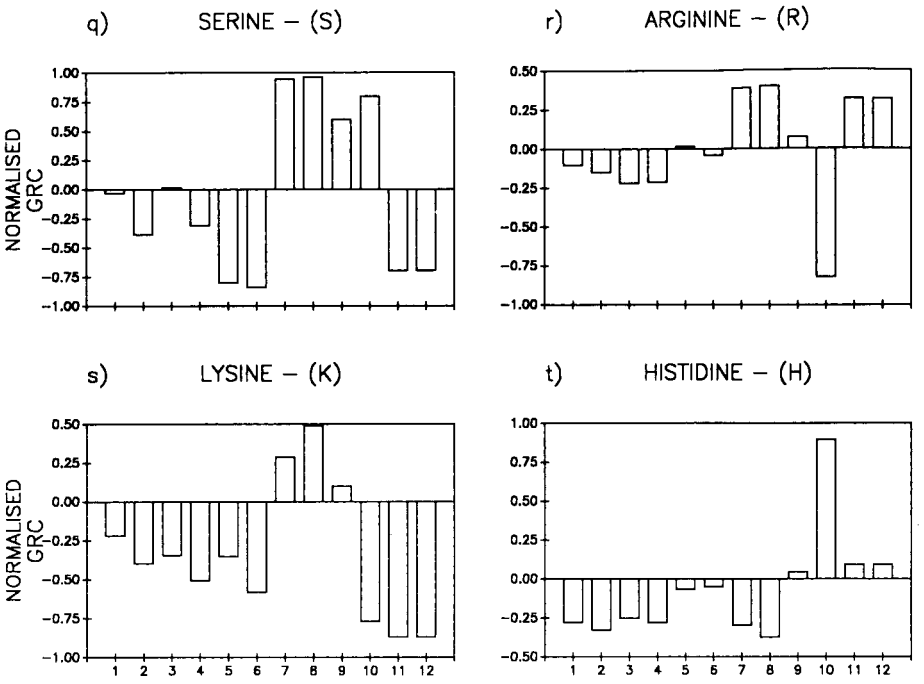

Fig. 3. Amino acid group retention coefficients (GRC) for each group. Groupings: 1 = MF; 2 = MFC18; 3 = MFTA; 4 = MFC18TA; 5 = MFCTF1; 6 = MFCTF1C; 7 = MFTPA; 8 = MFC18TPA; 9 = MFC4; 10 = MFC4TA; 11 = MFC8; 12 = MFC8TA. Table IV provides an explanation of these groupings.

groups of group retention coefficients. Examination of the histograms shown in Fig. 3 demonstrate that for each amino acid, a reasonably constant value for the group retention coefficients is obtained for groups 1–6. The range of R^2 values, as shown in Table III, indicate that all of the selection criteria have an effect on the group retention coefficients. However, once the stationary phase ligand and the mobile phase had been selected the other chromatographic parameters such as flow-rate and column length have only a marginal effect. The general agreement of the group retention coefficients amongst these columns therefore again confirms that the nature of the stationary and mobile phase and not the column length, gradient slope, flow-rate etc., are the dominant variables to be considered, and is consistent with the approach of data grouping used in this study.

The effect of mobile phase composition and alkyl chain length

Numerous investigations have examined various factors involved in the development and application of non-polar bonded stationary phases (for a compendium see refs. 25 and 26), but the underlying separation mechanisms for peptides and proteins are still poorly understood. One of the major factors which control the retention of peptide solutes in RP-HPLC is the relative eluotropicity of the organic modifier. Furthermore, a number of long range Van der Waals, London and Lifshitz intermolecular interations, as well as, dispersion forces, dipole polarisation and

hydrogen-bonding, can also occur between the sample and mobile phase molecules which further influence peptide retention behaviour. The present study considers the effect of two mobile phases aqueous, TFA–ACN and TFA–1-propanol–ACN, on the derived amino acid group retention coefficients. A statistical measure was used to estimate the relative interactive potential of each amino acid with aqueous TFA–ACN and TFA–1-propanol–ACN. This approach involved taking the difference between the coefficients for each amino acid for the pair of mobile phases. The mean and standard deviation of the difference coefficients were then determined according to:

$$\text{mean} = \frac{1}{20} \sum_{i=1}^{20} (XI_i - XII_i)$$

$$\text{standard deviation} = \frac{1}{20} \left\{ \sum_{i=1}^{20} [(XI_i - XII_i) - \text{mean}]^2 \right\}$$

where XI_i is mobile phase I coefficient of amino acid i, XII_i is mobile phase II coefficient and $XI_i - XII_i$ is difference coefficient ΔGRC. Those amino acids which have a difference coefficient, ΔGRC, further than 1 standard deviation from the mean are considered to have significantly different group retention coefficients in the two mobile phases. Table V lists the ΔGRC, the mean and standard deviations.

In changing the mobile phase from TFA–ACN to TFA–1-propanol–ACN the amino acids F, L, I, Y, C and A all have significant difference coefficients. Furthermore, when present within the peptide contact area F, L, Y and A interact more strongly with the octadecylsilica ligand when the mobile phase is TFA–ACN, while I and C interact more strongly when the mobile phase is TFA–1-propanol–ACN. This observation therefore provides an explanation for the experimental observation of selectivity changes or reversals which can occur with a group of peptides when the organic modifier is changed.

The relative interactive potential of the 20 naturally occurring amino acids was also examined through variation in the chain length of the bonded alkylsilica in particular, octadecylsilica, octylsilica and butylsilica. The same statistical measure used to analyse the change in mobile phase was also applied to the comparison of the three stationary phases.

A decrease in the alkyl chain length from 18 to 8 carbon atoms resulted in statistically significant ΔGRCs for the amino acids F, L, W, Q, M, A and D, as listed in Table V. Furthermore, the strongly hydrophobic amino acids F, L and W, all exhibit enhanced values when interacting with the octylsilica column rather than the octadecylsilica as shown in Fig. 3. These amino acids therefore, when present in the peptide contact area, all manifest an increased apparent hydrophobicity. Conversely, the hydrophobicity coefficients for the amino acids Q, M and D were found to be larger with the 18 carbon alkyl chain. Those amino acids that have significant ΔGRCs when comparing a 18- and 4-carbon alkyl chain are F, L, C and H. The two hydrophobic amino acids F and L again exhibited enhanced hydrophobicity with the octadecylsilica column, whereas the amino acids C and H show apparent hydrophobicity increases with the butylsilica. The final comparison between the octylsilica and butylsilica revealed statistically significant ΔGRCs for the amino acids F, L, C, M, A, R and H. In

TABLE V

DIFFERENCE COEFFICIENTS

The italicized numbers indicate those difference coefficients, ΔGRC, further than one standard deviation from the mean. The mean and standard deviation for each set are also given.

Amino acid[a]	C18 – C8	C18 – C4	C8 – C4	C18 – TPA[b]
F	*−4.44*	*6.16*	*10.16*	*2.24*
L	*−3.07*	*2.67*	*5.75*	*2.41*
I	−0.90	0.46	1.35	−3.78
W	*−3.62*	−0.32	3.30	−1.30
Y	0.50	−0.48	−0.98	*4.47*
V	−0.71	1.06	1.77	−0.48
P	−0.84	−2.41	−3.25	0.86
T	−1.17	−1.66	−0.50	0.46
C	−0.24	*−8.81*	*−8.57*	*−4.54*
Q	*2.00*	0.35	−1.66	0.14
N	1.52	−0.58	−2.10	−2.57
M	*3.34*	−4.05	*−7.38*	−0.41
G	1.36	2.06	0.70	1.27
A	*−2.56*	1.70	*4.26*	*2.40*
E	0.35	−1.29	−1.63	−1.40
D	*2.64*	−0.90	−3.54	0.28
S	0.78	−2.21	−2.99	−2.54
R	−2.11	2.44	*4.55*	−2.44
K	1.16	0.84	−0.32	*−3.19*
H	*−2.99*	*−9.41*	*−6.42*	0.75
Mean	−0.41	−0.84	−0.42	−0.40
S.D.	2.10	3.38	4.43	2.24

[a] For abbreviations see Fig. 3.
[b] C18 – TPA is RP-C18 and TFA–1-propanol–ACN.

particular, Fig. 3 shows that C, M and H increased GRC values with the *n*-butylsilica sorbent.

Currently, a full molecular rationalisation of the varying specificities of the different alkyl ligands in terms of specific ligand–solute interactions is not feasible. This difficulty is primarily due to limited amount of information available on the exact nature of the sorbent surface. The main physical and chemical parameters used to characterise chemically modified, microparticulate *n*-alkylsilicas are specific surface area, mean pore diameter, specific pore volume, mean particle size, alkyl chain length and alkyl ligand density. However, knowledge of these bulk parameters gives very little information in terms of how the ligand interacts with a solute. In particular, the exact nature of the dynamic structure of the bonded phase has not been fully characterised. However it has been demonstrated by NMR studies that under conditions typical of chromatographic separations, the alkyl chains may assume different conformations [27]. These depend on the interaction of the chains with themselves, with neighbouring chains, with the "capping" groups, *e.g.*, trimethylsilyl groups, with the mobile phase and finally the solute. It has also been demonstrated that increasing the polarity of the mobile phase increases the mobility of the bonded alkyl groups [28]. All of these factors

will therefore influence the affinity of the solute for the non-polar sorbent which is ultimately manifested as the experimental retention time. The range of values of the group retention coefficients generated with different stationary phases indicates that the chain length exerts a dramatic effect on the way in which the surface of a peptide solute is probed by the alkyl ligand during the retention process. In accord with the concepts of the solvophobic theory, these results confirm that the surface area of the peptide solute involved with the interaction with the non-polar sorbent will vary significantly with a change in the characteristics of either the stationary or the mobile phase.

The procedure of group retention contribution mapping also allows the interactive specificities for particular amino acids to be evaluated. For instance, F, L, I and W all have relatively similar group retention coefficients when their corresponding peptides are eluted in TFA–ACN–water, but the values of the group retention coefficients vary noticeably when the mobile phase is changed to TFA–1-propanol–ACN–water (Table V and Fig. 3, columns 4 and 8). Clearly the hydrophobic nature of an amino acid within a peptide is dependent on the solvated microenvironment in which it is located. For instance, within a peptide structure, the amino acid Y is manifestly more hydrophobic when eluted with TFA–ACN–water than with TFA–1-propanol–ACN–water. Many other amino acids show this same phenomenon as can be seen in Fig. 3. Changes in the stationary phase also have a comparable effect. The retention coefficient changes for amino acid M indicate that within a peptide structure, this amino acid is quite hydrophobic when interacting with a butylsilica column but becomes less so with an octylsilica sorbent.

One point of interest is that the amino acids A, C, F, H and L have significant ΔGRCs for at least three of the four comparisons. What feature is it that these amino acids have that make their retention on RP-HPLC so susceptible to a change in either stationary or mobile phase composition? Because of the atomic features of these amino acids, it would appear that these differences cannot be attributed to hydrogen bond interactions. Similarly, these differences cannot be ascribed to sensitivity to side chain ionisation phenomena. Since the dynamic structure of the stationary phase is not known at the requisite level of molecular definition the precise mechanism by which these amino acids within a peptide structure interdigitate with the hydrocarbonaceous ligand remains to be elucidated. Until this is studied in greater detail with even more comprehensive data bases than those used in the present study, fully mechanistic interaction models will be difficult to produce. However the emergence of such data bases and descriptive molecular interaction models would provide valuable additional insight into the physicochemical origin of the hydrophobic effect, which even after 30 years of intensive research by many groups of investigators still remains to be resolved.

CONCLUSION

This study presents and validates a new mathematical approach to the calculation of group retention coefficients. The establishment of a large database of peptide retention data for the generation of the group retention coefficients allowed the influence of a number of parameters on the group retention coefficients to be assessed. In particular it was found that to generate consistent group retention coefficients the retention data of at least 100 peptides is required. The database

contained peptide retention data from peptides eluted from a range of chemically modified *n*-alkylsilicas and aquo-organic mobile phases. This allowed the examination of the variation of the interaction of the individual amino acids with the alkyl ligands under a range of chromatographic conditions.

ACKNOWLEDGEMENTS

These investigations were supported by the Australian Research Council and National Health and Medical Research Council of Australia (M.T.W.H.). The support of the Potter Foundation and the Buckland Foundation is also gratefully acknowledged.

REFERENCES

1 M. A. Stadalius, H. S. Gold and L. R. Snyder, *J. Chromatogr.*, 296 (1984) 31.
2 M. I Aguilar, A. N. Hodder and M. T. W. Hearn, *J. Chromatogr.*, 327 (1985) 115.
3 M. T. W. Hearn and M. I. Aguilar, *J. Chromatogr.*, 359 (1986) 31.
4 M. T. W. Hearn and M. I. Aguilar, *J. Chromatogr.*, 392 (1987) 33.
5 M. T. W. Hearn and M. I. Aguilar, *J. Chromatogr.*, 352 (1986) 35.
6 S. J. Su, B. Grego, B. Niven and M. T. W. Hearn, *J. Liq. Chromatogr.*, 4 (1981) 1745.
7 R. F. Rekker and H. M. De Kart, *Eur. J. Med. Chem.*, 14 (1979) 479.
8 J. L. Meek and Z. L. Rosetti, *J. Chromatogr.*, 211 (1981) 15.
9 V. Pliska and M. Fauchere, in E. Gross (Editor), *Peptides, Structure and Biological Function*, Pierce, Rockford, IL, 1979, p. 249.
10 A. Segrest and R. Feldmann, *J. Mol. Biol.*, 87 (1974) 853.
11 K. J. Wilson, A. Honegger, R. P. Stotzel and G. J. Hughes, *Biochem. J.*, 199 (1981) 31.
12 C. A. Browne, H. P. J. Bennett and S. Solomon, in M. T. W. Hearn, F. E. Regnier and C. T. Wehr (Editors), *High Performance Liquid Chromatography*, Academic Press, New York, 1983, p. 65.
13 Y. Nazaki and C. Tanford, *J. Biol. Chem.*, 246 (1971) 2211.
14 T. Sasagawa, T. Okuyama and D. C. Teller, *J. Chromatogr.*, 240 (1982) 329.
15 D. Guo, C. T. Mant, A. K. Taneja, J. M. R. Parker and R. S. Hodges, *J. Chromatogr.*, 359 (1986) 499.
16 J. M. R. Parker, D. Guo and R. S. Hodges, *Biochem.*, 25 (1986) 5425.
17 V. Houghten and S. T. DeGraw, *J. Chromatogr.*, 386 (1987) 223.
18 C. T. Mant, N. E. Zhou and R. S. Hodges, *J. Chromatogr.*, 476 (1989) 363.
19 A. W. Purcell, M. I. Aguilar and M. T. W. Hearn, *J. Chromatogr.*, 476 (1989) 113.
20 A. W. Purcell, M. I. Aguilar and M. T. W. Hearn, *J. Chromatogr.*, 476 (1989) 125.
21 F. E. Regnier, *Science (Washington, D.C.)*, 228 (1987) 319.
22 M. L. Heinitz, E. Flanigan, R. C. Orlowsi and F. E. Regnier, *J. Chromatogr.*, 443 (1988) 229.
23 Cs. Horváth, W. R. Melander and I. Molnar, *J. Chromatogr.*, 125 (1976) 129.
24 P. Y. Chou and G. D. Fasman, *Ann. Rev. Biochem.*, 47 (1978) 251.
25 K. K. Unger, *Porous Silica*, Elsevier, Amsterdam, 1979.
26 K. K. Unger, *Packings and Stationary Phases in Chromatographic Techniques*, Marcel Dekker, New York, 1989.
27 E. Bayer, A. Paulus, B. Peters, G. Laupp, J. Reniers and K. Albert, *J. Chromatogr.*, 364 (1986) 25.
28 J. Nawrocki and B. Buszewski, *J. Chromatogr.*, 449 (1988) 1.
29 M. T. W. Hearn, *High Performance Liquid Chromatography of Peptide and Proteins: Separation, Analysis and Conformation*, CRC Press, Boca Raton, FL, 1990, in press.
30 G. E. Deibler, L. F. Boyd, R. E. Martenson and M. W. Kies, *J. Chromatogr.*, 326 (1985) 433.
31 S. James and H. P. I. Bennett, *J. Chromatogr.*, 326 (1985) 329.
32 H. W. Lahm and S. Stein, *J. Chromatogr.*, 326 (1985) 357.
33 M. D. Moore, P. Q. Behrens and A. F. Riggs, *J. Biol. Chem.*, 261 (1986) 10511.
34 I. Correas, D. W. Speicher and V. T. Marches, *J. Biol. Chem.*, 261 (1986) 13362.
35 J. A. Cromlish, N. G. Seidah and M. Chretien, *J. Biol. Chem.*, 261 (1986) 10859.

36 D. Barra, M. E. Schinina, W. H. Bannister, J. V. Bannister and F. Bossa, *J. Biol. Chem.*, 262 (1987) 1001.
37 H. C. Ludwig, F. Lottspeich, A. Henschen, R. Ladenstein and A. Bachen, *J. Biol. Chem.*, 262 (1987) 1016.
38 T. Sueyoshi, T. Miyata, N. Hashimoto, H. Kato, H. Hayashida, T. Miyata and S. Iwanaga, *J. Biol. Chem.*, 262 (1987) 2768.
39 H. S. Lu, P. J. Yuan and R. W. Gracy, *J. Biol. Chem.*, 259 (1984) 11958.
40 D. Barra, M. E. Schinina, M. Simmaco, J. V. Bannister, W. H. Bannister, G. Rotilio and F. Bossa, *J. Biol. Chem.*, 259 (1984) 12595.
41 P. H. Lai, R. Everett, F. F. Wang, T. Arakawa and E. Goldwasser, *J. Biol. Chem.*, 261 (1986) 3116.
42 P. J. Neame, J. E. Christner and J. R. Baker, *J. Biol. Chem.*, 261 (1986) 3519.
43 K. M. Zsebo, H. S. Lu, J. C. Fieschko, L. Goldstein, J. Davis, K. Duker, S. V. Suggs, P. H. Lai and G. A. Bitter, *J. Biol. Chem.*, 261 (1986) 5858.
44 H. Hirano, C. Fukazawa and K. Harada, *J. Biol. Chem.*, 259 (1984) 14371.
45 B. Grego, F. Lambrou and M. T. W. Hearn, *J. Chromatogr.*, 266 (1983) 89.
46 S. T. Davrat-Larrogue, K. Brew and R. E. Fenna, *J. Biol. Chem.*, 261 (1986) 3607.
47 T. Suzuki, *J. Biol. Chem.*, 261 (1986) 3692.
48 K. G. Linden and W. F. Benisek, *J. Biol. Chem.*, 261 (1986) 6454.
49 T. Yubisui, T. Miyata, S. Iwanaga, M. Tamura and M. Takeshita, *J. Biochem.*, 99 (1986) 407.
50 Y. Kitagawa, S. Tsunasawa, N. Tanaka and Y. Katsube, *J. Biochem.*, 99 (1986) 1289.
51 J. Hirabayashi, H. Kawasaki, K. Suzuki and K. Kasai, *J. Biochem.*, 101 (1987) 775.
52 T. Takagi and K. Konishi, *J. Biochem.*, 95 (1984) 1603.
53 M. Singhofer-Wowra, L. Clayton, P. Dawson, K. Gull and M. Little, *Eur. J. Biochem.*, 161 (1986) 669.
54 O. Markovic and H. Jornvall, *Eur. J. Biochem.*, 158 (1986) 455.
55 O. V. Beg, H. von Bahr-Lindstrom, Z. H. Zaidi and H. Jornvall, *Eur. J. Biochem.*, 159 (1986) 195.
56 H. Wada, T. Takai and T. Tanabe, *Eur. J. Biochem.*, 167 (1987) 13.
57 F. Tokunaga, T. Miyata, T. Nakamura, T. Morita, K. Kuma, T. Miyata and S. Iwanaga, *Eur. J. Biochem.*, 167 (1987) 405.
58 F. Schoentgen, F. Saccoccio, J. Jolles, I. Bernier and P. Jolles, *Eur. J. Biochem.*, 166 (1987) 333.
59 T. Miyata, K. Usui and S. Iwanaga, *J. Biochem.*, 95 (1984) 1793.
60 T. Nakamura, T. Hirai, F. Tokunaga, S. Kawabata and S. Iwanaga, *J. Biochem.*, 101 (1987) 1297.
61 T. Hirao and K. Takahashi, *J. Biochem.*, 96 (1984) 775.
62 Y. Hamazume, T. Mega and T. Ikenaka, *J. Biochem.*, 95 (1984) 1633.
63 S.-H. Kim, S. Hara, S. Hase, T. Ikenaka, H. Tada, K. Kitamura and N. Kaizuma, *J. Biochem.*, 98 (1985) 435.
64 A. J. P. Martin and R. L. M. Synge, *Biochem. J.*, 35 (1941) 1358.
65 T. Fujita, I. Iwaja and C. Hansch, *J. Am. Chem. Soc.*, 86 (1964) 5175.
66 L. P. Hammett and H. L. Pflunger, *J. Am. Chem. Soc.*, 55 (1933) 4079.

Journal of Chromatography, 536 (1991) 185–191
Elsevier Science Publishers B.V., Amsterdam

CHROMSYMP. 2001

Separation and study of corrinoid cobalt-ligand isomers by high-performance liquid chromatography

SUSAN H. FORD*, ALVA NICHOLS and JEAN M. GALLERY
Chicago State University, 95th Street at King Drive, Chicago IL 60628 (U.S.A.)

ABSTRACT

Vitamin B_{12} belongs to a group of complex organo-cobalt compounds, the corrinoids. "Complete" corrinoids, such as B_{12}, contain a nucleotide as the cobalt α-(lower)ligand. This nucleotide is also connected to the periphery of the corrin ring. The "incomplete" corrinoids, in contrast, contain simple cobalt α-ligands, such as water or cyanide. Using analytical reversed-phase and anion-exchange high-performance liquid chromatography (HPLC), we have been able to study the behavior of several aquocyano-"incomplete" corrinoids: three isomeric cobinic acid pentaamides, cobinamide, and cobyric acid, all of which exist as thermally unstable isomers, which separate during HPLC. All but one of these corrinoids gave isomer mixtures of 1:1, the exception giving mixtures of 2:1 to 3:1. The separated stereoisomers had different retention times and were collected from analytical columns for further study.

INTRODUCTION

Vitamin B_{12} (cyanocobalamin) is a member of a group of complex organo-cobalt compounds called the corrinoids. Vitamin B_{12} itself is a "complete" corrinoid, having not only the corrin ring, which supplies four bonds to the central cobalt atom, but also a fifth and sixth ligand. These ligands are a cyanide group on the β (upper) side of the corrin ring and a nucleotide loop, which is connected to the periphery of the ring at position *f* (see Fig. 1) on the α (lower) side of the ring. Although most of the biologically important corrinoids are "complete", there is a group of naturally occurring corrins which do not contain the α side nucleotide loop and are therefore

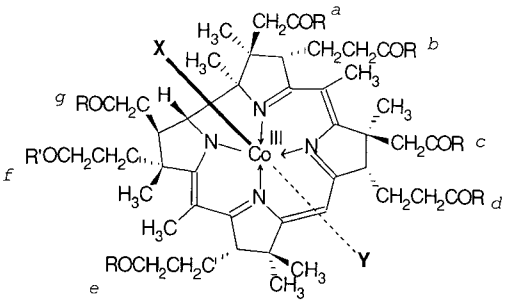

Fig. 1. Structure of the corrin ring.

0021-9673/91/$03.50

called "incomplete." Such corrinoids are of interest mainly as known or suspected cobalamin precursors, although one or two have also been identified as biologically active coenzymes [1]. In addition, study of the cobalt-ligand chemistry and reactivity in incomplete corrinoids has given insight into the mechanism of action of cobalamin-dependent enzymes [2].

The incomplete corrinoids, most of which are six-coordinate, may contain any two of a number of possible cobalt ligands in the α and β (axial, lower and upper, respectively) positions. Although water and/or cyanide are the ligands usually encountered, alkyl groups, carbohydrates, or amino acids can be attached as the sixth ligand under the right conditions [3,4]. When two different fifth and sixth ligands are present in incomplete corrinoids, then two different stereoisomers are possible. Fig. 1 illustrates the corrin ring, with the fifth and sixth ligands designated as X and Y. When these ligands are a water molecule and a cyanide group, the name of the corrinoid incorporates aquocyano as a prefix. The position of each of these ligands [*i.e.* whether α (lower) or β (upper)] is known to shift rather rapidly at room temperature, but the individual stereoisomers can be "frozen out" and separated during chromatography at 3°C, as was demonstrated by Friedrich [5,6] in the case of cobyric acid.

HPLC can be used to separate and identify many of the naturally occurring corrinoids from bacterial or mammalian materials [7,8]. Although the complete corrinoids are the ones usually targeted for identification, the incomplete corrinoids are often encountered in mixtures from natural sources. Since these corrinoids can exist as stereoisomers, they often appear as double peaks during high-performance liquid chromatography (HPLC), leading to possible confusion about purity and identity of corrinoid mixture components. This study was designed to investigate the formation/isomerization of the (aquocyano) incomplete corrinoid stereoisomers during HPLC.

EXPERIMENTAL

All solvents used for HPLC were of HPLC grade. Water for HPLC buffers and solutions was distilled, deionized in a Millipore (Milford, MA, U.S.A.) system, filtered through a 0.2-μm membrane, and then degassed. Other chemicals and solvents were of analytical reagent grade.

High-performance liquid chromatography

HPLC was performed with a Waters system (Millipore, Waters Chromatography Division, Milford, MA, U.S.A.), consisting of an automatic gradient controller, dual Model 501 high-pressure pumps, a Rheodyne injector (Rheodyne, Cotati, CA, U.S.A.) with a 20-μl injection loop, and a Model 441 fixed-wavelength detector with a 365-nm filter. Peak areas from the data print-out on a Kipp & Zonen (Delft, The Netherlands) BD41 flatbed recorder were used to estimate the percentage of individual components in mixtures and of individual, separated stereoisomers. Both ion-exchange (Waters -NH_2 or Whatman Partisil 5-SAX, Whatman, Clifton, NJ, U.S.A.) and reversed-phase (Waters μBondapak C_{18} or Alltech Adsorbosphere C_{18}, Alltech Assoc., Deerfield, IL, U.S.A.) columns were used. The guard column, inserted between the injector and the analytical column, was RCSS CN (Millipore, Waters Chromatography Division) for ion-exchange and RCSS C_{18} for reversed-phase

chromatography. The Waters -NH_2 and Alltech Adsobosphere C_{18} columns were 250 × 4.6 mm I.D. The Waters μBondapak C_{18} column was 300 × 4.6 mm I.D. and the Whatman Partisil 5-SAX was 100 × 4.6 mm I.D.

Solvents used for ion-exchange HPLC were water–tetrahydrofuran (96:4) pyridine acetate buffers at 80 m*M* or less, pH range 6.0–3.5. Solvents for reversed-phase chromatography were methanol with aqueous acetic acid or acetonitrile with aqueous pyridine acetate buffer. Use of these solvents was as described in the text. Corrinoids were dissolved in HPLC-grade water and syringe-filtered through a 0.2-μm PTFE membrane (Vanguard, Neptune, NJ, U.S.A.) before injection. The amounts of incomplete corrinoid were in the 1–2-nmol range in 20-μl water or 0.01% aqueous KCN.

Corrinoid preparation

Incomplete corrinoids were obtained by chemical degradation of cyanocobalamin (Sigma, St. Louis, MO, U.S.A.). Cobyric acid (Fig. 1: R = NH_2, R′ = OH) was prepared by the Renz method [9] and cobinamide (Fig. 1: R = NH_2, R′ = $NHCH_2$-$CHOHCH_3$) was obtained as a major side-product from that preparation. The cobinic acid pentaamides (isomers 1 or 2 or 3, respectively, Fig. 1: R(*d* or *b* or *e*) = OH, otherwise R = NH_2, R′ = $NHCH_2CHOHCH_3$) were prepared via weak-acid hydrolysis [10], followed by treatment with cerous hydroxide [9]. All of these compounds were purified by Whatman DE-53 (acetate) low-pressure column chromatography with 0.05% aqueous HCN/0.08% aqueous acetic acid. After desalting by phenol extraction, and drying under a nitrogen stream, the aquocyano form was obtained for each of these incomplete corrinoids as a powder or glass. This form of incomplete corrinoids has a characteristic electronic absorption spectrum, with the γ band (the most intense in the spectrum), located at *ca.* 350–354 nm.

Diaquocorrinoids were prepared, with some modifications, following the method of Baldwin *et al.* [11] for diaquocobinamide. These compounds were frozen in sealed vials in aqueous solution and stored under nitrogen to prevent oxidation [11].

Corrinoid standards

Small quantities of cobyric acid and cobinamide, were kindly supplied by H. C. Friedmann (University of Chicago, Chicago, IL, U.S.A.).

Electronic absorption spectrophotometry

This was performed in matched quartz cuvettes, using a Perkin-Elmer (Norwalk, CT, U.S.A.) Lambda 3B UV–VIS spectrophotometer (1 cm light path), and spectra were recorded on a PE R-100A Recorder.

Analytical thin-layer chromatography

This was performed on silica gel 60 plates (0.2 mm thickness) (E. Merck, Darmstadt, F.R.G.) with the solvents described in ref. 12.

RESULTS AND DISCUSSION

Table I shows the results of both ion-exchange and reversed-phase HPLC of both the aquocyano incomplete corrinoids and the diaquo forms. These results illustrate several important characteristics of the aquocyano stereoisomers. First, all of the incomplete corrinoids tested, with only a couple of exceptions, showed approximately equal percentages of the component stereoisomers, when cyanide was absent from the eluting solvent in both ion-exchange and reversed phase chromatography. The appearance of two peaks for each of the aquocyano- forms is as predicted by Friedrich and co-workers [6,13,14] who described the separation of the stereoisomers at 3°C by low-pressure column chromatography, and assigned structures according to their retention times: short retention corresponds to the α-aquo,

TABLE I

ISOCRATIC ION-EXCHANGE (IE) AND REVERSED-PHASE (RP) HPLC OF INCOMPLETE CORRINOID STEREOISOMERS

RP conditions: Alltech Adsorbosphere C_{18} column; 70% 80 m*M* pyridine acetate buffer in 4% aqueous tetrahydrofuran (pH 3.61) and 30% acetonitrile; 1.0 ml/min. IE Conditions: Whatman Partisil-5-SAX Column; 80 m*M* pyridine acetate buffer in 4% aqueous tetrahydrofuran (pH 3.62); 1.0 ml/min.

Corrinoid[a]	Retention time (min) (component % of total)		
	IE		RP,
	−KCN	+KCN	−KCN
(AqCN)Cobinamide R=NH_2, R′=$NHCH_2CHOHCH_3$	2.6(68) 3.7(32)	3.0(100)[b]	5.6(55) 6.3(45)
$(Aq)_2$Cobinamide	5.0(100)[c]	3.1(100)[b]	13.6(100)[c]
(AqCN)Cobyric acid R=NH_2, R′=OH	2.7(52) 3.8(48)	3.4(100)[b]	5.4(42) 6.0(58)
$(Aq)_2$Cobyric acid	3.6(100)[c]	–	–
(AqCN)Cobinic acid-1[d]	3.2(49) 4.9(51)	3.7(100)[b]	5.8(47) 6.6(53)
$(Aq)_2$Cobinic acid-1	5.7(100)[c]	3.6(100)[b]	–
(AqCN)Cobinic acid-2[e]	3.0(56) 4.3(44)	3.5(100)[b]	5.7(48) 6.3(52)
$(Aq)_2$Cobinic acid-2	5.1(100)[c]	–	12.6(100)[c]
(AqCN)Cobinic acid-3[f]	3.2(30) 5.0(70)	3.4(100)[b]	5.8(25) 6.5(75)
$(Aq)_2$Cobinic acid-3	5.1(100)[c]	–	–

[a] (AqCN)=Axial ligands on cobalt are water and cyanide (=aquocyano); $(Aq)_2$=both axial ligands on cobalt are water (=diaquo).

[b] In KCN both axial ligands on cobalt are cyanide (=dicyano).

[c] Single, *broad* peak centered at this retention time.

[d] Cobinic acid (*a,b,c,e,g*) pentaamide (=*d* OH, *f*=$NHCH_2CHOHCH_3$).

[e] Cobinic acid (*a,c,d,e,g*) pentaamide (=*b* OH, *f*=$NHCH_2CHOHCH_3$).

[f] Cobinic acid (*a,b,c,d,g*) pentaamide (=*e* OH, *f*=$NHCH_2CHOHCH_3$).

β-cyano stereoisomer (Fig. 1: X = CN, Y = OH_2) and long retention corresponds to the β-aquo, α-cyano isomer (Fig. 1: X = OH_2, Y = CN).

Second, when cyanide was present in the solvent, all of the incomplete corrinoids showed a single component, presumably the dicyano form. In all cases, this dicyano form had a retention time *in between* the retention times of the two aquocyano stereoisomers. This dicyano form was unstable, unless cyanide was present in the eluting solvent. When dicyanocobinamide was injected under the IE or RP conditions described in Table I, and no cyanide was present in the solvent, the major components formed were the two aquocyano stereoisomers. Only a small amount, if any, of the dicyano form persisted. Our observations in this regard correspond to those in ref. 7,

TABLE II

SEPARATION AND REFORMATION OF CORRINOID STEREOISOMERS ON ION-EXCHANGE HPLC

HPLC Conditions: Whatman Partisil-5-SAX Column, 80 m*M* pyridine acetate in 4% aqueous tetrahydrofuran (pH 5.97 or 3.48, as noted below); 1.0 ml/min. Stereoisomers collected directly from the detector effluent were concentrated under an N_2 stream before reinjection; only the highest part of each peak was collected.

Corrinoid[b]	Retention time (min) (Component % of Total)				
	Cpt.[a]	Original injection, pH 5.97	Reinjection		
			Cpt.	pH 5.97	pH 3.48
Cobinamide	I	3.8(43)	I	4.1(46)	2.9(64)
				6.1(54)	4.7(36)
	II	5.2(57)	II	4.1(32)	3.0(63)
				6.2(68)	4.6(37)
Cobyric acid	I	3.1(52)	I	3.1(31)	2.5(47)
				3.9(30)[c]	3.5(53)
	II	3.9(48)	II	3.1(28)	2.6(74)
				3.9(65)[c]	3.5(26)
Cobinic acid-1[d]	I	3.7(50)	I	3.8(33)	3.0(41)
				4.7(30)[c]	4.6(59)
	II	4.5(50)	II	3.7(16)	3.0(85)
				4.4(50)[c]	4.7(15)
Cobinic acid-2	I	3.3(49)	I	3.3(30)	3.0(56)
				4.1(38)[c]	4.5(44)
	II	4.1(51)	II	3.5(16)	2.9(88)
				4.2(73)[c]	4.6(12)
Cobinic acid-3	I	3.5(75)	I	3.5(34)	2.9(48)
				4.5(33)[c]	4.7(52)
	II	4.5(25)	II	3.5(12)	2.9(87)
				4.4(72)[c]	4.9(13)

[a] Designation for stereoisomers: Cpt. I and Cpt. II.

[b] All corrinoids were in the aquocyano form.

[c] Balance of % accounted for by a slow-moving component, which appears as a broad peak and is probably the diaquo form (see Table I).

[d] For nomenclature of the cobinic acid pentaamides, see Table I.

but contrast with those in ref. 15, where a single component of short retention time was reported when dicyanocobinamide was injected.

Third, the diaquo forms of all of the cobinic acid isomers and cobinamide exhibited longer retention times, whereas diaquocobyric acid showed an intermediate retention time.

Finally, cobinic acid-3 (the *a,b,c,d,g*-pentaamide) exhibited percentages of component stereoisomers that were very different from those of other incomplete corrinoids tested, the faster component being present at 1/2 to 1/3 of the amount of the slower component. According to refs. 16 and 17 this behavior may indicate a greater thermal stability of the α-cyano stereoisomer, or it may be due to the interaction of the corrin ring-peripheral carboxylic acid/carboxylate or amides (Fig. 1, R groups) with the α side cyanide (Fig. 1, Y ligand) [16].

Table II shows the result of collecting the stereoisomers from the analytical ion-exchange column and then reinjecting them at two different pH values. The original injection in this case was at pH 5.97. In all cases, except that of cobinic acid-3, the stereoisomers were formed in a ratio of about 1:1. When each individual component was then reinjected into the same column at the same or different pH, both isomers were again formed, but no longer in 1:1 ratio. At pH 5.97, the component with longer retention time usually predominated, and the diaquo form appeared. Reinjection at pH 3.48 usually showed the opposite: predominance of the component with the shorter retention time. These data clearly show that the stereoisomers were, in fact, thermally unstable, facile reformation of the "other" isomer occurring at room temperature, although the amount of each isomer formed was dependent on solvent pH and corrinoid structure. These results support the assertions in ref. 6 to the effect that the cyanide group can "migrate" from one corrinoid to another at elevated temperatures.

The separated stereoisomers were studied not only by HPLC, but also by thin-layer chromatography. As one would predict, each stereoisomer showed two or three components in thin-layer chromatography with 2-propanol–28% ammonia–water (7:1:2) [12]. R_F values always clustered in 3 areas: 0.5–0.6, 0.15–0.25 and 0.05, corresponding to, respectively, the two aquocyanostereoisomers (fast and slow), and the diaquo form.

Friedrich [6] described differences in the spectra of the separated aquocyano stereoisomers of cobyric acid. Our attempts to discern reproducible differences in the electronic absorption spectrum of each of the separated stereoisomers were unsuccess ful, however, as one would expect in light of the thermal instability of these compounds.

ACKNOWLEDGEMENT

This work was supported by Grant No. SO6GM08043(NIH).

REFERENCES

1 L. Ljungdahl, E. Irion and H. G. Wood, *Biochemistry*, 4 (1965) 2771.
2 B. P. Hay and R. G. Finke, *J. Am. Chem. Soc.*, 109 (1987) 8012.
3 D. Dolphin, *Methods Enzymol.*, 18c (1971) 41.
4 D. A. Baldwin, E. A. Betterton, S. M. Chemaly and J. M. Pratt, *J. Chem. Soc., Dalton Trans.*, (1985) 1613.

5 W. Friedrich, *Biochem. Z.*, 342 (1965) 143.
6 W. Friedrich, *Z. Naturforsch. B*, 21 (1966) 595.
7 E. Stupperich, I. Steiner and M. Ruhlemann, *Anal. Biochem.*, 155 (1986) 365.
8 D. W. Jacobsen, R. Green and K. L. Brown, *Methods Enzymol.*, 123 (1986) 14.
9 P. Renz, *Methods Enzymol.*, 18c (1971) 82.
10 D. L. Anton, H. P C. Hogenkamp, T. E Walker and N. A. Matriwiyoff, *J. Am. Chem. Soc.*, 102 (1980) 2215.
11 D. A. Baldwin, E. A. Betterton and J. M. Pratt, *J. Chem. Soc., Dalton Trans.*, (1983) 217.
12 T. Toraya, E. Krodel, A. S. Mildvan and R. H. Abeles, *Biochemistry*, 18 (1979) 417.
13 W. Friedrich and J. P. Nordmeyer, *Z. Naturforsch. B*, 23 (1968) 1119.
14 W. Friedrich and R. Messerschmidt, *Z. Naturforsch. B*, 24 (1969) 465.
15 D. W. Jacobsen, R. Green, E. V. Quadros and Y. D. Montejano, *Anal. Biochem.*, 120 (1982) 394.
16 K. L. Brown and S. Peck-Siler, *Inorg. Chem.*, 27 (1988) 3548.
17 K. L. Brown and J. M. Hakimi, *Inorg. Chem.*, 23 (1984) 1756.

Journal of Chromatography, 536 (1991) 193–201
Elsevier Science Publishers B.V., Amsterdam

CHROMSYMP. 2011

Use of ion-exclusion chromatography for monitoring fatty acids produced by bacterial anaerobic degradation of tetrachloroethene in ground water

N. CHAMKASEM*,[a] and K. D. HILL
NSI Technology Services, P.O. Box 1198, Ada, OK 74820 (U.S.A.)
and
G. W. SEWELL
R. S. Kerr Environmental Research Laboratory, U.S. Environmental Protection Agency, Ada, OK 74820 (U.S.A.)

ABSTRACT

A rapid method for the simultaneous quantification of non-volatile and volatile fatty acids in aqueous sample by ion-exclusion chromatography is described. The sample is directly injected into the column and detected by a chemically suppressed conductivity detector, connected in tandem with an UV detector at 210 nm. The method allows detection of fatty acid as low as 1 ppm with a linear dynamic range up to 1000 ppm. At least 13 fatty acids can be determined within 50 min. This technique has been used to monitor the common fermentation products (lactate, acetate, propionate and butyrate) of the reductive dehalogenation of tetrachloroethene by anaerobic bacteria.

INTRODUCTION

Gas chromatography (GC) has been used to determine non-volatile and volatile carboxylic acids in aqueous solution. [1]. Volatile fatty acids are extracted with ether prior to the analysis by GC. Then non-volatile fatty acids are derivatized to form dimethyl esters and are extracted into an organic solvent before GC analysis. Later, this time-consuming procedure was simplified by direct injection of the aqueous sample into the column [2]. Polar stationary phase, such as free fatty acid phase (FFAP) is used with either packed or capillary column. With this column, one can analyze both volatile and non-volatile fatty acids by using different conditions; therefore, separate analyses are required.

The simultaneous analysis of both type of fatty acids by high-performance liquid chromatography (HPLC) has been reported [3]. At least 20 *p*-nitrobenzyl (PNB) esters of fatty acids in coffee were determined with 20 min by gradient reversed-phase HPLC. This technique requires extensive sample cleanup to remove the excess deriv-

[a] Present address: National Food Processors Association, 6363 Clark Ave., Dublin, CA 94568, U.S.A.

0021-9673/91/$03.50

atizing agent. It is also unsuitable for samples containing chloride ions, because the formation of PNB chloride will interfere with the propionic acid PNB ester.

Ion-exclusion chromatography on a cation-exchange resin is widley used for the determination of fatty acids [4]. Strong-acid anions are excluded from the resin according to the Donnan principle and are eluted at the void volume of the column. Weaker-acid anions, existing largely in the molecular form, are retained on the stationary phase by a combination of ion exclusion, size exclusion and hydrophobic interactions. Typically, a mineral acid solution is used as the eluent to ensure that the fatty acids are predominantly in non-ionized form. However, water has also been used as eluent [5]. Detection of the eluted weak acids has been carried out by UV detection at 195–220 nm. A non-suppressed conductivity detector was also used with benzoic acid as the eluent to determine the C_1–C_4 aliphatic fatty acids [6]. Although this method can achieve detection limits from 60 ppb[a] to 1.4 ppm, the linearity is only one order of magnitude. Nadkarni and Brewer [2] reported the use of a chemically suppressed conductivity detector with ion-exclusion chromatography to determine volatile and non-volatile fatty acids in aqueous samples to obtain detection limits below 1 ppm with linearity over 2–3 orders of magnitude. However, resolution was not sufficient to determine more than 6 components simultaneously.

Contamination of aquifers with recalcitrant chlorinated compounds, including chloroethenes, creates a situation difficult to remedy. Although reductive dechlorination process can be effective in removing highly chlorinated compounds, as yet little is known about the factors controlling these reactions. In this study, the effects of the addition of common fermentation products (acetate, lactate, propionate and butyrate) on the reductive dehalogenation of tetrachloroethene (PCE) by anaerobic bacteria were examined. It was important that all four acids could be analyzed and quantified over the life of the experiment to identify changes in their concentrations and to compare those changes to the appearancce of chlorinated daughter products from the reduction of PCE.

EXPERIMENTAL

Reagents and chemicals

Pyruvic, malonic, methylmalonic, succinic, lactic, fumaric, acetic, propionic, butyric, isobutyric, valeric and isovaleric acids were purchased from Sigma (St. Louis, MO, U.S.A.). PCE, trichloroethenes (TCEs) and dichloroethenes (DCEs) were obtained from Aldrich (Milwaukee, WI, U.S.A.). Tetrabutyl ammonium hydroxide (TBAOH) and hexanesulfonic acid were high-purity grade and obtained from Dionex (Sunnyvale, CA, U.S.A.). Analytical reagent-grade sulfuric acid (H_2SO_4) (Fisher Scientific, Springfield, NJ, U.S.A.) was also used.

Reagent solutions

Sulfuric acid (0.05 *M*) was prepared by diluting concentrated sulfuric acid with deionized water (18 mΩ). This solution was used to prepare mobile phase at a concentration range from 1 to 7.5 m*M*. Hexanesulfonic acid 1 m*M* was prepared by diluting the stock solution (0.1 *M*) with deionized water. TBAOH (5 m*M*) was prepared by

[a] Throughout this article, the American billion (10^9) is meant.

pipetting 50 ml of the stock solution (100 m*M*) into a 1-liter volumetric flask and diluting to volume with deionized water. These solutions were filtered through a 0.45-μm Millipore filter before use. Fatty acids were dissolved in water, aqueous methanol or methanol in the concentration range 1–1000 ppm.

Liquid chromatography

The apparatus consisted of the following components: a Model M6000 pump (Waters Associates, Milford, MA, U.S.A.), a Waters Autosampler Model 710B, a chemically suppressed conductivity detector, equipped with an anion micromembrane suppressor, Model AMMS-ICE (Dionex) and a Waters UV detector Model 490 at 210 nm. A Series A pump (Eldex Labs., San Carlos, CA, U.S.A.) delivered a regenerant TBAOH 5 m*M*) into the suppressor at a flow-rate of 1 ml/min. A 100-μl sample loop was used for loading the sample on the Ionguard GC-801 guard column (Interaction Chemicals, Mountainview, CA, U.S.A.), attached to the Interaction Ion-300 fatty column (300 × 7.8 mm). The columns were kept at 70°C in a Waters electric column heater. For routine analysis of the fatty acids, the mobile phase was 1 m*M* hexane sulfonic acid at a flow-rate of 0.5 ml/min. The chromatograms from the two detector were recorded simultaneously by a Model 2600 integrator (PE Nelson, Cupertino, CA, U.S.A.).

Methods

Anaerobic slurries were made with aquifer solids and sterile sulfide-reduced spring water supplemented with nitrogen and phosphorus. Aquifer solids were collected using the aseptic/anaerobic coring procedure [7]. Sealed, collected cores were placed in an anaerobic chamber where 50 g each of saturated core material was added aseptically to sterile 160 ml serum bottles. They were then completely filled with sterilized spring water amended with ammonium phosphate (10 m*M* ammonium and 5 m*M* phosphate). Reducing conditions were maintained by the addition of sodium sulfide (1 m*M* final concentration) and resazurin was added as a redox indicator. These slurries were spiked with 30 μM PCE or were unamended. Four concentrations (0, 0.1, 1 and 10 m*M*) of mixed organic acids (lactate, acetate, propionate and butyrate) were tested. The slurries were incubated anaerobically at room temperature, protected from light. They were sampled periodically and analyzed for PCE and its degradation products (TCE and DCE) by a headspace analysis technique, using the HP5890A gas chromatograph, equipped with HP 19395A headspace sampler. The aqueous portions were also centrifuged at 14 000 *g* for 5 min and the supernatant (100 μl) was injected into the HPLC column.

RESULTS AND DISCUSSION

The retention of the organic acid on the ion-exclusion column was mainly controlled by the column temperature and the mobile phase concentration. The column temperature was varied between 40 to 60°C and the concentration of sulfuric acid was varied between 1 to 7.5 m*M*. The effect of column temperature on selectivity is shown in Fig. 1. At 40°C, fumaric acid is coeluted with acetic acid and lactic acid is not separated from succinic acid. On the other hand, fumaric acid and formic acid are unresolved at 60°C. When 3 m*M* sulfuric acid is used as the mobile phase, the opti-

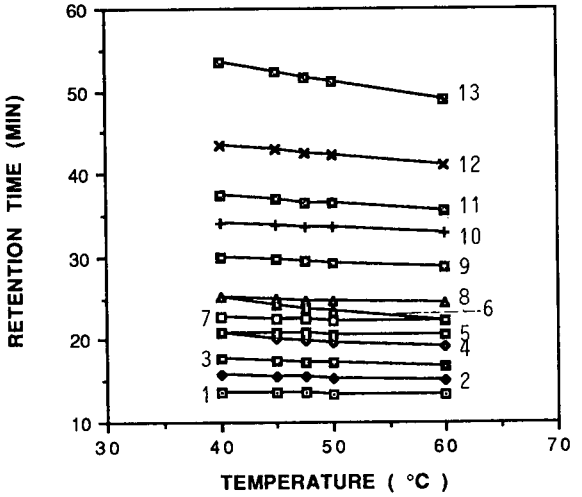

Fig. 1. Effect of column temperature on the retention times of fatty acids using 3 m*M* of sulfuric acid as the mobile phase. For compounds numbers, see Table I.

mum temperature lies between 45 and 50°C. Subsequently, the concentration of sulfuric acid was varied from 2.5 to 3.5 m*M* and the carboxylic acids were analyzed at 47.5°C (Fig. 2). To achieve good resolution of formic acid, fumaric acid and acetic acid at a column temperature of 47.5°C, the mobile phase concentration must be 3 m*M* (Fig. 3). Serial dilutions of fatty acid standard, having concentrations from 1 to 1000 ppm, were prepared and analyzed to construct the calibration curve. Table I shows the limit of detection and the linear range of 13 carboxylic acids when the UV detector is set at 210 nm.

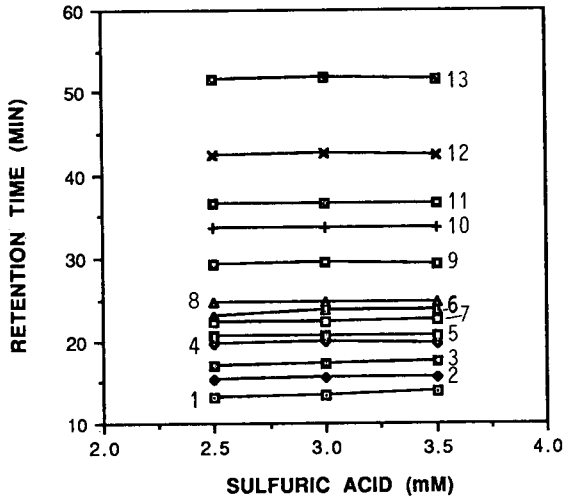

Fig. 2. Effect of sulfuric acid concentration used as the mobile phase on the retention time of fatty acids at 47.5°C.

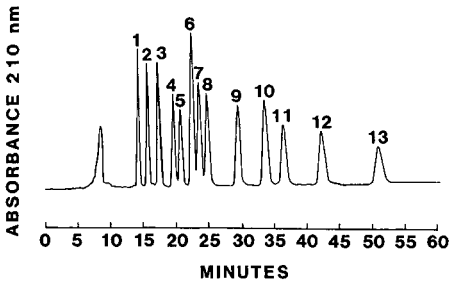

Fig. 3. Chromatogram of fatty acids on the I-300 fatty acid column. Mobile phase 3 mM H_2SO_4; flow-rate 1 ml/min; UV detector at 210 nm. Acids: 1 = pyruvic; 2 = malonic; 3 = methylmalonic; 4 = succinic; 5 = lactic; 6 = formic; 7 = fumaric; 8 = acetic; 9 = propionic; 10 = isobutyric; 11 = butyric; 12 = isovaleric; 13 = valeric.

Acidified ground water (200 ml of water + 2 drops of concentrated sulfuric acid), collected from Traverse city, MI U.S.A., was spiked with carboxylic acid mixtures at two concentration levels (Table II). Deionized water, spiked with the same amount of acid, was used as the control sample. Each sample was analyzed for carboxylic acids, along with blank sample. The recovery of pyruvic acid was low at both concentration levels. It may react with compounds in ground water and then be degraded to other by-products. The recoveries of other fatty acids were above 90% with a coefficient of variation of $< 5\%$ at the low concentration level and $< 1\%$ at the high concentration level. This ion-exclusion method works well for a determination of fatty acids in ground water at a detection limit above 10 ppm.

To improve the sensitivity of this technique, a chemically suppressed conductivity detector was connected to the UV detector in tandem. However, the sulfuric acid solution (3 mM) used as the mobile phase has such a high background conductivity

TABLE I

ANALYTICAL PERFORMANCE OF ION-EXCLUSION CHROMATOGRAPHY FOR THE DETERMINATION OF FATTY ACIDS WITH THE UV DETECTOR AT 210 nm

No.	Acid	Detection limit (ppm)	Upper dynamic range (ppm)
1	Pyruvic acid	0.3	100
2	Malonic acid	4	1000
3	Methylmalonic acid	3	1000
4	Succinic acid	7	1000
5	Lactic acid	5	1000
6	Fumaric acid	0.01	50
7	Formic acid	5	1000
8	Acetic acid	7	1000
9	Propionic acid	8	1000
10	Isobutyric acid	8	1000
11	Butyric acid	12	1000
12	Isovaleric acid	12	1000
13	Valeric acid	15	1000

TABLE II

RECOVERIES OF FATTY ACIDS FROM GROUND WATER

Acid	Spike level 1				Spike level 2			
	ppm	Average recovery (n = 3)	S.D.	C.V.	ppm	Average recovery (n = 3)	S.D.	C.V.
Pyruvic acid	4.0	27.5	10.4	27.7	40	14.3	3.6	25.3
Malonic acid	40.0	94.0	0.3	0.4	400	95.8	0.9	0.9
Methylmalonic acid	34.0	95.0	1.0	1.1	340	97.7	0.3	0.3
Succinic acid	73.0	97.0	0.4	0.4	730	99.5	0.4	0.4
Lactic acid	41.0	96.1	0.8	0.8	410	96.9	0.1	0.1
Fumaric acid	0.4	96.7	1.0	1.0	4	99.1	0.7	0.7
Formic acid	80.0	98.1	0.5	0.5	800	98.8	0.2	0.2
Acetic acid	80.0	103.5	1.1	1.0	800	100.6	0.2	0.2
Propionic acid	80.0	114.1	2.2	1.9	800	98.2	0.2	0.3
Isobutyric acid	80.0	102.5	1.9	1.8	800	96.8	0.2	0.2
Butyric acid	80.0	103.8	2.1	2.0	800	99.5	0.4	0.4
Isovaleric acid	80.0	106.9	5.9	5.5	800	109.9	0.3	0.3
Valeric acid	76.0	99.2	5.3	5.3	760	107.3	0.3	0.2

that it cannot be suppressed to an acceptable level. Hexane sulfonic acid (1 mM) was used as the mobile phase with TBAOH as the regenerant to suppress the background conductivity. Because the concentration of the hexane sulfonic acid was much less than the concentration of sulfuric acid previously used, the retention times of the carboxylic acids decreased. Since only four acids were investigated in the experiment, the column temperature was increased to 70°C to shorten the analysis time.

Applications

The method developed has been applied to the study of the reductive dechlorination processes of PCE in the presence of carboxylic acids, including lactate, acetate, propionate and butyrate. It is important that all four acids can be determined over the life of the experiment. The changes of their concentrations are compared with the changes in the chlorinated daughter products from the reduction of PCE. Fig. 4 shows the typical chromatograms of standard fatty acids detected by the conductivity detector and the UV detector. The benefit of having two detectors connected in tandem is that sensitivity and selectivity increase. The conductivity detector has an average detection limit of 1 ppm for fatty acids with a linear dynamic range up to 100 ppm. The UV detector has the average detection limit of 10 ppm with the linear dynamic range up to 1000 ppm. Therefore, the analyst can determine fatty acids over a much wider linear dynamic range with high sensitivity. For the sample that contains high concentrations of carbonate, it is difficult to quantify butyrate with the conductivity detector because carbonate peak overlaps the butyrate peak (Fig. 5). On the other hand, the UV detector can detect butyrate quite nicely.

Fig. 6A shows the change of the PCE concentration and the concentrations of its daughter products in the slurry containing 10 mM of carboxylic acids. The change of carboxylic acids concentrations, is shown in Fig. 6B for comparison. As the buty-

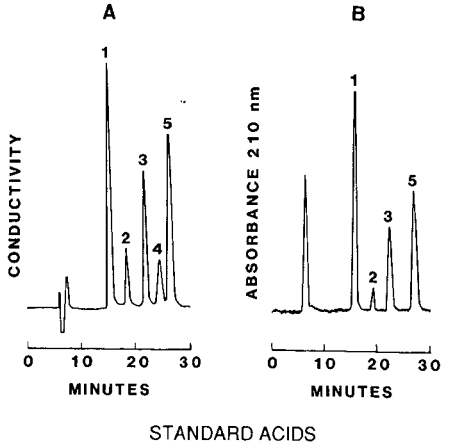

Fig. 4. Chromatograms of a mixture of standard fatty acids: 1 = lactic (82 ppm), 2 = acetic (13 ppm), 3 = propionic (47 ppm), 4 = carbonate (trace) and 5 = butyric (92 ppm) detected by (A) the chemically suppressed conductivitity detector and (B) the UV detector at 210 nm.

rate was oxidized to acetate, the PCE was reduced to TCE and DCE after 51 days of incubation. Lactate was used up after the first 20 days. There was no change in propionate concentration. The incubation times before reductive dechlorination of PCE was observed were 51 days (10 m*M* acids), 65 days (1 m*M* acids), 86 days (0.1 m*M* acids), and over 175 days (no acids added). After 175 days incubation, no PCE was detectable in any of the fatty acid-supplemented slurry, but 27 to 29 μM of combined tri- and dichloroethenes were detected. These results indicate that the avail-

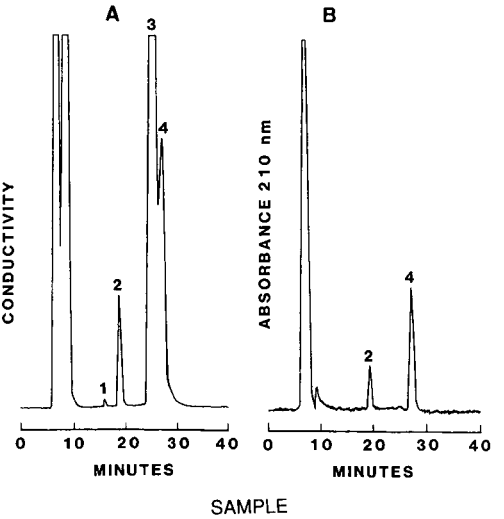

Fig. 5. Chromatograms of the slurry containing high concentration of carbonate detected by (A) the chemically suppressed conductivity detector and (B) the UV detector at 210 nm. Peaks: 1 = lactic acid; 2 = acetic acid; 3 = carbonate; 4 = butyric acid.

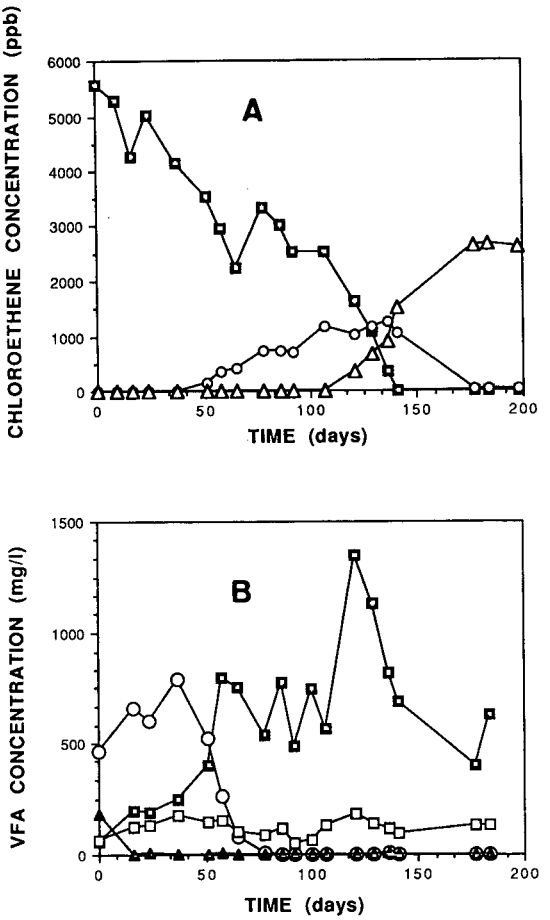

Fig. 6. (A) Relationship between the incubation period and the concentration of PCE with its daughter products in the slurry containing 10 m*M* of fatty acids: ◘ = PCE; ○ = TCE; △ = DCE; (B) Relationship between the incubation period and the fatty acids concentrations in the slurry. VFA = Volatile fatty acids. ◘ = Acetate; ○ = butyrate; ▲ = lactate; □ = propionate.

ability of organic electron donors are stimulatory to reductive dechlorination processes.

CONCLUSION

Ion-exclusion chromatography is suitable for the analysis of fatty acids in an aqueous sample. It requires neither sample cleanup nor precolumn derivatization. Two parameters, column temperature and mobile phase concentrations, play an important role in a successful separation. To increase the sensitivity and selectivity of the analysis, connecting a chemically suppressed conductivity detector and a UV detector in tandem is recommended.

REFERENCES

1 L. V. Holdeman, E. P. Cato and W. E. C. Moore, *Anaerobe Laboratory Manual,* Virginia Polytechnic Institute and State University, Blacksburg, VA, 4th ed., 1977, p. 187–221.
2 R. A. Nadkarni and J. M. Brewer, *Am. Lab.,* 2 (1987) 50.
3 R. L. Patience and J. D. Thomas, *J. Chromatogr.,* 249 (1982) 183.
4 H. Waki and Y. Tokunaga, *J. Chromatogr.,* 201 (1980) 259.
5 K. Tanaka, T. Ishizuka and H. Sunahara, *J. Chromatogr.,* 174 (1979) 153.
6 K. Tanaka and J. S. Fritz, *J. Chromatogr.,* 361 (1986) 151.
7 L. L. Leach, F. P. Beck, J. T. Wilson and D. H. Kampbell, *Proceedings of the Second National Outdoor Action Conference on Aquifer Restoration, Ground Water Monitoring and Geophysical Methods, Las Vegas, NV,* Vol. 1, U.S. EPA EMSL, Las Vegas, NV, 1988.

Journal of Chromatography, 536 (1991) 203–209
Elsevier Science Publishers B.V., Amsterdam

CHROMSYMP. 2007

Evaluation of chemical structural heterogeneity of cationic acrylamide copolymers by high-performance liquid chromatography

SHYHCHANG S. HUANG
Hercules Incorporated, Research Center, Wilmington, DE 19808 (U.S.A.)

ABSTRACT

The chemical structural heterogeneities of two cationic acrylamide copolymers, methacryloxyethyl trimethylammonium chloride–acrylamide (AAM) and diallyldimethyl ammonium chloride–AAM, have been determined by high-performance liquid chromatography. In this method aqueous size-exclusion chromatography is combined with ion-exchange chromatography. Gradient elution with a sodium chloride solution is used. The resulting chromatogram shows the heterogeneity between polymer chains in solution. A comparison of the chromatograms of the original copolymer and its degradation product showed the heterogeneity along the copolymer chains.

INTRODUCTION

Cationic acrylamide copolymers, such as diallyldimethylammonium chloride (DADMAC)–acrylamide(AAM) copolymer and methacryloxyethyl trimethylammonium chloride (MTMAC)–AAM copolymer, have been used extensively in paper manufacture and water treatment [1]. Differences in the performance of some copolymers with the same molecular weight and content of cationic groups have recently been found. Chemical structural heterogeneity of the copolymers may be one of the important factors in the performance.

DADMAC-AAM

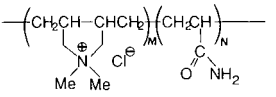

MTMAC-AAM

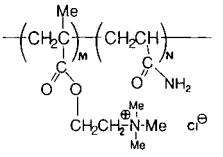

Me = methyl

The by far most often used technique to elucidate the chemical structure of copolymers is ^{13}C NMR [2]. However, ^{13}C NMR is difficult to use for studying the chemical structure of cationic acrylamide copolymers. Firstly, the content of the cationic groups of this type of copolymers is normally very low, *i.e.*, less than 10 mol%, and the NMR signal of "effective" carbons becomes very low. Secondly, because this type of copolymer normally has a very high molecular weight (in millions), it is very difficult to prepare sample solutions of sufficiently high concentration for an increased NMR signal. Thirdly, also because of the high molecular weight of the polymer, the NMR peaks are usually broad.

The purpose of this paper is to introduce a new method for studying the chemical heterogeneity of cationic acrylamide copolymers by high-performance liquid chromatography (HPLC).

THEORY

Assume a polyelectrolyte chain having a homogeneous charge distribution. Charges are randomly distributed throughout the chain (Fig. 1). If this chain is degraded to several shorter chains, each resulting chain should also have a homogeneous charge distribution. On the other hand, if the original polyelectrolyte chain is heterogeneous, the degraded product will consist of some highly charged chains and some slightly charged chains.

HPLC has been used to fractionate copolymers according to their chemical composition [3]. The differences between the degradation products of homogeneous and heterogeneous polyelectrolytes should be readily distinguishable by HPLC. Assuming that the retention in HPLC is due to the number of cationic groups on the chains, the anticipated chromatograms of a polyelectrolyte and its degradation product will be as shown in Fig. 2. If the polyelectrolyte is homogeneous, the degradation product will consist of shorter, but homogeneous polyelectrolyte chains. The chromatogram of such product should show a single peak, eluted earlier than the original sample. If the polyelectrolyte is heterogeneous, the degradation product may contain polymer chains with a different number of charges, and even some uncharged polymers. Therefore, the HPLC may be multimodal and show very broad peaks.

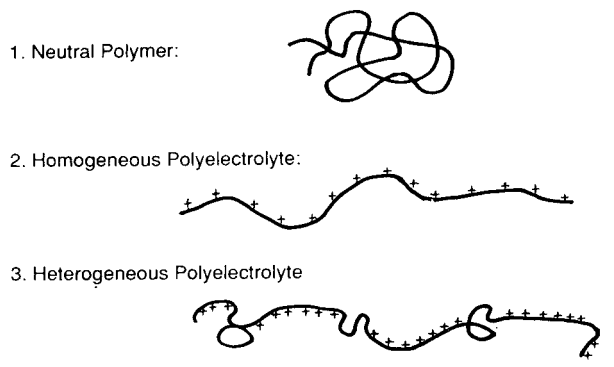

Fig. 1. Polymer chains in salt-free solution.

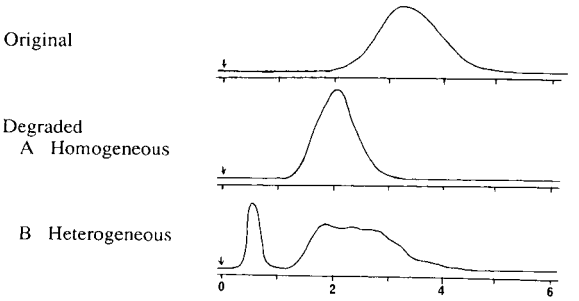

Fig. 2. Theoretical HPLC results of homogeneous and heterogeneous polyelectrolytes.

EXPERIMENTAL

The DADMAC–AAM and three MTMAC–AAM copolymers are experimental samples used at the Hercules Research Center, The DADMAC–AAM copolymer contains *ca.* 6 mol% of DADMAC. Three MTMAC–AAM copolymers contain about 5, 7.5 and 10 mol% of MTMAC, respectively.

The water used in the size-exclusion chromatography (SEC) and HPLC studies was purified with a Milli-Q reagent-grade water system (Millipore, Milford, MA, U.S.A.) and vacuum-filtered through a 0.2-μm nylon 66 membrane filter (Rainin 38-111) before chromatography. The GR crystal-grade sodium chloride was purchased from EM Chemicals (Gibbstown, N.J., U.S.A.).

A Bransonic 12 (Branson Ultrasonic, Danbary, CT, U.S.A.) ultrasonic cleaning bath was used to degrade the copolymers. SEC of polymers was performed with a Waters 510 (Milford, MA, U.S.A.) pump, which was equipped with a Rheodyne (Cotati, CA, U.S.A.) 7125 injector and a Waters 401 differential refractometer. Polymers were fractionated on a TSK PWH guard column and a PWXL mixed-bed column (both from Tosoh, Tokyo, Japan), in 0.24 *M* sodium formate aqueous solution (pH 3.7) as the mobile phase.

A Perkin-Elmer (Norwalk, CT, U.S.A.) Series 4 LC, equipped with a Rheodyne 7125 injector and a Schoeffel (Kratos, F.R.G.) 770 UV monitor were used in the HPLC analysis. Polymers were separated on a TSK PWH guard column, which was packed with cross-linked hydroxylated polyether gel having a low degree of residual carboxyl groups.

The infrared (IR) spectra were taken with a Perkin-Elmer Model 983 dispersive IR spectrometer. The samples were first dissolved in water, cast on germanium plate and then dried in a vacuum oven at room temperature.

RESULTS AND DISCUSSION

Molecular-weight reduction (degradation) of polyelectrolytes

High-molecular-weight polymer chains in solution can be degraded by ultrasonic vibration [4]. Fig. 3 shows the SEC curves of DADMAC–AAM copolymers at different ultrasonication times. The peak maximum of the original sample was at *ca.* 7.6 ml, which is the exclusion limit of this column set. When polymers were degraded

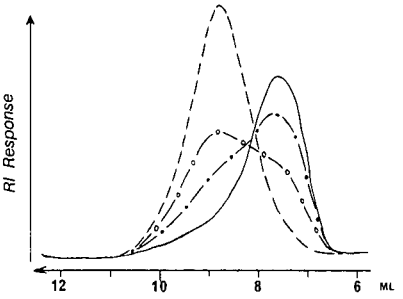

Fig. 3. Size-exclusion chromatography of a DADMAC–AAM copolymer and its degradation products after different ultrasonication times. Column: TSK PWH guard column (7.5 cm × 7.5 mm I.D., 13 μm particle size) plus TSK PWXL mixed-bed column (30 cm × 7.5 mm I.D.; 13 μm particle size); mobile phase: 0.24 *M* aqueous sodium formate (pH 3.7), 1.0 ml/min; detector: differential refractometer; ultrasonication equipment: Bransonic 12 ultrasonic cleaning bath. ——— = Original sample, ●—● = 0.5 h, ○—○ = 1.0 h, – – – = 3.0 h. RI = Refractive index.

by ultrasonic treatment, a new peak appeared at 8.8 ml, which corresponds to a molecular weight of $5 \cdot 10^5$, based on poly(ethylene oxide) calibration. After 3 h of ultrasonication, the high-moleular-weight peak almost completely disappeared. The polymer showed a narrow peak at 8.8 ml. The degradation of MTMAC–AAM copolymer by ultrasonic treatment also resulted in a narrow peak in SEC. These narrow molecular-weight distributions are very helpful for the interpretation of HPLC data.

HPLC

Many HPLC columns and different solvent gradient programs were tested for these low-charge-density, high-molecular-weight polyelectrolytes. The best choice from my experience was a TSK PWH guard column, which is packed with cross-linked hydroxylated polyether gel having a low degree of residual carboxyl groups. The solvent gradient program was from water to 0.2 *M* aqueous sodium chloride solution. Retention is probably based on an ion-exchange mechanism with some contribution of size-exclusion and reversed-phase partition chromatography. Since the concentration of negative charges (the residual carboxyl groups) on the gels is very low, the retention of multi-charge species, polyelectrolytes, is not as long as in normal ion-exchange chromatography. Because the retention of high polymers in liquid chromatography, except SEC, is strongly dependent on mobile phase composition, but not on column length [5], chromatography of this polymeric material does not require a long column. A short guard column was thus selected. This short SEC column also reduced the size-exclusion effect.

MTMAC–AAM

The chromatogram of a MTMAC–AAM copolymer under the above conditions is shown in Fig. 4. The sharp peak at 1.2 min was eluted by size-exclusion without other retention contribution. It should be due to high-molecular-weight polymer without, or almost without, positive charges. The second peak at 2.5 min is the peak of solvent impurity, such as acetone (introduced during polymer purification). Neutral polymers

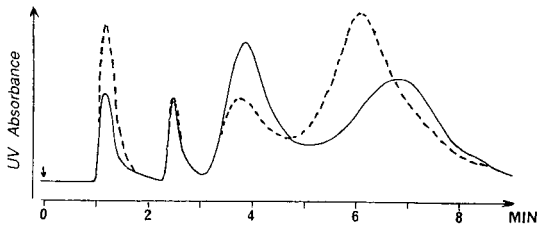

Fig. 4. Chromatograms of a MTMAC–AAM copolymer and its degradation product. Column: TSK PWH guard column (7.5 cm × 7.5 mm I.D., 13 μm particle size); mobile phase: linear gradient elution from water to 0.2 *M* aqueous sodium chloride in 10 min, 0.5 ml/min; detector: UV monitor at 230 nm; sample size: 50 μl of 0.2% solution. ——— = Original sample, – – – = degradation product.

will be eluted between these two peaks, depending on their molecular weight. After 2.5 min, the retention will be mainly due to ion exchange. Therefore, the longer the retention time, the more positive charges the polymer has. The chromatogram of the original sample in this figure (solid line) reveals two peaks in this area, which indicates that the sample probably contained two "types" of polyelectrolytes, one having much less positive charges and the other having much more positive charges. It should be mentioned that the high-molecular-weight (*ca.* one million or higher) polymers may be shear degraded during chromatography. Therefore, one should interpret the chromatogram with caution.

The dotted curve in Fig. 4 shows the chromatogram of the degraded sample. Since most of the degraded neutral polymers had a larger molecular size than the exclusion limit of this column, the peak at 1.2 min was still sharp. As this neutral polymer peak became larger, the less charged peak (3.7 min) became smaller and the highly charged peak (at *ca.* 6 min) shifted toward a shorter retention time. The peak at *ca.* 6 min is probably due to polymers with relatively homogeneous charge distribution or randomly distributed ionic groups. The polymer chains were degraded to shorter and still relatively homogeneous polyelectrolyte chains. The peak at *ca.* 3.7 min is probably due to the polymer with some ionic groups in one segment of the polymer chain and almost pure polyacrylamide in another segment of the chain side. Therefore, after degradation, this peak shifted only slightly. The intensity (corresponding to the polymer concentration) of this peak was reduced and that of the first peak (1.2 min) was increased.

The assignments of these peaks can be used to explain the chromatograms of different MTMAC–AAM copolymer samples shown in Fig. 5. The retention times of peaks a, b and c in Fig. 5A and B are about the same. However, the ratios of the peak sizes are different. Fig. 5A (the copolymer with 5 mol% of MTMAC) shows more neutral polymer (peak a) and less charged polyelectrolytes (peak b) than Fig. 5B (the copolymer with 7.5 mol% of MTMAC). It should be pointed out that the UV absorption of these peaks is due to a combination of amide and ester groups. Therefore, it is very difficult to calculate the composition of the polymers of the three peaks in each sample. On the other hand, Fig. 5C (10 mol% MTMAC) shows longer retention times of both peaks b and c than the corresponding peaks in Fig. 5A and B, which indicates that the 10 mol% copolymer sample has more ionic groups on both types of polyelectrolyte chains (peaks b and c).

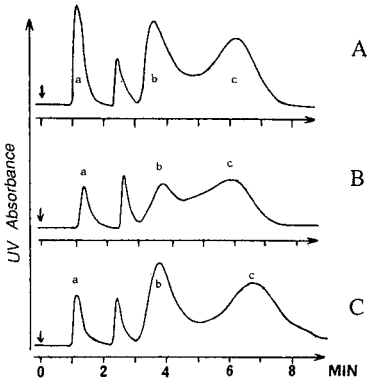

Fig. 5. Chromatograms of three MTMAC–AAM copolymers with different MTMAC content. Some chromatographic conditions as in Fig. 4. A = 5 mol% MTMAC; B = 7.5 mol% MTMAC and C = 10 mol% MTMAC.

Ultrasonic wave generates high temperature (*ca.* 2000 K) at micro-region in liquid phase [6]. Since the ester group of MTMAC is unstable at high temperature [7], there was concern that degradation by using ultrasonic treatment may induce hydrolysis of the ester to acid. The acid could then react with the adjacent amide group to form an imide [7]. The IR spectrum of an ultrasonically degraded MTMAC–AAM copolymer (Fig. 6) was compared with that of the original material. The two spectra were very similar except for a slight difference at 1720 cm^{-1}. Therefore, ultrasonication did not induce significant hydrolysis of the ester. Fig. 6 also shows the spectrum of a sample that was shear degraded by using a blender. This spectrum is essentially the same as that of the original sample. The chromatogram of ultrasonically

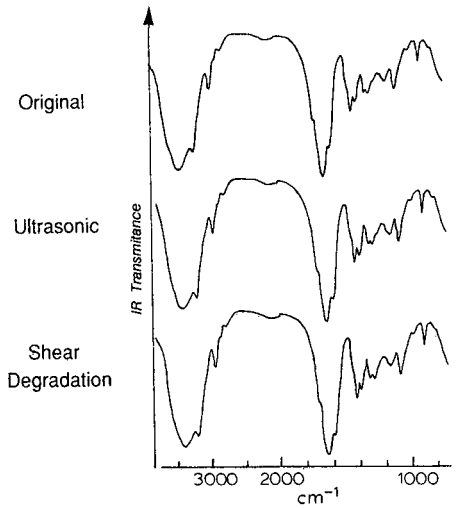

Fig. 6. Infrared spectra of an MTMAC–AAM copolymer and its degradation products. Samples were cast on germanium plates.

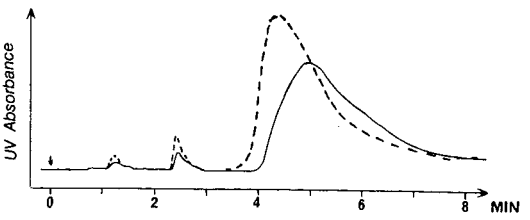

Fig. 7. Chromatograms of a DADMAC–AAM copolymer and its degradation products. Same chromatographic conditions as in Fig. 4. ——— = Original, – – – = degradation product.

degraded MTMAC–AAM copolymer was about the same as that of shear degraded product.

DADMAC–AAM copolymer

The chromatogram of DADMAC–AAM copolymer is much simpler. The original sample gave only one broad peak after 4.0 min (Fig. 7). There was almost no uncharged polymer. After degradation, the broad peak became narrower and was eluted earlier. These two chromatograms indicated that this DADMAC–AAM sample was chemically homogeneous. The broad HPLC peak of the original sample was probably due to a broad molecular weight distribution.

REFERENCES

1 W. M. Thomas and D. W. Wang, *Encyclopedia of Polymer Science and Engineering*, Vol. 1, Wiley, New York, 1985, p. 196.
2 E. D. Becker, *High Resolution NMR, Theory and Chemical Applications*, Academic Press, New York, 2nd ed., 1980, p. 116.
3 G. Glöckner, *Polymer Characterization by Liquid Chromatographiy (Journal of Chromatography Library*, Vol. 34), Elsevier, Amsterdam, 1986, p. 373.
4 A. M. Basedow and K. Ebert, *Adv. Polym. Sci.*, 22 (1977) 83.
5 L. R. Snyder, M. A. Stadalius and M. A. Quarry, *Anal. Chem.*, 55 (1983) 1413A.
6 K. S. Suslick, D. A. Hammerton and R. E. Cline, *J. Am. Chem. Soc.*, 108 (1988) 5641.
7 R. Aksberg and L. Wågberg, *J. Appl. Polym. Sci.*, 38 (1989) 297.

Journal of Chromatography, 536 (1991) 211–216
Elsevier Science Publishers B.V., Amsterdam

CHROMSYMP. 2031

High-performance liquid chromatographic separation of the three stereoisomers of diaminopimelic acid in hydrolysed bacterial cells

M. ZANOL* and L. GASTALDO
Merrell Dow Research Institute, Lepetit Research Centre, 21040 Gerenzano (VA) (Italy)

ABSTRACT

A high-performance liquid chromatographic method able to separate the three stereoisomers of diaminopimelic acid (DAP) was developed. It consists of the reaction of DAP with 1-fluoro-2,4-dinitrophenylalanine amide (FDAA), followed by chromatographic analysis of the diastereomers under reversed-phase conditions. With this method whole cell hydrolysates of different bacterial strains were analysed. The DAP derivatives can be resolved from one another and from complex mixtures of other amino acids. The precision of the derivatization and the day-to-day reproducibility were calculated and were in the range 0.5–2%. The lower limit of sensitivity is *ca.* 600 ng for a mixture of the three isomers, which is sufficient for the detection of DAP even starting from small amounts of biological material. The method was applied to the analysis of the whole cell hydrolysate of *Kineosporia aurantiaca*, an unusual strain in which L,L- and "*meso*"-isomers are both present.

INTRODUCTION

Actinomycetes, the most important producers of antibiotics, have been taxonomically separated into groups by utilizing morphological, physiological and chemical criteria [1,2]. The chemical composition of the cell wall has been found to be a particularly useful tool in actinomycete taxonomy [3]. The majority of actinomycete strains have, as a cell wall constituent, a peptidoglycan containing diaminopimelic acid (DAP). This amino acid can occur in three isomeric forms, D,D, L,L and D,L (*meso*). The L,L-isomer is present in the cell wall of strains belonging to the genus *Streptomyces*, the most important antibiotic-producing actinomycetes, while other strains may contain the *meso* form. The separation of two of the isomers, the D,L and the L,L forms, in hydrolysates of whole cells has been reported using paper chromatography [4], thin-layer chromatography (TLC) [5] and high-performance liquid chromatography (HPLC) [6]. The D,D-isomer is not readily separable from the *meso* form and is of unknown taxonomic significance. Of these methods, HPLC gives a resolution superior to that of TLC, which is, however, still widely employed for rapid DAP isomer detection.

In this paper we report an improved HPLC separation method. It consists of a reaction with 1-fluoro-2,4-dinitrophenyl-5-L-alanine amide (FDAA) as described

0021-9673/91/$03.50

elsewhere [7], with consequent formation of diastereomers. The reaction is easy to perform and separation occurs in the reversed-phase mode without the employment of columns with optically active sites; the three isomers of DAP are clearly resolved. We applied it to two standard strains and to identify the DAP isomers of a new actinomycete strain, *Kineosporia aurantiaca* [8], which was isolated in our laboratories in the course of an extensive screening programme aimed at discovering new antibiotics from non-*Streptomyces* strains.

EXPERIMENTAL

Chemicals

DAP was obtained from Sigma (St. Louis, MO, U.S.A.) as a mixture of the three isomers (L,L, D,D and *meso*). FDAA was purchased from Pierce (Rockford, IL, U.S.A.). All the solvents and salts were of analytical-reagent grade.

Bacterial strains

The actinomycete strains utilized in the study were *Streptomyces coelicolor* ATCC 19832, *Nocardia lurida* ATCC 14930 and *Kineosporia aurantiaca* ATCC 29727. *Streptomyces coelicolor* and *Nocardia lurida* were chosen as markers for L,L- and *meso*-DAP, respectively.

Growth conditions

Stock cultures of microorganism were maintained on oatmeal agar slants and used to inoculate 500-ml erlenmeyer flasks containing 100 ml of V6 medium having the following composition: ACAS meat extract, 0.5%; yeast hydrolysate, 0.5%; peptone, 0.5%; casein hydrolysate, 0.3%; dextrose, 2%; sodium chloride, 0.15%. Flasks were incubated at 28°C for 3 days on a rotary shaker at 200 rpm, then the mycelium was collected by centrifugation and thoroughly washed with distilled water. The washed mycelium was resuspended in ethanol, dried under an air flow at room temperature and stored in dark vials.

Preparation of the whole cell hydrolysate

The whole cell hydrolysate was obtained according to Becker *et al.* [4]: *ca.* 20 mg of dried mycelium were placed in small ampoules with 1 ml of 6 *M* hydrochloric acid. The sealed ampoules were kept at 100°C overnight and, after cooling, the contents were filtered through Whatman No. 1 paper and the filtrate was evaporated to dryness under vacuum. The residue was dissolved in 0.3 ml of distilled water and used for the chromatographic analysis.

HPLC apparatus

A Model 1090 liquid chromatograph (Hewlett-Packard) equipped with a diode-array detector (DAD) and a Model 79994A workstation was used.

The chromatographic conditions were as follows: column, Ultrasphere ODS, 5 μm (25 cm × 4.6 mm I.D.) (Beckman); eluent, (A) 0.05 *M* triethylamine phosphate (pH 3)–acetonitrile (95:5) and (B) acetonitrile; flow-rate, 1 ml/min; gradient, 0 min 20%, 15 min 30%, 30 min 80%, 32 min 80%, 33 min 20% B and 34 min stop; DAD, monitored at 325, 254, 220 and 400 nm; UV spectra, measured between 220 and 450 nm.

Standard preparation

The derivatization procedure employs FDAA according to Marfey [7]: to 5 μmol of DAP in 100 μl of water, 100 μl of a 1% acetone solution of FDAA and 40 μl of a 1 *M* sodium hydrogencarbonate solution were added. After 1 h at 40°C, 20 μl of 2 *M* hydrochloric acid were added and, after degassing to remove bubles of carbon dioxide, the solution was injected under the conditions described above.

Sample preparation

To 50 μl of the hydrolysed whole cell, a saturated solution of sodium carbonate was added to bring the pH to 8–9. After addition of 100 μl of a 1% acetone solution of FDAA, the sample was treated as the standard and injected.

RESULTS AND DISCUSSION

A typical chromatogram of the standard stereoisomer mixture of DAP, derivatized with FDAA, is shown in Fig. 1. The peaks with retention times between 19 and 22 min are due to the three D,D-, D,L (*meso*) and L,L-stereoisomers. As no isolated stereoisomers are commercially available, peak assignment was achieved by comparison with hydrolysed whole cell samples of *Nocardia lurida* and *Streptomyces lividans*, which are known to contain D,L- and L,L-DAP, respectively. Figs. 2 and 3 show the chromatograms obtained. The peak at 19 min in Fig. 2 corresponds to the D,L-DAP derivative and that at 22 min in Fig. 3 is due to the L,L-DAP isomer. The reproducibility (precision) of derivatization of the standard solution was determined in the following way: two aliquots (1 and 2) of 5 μmol of DAP were derivatized as described above and injected five times each. The same samples were reinjected five times after 24 h. The precision is expressed as the relative standard deviation (R.S.D.) of the groups of

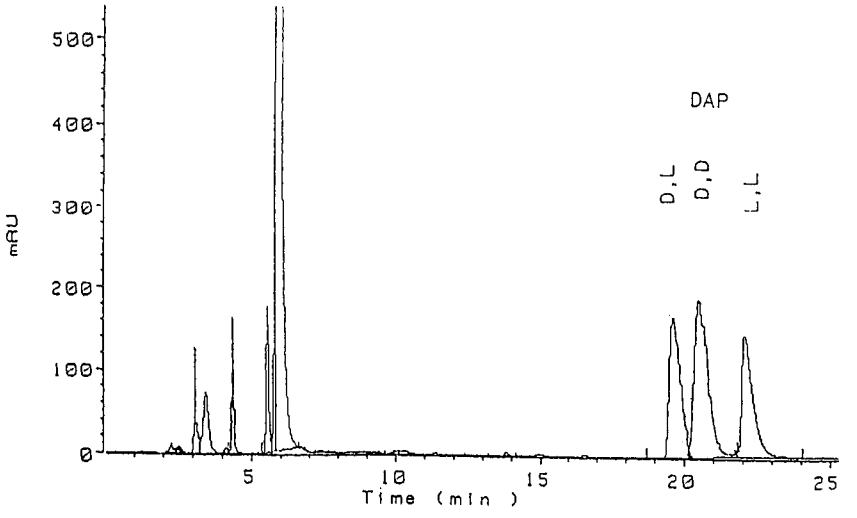

Fig. 1. Chromatogram of the three stereoisomers of diaminopimelic acid after derivatization with FDAA. An RP-18 column was used under gradient conditions. Detection at 325 nm.

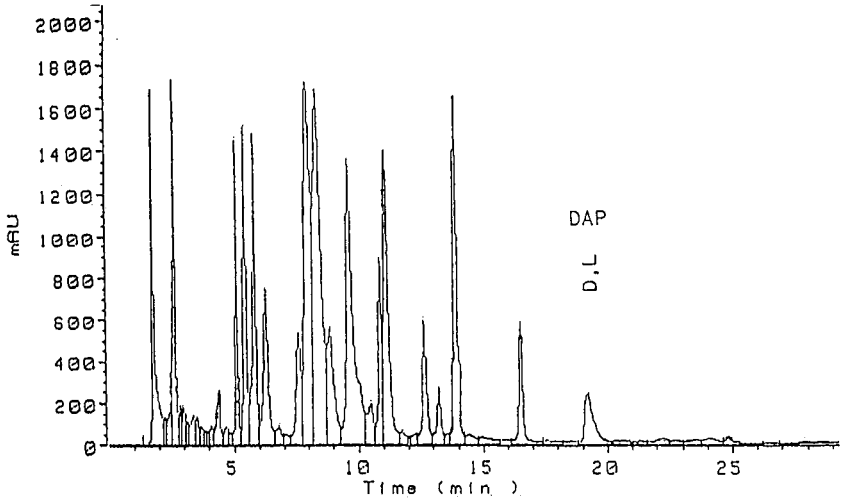

Fig. 2. Chromatogram of amino acid derivatives from whole cell hydrolysates of *Nocardia lurida*.

values reported in Table I. The instrumental precision, the reaction precision and the day-to-day reproducibility are therefore indicated.

The method was applied to verify the presence of DAP acid in *Kineosporia aurantiaca*. The hydrolysed whole cell clearly contained both the L,L and D,L forms. The resulting chromatogram is shown in Fig. 4.

The occurrence of a mixture of DAP isomers in the cell wall of bacteria is rare and in the actinomycetes is limited to the genus *Kitasatosporia* [9,10] in which the L,L form is present in major amounts in the aerial mycelium whereas the *meso* form is mostly present in the vegatative mycelium. *Kineosporia aurantiaca* does not develop

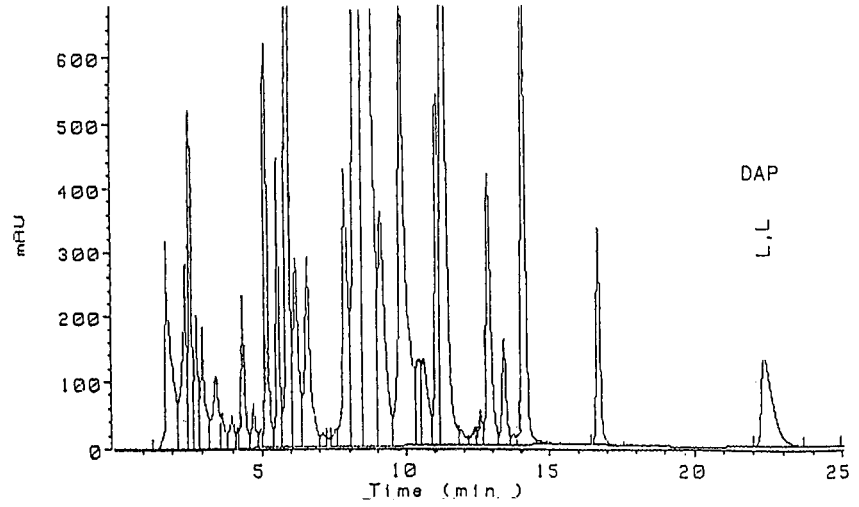

Fig. 3. Chromatogram of amino acid derivatives from whole cell hydrolysates of *Streptomyces lividans*.

TABLE I

PRECISION OF HPLC DETERMINATION OF DIAMINOPIMELIC ACID

Sample	Injections	R.S.D. (%)		
		D,L	D,L	L,L
1	5, 1st day	1.9	3.5	3.3
1	5, 2nd day	1.2	2.2	1.9
1	10, 1st + 2nd day	1.8	3.0	2,8
2	5, 1st day	0.4	1.0	1.0
2	5, 2nd day	1.1	2.6	2.7
2	10, 1st + 2nd day	1.3	1.9	1.5
1+2	10, 1st day	2.4	2.6	2.5
1+2	10, 2nd day	2.1	3.4	3.1

aerial mycelium but forms spores when grown on agar media. To check if the two isomers are present also during morphological cell differentiation, we separated by centrifugation and filtration the spores from the mycelium and both fractions were subjected to the hydrolysis. The result obtained with the spore-free mycelium fraction was the same as that obtained with the whole cell hydrolysate, indicating that both isomers are constitutively present in the cell wall. Attempts to identify DAP in purified spores failed even when a hydrolysate was obtained from *ca.* 200 mg of biomass (see Fig. 5). This indicates that the DAP spore content is at least two orders of magnitude lower than that of mycelium.

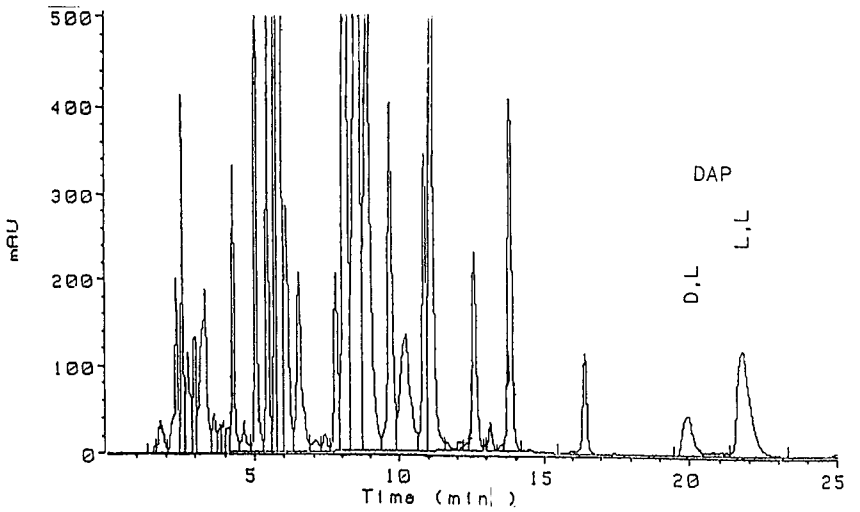

Fig. 4. Chromatogram of amino acid derivatives from whole cell hydrolysates of *Kineosporia aurantiaca.*

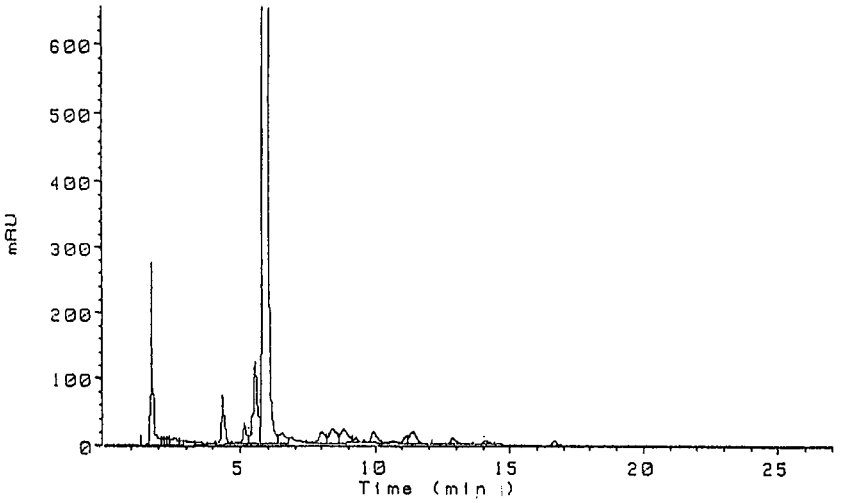

Fig. 5. Chromatogram of amino acid derivatives from purified spores of *Kineosporia aurantiaca*.

CONCLUSIONS

The method described here has several advantages: first, it is simple and reproducible, and second, very good resolution is obtained under the described chromatographic conditions. As can be seen in the figures, the peaks due to the three isomers of DAP are well resolved from one another and from other amino acids even in complex mixtures. Moreover, the derivatized diastereomers have a good response factor. The limit of detection is of the order of 600 ng of a mixture of the three isomers. The method is therefore sensitive enough to give information on DAP content starting from very small amounts of biological material. In addition, resolution of the D,D-isomer could provide further information of use in actinomycete taxonomy, given the hypothesis that this isomer may be present in some strains.

ACKNOWLEDGEMENTS

The authors are indebted to Franco Recupero for his valuable contribution to the HPLC work and to James Parlett for his accurate revision of the text.

REFERENCES

1 T. Cross and M. Goodfellow, in G. Sykes and F. A. Skinner (Editors), *Actinomycetales*, Academic Press, London, 1973, p. 76.
2 H. A. Lechevalier and M. P. Lechevalier, *Annu. Rev. Microbiol.*, 21 (1967) 71.
3 H. A. Lechevalier, M. P. Lechevalier and N. N. Gerber, *Adv. Appl. Microbiol.*, 14 (1971) 47.
4 B. Becker, M. P. Lechevalier, R. E. Gordon and H. A. Lechevalier, *Appl. Microbiol.*, 12 (1964) 421.
5 J. L. Staneck and G. D. Roberts, *Appl. Microbiol.*, 28 (1974) 226.
6 P. A. Tisdall and J. P. Anhalt, *J. Clin. Microbiol.*, 10 (1979) 503.
7 P. Marfey, *Carlsberg Res. Commun.*, 49 (1984) 591.
8 H. Pagani and F. Parenti, *Int. J. Syst. Bacteriol.*, 28 (1978) 401.
9 A. Omura, Y. Iwai, Y. Takahashi, K. Kojima, K. Otoguro and R. Oiwa, *J. Antibiot.*, 34 (1981) 1633.
10 S. Omura, Y. Tagahashi, Y. Iwai and H. Tanaka, *J. Antibiot.*, 35 (1982) 1013.

Journal of Chromatography, 536 (1991) 217–222
Elsevier Science Publishers B.V., Amsterdam

CHROMSYMP. 2010

Post-column reaction for simultaneous analysis of chromatic and leuco forms of malachite green and crystal violet by high-performance liquid chromatography with photometric detection

JOHN L. ALLEN* and JEFFERY R. MEINERTZ

U.S. Fish and Wildlife Service, National Fisheries Research Center, P.O. Box 818, La Crosse, WI 54602-0818 (U.S.A.)

ABSTRACT

The chromatic and leuco forms of malachite green and crystal violet were readily separated and detected by a sensitive and selective high-performance liquid chromatographic procedure. The chromatic and leuco forms of the dyes were separated within 11 min on a C_{18} column with a mobile phase of 0.05 *M* sodium acetate and 0.05 *M* acetic acid in water (19%) and methanol (81%). A reaction chamber, containing 10% PbO_2 in Celite 545, was placed between the column and the spectrophotometric detector to oxidize the leuco forms of the dyes to their chromatic forms. Chromatic and leuco malachite green were quantified by their absorbance at 618 nm; and chromatic and leuco Crystal Violet by their absorbance at 588 nm. Detection limits for chromatic and leuco forms of both dyes ranged from 0.12 to 0.28 ng. A linear range of 1 to 100 ng was established for both forms of the dyes.

INTRODUCTION

Malachite green oxalate {N-[4-[[4-(dimethylamino)-phenyl]phenylmethylene]-2,5-cyclohexadien-1-ylidine]-N-methylmethanaminium oxalate} has been used to treat external fungal and protozoan infections in fish since 1933 [1]. Crystal violet (hexamethylpararosaniline chloride) has long been used to inhibit mold and fungal growth in poultry feeds, control fungal and intestinal parasites in humans, and combat microbial infections in domestic animals. Both chemicals belong to the triphenylmethane class of dyes, some of which are animal carcinogens [2]. Meyer and Jorgenson [3] demonstrated that malachite green caused significant developmental abnormalities when administered to eggs of Rainbow trout (*Oncorhynchus mykiss*) and to pregnant New Zealand white rabbits (*Oryctolagus cuniculus*). Crystal violet was determined to be mutagenic to *Bacillus subtilis*, *Escherichia coli*, and *Salmonella typhimurium* [4] and cytotoxic to mammalian cells [5].

Animals reduce malachite green and crystal violet to their leuco forms [6–8]. However, the leuco forms of these dyes are also their precursors during production and could be contaminants of commercial preparations of the dyes. Although the leuco forms of these dyes have no acute adverse effects in animals, Roybal *et al.* [9]

0021-9673/91/$03.50

quoting the National Center for Toxicological Research, stated that 'This leuco derivative is then structurally similar to the classical aromatic amine carcinogens'.

Concern about the health risks associated with the use of malachite green and crystal violet and their metabolites requires that methods be developed to monitor these residues. The chromatic and leuco forms of the dyes can now be analyzed simultaneously by high-performance liquid chromatography (HPLC) only with electrochemical detection [9]. Bauer *et al.* [10] analyzed for malachite green and leuco malachite green by splitting the sample and oxidizing half of the sample to all malachite green with PbO_2. The amount of leuco malachite green in the sample was determined by the difference in the malachite green found in the subsamples. We here present a method of separating the chromatic and leuco forms of two triphenylmethane dyes by HPLC, with oxidation of the leuco forms to the chromatic forms (Fig. 1), and detection of both forms by visible spectrophotometry. Detection in the visible region of the spectrum has the advantage of increased specificity as few potential interferences adsorb light in this area of the spectrum.

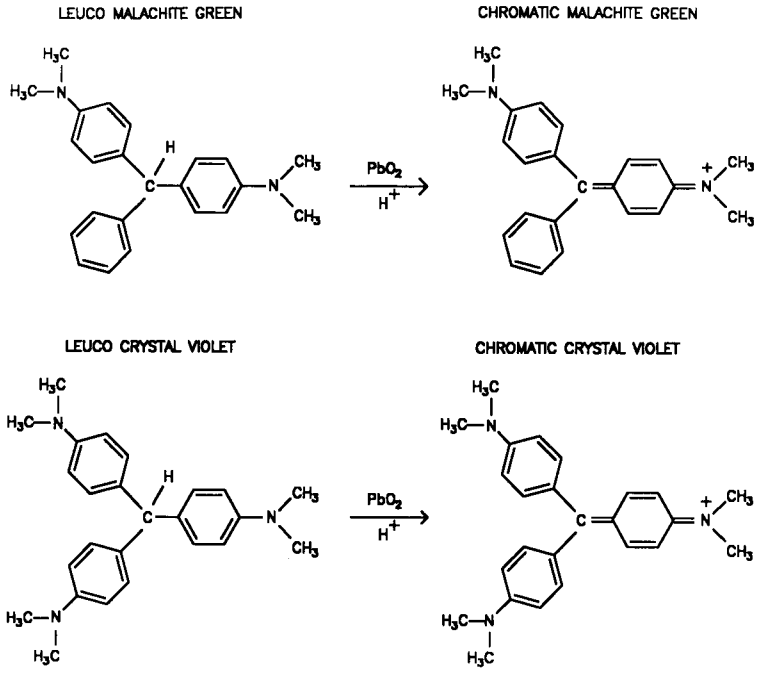

Fig. 1. Leuco malachite green and leuco crystal violet, when mixed with PbO_2 in the presence of acid, are oxidized to the chromatic dye forms.

EXPERIMENTAL[a]

Chemicals and reagents

All chemicalls were of reagent grade. Malachite green oxalate and leuco malachite green [4,4'-benzylidenebis-(N,N-dimethylaniline)] were obtained from Eastman Kodak (Rochester, NY, U.S.A.). Crystal violet {N-[4-[bis[4-(dimethylamino)-phenyl]-methylene]-2,5-cyclohexadien-1-ylidine]-N-methyl-methanaminium chloride}, leuco crystal violet [4,4',4''-methylidynetris (N,N-dimethylaniline)] and anhydrous acetic acid, sodium salt, were obtained from Aldrich (Milwaukee, WI, U.S.A.). Glacial acetic acid, toluene sulfonic acid, and all solvents were of HPLC grade (Baker, Phillipsburg, NJ, U.S.A.). Celite 545 was obtained from Fisher Scientific and reagent grade lead dioxide (PbO_2, powder) was obtained from Mallinckrodt.

HPLC

Chromatographic separations of the triphenylmethane dyes and their reduced forms were achieved with a μBondapak C_{18} column (300 mm × 3.9 mm I.D., Waters, Milford, MA, U.S.A.), particle size 10 μm, and an isocratic, degassed mobile phase (flow-rate 1.5 ml/min) of methanol–water (81:19), buffered with 0.05 *M* sodium acetate and 0.05 *M* glacial acetic acid. The resulting solution had a pH of 6.0. A Beckman fixed-loop (10-μl) injector delivered the analyte to the column. A Waters Lambda-Max, Model 481 spectrophotometer was operated at 618 nm for malachite green analysis, 588 nm for crystal violet analysis, and 600 nm for analysis of a combination of two chemicals. Chromatographic data from injections were collected and analyzed with System Gold chromatographic software (Beckman, Arlington Heights, IL, U.S.A.). The detection limit was determined by using the 1984 U.S. Environmental Protection Agency (EPA) method [11]. Solutions of the triphenylmethane dyes and their leuco forms were prepared in 0.05 *M* toluenesulfonic acid in methanol. Solutions of the dyes and their leuco forms should be protected from light.

Oxidation of reduced forms of dyes

The leuco forms of the chemicals were oxidized to the chromatic forms in a post-column reactor (stainless-steel tube, 32 mm long, 4 mm I.D.) capped with guard column fittings and packed with 10% PbO_2 suspended in Celite 545. The post-column reactor was packed with the dry mixture of PbO_2 in Celite 545 by gently tamping with a glass rod and placed in line between the HPLC column and the spectrophotometric detector.

RESULTS AND DISCUSSION

The chromatic forms of malachite green and crystal violet are separated from their leuco forms by HPLC on a reversed-phase column. The high absorbance of the dyes in the visible spectrum and the lack of absorbance by contaminants allows easy and specific detection by visible spectrophotometry. The leuco forms of the dyes are colorless and not detectable by visible spectrophotometry. Oxidation of the leuco

[a] Reference to trade names or manufacturers does not imply U.S. Government endorsement of commercial products.

form of the dye to the chromatic form after HPLC separation allows simultaneous analysis of the chromatic and leuco forms of the dyes with excellent sensitivity and specificity.

The detector response was about equal on a mol/mol basis when both chromatic and leuco crystal violet were analyzed with the spectrophotometric detector set at 588 nm (Fig. 2). The relative response indicates near complete conversion of the leuco to the chromatic form of the chemical. We prepared separate calibration curves, using this system with both the chromatic and leuco forms of crystal violet, that were linear over the range, of 1 to 100 ng, $r^2 = 0.998$. The minimum detection limits for the HPLC systeme, as estimated by the EPA method, were 0.13 ng for chromatic crystal violet and 0.16 ng for leuco crystal violet.

The detector response was lower for chromatic malachite green oxalate than for its leuco form due to the different molecular weight (Fig. 3). The calibration curves for both the chromatic and leuco forms of malachite green were linear over the range of 1 to 100 ng, $r^2 = 0.998$. The minimum detection limit was estimated to be 0.28 ng for chromatic malachite green oxalate and 0.12 ng for leuco malachite green.

We attempted to separate crystal violet, malachite green oxalate, and their leuco forms. Although a good response was obtained for all four chemicals, the leuco forms were poorly resolved (Fig. 4).

Roybal *et al.* [9], using electrochemical detection, achieved good sensitivity and selectivity for both chromatic and leuco crystal violet. Although an electrochemical detector yielded good sensitivity and selectivity for a triphenylmethane dye, UV–visible detectors are readily available and widely used in HPLC analysis. Our use of a

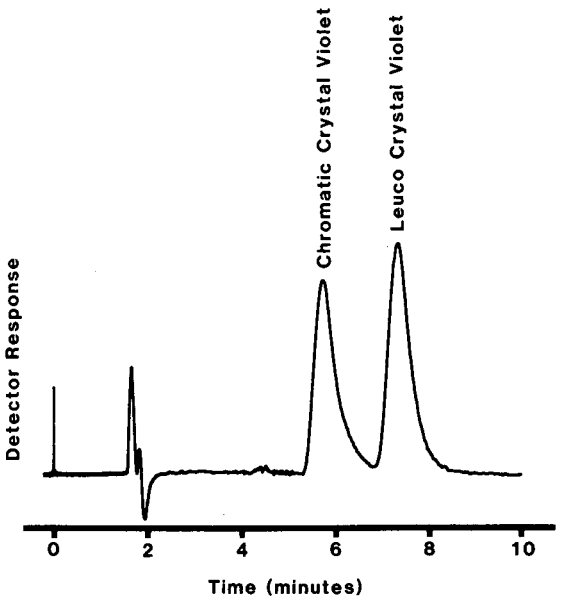

Fig. 2. Chromatogram of 10 ng each of chromatic crystal violet and leuco crystal violet on a C_{18} column with 1.5 ml/min of methanol–water (81:19) buffered with 0.05 *M* sodium acetate and 0.05 *M* glacial acetic acid at 588 nm and a sensitivity of 0.005 a.u.f.s., with post-column oxidation.

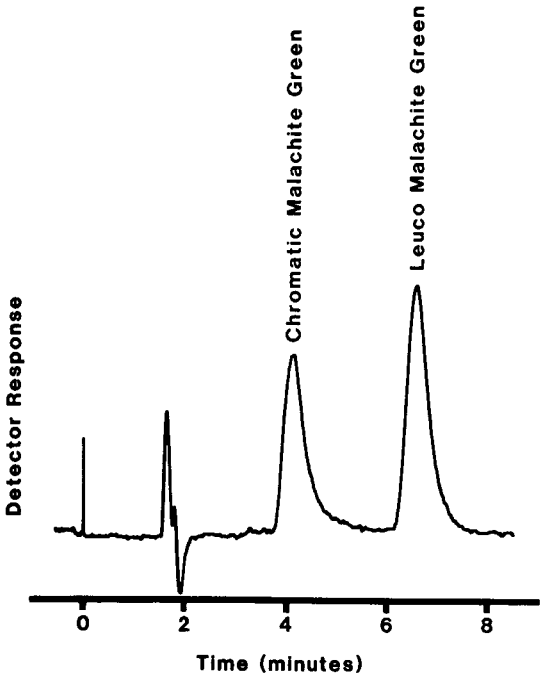

Fig. 3. Chromatogram of 10 ng each of chromatic malachite green and leuco malachite green on a C_{18} column with 1.5 ml/min of methanol–water (81:19), buffered with 0.05 *M* sodium acetate and 0.05 *M* glacial acetic acid at 618 nm and a sensitivity of 0.005 a.u.f.s., with post-column oxidation.

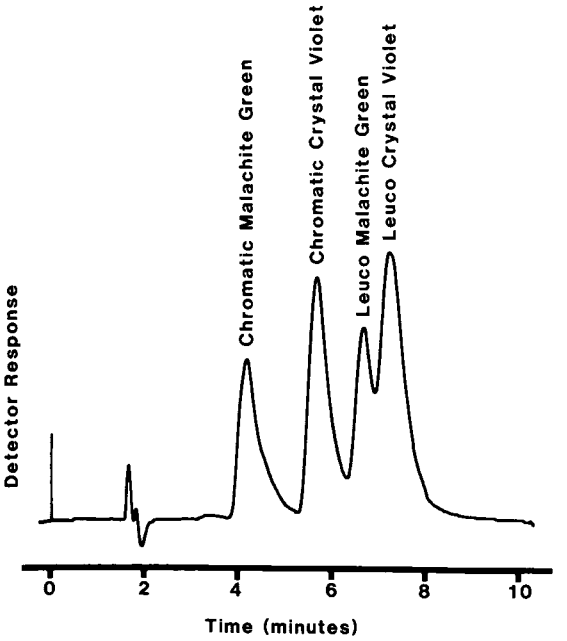

Fig. 4. Chromatogram of 10 ng each of chromatic malachite green, leuco malachite green, chromatic crystal violet, and leuco crystal violet on a C_{18} column with 1.5 ml/min of methanol–water (81:19), buffered with 0.05 *M* sodium acetate and 0.05 *M* glacial acetic acid at 600 nm and a sensitivity of 0.01 a.u.f.s., with post-column oxidation.

reaction chamber, containing PbO_2 between the HPLC column and the spectrophotometric detector, permitted simultaneous analysis of the parent dyes and their leuco forms at a single wavelength. Bauer *et al.* [10] used PbO_2 oxidation to analyze fish tissue for chromatic and leuco malachite green, but both the quantitative and qualitative information were obtained from the difference of two injections. The calibration curves indicate that the oxidation in the reaction chamber is reproducible over the range of 1 to 100 ng for the leuco forms of both dyes with the chromatographic conditions used. Although the reaction chamber increased the deadvolume of the chromatographic system, we achieved good sensitivity for all four components. The reaction chamber is able to convert these dyes form the leuco to the chromatic form after 400 injections; however, the efficiency of the conversion should be checked periodically using standards of the leuco forms of the dyes to ensure that the PbO_2 has not ben depleted.

REFERENCES

1 F. J. Foster and L. Woodbury, *Prog. Fish-Cult.*, 18 (1936) 7.
2 L. G. Rushing and M. C. Bowman, *J. Chromatogr. Sci.*, 18 (1980) 224.
3 F. P. Meyer and T. A. Jorgenson, *Trans. Am. Fish. Soc.*, 112 (1983) 818.
4 H. Fujita, A. Mizuo and K. Hiraga, *Tokyo Toritsu Eisei Kenkyusho Kenkyu Nempo*, 27 (1976) 153.
5 K. Norrby and H. Mobacken, *Acta Derm. Venereol.*, 52 (1972) 476.
6 J. J. McDonald and C. E. Cerniglia, *Drug Metab. Dispos.*, 12 (1984) 330.
7 W. E. Poe and R. P. Wilson, *Prog. Fish-Cult.*, 45 (1983) 228.
8 G. Werth and A. Boiteux, *Arzneim. Forsch.*, 17 (1967) 155.
9 J. E. Roybal, R. K. Munns, J. A. Hurlbut and W. Shimoda, *J. Chromatogr.*, 467 (1989) 259.
10 K. Bauer, H. Dangschat, H. O. Knoeppler and J. Neudegger, *Arch. Lebensmittelhyg.*, 39 (1988) 97.
11 U.S. Environmental Protection Agency, *Fed. Reg.*, 49 (1984) 198.

Journal of Chromatography, 536 (1991) 223–228
Elsevier Science Publishers B.V., Amsterdam

CHROMSYMP. 2025

Simplified high-performance liquid chromatography method for the simultaneous analysis of tebuthiuron and hexazinone

JOHN LYDON*, BEATRIZ F. ENGELKE and CHARLES S. HELLING
U.S. Department of Agriculture, Agricultural Research Service, Tropical Plants Research Laboratory, Beltsville, MD 20705 (U.S.A.)

ABSTRACT

A simplified, high-performance liquid chromatography (HPLC) method for the simultaneous measurement of the herbicides tebuthiuron and hexazinone was developed. Separation was achieved on a Nova-Pak® phenyl (4 μm) 10 × 0.8 cm column with methanol–water (50:50 v/v) as eluent and on-line detection at 254 nm for tebuthiuron and 249 nm for hexazinone. At a flow-rate of 2.5 ml min^{-1}, the retention times were approximately 4.5 and 6.3 min for tebuthiuron and hexazinone, respectively. The procedure was used successfully for the analysis of residues of these herbicides in soil and plant tissues. A comparison with published procedures for the individual analysis of tebuthiuron and hexazinone is presented.

INTRODUCTION

The urea herbicide tebuthiuron {N-[5-(1,1-dimethylethyl)-1,3,4-thiadiazol-2-yl]-N,N′-dimethylurea} and the triazine herbicide hexazinone [3-cyclohexyl-6-(dimethylamino)-1-methyl-1,3,5-triazine-2,4(1H,3H)-dione] are used on non-cropland areas for the control of grasses, broadleaf weeds, and woody plants for brush control [1]. Because they have similar applications, there is the potential for plant and soil samples from sites undergoing brush control to contain residues of both tebuthiuron and hexazinone. High-performance liquid chromatographic (HPLC) methods have been developed for the separate analysis of residues of these herbicides in water, soil, and leaf tissue [2–6]. Two HPLC methods have been developed for the analysis of tebuthiuron, one utilizing a normal-phase column and the other a reversed-phase C_{18} column [2,3]. All the HPLC methods developed for analysis of hexazinone residues utilize reversed-phase columns with C_8 or C_{18} stationary phases, the latter methods requiring a column heater [4–7].

Although applicable for the individual analysis of tebuthiuron or hexazinone, the methods that use reversed-phase columns without column heaters did not adequately separate these analytes when both were present in the sample. This report presents a simple HPLC procedure for the separation and simultaneous analysis of tebuthiuron and hexazinone residues in water, soil and plant samples.

0021-9673/91/$03.50

EXPERIMENTAL[a]

Plant propagation and treatment

Pigweed (*Amaranthus retroflexus* L.) plants were started from seed in 0.32-l pots filled with 240 g of sandy-loam, greenhouse soil (pH 7.0, 3.9% organic matter). Plants were grown under a 16-h photoperiod with a photosynthetic photon flux density of 335 μmol m^{-2} s^{-1} and a day/night temperature of 25/20°C, watered as needed, and fertilized (after seedling establishment) every other watering with a dilute solution of 20-20-20 (N-P-K) fertilizer (0.25 g l^{-1}). Two weeks after emergence, the plants were thinned to 1 plant per pot.

Sixty-day-old plants (three replicates per treatment) were soil-treated with commercial formulations of tebuthiuron (Spike® 20 P, Elanco Products, Indianapolis, IN, U.S.A.) and hexazinone (Pronone® 75 P, Pro-Serve, Memphis, TN, U.S.A.) at 2.75 mg active ingredient (a.i.) per pot, which is equivalent to 3.36 kg ha^{-1} a.i. based on the surface area of the pot. Seven days after treatment, when the leaves began to abscise, the remaining leaves were removed from the stem, dipped into liquid nitrogen, freeze-dried, and stored at −5°C over silica gel. Stem tissue was removed at the soil line and discarded. A subsample of soil was dried at 105°C to determine moisture content, the roots separated from the soil, and the remaning soil stored at −5°C. Roots were washed with deionized water, lightly blotted dry, freeze-dried, and stored over silica at −5°C.

Extraction and partial purification

Soil (20 g equivalent dry weight) was extracted with 75 ml methanol–water (80:20, v/v) at room temperature by shaking for 1 h. The slurry was suction filtered through a Whatman 934-AH glass fiber filter, the soil re-extracted with 25 ml methanol–water (80:20, v/v) for 15 min, suction filtered, and the two extracts combined. The combined extracts were reduced to 2–3 ml at 45°C on a rotary evaporator, brought to a final volume of 4 ml with methanol, and filtered through a 0.45-μm polytetrafluoroethylene (PTFE) membrane syringe filter.

Plant tissue was milled to 0.5 mm in a Brinkmann (Westbury, NY, U.S.A.) ZM-1 centrifugal grinding mill, and extracted twice with shaking for 1 h in methylene chloride at a ratio of 1:100 (tissue–methylene chloride, w/v) at room temperature. The extracts were filtered through Whatman No. 1 filter paper, combined, evaporated to dryness under vacuum at room temperature, resuspended in 10 ml methylene chloride–hexane (50:50, v/v), and filtered through a 5-μm PTFE syringe filter. Semi-purification of extracts was obtained using gel permeation chromatography (GPC), [8] with 5 ml of extract loaded on a 2.5 mm (I.D.) GPC column packed with 60 g of Bio-Beads® SX-3 (Bio-Rad, Richmond, CA, U.S.A.) in methylene chloride–hexane (50:50, v/v), providing a final bed length of 39 cm; the eluting solvent was methylene chloride–hexane (50:50, v/v) at a flow-rate of 5 ml min^{-1}. The first 125 ml of eluting solvent was discarded and the following 30 ml collected, evaporated to dryness under

[a] Mention of a trademark, proprietary product or vendor does not constitute a guarantee or warranty of the product by the U.S. Department of Agriculture and does not imply its approval to the exclusion of other products or vendors that may also be suitable.

vacuum at room temperature, resuspended in 5 ml methylene chloride, evaporated to dryness under vacuum at room temperature, resuspended in 500 μl of methanol, and filtered through a 0.2-μm PTFE syringe filter.

HPLC analysis

The HPLC system was composed of Waters Assoc. HPLC components: a system controller (Model 600E), an autosampler (Model 712), and a scanning, photodiode array UV detector (Model 990). The columns, solvents, and flow-rates used in this study are listed in Table I. Sample injection volumes were 50 μl for soils, roots, and leaves (untreated controls only), and 15 μl for leaf extracts from herbicide-treated plants. Detection was monitored from 220 to 300 nm, while the concentrations of tebuthiuron and hexazinone were determined based on their individual absorption maxima, *i.e.*, 254 and 249 nm for tebuthiuron and hexazinone, respectively. Plots of peak response *versus* amount of herbicide in the range of 1.25 to 2000 ng consistently gave linear responses with correlation coefficients of 0.98 or greater for both herbicides. (For presentation purposes, chromatograms were reproduced at an intermediate wavelength, *i.e.*, 252 nm).

RESULTS AND DISCUSSION

The published, reversed-phase methods for the individual analysis of tebuthiuron and hexazinone failed to provide adequate separation of these two compounds (Fig. 1). The two methods utilizing a C_8 column (Fig. 1 A and B) gave partial, but not baseline, separation of tebuthiuron and hexazinone. The C_{18} method resulted in tebuthiuron and hexazinone co-eluting, as determined by the increased peak height and absorption spectra. Of the methods tested, only the phenyl column gave baseline separation of tebuthiuron and hexazinone, with retention times of 4.5 and 6.3 min, respectively. The phenyl column method was used successfully in analyzing residues

TABLE I

HPLC COLUMNS AND SOLVENT SYSTEMS USED IN TESTING FOUR METHODS FOR THE SEPARATION OF TEBUTHIURON AND HEXAZINONE

Columns and prefilters are products of Waters Assoc.

Method	Column dimensions and packing	Eluent (v/v)	Prefilter	Flow-rate (ml min^{-1})	Ref.
A	10 cm × 8 mm (I.D.) Radial-Pak® C_8, 10-μm spherically shaped silica	acetonitrile–water (50:50)	C_{18} Guard-Pak®	1.2	5
B	10 cm × 8 mm (I.D.) Radial-Pak C_8, 10-μm spherically shaped silica	acetonitrile–water (45:55)	none	1.0	4
C	30 cm × 3.9 mm (I.D.) C_{18}, μBondapak®, 10-μm irregularly shaped silica	methanol–water (50:50)	none	1.0	3
D	10 cm × 8 mm (I.D.) Nova-Pak phenyl, 4-μm spherically shaped silica	methanol–water (50:50)	Phenyl Guard-Pak	2.5	This report

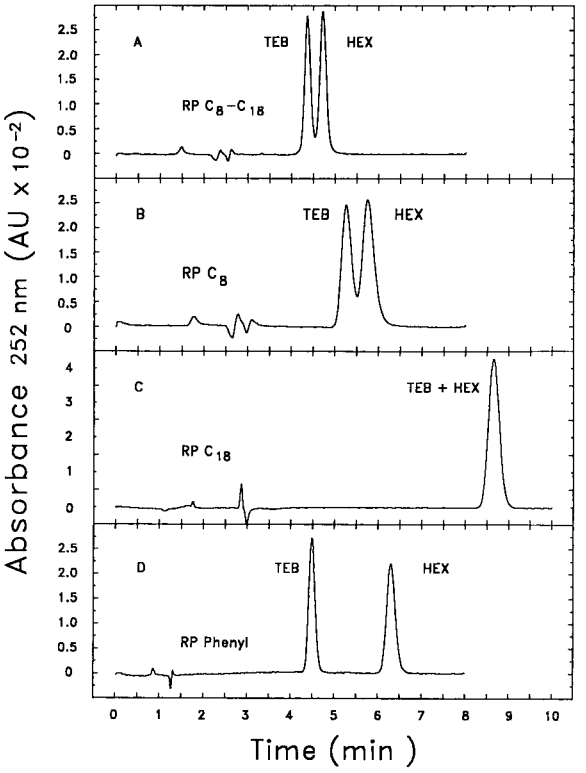

Fig. 1. Chromatographic separation of tebuthiuron (TEB) and hexazinone (HEX) using the HPLC methods described in Table I. Each chromatogram respresents an injection of 0.12 μg of each herbicide.

of these herbicides in soil and plant tissue (Fig. 2). Given a detection limit (based upon peak response for spiked, control extracts) of 1.25 ng, the amount of material extracted, and the final volume of the extracts, the minimum detection limit for tebuthiuron and hexazinone on the phenyl column system was 0.1, 0.02, and 0.005 μg g^{-1} for roots, leaves, and soil, respectively. The recovery rates of tebuthiuron and hexazinone, from control soil and leaf samples (two replicates each) spiked with 1 μg each of tebuthiuron and hexazinone and extracted and partially purified as described above, were 99 and 100 ± 2% and 98 and 102 ± 2%, respectively. These recovery rates are higher than those reported for other HPLC methods for tebuthiuron [3] and hexazinone [5], but similar to that reported for a gas chromatographic method for hexazinone [7].

Seven days after treatment with 3.36 kg ha^{-1} of each herbicide, tebuthiuron and hexazinone were more concentrated in the leaves than in the roots or soil (Table II). The distribution of tebuthiuron and hexazinone in pigweed was similar to that reported for tebuthiuron in common ragweed (*Ambrosia artemisiifolia* L.) and rye (*Secale cereale* L. 'Elbon') 1 day after treatment [9], but the reverse of that reported for tebuthiuron and hexazinone in bur oak (*Quercus macrocarpa* Michx.) and eastern redcedar (*Juniperus virginiana* L.) 3 days after treatment [10].

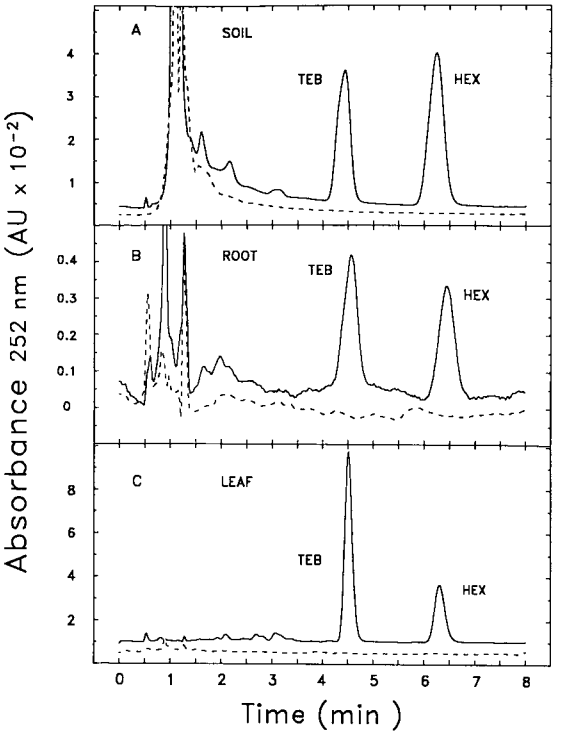

Fig. 2. Chromatograms of extracts from soil (A) and pigweed (*Amaranthus retroflexus* L.) root (B) and leaf (C) tissue 7 days after treatment with 3.36 kg ha^{-1} (a.i.) of soil-applied tebuthiuron (TEB) and hexazinone (HEX). Dotted lines represent untreated control samples and solid lines represent herbicide-treated samples.

TABLE II

RESIDUES OF TEBUTHIURON AND HEXAZINONE IN SOIL AND PIGWEED (*AMARANTHUS RETROFLEXUS* L.) TISSUES SEVEN DAYS AFTER TREATMENT WITH 3.36 kg ha^{-1} (A.I., SOIL-APPLIED) OF EACH HERBICIDE

Values represent the average of three replicates ± 1 standard error of the mean.

Sample		Tebuthiuron (μg g^{-1})	Hexazinone (μg g^{-1})
Soil			
	Control	0	0
	Treated	1.83 ± 0.30	2.06 ± 0.30
Roots			
	Control	0	0
	Treated	3.68 ± 0.68	4.72 ± 1.32
Leaves			
	Control	0	0
	Treated	21.4 ± 8.2	8.9 ±2.9

The method described here, which utilizes a reversed-phase phenyl column and an isocratic mobile phase of methanol–water (50:50, v/v), gave excellent separation of tebuthiuron and hexazinone, and is applicable to the simultaneous analysis of these herbicides in soil and plant tissue.

ACKNOWLEDGEMENTS

We thank Cheryl M. Patterson and Michael A. Doherty for their expert technical assistance.

REFERENCES

1 N. E. Humburg (Editor), *Herbicide Handbook of the Weed Science Society of America*, Weed Science Society of America, Champaign, IL, 6th ed., 1989.
2 A. Loh, R. Frank and O. D. Decker, *Anal. Methods Pestic. Plant Growth Regul.*, 11 (1980) 351.
3 A. E. Smith, Jr., L. M. Shuman and N. Lokey, *J. Agric. Food Chem.*, 32 (1984) 416.
4 C. E. Parker, C. A. Haney, D. J. Harvan and J. R. Hass, *J. Chromatogr.*, 242 (1982) 77.
5 D. C. Bouchard and T. L. Lavy, *J. Chromatogr.*, 270 (1983) 396.
6 T. H. Byast, *J. Chromatogr.*, 134 (1977) 216.
7 C. L. McIntosh, D. D. Schlueter and R. F. Holt, *Anal. Methods Pestic. Plant Growth Regul.*, 13 (1984) 267.
8 M. L. Hopper, *J. Agric. Food Chem.*, 30 (1982) 1038.
9 W. G. Steinert and J. F. Strizke, *Weed Sci.*, 25 (1977) 390.
10 W. K. McNeal, J. F. Strizke and E. Basler, *Weed Sci.*, 32 (1984) 739.

Journal of Chromatography, 536 (1991) 229–236
Elsevier Science Publishers B.V., Amsterdam

CHROMSYMP. 2063

Determination of neurochemicals in biological fluids by using an automated high-performance liquid chromatographic system with a coulometric array detector

VITTORIA RIZZO and GIANVICO MELZI D'ERIL*
Servizio Analisi Chimico Cliniche e Neurochimica, IRCCS Istituto Neurologico "C. Mondino", Università di Pavia, Via Palestro 3, 27100 Pavia (Italy)
and
GUIDO ACHILLI and GIAN PIERO CELLERINO
ESA International, Parabiago (Italy)

ABSTRACT

The chromatographic separation of 33 neurochemicals was achieved by using a combined gradient of organic modifier, pH and counter-ion. A secondary separation of unresolved analytes was obtained by using electrochemical detection with a coulometric array of sixteen electrodes. The stability of the analytes was studied and data on analytical performance are reported in addition to a list of neurochemicals detected in a normal plasma sample.

INTRODUCTION

Electrochemical detection has been used with high-performance liquid chromatography (HPLC) for more than 10 years. This technique is often used for the detection of electrochemically active neurotransmitters, and over the years many new applications have been described, covering various fields of the reversed-phase HPLC and in some instances normal-phase HPLC [1–6]. While amperometric and coulometric electrochemical techniques have been used extensively, the selectivity available with full conversion of the analyte has only been described for coulometric detectors [7].

Multiple coulometric electrodes in series can be used for characterizing molecules passing through them. This is possible by operating the cells at different potentials on the current–voltage curve of the analyte, thereby generating multiple chromatograms. From these chromatograms it is possible to obtain the ratio of the peak heights measured at different detector potentials; this ratio is typical of a pure molecule, and any deviation from this value will indicate the presence of a contaminant [7].

The ratio of the measured peaks can be obtained with a normal cell, containing two coulometric measuring electrodes in series; greater selectivity is achieved by increasing the number of electrodes in series, *e.g.*, cells containing a set of four

0021-9673/91/$03.50

coulometric electrodes potted in a single pack. Several packs of four electrodes are used in series, forming arrays of eight, twelve and sixteen electrodes [8].

As each cell in the array will react with the total amount of analyte pertinent to its potential, the concentration of the component reaching the next electrode will be decreased by the same amount. Following subsequent reactions, the component will be fully transformed when it leaves the element located in the plateau of the current–voltage curve. In a symmetric array the maximum signal will be generated by the electrode whose potential is the closest to the half-wave potential; the corresponding channel is known as the dominant channel (T_d). The channels immediately before and after the dominant channel are called sub-dominant channels (T_s).

In this way the component, will be described not only as a function of its elution time, but also as a function of its behaviour according to the potential of the reaction; this increases the selectivity of the system to help in the correct identification of the measured peaks.

In fact, the coulometric efficiency of each element of the array allows a complete separation of analytes as a function of their reaction potential, and some peaks may therefore be resolved by the detector even if they are unresolved when they leave the chromatographic column. This principle was applied to a new instrument to increase the number of species simultaneously resolved in a single analysis. By coupling the array selectivity to a gradient capability, it is possible to generate a complete picture of the components present in very complex mixtures. The first practical applications have been developed in the neurochemistry field, for different matrices, such as cerebrospinal fluid, plasma and brain tissues [9–11].

The purpose of this work was to verify the suitability of this automated system for the analysis of human plasma samples.

EXPERIMENTAL

Chemicals

The eluents used in gradient elution were purchased from ESA (Bedford, MA, U.S.A.). Mobile phase A consisted of 34.7 μM sodium dodecyl sulphate (SDS)–0.1 M monobasic sodium phosphate–50 nM nitrilotriacetic acid (pH 3.35). Mobile phase B consisted of 173 μM SDS–0.1 M monobasic sodium phosphate–50 nM nitrilotriacetic acid–50% aqueous methanol (pH 3.45).

Apparatus

The analytical apparatus used was a Coulochem Electrode Array System (CEAS) (ESA). The instrument consists of an autosampler, capable of variable-volume injections, equipped with a 100-μl loop and a circulating glycol bath, which maintains sample vials at a temperature between 0 and 4°C prior to the injection, and two HPLC pumps capable of gradient operation from 0.05 to 10 ml/min. The output of the pumps is connected to a dynamic gradient mixer. The analytical column (80 mm × 4.6 mm I.D.) contained HR80 (C_{18}), 3 μm (ESA).

The detection system consisted of four cell packs in series, each containing four porous graphite working electrodes with associated palladium reference electrodes and platinum counter electrodes. The detector, column and one pulse damper were housed in a temperature-controlled compartment. Two additional pulse dampers were placed before the column and cell compartment.

The autosampler, pumps, detectors, temperature-controlled box and all associated electronic circuitry were monitored and controlled by the CEAS software, installed in a Model 286 computer equipped with a 32-megabyte hard disk and one 1.2-megabyte floppy disk drive. The computer was coupled with a high-resolution colour monitor with a "touch screen" interface and a matrix graphic printer.

This computer system performed the data storage, analysis and report generation. An appropriate software package was used for summary reports of the final data.

Chromatographic method

The compounds investigated were predominantly from the tyrosine, tryptophan and purine metabolic pathways and were uric acid (URIC), vanillylmandelic acid (VMA), xanthine (XANT), methionine (METH), 3,4-methoxyhydroxyphenyl glycol (MHPG), 3-(3,4-dihydroxyphenyl)alanine (DOPA), noradrenaline (NE), 3,4-dihydroxyphenylacetic acid (DOPAC), xanthurenic acid (XANTHURENIC), 4-hydroxyphenyllactic acid (4-HPLA), 3-hydroxyanthranilic acid (3-HANTR), 3-hydroxykynurenine (3-HKIN), 4-hydroxybenzoic acid (4-HBAC), *p*-tyrosine (TY), adrenaline (E), 4-hydroxyphenylacetic acid (4-HPAC), 5-hydroxyindoleacetic acid (5-HIAA), normetanephrine (NMN), homovanillic acid (HVA), kynurenine (KYN), 5-hydroxytryptophan (5-HTP), *o*-tyrosine (O-TY), dopamine (DA), metanephrine (MN), tyramine (TYR), serotonin (5-HT), 3-methoxytyramine (3-MT), melatonin (MEL), tryptophan (TP), octopamine (OCT), guanosine (GUAN), homogentisic acid (HGA) and *n*-acetylserotonin (NA-5HT).

The instrumental parameters of the separation method were as follows: cell box and column temperature, 35°C; full-scale sensitivity of all channels, 100 μA; and potentials of each of the 16 channels, starting with channel 1, −50, 60, 120, 180, 240, 300, 360, 420, 480, 540, 660, 780, 800, 825, 850, 900 mV.

The gradient profile is shown in Fig. 1. The total analysis time was 35 min, including 5 min for stabilization between injections, at a flow-rate of 1 ml/min.

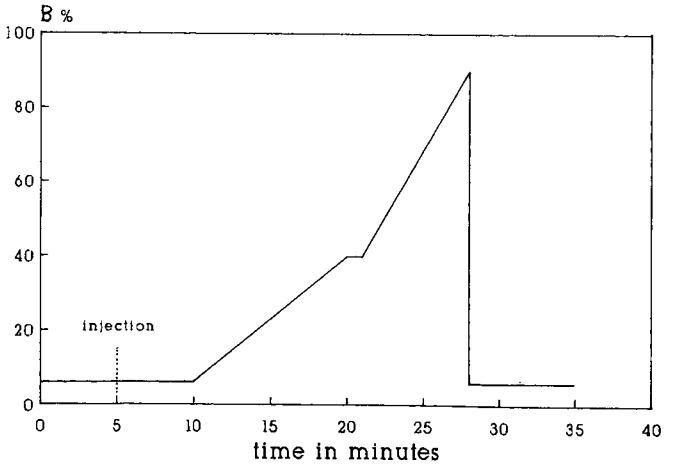

Fig. 1. Time line showing the gradient profile used in the separation.

Peak identification and confirmation

Peak identification was performed automatically on the basis of the traditional criterion of a retention time matching window. The peak identity confirmation was achieved by comparing the matching ratio (R) between a standard and the actual sample. The controlling software used a relative number to express the matching: 100% matching, $R = 1$; no matching, $R = 0$ [8].

Standard and sample preparation

The primary standard solutions were prepared by dissolving 10 mg of the components in a solution of 0.1 *M* hydrochloric acid–0.05% sodium metabisulphite–50% aqueous methanol. For uric acid, 0.05 *M* sodium hydroxide solution was used in place of hydrochloric acid. Individual secondary stock solutions were prepared by diluting each component with the saline solution to give a concentration of 1 μg/ml. These concentrates were subdivided into 1-ml portions. All solutions were stored at −30°C and thawed when necessary at 4°C.

A 33-component working standard was prepared by combining and diluting an aliquot of each of the concentrated mixtures (final concentration 100 ng/ml).

All plasma samples, immediately upon collection, were filtered through PM 10 membranes (Amicon, Denver, MA, U.S.A.). The filtered samples (40 μl) were injected into the CEAS.

Precision

To investigate the maximum analytical precision available, twenty sets of pure standards (containing 5 ng of each component) were injected and analysed under different analytical conditions.

Under strictly controlled conditions, the column compartment was thermostated at 35°C and the samples were refrigerated prior to analysis (4°C). The instrument was operated in the dark.

Under partially controlled conditions, artificial and natural light were allowed in the sample tray, the column compartment was kept at room temperature, where fluctuations of more than 5°C were observed (average value 27°C), and samples awaiting analysis were kept at room temperature.

For this quality control we tested only ten of the 33 molecules used as standards when analysing the plasma samples, *viz.*, OCT, NE, 5-HIAA, KYN, DA, MHPG, TY, 5-HT, TP and HVA.

This choice followed the criterion of evaluating a selection of molecules with different retention times, potentials and chemical characteristics representing all the other molecules considered. For all the tested substances the value of R was measured.

RESULTS

Fig. 2 shows the chromatogram of a 50-μl sample containing 5 ng each of the 33 components as external standard. The total analysis time was less than 35 min.

The reproducibility of the method was tested by repeated injections (20 times) of a standard solution containing 5 ng each of the ten substances chosen for this experiment under the conditions given under Experimental. Under the fully controlled conditions, the within-run concentration variability [relative standard deviation

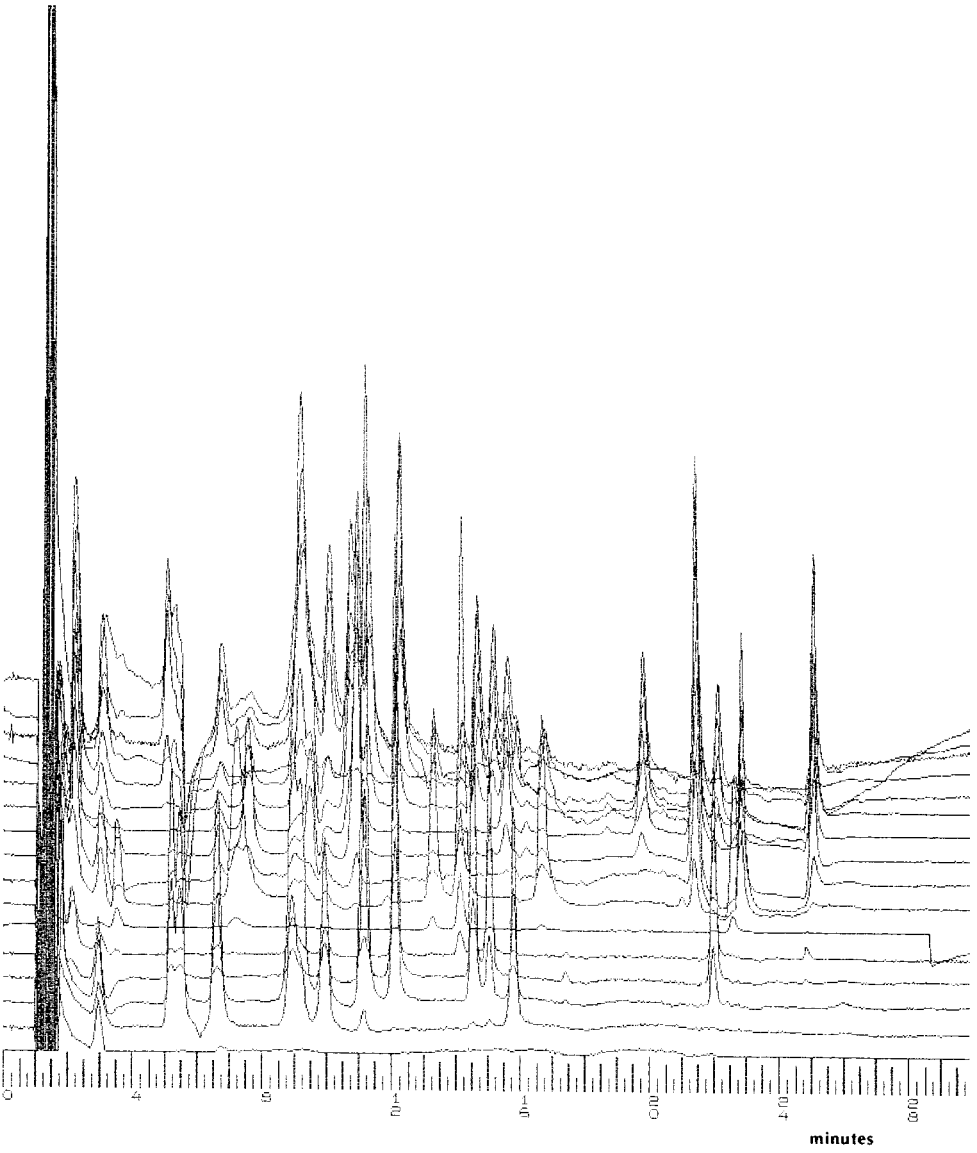

Fig. 2. Chromatogram of the 32-component standard mixture, 5 ng of each. The lines represent the signals of the sixteen electrodes. The potentials of the traces from the bottom to the top follow the values given under Experimental.

(R.S.D.)] ranged from 1 to 3% for all the substances investigated. Under the partially controlled conditions the R.S.D. was up to 10% in some instances. In particular, we observed and confirmed that 5-HIAA is degraded under the partially controlled conditions.

The results of this investigation are summarized in Table I. For each component the retention time, the standard deviation, the number of T_d and of T_s used for the

TABLE I

MAIN PARAMETERS FOR IDENTITY CONFIRMATION

$t_R \pm$ S.D., retention time $\pm$ standard deviation; T_d, dominant channel number; T_s, subdominant channel number; R, ratio matching; R.S.D. (%), within-assay precision; DL, detection limit.

Molecule	$t_R \pm$ S.D. (min)	T_d	T_s	R	R.S.D. (%)	DL (pg)
URIC	1.73	4	3	–	–	4.0
VMA	2.30	9	8	–	–	4.0
XANT	2.34	14	13	–	–	20.0
MHPG	2.63 ± 0.03	7	6	0.97	2.14	8.0
HGA	3.42	1	2	–	–	4.0
NE	3.51 ± 0.02	2	1	0.97	1.35	6.3
GUAN	5.43	14	15	–	–	27.0
DOPAC	6.35	2	3	–	–	5.0
METH	6.35	15		–	–	35.0
DOPA	6.35	3	4	–	–	7.0
OCT	6.38 ± 0.04	11	10	0.97	1.87	90.0
4-HPLA	7.40	9	10	–	–	19.0
XANTHURENIC	7.71	7	6	–	–	18.0
TY	8.23 ± 0.09	10	9	0.96	1.40	28.9
4-HBAC	9.31	12	11	–	–	25.0
E	9.87	2		–	–	11.3
3-HANTR	10.12	3		–	–	13.1
3-HKYN	10.50	3		–	–	31.0
4-HPAC	10.85	9	10	–	–	6.5
5-HIAA	11.12 ± 0.12	4	3	0.93	3.13	13.0
HVA	13.40 ± 0.13	7	6	0.88	1.63	6.5
DA	13.73 ± 0.10	2	1	0.90	1.24	12.0
NMN	14.65	6	7	–	–	26.0
KYN	15.86 ± 0.10	14	13	0.45	2.34	34.5
5-HTP	18.43	5	4	–	–	10.3
O-TY	18.93	10	9	–	–	58.0
5-HT	19.02 ± 0.10	4	3	0.96	2.17	12.5
MN	20.48	7	6	–	–	27.0
TP	23.42 ± 0.16	11	10	0.97	5.16	10.4
TYR	23.59	11	10	–	–	59.0
NA-5HT	26.80	7	6	–	–	7.2
3-MT	28.25	7	6	–	–	20.3
MEL	30.09	10	9	–	–	7.5

quantification, the R, the within-run precision (R.S.D.) and the detection limit are reported.

A chromatogram of a sample of human plasma is shown in Fig. 3, where the great complexity of the matrix can be seen. The automated data processing supplied by the CEAS allows a relatively easy collection and report of the selected analytical results.

The automatic calculation provided by the system gave the following concentrations as averages of four analyses of the same sample (40 μl), expressed in ng per injection: URIC 438.32, VMA 7.90, XANT 1295.49, MHPG 0.035, GUAN 15.21, NE

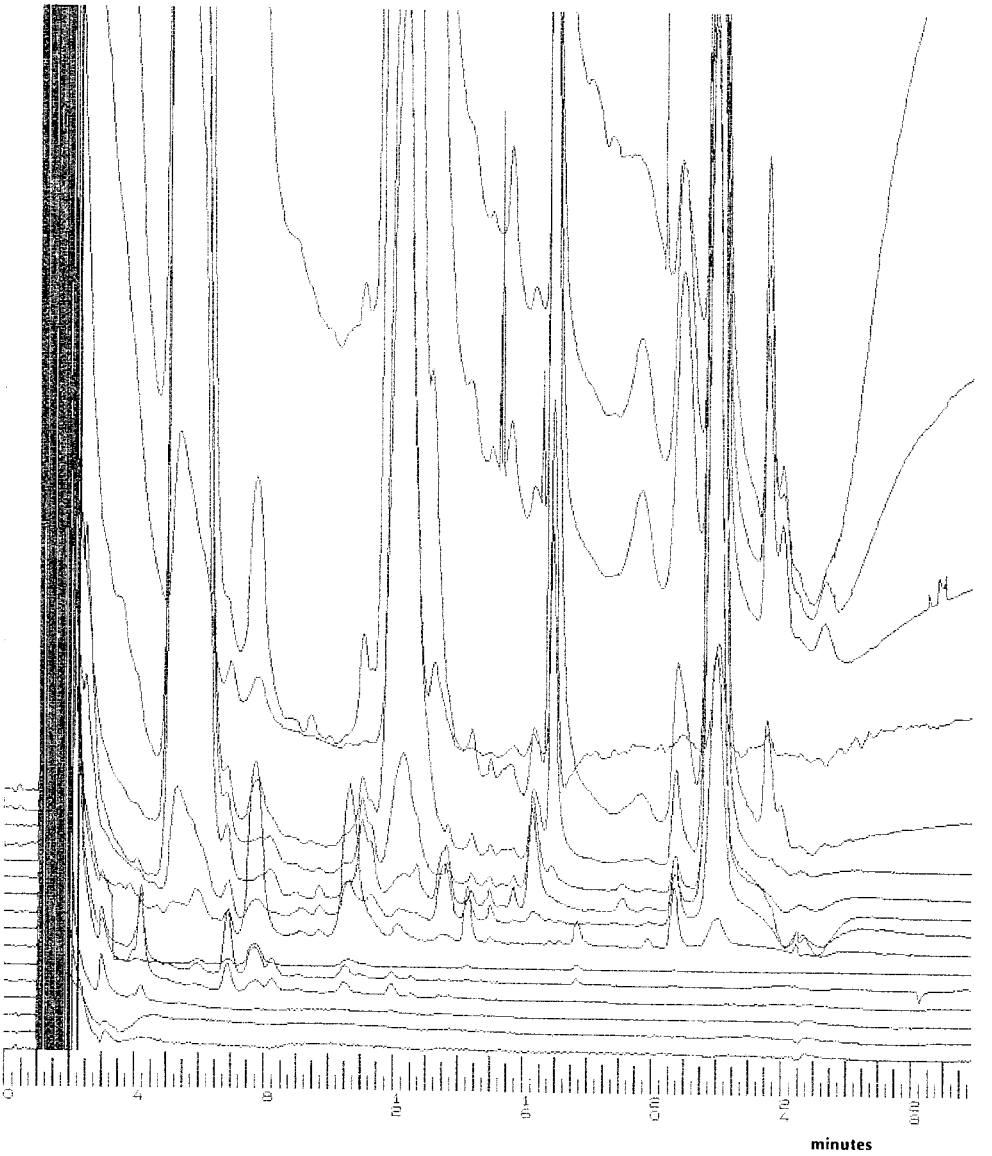

Fig. 3. Chromatogram of human plasma (40 μl), ultrafiltered with a PM 10 membrane.

0.087, METH 8.68, 4-HPLA 0.81, XANTHURENIC 0.16, OCT 0.69, 3-HANTR 0.08, 4-HPAC 4.94, 5-HIAA 0.31, NMN 0.39, HVA 0.098, O-TY 0.61, MN 0.22, KYN 133.46, NA-5HT 0.04, 5HT 0.05 and TP 53.91. Components not found in this sample were: HGA, DOPA, DOPAC, 4-HBAC, E, 3-HKYN, TY, 5-HTP, DA, TYR, 3-MT and MEL. The components not found may, of course, be present, but at concentrations lower than the detection limits indicated in Table I.

DISCUSSION AND CONCLUSIONS

The use of the CEAS for determining neurochemicals in tissues has been reported [10,11]. In this study we have demonstrated the applicability of this technique to the analysis of biological fluids. We have presented an application to plasma, where no sample pretreatment was needed other than filtration, owing to the high selectivity of the analytical system. With reference to molecules present in very low concentrations, an enrichment step can be used as in traditional HPLC electrochemical detection, *e.g.*, alumina extraction. With the present method, we can separate 33 species in less than 35 min; in a plasma sample we were able to measure 21 of the 33 molecules searched for, and many others were detected, but not identified or quantified.

In a complex mixture such as plasma, there are several unresolved molecules, hence the retention time is not a sufficient criterion for component confirmation. Therefore, R is used as a second criterion to be matched for automatic confirmation of the peaks. The closer R is to unity, the better the selectivity match will be. As this is very useful information in doubtful cases, it is important to establish R in an appropriate way. In order to obtain a significant R, two conditions must be satisfied: T_s should have at least 10% of the signal measured in T_d, and this signal should be at least ten times greater than the detection limit. In this study, not all the molecules satisfied the first condition. This can be observed from their abnormal value for R (*e.g.*, kynurenine), as the potential choice in this study was the result of the best compromise for all molecular species and gives too low a value for T_s.

REFERENCES

1 S. F. Mitchell and P. J. Rennie, *Chromatogr. Int.*, 125 (1986) 19.
2 Y. Haroon, C. A. Schubert and P. V. Hauschka, *J. Chromatogr. Sci.*, 22 (1984) 89.
3 M. L. Chen and W. L. Chiou, *J. Chromatogr.*, 278 (1983) 91.
4 G. H. Chiang, *J. Food Sci.*, 51 (1986) 499.
5 G. A. Qureshi and A. Eriksson, *J. Chromatogr.*, 441 (1988) 197.
6 R. T. Krause, *J. Chromatogr.*, 442 (1988) 333.
7 L. Volicer, P. J. Langlais, W. R. Matson, K. A. Mark and P. H. Gamache, *Arch. Neurol.*, 42 (1985) 1158.
8 W. R. Matson, P. Langlais, L. Volicer, P. H. Gamache, E. Bird and K. A. Mark, *Clin. Chem.*, 9 (1984) 1477.
9 W. R. Matson, P. G. Gamache, M. F. Beal and E. D. Bird, *Life Sci.*, 41 (1987) 905.
10 K. J. Swartz and W. R. Matson, *J. Neurochem.*, in press.
11 C. N. Svendsen and E. D. Bird, *Neurosci. Lett.*, Suppl., 35 (1989) 49.

Journal of Chromatography, 536 (1991) 237–243
Elsevier Science Publishers B.V., Amsterdam

CHROMSYMP. 2048

High-performance liquid chromatography of deoxyribonucleoside di- and triphosphates in tomato roots

INDRANI DUTTA*, PROBIR K. DUTTA, DON W. SMITH and GERARD A. O'DONOVAN
Department of Biological Sciences, University of North Texas, Denton, TX 76203 (U.S.A.)

ABSTRACT

The levels of endogenous deoxyribonucleotides in plants are greatly affected by the absence of the micronutrient boron. Described here is a high-performance liquid chromatographic assay for quantitating deoxyribonucleoside di- and triphosphates in tomato root tip tissues under boron-sufficient and boron-deficient conditions. The extraction procedure consists of (a) removing phenols from the tomato root tips by grinding frozen tissue in 6% trichloroacetic acid containing polyvinylpolypyrrolidone, (b) neutralizing the extract with freon-amine, (c) selective degradation of ribonucleotides with periodate, followed by (d) treatment with rhamnose and methylamine prior to injection of the deoxyribonucleotides into an anion-exchange column. Results indicate that the eight deoxyribonucleoside di- and triphosphates can be reproducibly resolved and quantified. By this extraction procedure, column life was extended to more than 70 runs per cartridge. This assay technique can be used with less than 500 mg of fresh root tip tissue and allows quantitation of plant deoxyribonucleotides in the picomole range.

INTRODUCTION

Boron is required as an essential micronutrient for the growth of vascular plants [1,2] and influences nucleic acid metabolism in all plants [3–5]. One way to monitor changes in nucleic acid metabolism is to compare the concentrations of ribo- and deoxyribonucleotides in boron-sufficient and boron-deficient plants. We have reported earlier on the effects of boron deficiency on the ribonucleotide pools [3] as determined by high-performance liquid chromatography (HPLC). Results of that study have led us to believe that the level of the deoxyribonucleotide pools in the boron-deficient plants would be simultaneously affected, since deoxyribonucleotides are required in the micromolar range for DNA replication and cellular nucleotide metabolism [3]. HPLC is the method of choice for monitoring such deoxyribonucleotide pool changes in animal systems [4,5]. Although HPLC can be readily used for quantifying plant ribonucleotides in boron-sufficient plants [3,6–9], there have been no published reports on deoxyribonucleotide pools in plant cells. It is therefore important to address some of the existing problems in analyzing deoxyribonucleotides in plant cells. These problems include: (a) There is a large excess of ribonucleoside triphosphates (rNTPs) over deoxyribonucleoside triphosphates (dNTPs). As a result, several methods of selective degradation of ribonucleotides in cell extracts and subsequent analysis by HPLC have been reported [4,5,10–12]. (b) The chromato-

0021-9673/91/$03.50

graphic separation and UV determination of deoxyribonucleotides in plant extracts are greatly hindered in tomato roots by the interference of phenols [3,13,14,16].

In the present experiments, we report an improved method for absorbing phenols by water-insoluble polymers having hydrogen-bonding capability, such as polyvinylpolypyrrolidone (PVPP) [3,14,15], and a modified selective degradation procedure of ribonucleotides from boron-deficient root tissues. Herein, we describe such a method, which affords detection of nanomolar concentrations of deoxyribonucleotides from 500 mg tomato root tips by anion-exchange HPLC.

EXPERIMENTAL

Chemicals and reagents

Nucleotides, trichloroacetic acid (TCA), PVPP, tri-*n*-octylamine, sodium periodate, methylamine and rhamnose were from Sigma (St. Louis, MO, U.S.A.); 1,1,2-trichloro-1,2,2-trifluoroethane (freon) and monobasic ammonium phosphate were from Mallinckrodt (Paris, KY, U.S.A.) and potassium chloride was from Eastman Kodak (Rochester, NY, U.S.A.). All other chemicals were of analytical grade and were purchased from Fisher Scientific (Fairlawn, NJ, U.S.A.).

Plant material

Tomato seeds (*Lycopersicon esculentum* Mill., cv. Improved Summertime) were obtained from Texas A & M University Experiment Research Station (College Station, TX, U.S.A.). Seeds were germinated in plastic Petri plates (9 cm in diameter) after a disc of Whatman No. 1 filter paper had been inserted into each dish. The filter paper was moistened with water, which had been deionized with a Milli-Q water system (Millipore, Bedford, MA, U.S.A.). Petri dishes were incubated for 5–7 days under UV radiation at 26 $\pm$ 2°C until the first true leaf pairs emerged. Seedlings about 5 cm in length with 2 or 3 small leaves, were transplanted to an aerated, full-strength, complete nutrient solution [17]. The pH of the nutrient solution was adjusted to 4.7 by either 0.1 *M* sodium hydroxide or 0.1 *M* hydrochloric acid. Two plants were mounted in a two-holed No. 6 rubber stopper. Fresh nutrient solutions were used after every 5 days. When the plants were 20 cm in height (measured from the cotyledons to the apical meristems), they were used as experimental materials. At the desired time interval of treatment, the roots were measured and the tips were harvested for nucleotide analysis or returned to the solution for later measurement and analyses.

Extraction of deoxyribonucleotides

Excised root tips were washed, weighed and frozen in liquid nitrogen. The frozen root tissue was stored at −80°C until ready for purification, when it was powdered in a mortar precooled by liquid nitrogen. The powdered root tissue was homogenized in chilled 6% (w/v) TCA, containing PVPP (0.5 g/10 ml), and incubated on ice in a gyrating shaker (New Brunswick Sci. Co., Edison, NJ, U.S.A.) for 30 min before centrifugation at 14 000 *g* for 12 min. The acid extract, containing nucleotides, was neutralized with an equal volume of ice-cold freon-amine [18] solution. The freon-amine mixture was agitated on a vortex mixer for 1 min and allowed to separate while standing at 4°C for 10 min. The top aqueous layer, which contained the deoxyribonucleotides, was removed with a 5-ml syringe and frozen at −80°C until ready for use.

Modified selective degradation of ribonucleotides [4,5]

To 160 μl of neutralized extract, 40 μl of 0.25 *M* $NaIO_4$ were added and incubated for 5 min at 37°C. The mixture was then centrifuged at 8000 *g* for 2 min. Next, 60 μl of 4 *M* methylamine and 14 μl of 1 *M* rhamnose were added before incubation on ice for 2 min. The mixture was then incubated for 30 min at 37°C before centrifugation at 8000 *g* for 2 min. This extract was then filtered through a 0.45-μm ACRO LC3A filter (Gelman, Ann Arbor, MI, U.S.A.) and kept frozen at −20°C until used.

Chromatographic apparatus and conditions

The HPLC equipment (Waters, Milford, MA, U.S.A.) consisted of two Model 510 pumps, a Model 680 automated gradient controller, a U6K injector and a Model 481 LC spectrophotometer. Deoxyribonucleotides were detected by monitoring the column effluent at 254 nm with the sensitivity fixed at 1 V a.u.f.s. (absorbance unit full scale). Separations were performed on a Beckman Ultrasil AX (10 μm) column (25 cm × 4.6 mm I.D.). The elution buffer system used consisted of eluent A, 7 m*M* $NH_4H_2PO_4$ (pH 3.8), and eluent B, 250 m*M* $NH_4H_2PO_4$ (pH 4.5) with 500 m*M* potassium chloride [3].

Deoxyribonucleotide samples (100 μl) obtained from plant root tips were injected into the column. A linear gradient of eluent A to eluent B was applied for 40 min, followed by an isocratic period of 20 min with eluent B. The column was re-equilibrated by washing with 30 ml of eluent A. The flow-rate was maintained at 1 ml/min. Analyses were performed at ambient temperature. Peaks were integrated either manually on a Cole-Palmer (Chicago, IL, U.S.A.) strip-chart recorder or on a Waters 740 data module.

Individual components of the deoxyribonucleotide pool mixture were identified on the basis of their retention time as compared with standards and by injecting known internal standards. The recoveries of deoxyribonucleotides from solutions of deoxyribonucleotide standards were determined by measuring peak heights before and after the extraction procedures. The percentage recoveries of added deoxyribonucleoside diphosphate (dNDP) and dNTP were [mean of two experiments ± standard error of the mean (S.E.M.)]: dTDP, 95 ± 2.1; dCDP, 97 ± 2.8; dADP, 97 ± 4.1; dGDP, 95 ± 1.8; dTTP, 96 ± 6.1; dCTP, 89 ± 2.4; dATP, 98 ± 3.1 and dGTP, 98 ± 1.8.

The concentration of the sample was calculated by comparing its peak height to the standard, for which the concentration was known (1 m*M*). The deoxyribonucleotide concentration in all samples, expressed as nanomoles per gram fresh weight was computed as follows:

$$\frac{S_a}{S_t} C \frac{V_{st}}{V_{sa}} \frac{V}{FW}$$

where S_a is the peak height of the sample, S_t the peak height of the standard, C is the amount (gram) of compound in the standard divided by the molecular weight of the compound, V is the total volume of the sample, V_{sa} the volume of injected sample, V_{st} the volume of injected standard and FW the fresh weight (gram) of the sample.

RESULTS AND DISCUSSION

A major problem associated with determining the level of ribo- and deoxyribonucleotides in plant tissue arises from the severe interference by low-molecular-weight material, such as phenolic compounds and precursors or degradation products of chlorophyll, which are extracted along with the nucleotides [6]. In this research, the small quantity of available root tissue, typically less than 500 mg, was an additional obstacle. As was the case for the ribonucleotides [3], experiments in our laboratory with various extraction techniques have shown that 6% (w/v) TCA produced the most reproducible results. Grinding of the frozen tissue in a precooled mortar proved to be a very useful as well as convenient method of homogenization for the extraction of the deoxyribonucleotides. This was the case also with ribonucleotides [3,8].

Tomato plants are especially rich in phenols. This makes nucleotide determinations very difficult under any circumstance [3]. This was further complicated by the fact that in these experiments the phenol content of the tomato plant tissues increased enormously when they were starved for boron [19]. In order to remove phenol, PVPP was added to the 6% (w/v) TCA solution and used in the homogenization buffer. It was critical that after extraction the samples be shaken on ice for at least 30 min before centrifugation. In this procedure all the phenols are adsorbed and this results in much greater yield of deoxyribonucleotides. Samples prepared by this technique did not affect column life. Of vital importance here was the fact that after this preparation, it was possible to quantitate more than 70 samples on the same Ultrasil AX column without any loss of sensitivity.

There is a previous report [8] which shows that freon-amine neutralization led to lower recovery. In our case, neutralization with potassium hydroxide, followed by removal of the potassium chloride precipitate by centrifugation resulted in a distortion of peaks and decreased column life. Accordingly, the freon-amine neutralization step [18] was used throughout the experiments despite the minor loss (3%) in recovery.

There are some limitations to the measurement of deoxyribonucleotides, which are present in very low concentrations. In order to overcome these limitations, selective degradation of ribonucleotides prior to HPLC has been devised. Using three previously described methods [4,5,19], total nucleotide pool extracts were treated to destroy the ribonucleotides in the sample. All three methods had to be modified so that HPLC could be used for tomato root tips. Analysis of the ribonucleotide standards showed that these methods effectively destroyed the ribonucleotides. Analysis of mixed deoxyribonucleotide standards, treated in the same way, showed that the recovery of deoxyribonucleotides was not reduced and that the chromatography of these compounds was not altered. Treatment of sample labelled with ^{3}H-dTTP showed that the retention of this compound was not altered.

Because previous methods [4,5] appeared to reduce the resolving power of the column after about 10 runs, we devised a new technique, based on an earlier method [5] which proved to be very successful for plant dNDP and dNTP. This is described under *Modified Selective Degradation of Ribonucleotides*, above. We applied this method to a standard mixture of the eight ribonucleotides and the eight deoxyribonucleotides, using concentrations typical of those found in plant tissue extracts. All ribonucleotides were degraded completely, and this gave highly reproducible and accurate results (data not shown). In the present method, the nucleotide pool extract was incubated for 5 min

before methylamine and rhamnose were added. All solutions were added without altering the pH of any mixtures.

Fig. 1A shows the chromatogram of a mixture of the eight dNDP and dNTP standards. In order to avoid errors in identification due to any variation in retention times, a mixed standard was injected between every sample run. Regardless of individual variation, retention times always fell in the pattern: diphosphates < triphosphates. As seen in Fig. 1A, all eight deoxyribonucleoside di- and triphosphates were separated. The quantitative HPLC data are presented in Table I. Extracts were prepared from the roots of boron-sufficient (B^+, positive control) and boron-deficient (B^-, negative control) tomato plants. As can be seen from Table I, there was a significant decrease in the levels of all deoxyribonucleotides in the boron-deficient plants. When tomato plants were starved of boron for longer than two days, their roots did not recover and the plants died. When boron was provided to plants after they had been starved of boron for two days, recovery, as reflected in the nucleotide levels, was not at all certain (see Table I, column 3). Though the plants seemed to survive, they were unable to replenish their nucleotide pools to the boron-sufficient levels. It is noteworthy that addition of the pyrimidine base, uracil, to boron-deficient nutrient

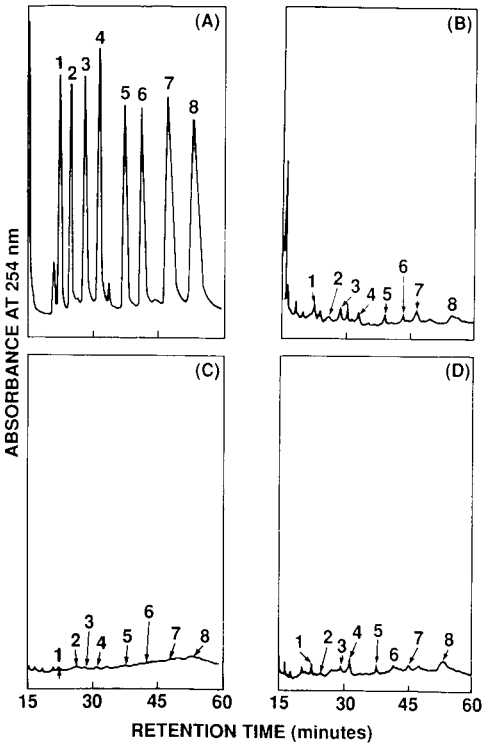

Fig. 1. Representative anion-exchange chromatograms of deoxyribonucleotides on a Beckmans Ultrasil AX column. (A) Standard dNDP and dNTP mixture (100 μl), consisting of 10^{-6} M of each deoxyribonucleotide. (B) Sample (100 μl) from tomato plant root tip tissue grown in boron-sufficient, (C) boron-deficient, (D) uracil-containing boron-deficient media, respectively. Peaks: 1 = dTDP; 2 = dCDP; 3 = dADP; 4 = dGDP; 5 = dTTP; 6 = dCTP; 7 = dATP and 8 = dGTP.

TABLE I

CONCENTRATIONS OF DEOXYRIBONUCLEOSIDE DI- AND TRIPHOSPHATES FROM TOMATO ROOT TIPS (nmol/g FRESH WEIGHT)

All values are the averages of two separate analyses.

	+B[a]	−B[b]	−B +B[c]	−B +U[d]	−B +U[e]
dTDP	3.12	0.83	1.01	1.04	1.02
dCDP	0.97	0.41	0.21	0.83	0.39
dADP	2.67	0.46	0.91	0.36	1.09
dGDP	0.68	0.28	0.51	0.29	0.61
dTTP	2.81	0.61	0.55	0.44	1.87
dCTP	4.31	0.49	0.67	0.97	2.95
dATP	5.40	0.13	4.10	6.01	9.72
dGTP	8.41	0.64	5.31	7.33	8.42

[a] +B = Positive control, boron present at all times.
[b] −B = Negative control, plants grown in boron-free medium for 2 days.
[c] Plants, grown without boron for 2 days, were given boron for an additional 2 days.
[d] Plants, grown without boron for 2 days, were given uracil (0.1 m*M*) for an additional 2 days.
[e] Plants, grown without boron for 2 days, were given uracil (0.1 m*M*) at the time boron was removed.

solution [16] restored the nucleotide pools close to their boron-sufficient level (Fig. 1D and Table I).

Data in Table I demonstrate the following points: (a) Boron starvation depletes the dCTP and dTTP pools much more than it does the dATP and dGTP pools. Indeed, dGTP levels seem almost resistant to boron depletion. This suggests that pyrimidine nucleotides are more susceptible to boron starvation than purine nucleotides. (b) It is not possible to restore the boron-sufficient levels by the re-addition of boron after two days of starvation. This suggests that cell permeability might have been impaired. (c) It is also not possible to restore the boron-sufficient levels by adding uracil after two days of boron starvation. This suggests that the cells can no longer concentrate uridine nucleotides. (d) The inclusion of uracil as soon as boron was removed allowed the restoration of the deoxyribonucleotides to their boron-sufficient levels. This implicates uridine compounds in restoring nucleotide levels to their boron-sufficient state.

The method of selective destruction of the ribonucleotides described here was based on the reactivity of 2′,3′-*cis*-diol of ribonucleotides with periodate. After the inactivation of periodate with rhamnose, the reaction of methylamine caused N-glycosyl bond cleavage with β-elimination of phosphate [20,21]. During the above treatment, ribonucleotides were completely (>99.99%) destroyed to give the bases, while the deoxyribonucleotides were not affected (data not shown). The reaction mixture could then be injected directly into the anion-exchange Ultrasil AX column for analysis. All peaks were identified except one which appeared between dATP and dGTP. So far we have not been able to identify this peak.

The following general statements are made regarding deoxyribonucleotide measurements from the roots of tomato plants: (1) dNDP and dNTP pool levels always paralleled the root elongation data. (2) The four deoxyribonucleoside diphosphates were quantitated in the boron-sufficient samples. (3) Their levels

appeared to be particularly responsive to boron deprivation. (4) The levels of the four dNTPs were higher than those for the dNDPs, regardless of how the samples were prepared (data not shown). (5) As has typically been observed for other systems [22], the dGTP level was the greatest of the four dNTPs though its value in the root was only 8.41 nmol/g fresh weight. (6) This assay procedure could be used to quantitate deoxyribonucleosides at nanomolar concentrations. (7) This method is simple and rapid when compared to other current methods of quantifying deoxyribonucleotides such as the *in vitro* polymerizing system [23] and $^{32}PO_4$ label in thin-layer chromatography [10]. We believe that our method provides a direct and unambiguous measurement of the deoxyribonucleotide concentrations without the necessity of working with ^{32}P. It is rapid and simple. This technique should be of great value in plant physiology experiments where deoxyribonucleotide concentrations need to be measured.

ACKNOWLEDGEMENT

This research was supported by a Texas Advanced Technology Research Grant to G. A. O'Donovan.

REFERENCES

1 W. M. Dugger, *Adv. Chem. Ser.*, 123 (1973) 112.
2 D. T. Clarkson and J. B. Hanson, *Annu. Rev. Plant. Physiol.*, 31 (1980) 239.
3 I. Dutta, G. A. O'Donovan and D. W. Smith, *J. Chromatogr.*, 444 (1988) 183.
4 C. Garrett and D. V. Santi, *Anal. Biochem.*, 99 (1979) 268.
5 K. Tanaka, A. Yoshioka, S. Tanaka and Y. Wataya, *Anal. Biochem.*, 139 (1984) 35.
6 R. H. Nieman, D. L. Pap and R. A. Clark, *J. Chromatogr.*, 161 (1978) 137.
7 R. H. Nieman and R. A. Clark, *J. Chromatogr.*, 317 (1984) 271.
8 R. Meyer and K. G. Wagner, *Anal. Biochem.*, 148 (1985) 269.
9 R. Meyer and K. G. Wagner, *Physiol. Plant.*, 67 (1986) 666.
10 C. D. Yegian, *Anal. Biochem.*, 58 (1974) 231.
11 B. Ullman, L. J. Gudas, S. M. Clift and D. W. Martin, Jr., *Proc. Natl. Acad. Sci. USA*, 76 (1979) 1074.
12 E. J. Ritter and L. M. Bruce, *Biochem. Med.*, 21 (1979) 16.
13 R. M. Reeve, *Am. J. Bot.*, 46 (1959) 210.
14 R. Watanabe, W. J. McIlrath, J. Skok, W. Chorney and S. H. Wender, *Arch. Biochem. Biophys.*, 94 (1961) 241.
15 W. D. Loomis and J. Battaile, *Phytochemistry*, 5 (1966) 423.
16 R. A. Anderson and J. A. Sowers, *Phytochemistry*, 7 (1968) 293.
17 D. I. Arnon and D. R. Hoagland, *Soil Sci.*, 50 (1940) 463.
18 J. X. Khym, *Clin. Chem. (Winston-Salem, N.C.)*, 21 (1975) 1245.
19 H. J. Perkins and S. Aronoff, *Arch. Biochem. Biophys.*, 64 (1956) 506.
20 J. X. Khym and W. E. Cohn, *J. Biol. Chem.*, 236 (1961) PC9.
21 D. H. Rammler, *Biochemistry*, 10 (1971) 4699.
22 R. L. Hopkins and M. F. Goodman, *J. Biol. Chem.*, 260 (1985) 6618.
23 U. Lindberg and L. Skoog, *Anal. Biochem.*, 34 (1970) 152.

Journal of Chromatography, 536 (1991) 245–249
Elsevier Science Publishers B.V., Amsterdam

CHROMSYMP. 2032

Liquid chromatographic separation of isomeric phenanthrols on monomeric and polymeric C_{18} columns

ZIPING BAO and SHEN K. YANG*

Department of Pharmacology, F. Edward Hébert School of Medicine, Uniformed Services University of the Health Sciences, Bethesda, MD 20814-4799 (U.S.A.)

ABSTRACT

Separations of all five possible isomeric phenanthrols by reversed-phase high-performance liquid chromatography using a monomeric Zorbax C_{18} column and a polymeric Vydac C_{18} column were compared. With identical elution solvents and flow-rates, the phenanthrols were separated with shorter retention times on the latter column. The elution orders of the phenanthrols were different on the two columns. Ultraviolet absorption spectral properties of the phenanthrols in methanol and in alkaline methanol are reported.

INTRODUCTION

Metabolism of phenanthrene yields phenolic products which are formed by spontaneous isomerization of the metabolically formed epoxide intermediates [1–3]. A satisfactory chromatographic method has previously not been available to separate all five possible phenanthrols efficiently. We describe in this paper the reversed-phase high-performance liquid chromatographic (HPLC) separation of all five isomeric phenanthrols by the sequential use of a polymeric Vydac C_{18} column and a monomeric Zorbax ODS (C_{18}) column. Ultraviolet absorption properties of chromatographically pure phenanthrols are reported.

EXPERIMENTAL

Materials

9-Phenanthrol was purchased from Aldrich (St. Louis, MO, U.S.A.). Phenanthrene *trans*-1,2- and *trans*-3,4-dihydrodiols were isolated by normal-phase HPLC (see below) from a mixture of products formed by incubation of phenanthrene with rat liver microsomes [2,3], 1- and 2-phenanthrols were obtained by dehydration of phenanthrene *trans*-1,2-dihydrodiol with dilute HCl in acetone at 37°C for 1 h and 3- and 4-phenanthrols were similarly obtained by dehydration of phenanthrene *trans*-3,4-dihydrodiol. All phenanthrols used for UV absorption spectral measurement were eluted as a single peak by reversed-phase HPLC.

Phenanthrene *trans*-1,2- dihydrodiol, obtained by incubation of phenanthrene

0021-9673/91/$03.50

with rat liver microsomes and isolated by normal-phase HPLC (see below), was dehydrated by acid in acetone to form 1-phenanthrol and 2-phenanthrol, which were separated on the Vydac C_{18} column. The area ratio of the chromatographic peaks, detected at 254 nm, of 1- and 2-phenanthrol was 64:36, which is in close agreement with the ratio of 66:34 reported by Jerina *et al.* [4]. Phenanthrene *trans*-3,4.dihydrodiol, obtained as a metabolite of phenanthrene, was dehydrated by acid in acetone to form 3- and 4-phenanthrol, which were separated on the Vydac C_{18} column. The area ratio of the chromatographic peaks, detected at 254 nm, of 3- and 4-phenanthrol was 65:35, which is consistent with the ratio of 59:41 reported by Jerina *et al.* [4].

High-performance liquid chromatography

HPLC was performed using a Waters Assoc. (Milford, MA, U.S.A.) liquid chromatograph consisting of a Model 6000A solvent-delivery system, a Model M45 solvent-delivery system, a Model 660 solvent programmer and a Model 440 absorbance detector. Samples were injected via a Valco (Houston, TX, U.S.A.) Model N60 loop injector. Retention times and ratios of areas under the chromatographic peaks were recorded with a Hewlett-Packard Model 3390A integrator.

Normal-phase HPLC

The dihydrodiol metabolites of phenanthrene were separated on a DuPont (Wilmington, DE, U.S.A.) Zorbax SIL column (25 cm × 6.2 mm I.D.) with tetrahydrofuran–hexane (1:3, v/v) at a flow-rate of 2 ml/min. Under these conditions the retention times were phenanthrene 3.8, phenanthrols 5.0, phenanthrene *trans*-9,10-dihydrodiol 6.8, phenanthrene *trans*-1,2-dihydrodiol 9.0 and phenanthrene *trans*-3,4-dihydrodiol 13.1 min. Efficient separation of the three phenanthrene *trans*-dihydrodiols was also achieved by using a DuPont Golden SIL column (8 cm × 6.2 mm I.D.), eluted with 2.5% of ethanol–acetonitrile (2:1, v/v) in hexane at a flow-rate of 2 ml/min. For the purpose of preparing relatively large amount of phenanthrene dihydrodiol metabolites, normal-phase HPLC is preferred to reversed-phase HPLC [2] because of relative ease of removal or organic solvents.

Reversed-phase HPLC

A monomeric Zorbax ODS column (25 cm × 4.6 mm I.D.; DuPont) or a polymeric Vydac C_{18} columns (25 cm × 4.6 mm I.D.; Separations Group, Hesperia, CA, U.S.A.) was used. Phenanthrols were eluted with methanol–water (3:2 or 1:1, v/v) at a flow-rate of 1.2 ml/min.

Absorption spectra

Ultraviolet absorption spectra of phenanthrols in methanol and in alkaline methanol (*ca.* 0.05 ml of 0.5 *M* NaOH in methanol) were determined using a 1-cm path length quartz cuvette with a Beckman Model 25 spectrophotometer.

RESULTS AND DISCUSSION

Retention times of phenanthrols by reversed-phase HPLC on the monomeric Zorbax ODS column and the polymeric Vydac C_{18} column using methanol-water (3.2, v/v) are shown in Fig. 1. With identical elution solvents and flow-rates, the

phenanthrols are retained longer on the monomeric Zorbax ODS column. Further, the elution orders of the phenanthrols on the monomeric and polymeric columns are different. The elution order on the Zorbax ODS column is 2- <3- <9- <1- <4-phenanthrol, whereas on the Vydac C_{18} column the elution order is 3- <2- <9- <4- <1-phenanthrol. The peaks of the phenanthrols on the monomeric Zorbac ODS column are generally broader (peak width at half height $\geq$1.3 min) and the elution order is similar to that on a DuPont Permaphase ODS (1-m) column [4]. On the other hand, the peaks of the phenanthrols on the polymeric Vydac C_{18} column are relatively sharper and more symmetrical (Fig. 2). By using a lower concentration of methanol (methanol–water, 1:1), 2-, 3.- and 9-phenanthrol are better separated, whereas 4- and 1-phenanthrol are partially separated (Fig. 2). In comparison, 9-phenanthrol is well separated from 2- and 3-phenanthrol on the monomeric Zorbax ODS column (Fig. 1). Similarly, 1- and 4-phenanthrol are also better separated on the monomeric Zorbax ODS column. Hence, it is possible to separate all five isomeric phenanthrols by sequential use of the monomeric and polymeric C_{18} columns.

All phenanthrols have UV absorption maxima at *ca.* 250 nm (Fig. 3). Each phenanthrol has distinct and chracteristic UV absorption properties. Differences in the UV absorption properties of 3-, 4- and 9-phenanthrol in methanol are small and subtle. However, when their UV absorption properties in alkaline methanol are viewed together, the differences become apparent. The UV absorption properties of 1- and 2-phenanthrol in methanol and alkaline methanol are different from each other and from other isomeric phenanthrols. Subtle differences in the UV absorption properties among isomeric phenanthrols are difficult to differentiate if the absorption properties are tabulated in terms of molar absorptivities and wavelengths. The UV absorption spectra described in this paper should be useful in the identification of isomeric phenanthrols.

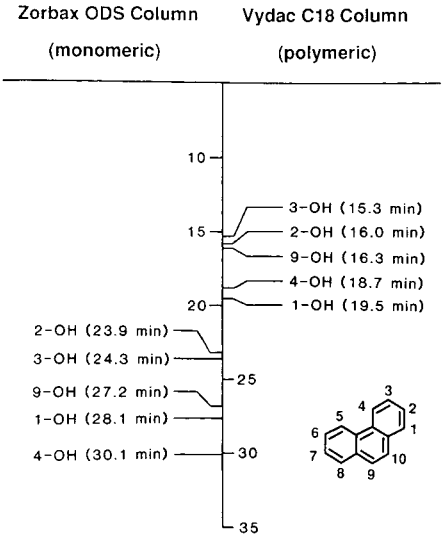

Fig. 1. Retention times of phenanthrols on the monomeric Zorbax ODS and the polymeric Vydac C_{18} columns. Eluent: methanol–water (3:2, v/v) at a flow-rate of 1.2 ml/min.

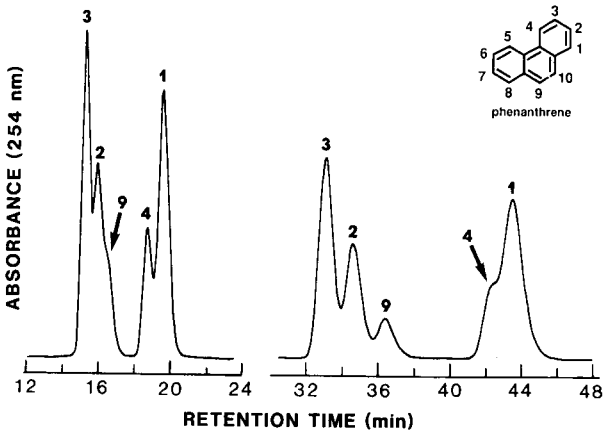

Fig. 2. Reversed-phase HPLC separation of phenanthrols on a polymeric Vydac C_{18} column. Eluents: methanol–water (3:2, v/v) (left) and methanol–water (1:1, v/v) (right) at a flow-rate of 1.2 ml/min. Numbers on peaks indicate the positions of the hydroxyl group on the phenanthrene molecule.

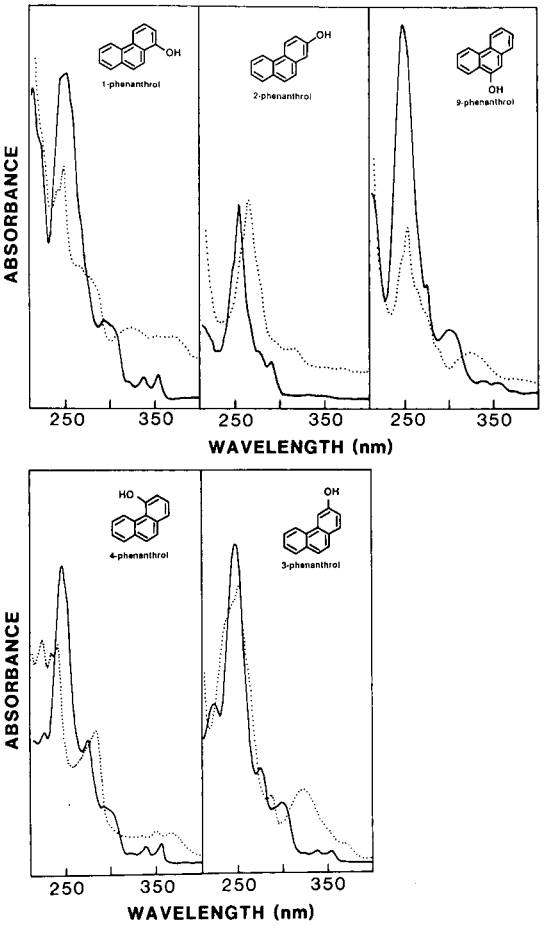

Fig. 3. Ultraviolet absorption spectra of phenanthrols in methanol (solid curves) and in alkaline methanol (dotted curves).

We have previously reported the separation of isomeric phenols of chrysene, benz[*a*]anthracene, and benzo[*a*]pyrene using monomeric and polymeric C_{18} columns [5]. It appears that the polymeric Vydac C_{18} column is generally more useful in the separation of isomeric phenols of polycylic aromatic hydrocarbons.

ACKNOWLEDGEMENTS

This work was supported by USUHS protocol RO7502. The opinions or assertions contained herein are the private ones of the authors and are not to be construed as official or reflecting the views of the Department of Defense or the Uniformed Services University of the Health Sciences.

REFERENCES

1 P. Sims and P. L. Grover, *Adv. Cancer Res.*, 20 (1974) 165–274.
2 M. Nordqvist, D. R. Thakker, K. P. Vyas, H. Yagi, W. Levin, D. E. Ryan, P. E. Thomas, A. H. Conney and D. M. Jerina, *Mol. Pharmacol.*, 19 (1981) 168–178.
3 S. Chaturapit and G. M. Holder, *Biochem. Pharmacol.*, 27 (1978) 1865–1871.
4 D. M. Jerina, H. Selander, H. Yagi, M. C. Wells, J. F. Davey, V. Mahadevan and D. T. Gibson, *J. Am. Chem. Soc.*, 98 (1976) 5988–5996.
5 M. Mushtaq, Z. Bao and S. K. Tang, *J. Chromatogr.*, 385 (1987) 293–298.

Journal of Chromatography, 536 (1991) 251–254
Elsevier Science Publishers B.V., Amsterdam

CHROMSYMP. 2056

Gel permeation chromatographic determination of starches using alkaline eluents

T. SUORTTI* and E. PESSA
Technical Research Centre of Finland, Food Research Laboratory, Biologinkuja 1, SF-02150 Espoo (Finland)

ABSTRACT

By using a dilute solution of sodium hydroxide as eluent in a gel permeation chromatography analysis of natural and modified starches, many of the difficulties encountered with less basic eluent (so-called ghost peaks or memory effects) or with the instability of columns encountered with dimethylsulphoxide, are avoided. The system is shown to give reproducible results and no problems with column stability are encounterd after several months' use. Either ordinary refractive index detection or after-column complexation with iodine and spectrophotometric detection are used. The latter system is especially suited for the analysis of changes that occur on amylose during various treatments (entsymatic or acid hydrolysis or extrusion).

INTRODUCTION

Starches are used in foodstuffs and in various technological applications. For technological purposes, starches are often modified by various chemical, enzymatic or physical treatments, which change their molecular weight distribution and the ratio between the two major components, namely amylose and amylopectin.

The two principal problems in the determination of starches are their high molecular weights and their solubility. On account of the high molecular weight, most liquid chromatographic analyses have been carried out using soft gels and aqueous alkaline eluents, which has meant analysis times of several hours [1–6]. Most work in which modern columns have been employed has been done by using dimethyl sulphoxide (DMSO) as the eluent. The packing materials used have been either silica-based [7,8] or porous glass [9], both showing low capacity and limited separation capability. In the use of styrene–divinylbenzene resins, problems have been encountered with the instability of the column packing material with DMSO [10]. The dissolution of starches into DMSO is also slow, normally requiring several days, and the sensitivity of a refractive index (RI) detector with DMSO is less than that with alkaline aqueous eluents. The use of most water-compatible rigid packings has been handicapped by their low pH stability, which in one experiment led to ghost peaks or a memory effect, obviously due to the low solubility of the samples [11].

0021-9673/91/$03.50

We have been studying the chromatography of starches on μHydrogel columns (cross-linked hydroxylated polymethacrylate gel with residual carboxyl groups). The pH stability of the columns has made it possible to use eluents that are alkaline enough (pH 12.5) for good solubility of the samples and thus no ghost peaks or memory effects are encountered.

The ability of starches to form complexes with iodine has been used for a long time to determine the ratio between amylose and amylopectin [12–14], the complexes showing different absorbance maxima (640 and 525 nm, respectively). We used this for on-line detection by pumping iodine solution into the eluent after separation and utilizing a UV–VIS detector. By utilizing this detection system in addition to ordinary RI detection, we have been able to monitor more precisely what happens to different components of starches during their treatment.

EXPERIMENTAL

The high-performance liquid chromatograph consisted of a Model M-6000A pump, a Model M-710B automatic injector, μHydrogel 2000 and 250 columns (300 × 7.8 mm I.D.) connected in series, a column thermostat and an M-411 refractive index detector.

For detection with iodine complexation, a second Model M-6000A pump was used to pump 1.2 m*M* iodine solution (0.14 g of iodine and 0.34 g of potassium iodide per litre of aqueous 0.5% orthophosphoric acid) at a flow-rate of 0.3 ml/min through a mixing tee, which was situated between the column exit and the M-440 UV–VIS detector monitoring at 658 and 546 nm. All the components that were in contact with iodine solution were carefully passivated by flushing with nitric acid diluted 1:5.

The mobile phase was 50 m*M* sodium hydroxide solution, at a flow-rate of 0.5 ml/min. The mobile phase was carefully deaerated and purged with helium. Samples were dissolved at room temperature in 1 *M* sodium hydroxide solution with a magnetic stirrer for 4 h and then diluted 1:10 with water. All the solutions were carefully deaerated and the samples were stored under an argon blanket. The instrument was controlled and data were processed with a Model M-820 Maxima data station. All the instrumentation was supplied by Millipore–Waters (Milford, MA, U.S.A.).

RESULTS AND DISCUSSION

The molecular weights of most of the samples exceeded the highest commercially available polysaccharide molecular weight standards (dextran T2000 from Pharmacia and pullulan P-800 from Shodex), so only comparisons could be made with the available instrumentation.

With RI detection, the peak area changed linearly in the concentration range 4000–1000 mg/l for both amylose and amylopectin ($r^2 = 0.97$ and 0.99, respectively) and also for injection volumes between 50 and 200 μl. The peak profiles did not change when the column temperature was changed from 60 to 80°C. When a column temperature of 45°C was used, the peaks were less sharp. The remainder of the experiments were therefore carried out at 60°C.

In the detection system where iodine addition was employed, the peak areas

changed linearly for amylopectin in the concentration range 2000–200 mg/l for detection at both 546 and 658 nm (r^2 = 0.97 and 0.99). Moreover, amylose showed linear calibration graphs at 546 and 658 nm (r^2 = 0.97 and 0.99, respectively) in the same concentration range. In all instances the relative standard deviation was less than 8% in triplicate injections, and in most instances the values were less than 3%.

An increase in iodine concentration from 1.2 to 2.4 m*M* did not result in an increase in peak areas but in a slightly inferior baseline at 546 nm because of the increased absorbance of iodine solution at 546 nm. Lowering of the iodine concentration from 1.2 to 0.3 m*M* markedly lowered the detector response for amylopectin samples and also changed the ratio between absorbance at 546 and 658 nm. The detector response for amylose samples, however, remained unchanged. An increase in iodine flow-rate from 0.3 to 0.6 ml/min lowered the peak areas in proportion to the increased dilution, but had no other effect. To check the sufficiency of the reaction time, an additional capillary was added between the mixing tee and the UV–VIS detector, which increased the reaction time from *ca.* 1 to *ca.* 10 s. This did not, however, increase the peak areas, indicating that the original reaction time was sufficient.

With this elution and these detection systems, some commercial amylopectin standards showed two peaks, one of which was in the molecular weight range of several millions and the other *ca.* 80 000, or one peak of molecular weight *ca.* 80 000, which probably means that during their isolation they were seriously degraded. These breakdown products also show an absorbance ratio of 2.2 between detection at 546 and 658 nm. For the peak that eluted with an elution volume indicating a molecular weight of several millions, the absorbance ratio was 1.3 (whereas amylose shows a ratio of 0.5) (Fig. 1). A molecular weight of several millions and a similar absorbance ratio was also obtained for the main peak of a waxy maize sample (containing mostly

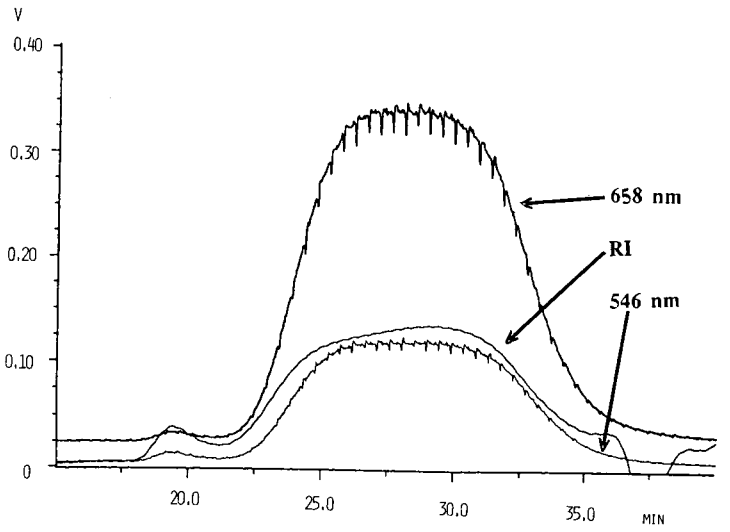

Fig. 1. Chromatogram of amylose from a commercial source. Detection with a refractive index detector (RI) and by spectrophotometry at 546 and 658 nm after complexation with iodine. For other details, see text. A dextran standard of molecular weight 500 000 eluted at 32.0 min. The exclusion volume was 8.7 ml (amylopectin) and the total permeation volume was 19.3 ml (glucose).

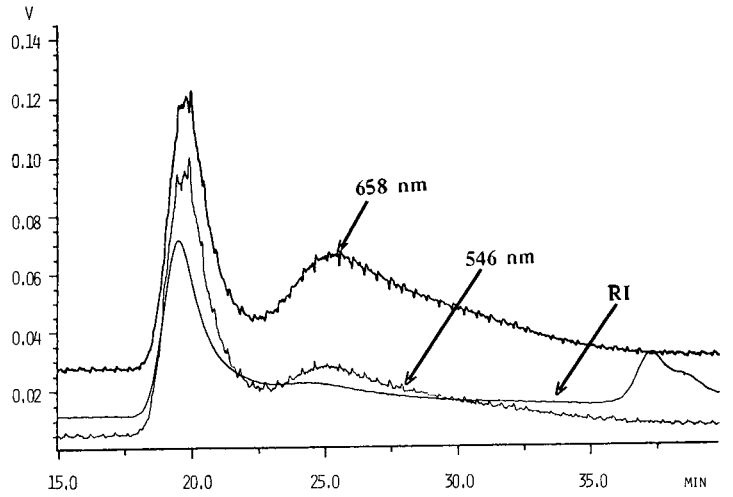

Fig. 2. Chromatogram of potato amylopectin isolated by the method of Schoch [15,16]. Detection with a refractive index detector (RI) and by spectrophotometry at 546 and 658 nm after complexation with iodine. For other details, see text. A dextran standard of molecular weight 500 000 eluted at 32.0 min.

amylopectin) and an amylopectin sample isolated according to the procedure of Schoch [15,16] (Fig. 2). The relative response was 8.8 times higher for amylose at 658 nm than for amylopectin. At 546 nm amylose was detected 2.9 times more sensitively than amylopectin.

We have used this analysis system for several weeks during the last year and the alkaline eluent had no deleterious effect on the column, nor did the iodine solution cause corrosion of the stainless-steel. Moreover, the system has provided valuable information regarding the changes in molecular weight and the different constituents of starches in the native state and after different chemical, enzymatic and physical treatments.

REFERENCES

1 T. Yamada and M. Taki, *Starch/Stärke*, 28 (1976) 374.
2 C. D. Biliaderis, D. R. Grant and J. R. Vose, *Cereal Chem.*, 56 (1979) 475.
3 S. A. Craig, S. Stark and J. R. Stark, *Starch/Stärke*, 36 (1984) 127.
4 W. Praznik and R. Ebermann, *Starch/Stärke*, 31 (1979) 288.
5 C. D. Boyer, P. A. Damewood and E. K. G. Simpson, *Starch/Stärke*, 33 (1981) 125.
6 W. Praznik, G. Burdicek and R. H. F. Beck, *Starch/Stärke*, 38 (1986) 181.
7 S. Kobayashi, S. J. Schwarz and D. R. Lineback, *J. Chromatogr.*, 319 (1985) 205.
8 P. Reinikainen, T. Suortti, J. Olkku, Y. Mälkki and P. Linko, *Starch/Stärke*, 30 (1986) 20.
9 F. Meuser, R. W. Klingler and E. A. Niediek, *Getreide Mehl Brot* 33 (1979) 295.
10 W. Cai, C. Athanasoulias and L. L. Diosady, *Acta Aliment.*, 17 (1988) 319.
11 P. Lehtonen, *Chromatographia*, 26 (1988) 157.
12 R. Ebermann and R. Schwarz, *Starch/Stärke*, 27 (1975) 361.
13 J. H. M. Hovenkamp-Hermelink, J. N. De Vries, P. Adame, E. Jacobsen, B. Witholt and W. J. Feenstra, *Potato Res.*, 31 (1988) 241.
14 J. Chrastil, *Carbohydr. Res.*, 159 (1987) 154.
15 T. J. Schoch, *J. Am. Chem. Soc.*, 64 (1942) 2957.
16 R. L. Whistler, in R. L. Whistler and E. F. Paschall (Editors), *Starch: Chemistry and Technology*, Academic Press, New York, London, 1965, p. 331.

Journal of Chromatography, 536 (1991) 255–264
Elsevier Science Publishers B.V., Amsterdam

CHROMSYMP. 2012

Liquid chromatographic analysis of a potential polymeric-pendant drug delivery system for peptides

Application of high-performance size-exclusion chromatography, reversed-phase high-performance liquid chromatography and ion chromatography to the evaluation of biodegradable poly[(chloromethoxytrialanine methyl ester) phosphazenes]

W. MARK EICKHOFF* and GARY G. LIVERSIDGE
Department of Drug Delivery, Sterling Research Group, Great Valley, PA 19355 (U.S.A.)
and
R. MUTHARASAN
Department of Chemical Engineering, Drexel University, Philadelphia, PA 19104 (U.S.A.)

ABSTRACT

A novel water-soluble polymer, poly[(chloromethoxytrialanine methyl ester)phosphazene] (poly-Tame), was characterized and evaluated using high-performance size-exclusion chromatography, gradient reversed-phase high-performance liquid chromatography and ion chromatography. These novel liquid chromatographic methods were validated for application to *in vitro* biodegradation experiments of poly-Tame in aqueous solutions. Results from method validation experiments are presented.

INTRODUCTION

Water-soluble macromolecular conjugates are becoming increasingly important as drug delivery platforms for therapeutic agents [1,2]. The structural complexity and diversity of these polymeric molecules requires a sophisticated array of analytical methodologies to evaluate their performance as drug delivery systems. Liquid chromatographic methods have been used by Larsen *et al.* [3] to measure the disappearance of dextran-metronidazole ester conjugates and the release of metronidazole from the hydrolyzed polymeric pro-drug *in vitro*. Kurtzhals *et al.* [4] applied high-performance size-exclusion chromatography, (HPSEC) to *in vitro* and *in vivo* evaluations of dextran–fluoresceinyl isothiocyanate (FITC) conjugates.

Similar liquid chromatographic methods are needed for polyphosphazenes, a class of inorganic polymers proposed as macromolecular conjugates for drug delivery

0021-9673/91/$03.50

of a wide variety of covalently attached and biologically active side groups [5]. Grollemand and co-workers [6,7] measured the *in vitro* and *in vivo* release of naproxen with a lysine spacer conjugated to an implantable poly(glycine ethyl ester)phosphazene device using reversed-phase high-performance liquid chromatography (RP-HPLC) and determined the molecular weight (MW) of the polymers using gel permeation chromatography (GPC). Goedemoed and De Groot [8] used RP-HPLC with pre-column amino acid derivatization to measure the release of amino acid from a bioerodible poly(amino acid ester) phosphazene device and monitored the diffusion of melphalan from the polymer matrix using RP-HPLC.

The biodegradation of the poly[(peptide ester)phosphazene] (Fig. 1), will ultimately lead to the formation of ammonia, phosphate, alanine, methanol and hydrochloric acid. However, the release of free tripeptide, trialanine methyl ester (Tame) or trialanine (Tala), used here as model peptides, could occur during intermediate degradation processes under physiological conditions. Furthermore, the degradation mechanism for poly[(amino and amino acid ester)phosphazenes] have been postulated based on spectroscopic and qualitative chemical analyses of hydrolyzed cyclic and polymeric phosphazenes in aqueous solutions [9,10]. However, these techniques are incapable of measuring changes in MW and are not sensitive or selective enough to measure pendant release at low concentrations. The interdependent kinetics of side chain release with polymeric degradation is a relationship best determined using HPSEC and RP-HPLC.

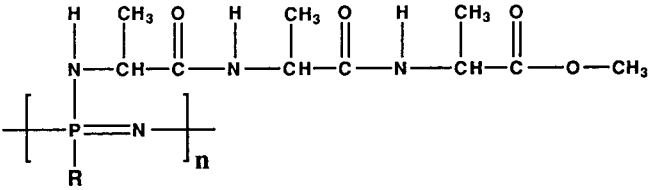

Fig. 1. Structure of polyTame. R = Tame, OCH_3 or Cl.

Evaluating the hydrolytic stability and determining the degradation mechanism for polyTame in aqueous solutions is predicated on the development of validated analytical procedures for degradation intermediates. These methods should identify and quantitate polyTame and its potential hydrolysis products and probably would utilize both spectroscopic and chromatographic techniques. The components necessary for quantitation and characterization of this polymer with liquid chromatographic methods include MW calculations of number-average MW ($\bar{M}_n$), weight-average MW ($\bar{M}_w$), MW distribution (MWD) and polyTame concentrations using HPSEC. The degree of substitution of Tame and release of both Tame and Tala from the polyphosaphazene backbone will be characterized using RP-HPLC. The amount of unreacted chloride and the amount bound to the polymeric backbone as the hydrochloride salt will be determined by inorganic anion analysis using ion chromatography (IC). Monitoring the formation of phosphate and release of unreacted chloride during polyTame hydrolysis will be achieved using the same IC method.

EXPERIMENTAL

Materials

The HPLC grade reagents used were methanol, acetonitrile and ammonium acetate from J.T. Baker (Phillipsburg, NJ, U.S.A.), trifluoroacetic acid (TFA) and triethylamine (TEA) from Pierce (Rockford, IL, U.S.A.) and octanesulfonic acid sodium salt from Kodak (Rochester, NY, U.S.A.). HPLC-grade water was obtained from a Milli-Q Plus water system (Millipore, Milford, MA, U.S.A.).

The narrow molecular weight standards used for external calibrations of the HPSEC were poly(ethylene glycol)(PEG) (Polymer Lab., U.K.), poly(ethylene oxide) (PEO) (Polymer Labs.) and poly(2-vinlypyridine) (PVP) (Pressure Chemical, Pittsburgh, PA, U.S.A.).

Ala–Ala–Ala–CH_3 (Tame), Ala–Ala–Ala (Tala) and other peptides and amino acids were obtained from Sigma (St. Louis, MO, U.S.A.). Gold label phthalic acid and 4-hydroxybenzoic acid were purchased from Aldrich (Milwaukee, WI, U.S.A.). Chloride and phosphate standards were prepared from a standardized 1.00 *M* hydrochloric acid volumetric solutions and reagent grade sodium phosphate dibasic, respectively (J.T. Baker).

The poly [(chloromethoxytrialanine methyl ester) phosphazene] polymer (poly-Tame) was synthesized in-house (Sterling Research Group, Malvern, PA, U.S.A.) as described elsewhere [11].

Instrumentation and chromatographic conditions

The chromatographic system included a Waters 840 multisystem controller (Waters Chromatography Division/Millipore, Milford, MA, U.S.A.) for control of three independent liquid chromatographs (version 6.21A software). Raw data were automatically transferred to a Waters 860 software system (version 2.1) with LC/GPC software capability located on a VAX 8250 (Digital Equipment, Maynard, U.S.A.) for subsequent analyses and reduction.

The HPSEC system consisted of a Waters 712 autosampler with cooling unit maintained at 20°C, a Waters Model 510 pump with pulse dampener and high sensitivity noise filter and a Waters 490E UV–VIS detector set a 225 nm connected in series with a Waters 410 differential refractometer (sensitivity = 128, internal temperature = 40°C). Chromatographic size exclusion was achieved by employing a mobile phase of 0.1 *M* ammonium acetate in methanol at a flow-rate of 2.0 ml/min through Zorbax GF-250 and GF-450 (25 cm × 9.4 mm I.D., 5μm) HPSEC columns (DuPont, Wilmington, DE, U.S.A.) maintained at 50°C in a Waters column oven. Integration of size-exclusion chromatograms was determined by peak slicing at 20 slices/min from the beginning of the peak to the end of the peak with baselines projected horizontally from a stable baseline point before the exclusion limit (usually at 6 min) to a stable baseline point after the void volume (usually at 17 min).

The RP-HPLC gradient system consisted of a Waters 712 autosampler with cooling unit maintained at 20°C, two Waters 510 pumps and a Spectroflow 783 UV–VIS detector (Applied Biosystems, Ramsey, NJ, U.S.A.) with the wavelength set at 210 nm. The analytical column was a Zorbax C_8 reliance cartridge (4 cm × 6 mm I.D., 3 μm) with Zorbax C_8 guard cartridge (1 cm × 3.2 mm I.D., 5 μm) (DuPont). A linear gradient profile of 100 to 40% A over 8 min at a flow-rate of 2.0 ml/min

through was used with a 3-min re-equilibration period between injections. The mobile phases employed for gradient reversed-phase separation of Tame and potential hydrolysis products were: (A) 5.0 m*M* octanesulfonic acid sodium salt and 0.05% (v/v) TFA in water, and (B) 0.05% (v/v) TFA in acetonitrile–water (60:40, v/v).

THe IC system consisted of a Waters 712 autosampler with cooling unit maintained at 20°C, a Waters Model 510 pump and a Waters 484 UV–VIS detector set at 270 nm connected in series with a Waters 430 conductivity detector. The mobile phase was prepared by dissolving 1.0 mmol of phthalic acid in 50 ml of methanol and adding 950 ml of water and 300 μl of TEA. The pH of this solution was adjusted to pH 6.3–6.5 with 50 m*M* 4-hydroxybenzoic acid dissolved in methanol. The mobile phase was prepared fresh daily. Separation and analysis of free chloride and phosphate from hydrolyzed polyphosphazene polymers was achieved with a flow-rate of 3.0 ml/min through a Vydac 300 IC anion exchange column (5 cm × 4.6 mm I.D., 5 μm) with Vydac 300 IC guard cartridge (2.5 cm × 4.6 mm I.D., 5 μm), (The Separations Group, Hesperia, CA, U.S.A.).

RESULTS AND DISCUSSION

Development and validation of HPSEC method

PolyTame is a cationic polymer capable of strong ionic, adsorptive and hydrophobic interactions with chromatographic supports. Thus the development of a rugged and precise HPSEC method requires that all interactions between the polymer and stationary phase are minimized so that MW separation is based on pore diffusion only. Attempts to chromatograph polyTame using standard aqueous buffered mobile phases and silica columns were unsuccessful. In addition, polyTame could not be chromatographed with strong organic mobile phases and standard resin-based GPC columns. In both cases, polyTame failed to elute from the columns presumably due to

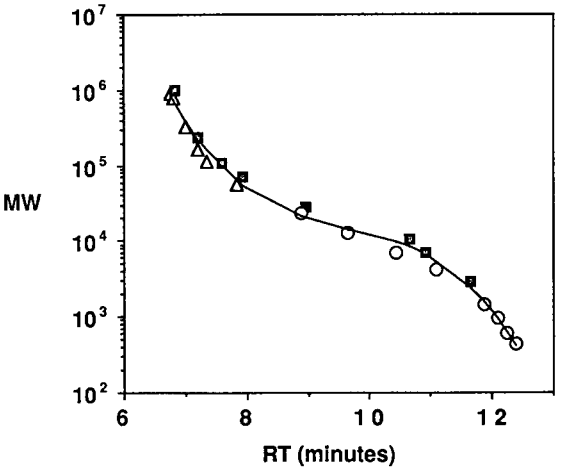

Fig. 2. HPSEC narrow standard calibration curve for MW determination of polyTame. △ = PEO standards; ■ = PVP standards; ○ = PEG standards. Curve fit to third order polynominal: $MW = 50.76 \cdot RT^3 - 14.08 \cdot RT^2 + 1.44 \cdot RT - 0.05$ ($R^2 = 0.992$); RT = Retention time (min). Conditions are described in the Experimental section.

strong interactions with the stationary phase. These interactions were minimized when a mobile phase of methanol, an excellent solvent for polyTame, and a hydrophilic diol stationary phase on a silica support were used. Because of the polymer's cationic nature and the unknown stability of the 'protected' diol stationary phase, ammonium acetate was added in the mobile phase to suppress potential ionic interactions with any free silanol groups.

The HPSEC method was calibrated using narrow MW neutral and cationic polymers that were methanol soluble. The PEO, PEG and PVP standards from 440 to $1 \cdot 10^6$ dalton were dissolved in methanol at about 1 mg/ml and 25μl injected into the HPSEC. The results illustrated in Fig. 2 indicate a good correlation between retention time and MW for these three classes of polymers over the MW range. The calibration was fit to a third order polynomial ($R^2 = 0.992$) with a mean residual error of 17% between calculated and actual MWs. Although values for PVP appear to deviate slightly from PEO and PEG, this is not surprising considering the difference in chemical structure. PVP is a linear, short branched, cationic polymer with physico-chemical characteristics more similar to polyTame than the other linear, neutral polymers, PEO and PEG. Therefore, in the absence of a 'universal' calibration, it is believed that the use of all three sets of standards represents the best 'average' external calibration for polyTame. Absolute MW determinations using this procedure can only be considered to be approximate. However, HPSEC time course evaluations measuring polymeric degradation of polyTame will not be significantly affected by the choice of external calibration since only differences in MW are important.

Separation of standards over the entire MW range demonstrates the high efficiency of this system (Fig. 3). The reproducibility of the method was determined by

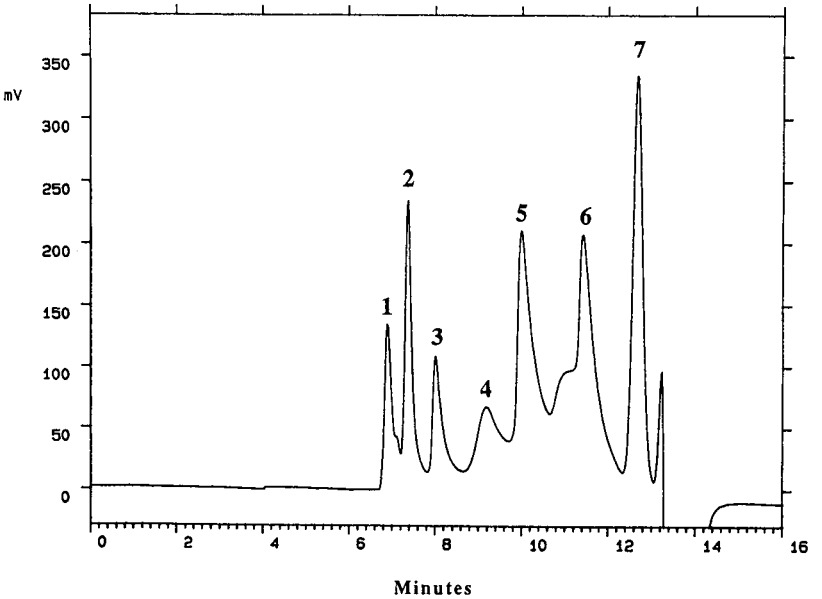

Fig. 3. HPSEC separation of narrow MW standards in methanol solution, 25 μl per injection. Peaks: 1 = PEO, MW = 900 000, 0.75 mg/ml; 2 = PVP, MW = 240 000, 0.75 mg/ml; 3 = PEO, MW = 56 300, 1.25 mg/ml; 4 = PVP, MW = 28 000, 0.5 mg/ml; 5 = PEG, MW = 12 600, 3.0 mg/ml; 6 = PEG, MW = 4250, 1.7 mg/ml; 7 = PEG, MW = 440, 1.7 mg/ml. Conditions are described in the Experimental section.

analyzing MW, peak area and peak height following repetitive injections of a polyTame-in-methanol solution. The precision of the method was better than 5% coefficient of variation (C.V.) ($n = 15$) over 3 days (Table I) for all variables monitored. The application of this method for studying the hydrolysis of polyTame is illustrated in Fig. 4. In a 0.8 *M* hydrochloric acid solution, polyTame undergoes rapid MW decline, a significant change in the MWD and a high disappearance of polymer over a 14-h period at 20°C.

TABLE I

HPSEC PRECISION OF POLYTAME ANALYSES

Analyses of 100 μg/ml polyTame in methanol, 25 μl per injection. Conditions as described in the Experimental section. $\bar{M}_p$ is peak MW.

Time (days)	$\bar{M}_n$	$\bar{M}_w$	$\bar{M}_p$	Peak height	Peak area
0.02	33 416	58 017	120 867	23 592	1 967 650
0.11	32 632	58 362	120 867	23 210	1 817 827
0.21	32 795	57 297	120 867	23 336	1 879 397
0.30	31 498	55 414	109 668	23 574	1 957 417
0.40	33 238	59 075	120 867	23 758	1 938 014
0.49	32 806	55 988	120 867	23 369	1 947 826
0.59	32 580	56 578	120 867	23 699	1 927 924
0.69	32 505	55 937	109 668	23 670	1 915 044
0.78	31 644	56 329	109 688	23 247	2 050 452
1.44	30 723	55 173	120 867	23 210	1 897 355
1.68	33 092	58 812	120 867	23 198	1 900 700
1.76	32 940	58 075	120 867	24 022	2 122 675
1.84	29 968	52 834	109 668	23 096	1 997 348
2.96	32 105	55 318	109 668	22 295	1 853 547
3.04	33 792	57 810	109 668	24 093	2 041 558
Mean ($n = 15$)	32 382	56 735	116 388	23 425	1 947 649
C.V. (%)	3.2	3.0	4.9	1.9	4.1

Development and validation of RP-HPLC method

Traditional methods for the separation of peptides by RP-HPLC based on a gradient of TFA in water and acetonitrile lacked the selectivity necessary for the separation of Tame from its major hydrolysis product, Tala. However, when a more hydrophobic ion-pairing agent such as octanesulfonic acid was incorporated into the aqueous mobile phase, the selectivity was improved such that Tame and Tala were easily resolved. In addition, the use of short 4 cm, 3-μm particle size C_8 columns at relatively high flow-rates greatly reduced the run time without compromising the efficiency compared to standard dimension columns. This approach has also been applied to the rapid separation of much higher MW vasopressin peptides from intestinal metabolites [12].

Separation of Tame from its major hydrolysis product, Tala, and other low-MW peptides and amino acids illustrated in Fig. 5 demonstrates the selectivity of this

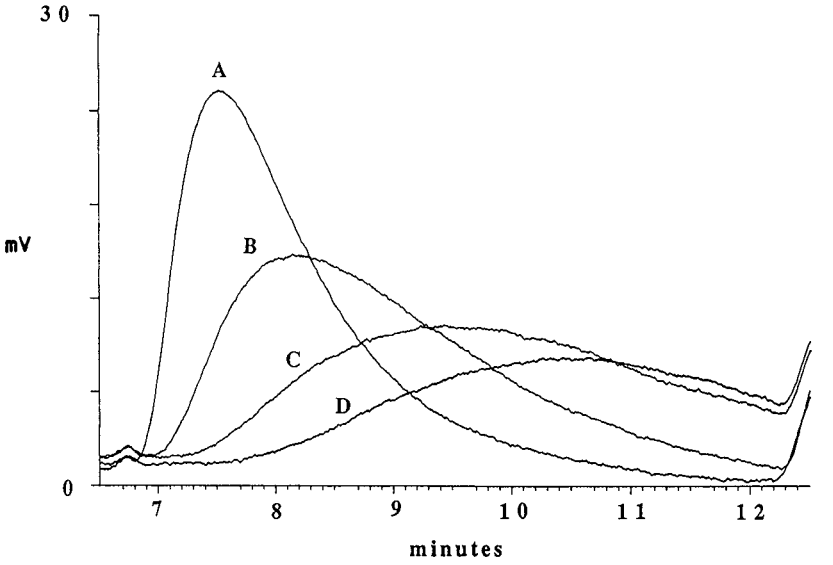

Fig. 4. HPSEC chromatograms of a polyTame sample in a 0.8-*M* hydrochloric acid solution at 20°C: (A) after 0.5 h, $(\bar{M}_n\bar{M}_w)^{1/2}$ = 39 542; (B) after 7.4 h, $(\bar{M}_n\bar{M}_w)^{1/2}$ = 25 626; (C) after 12.0 h, $(\bar{M}_n\bar{M}_w)^{1/2}$ = 18 818; (D) after 14.3 h, $(\bar{M}_n\bar{M}_w)^{1/2}$ = 14 137. The small peaks before the exclusion limit at a retention time of 6.85 min are 'unknown system peaks' and have not been included in MW calculations. Conditions are described in the Experimental section.

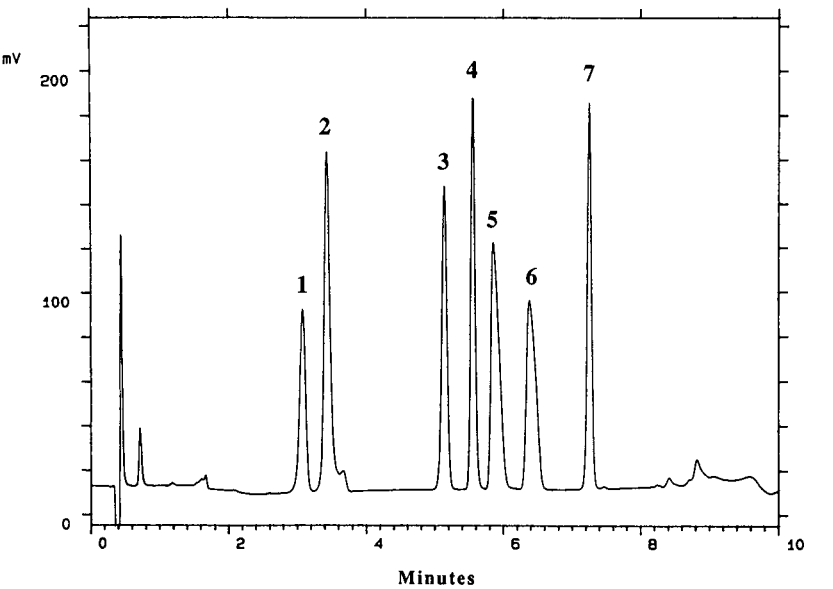

Fig. 5. RP-HPLC separation of Ala–Ala–Ala–CH_3 (Tame) from its hydrolysis product Ala–Ala–Ala (Tala) and similar dipeptides and amino acids. Peaks: 1 = Gly–Gly–NH_2, 1.5 m*M*; 2 = Gly–Gly, 3.7 m*M*; 3 = Ala–Ala, 2.0 m*M*; 4 = Tala, 1.0 m*M*, capacity factor (k') = 12.7; 5 = Ala–CH_3, 46 m*M*; 6 = Gly–CH_2–CH_3, 48 m*M*; 7 = Tame, 1.0 m*M*, k' = 17.0. The resolution between Tala and Tame is 11. Conditions are described in the Experimental section.

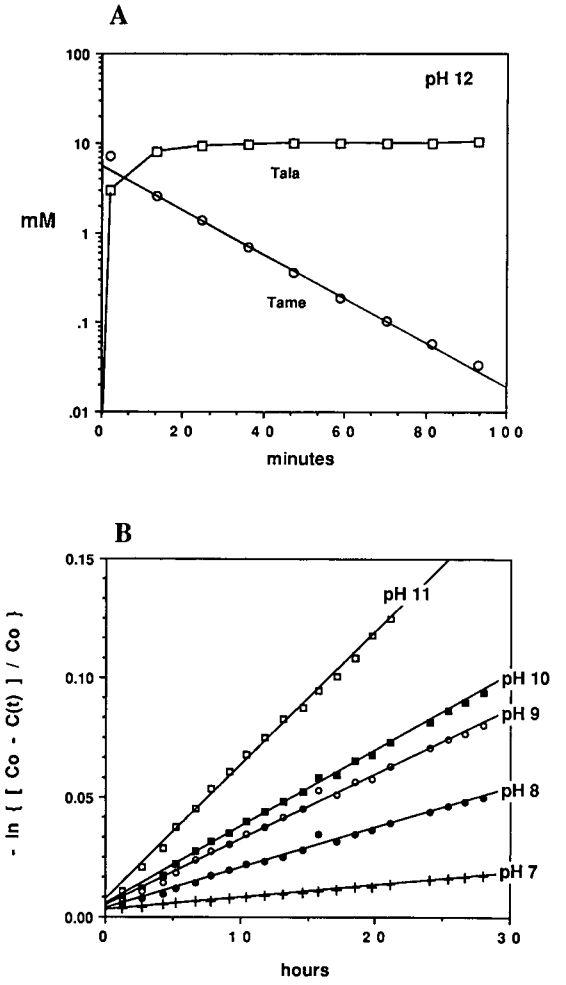

Fig. 6. Effect of pH on the hydrolysis of Tame to Tala at 20°C. Solutions were prepared in 0.05 *M* K_2PO_4 and adjusted to the appropriate pH with concentrated hydrochloric acid or sodium hydroxide. The initial concentration (Co) is 10 m*M* Tame. (A) Disappearance of Tame (○) and appearance of Tala (□) at pH 12, first order rate constant, $k = 3.485\ h^{-1}$, $t_{1/2} = 0.20$ h. (B) First order initial rate plot of Tame disappearance based on appearance of Tala, C(t); pH 11, $k = 5.59 \cdot 10^{-3}\ h^{-1}$, $t_{1/2} = 124$ h; pH 10, $k = 3.20 \cdot 10^{-3}\ h^{-1}$, $t_{1/2} = 216$ h; pH 9, $k = 2.76 \cdot 10^{-3}\ h^{-1}$, $t_{1/2} = 252$ h; pH 8, $k = 1.70 \cdot 10^{-3}\ h^{-1}$, $t_{1/2} = 408$ h; pH 7, $k = 5.06 \cdot 10^{-4}\ h^{-1}$, $t_{1/2} = 1370$ h.

method. Standard solutions of Tame and Tala were prepared in 0.05% (v/v) acetic acid–water and 20 μl injected for analyses. The detector response was linear ($R^2 = 0.999$) over the concentration range from 0.1 to 5.0 m*M* for both Tame and Tala based on peak area. The intra-day precision over this concentration range was 0.6% C.V. ($n = 4$). The inter-day reproducibility of the method was determined by repetitive analyses over 23 days ($n = 27$) of a 3.65-m*M* Tame solution in water during the course of hydrolysis experiments and was better than 1.0% C.V. The minimum quantifiable

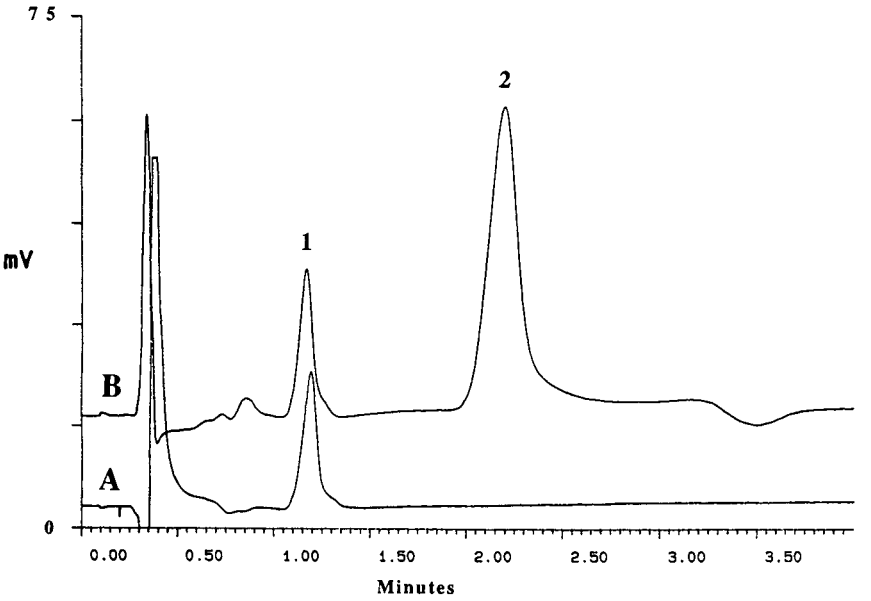

Fig. 7. IC chromatograms of hydrolyzed polyTame in water after (A) 3 days at 20°C, 1.49 m*M* chloride, capacity factor (k') = 2.9 and (B) 4 days at 160°C, 1.53 m*M* chloride, k' = 3.0, and 5.92 m*M* phosphate, k' = 6.4. Peaks: 1 = chloride; 2 = phosphate. The resolution between chloride and phosphate is 4.2. Conditions are described in the Experimental section.

concentration is 0.01 m*M* with a signal-to-noise ratio of 3:1. This method was applied to the base hydrolysis of Tame in aqueous solutions. The results shown in Fig. 6 indicate that Tame hydrolysis occurs mainly at the C-terminal ester, follows first order disappearance kinetics and is strongly pH dependent. Application of this method for the determination of Tame/Tala N-terminal hydrolysis from the polyTame backbone is presented elsewhere [11].

Development and validation of IC method

The IC method was a modification of the procedure supplied by the column manufacturer for inorganic anions. The chromatographic conditions were optimized for the separation of chloride and phosphate with indirect UV detection. Electronically suppressed conductivity detection could not be used because of a poor signal-to-noise ratio for phosphate.

The method was calibrated by injecting 20 μl of chloride and phosphate standard solutions prepared in water from 0.1 to 3 m*M* chloride and 0.05 to 2.5 m*M* phosphate. The indirect UV detector response is linear for chloride (R^2 = 0.999) and phosphate (R^2 = 0.998) based on peak area. The standards were injected in triplicate and the precision over the concentration range was better than 3% C.V. (n = 12) for chloride and 6% C.V. (n = 18) for phosphate. Because of the inter-day variability in column retention, (*e.g.* note change in retention for chloride in Fig. 7), the IC system was calibrated immediately prior to sample analysis. Minimum quantifiable concentrations based on a signal-to-noise ratio of 3:1 for chloride and phosphate are 0.01

and 0.025 m*M*, respectively. Sample chromatograms of polyTame samples hydrolyzed in water at 20 and 160°C illustrate the application of the IC method to *in vitro* degradation experiments (Fig. 7).

REFERENCES

1 J. Drobnik, *Adv. Drug Delivery Rev.*, 3 (1989) 229.
2 H. Sezaki, Y. Takakura and H. Hashida, *Adv. Drug Delivery Rev.*, 3 (1989) 247.
3 C. Larsen, P. Kurtzhals and M. Johansen, *Acta Pharm. Suec.*, 25 (1988) 1.
4 P. Kurtzhals, C. Larsen and M. Johansen, *J. Chromatogr.*, 491 (1989) 117.
5 H. R. Allcock, *ACS Symp. Ser.*, 232 (1983) 49–67.
6 C. W. J. Grolleman, A. C. de Visser, J. G. C. Wolke, H. van der Goot and H. Timmerman, *J. Controlled Release*, 4 (1986) 119.
7 C. W. J. Grolleman, A. C. de Visser, J. G. C. Wolke, C. P. A. T. Klein, H. van der Groot and H. Timmerman, *J. Controlled Release*, 4 (1986) 133.
8 J. H. Goedemoed and K. de Groot, *Makromol. Chem. Macromol. Symp.*, 19 (1988) 341.
9 H. R. Allcock, T. J. Fuller, D. P. Mack, K. Matsumura and K. M. Smeltz, *Macromolecules*, 10 (1977) 824.
10 H. R. Allcock, T. J. Fuller and K. Matsumura, *Inorg. Chem.*, 21 (1982) 515.
11 W. M. Eickhoff, G. G. Liversidge and R. Mutharasan, *Proc. Int. Symp. Control. Rel. Bioact. Mater.*, Vol. 17, Controlled Release Society, 1990, p. 160.
12 W. M. Eickhoff, G. G. Liversidge and K. C. Cundy, *Pharm. Res.*, 6 (1989) S-114.

Journal of Chromatography, 536 (1991) 265–272
Elsevier Science Publishers B.V., Amsterdam

CHROMSYMP. 2020

Quantitation of adenosine, inosine and hypoxanthine in biological samples by microbore-column isocratic high-performance liquid chromatography

R. H. GAYDEN

Division of Cardiology, Department of Internal Medicine, University of Texas, Health Science Center at Houston, Houston, TX 77030 (U.S.A.)

B. A. WATTS, III and R. E. BEACH

Division of Nephrology, Department of Internal Medicine, University of Texas, Medical Branch, Galveston, TX 77550 (U.S.A.)

and

C. R. BENEDICT*

Division of Cardiology, Department of Internal Medicine, University of Texas, Health Science Center at Houston, Houston, TX 77030 (U.S.A.)

ABSTRACT

This paper describes a simple and sensitive high-performance liquid chromatographic method for measuring adenosine, inosine and hypoxanthine in cell suspensions. The method involves direct injection of the filtered sample on a microbore C_{18} reversed-phase column with UV detection at 259 nm. The mobile phase consisted of 125 m*M* potassium dihydrogenphosphate, 1.0 m*M* tetrabutylammonium hydrogensulfate, 1.5% acetonitrile and 20 m*M* triethylamine, pH 6.5. The minimum detectable amounts (signal-to-noise ratio of 3:1) were 2.0 pmol of adenosine, 2.5 pmol inosine and 3.5 pmol of hypoxanthine. The limits of quantitation were 2.9 ± 0.2 pmol for adenosine, 4.2 ± 0.3 pmol for inosine and 4.9 ± 0.4 pmol for hypoxanthine. This method was used to quantitate adenosine release by dispersed rat renal outer medullary cells (tubules) under conditions of normoxia and hypoxia.

INTRODUCTION

Adenosine (Ado) is a potent extracellular messenger in a variety of systems. It causes vascular smooth muscle relaxation [1], regulates regional blood flow in brain [2], inhibits norepinephrine release from sympathetic nerve endings [3] and in the kidney alters renal hemodynamics and renin secretion [4–6]. The increase in our knowledge of the actions of Ado has been accompanied by the elucidation of the biochemical pathways for Ado metabolism. It is known that Ado can be formed intra- or extra-cellularly and that both adenosine monophosphate and S-adenosylhomocysteine can serve as the immediate precursors for Ado [7].

These findings have lead to attempts at delineating the specific sites of Ado production and its regulation in various organs under conditions of hypoxia or ischemia. Adenosine and its enzymatic breakdown products inosine (Ino) and hypoxan-

0021-9673/91/$03.50

thine (Hyp) have been previously measured predominantly by high-performance liquid chromatography (HPLC) with UV detection [8–13]. However, these methods are of limited usefulness for studying the metabolic pathways of Ado in isolated cells or cell suspensions as they lack reliability to quantitate Ado, Ino and Hyp at a concentration range of 3–5 pmol. An isocratic method is described for the determination of Ado, Ino and Hyp by the use of reversed-phase HPLC on a 2.1-mm I.D. C_{18} column with UV detection at 259 nm. Adenosine production by renal outer medullary cells under conditions of normoxia and hypoxia was measured by this method to demonstrate its sensitivity and precision.

METHODS

HPLC

The system consisted of Waters 6000A (Milford, MA, U.S.A.) pump with microflow modifications, a Waters U6K injector with 10-μl injection loop and a Kratos Spectroflow 783 UV detector (Kratos Analytical, Ramsey, NJ, U.S.A.) equipped with a 2.4-μl flow cell operated at 259 nm. A Brownlee RP-18 column (220 × 2.1 mm I.D.) attached to a Brownlee RP-18 (15 × 2.1 mm) guard precolumn was used for chromatographic separations (Santa Clara, CA, U.S.A.). To obtain high sensitivity and to minimize the peak broadening the connection tubings were kept as short as possible, the microbore manifold was installed on the detector to connect the column directly to the detector cell and a 2.4-μl analytical flow cell was used. Data were collected and peaks integrated using IBM PC/AT and Nelson Analytical 2600 Series chromatography software (Cupertino, CA, U.S.A.).

The chemicals used were of HPLC/analytical grade. Acetonitrile was obtained from Aldrich (Milwaukee, WI, U.S.A.). Potassium dihydrogenphosphate, potassium hydroxide, tetrabutylammonium hydrogensulfate (TBAHS) and triethylamine (TEA) were obtained from Fluka (Ronkonkoma, NY, U.S.A.). Ado, Ino and Hyp standards were obtained from Sigma (St. Louis, MO, U.S.A.). Collagenase, hyaluronidase and dipyridamole were also obtained from Sigma. *erythro*-9-(2-Hydroxy-3-nonyl)adenine (EHNA) was a gift from Wellcome Research Labs. (Research Triangle Park, NC, U.S.A.). Milli-Q Water (Millipore, Bedford, MA, U.S.A.) was used for preparation of the mobile phase. Kidneys were obtained from male Spraque-Dawley rats (Taconic Farms, Germatown, NY, U.S.A.), 250–350 g, that received standard rat chow (Purina, St. Louis, MO, U.S.A.) and tap water *ad libitum*.

Mobile phases contained 125 m*M* potassium dihydrogenphosphate, 1.5% (v/v) acetonitrile, 20 m*M* triethylamine and 1.0 m*M* TBAHS (pH 6.5) and adjusted to pH 6.5 with 8 *M* potassium hydroxide. This solution was filtered using a 0.45-μm nylon filter (Ranin Instruments, Woburn, MA, U.S.A.) and degassed under vacuum with sonication for 10 min before use. Chromatography was carried out at room temperature using a mobile phase flow-rate of 0.5 ml/min and sample injections of 10 μl. Generally, equilibration of the column with stable chromatographic conditions was assumed when a steady baseline was observed at 0.002 a.u.f.s. with a rise time of 0.1 s for at least 60 min. Standard curves for Ado, Ino and Hyp prepared in the incubation media were constructed for each assay. The standards encompassed a range from 3 to 50 pmol. At the end of each day the column was run overnight with methanol to elute any retained materials.

Suspensions of outer medulla

Suspensions of outer medulla (tubules) (OM) were prepared by the method of Chamberlin *et al.* [14], with minor modifications. Animals were anesthetized by intraperitoneal pentobarbital, 50 mg/kg. The kidneys were perfused retrograde through the aorta with a hypertonic mannitol solution (solution A: NaCl, 115 m*M*; $NaHCO_3$, 25 m*M*; NaH_2PO_4, 0.2 m*M*; KCl, 8.0 m*M*; $CaCl_2$, 0.25 m*M*; $MgSO_4$, 1.0 m*M*; sodium lactate, 5.0 m*M*; L-alanine, 1.0 m*M*; glucose, 5.0 m*M*; dextran, 0.3%; and mannitol, 25 m*M*) at 4°C until the kidneys were were completely blanched of blood and brisk urine flow was established. The kidneys removed, longitudinally bisected and the inner strip of the outer medulla dissected free and minced. The minced tissue was digested at 37°C for three 10-min periods in solution A that contained 110 U/ml collagenase Type IV and 297 U/ml hyaluronidase. The digested solution was stirred continuously and bubbled with oxygen–carbon dioxide (95:5). Following each of the first two digestion periods, the digested material was filtered through a 105-μm polypropylene filter (Spectrum, Los Angeles, CA, U.S.A.) and the undigested tissue was resuspended in fresh enzyme solution. At the end of the third digestion period, the suspension was aspirated through an 18-gauge needle to separate completely any remaining tissue aggregates. This tissue was washed with incubation fluid (NaCl, 115 m*M*; $NaHCO_3$, 25 m*M*; NaH_2PO_4, 2.0 m*M*; KCl, 5.0 m*M*; $CaCl_2$, 1.0 m*M*; $MgSO_4$, 1.0 m*M*; sodium lactate, 5.0 m*M*; glucose, 5.0 m*M*; dipyridamole, 0.02 m*M*; and EHNA, 0.01 m*M*) examined with a light microscope to insure a homogeneous tubule population, and kept at 4°C as the OM suspension. Alternatively, some suspensions were washed with the incubation fluid which did not contain the dipyridamole and EHNA in order to determine the need for the inhibitors of adenosine metabolism. An aliquot of the suspension was assayed for protein concentration by the Lowry method [15] for standardization of Ado release. The protein concentration in these suspensions were between 0.6 mg to 3 mg/ml.

Incubation protocol

Incubation fluid 0.8-ml aliquots, containing dipyridamole and EHNA was preequilibrated for at least 20 min with 0% or 8% oxygen and 5% carbon dioxide (balance nitrogen). Following this equilibration period, 0.1 ml of OM suspension (0.06 to 0.3 mg of protein) was added to each aliquot and incubated for 0.5 or 8 min while being bubbled with either 0% or 8% oxygen gas mixtures. The incubation fluid was rapidly filtered through 0.45-μm HA syringe filters (Millipore) to separate the supernatant from the medullary tissue. In addition, to determine whether Ado release occurred prior to incubation, an aliquot of the suspension (0.1 ml) was added directly into a syringe containing 0.8 ml incubation fluid and immediately filtered. No Ado could be detected in these samples ($n=8$). The experimental samples were stored at -70°C for less than two weeks until quantitated by HPLC. The amount of Ado released was expressed in terms of the amount of protein present in the total sample (suspension) (pmoles Ado/μg protein).

Oxygen tensions in the suspensions were measured by rapidly aspirating the incubation fluid into sealed glass syringes and analyzing on a Corning blood gas analyzer Model 165/2 (Medfield, MA, U.S.A.) calibrated using 0 and 20% oxygen standards. Oxygen tension measured in fluid equilibrated with nominally 0% oxygen was 16 mmHg (2.2%) and at 8% oxygen was 61 mmHg (8.2%). The small differences

between measured and nominal values presumably reflect gain or loss of oxygen from the air due to the open system. Nominal values are used in the text for simplicity.

Statistical analysis

All the result are expressed as mean ± 1 S.D. Adenosine concentrations from OM suspensions were analyzed by ANOVA for the effect of time and oxygen concentrations, and the differences between means were compared by Newmann–Keuls multiple comparison procedure [16]. Differences between means were considered significant at the $p < 0.05$ level.

RESULTS

When an Ado, Ino and Hyp standard mixture prepared in the mobile phase was injected, Ado eluted at 10.2 min with a capacity factor, $k' = 8.8$, Ino eluted at 3.8 min with a $k' = 2.6$ and Hyp eluted at 1.9 min with a $k' = 0.8$ (Fig. 1A). Similar results were obtained by injecting standards prepared using incubation fluid or cell suspen-

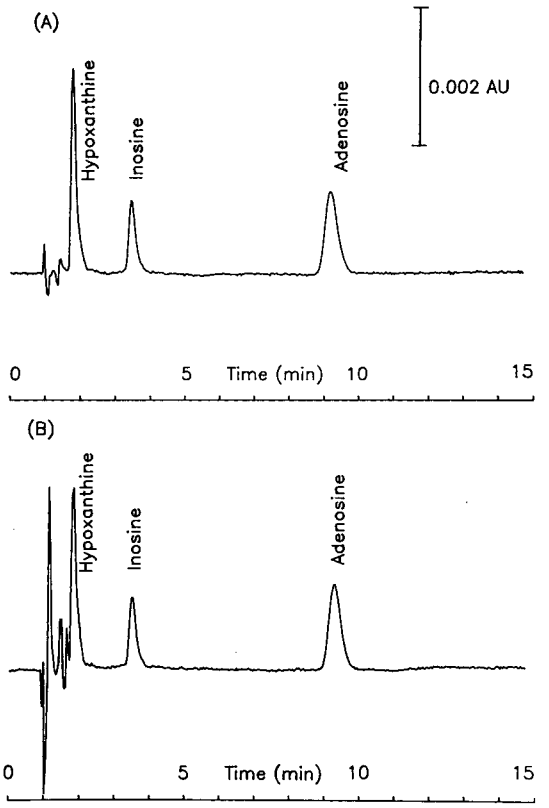

Fig. 1. Chromatogram showing the retention time for Ado (22.45 pmols), Ino (22.37 pmol) and Hyp (44.08 pmol). Mobile phase: 125 m*M* potassium dihydrogen phosphate, 1.5% (v/v) acetonitrile, 20 m*M* triethylamine and 1.0 m*M* TBAHS (pH 6.5). Flow-rate: 0.5 ml/min. (A) Standard prepared in mobile phase. (B) Standard prepared in incubation fluid or cell suspension media (Solution A).

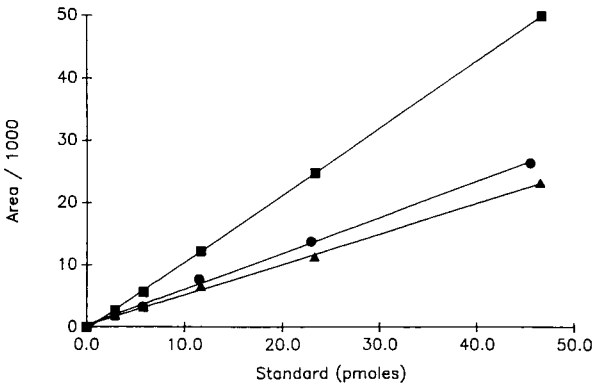

Fig. 2. Standard curve for Ado (■), Ino (▲) and Hyp (●) from 3 to 50 pmol ($r = 0.99$, $p < 0.001$ for all three compounds) ($n = 4$ with C.V. < 3% for all three compounds).

sion media (solution A) (Fig. 1B). The standard curve was linear throughout the range tested ($r = 0.99$; $p < 0.001$) (Fig. 2). The minimum detectable amounts (at a signal-to-noise ratio of 3:1) were 2.0 pmol of Ado, 2.5 pmol Ino and 3.5 pmol Hyp. The limits of quantitation were 2.9 ± 0.2 pmol for Ado, 4.2 ± 0.3 pmol for Ino and 4.9 ± 0.4 pmol Hyp. The interassay coefficient of variation (C.V.), was determined by injecting 5.0 ng of Ado (22.45 pmol), Ino (22.37 pmol) and Hyp (44.08 pmol) added to four different preparations of incubation fluid on four different days. The C.V. of the integrated areas was less then 4% for all three compounds. The purity of the detected Ado was determined by two methods: (1) The peak areas were increased in direct proportion to exogenously added Ado, Ino and Hyp; (2) absorptions at 259 and 280 nm were compared for all three compounds. The mean (± S.D.) $area_{259}/area_{280}$ ratios for all three compounds were similar between the sample peaks (6.30 ± 0.15 for Ado, 7.76 ± 0.18 for Ino and 22.5 ± 0.85 for Hyp) and the injected authentic standards (6.38 ± 0.12 for Ado, 7.70 ± 0.19 for Ino and 23.1 ± 0.73 for Hyp). These results indicate that there was negligible interference by impurities or components in the incubation media.

Chromatographic parameters were examined to improve peak separation, especially Hyp without significantly increasing the analysis time for each sample. Fig. 3

TABLE I

THE EFFECT OF GRADED OXYGEN TENSION ON ADENOSINE RELEASE IN SUSPENSIONS OF RAT OUTER RENAL MEDULLA

Nominal oxygen concentration (%)	Adenosine relaese (pmol of adenosine/μg protein)	
	Time of incubation (min)	
	0.5	8
8	0.78 ± 0.30 ($n = 7$)	2.69 ± 0.34 ($n = 13$)
0	1.46 ± 0.37 ($n = 5$)	5.24 ± 0.78[a] ($n = 8$)

[a] $p < 0.05$ compared to 8 and 0% oxygen, ANOVA with Dunnett's multiple comparisons test [16].

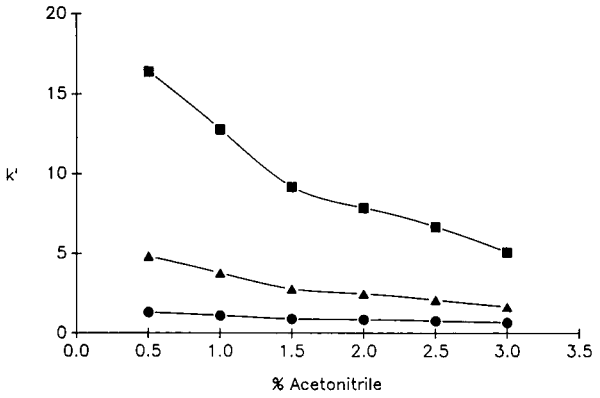

Fig. 3. Change in capacity factors for Ado (■), Ino (▲) and Hyp (●) with variations in acetonitrile concentration. Other components: 125 m*M* potassium dihydrogenphosphate, 1.0 m*M* TBAHS, 20 m*M* triethylamine (pH 6.5). Flow-rate: 0.5 ml/min.

shows the effect of change in acetonitrile percentage on k' of Ado, Ino and Hyp. Fig. 4 shows the effect on k' of Ado, Ino and Hyp with different concentrations of TBAHS.

Adenosine release was measured in OM suspensions incubated with 0 (hypoxic) or 8% (normal medullary) oxygen concentrations for 0.5 or 8 min (Table I). Ado concentrations after 8 min were significantly greater in incubation fluid of suspensions maintained with 0% oxygen than in fluid from suspensions 8% oxygen. In samples were EHNA and dipyridamole were not added, the Ado concentration was significantly reduced from 5.24 ± 0.78 pmol/μg of protein to 2.69 ± 0.83 pmol/μg of protein ($p < 0.05$) and Hyp (1.75 ± 0.40 pmol/μg of protein) and Ino (0.42 ± 0.01 pmol/μg of protein) were detected.

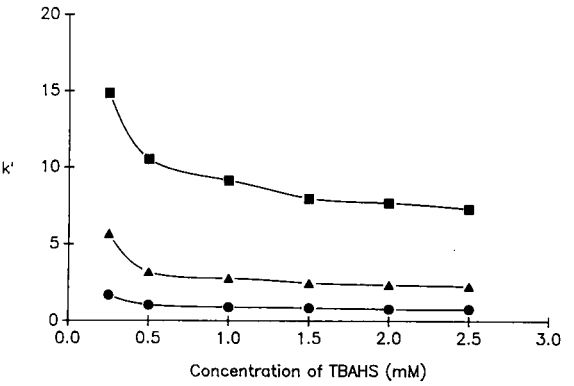

Fig. 4. Change in capacity factors for Ado (■), Ino (▲) and Hyp (●) with variations in TBAHS concentration. Other components: 125 m*M* potassium dihydrogenphosphate, 1.5% (v/v) acetonitrile, 20 m*M* triethylamine (pH 6.5). Flow-rate: 0.5 ml/min.

DISCUSSION

It is well known that application of gradient elutions to routine quantitative analysis can impair reproducibility of peak retention times since changes in the column equilibria between analyses easily results in peak shifting [17,18]. Therefore for the simultaneous measurement of Ado, Ino and Hyp, a highly sensitive isocratic, reversed-phase method was developed by optimization of the concentrations of ion-pairing reagent and percentages of acetonitrile used.

A low concentration of the ion-pairing reagent TBAHS was used to enhance peak separation and to eliminate peak asymmetry seen with mobile phases prepared with acetonitrile alone. Tetrabutylammonium ions (TBA) bind to the stationary phase of the C_{18} column due to hydrophobic interactions between the aliphatic groups of the packing material with the butyl groups of TBA. Consequently, positively charged groups arise on the stationary phase which should greatly modulate the retention of nucleotides (due to strong interactions with phosphate groups) and only slightly modulate the retention nucleosides (due to weaker interactions with oxygens or nitrogens with lone pair electrons) [19]. The use of ion-pairing reagent effectively reduced the strong hydrophobic interactions of the C_{18} stationary phase with the nucleosides. This improved peak symmetry and allowed better peak separations (elimination of tailing). In agreement with this, we found that increasing the concentration of TBAHS produced a decrease in the k' for Ado and Ino, and a smaller decrease in the k' for Hyp.

As the concentration of acetonitrile was increased, the k' values for Ado, Ino and Hyp decreased. Predictably, as the hydrophobicity of the solvent increased the nucleosides eluted earlier. No significant effect on retention times was seen at different pH value encompassing a range of 5.5 to 7.5, and the selected pH of 6.5 did not alter the retention characteristics of the column even after several months of use ($>$ 1000 sample injections).

It is known that underivatized surface silanols may react with solutes. Basic compounds often suffer from severe peak asymmetry and therefore poor column efficiency due to strong interactions of the nitrogen lone pair electrons with free silanol groups [19,20]. The effect of these silanol groups was modified with triethylamine (TEA) which was added to mobile phases as a silanol blocking or masking agent. When TEA was not added to the mobile phase, tailing of the peaks were observed suggesting that the column was not fully masked [19]. Tailing was not observed when 20 m*M* TEA was used.

Using this method, we examined the effects of hypoxia on Ado production by the outer medulla by measuring the Ado release during incubation of the OM suspension at two different *in vitro* oxygen contents. The oxygen concentrations used in the present studies are physiologically relevant because *in vivo* oxygen tensions previously determined in the renal medulla under control conditions have ranged from 30–60 mmHg [21]. This range is comparable to the oxygen tensions (61 mmHg) achieved in the present study in suspensions equilibrated with 8% oxygen. As shown in Table I, reduction to 16 mmHg (0% oxygen), a value comparable to that reported during hypoxia [19] was associated with an increase in Ado release.

In summary, a highly sensitive, isocratic HPLC method is described for the concurrent determination of Ado, Ino and Hyp in a suspension of OM cells. Using

this method Ado release by the cells in the renal outer medulla was demonstrated. When dipyridamole and EHNA was omitted in the incubation media, a major portion of the Ado released was metabolized to Ino and Hyp. The Ado release is increased by *in vitro* hypoxic conditions that are similar to those that are expected *in vivo* in the renal medulla during ischemic injury. This increased Ado release by hypoxia may have physiologic actions that may protect the medullary nephrons from ischemic injury by increasing renal medullary blood flow due to its vasodilatory effects.

ACKNOWLEDGEMENTS

This work was supported by RO1 34837, RO1 HL39916 and RO1 HL39165 (C.R.B.) and the John Sealy Memorial Endowment and Texas Heart Association (R.E.B.). C.R.B. is an Established Investigator of the American Heart Association.

REFERENCES

1 R. L. Schanarr and H. V. Sparks, *Am. J. Physiol*, 223 (1972) 223.
2 S. Moric, A. C. Ngain and H. R. Winn, *J. Cereb. Blood Flow Metab.*, 6 (1986) 34.
3 R. H. Verhalghe and P. M. Vanhoutte, *Circ. Res.*, 40 (1977) 208.
4 P. C. Churchil and A. Bidani, *Am. J. Physiol.*, 252 (1987) F299.
5 M. Miyamota, Y. Yagil, T. Larson, C. Robertson and R. L. Jamison, *Am. J. Physiol.*, 255 (1988) F1230.
6 W. S. Spielman and C. I. Thompson, *Am. J. Physiol.*, 242 (1982) F423.
7 J. Schrader, in R. M. Derne, T. W. Rall and R. Rulio (Editors), *Regulatory Functions of Adenosine*, Martinus Nijhoff, Boston, 1983, p. 133.
8 E. Juengling and H. Kammermeier, *Anal. Biochem.*, 102 (1980) 358.
9 D. W. Neirenberg, A. L. Pogolotti, Jr. and D. V. Santi, *J. Chromatogr.*, 190 (1980) 212.
10 B. Levitt, R. J. Head and D. P. Westfall, *Anal. Biochem.*, 137 (1984) 93.
11 G. Crescentini and V. Stocchi, *J. Chromatogr.*, 290 (1984) 393.
12 G. K. Bedford and M. A. Chiong, *J. Chromatogr.*, 305 (1984) 183.
13 Z. Olempska-Beeer and E. B. Freese, *Anal. Biochem.*, 140 (1984) 236.
14 M. E. Chamberlin, A. Lefurgey and L. J. Mandel, *Am. J. Physiol.*, 247 (1984) F955.
15 O. H. Lowry, N. J. Rosenbrough, A. L. Farr and R. J. Randall, *J. Biol. Chem.*, 193 (1951) 265.
16 J. H. Zar, in W. D. McElroy and C. P. Swanson (Editors), *Biostatistical Analysis*, Prentice-Hall, Englewood Cliffs, NJ, 1974, pp. 151–162.
17 V. Stocchi, L. Cucchiarini, M. Magnani, L. Chiarantini, P. Palma and G. Crescentini, *Anal. Biochem.*, 146 (1985) 118.
18 D. DeKorte, W. A. Haverkort, A. H. Van Gennip and D. Roos, *Anal. Biochem.*, 147 (1985) 197.
19 S. S. Yang and R. K. Gilipin, *Anal. Chem.*, 59 (1987) 2750.
20 J. Stahlberg and I. Hagglund, *Anal. Chem.*, 60 (1988) 1958.
21 H. Baumgarte, H. P. Leichtweiss, D. W. Lubbers, C. H. Weiss and H. Huland, *Microvascular Res.*, 4 (1972) 247.

Journal of Chromatography, 536 (1991) 273–282
Elsevier Science Publishers B.V., Amsterdam

CHROMSYMP. 2039

High-performance liquid chromatographic detection of hydroxylated benzoic acids as an indirect measure of hydroxyl radical in heart: its possible link with the myocardial reperfusion injury

DIPAK K. DAS* and GERALD A. CORDIS

Cardiovascular Division, Department of Surgery, University of Connecticut School of Medicine, Farmington, CT 06030 (U.S.A.)

PARINAM S. RAO

Department of Cardiothoracic Surgery, Long Island Jewish Medical Center, Albert Einstein Medical Center, New Hyde Park, NY 11042 (U.S.A.)

and

XIEKUN LIU and SWAPNA MAITY

Cardiovascular Division, Department of Surgery, University of Connecticut School of Medicine, Farmington, CT 06030 (U.S.A.)

ABSTRACT

The present report describes a method suitable for the indirect assay of hydroxyl radical ($OH^{\cdot}$), which is likely to be produced during reperfusion of ischemic myocardium. Isolated rat heart perfused by the Langendorff technique was subjected to 30 min of ischemia, followed by 30 min of reperfusion. Salicylic acid (2 m*M*) was added to the perfusion circuit to trap any $OH^{\cdot}$ radical generated during the experiment. 2,5- and 2,3-dihydroxybenzoic acids (hydroxylated products of salicylic acid) were identified by authentic standards as well as by pure $OH^{\cdot}$-generating system using high-performance liquid chromatography with electrochemical detection. In addition to serving as a chemical trap for the detection of $OH^{\cdot}$, salicylate attenuated myocardial reperfusion injury as evidenced by reduced formation of creatine kinase, decreased lipid peroxidation, and improved myocardial contractile functions during reperfusion. These results thus provide direct evidence for the presence of $OH^{\cdot}$ in heart and link it to the myocardial reperfusion injury.

INTRODUCTION

Oxygen-derived free radicals have been linked to ischemic and reperfusion injury in a variety of tissues including heart [1–5]. Once these free radicals are formed, they presumably attack the polyunsaturated fatty acids of membrane phospholipids and cause lipid peroxidation [6,7], which has been accepted as an indirect, yet presumptive, marker for free radical production [8–10]. Recently, electron paramagnetic resonance spectrometry (EPR) has been used to directly demonstrate the presence of these free radicals. To date, the EPR method remains the only method of choice for this purpose [11–14].

0021-9673/91/$03.50

However, there are certain disadvantages regarding the use of EPR. First, it is very expensive and is not readily available to many investigators. Second, chemical interconversions between spin-trap radical adducts occasionally lead to confusion in properly identifying radical species. Third, interpretation of the data is extremely difficult and frequently computer assistance is essential. Finally, and most importantly, oxygen free radicals may be generated in biological tissues in such small quantities that they are overpowered by other free radical signals, making the proper identification difficult.

During recent years, a number of investigators, including Floyd *et al.* [15], Grootveld and Halliwell [16], and Pritsos *et al.* [17], described high-performance liquid chromatography (HPLC) methods to detect oxygen-free radicals. These methods are easily adaptable, and some of them are extremely sensitive in detecting very low levels of hydroxyl radical ($OH^{\cdot}$). We have adapted one of these methods using salicylate to trap $OH^{\cdot}$ and subsequent analysis of the hydroxylated products by HPLC using an electrochemical detector as our method of choice to confirm the role of $OH^{\cdot}$ in myocardial ischemic and reperfusion injury.

MATERIALS AND METHODS

Materials

All chemicals used in this study were of analytical grade. Salicylic acid and its hydroxylated derivatives, 2,3-dihydroxybenzoic acid (2,3-DHBA) and 2,5-dihydroxybenzoic acid (2,5-DHBA), were obtained from the Aldrich (Milwaukee, WI, U.S.A.). Dimethyl thiourea (DMTU), dimethyl sulfoxide (DMSO), hypoxanthine, and xanthine oxidase (XO) were all purchased from Sigma (St. Louis, MO, U.S.A.). Water was purified with a Milli-Q filtration system (Millipore, Bedford, MA, U.S.A.). Chelex resin was obtained from Bio-Rad (Richmond, CA, U.S.A.). All of the solutions were made up in Chelex-treated Milli-Q water, unless mentioned otherwise.

Methods

Preparation of isolated heart. Male Sprague-Dawley rats weighing 250–300 g were anesthetized with an intravenous injection of sodium pentobarbital (6.5 mg/100 g). Hearts were removed and perfused with Krebs-Henseleit bicarbonate buffer equilibrated with a gas mixture of 95% oxygen and 5% carbon dioxide (pH 7.4), using Langendorff's non-recirculating mode [18]. Heart was perfused for 15 min at 37°C in the presence of 2 m*M* salicylate at 100 cm water perfusion pressure for stabilization. Flow was reduced to about 0.1 ml/min, and the heart was rendered ischemic for 30 min. Following 30 min of ischemia, reperfusion was performed for 30 min with non-recirculating Krebs-Henseleit bicarbonate buffer containing 2 m*M* salicylate.

To monitor the myocardial functions during the experiment, a polyethylene catheter was inserted into the left ventricle through the apex. This, in turn, was connected to a Model P23 pressure transducer (Gould Inc., Oxnard, CA, U.S.A.) to measure left ventricular developed pressure (LVDP) and its first derivative (LV$dp/dt$), as described previously [5].

Myocardial cellular injury was monitored by assaying the release of creatine kinase (CK) from heart. CK was assayed enzymatically using an assay kit obtained from Sigma [5].

The extent of lipid peroxidation was measured in the perfusate buffer by assaying malondialdehyde (MDA) formation as described previously [10]. In brief, 1 ml of perfusate was treated with 1 ml of ice-cold 30% $HClO_4$ and 1 ml of 0.75% thiobarbituric acid (TBA) dissolved in 0.5% sodium acetate. The samples were boiled for 20 min and centrifuged to remove the pellet. The color of the supernatant was read at 535 nm. The concentration of the supernatant was measured using a molar extinction coefficient of 156 mM^{-1} cm^{-1}.

To examine whether the generated free radical was indeed $OH^{\cdot}$, parallel experiments were performed by simultaneously adding a specific scavenger of $OH^{\cdot}$ (deferoxamine) along with salicylate. The experiments were terminated at different points: prior to ischemia, after 30 min of ischemia, and after 1, 2, 5, 15 and 30 min of reperfusion. At least ten experiments were performed for each time frame. Perfusates and hearts were processed as described below.

Subcellular fractonation of heart. Hearts were homogenized in Krebs-Henseleit bicarbonate buffer using a Polytron homogenizer (Brinkman, NY, U.S.A.). The homogenate was centrifuged at 100 *g* to remove nuclear debris. The supernatant was then centrifuged at 10 000 *g* to collect mitochondria. Mitochondria-free supernatant was centrifuged at 100 000 *g* to precipitate microsomal fraction. Mitochondria (500–6500 *g*) and microsomes (10 000–100 000 *g*) were further purified by repeated precipitation and washing as described elsewhere [19]. Marker enzymes were assayed to judge the purity of the preparation [20]. Nuclear fraction was purified by sucrose density gradient as described previously [20].

Analyis of hydroxylated benzoic acids by HPLC. Each subcellular fraction as well as whole homogenate were suspended in 1 ml Tris–sucrose buffer and 800 μl homogenate was treated with 40 μl 3 *M* hydrochloric acid. The precipitate was removed by centrifugation and the supernatant was filtered though Rainin nylon-66 membrane filter (0.22 μm pore size) (Rainin, Woburn, MA, U.S.A.). To examine the presence of hydroxylated benzoic acids in the perfusate buffer, 1 ml of the perfusate was similarly treated. A 20-μl volume of the sample was injected onto an Altex Ultrasphere 3 μm ODS (75 mm × 4.6 mm) (Rainin) equipped in a Waters Assoc. (Millford, MA, U.S.A.) HPLC unit consisting of a Model 510 pump and a Model 460 electrochemical detector. 2,5-DHBA and 2,3-DHBA (hydroxylated products of salicylic acid after interaction with $OH^{\cdot}$ were eluted by buffer containing 0.03 *M* sodium acetate and 0.03 *M* citric acid (pH 3.6) at a flow-rate of 1 ml/min [21]. The detection potential was maintained at 0.6 V, employing the Ag/AgCl reference electrode. Peaks were identified by authentic standards as well as by injecting the hydroxylated products of salicylic acid from a pure $OH^{\cdot}$-generating system [7].

Statistical analysis. For comparison between two groups, the Student's *t*-test was used for the statistical analysis. For the comparison between several independent groups, analysis of variance followed by Scheffe's test was performed. Results were considered significant when $p < 0.05$.

RESULTS

Generation of $OH^{\cdot}$ during reperfusion of ischemic myocardium

Whole heart as well as each subcellular fraction were subjected to HPLC for the detection of $OH^{\cdot}$ radical by measuring hydroxylated benzoic acids. Both heart (Fig. 1)

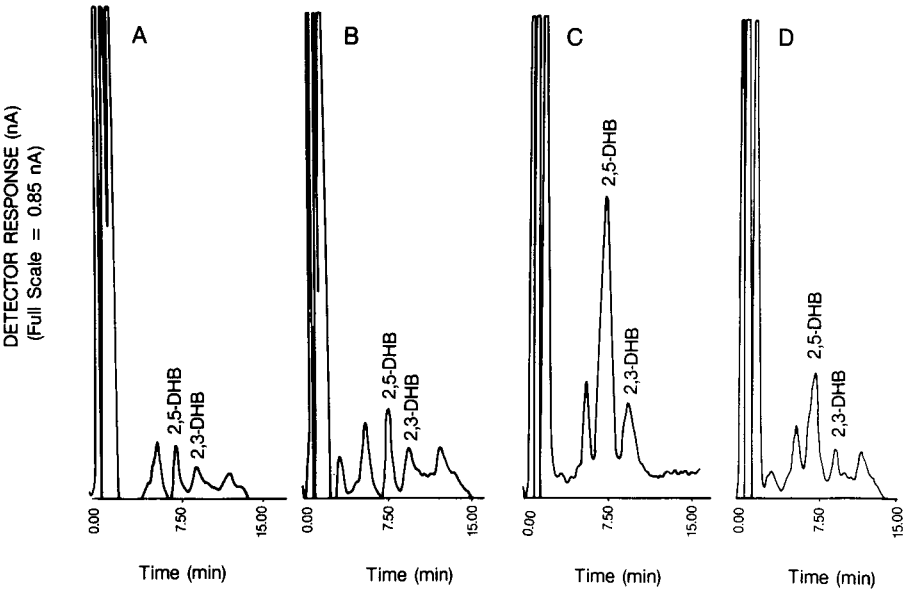

Fig. 1. Indirect detection of OH$^{\bullet}$ as 2,3- and 2,5-dihydroxybenzoic acid (DHB) in the ischemic and reperfused rat heart. (A) Isolated rat heart was perfused in the presence of 2 m*M* salicylate for 30 min; (B) Isolated rat heart was perfused in the presence of 2 m*M* salicylate for 15 min, and then the heart was made ischemic for 30 min; (C) Isolated rat heart was preperfused for 15 min, followed by 30 min of ischemia and 2 min of reperfusion. Salicylic acid (2 m*M*) was added to the perfusion circuit after ischemia and at the onset of reperfusion; (D) Isolated rat heart was preperfused for 15 min, followed by 30 min of ischemia. Ischemic heart was then reperfused for a further period of 2 min with a buffer containing 2 m*M* salicylate and 0.6 m*M* deferoxamine.

and mitochondrial fraction (not shown) demonstrated peaks during reperfusion corresponding to OH$^{\bullet}$ (Table I). The intensity of the 2,3- and 2,5-DHBA signals was higher in the mitochondria compared to that for the whole heart. The cell-free cytosolic fraction also exhibited a very small peak corresponding to OH$^{\bullet}$ (not shown). The peaks corresponding to the 2,3- and 2,5-DHBA signals were reduced significantly when hearts were perfused in the presence of deferoxamine, which inhibits OH$^{\bullet}$ formation by chelating free iron. This suggests that the DHBA signals generated in the reperfused hearts were indeed due to the formation of OH$^{\bullet}$.

We also examined the perfusate for the presence of 2,3- and 2,5-DHBA. In concert with the heart, perfusates from reperfused heart also demonstrated the presence of hydroxylated benzoic acid peaks when analyzed by HPLC (Table I). The intensities of these peaks, however, were smaller compared to those found in heart. These peaks were also completely abolished when hearts were preperfused in the presence of deferoxamine.

Analysis of OH$^{\bullet}$-salicylate reaction products by HPLC

To further confirm the identity of the hydroxylated benzoic acid signals found in heart and in perfusate samples, we produced pure OH$^{\bullet}$ radical from the reaction of hypoxanthine (100 μM), XO (8 mU),$FeCl_3$ (100 μM), and EDTA (100 μM). When these reactions were carried out in the presence of salicylate (2 m*M*) and injected into

TABLE I

GENERATION OF OH· IN ISCHEMIC MYOCARDIUM AS A FUNCTION OF THE DURATION OF REPERFUSION

Results are expressed as means ± S.E. of at least 5 experiments in each group. Generation of OH· is measured indirectly by measuring 2,3- and 2,5-DHBA using HPLC.

	Concentration of 2,3- and 2,5-DHBA (nmol/ml)				
	Duration of reperfusion (min)				
	1	2	5	15	30
Whole heart	0.69 ± 0.07	0.63 ± 0.05	0.47 ± 0.09	0.31 ± 0.06	0.18 ± 0.03
+ deferoxamine	0.16 ± 0.01	0.15 ± 0.02	0.09 ± 0.01	0.8 ± 0.01	0.08 ± 0.01
Mitochondrial fraction	2.11 ± 0.44	2.0 ± 0.39	1.65 ± 0.25	0.82 ± 0.17	0.30 ± 0.09
+ deferoxamine	0.11 ± 0.02	0.09 ± 0.01	0.10 ± 0.02	0.07 ± 0.01	0.08 ± 0.02
Perfusate	0.28 ± 0.05	0.27 ± 0.06	0.17 ± 0.04	0.09 ± 0.02	0.08 ± 0.02
+ deferoxamine	0.07 ± 0.02	0.07 ± 0.01	0.06 ± 0.02	0.05 ± 0.01	0.05 ± 0.02

the HPLC system, peaks for hydroxylated benzoic acids emerged at the identical positions having the same retention times (Fig. 2). Since OH· reacts with salicylic acid and produces 2,3-DHBA and 2,5-DHBA, we also analyzed the authentic standards of

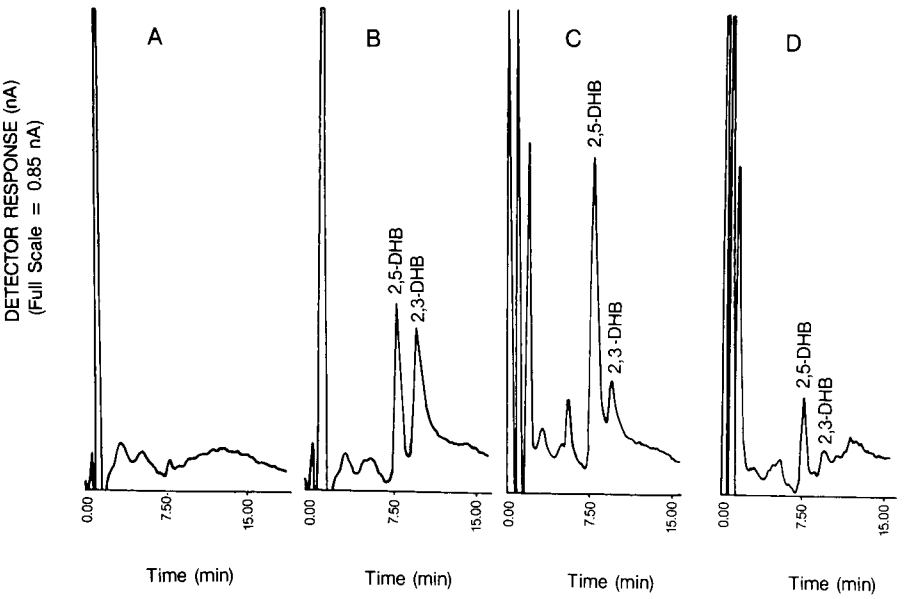

Fig. 2. Indirect *in vitro* detection of OH· radical as 2,3- and 2,5-dihydroxybenzoic acid (DHB) by the use of HPLC. (A) 25 μl of reaction blank: hypoxanthine + $FeCl_3$ + EDTA + salicylate; (B) 25 μl of 125 μM 2,5-DHB and 250 μM 2,3-DHB authentic standards; (C) 25 μl of chemically generated OH· (hypoxanthine + xanthine oxidase + $FeCl_3$ + EDTA) + salicylate; (D) Same reaction mixture as C + 0.6 mM deferoxamine.

these two hydroxylated benzoic acids. As show in Fig. 2, these two standards had identical retention times. Adding deferoxamine to the OH·-generating system removed these peaks completely. We also spiked the hydroxylated benzoic acid peaks obtained from the heart extract with authentic standards. The results shown in Fig. 3 demonstrate that these peaks indeed are identical with 2,5-DHBA and 2,3-DHBA.

Generation of OH· as a function of duration of reperfusion

Since oxygen free radicals are known to appear at the onset of reperfusion, we examined the presence of OH· by measuring 2,3- and 2,5-DHBA as a function of reperfusion time. As expected, OH· was reduced as reperfusion progressed (Table I). A slight reduction of hydroxylated benzoic acids was noted after 2 min of reperfusion in heart as well as in its mitochondrial fraction. Reduction of hydroxylated benzoic acid signals was significant after 15 and 30 min of reperfusion in both whole heart and mitochondria. The intensity of hydroxylated benzoic acids in the perfusate followed a different pattern. The amount of hydroxylated benzoic acids remained unchanged after 15 min of reperfusion. No hydroxylated benzoic acid signal was recovered from hearts after 30 min of reperfusion.

Effects of salicylate on myocardial preservation

Since the release of CK directly relates to cellular injury, the perfusate from perfused heart was assayed for the presence of CK activities. Release of this enzyme was markedly increased during reperfusion in both groups, as expected (Table II).

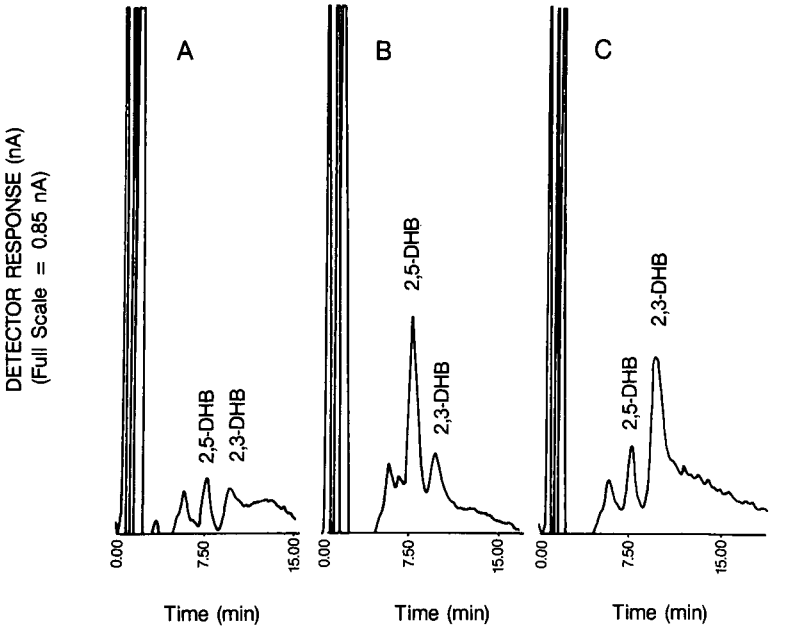

Fig. 3. 2,3- and 2,5-dihydroxybenzoic acid (DHB) in reperfused heart in the presence of spiked standards. (A) Isolated rat heart was perfused for 15 min in the presence of 2 m*M* salicylate; (B) Same as A, but spiked with 2,5-DHB authentic standard; (C) Same as A, but spiked with 2,3-DHB authentic standard.

TABLE II

EFFECTS OF SALICYLATE ON MYOCARDIAL CELLULAR INJURY, LEFT VENTRICULAR FUNCTIONS AND LIPID PEROXIDATION DURING ISCHEMIA AND REPERFUSION

Results are expressed as means ± S.E. of seven experiments in each group.

	CK Release[a] (IU/l)		LVDP[b] (mmHg)		LV Max dp/dt[b] (mmHg/s)		MDA[a] (nmol/g)	
	−sal[b]	+sal	−sal	+sal	−sal	+sal	−sal	+sal
Baseline	0.05 ± 0.04	0.07 ± 0.05	95 ± 2	92 ± 6	1298 ± 75	1177 ± 101	21.5 ± 2.2	20.3 ± 1.9
30 min ischemia	11 ± 2.5	10 ± 2.7	59 ± 7	57 ± 9	1005 ± 118	987 ± 135	24.1 ± 3.5	23.6 ± 2.8
30 min reperfusion	32 ± 5.2	17[c] ± 3.4	55 ± 4	68[c] ± 3	742 ± 89	1169[c] ± 78	62.7 ± 9.4	38.0[c] ± 7.6

[a] CK = Creatine kinase; MDA = malondialdehyde.
[b] LVDP = Left ventricular developed pressure; LV max dp/dt = maximum first derivative of left ventricular developed pressure; sal = salicylic acid.
[c] $p < 0.05$ compared to corresponding untreated group.

However, the amount of CK release was significantly lower in the salicylate group compared to the untreated control group.

Similarly, both LVDP and LV$dp/dt$ were decreased after ischemic insult and during reperfusion. Again, reduction in the left ventricular functions was sigificantly inhibited by salicylic acid, indicating the ability of salicylic acid to preserve myocardial contractile functions.

Malondialdehyde formation, a presumptive marker for lipid peroxidation, was also enhanced during reperfusion of ischemic myocardium in both groups. Similar to other parameters malondialdehyde formation was also lower in the salicylic acid group, suggesting that this compound interfered with $OH^{\cdot}$–lipid interaction.

DISCUSSION

Reports linking the oxygen-derived free radicals with myocardial ischemic and reperfusion injury are overwhelming [1–5]. However, direct evidence demonstrating oxygen free radicals as mediators of reperfusion injury has yet to be shown. Most of the evidence is based on the fact that reperfusion of ischemic myocardium is associated with the formation of malondialdehyde, a presumptive marker for lipid peroxidation [6,7], and that scavengers of free radicals such as superoxide dismutase (SOD) and catalase can attenuate reperfusion injury [22–24]. Although spin-trapping of the free radicals and subsequent determination by EPR confirmed their presence in reperfused heart [11–14], direct demonstration of linking these free radicals with reperfusion injury is not possible by this technique. Spin-trapped free radicals are still extremely short-lived, and they must be handled in a special way in order to show their presence with EPR.

The method described in this study utilized a chemical trap, such that the free radical interaction products are extremely stable and can be subjected to various treatments in order to study their direct role in reperfusion injury. The results of our study confirmed the previous reports concerning the presence of $OH^{\cdot}$ in the ischemic-reperfused heart and further demonstrated their presence in the perfusate, suggesting that $OH^{\cdot}$ is indeed formed during reperfusion of ischemic myocardium. In addition, this study demonstrated for the first time the presence of $OH^{\cdot}$ in the mitochondrial fraction of heart. The reduction of reperfusion injury by salicylic acid with the simultaneous presence of hydroxylated products strongly indicates a direct link of $OH^{\cdot}$ with myocardial reperfusion injury.

A substantial body of evidence now suggests that O_2^- produced initially from molecular oxygen undergoes dismutation, forming hydrogen peroxide as indicated below:

$$O_2 + e^- \rightarrow O_2^- \quad (1)$$

$$2O_2^- + 2H^+ \rightarrow O_2 + H_2O_2 \quad (2)$$

The O_2^- was thought to undergo a Haber-Weiss reaction in the presence of hydrogen peroxide, forming $OH^{\cdot}$:

$$O_2^- + H_2O_2 \rightarrow O_2 + OH^- + OH^{\cdot} \quad (3)$$

Although this reaction is thermodynamically feasible, and the overall stoichiometry is widely accepted under *in vitro* conditions, the reaction is kinetically very slow or even negligible. The modified reaction has been suggested to occur in two steps by iron-catalyzed Fenton-type reactions, as described below:

$$O_2^- + Fe^{3+} \rightarrow O_2 + Fe^{2+} \quad (4)$$

$$Fe^{2+} + H_2O_2 \rightarrow Fe^{3+} + OH^- + OH^\cdot \quad (5)$$

$$O_2^- + H_2O_2 \rightarrow O_2 + OH^- + OH^\cdot \quad (4+5)$$

With present technology, it is virtualy impossible to identify O_2^- in an *in vivo* system, even if it may be produced in mitochondia. O_2^- has a extremely short half-life which rapidly undergoes dismutation, yielding hydrogen peroxide. O_2^- than undergoes a Fenton-type reaction catalyzed by a metal ion such as iron(III). The exact source of iron to catalyze this reaction remains highly speculative [25]. A recent study from our laboratory suggested oxygen-carrying heme proteins as a potential source of iron [26].

Chemically generated $OH^\cdot$ radical (Fenton system), when allowed to react with salicylate, produces three different products: catechol, 2,3-DHBA, and 2,5-DHBA [16]. The hydroxylated benzoic acids can be detected in femtomoles using the above-described HPLC technique [15]. The rate constant of the interaction between $OH^\cdot$ and salicylate is about $5 \cdot 10^9$ to 10^{10} M^{-1} s^{-1} [27]. Because we used an isolated rat heart weighing approximately 1 g, 2 m*M* salicylic acid is expected to react with most of the $OH^\cdot$ formed in this system. Our results not only showed the presence of $OH^\cdot$ in the reperfused myocardium, but it further demonstrated that the mitochondrial fraction was the locus of free radical production. The intensity of generated $OH^\cdot$ drops as reperfusion progresses. The presence of hydroxylated benzoic acid products in the perfusate further suggests that $OH^\cdot$ is indeed formed in the heart during reperfusion, and that it leaches out of heart as a result of the washout.

The attenuation of reperfusion injury as indicated by the reduction of CK release and better preservation of myocardial contractile functions suggests that salicylic acid itself may have some cardioprotective effect. Furthermore, it reduced the extent of lipid peroxidation, indicating its effectiveness in interfering with free radical–lipid interactions. Salicylic acid is a well-known anti-inflammatory agent which functions by inhibiting cyclooxygenase pathway [28]. It is possible that the beneficial effects of salicylate observed during reperfusion of ischemic myocardium are due to its anti-inflammatory actions. However, at a rate constant on the order of $5 \cdot 10^9$ to 10^{10} M^{-1} s^{-1}, salicylate is likely to react with $OH^\cdot$ before it attacks any other compounds and functions by some other mechanisms. $OH^\cdot$ is extremely reactive, and it reacts with virtually almost any compound including lipids, proteins and nucleic acids. Breakdown of phospholipids and its peroxidation has been indicated in ischemic-reperfused myocardium [29]. Lipid peroxidation is presumably one of the major causes for myocardial dysfunction observed during reperfusion.

The major finding of this study is that salicylate can be used as a chemical trap to demonstrate the presence of $OH^\cdot$ in the pathogenesis of myocardial reperfusion injury. The attenuation of reperfusion injury with salicylate in concert strongly suggests a direct link of $OH^\cdot$ as a mediator of reperfusion injury.

ACKNOWLEDGEMENTS

This study was supported by USPHS NIH HL 22559, HL 33889 and HL 34360, and by a grant from the United States Department of the Navy. We are grateful to Joanne D'Aprile for her skillful secretarial assistance.

REFERENCES

1 D. N. Granger, M. E. Höllwarth and D. A. Parks, *Acta Physiol. Scand.*, suppl. 548 (1986) 47–63.
2 J. H. Kramer, C. M. Arroyo, D. F. Dickens and W. B. Weglicki, *Free Radical Biol. Med.*, 3 (1987) 153–159.
3 I. E. Blasig, B. Ebert, G. Wallukat and H. Loewe, *Free Radical Res. Common.*, 6 (1989) 303–310.
4 D. K. Das, R. M. Engelman, J. A. Rousou, R. H. Breyer, H. Otani and S. Lemeshow, *Basic Res. Cardiol.*, 81 (1986) 155–166.
5 H. Otani, R. M. Engelman, J. A. Rousou, R. H. Breyer, S. Lemeshow and D. K. Das, *Circulation*, 76 (suppl. V) (1987) 161–167.
6 J. F. Mead, *Free Radicals in Molecular Biology, Aging and Disease*, Raven Press, New York, 1984, pp. 53–66.
7 H. Otani, R. M. Engelman, J. A. Rousou, R. H. Breyer and D. K. Das, *J. Mol. Cell. Cardiol.*, 18 (1986) 953–961.
8 F. Z. Meerson, V. E. Kagan, Y. P. Kozlov, L. M. Belkina and Y. V. Arkhipenko, *Basic Res. Cardiol.*, 77 (1982) 465–485.
9 D. K. Das, R. M. Engelman, D. Flansaas, H. Otani, J. Rousou and R. H. Breyer, *Basic Res. Cardiol.*, 82 (1987) 36–50.
10 T. F. Slator, *Biochem. J.*, 222 (1984) 1–15.
11 J. E. Baker, C. C. Felix, G. N. Olinger and B. Kalyanaraman, *Proc. Natl. Acad. Sci. U.S.A.*, 85 (1988) 2786–2789.
12 R. Bolli, B. S. Patel, M. O. Jeroudi, E. K. Lai and P. B. McCay, *J. Clin. Invest.*, 82 (1988) 476–485.
13 D. J. Hearse and A. Tosaki, *J. Cardiovasc. Pharmacol.*, 9 (1987) 641–650.
14 D. K. Das, R. M. Engelman, R. Clement, H. Otani, M. R. Prasad and P. S. Rao, *Biochem. Biophys. Res. Commun.*, 148 (1987) 314–319.
15 R. A. Floyd, R. Henderson, J. J. Watson and P. K. Wong, *Free Radic. Biol. Med.*, 2 (1986) 13–18.
16 M. Grootveld and B. Halliwell, *Biochem. J.*, 237 (1986) 499–504.
17 C. A. Pritsos, P. P. Constantinides, T. R. Trilton, D. C. Heimbrook and A. C. Sartorell, *Anal. Biochem.*, 150 (1985) 294–299.
18 B. N. Srimani, R. M. Engelman, R. Jones and D. K. Das, *Circ. Res.*, 66 (1990) 1535–1543.
19 D. K. Das, R. M. Engelman, J. A. Rousou, R. H. Breyer, H. Otani and S. Lemeshow, *Am. J. Physiol.*, 251 (1986) H71–H79.
20 D. K. Das and H. Steinberg, *Am. J. Physiol.*, 248 (1985) E58–E63.
21 R. A. Floyd, C. A. Lewis and P. K. Wong, *Methods Enzymol.*, 105 (1984) 231–237.
22 H. Otani, R. M. Engelman, J. A. Rousou, R. H. Breyer, S. Lemeshow and D. K. Das, *J. Thorac. Cardiovasc. Surg.*, 91 (1986) 290–295.
23 C. L. Myer, S. J. Weiss, M. M. Kirsh, B. M. Shepard and M. Shlafer, *J. Thorac. Cardiovasc. Surg.*, 91 (1986) 281–289.
24 S. W. Werns, M. J. Shea, S. E. Mitsos, R. C. Dysko, J. C. Fantone, M. A. Schork, G. D. Abrams, B. Pitt and B. R. Lucchesi, *Circulation*, 73 (1986) 518–524.
25 C. E. Thomas, L. A. Morehouse and S. D. Aust, *J. Biol. Chem.*, 260 (1985) 3275–3280.
26 M. R. Prasad, R. M. Engelman, R. M. Jones and D. K. Das, *Biochem. J.*, 263 (1989) 731–736.
27 K. D. Hiller, P. L. Hodd and R. L. Wilson, *Chem. Biol. Interact.*, 47 (1983) 293–305.
28 T. M. Brody, *Ann. Soc. Pharmacol. Exp. Ther.*, 115 (1955) 39–51.
29 D. K. Das and R. M. Engelman, *Oxygen Radicals: Systemic Events and Disease Processes*, S. Karger, Basel, 1989, pp. 97–120.

Journal of Chromatography, 536 (1991) 283–288
Elsevier Science Publishers B.V., Amsterdam

CHROMSYMP. 2036

Determination of 3-methylhistidine in hydrolysed proteins by fluorescamine derivatization and high-performance liquid chromatography

L. DALLA LIBERA
CNR Unit of Muscle Biology and Physiopathology, Institute of General Pathology, University of Padova, Via Trieste 75, 35131 Padova (Italy)

ABSTRACT

A method is described for the determination of the 3-methylhistidine content in myofibrilar proteins (myosin and actin) using reversed-phase high-performance liquid chromatography with ultraviolet detection. Proteins were hydrolysed and free amino acids were derivatized with fluorescamine. Elution was performed isocratically with acetonitrile–water (24:76). This method allows the detection of picomole amounts of 3-methylhistidine in myosin and actin.

INTRODUCTION

The unusual amino acid 3-methylhistidine (3MH) is present in the myofibrillar proteins myosin and actin [1,2]. It has been shown that the methyl group is added after the histidine residue has been incorporated into the polypeptide chains [3]. The 3MH content of actin appears to be much more constant than is the case with myosin. In fact, 3MH is present in about the same amount in all the actins so far analysed [1]. In contrast, 3MH is present in adult white skeletal muscle mysosin and is absent from cardiac and slow muscle myosins and from white skeletal muscle myosin of newborn animals [4]. With the methods so far available, large amounts of protein are necessary for 3MH detection [1] and then it is impossible or very difficult to work with small amounts of material when, for example, human biopsies are to be analysed. For this purpose we have separated and detected 3MH utilizing high-performance liquid chromatography (HPLC) in hydrolysates of nanomole amounts of actin and myosin isolated from rat and rabbit muscles. The method used here was originally described by Wassner and co-workers [5,6] for 3MH determination in plasma and urine and in this work it was adapted to protein hydrolysates. The results obtained for rabbit actin and myosin are in good agreement with those reported in the literature. Further, we have determined for the first time the 3MH content of myosins isolated from rat muscles.

0021-9673/91/$03.50

EXPERIMENTAL

Reagents

Histidine, 3-methylhistidine, N-methyllysine and fluorescamine were obtained from Sigma (St. Louis, MO, U.S.A.). The amino acid standard was from Bio-Rad Labs. (Richmond, CA, U.S.A.). Acetonitrile (HPLC grade), thiodiglycol, *n*-caprylic acid and perchloric acid were purchased from Carlo Erba (Milan, Italy). Glass-distilled water was filtered through a 0.45-μm Millipore filter before use.

Proteins preparation

Myosin was prepared from rabbit and rat muscles according to Dalla Libera *et al.* [7]. Actin was prepared from rabbit muscle according to Leadbeater and Perry [8].

About 1 mg of purified protein was precipitated with 10% trichloroacetic acid, washed with ethanol and diethyl ether and hydrolysed for 22 h in 6 *M* HCl at 110°C under vacuum. Then the vials were opened and the HCl was removed with a rotary evaporator connected to a water pump. The hydrolysate was solubilized in a small amount (0.2–0.4 ml) of a buffer which contained 67 m*M* sodium citrate–0.63 m*M* *n*-caprylic acid–48 m*M* thiodiglycol (pH 2.2) and filtered through a 0.22-μm filter.

Preparation of derivatives

Standard solutions of histidine, 3-MH and N-methyllysine of 1 μmol/ml were prepared. The amino acid standard was diluted 1:10 with water to a concentration of about 5 μmol/ml total amino acid. Fluorescamine derivatives were prepared using standards or hydrolysed protein according to Wassner *et al.* [5]. Briefly, to 100 μl of standards or hydrolysed protein were added 250 μl of sodium borate solution (0.8 *M* boric acid adjusted to pH 12.2 with NaOH). Then 250 μl of fluorescamine solution (160 mg per 100 ml in acetonitrile) were added with vigorous agitation. After the addition of 35 μl of concentrated perchloric acid the sample were incubated at 80°C for 1 h. After cooling at room temperature 100 μl of 0.5 *M* morpholinopropanesulphonic acid (MOPS) in 3 *M* NaOH were added to the samples just before analysis. Aliquots of 20–30 μl of the resulting solution were injected into the HPLC system.

Apparatus

A Perkin-Elmer (Norwalk, CT, U.S.A.) Series 3B HPLC system was used. A Sigma 10 data station was employed. Separation was achieved with a μBondapak C_{18} (Waters Assoc., Milford, MA, U.S.A.) or RP-8 and RP-18 (Merck, Darmstadt, F.R.G.) of Rosil C_{18} (Alltech, Deerfield, IL, U.S.A.). All columns were 25 cm × 0.46 cm I.D. A guard obtained from Upchurch (Oak Harbour, WA, U.S.A.) was always used to protect the main column. Elution was performed isocratically with acetonitrile–water (24:76) at 1.5 ml/min at room temperature. The derivative can be monitored either at 254 nm (Fig. 1) or 365 nm (Fig. 2); we prefer the latter wavelength as it results in clearer chromatograms, especially in the 3MH area. Peak areas were quantitated by the method of external standardization using 3MH. The molecular weights of actin and myosin were assumed to be 45 and 500 kilodalton, respectively.

RESULTS

Fig. 1A shows a chromatogram of 1360 pmol of 3MH. After a large early-eluting peak and a minor peak at about 10 min, which are also present in all blank runs, a large

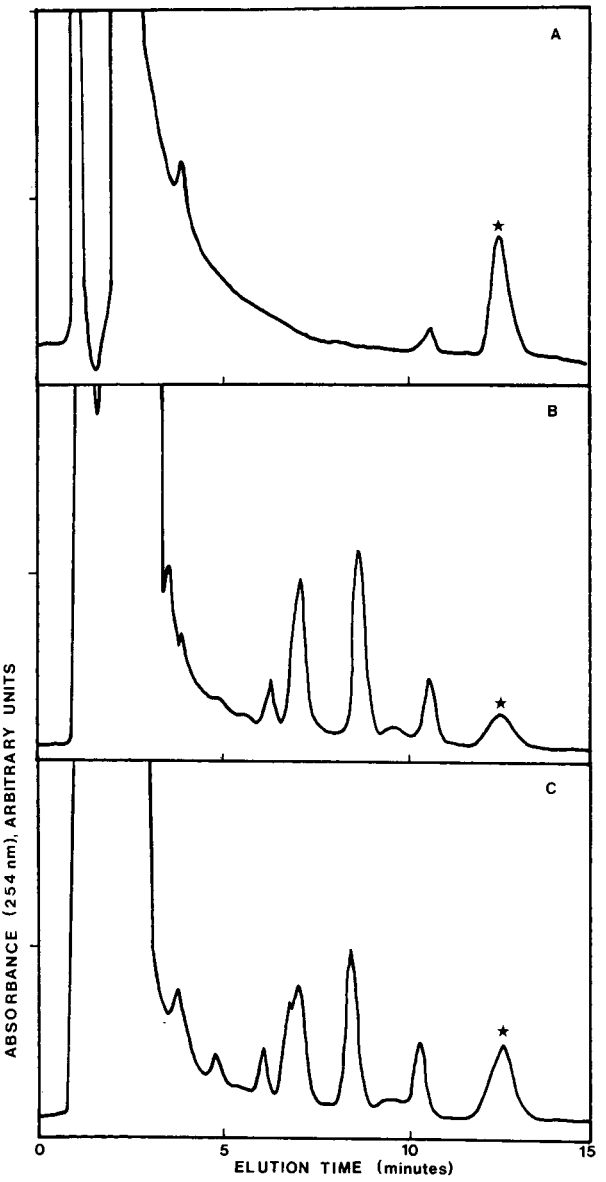

Fig. 1. Chromatograms of 3-methylhistidine from a standard solution and an actin sample. (A) 1360 pmol of 3MH standard; (B) 30 μl of actin prepared as described in the text, containing 520 pmol of 3MH; (C) 30 μl of actin (520 pmol of 3MH) and 680 pmol of 3MH standard. The effluents were monitored at 254 nm. The asterisk indicates the 3MH peak.

peak elutes at about 12–13 min. This peak correspond to the 3MH fluorescamine derivative. Peak areas were linear over the range *ca.* 100–1500 pmol. The reproducibility was 1.5%. Fig. 1B shows a chromatogram of an actin sample hydrolysate. In addition to the blank and 3MH peaks, other unidentified peaks are seen. These peaks, which do not correspond to any of the amino acids present in the amino acid standard, may be the result of degradation products of fluorescamine. The identification of the 3MH peak in the actin chromatogram was based not only on retention times but also on standard addition experiments. In Fig. 1C such an elution is show and it is evident that the area of the peak corresponding to 3MH is enhanced by the adding 3MH. We observed that the best separations were obtained using the μBondapak C_{18} or Rosil C_{18} columns.

Fig. 2 shows representative chromatograms for the detection of 3MH in myosins from different rat muscles. As with actin hydrolysates, several peaks elute before 3MH. However, the area where 3MH elutes is sufficiently clear for it to be identified. As it is well known that myofibrillar proteins contain large amounts of histidine and also lysines methylated to a variable extent [2,9], hystidine and N-methyllysine were derivatized and chromatographed as described under Experimental section. No peak was visible in the elution time range of 3MH (results not shown). Moreover, to rule out the possibility that artifacts originating during the hydrolysis procedure might affect the 3MH area in subsequent chromatograms, proteins that do not contain 3MH, *viz.*, casein, albumin, trypsin and chymotrypsin, were treated exactly as the myofibrillar protein samples. Again, no peak in the position of 3MH was visible during the chromatographic separation (results not shown).

In Table I are reported the concentrations of 3MH determined in rat and rabbit actin and several myosin of different muscles of rat and rabbit. The values (0.8 residues per mole) for actins determined with the assay here reported are close to those calculated with conventional nynhydrin-based amino acid analysers either from total protein hydrolysates [1,2,4] or in sequence studies [10].

As far as rabbit myosin is concerned, myosin prepared from fast-contracting muscle (adductor) contains about two residues of 3MH per molecule (one residue per heavy chain) whereas myosin prepared from slow-contracting muscle (soleus) does not contain 3MH. The results are in agreement with the data reported previously [2]. With rat myosin we found that the pattern of distribution of 3MH is similar to that observed in the rabbit. In fact, predominantly fast-contracting muscles, *i.e.*, the masseter and the EDL, contain about 1.5 residues of 3MH. Interestingly, the 3MH content of myosin from the diaphragm, which is a mixed muscle (fast and slow), was less than that observed for a pure fast muscle, 0.9 *vs.* 1.4 residues per mole, respectively.

DISCUSSION

The method described here was first used for the detection of 3MH in urine and plasma [5,6]. In this work it was used for the identification of 3MH in a mixture of amino acids obtained from the acidic hydrolysis of small amounts (less than 1 mg) of the two major myofibrillar proteins, actin and myosin. It is evident that in the case of protein hydrolysates the fluorescamine derivatization is achieved on the condition that the pH of the solution is not acidic. In fact, it is known that the reaction of amino acids with fluorescamine takes place only at alkaline pH [11]. For this reason, it is necessary

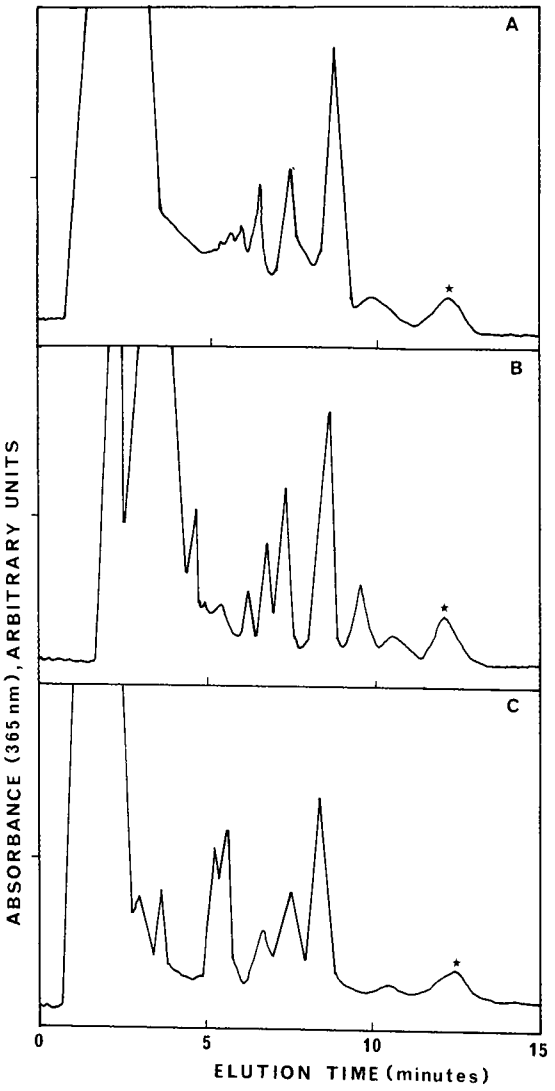

Fig. 2. Chromatograms of 3-methylhistidine from rat myosin samples. (A) Diaphragm muscle; (B) extensor digitorum longus muscle; (C) embryonic muscles. The effluents were monitored at 365 nm. The asterisk indicates the 3MH peak.

to dry the acidic hydrolysates with a vacuum evaporator in order to eliminate all the HCl present.

When less than 30 nmol of actin are available (1 mg), it is possible to perform the hydrolysis and the subsequent derivatization with florescamine and obtain a measurable peak of 3MH on the chromatogram. The values so obtained are in good agreement with the data reported previously [1,2,4,10], indicating that no interfering component, such as histidine, contributes to the 3MH peak area.

We have applied this method to the study of the other major myofibrillar

TABLE I

3MH CONTENTS OF MYOFIBRILLAR PROTEINS

Sample	3MH concentration[a]	Literature value
Actin (rabbit)	0.75 (6)	1.0 [1,2,4,10]
Actin (rat)	0.8 (2)	
Myosin (rabbit):		
Adductor muscle	1.6 (1)	1.5 [2,4]
Soleus muscle	0 (2)	0 [2,4]
Myosin (rat):		
Masseter muscle	1.4 (2)	
Extensor digitorum longus muscle	1.3 (2)	
Diaphragm muscle	0.9 (3)	
Embryonic muscle	0.8 (2)	

[a] Values are expressed as residues of 3MH per mole. The number of observations is given in parentheses.

protein, *i.e.*, myosin. We investigated the 3MH content of myosin not only from already studied tissues such as rabbit fast and slow muscles, but also from a yet unstudied species, the rat. In this latter instance the limiting factor is the amount of available starting material, which is too low to perform the analysis of 3MH with conventional ion-exchange chromatographic techniques.

In conclusion, the method appears particularly suitable for the rapid evaluation of 3MH at picomole levels in actin and myosin available in small amounts as in the case of small muscles or biopsies.

ACKNOWLEDGEMENTS

The skilful technical assistance of Mr. S. Belluco is gratefully acknowledged.

REFERENCES

1 P. Johnson and S. V. Perry, *Biochem. J.*, 119 (1970) 293–298.
2 W. M. Kuehl and R. S. Adelstein, *Biochem. Biophys. Res. Commun.*, 39 (1970) 956–964.
3 V. R. Young, S. D. Alexis, B. S. Baliga and H. N. Munro, *J. Biol. Chem.*, 247 (1972) 3592–3600.
4 G. Huszar, *Nature New Biol.*, 240 (1972) 260–264.
5 S. J. Wassner, L. Schlitzer and J. B. Li, *Anal. Biochem.*, 104 (1980) 284–289.
6 J. B. Li and S. J. Wassner, *Kidney Int.*, 20 (1981) 321–325.
7 L. Dalla Libera, A. Margreth, I. Mussini, C. Cerri and G. Scarlato, *Muscle Nerve*, 1 (1978) 280–291.
8 L. Leadbeater and S. V. Perry, *Biochem. J.*, 87 (1963) 233–238.
9 M. F. Hardy, C. I. Harris, S. V. Perry and D. Stone, *Biochem. J.*, 120 (1970) 653–660.
10 M. Elzinga, J. H. Collins, W. M. Kuehl and R. S. Adelstein, *Proc. Natl. Acad. Sci. U.S.A.*, 70 (1973) 2687–2691.
11 S. Udenfriend, S. Stein, P. Bohlen, W. Dairman, W. Leimgruber and M. Weigle, *Science*, 178 (1972) 871–872.

Journal of Chromatography, 536 (1991) 289–301
Elsevier Science Publishers B.V., Amsterdam

CHROMSYMP. 2002

Refractive index gradient detection of biopolymers separated by high-temperature liquid chromatography

CURTISS N. RENN and ROBERT E. SYNOVEC*
Center for Process Analytical Chemistry, Department of Chemistry, BG-10, University of Washington, Seattle, WA 98195 (U.S.A.)

ABSTRACT

A refractive index gradient (RIG) detector has been successfully applied in both mobile phase gradient (MPG) and thermal gradient (TG) microbore liquid chromatography (μLC). The RIG detector is based upon probing the radial RIG of the material passing through a small-volume *z*-configuration flow cell with a 390-μm internal radius. The optimum RIG sensitivity was at a position of 225 μm offset parallel to the flow cell center axis. This optimum position was probed by a 200-μm diameter collimated laser beam produced by fiber optic techniques. The performance of MPG-μLC and TG-μLC with RIG detection was evaluated using mixtures of *n*-alkanes and 1,2-diacylphosphatidylcholines (a class of phospholipid biopolymers). Baseline drift for the gradient separations was found to be quite small, in contrast to the performance one would obtain using conventional RI detection. Furthermore, the detection limit for the integrated RIG signal was routinely $2 \cdot 10^{-8}$ RI units ($3 \times$ baseline root mean square noise). The technique of TG-μLC with RIG detection was found to dramatically reduce the analysis time for the biopolymer separation, while providing detection limits below 100 ng injected phospholipid.

INTRODUCTION

High-temperature–high-performance liquid chromatography (HT-HPLC) is gaining interest as a useful technique for rapidly separating large molecules [1]. The rapid analysis of complex biopolymer samples by HPLC also requires a suitable detector. The analytical challenge is in developing new techniques and instrumentation to meet the need of rapid and confident quantitative analysis in the biotechnology field. While isocratic separations are straightforward, the need to optimize the information content per unit time necessitates the application of gradient elution HPLC [2]. The traditional approach in HPLC employs a mobile phase gradient (MPG), minimally a time-dependent mixing of two solvents of differing elution strength. The need for both rapid separation and rapid recovery to initial mobile phase conditions in the column may make thermal gradient (TG) elution in LC an useful alternative to the conventional MPG, where temperature instead of mobile phase composition is changed with time [3]. One of the experimental considerations in TG elution is the requirement for rapid thermal "equilibration" of the column as

0021-9673/91/$03.50

a function of temperature. Microbore columns meet this requirement, thus the technique of thermal gradient microbore liquid chromatography (TG-μLC) should be well suited for rapid process analysis of biopolymers.

Detection of biopolymers and related species separated by HPLC has been difficult, since many analytes of interest do not exhibit an useful chromophore, inhibiting direct absorbance and fluorescence detection [4]. While derivatization with a chromophore is possible, the approach is often time consuming and compatibility with gradient elution is seldom developed. The conventional refractive index (RI) detector is not compatible with either MPG-μLC or TG-μLC primarily due to two factors. First, large baseline drifts result from the detection mechanism, *i.e.*, the bulk RI of the effluent is measured [5]. Second, the need to minimize band broadening prohibits the application of sequential differential RI detection [6,7]. Nonetheless, the universal nature of the RI detector response is appealing. To solve many of these deficiencies, a mass detector based upon light scattering from non-volatile solute particles following preferential evaporation of the mobile phase (solvent) has been developed [8,9]. The mass detector works quite well for MPG-μLC separations for several biopolymer samples, but is hampered by the requirement that the mobile phase be volatile to function properly, thus mobile phase selection is generally limited to volatile organics, precluding the application of popular aqueous buffers. Indirect detection also provides universal detection of analytes with absolute quantitation [10,11]. While indirect detection may also prove useful for gradient elution μLC, demonstration has not been reported and baseline stability may be a problem. All of the previously mentioned detectors have not been hyphenated to TG-μLC, although work in this direction might prove fruitful once the technical problems have been addressed [3], as is the focus of the work reported here.

A sensitive universal detector that is readily amenable to both MPG-μLC and TG-μLC, and can be applied in conjunction with popular aqueous buffers, would be quite useful for many biopolymer separations. The refractive index gradient (RIG) detector, which is not to be confused with the conventional RI detector, meets these criteria. While the RIG detector development has a complicated past, the first report was made by Betteridge *et al.* [12] where the authors provided a concise, yet qualitative, description of the detection mechanism. Later, Pawliszyn [13–15] provided a more detailed description of a RIG detector for HPLC, where the RIG along the direction of the effluent flow (axial) is probed. The RIG detector that we have been developing [16–18] involves carefully probing the radial concentration gradient [12,19], not the axial concentration gradient, resulting in a considerable improvement in detection sensitivity, and thus ease in detector design and application. Since the detection mechanism results in probing the RIG in the flow cell, there is a sensitivity "preference" for spatially sharp concentration profiles, such as chromatographic peak, while slowly changing concentration profiles, such as a MPG or TG contribute a minimal extent to the detected signal. While the merits of the RIG detector for HPLC were clearly outlined in the work of Pawliszyn [13], experimental evidence of a RIG detector performing in gradient elution HPLC has not been published.

In this paper we report the first use of RIG detection for MPG-μLC and TG-μLC. A test mixture of *n*-alkanes is separated by reversed-phase (RP) μLC in order to evaluate the detector performance under isocratic, binary MPG, and TG separation conditions. The relationship between the MPG program and the RIG-detected

baseline is examined with guidelines reported, and compared in principle to the baseline one would observe with a conventional RI detector. Results will demonstrate that indeed the technique of TG-μLC with RIG detection is simple, yet effective, in providing optimized resolving power with sensitive, universal detection. Thus, TG-μLC was applied to a RP separation of a test mixture of high molecular weight 1,2-diacylphosphatidylcholines (DAPCs), a class of phospholipids known to be difficult to analyze by HPLC due to solubility difficulties, and by gas chromatography due to the required, tedious sample derivatization and pretreatment procedures [4,9,20]. The technique of RP-TG-μLC is shown to not require the ion pairing reagent choline chloride, commonly added to improve elution behavior [4]. Essentially, the TG technique is shown to dramatically improve the separation through "programmed solubility" of the DAPCs. Further, the RIG detector is shown to perform admirably with the TG-μLC separation of DAPCs. Other details that are addressed include RIG detector design in the context of minimizing band broadening, optimization of the sensitivity, and the detection limit for the device.

EXPERIMENTAL

Refractive index gradient detector

A schematic of the apparatus used in this work is shown in Fig. 1a. The 633-nm, 5-mW continuous wave (cw) output from a HeNe laser (1305 P; Uniphase, Sunnyvale, CA, U.S.A.) was focused by a 20× microscope objective (M-20×; Newport Corp., Fountain Valley, CA, U.S.A.) onto an optical fiber (6 μm core, 125 μm clad, 175 μm

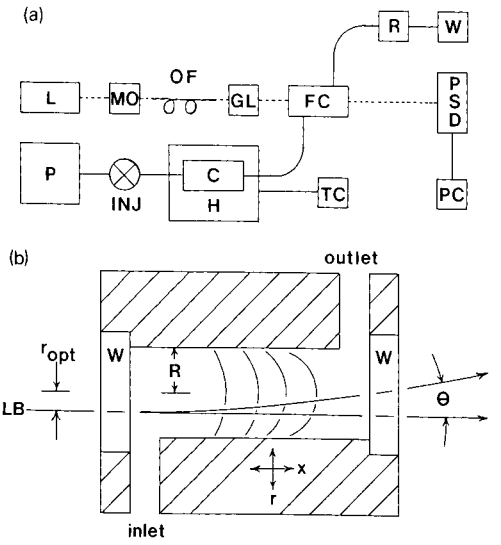

Fig. 1: (a) Apparatus for both MPG-μLC and TG-μLC with RIG detection. L = Laser; MO = microscope objective; OF = optical fiber; GL = GRIN-lens; FC = flow cell; PSD = position-sensitive detector; PC = personal computer; P = MPG syringe pump system; INJ = injection valve; H = heater; C = column; TC = temperature controller; R = pressure restrictor; W = waste. (b) z-Configuration flow cell. LB = Laser beam; r_{opt} = optimum radial position of probe beam; W = quartz window; R = radius of flow cell; θ = angular deflection of probe beam; r = radial axis of flow cell; x = length axis of flow cell.

jacket) that was designed for single-mode operation at 633 nm (SM 6/125 Al coated; Fujikura, Tokyo, Japan). A collimated probe beam was produced by interfacing the optical fiber output to a graded refractive index (GRIN) lens that was quarter pitch at 633 nm (NSG America, Somerset, NJ, U.S.A.). The optical fiber and GRIN-lens combination was chosen to obtain a small-diameter, collimated beam to selectively probe the most sensitive radial position for RIG detection in the flow cell. Careful measurement of the beam intensity profile indicated that the probe beam full angle divergence was 3.5 mrad, with an initial diameter of 110 μm, defined as 95% of the beam intensity, at the GRIN-lens output face. The probe beam was directed through a z-configuration flow cell (made in-house) mounted to a high precision x–y–z translational stage (460-XYZ Newport Corp.) with a 2 cm distance separating the flow cell and the GRIN-lens. The flow cell was constructed of polyetheretherketone (PEEK) with a 6 mm optical pathlength and a 780-μm internal diameter, comprising a total internal volume of 2.9 μl, with liquid flow entering and exiting in the vertical plane. The probe beam was aligned at the optimum radial position for maximum RIG detection sensitivity as shown in Fig. 1b, and on the horizontal axis to avoid possible flow perturbations at the flow inlet and outlet positions. The probe beam was at an average diameter of 200 μm in the flow cell so we could selectively probe the most sensitive radial position. For the flow cell used in this work, the optimal radial position, r_{opt}, was 225 μm. The measured length variance of a chromatographic peak (s_x^2) in the context of the flow cell can be calculated by the sum of the length variance of the peak before detection (s_v^2) plus the length variance contribution of the flow cell by

$$s_x^2 = \left(\frac{s_v}{\pi R^2}\right)^2 + \frac{R^2 L v}{24 D_m} \tag{1}$$

where R is the radius of the flow cell, L the length of flow cell, v the linear flow velocity in the flow cell, and D_m the diffusion coefficient of the analyte of interest. Given a typical μLC peak width of 40 μl at the base, standard deviation (s) = 10 μl, and given R = 390 μm, v = 3.48 mm/s in the flow cell (for a typical volumetric flow-rate of 100 μl/min), and $D_m = 5 \cdot 10^{-3}$ mm^2/s, the length variance of the peak is 438 mm^2 and 465 mm^2 before and after detection, respectively, corresponding to only 3% additional band broadening due to the flow cell. Using pure acetonitrile as the solvent, the calculated Reynolds number for the flow cell is 2.6, well within the Poiseuille flow range required to obtain consistent detector performance. Quartz windows were placed over the ends of the flow cell and sealed with polymer O-rings to provide an optical window and high pressure flow cell. After the collimated probe beam passed through the flow cell, it was incident on a position-sensitive detector (S1352; Hamamatsu, Hamamatsu, Japan) with dimensions of 33 mm × 2.5 mm, placed a distance of 83 cm from the flow cell.

Microbore HPLC system

For the MPG separation, the solvent delivery system consisted of two syringe pumps (μLC-500; ISCO, Lincoln, NE, U.S.A.) to deliver the chromatographic mobile phase to a microscale mixer (Upchurch, Oak Harbor, WA, U.S.A.) with an internal volume of 3.2 μl. A 152-cm coiled length of 1/16 in. O.D. × 0.020 in. I.D. PEEK tubing (Upchurch) followed the mixer to provide additional mixing for use with the MPG.

The injection valve (7520; Rheodyne, Cotati, CA, U.S.A.) fitted with a 1-μl injection disk. A μLC column was connected to the microbore injection valve via a 5-cm length of 1/16 in. O.D. × 0.005 in. I.D. PEEK tubing (Upchurch). A 250 mm × 1 mm column with 5 μm, silica based octyl packing (Deltabond; Keystone, Bellefonte, PA, U.S.A.) was used with the separations of *n*-alkanes, and a 200 mm × 1 mm column packed with PRP 10-μm resin (Suprex, Pittsburgh, PA, U.S.A.) was used with the TG-μLC separation of phosphatidylcholines. The columns were placed on a heating strip (SS2181; Wellman, Shelbyville, IN, U.S.A.) with thermal contact to the heater accomplished via thermal joint compound and the temperature controlled by a FIAtron controller (TC-55; FIAtron, Oconomowoc, WI, U.S.A.) used only for the TG-μLC separations. The effluent from the column was delivered to the flow cell via a short length of low-dispersion tubing. After exiting the flow cell, the column effluent passed through a pressure restrictor (Upchurch) rated at 250 p.s.i.g. and subsequently to waste.

Chromatographic conditions and reagents

The MPG-μLC separation of *n*-alkanes consisted of a binary mixture with a composition by %(v/v) of A (acetonitrile–diethyl ether, 90:10) and B (water–acetonitrile–diethyl ether, 50:45:5) at a constant flow-rate of 100 μl/min, with the A–B ratio given in the figure captions. In all cases, the MPG was linear from A–B (80:20) to 100% A over the time specified in the figure captions. The TG-μLC separation of *n*-alkanes consisted of A–B (70:30) at a flow-rate of 100 μl/min with the temperature profiles given in the respective figure. The isothermal (25°C) and TG-μLC separation of DAPCs consisted of 100% methanol at 50 μl/min. All mobile phases consisted of HPLC-grade solvents (Baker Analyzed; J. T. Baker, Phillipsburg, NJ, U.S.A.). Reagent-grade DAPCs and *n*-alkanes (Sigma, St. Louis, MO, U.S.A.) were used as test mixtures.

Data collection and analysis

Chromatographic data were collected via laboratory interface (DASH-16; Metra Byte, Taunton, MA, U.S.A.), which facilitated the analog-to-digital (A/D) conversion of the signal from the position-sensitive detector and subsequently stored on a personal computer (IBM-XT, Armonk, NY, U.S.A.) for further data processing. The data collected for the alkane separations were not at an optimal signal-to-noise ratio (S/N) due to a noisy data acquisition input; however, the absolute angular deflection is accurate and therefore the operation of the RIG detector can be objectively investigated with TG- and MPG-μLC separations. Subsequent analysis of DAPCs was optimized for S/N considerations with detection limits expressed as three times the standard deviation of the baseline noise.

RESULTS AND DISCUSSION

Mobile phase gradient and isocratic separations

The use of the RIG detector with μLC will be illustrated by working through isocratic separations of *n*-alkanes, with subsequent optimization by MPG-μLC. An isocratic RP-μLC separation of *n*-alkanes using a relatively strong mobile phase is shown in Fig. 2a where the injection disturbance at 2 min marked the elution time of an

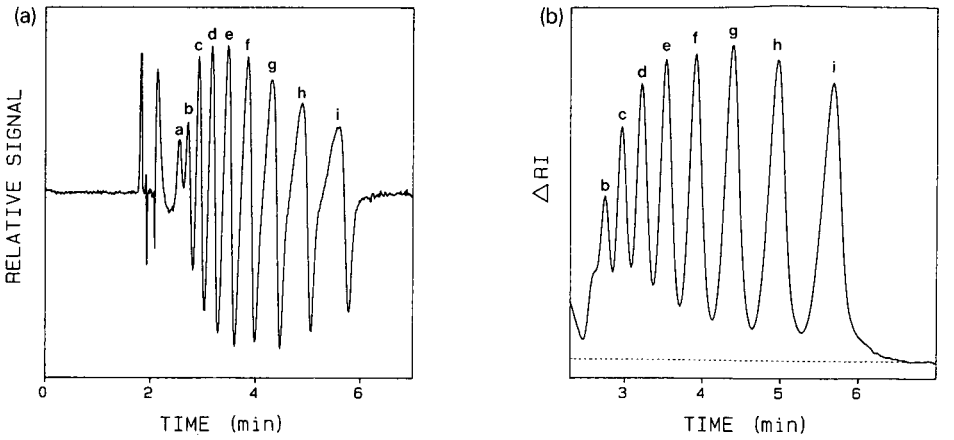

Fig. 2. (a) Microbore isocratic separation of *n*-alkanes at room temperature (25°C) with RIG detection. Peaks: a = *n*-pentane; b = *n*-hexane; c = *n*-heptane; d = *n*-octane; e = *n*-nonane; f = *n*-decane; g = *n*-undecane; h = *n*-dodecane; i = *n*-tridecane. Mobile phase, 100% A (as defined in Experimental section) at 100 μl/min. (b) Running total integration of the chromatogram shown in (a).

unretained analyte. The analytical signal consisted of a positive and negative going peak as previously described [12–19], corresponding to the derivative of the RI profile eluted from the μLC column. This unconventional signal can be cast into a more familiar form by performing the running total integration (RTI) [14,21,22] to obtain the RI profile eluting from the μLC column as shown in Fig. 2b. Baseline resolution is given by the dashed line on the bottom of the figure, indicating incomplete resolution for all of the analytes with *n*-pentane forming a shoulder on the side of *n*-hexane, furthermore, complicated by *n*-pentane falling on the tail of the injection disturbance, precluding confident quantitation. The RTI algorithm was successfully applied to all chromatograms, however for subsequent chromatograms only the RIG signal will be shown for brevity.

A simple solution to the lack of chromatographic resolution is to decrease the strength of the mobile phase, thus increasing the water content of the mobile phase resulted in the chromatogram shown in Fig. 3. Inspection of the integrated chromatogram from Fig. 3, not shown for brevity, indicated baseline resolution for all the analytes, *n*-pentane through *n*-tridecane. The limitation of this approach to increase chromatographic resolution is long analysis time, nearly 20 min for the same analyte mixture, and excessive peak broadening of the later eluting peaks, resulting in inferior detectability.

An alternative solution to increasing chromatographic resolution is to perform a MPG to dynamically change the retention behavior of later eluting analytes, allowing the optimization of resolution throughout the entire chromatogram. The MPG should provide a shorter analysis time while not sacrificing resolution for early eluting analytes and optimizing detection for later eluting analytes [2]. Traditionally, MPG-μLC separation capability was not compatible with RI detection since the measured analytical signal was proportional to the bulk RI of the column effluent [5]. It was therefore prohibitively difficult to keep the signal for a conventional RI detector on scale for a typical MPG separation of interest. For RP-μLC separations, a large

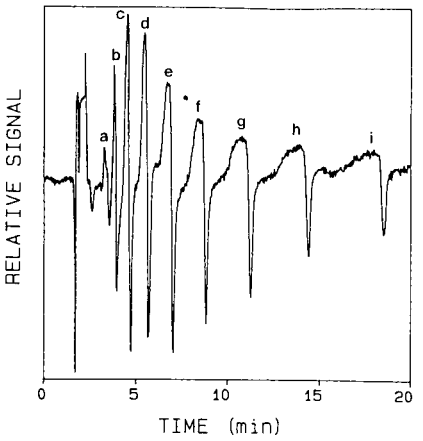

Fig. 3. Isocratic separation of *n*-alkanes at room temperature (25°C) with RIG detection. Mobile phase, A–B (80:20, v/v) (as defined in Experimental section) at 100 μl/min. Peaks as in Fig. 2a.

change in solvent strength would be to start with 100% water and finish with 100% methanol, comprising a RI change of 0.0046, much too large of a RI change to be useful for a conventional RI detector. Furthermore, the problem of poor sensitivity and limited dynamic range for conventional RI detection cannot be solved by injecting a high concentration, since overloading of the column will occur. Thus, the inherent sensitivity and limited dynamic detection range of conventional RI detection precludes the application of a MPG in μLC.

The first published report of a MPG-μLC separation with RIG detection is presented in Fig. 4a with the entire analysis time under 10 min for baseline resolution of all *n*-alkanes. The MPG started with the same composition as the chromatogram in Fig. 3 to obtain baseline resolution of the early eluting analytes with a linear change of the mobile phase composition to the stronger eluent used for Fig. 2 to optimize resolution of later eluting analytes. Collection of the MPG baseline (Fig. 4b) and MPG-μLC separation (Fig. 4a) on a computer allowed further data analysis by subtraction of the MPG baseline from the MPG separation to remove the baseline drift as shown in Fig. 4c. This simple data manipulation technique allows baseline correction for subsequent integration and further inspection of the separation.

A more critical evaluation of the baseline signal obtained in MPG-μLC as shown in Fig. 4b is warranted. Integration of Fig. 4b yields the total RI change for the mobile phase gradient as shown by Fig. 5, trace B. Additionally, 2.5- and 10-min gradients were also collected and integrated as shown by traces A and C, respectively. Integration to essentially the same RI value indicates that the RI signal is conserved and independent of the steepness of the gradient formation, providing evidence that the RIG detector is functioning properly.

From Fig. 5, the RI changed by $6 \cdot 10^{-4}$ RI over the 5-min linear MPG, shown in Fig. 4B, corresponding to an angular deflection of the baseline by only 600 μrad as given in Table I. The RIG detector signal was found to be well-behaved to 10 mrad, indicating a maximum useable eluent range of 0.01 RI for a 5 minute gradient. As

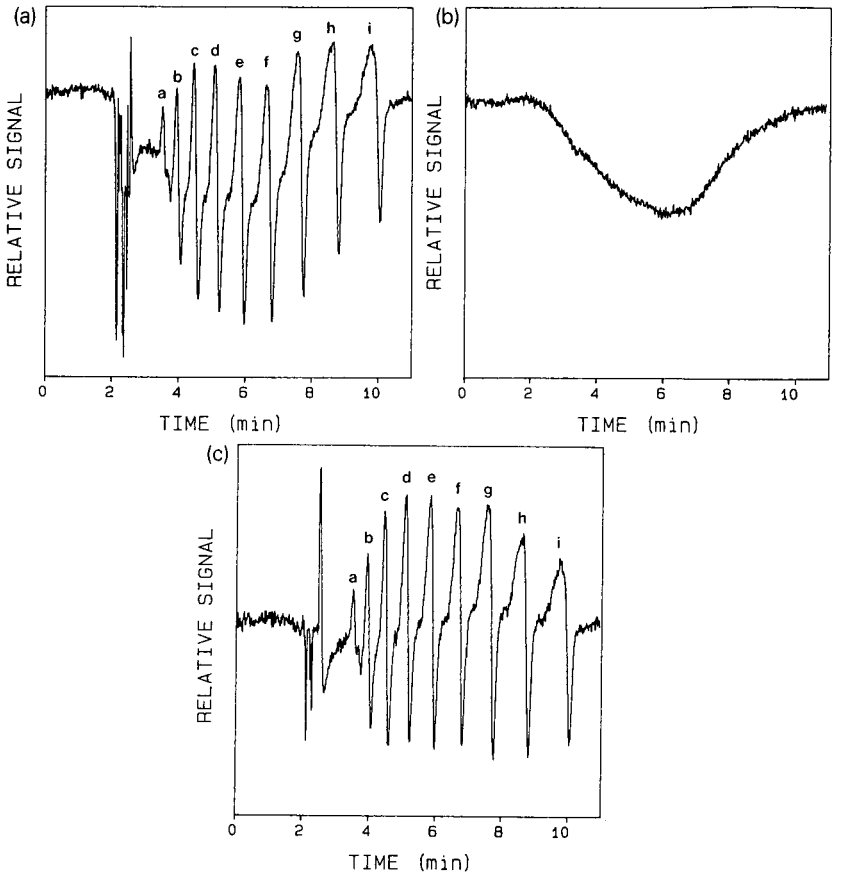

Fig. 4. (a) MPG-μLC separation of *n*-alkanes at room temperature (25°C) with RIG detection. Linear MPG from A–B (80:20) to 100% A (as defined in Experimental section) over 5-min interval at 100 μl/min. Peaks as in Fig. 2a. (b) Baseline for MPG-μLC with RIG detection. No sample injected. Chromatographic conditions as in (a). (c) Baseline corrected MPG-μLC separation of *n*-alkanes with RIG detection [(a) minus (b)]. Peaks as in Fig. 2a.

indicated by Table I, a longer gradient delivery time results in a reduced baseline response, thereby increasing the useful RI range that can be accommodated. For instance, a 10-min MPG program would result in a maximum allowable baseline angular deflection of 10 mrad if the absolute RI change is 0.02 RI, well beyond the RI change resulting from a 100% water to 100% methanol MPG (0.0046 RI change). Compared to conventional RI detection there is a considerable increase in useful dynamic range for mobile phase composition change using RIG detection.

Thermal gradient separations of n-alkanes

A more attractive solution to reduce analysis time while optimizing the column resolving power is to perform a thermal gradient (TG-μLC) separation. A potential benefit of TG-μLC is reproducible temperature control and thus reproducible

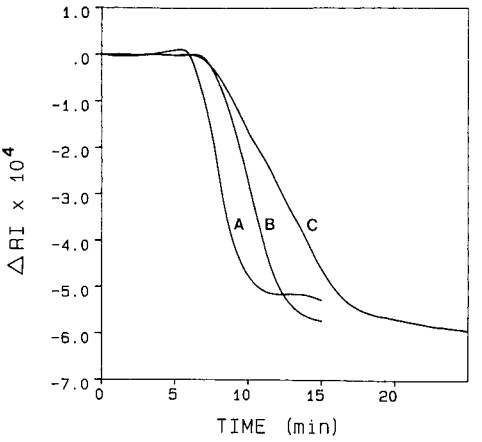

Fig. 5. Integrated RIG detected baseline drift from MPGs. A = 2.5-min gradient; B = 5.0-min gradient; C = 10.0-min gradient. Linear MPG from A–B (80:20) to 100% A (as defined in Experimental section) at 100 μl/min over specified time intervals.

separation conditions, in contrast to the difficulties often encountered with reproducible MPG formation. Another distinct advantage of TG-μLC is the simplicity of the instrumentation, requiring only one pump, heater and temperature controller, in contrast to MPG-μLC requiring two syringe pumps, microscale mixer and gradient pump controller. To perform sensitive detection via conventional RI detection, commonly requires thermostating the column and detector in an oven by ± 0.01 C, preventing the use of conventional RI detection with TG-μLC.

The first report of a TG-μLC separation with RI-based detection is shown in Fig. 6 for the same *n*-alkane mixture used in the isocratic and MPG-μLC separations. Comparing the analysis time in Fig. 4a and Fig. 6 clearly indicates that TG-μLC is an effective alternative to MPG-μLC. The temperature profile of the TG program is given by the dashed line in Fig. 6. Even though no attempt was made to thermostat the flow cell to the temperature of the incoming column effluent, the baseline drift of 500 μrad was less than observed for the MPG-μLC separation for a similar analysis time. Future improvements to the instrument will include placement of the flow cell in the same temperature environment as the column, eliminating any problems due to non-equilibrium temperature conditions between the flow cell and the column effluent. The

TABLE I

BASELINE DRIFT WITH RIG DETECTION AT VARIOUS MPG RATES

Gradient conditions given in Experimental section.

Gradient (min)	Baseline drift[a] (μrad)
2.5	900
5.0	600
10	280

[a] Drift defined by RIG maximum to minimum baseline signal for MPG.

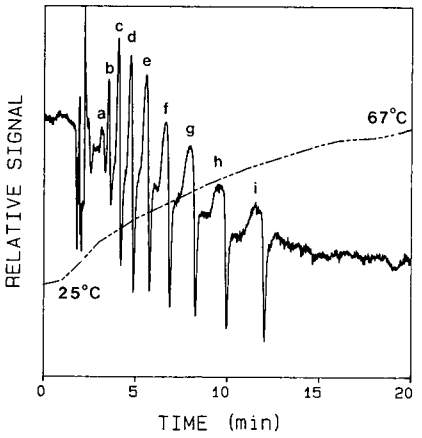

Fig. 6. TG-μLC separation of n-alkanes with RIG detection. Temperature program given by dashed line. Mobile phase, A–B (70:30) (as defined in Experimental section) at 100 μl/min. Peaks as in Fig. 2a.

technique of subtracting the TG-μLC baseline drift from the TG-μLC separation can be used to correct the data for baseline drift, as described for the MPG-μLC separation.

Bioseparations

A resin-based μLC column was chosen for the separation of DAPCs to allow separation of DAPCs without the use of modifiers or buffers typically used with reversed-phase silica-based columns [4]. Furthermore difficulties associated with dissolution of silica column packing material were eliminated by using a polymer-based column. A generic structure of a DAPC is shown in Fig. 7, with the largest DAPC used in this study approaching a molecular weight of 800 g/mole. Four DAPCs, as defined by Fig. 7 and Table II, were used as a test mixture. An isothermal separation of DAPCs is shown in Fig. 8, clearly indicating the need for gradient separation capability, evident by near baseline resolution at the beginning of the separation with excessive resolution and long analysis time for the complete separation [4,9,20] with the last peak severely broadened. The detection limit for DLPC was 36 ng injected mass, with an angular detection limit of 2 μrad, and a RI detection limit of $2 \cdot 10^{-8}$ RI. In principle, one could utilize a PSD with a better angular sensitivity to achieve a better

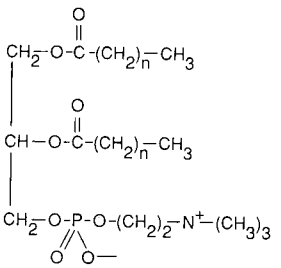

Fig. 7. General structure of 1,2-diacylphosphatidylcholine. See Table II for definition of species analyzed.

TABLE II

IDENTIFICATION OF 1,2-DIACYLPHOSPHATIDYLCHOLINES (DAPCs)

These four DAPCs comprise a mixture defined according to the value of n, as applied in Fig. 7.

n	Common name[a]	Abbreviation
10	Dilauryl	DLPC
12	Dimyristyl	DMPC
14	Dipalmityl	DPPC
16	Distearyl	DSPC

[a] Fatty acid chain = $n+2$, (diacyl-).

RI and mass detection limit, however, in practice the angular detection limit is not limited by the sensitivity of the position-sensitive detector but rather limited by minor flow perturbations in the flow cell.

Previous work with the RIG detector [16] has shown RI detectability to be inversely proportional to the peak width and analyte detectability to be inversely proportional to the peak variance and therefore an more efficient separation is a viable solution to yield better detectability. The polymer column used for this work was chosen for potential use with low-pressure LC instrumentation and therefore efficiency was traded for low column back pressure. The pressure for the isothermal separation of DAPCs was only 600 p.s.i. including the 250-p.s.i. pressure restrictor, thereby allowing a wide variety of solvent delivery and injection systems compatible with the column and RIG detector. Alternatively, where detection limits are a major concern, selection of a higher efficiency column yielding peak widths of 25 μl at the base instead of 100 μl would result in mass detection limits 16 times lower, or 2 ng injected DLPC.

Rapid analysis of the same DAPC mixture shown in Fig. 8 by TG-μLC with RIG detection is shown in Fig. 9 with the analysis time reduced by a factor of about 2.5 from

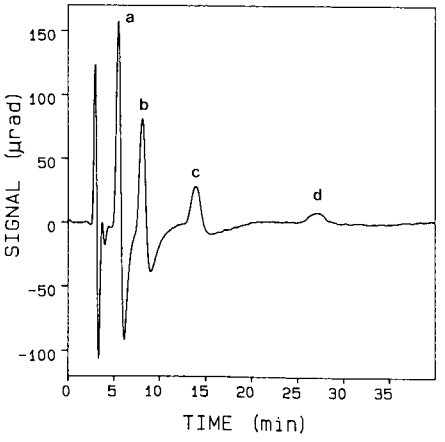

Fig. 8. Isothermal (25°C) separation of DAPCs defined in Table II and Fig. 7. Peaks: a = DLPC; b = DMPC; c = DPPC; d = DSPC. Mobile phase, 100% methanol at 50 μl/min. Injected mass, 8 μg of each DAPC.

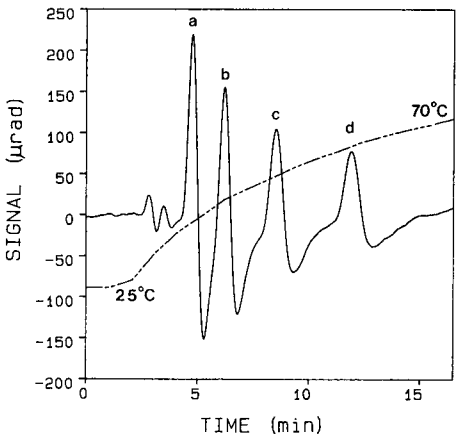

Fig. 9. TG-μLC separation of the same mixture of DAPCs shown in Fig. 8. Temperature profile given by dashed line. Mobile phase, 100% methanol at 50 μl/min. Peaks as in Fig. 8.

the room temperature separation. The capacity factor for DSPC changed from 9.0 to 3.2 from the isothermal separation to the TG-μLC separation. Furthermore, detectability of DSPC for the TG separation relative to the isothermal separation is better by a factor of 14 due to a reduction in peak width. The decreased analysis time or increased solvent strength of the TG separation also indicates the capability to elute larger DAPCs normally present in biological samples without loss of resolution for earlier eluting DAPCs. Inspection of Fig. 9 also indicates the baseline drift to be less than 10 μrad, clearly an improvement over the TG-μLC separation of *n*-alkanes (Fig. 6), with a baseline drift of 500 μrad. The primary experimental difference between the DAPC and *n*-alkane separation was the flow-rate of the eluent, indicating a strong flow-rate dependence of non-equilibrium temperature conditions manifested as baseline drift for TG-μLC with RIG detection. This apparent advantage requires further investigation. In general, the technique of TG-μLC with RIG detection appears to be very promising for routine analysis of biopolymers where rapid characterization and confident quantitation is required.

ACKNOWLEDGEMENT

We thank the NSF Center for Process Analytical Chemistry for support of this work (Project Number 89-5).

REFERENCES

1 F. D. Antia and Cs. Horváth, *J. Chromatogr.*, 435 (1988) 1.
2 B. L. Karger, L. R. Snyder and Cs. Horváth, *An Introduction to Separation Science*, Wiley, New York, 1973, p. 161.
3 W. R. Biggs and J. C. Fetzer, *Anal. Chem.*, 61 (1989) 236.
4 A. D. Postle, *J. Chromatogr.*, 415 (1987) 241.
5 M. Munk, in T. Vickers (Editor), *Liquid Chromatographic Detectors*, Marcel Dekker, New York, 1983.

6 S. Banerjee and E. J. Pack, Jr., *Anal. Chem.*, 54 (1982) 324.
7 S. D. Woodruff and E. S. Yeung, *J. Chromatogr.*, 260 (1983) 363.
8 A. S. Stolyhwo, H. Colin and G. Guiochon, *Anal. Chem.*, 57 (1985) 1342.
9 N. Sotirhos, C. Thorngren and B. Herslof, *J. Chromatogr.*, 331 (1985) 313.
10 H. Small and T. E. Miller, *Anal. Chem.*, 54 (1982) 462.
11 D. R. Bobbit and E. S. Yeung, *Anal. Chem.*, 56 (1984) 1577.
12 D. Betteridge, E. L. Dagless, B. Fields and N. F. Graves, *Analyst (London)*, 103 (1978) 897.
13 J. Pawliszyn, *Anal. Chem.*, 58 (1986) 243.
14 J. Pawliszyn, *Anal. Chem.*, 58 (1986) 2307.
15 J. Pawliszyn, *Anal. Chem.*, 60 (1988) 2796.
16 D. O. Hancock and R. E. Synovec, *Anal. Chem.*, 60 (1988) 1915.
17 D. O. Hancock and R. E. Synovec, *Anal. Chem.*, 60 (1988) 2812.
18 D. O. Hancock and R. E. Synovec, *J. Chromatogr.*, 464 (1989) 83.
19 C. E. Evans and V. L. McGuffin, *J. Chromatogr.*, 459 (1988) 119.
20 E. W. Hammond, *Trends Anal. Chem.*, 8 (1989) 308.
21 R. E. Synovec and E. S. Yeung, *Anal. Chem.*, 57 (1985) 2162.
22 R. E. Synovec and E. S. Yeung, *Anal. Chem.*, 58 (1986) 2093.

Journal of Chromatography, 536 (1991) 303–308
Elsevier Science Publishers B.V., Amsterdam

CHROMSYMP. 2064

Size-exclusion chromatography of lignocellulosics in wheat straw

GUIDO C. GALLETTI*
Centro di Studio per la Conservazione dei Foraggi, CNR, Via F. Re 8, 40126 Bologna (Italy)
and
GIUSEPPE CHIAVARI
Dipartimento di Chimica "G. Ciamician", Università di Bologna, Via F. Selmi 2, 40126 Bologna (Italy)

ABSTRACT

The application of Fractogel TSK HW-40, a semi-rigid, hydrophilic vinyl polymer, and Vydac 214 TP, a wide-pore high-performance liquid chromatographic packing, to the fingerprinting of extracts of wheat straw, both untreated and treated with sodium hydroxide, is reported. Whereas separation on Fractogel TSK is typical size-exclusion chromatography, chromatography on the Vydac column is influenced by both adsorption effects and the molecular size of the solutes. Chromatograms showing significant differences among samples are discussed in relation to sample pretreatment and extraction, molecular weight distribution and electrochemical properties of the main peak.

INTRODUCTION

Lignocellulosic materials, such as wood, agricultural residues and industrial by-products, are an economical and renewable source of energy and raw material in areas of application as diverse as the chemical industry, fibre and paper manufacture, livestock feeding and even environmental decontamination from toxic chemicals. Lignocellulose resources represent about 95% of the world biomass [1]. Cellulose, hemicellulose and lignin are the three main constituents of lignocellulose. Lignin is a polymer with phenylpropane units, linked to each other by carbon–carbon and ether bonds. Lignin forms complex structures with cell-wall polysaccharides (lignin–carbohydrate complexes, LCC) through hydrogen and ether bonding [2]. Lignin depolymerization and/or disaggregation of the complexes with polysaccharides is often the basis of practical processes of lignocellulose exploitation, such as animal feeding with straw, where an improved digestibility of structural carbohydrates can be achieved by treating straw with alkali or lignin-degrading organisms.

Lignin degradation products have been successfully analysed by gas chromatography (GC) [3] and reversed-phase high-performance liquid chromatography (HPLC) [4–6]. Direct analysis of lignocellulosic substrates has been carried out by Fourier transform infrared (FTIR) spectrometry [7], ^{13}C nuclear magnetic resonance (^{13}C NMR) [8] and pyrolysis–gas chromatography–mass spectrometry (Py–GC–MS)

0021-9673/91/$03.50

[9]. These techniques provide data on the phenolic monomers related to lignin, allowing chemical characterization and significant comparisons among treated and untreated materials, but give no information on the molecular weight distribution of native lignin, oligomers derived from lignin degradation or lignin–carbohydrate complexes.

Size-exclusion chromatography (SEC) and high-performance SEC (HPSEC) are well established methods for determining the molecular weight distribution of industrial lignins, although relatively few publications have dealt with SEC of lignin from gramineous plants and LCC [10]. Molecular weight determination is not as straightforward for lignins and LCCs as for synthetic polymers, owing to a lack of standard compounds with a chemical nature similar to that of lignin (for column calibration) and possible effects that disturb the relationship between column elution volume and polymer hydrodynamic volume, such as adsorption, aggregation and ionic/hydrophobic interactions [11]. Separation media used for the SEC of lignins and LCCs from gramineous plants include soft and semi-rigid gels such as Sephadex, Sepharose and Sephacryl types, whereas HPSEC has been performed on rigid gels after various modes of chemical deactivation, such as μStyragel (polystyrene–divinylbenzene), μBondagel E (bonded silica) and Zorbax PSM (silica) [10,11].

The aim of this work was to establish whether significant fingerprintings of wheat straw samples were obtainable by using two packing materials so far not reported for the characterization of molecular weight distributions in lignocellulose from gramineous plants. Extracts of wheat straw, both untreated and treated with sodium hydroxide to upgrade its digestibility by ruminants, were chromatographed on Fractogel TSK HW-40(S) and on Vydac 214 TP. This chromatographic support is a porous spherical gel with high chemical and mechanical stability for SEC and Vydac 214 TP is a wide-pore (300 Å) short-chain (C_4)-bonded support designed for the reversed-phase separation of peptides and other large molecules.

EXPERIMENTAL

Sample preparation

A 200-mg amount of each of an untreated sample (control, C) and a sample treated with sodium hydroxide (3% of dry matter), ground to pass a 0.2-mm sieve, was extracted with 10 ml of buffer [26.3 m*M* EDTA disodium salt dihydrate–58.2 m*M* KH_2PO_4–40.6 m*M* $Na_2HPO_4 \cdot 2H_2O$ (pH 7)] for 1 h under reflux. After cooling and centrifugation, the supernatant was decanted, filtered through a 0.22-μm cartridge filter (Millipore), diluted to 25 ml with the eluent and injected into the liquid chromatograph. The residue was extracted with 10 ml of 0.1 *M* sodium hydroxide solution for 10 min at 120°C and subjected to the same procedure as above, prior to injection into the liquid chromatograph.

Chromatographic conditions

Condition 1. Fractogel TSK HW-40(S) (swollen particle size 25–40 μm) (Merck, Darmstadt, F.R.G.) was packed into a Merck Superformance glass column (300 × 10 mm I.D.) and connected to a liquid chromatographic system, consisting of a Model 590 pump (Waters Assoc., Millford, MA, U.S.A.), a Rheodyne Model 7010 sample injector (100-μl loop), a Waters Assoc. Model 440 UV detector (set at 280 nm)

and a Model 5011 dual-cell detector (ESA, Bedford, MA, U.S.A.) controlled by an ESA Coulochem 5100 A module. Chromatograms were displayed on a Model 561 recorder (Perkin-Elmer, Beaconsfield, U.K.). The mobile phase was 1.2 m*M* perchloric acid at 1 ml/min. Analyses were performed at room temperature.

Condition 2. A Vydac 214 TP 54 column (300 × 4.6 mm I.D.) was connected to a Perkin-Elmer LC 4 liquid chromatograph with a Rheodyne 7125 S injector (6-μl loop), equipped with a Perkin-Elmer LC 95 variable-wavelength UV–VIS detector set at 280 nm. The mobile phase was water–acetonitrile (9:1) containing 0.5% trifluoroacetic acid at a flow-rate of 0.8 ml/min.

RESULTS AND DISCUSSION

Fractogel TSK is a semi-rigid gel, consisting of hydrophilic vinyl polymers with numerous hydroxyl groups on the matrix surface. Fractogel TSK is therefore completely different, in both its chemical structure and microstructure, from the usual gels based on dextran, agarose and polyacrylamide [12].

The molecular weight (MW) operating range of Fractogel TSK HW-40 is from 100 to 8000 for dextrans and from 100 to 2000 for polyethylene glycols. Oligomers detected in studies on lignin degradation were of such an MW order [11]. It therefore seemed appropriate to start this study on SEC of lignocellulose with this medium.

Considering that SEC of lignocellulose suffers from a lack of proper calibration compounds, the column was calibrated under condition 1 (see Experimental) with dextrans and sugars (Sigma, St. Louis, MO, U.S.A.) using a refractive index detector. Calibration results were as follows: blue dextran, void volume (V_0) 6.6 min; dextran with average MW 9000, 7.00 min; dextran tetramer–decamer mixture with MW from *ca.* 660 to *ca.* 1630, 9.9 min; dextran with MW 500, 12.4 min; sucrose with MW 342, 13.3 min; and glucose with MW 180, 14.5 min.

An acidic eluent was used in previous work [4–7] because it prevents adsorption effects of phenolic substances on reversed-phase packings. In this work, acidic eluents were used for both size-exclusion and reversed-phase chromatography in order to make a homogeneous comparison of the two packings.

Fig. 1 shows the four chromatograms corresponding to the sample preparations described under Experimental. The comparison between pH 7 buffer extracts of the control and sodium hydroxide-treated wheat straw (Fig. 1a and b) showed a lower total response in the control than in the treated sample, owing to the presence in the latter of more extractables, derived from sodium hydroxide hydrolysis of cell-wall polymers. There were also differences in the relative distributions of the molecular weights of the minor compounds (peaks A, C and D), corresponding approximately to the MW at the size-exclusion limit, 900 and 400 (dextran calibration). The main peak, B, corresponds to an MW of *ca.* 2300 (dextran calibration). In addition to the absorption at 280 nm, peak B had an electrochemical activity that proved its phenolic nature. The study of the voltammetric behaviour of an HPLC peak is generally performed by recording its hydrodynamic voltammogram (HV). The HV of peak B, determined by repeated injections at different detector potentials, showed a minimum detectable oxidation response at +0.45 V and a maximum at +1.00 V, with an intermediate plateau between +0.60 and +0.70 V, which suggests the presence of hydroxyl substituents in *ortho* and *meta* positions.

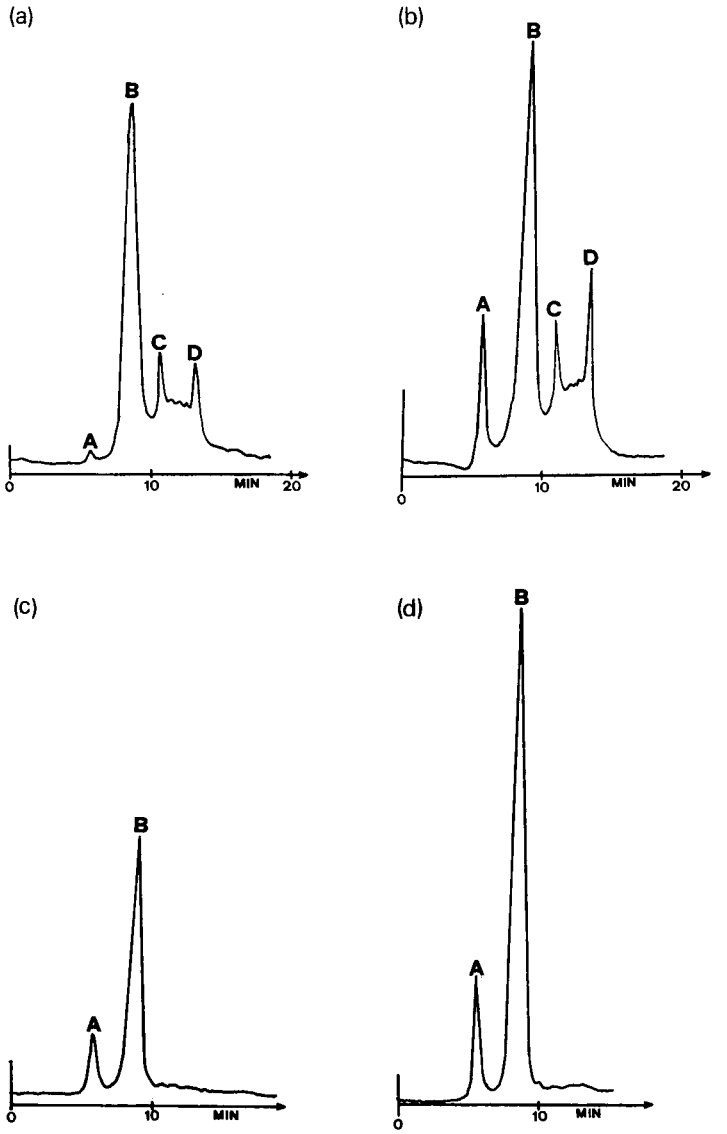

Fig. 1. Chromatograms obtained on a Fractogel TSK HW-40(F) column (300 × 10 mm I.D.) with detection at 280 nm of pH 7 buffer extracts of (a) control and (b) sodium hydroxide-treated wheat straw, and of the sodium hydroxide extracts of the corresponding residues (c) and (d). The sensitivity of (a) and (b) is double that of (c) and (d). Eluent, 1.2 m*M* perchloric acid; flow-rate, 1 ml/min.

In the sodium hydroxide extracts (Fig. 1c and d) there is a marked simplification of the chromatograms and an increased response in comparison with the previous two. Only peaks A and B are present. As observed with the other extracts, the treated sample showed a higher total response than the control. The lower molecular weight components (peaks C and D) are not present in the sodium hydroxide extracts,

probably because they are compounds loosely bound to the cell-wall polymers and, therefore, easily removed by the pH 7 buffer.

Wide-pore (300-Å) packings can be used for the reversed-phase separation of high-molecular-weight biological substances, such as proteins [13]. As no application of such columns to the characterization of the MW distribution in lignocellulose samples has been reported, it seemed interesting to perform a chromatographic separation of the same extracts on a column of this type.

Fig. 2 shows the elution profiles of the same extracts as in Fig. 1, obtained on a Vydac 214 TP C_4 column. The two columns show a consistent behaviour in terms of relative enhancement of response when sodium hydroxide-treated straw and sodium hydroxide extracts are compared with control straw and pH 7 buffer extracts, respectively. However, chromatographic separations on such columns can be affected by both adsorption effects and the molecular size of the solute. It is therefore more difficult to attribute chromatographic peaks to a certain molecular weight distribution in the sample, especially with lignocellulose owing to the already cited lack of calibration standards of appropriate structure. Nevertheless, given the differences in the fingerprinting of different straw samples, such a column is worthy of further study.

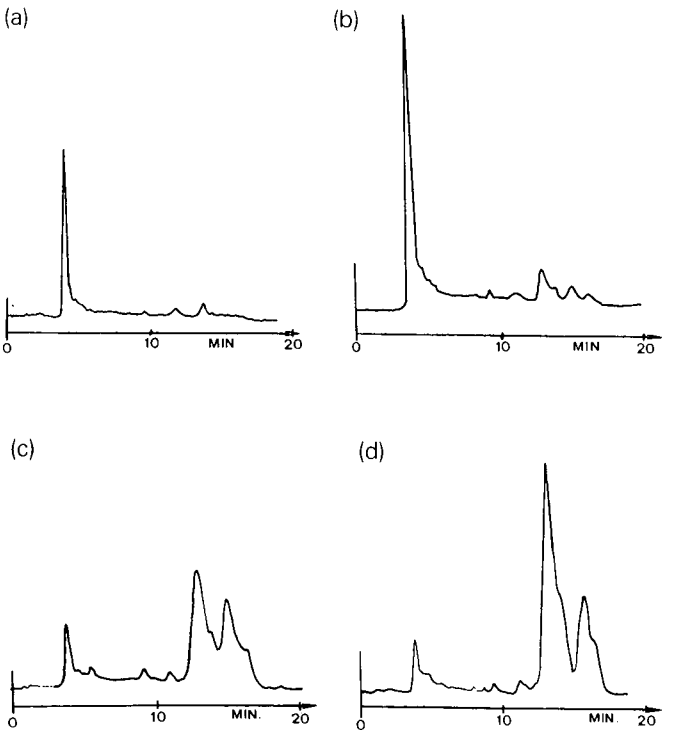

Fig. 2. Same extracts as in Fig. 1, chromatographed on a Vydac 214 TP column (300 × 4.6 mm I.D.) with detection at 280 nm. Eluent, water–acetonitrile (9:1) containing 0.5% trifluoroacetic acid; flow-rate, 0.8 ml/min.

CONCLUSION

Molecular weight determinations are tenuous on the basis of conventional chromatographic standards and, therefore, further analyses of the collected fractions should be performed in order to obtain absolute data. However, a fingerprinting comparison is satisfactory when only relative MW distributions or changes due to sample treatments have to be determined. The analysed samples, although small in number, allow the conclusion that TSK HW-40 is a useful gel for the SEC of lignocellulosic samples. Separations are rapid in comparison with the classical gels used for low-pressure SEC, and a rough MW distribution of these samples is obtainable. Vydac 214 TP chromatograms are interesting but more difficult to interpret. This kind of approach is now common in the study of LCCs and should be investigated further for application to lignocellulosic samples.

REFERENCES

1 H. Janshekar and A. Fiechter, in A. Fiechter (Editor), *Advances in Biochemical Engineering/Biotechnology*, Springer, Berlin, 1983, p. 119.
2 T. Watanabe, J. Onishi, Y. Yamasaki, S. Kaizu and T. Koshijima, *Agric. Biol. Chem.*, 53 (1989) 2233.
3 J. O. Fritz and K. J. Moore, *J. Agric. Food Chem.*, 35 (1987) 710.
4 G. C. Galletti, R. Piccaglia, G. Chiavari and V. Concialini, *J. Agric. Food Chem.*, 37 (1989) 985.
5 G. C. Galletti, R. Piccaglia, G. Chiavari, V. Concialini and J. G. Buta, *Chromatographia*, 26 (1988) 191.
6 G. Chiavari, V. Concialini and G. C. Galletti, *Analyst (London)*, 113 (1988) 91.
7 J. G. Buta, F. Zadrazil and G. C. Galletti, *J. Agric. Food Chem.*, 37 (1989) 1382.
8 H. G. Jung and D. S. Himmelsbach, *J. Agric. Food Chem.*, 37 (1989) 81.
9 G. Chiavari, O. Francioso, G. C. Galletti, R. Piccaglia and F. Zadrazil *J. Anal. Appl. Pyrol.*, 15 (1989) 129.
10 W. Zimmermann, in G. C. Galletti (Editor), *Lignocellulosic Utilization, proceedings of a workshop held in Reggio Emilia, May 16–19, 1990, Commission of the European Communities, COST 84/bis*, Elsevier, Amsterdam, in preparation.
11 M. Kuwahara, in H. F. Linskens and J. F. Jackson, *Plant Fibers*, Springer, Berlin, 1989, p. 186.
12 *Fractogel TSK Technical Bulletin*, E. Merck, Darmstadt, p. 1.
13 *Supelco Technical Bulletin*, Supelco, Bellefonte, PA, 1990.

Journal of Chromatography, 536 (1991) 309–317
Elsevier Science Publishers B.V., Amsterdam

CHROMSYMP. 2065

High-performance liquid chromatographic detection of myocardial prostaglandins and thromboxanes

GERALD A. CORDIS and DIPAK K. DAS*

Surgical Research Center, Cardiovascular Division, Department of Surgery, University of Connecticut School of Medicine, Farmington, CT 06030 (U.S.A.)

ABSTRACT

Reperfusion of ischemic myocardium is associated with the breakdown of membrane phospholipids and a corresponding increase in arachidonic acid, ultimately resulting in the production of prostaglandins (PGs) and thromboxanes (TXs). However, quantification of these arachidonic acid metabolites has been limited to radioimmunoassay because of their presence in extremely low amounts. In this report, we describe a method suitable to detect sub-picogram levels of 6-keto-$PGF_{1\alpha}$, $PGF_{1\alpha}$, PGE_2 and TXB_2 in myocardial perfusates by high-performance liquid chromatography (HPLC) with a high-gain photomultiplier and a xenon–mercury arc lamp. Strong Raleigh scatter of the lamp was eliminated by both interference and long-pass cut-off filters. Improved sample clean-up and HPLC separation were achieved by an HPLC system with an Ultrasphere 3-μm C_{18} column.

INTRODUCTION

Arachidonic acid metabolites, prostaglandins (PGs), thromboxanes (TXs), and leukotrienes, commonly known as eicosanoids, play an important role in the regulation of a variety of physiological and biological functions [1,2]. These oxygenated fatty acids are not stored in tissues; rather, they are formed from the membrane phospholipids during cell membrane perturbation under certain pathophysiological conditions [3,4]. Recent studies demonstrated the formation of PGs and TXs in ischemic and reperfused tissues including heart [5,6]. Because of their powerful biological activity in the cardiovascular system, there is a growing body of interest in their isolation from and quantification in heart.

However, because of their presence in extremely low quantities, it has not been possible to accurately estimate PG and TX levels in biological tissues, such as heart. Sophisticated and time-consuming methods, such as gas chromatography–electron-capture detection [7], gas chromatography–mass spectrometry [8] and radioimmunoassay (RIA) [5,9,10], are used to detect picogram levels of these eicosanoids in tissues. Although RIA offers excellent sensitivity in the picogram range, this method is not suitable to the analysis of multiple components in a single experiment.

Recently, high-performance liquid chromatography (HPLC) methods have

0021-9673/91/$03.50

been described for the quantification of PGs and TXs [11–15]. Detection limits of these procedures vary from nanogram to 60 picogram levels of injected dose. Unfortunately, PGs and TXs occasionally are present in sub-picogram quantity in tissues, which make these methods unsuitable.

We report here a method for detection of picogram quantities of PGs and TXs in heart by HPLC. This method, based on several previously published methods [11,12,15], has been modified extensively with respect to extraction techniques as well as in HPLC detection. Using this method, we have been able to detect sub-picogram levels of PGs and TXs in heart.

EXPERIMENTAL

Materials

Radioactive PGE_2 was obtained from Amersham (Arlington Heights, IL, U.S.A.). The authentic standards of 6-keto-$PGF_{1\alpha}$, $PGE_{1\alpha}$, PGE_2 and TxB_2 were purchased from Serdary Research Labs. (Port Huron, MI, U.S.A.). Panacyl bromide was obtained from Molecular Probes (Eugene, OR, U.S.A.) and was purified by adding 10 mg of this compound to 10 ml of acetonitrile–water–acetic acid (55:45:0.1, v/v/v). The mixture was vortex-mixed and centrifuged at low speed at room temperature, and the supernatant was collected. This procedure was repeated three times. The pooled supernatant was applied to a C_{18} Sep-Pak cartridge (Waters Assoc., Milford, MA, U.S.A.) and washed with 10 ml of acetonitrile–water–acetic acid (55:45:0.1 v/v/v). The eluted panacyl bromide was extracted with equal volumes of diethyl ether and centrifuged, and the ether supernatant was dried under a stream of nitrogen at 40°C. All the solvents used in this experient were of HPLC grade (Burdick & Jackson, Muskegon, MI, U.S.A.). Water was purified with a Milli-Q system. All other chemicals were of analytical grade.

Methods

Sample collection. Isolated rat heart was perfused by the Langendorff technique, using Krebs–Henseleit bicarbonate buffer (KHB) (pH 7.4) as described elsewhere [16]. Hearts were initially perfused for 15 min to allow stabilization and for collection of perfusate samples for baseline measurements. Global ischemia was then induced by terminating the coronary flow for 60 min, which was followed by 60 min of reperfusion. Perfusate samples were also withdrawn after the ischemic insult and during the reperfusion phase. Samples were collected in test tubes containing indomethacin (10 μg/ml).

Extraction. A 3-ml volume of perfusate sample was acidified to pH 3 with hydrochloric acid and applied to a preconditioned Sep-Pak C_{18} cartridge (Waters Assoc.) for extraction of PGs and TXs according to the method described by Powell [13,14]. The samples were washed with 20 ml of water, 15% aqueous ethanol, light petroleum (30–60°C) and finally with light petroleum–chloroform (65:35, v/v). PGs and TXs were eluted with 10 ml of methyl formate and then evaporated under nitrogen at 40°C.

Derivatization and sample clean up. The evaporated samples were derivatized with panacyl bromide according to the method described by Engels *et al.* [11] and Watkins and Peterson [15]. The dried extract was redissolved in 400 μl of acetonitrile

and allowed to react with 75 μl of panacyl bromide in tetrahydrofuran (0.1 mg/ml) and 2 ml of triethylamine (Fluka, Ronkonkoma, NY, U.S.A.) at 40°C for 2 h. The samples were then loaded onto a preconditioned silica Sep-Pak cartridge, washed with a mixture of 10 ml of dichloromethane–methanol (100:1, v/v), and eluted with 3 ml of acetonitrile–methanol (85:15, v/v). The fluorescent PGs and TXs were dried under nitrogen at 40°C, brought up in 0.5 ml dichloromethane–methanol (100:1, v/v), and re-extracted on a new preconditioned silica Sep-Pak cartridge.

The eluates were dried under nitrogen at 40°C and derivatized according to the method described by Pullen *et al.* [12]. A 200-μl volume of 2% methoxamine hydrochloride in pyridine (Pierce, Rockford, IL, U.S.A.) was added to the evaporated extract, vortex-mixed for *ca.* 1 min, and allowed to react for 16 h. The pyridine was evaporated at 40°C under nitogen, and 1 ml of water and 2 ml of diethyl ether were added, mixed for 1 min, and then centrifuged. The ether layer was saved, whereas the water layer was re-extracted with 2 ml of diethyl ether. The pooled ether layers were evaporated under nitrogen at 40°C and redissolved in 200 μl of acetonitrile.

HPLC. A 25-μl volume of the sample was injected into a Beckman Ultrasphere ODS C_{18} (3-μm particle size, 7.5 cm × 4.6 mm I.D.) column in a Waters chromatograph, equipped with a Model 820 full-control Maxima computer system, satellite Wisp Model 700 injector, Model 490 programmable multi-wavelength UV detector (set at 253 nm), two Model 510 pumps and a Bondapak C_{18} Guard-Pak pre-column. The fluorescent derivatives were detected by a McPherson Model FL-750 fluorescent detector with a high-gain photomultiplier and a xenon–mercury arc lamp. The fluorescent signal was increased due to a lamp emission maximum overlapping the panacyl bromide derivative absorption maximum at 365 nm. Strong Raleigh scatter of the lamp was eliminated by both interference and long cutoff filters to further improve the signal-to-noise ratio.

Radioactive [^{14}C]PGE_2 was used as internal standard. Radioactivity was detected by a Berthold LB506C radioactive monitor and NEC Powermate I computer.

The flow-rate was adjusted to 1 ml/min. Samples were eluted for 40 min with acetonitrile–water–acetic acid (55:45:0.1, v/v/v), and then a linear gradient to acetonitrile–water–acetic acid (75:25:0.1, v/v/v) was applied for the next 29 min. Hydroxy fatty acids were eluted with acetonitrile–acetic acid (100:0.1, v/v). The column was then equilibrated with acetonitrile–water–acetic acid (55:45:0.1, v/v/v) for 20 min.

RESULTS

Separation of prostaglandins and thromboxanes

The methoxamine panacyl derivatives of PG and TX standards were separated by HPLC as shown in Fig. 1. Each standard resulted in two methoxamine derivatives [12], with the retention times of 6-keto-$PGF_{1\alpha}$, $PGF_{1\alpha}$, PGE_2, and TXB_2 being 24.5 and 29.0 min, 26.5 and 32.0 min, 45.0 and 52.0 min, and 63.5 and 65.5 min, respectively, making the analysis time *ca.* 105 min. In this chromatogram, 8 fmol of each of the above compounds were injected into the HPLC system.

Construction of calibration curve

Using the HPLC system and the fluorescence detector as described in the Experimental section, and employing the Maxima 820 software, a calibration curve for

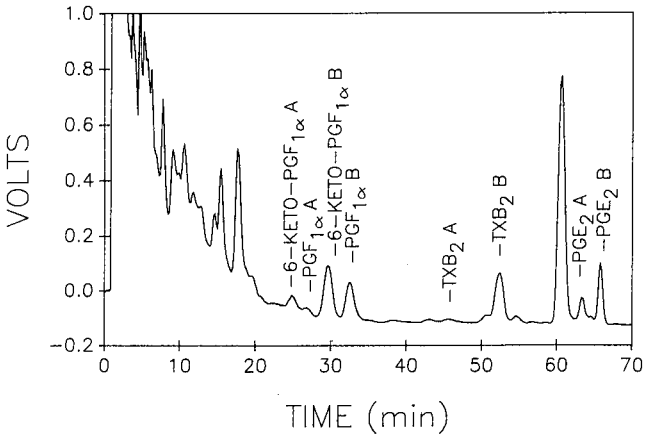

Fig. 1. Separation of methoxamine panacyl derivatives of 6-keto-$PGF_{1\alpha}$, $PGF_{1\alpha}$, TXB_2 and PGE_2 standards by reversed-phase HPLC. A volume of 25 μl of a solution, containing 8 fmol of each standard, was injected into a C_{18} column and measured by fluorescent detection, as described in the Experimental section.

each of the following was produced: 6-keto-$PGF_{1\alpha}$, $PGF_{1\alpha}$, PGE_2 and TXB_2. At least five different concentrations in the four- to ten-fold ranges for each standard were injected and chromatographed as described in the Experimental section. The concentrations of each standard, 6-keto-$PGF_{1\alpha}$, $PGF_{1\alpha}$, TXB_2 and PGE_2, were plotted against the peak area obtained. The peak area for each standard was the total area for two methoxamine derivative peaks. In each case, the calibration line was linear, with all points having a small standard deviation and falling on the line. The *r* values were 0.9823 for 6-keto-$PGF_{1\alpha}$, 0.9828 for $PGF_{1\alpha}$, 0.9815 for TXB_2 and 0.9935 for PGE_2. The major peak seen eluting just before the two methoxamine panacyl derivative peaks of PGE_2 is a reagent peak.

Quantitative estimation of prostaglandins and thromboxanes in heart

Since PGs and TXs are known to be formed from the accumulated arachidonic acid during reperfusion of ischemic myocardium, we assayed these compounds in the perfusate, obtained from the control heart (A), ischemic heart (B) and reperfused heart (C), as shown in Fig. 2. The perfusates collected over indomethacin were quickly frozen and processed, as described in *Methods*, and the methoxamine panacyl derivatives of PGs and TX were loaded onto an HPLC column equipped with a fluorescence detector. As shown in Fig. 2, even though the amounts of TX and PGs were extremely low, they were still detected with reasonable peak heights enough to obtain accurate estimates. As expected, the values of these compounds were near zero in the preischemic control hearts, and they increased slightly after 60 min of ischemic insult. A significant increase in these values was obtained after 60 min of ischemia, followed by 60 min of reperfusion. The accuracy of this method was determined by standard addition technique. Addition of even 5 fmol of any of these compounds were accurately reflected in the peak heights. The limits of detection for 6-keto-$PGF_{1\alpha}$, $PGF_{1\alpha}$, TXB_2 and PGE_2 were 0.2, 0.33, 0.2 and 0.5 fmol injected, respectively. The

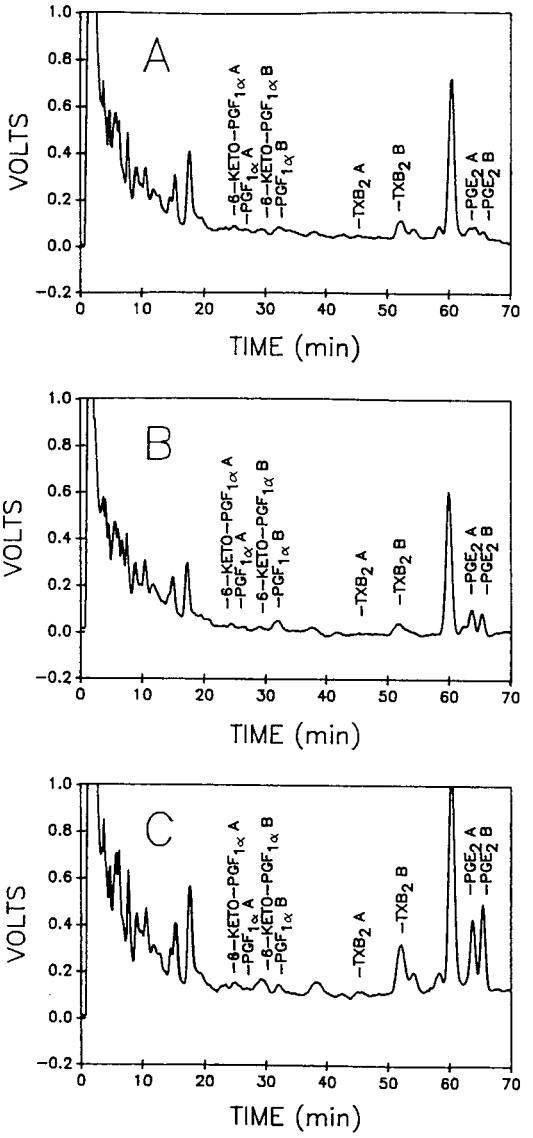

Fig. 2. Separation of derivatized prostaglandins and thromboxane from perfusates of isolated rat hearts. Rat heart perfusates were collected, derivatized, and chromatographed as described in the Experimental section. The injection volume was 25 μl, and the range of the fluorescent detector was 0.1 a.u.f.s. (A) Baseline perfusate; (B) after 60 min of ischemia; (C) after 60 min of reperfusion.

exact values of these compounds as a function of duration of ischemia and reperfusion are shown in Table I. Using [^{14}C]PGE_2 in the collected perfusates, recovery was found to be 17%.

TABLE I

RELEASE OF PROSTAGLANDINS AND THROMBOXANES FROM ISOLATED AND PERFUSED RAT HEART DURING ISCHEMIA AND REPERFUSION

	Baseline	60 min ischemia (pmol/ml perfusate)	60 min reperfusion
6-Keto-$PGF_{1\alpha}$	0.87 ± 0.20	0.85 ± 0.18	2.80 ± 0.47[a]
$PGF_{1\alpha}$	0.19 ± 0.02	0.24 ± 0.04	0.18 ± 0.03
TXB_2	0.87 ± 0.16	0.63 ± 0.11	8.58 ± 0.78[a]
PGE_2	1.45 ± 0.32	2.99 ± 0.44	9.70 ± 0.92[a]

[a] $p < 0.05$ compared to baseline. Results (pmol/ml perfusate) are expressed as mean ± S.D. of six experiments in each group.

DISCUSSION

The method described in this report is capable of giving an estimate of virtually all the arachidonic acid metabolites of heart via cyclooxygenase pathway that are of major interest in picogram quantities. This method is based on several previously published methods. Several modifications enhance the detection limit so as to allow

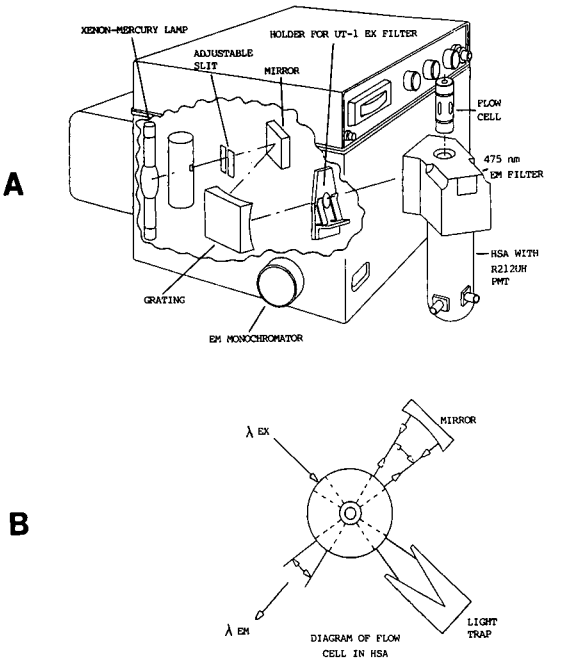

Fig. 3. Diagrams of McPherson FL-450 fluorescent detector with a high-sensitivity accessory (HSA). (A) Diagram of FL-450 fluorescent detector with its filters and HSA; (B) diagram of flow cell in HSA.

detection of PGs and TXs in the range present in the heart. For example, in contrast to the method described by Engels *et al.* [11], we performed fluorescent derivatization first, followed by methoxamination. The clean-up process was also modified using a second silica Sep-Pak chromatography prior to methoxamination. By these modifications, we were able to detect sub-picogram quantities of injected prostaglandins and thromboxanes compared to a minimum detection limit of about 60 pg, as reported previously [11,12,15]. In addition, we noticed some impurity in panacyl bromide, which interfered with the assay procedure by contaminating the derivatized PG peaks. We solved this problem by purifying the reagent as described in the *Methods* section.

The major modification performed was to enhance the sensitivity of the detection system by using a high-gain photomultiplier and a xenon–mercury arc lamp. High-pressure xenon–mercury arc lamp provided a high photon energy near the absorption maximum of the compound, *i.e.* 365 nm. Holographic excitation grating was used to tune the lamp emission maximum to 365 nm. The UV transmitting filter, UT-1, used in this experment can maximally transmit at 275–375 nm. This can eliminate the stray light and second-order effects resulting from grating (n), where $n = 1, 2, 3$, etc. Thus, without this stray light, the high-gain photomultiplier tube is likely to be able to eliminate excessive noise. In addition, this fluorescent detecting system is equipped with a excitation light trap and a reflecting mirror to double the collection efficiency. A larger angle of light collection is eliminated, since increased scatter noise relative to signal exists at angles other than 90°. Also, the long-pass emission filter was able to eliminate both Raleigh and Raman scatter. The photomultiplier tube in the high-sensitive accessory was a tube with high quantum efficiency at the emission wavelength of interest. The fluorescent detecting system used in this experiment (McPherson, Acton, MA, U.S.A.) is diagrammatically shown in Fig. 3. The output spectrum of the xenon–mercury lamp (Oriel Corp., Stratford, CT, U.S.A.) is shown in Fig. 4. This instrument system also improved the signal

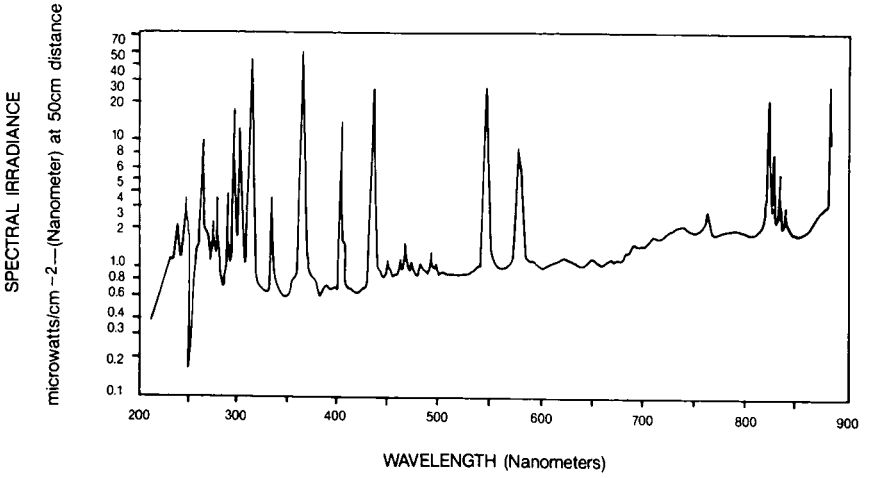

Fig. 4. Output spectra of a 200-W xenon–mercury lamp. Spectral irradiance of a xenon–mercury lamp is plotted against wavelength. Note the spike around 365 nm.

(*S*)-to-noise (*N*) ratio significantly, allowing us to measure very low levels of PGs and TXs as described below:

$$\frac{S}{N} = \frac{S}{\sigma_n} \frac{2.3 I_0 \theta F(\theta) g(\lambda) elc}{(\sigma^2 s + \sigma^2 f + \sigma^2 dc + \sigma^2 b)^{1/2}}$$

where

I_0 = source intensity: xenon–mercury lamp provides 100-fold excess energy
θ = photoluminescence efficiency: this was improved by improved clean-up technique
$F(\theta)$ = solid angle of fluorescence: this was improved by increasing light collection of high-sensitive accessory, because signal was collected only at 90° and 270° to the incident light (these angles have lowest scatter)
$g(\lambda)$ = detector efficiency at emission wavelength
e = extinction coefficient of the compound
l = path length
c = concentration
σ = standard deviation of the noise
σ^2 = variance
dc = dark current
f = flicker noise of lamp
s = shot noise of lamp
b = back ground noise of the mobile phase

Reperfusion of ischemic tissue is known to be associated with the accumulation of arachidonic acid released from the membrane phospholipids [5,6,17]. This is particularly important in the heart, because the accumulated arachidonic acid leads to the formation of several arachidonic acid metabolites via the cyclooxygenase pathway [18]. Some of these eicosanoids are beneficial to the heart, whereas others may cause further injury to the heart by several different mechanisms. Despite many investigations the precise mechanisms of the myocardial reperfusion injury are not known [19]. It is quite possible some of these metabolites contribute to reperfusion injury either directly or indirectly through the formation of cytotoxic oxygen-derived free radicals. It has been extremely difficult to examine the pathogenesis of such injury because of the lack of proper methods for identifying these arachidonic acid metabolites in such a low amount. In this paper, we have described a method suitable for assaying picogram quantities of the four major PGs and TXs, generated during reperfusion of ischemic myocardium, which are likely to play a role in the pathogenesis of ischemic and reperfusion injury.

ACKNOWLEDGEMENTS

This study was supported in part by grants from the National Institutes of Health (NIH HL 21818 and HL 34360).

REFERENCES

1 S. J. Coker, J. R. Paratt, I. M. Ledingham and I. L. Zeitlin, *J. Mol. Cell. Cardiol.*, 14 (1962) 483.
2 V. P. Addonizio, J. B. Smith, J. F. Strauss III, R. W. Colman and L. H. Edmunds, *J. Thorac. Cardiovasc. Surg.*, 79 (1980) 91.
3 F. A. Kuehl, J. L. Humes, E. A. Ham, R. W. Egan and H. W. Dougherty, *Adv. Prostaglandin Thromboxane Leukotriene Res.*, 6 (1980) 77.
4 R. Franson, M. Waite and W. Weglicki, *Biochemistry*, 11 (1972) 472.
5 H. Otani, R. M. Engelman, J. A. Rousou, R. H. Breyer and D. K. Das, *J. Mol. Cell. Cardiol.*, 18 (1986) 953.
6 W. Hsueh and P. Needleman, *Prostaglandins*, 16 (1978) 661.
7 S. E. Barrow, K. A. Waddell, M. Ennis, C. T. Dollery and I. A. Blair, *J. Chromatogr.*, 239 (1982) 71.
8 M. Claeys, C. van Hove, A. Duchateau and G. A. Herman, *Biomed. Environ. Mass Spectrom.*, 7 (1980) 544.
9 E. Granström and H. Kindahl, *Adv. Prostaglandin Thromboxane Leukotriene Res.*, 5 (1978) 119.
10 J. A. Salmon, *Br. Med. Bull.*, 39 (1983) 227.
11 W. Engels, M. A. F. Kamps, P. J. M. R. Lemmens, G. J. van der Vusse and R. S. Reneman, *J. Chromatogr.*, 427 (1988) 209.
12 R. H. Pullen, J. A. Howell and J. W. Cox, *Prostaglandins, Leukotrienes Med.*, 29 (1987) 205.
13 W. S. Powell, *Prostaglandins*, 20 (1980) 947.
14 W. S. Powell, *Methods Enzymol.*, 86 (1982) 467.
15 W. D. Watkins and M. B. Peterson, *Anal. Biochem.*, 125 (1982) 30.
16 H. Otani, M. R. Prasad, R. M. Engelman, H. Otani, G. A. Cordis and D. K. Das, *Circ. Res.*, 63 (1988) 930.
17 H. Otani, M. R. Prasad, R. M. Jones and D. K. Das, *Am. J. Physiol.*, 257 (1989) H252.
18 J. Nowak, L. Kaijser and A. Wennmalm, *Prostaglandins Leukotrienes Med.*, 4 (1980) 205.
19 D. K. Das and R. M. Engelman, in D. K. Das and W. B. Essman (Editors), *Oxygen Radicals: Systemic Events and Disease Processes*, S. Karger, Basel, 1989, p. 97.

Journal of Chromatography, 536 (1991) 319–325
Elsevier Science Publishers B.V., Amsterdam

CHROMSYMP. 2067

Rapid and simple high-performance liquid chromatographic determination of tricyclic antidepressants for routine and emergency serum analysis

MARIA PIA SEGATTI*, GIUSEPPE NISI, FLAVIA GROSSI and MARIANGELA MANGIAROTTI
Laboratorio di Analisi Chimico Cliniche, Ospedale Infantile "Burlo Garofolo", Via dell'Istria 65/1, Trieste (Italy)
and
CLAUDIO LUCARELLI
Laboratorio Biochimica Clinica, Istituto Superiore di Sanità, Via le R. Elena 299, Rome (Italy)

ABSTRACT

An isocratic reversed-phase high-performance liquid chromatographic procedure is presented for the simultaneous detection of desipramine, nortriptyline, imipramine, amitriptyline and clomipramine in serum. Drugs are extracted after sample alkalinization and separated from each other on an octyl reversed-phase with *n*-butylamine as mobile phase modifier. Detection is achieved at 254 nm. The recovery of tricyclic antidepressants (92–110%) has good precision, with a relative standard deviation of less than 5%. Being rapid and simple, the method is suitable for the emergency clinical laboratory.

INTRODUCTION

Tricyclic antidepressants (TCAs) are commonly used for the treatment of depressive disorders, as their efficacy in alleviating depression has been well established [1–4]. Many studies have indicated that the clinical outcome for this group of compounds might be concentration dependent, and also should show a marked variation among subjects in achieving a steady-state dose [5–7]. Therefore, it is desirable to monitor the concentrations of these drugs and their active metabolites in serum in order to minimize side-effects and avoid toxic reactions [8].

Many methods have been used for the determination of TCAs, including immunoenzymatic techniques and gas chromatography [9–12], but high-performance liquid chromatography (HPLC) is now widely used in routine application owing to its sensitivity, specificity and low cost [13–16].

The aim of this work was to develop a method that allows the simultaneous determination of five commonly prescribed TCAs: desipramine (DESI), nortriptyline (NOR), imipramine (IMI), amitriptyline (AMI) and clomipramine (CLO). Even though these drugs are never administered together, the availability of a single chromatographic method, suitable for their simultaneous detection, is very useful for

0021-9673/91/$03.50

the clinical laboratory, as the maintenance of separate chromatographic methods for each drug would be more expensive.

Of the relevant HPLC methods reported in the literature, we considered only those concerning the above-mentioned TCAs. Proelss *et al.* [17] described a technique involving ion-pair chromatography, but the recoveries at a concentration of 75 ng/ml were unsatisfactory (68–76%). Koteel *et al.* [15] needed an automated sample processor for a precision assay. Likewise, Lensemeyer and Evenson [14] and Lin and Frade [18] employed a set of disposable solid-phase cyanopropyl columns and a vacuum-elution system, respectively. Moreover, none of them considered the detection of clomipramine (CLO). In Matsumoto *et al.*'s method [19], automated column switching is necessary, the analysis time is long (CLO retention time = 30 min) and the day-to-day relative standard deviations (R.S.D.) at the 500 ng/ml level were higher than values obtained at the lower level (100 ng/ml).

In this paper, we propose a reversed-phase HPLC method for resolving the above TCAs within 15 min. The measurement of TCA serum levels is based on peak-area ratios of drug to internal standard at 254 nm. The pretreatment is simple and rapid, involving a single-step solvent extraction.

EXPERIMENTAL

Materials

All reagents were of analytical-reagent grade. Acetonitrile was purchased from J. T. Baker (Deventer, The Netherlands), hexane, sodium dihydrogenphosphate and *n*-butylamine from Merck (Darmstadt, F.R.G.) and sodium borate, sodium hydroxide and phosphoric acid from Carlo Erba (Milan, Italy). Desipramine hydrochloride and clobazam were obtained from Chiesi Farmaceutici (Parma, Italy), maprotiline, clomipramine, desmethylclomipramine and imipramine hydrochloride from Ciba Geigy (Varese, Italy), nortriptyline hydrochloride from Recordati (Milan, Italy) and amitriptyline from Roche (Milan, Italy). TCA stock standards (1 g/l) were prepared by dissolving the drugs in methanol.

Chromatography

The HPLC equipment consisted of a Model S2 pump (Perkin-Elmer, Norwalk, CT, U.S.A.), a Rheodyne Model 7105 injection valve, fitted with a 175-μl sample loop, and a Perkin-Elmer LC 75 UV spectrophotometric detector, set at 254 nm and 0.04 a.u.f.s. The analytical column was reversed-phase C_8 (150 mm × 4.6 mm I.D.), particle size 5 μm, connected to a 2-cm long Pelliguard LC-8 guard column with 40-μm packing, both from Supelco (Bellefonte, PA, U.S.A.).

The mobile phase was a modification of that proposed by Gill and Wanagho [20], consisting of acetonitrile–phosphate buffer (pH 3) in a 50:50 (v/v) mixture at a flow-rate of 1 ml/min. The buffer was obtained by adding 1.2 ml/l of butylamine to 0.01 *M* aqueous sodium dihydrogenphosphate and then adjusting the pH to 3 with phosphoric acid.

Extraction

To a screw-capped glass tube containing 1 ml of serum were added 3 μl of working internal standard solution (clobazam, 20 ng/ml), 1 ml of saturated sodium

borate (pH adjusted to 11 with 6 *M* sodium hydroxide) and 5 ml of *n*-hexane. The contents of the tube were mixed for 2 min and centrifuged for 10 min at 3000 *g*.

The organic phase was separated and evaporated to dryness under a stream of helium at 30°C. The residue was reconstituted in 20 μl of mobile phase and 10 μl were injected into the HPLC system.

RESULTS

Table I lists the capacity factors (k') of antidepressants most commonly used in the treatment of mood disorders in Italy and those of benzodiazepines, which may be administered simultaneously with TCAs in medical practice. Even if benzodiazepines had been extracted in a basic medium, as our method recommends, we observed no interference among benzodiazepines and the group of TCAs considered.

Table II gives the regression equations and correlation coefficients for the TCAs tested. The calibration graph was obtained by the plotting peak-area ratios (drug/internal standard) *versus* concentrations (ng/ml) of the drugs after analysing serum samples spiked with various amounts of TCAs (25–1000 ng/ml) and a fixed amount of internal standard (clobazam, 3 μl of 20 ng/ml solution). The relationship was linear over the range considered. The detection limit was *ca.* 10 ng/ml, sufficiently below the lowest therapeutic concentration (50 ng/ml). Nevertheless, it is possible to improve this limit by increasing the detector sensitivity or analysing a larger sample (>2 ml).

Table III shows the results of an analytical recovery study in which known amounts of drugs and internal standard were added to 1 ml of drug-free serum and carried out through the entire procedure. Reproducibility was assessed by reporting within- and between-assay results. The latter were calculated in a 5-day sequence over a 1-month period. As shown in Table IV, the within-day R.S.D. was <7% at 100 ng/ml, <4% at 250 ng/ml and <3% at 500 ng/ml. The between-assay R.S.D. ranged from 9.8% at 100 ng/ml to 3.9% at 500 ng/ml.

Fig. 1 illustrates chromatograms of a blank serum used for recovery and precision studies and the same serum supplemented with TCA standard (100 ng/ml). Fig. 2 shows representative chromatograms obtained from a child who had

TABLE I

RETENTION BEHAVIOUR OF TCAs AND OTHER DRUGS COMMONLY PRESCRIBED IN PSYCHIATRIC DISORDERS: INTERFERENCE STUDY AT 254 nm

Drug	k'	Drug	k'
Nitrazepam	0.831	Diazepam	1.830
Lorazepam	0.853	Haloperidol	1.976
Clonazepam	0.916	Desipramine	2.282
Triazolam	1.009	Nortriptyline	2.460
Desmethylclomipramine	1.092	Maprotiline	2.613
Flunitrazepam	1.185	Imipramine	3.025
Alprazolam	1.200	Amitriptyline	3.333
Clobazam	1.344	Clomipramine	4.085

TABLE II

LINEAR REGRESSION AND CORRELATION PARAMETERS DETERMINED BETWEEN 25 AND 1000 ng/ml

y = Peak area ratio drug/internal standard; x (ng/ml) = concentration of TCA.

Drug	Regression equation	r
Desipramine	$y = 0.0132x - 0.105$	0.98
Nortriptyline	$y = 0.0127x - 0.050$	0.99
Imipramine	$y = 0.0235x - 0.011$	0.99
Amitriptyline	$y = 0.0138x - 0.104$	0.99
Clomipramine	$y = 0.0196x - 0.033$	0.99

accidentally ingested an unknown number of clomipramine pills. The chromatograms correspond to two blood samples collected 2 h (left) and 5 h (right) after the pills had been swallowed. The results were obtained 30 min after the child was admitted to the emergency room.

DISCUSSION AND CONCLUSIONS

The method proposed for TCA determination involves a one-step clean-up and a resolution on a C_8 reversed-phase column with a binary mixture of acetonitrile and a phosphate buffer (pH 3) and *n*-butylamine as mobile phase modifier. For sample pretreatment, a single-step liquid–liquid extraction was preferred to a solid-phase extraction [15,18,19] because it does not require any special apparatus. Several efforts were made using different combinations of extractants; *n*-hexane–ethyl acetate or *n*-hexane–isoamyl alcohol were evaluated in order to improve the efficiency and avoid

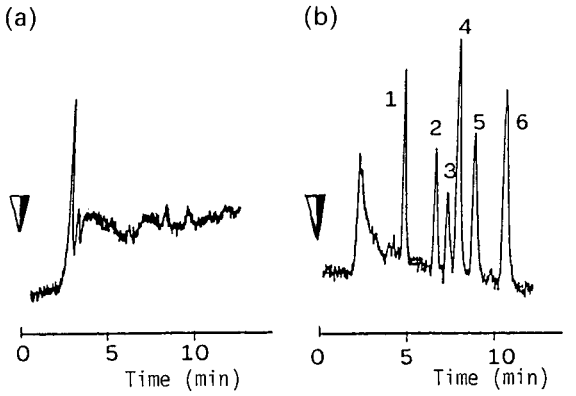

Fig. 1. Chromatogram of 10 µl of (a) drug-free human serum extract and (b) extract of serum, containing 100 ng/ml of each the tricyclic antidepressants analysed. Peaks: 1 = clobazam (internal standard); 2 = desipramine; 3 = nortriptyline; 4 = imipramine; 5 = amitryptyline; 6 = clomipramine. Mobile phase, acetonitrile–phosphate buffer (pH 3) (3:2); column, RP-C_8, 150 mm × 4.6 mm I.D.; flow-rate, 1 ml/min; detection, 254 nm (0.04 a.u.f.s.).

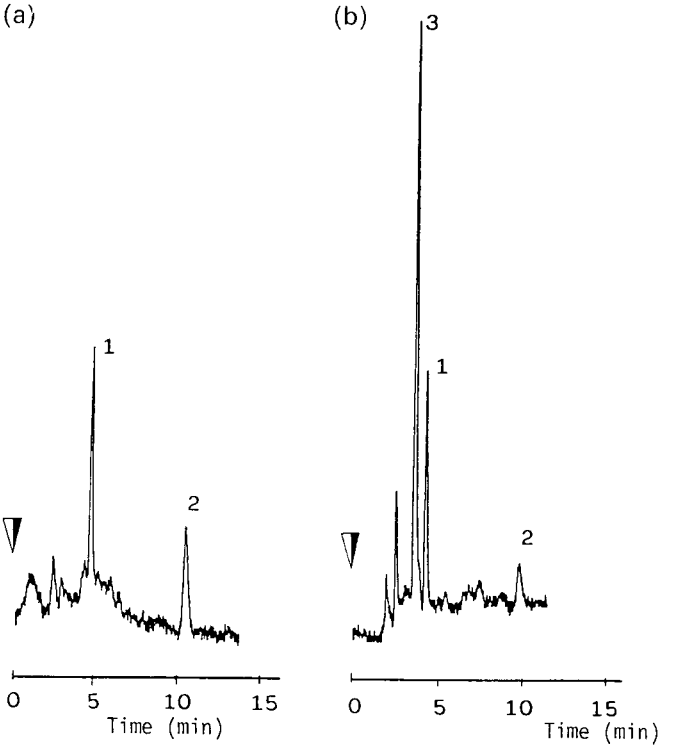

Fig. 2. Chromatograms of a serum extract obtained from a child who had accidentally ingested clomipramine. Sampling time: (left) 2 h and (right) 5 h after drug ingestion. Peaks: (a) 1 = clobazam (I.S.); 2 = clomipramine (50 ng/ml); (b) 1 = clobazam (I.S.); 2 = clomipramine (14.5 ng/ml); 3 = desmethylclomipramine. HPLC conditions as in Fig. 1.

TABLE III

ANALYTICAL RECOVERY OF TRICYCLIC ANTIDEPRESSANTS IN FORTIFIED SERUM AFTER EXTRACTION (n = 30)

Drug	Level (ng/ml)	Recovery (%)	R.S.D. (%)
Desipramine	100	94.6	6.4
Nortriptyline		93.2	6.7
Imipramine		95.4	5.7
Amitriptyline		96.1	7.5
Clomipramine		91.7	8.4
Desipramine	250	97.1	3.8
Nortriptyline		96.8	5.3
Imipramine		96.4	4.8
Amitriptyline		97.5	5.1
Clomipramine		102.6	4.1
Desipramine	500	108.2	4.0
Nortriptyline		105.5	3.8
Imipramine		98.9	3.4
Amitriptyline		104.5	4.5
Clomipramine		110.6	4.1

TABLE IV

PRECISION

Data pertain to a serum supplemented with three different amounts of TCAs.

Drug	Concentration added (ng/ml)	Within-day (n = 6)		Between-day (n = 5)	
		Concentration found (ng/ml)	R.S.D. (%)	Concentration found (ng/ml)	R.S.D. (%)
Desipramine	100	93.4	4.2	95.1	5.2
	250	257.3	2.8	234.6	4.2
	500	537.9	2.0	554.1	4.7
Nortryptiline	100	92.8	4.0	93.6	6.0
	250	248.9	2.7	235.2	5.9
	500	536.3	1.8	512.4	4.2
Imipramine	100	94.6	4.5	95.0	7.1
	250	225.6	3.1	236.4	5.2
	500	502.3	2.1	489.2	3.9
Amitriptyline	100	96.9	3.8	95.1	6.9
	250	251.2	2.9	237.3	4.7
	500	501.5	2.0	537.4	4.0
Clomipramine	100	92.1	5.3	91.3	9.8
	250	269.2	3.8	225.7	4.6
	500	547.1	2.9	569.2	5.1

emulsions or endogenous impurities. n-Hexane alone was found to be adequate, the recovery being close to 100% at several widely different concentrations. We found a discrepancy with a previously published paper [17], in that we did not notice any losses of the analysed drugs if isoamyl alcohol was absent from the extraction procedure. This was also confirmed by the high recoveries. Extracts prepared from TCA-free serum yielded no endogenous peaks with retention times similar to those of the antidepressant tricyclic drugs. Consequently, further purification as described by other workers [17] is not required.

In the elution of TCAs, the strong hydrogen-bonding interaction between the amino side-chain of TCAs with the possible free silanol group of the silica support of the reversed-phase packing broadens the peaks. The use of n-butylamine in the mobile phase improves the resolution and peak shape. Variables of the composition of the mobile phase, such as pH, buffer strength, concentration of amine added and acetonitrile percentage were considered in order to determine their effectiveness in recovering the TCAs. Retention of drugs and their separation from interfering substances on the C_8 column were not influenced by the pH or buffer strength of the eluent mixture, but the concentration of acetonitrile in particular had a very significant effect on k'. We found that the resolution of TCA also increased as the concentration of n-butylamine increased.

The choice of wavelength required a compromise between sensitivity and baseline noise, since at 254 nm the background noise, due to the mobile phase modifier,

is less than that at lower wavelengths, whereas the sensitivity is sufficiently high to determine serum TCAs at therapeutic levels. There is no interference from drugs, such as benzodiazepines or TCA metabolites, an observation made also by other workers [18]. In developing the assay, it was difficult to obtain an internal standard that would behave in a manner similar to TCAs in the extraction procedure and yet have acceptabe absorption at 254 nm and chromatographic retention times. As benzodiazepines were suitable for this purpose, we propose clobazam as an internal standard. For clinical use, when clobazam is simultaneously administered as medication, an alternative internal standard may be used, such as another TCA, as situations in which more than one TCA is administered at the same time are rare.

REFERENCES

1 L. E. Holister, *Drugs*, 22 (1981) 129.
2 J. T. Biggs, *Hosp. Pract.*, 13 (1978) 79.
3 J. P. Moody, A. C. Tait and A. Todrick, *Br. J. Psychiatry*, 13 (1967) 183.
4 A. Viala, J. P. Cano and A. Durand, *Encephale*, 6 (1980) 316.
5 V. E. Ziegler, L. T. Wylie and J. T. Biggs, *J. Pharm. Sci.*, 67 (1978) 554.
6 M. Asberg and F. Sjoquist, *Commun. Psychopharmacol.*, 2 (1978) 381.
7 M. Dugas, E. Zarifian, M. F. Leheuzey, V. Rovey, G. Durand and P. L. Morselli, *Ther. Drug. Monit.*, 2 (1980) 307.
8 APA, Task Force Report, *Am. J. Psychiatry*, 142 (1985) 155.
9 S. Pankey, C. Collins and A. Jaklitsh, *Clin. Chem.*, 32 (1986) 768.
10 M. C. Haven, D. J. Orsulak, J. A. Huth and R. S. Markin, *Clin. Chem.*, 33 (1987) 1472.
11 D. Bailey and P. Jatlow, *Clin. Chem.*, 22 (1976) 1697.
12 H. B. Hucker and S. C. Stauffer, *J. Chromatogr.*, 138 (1977) 437.
13 S. H. Wong, *Clin. Chem.*, 34 (1986) 848.
14 G. L. Lensemeyer and M. A. Evenson, *Clin. Chem.*, 30 (1984) 1774.
15 P. Koteel, R. E. Mullins and R. H. Gadsden, *Clin. Chem.*, 28 (1982) 462.
16 E. L. Crampton, R. C. Glass, B. Marchant and J. A. Rees, *J. Chromatogr.*, 183 (1980) 141.
17 H. Proelss, H. Lohmann and D. Miles, *Clin. Chem.*, 24 (1978) 1948.
18 W. Lin and P. Frade, *Ther. Drug. Monit.*, 9 (1987) 448.
19 K. Matsumoto, S. Kanba, H. Kubo, G. Yagi, H. Iri and H. Yuki, *Clin. Chem.*, 35 (1989) 453.
20 R. Gill and S. O. Wanagho, *J. Chromatogr.*, 391 (1987) 461.

Journal of Chromatography, 536 (1991) 327–335
Elsevier Science Publishers B.V., Amsterdam

CHROMSYMP. 2068

High-performance liquid chromatographic evaluation of 2-(α-thenoylthio)propionylglycine and its two metabolites in biological fluids

A. MARZO*, E. ARRIGONI MARTELLI, G. BRUNO and D. NAVA
Sigma-Tau SpA, Via Pontina Km. 30.400, 00040 Pomezia, Rome (Italy)
and
A. MIGNOT, R. VIDAL and M. A. LEFEBVRE
Centre d'Etudes et de Recherche en Pharmacie Clinique, Avenue du Haut de la Chaume, 86280 Saint Benoit (France)

ABSTRACT

A high-performance liquid chromatographic (HPLC) method for determining 2-(α-thenoylthio)propionylglycine (TTPG) and its two main metabolites, thiophenecarboxylic acid and thiopronine, in biological samples was developed. TTPG and its metabolites were extracted by solvent partition and then determined by reversed-phase HPLC with UV detection at 245, 295 and 360 nm. This procedure was validated in order to allow the assay of these compounds in plasma and urine samples with sufficiently low detection limits (50 ng/ml for TTPG and TCA and 100 ng/ml for thiopronine) and with good linearity within the concentration range investigated. It was applied to a comprehensive pharmacokinetic investigation of TTPG in healthy volunteers.

INTRODUCTION

2-(α-Thenoylthio)propionylglycine (TTPG) is a mucolytic agent which modifies bronchial secretion [1,2]. In man, it reduces mucus viscosity. In order to evaluate the pharmacokinetics of TTPG and its two main systemic metabolites, thiophene-2-carboxylic acid (TCA) and 2-mercaptopropionylglycine (thiopronine), a high-performance liquid chromatographic (HPLC) method was developed.

TTPG

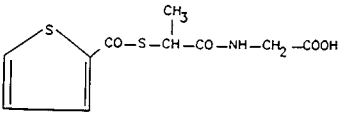

TCA

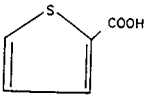

Thiopronine

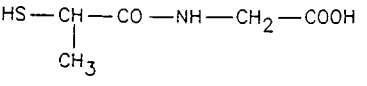

0021-9673/91/$03.50

Owing to the differences in the chemical and physical properties of the three substances, it is not possible to evaluate all of them by the same method. Two HPLC techniques with UV detection have been described previously, but only for TTPG in biological samples [3,4]. Few methods for the determination of thiol compounds by derivatization for fluorimetric or UV detection have been reported [5–8]. Our technique was based on reversed-phase HPLC, following a two-step extraction process, which enabled both TTPG and TCA to be determined with UV detection at 295 and 245 nm, respectively, and thiopronine to be determined with UV detection at 360 nm after derivatization with 2,4-dinitrofluorobenzene.

EXPERIMENTAL

Materials

TTPG and thiopronine were supplied by Sigma Tau Labs. and trichloroacetic acid (TCA), thiopheneacetic acid (TAA) and N-acetylcysteine by Janssen Chimica (Beerse, Belgium). All chemicals and HPLC-grade solvents were purchased from Merck (Bracco, Milan, Italy). The liquid chromatograph consisted of a Waters Assoc. Model M 590 pump (Millipore, Milford, MA, U.S.A.), an Waters Assoc. Wisp 710 B automatic injector and a Model 2550 variable-wavelength UV detector (Varian, Sunnyvale, CA, U.S.A.). The chromatographic columns were Nucleosil C_{18}, 5 μm (125 × 4.6 mm I.D.), purchased from Bischoff (Lymark, Roissy Charles de Gaulle, France) for TTPG and TCA and Hypersil ODS, 5 μm (250 × 4.6 mm I.D.), purchased from Shandon (Runcorn, U.K.) for thiopronine.

Assay of TTPG and TCA

Extraction procedure. In a 20-ml test-tube, 1 g of sodium chloride, 1 ml of plasma, 50 μl of a 15 μg/ml methanolic solution of TAA, 50 μl of a suitable standard solution of TTPG, TCA (calibration or control) or 100 μl of methanol (plasma samples) and 1 μl of buffer (pH 1.0) were successively introduced. After mixing for 10 s, the extraction solvent (5 ml), consisting of diethyl ether–hexane (50:50), was added. The tube was shaken for 15 min and centrifuged (10 min, 2000 *g*). The organic phase (4 ml) was transferred into a 10-ml tube containing 0.04 *M* disodium hydrogenphosphate solution (300 μl). After shaking for 5 min and centrifuging (5 min, 2000 *g*), the organic phase was discarded. An aliquot of the aqueous layer (200 μl) was transferred into a tube containing 20 μl of 10 *M* hydrochloric acid. The tube was shaken for 10 s and the mixture was ready for injecton into the HPLC system. Extraction from urine was carried out as described for plasma, with the addition of a washing step (3 ml of ethyl acetate) after the back-extraction of TTPG and TCA with the disodium hydrogenphosphate solution.

Preparation of standard solutions and eluent. Stock solutions of TTPG and TCA were prepared by dissolving the analytical standard (50 mg) in methanol (50 ml) in order to obtain a (1000 μg/ml) solution. The internal stock standard solution (TAA) was prepared by dissolving the analytical standard (15 mg) in methanol (100 ml) in order to obtain a 150 μg/ml solution. Mobile phase was prepared by adding acetonitrile (150 ml), potassium dihydrogenphosphate (1.36 g) and orthophosphoric acid (1 ml) and water to give a 1000 ml volume.

HPLC analysis. HPLC was performed under isocratic conditions at a flow-rate

of 1 ml/min and room temperature; a change of the wavelength was used for the detection of TCA and TAA at 245 nm (0–15 min) and TTPG at 295 nm (5–25 min). Under these conditions the retention times of TCA, TAA and TTPG were 8, 9.3 and 25 min, respectively.

Preparation of calibration graphs. Calibration graphs were obtained from drug-free blank plasma or urine. To each 1 ml of blank plasma or urine 50 μl of the appropriate solution were added to achieve final concentrations of TTPG and TCA of 2000, 1000, 500, 100 and 50 ng/ml. The blank sample was obtained by adding 100 μl of methanol to 1 ml of plasma. Reproducibility was assessed using blank plasma samples spiked with concentrations of the analytes (TCA or TTPG) of 2000, 500, 100, 50 and 0 ng/ml.

Assay of thiopronine

Extraction procedure. In a 20-ml test-tube, 1 ml of plasma, 100 μl of a 10 μg/ml solution of N-acetylcysteine containing 50 μg/ml dithiothreitol (DTT), 100 μl of the appropriate solution (calibration or control) or 100 μl of water containing 50 μg/ml DTT (plasma samples), 1 ml of water and 100 μl of 5 *M* hydrochloric acid were successively introduced. After mixing for 10 s, the extraction solvent (4 ml) consisting of diethyl ether–methylene chloride (60:40) was added. The tube was shaken and centrifuged (10 min, 2000 *g*). Then they were kept at −20°C for 10 min. The organic phase was discarded. This operation was repeated once. The aqueous phase (2.2 ml) was transferred to another tube and 0.5 ml of 0.5 *M* sodium carbonate solution was added. After mixing for 10 s, 400 μl of a 5 mg/ml aqueous solution of DTT were added. Then 0.269 *M* 2,4-dinitrofluorobenzene solution (125 μl) was added and the mixture was heated for 40 min at 60°C. The tube was cooled and hexane (5 ml) was added. After shaking for 10 min and centrifuging (5 min, 2000 *g*), the organic phase was discarded. To the aqueous phase 5 *M* hydrochloric acid (100 μl) and the extraction solvent (7 ml) were added. The tube was mixed for 10 min and centrifuged (5 min, 2000 *g*). The organic phase was transferred to a 10-ml tube, then evaporated to dryness under a gentle stream of nitrogen (40°C). The residue was resuspended in the mobile phase (250 μl) and the sample was ready for injection into the HPLC system. Extraction from urine was the same as described for plasma, except that 1 *M* $NaHCO_3$ was used instead of 0.5 *M* Na_2CO_3, the residue being dissolved in 1 ml of mobile phase.

Preparation of standard solutions and eluents. Stock solutions of thiopronine and of N-acetylcysteine were prepared by dissolving analytical standards (50 mg) in water containing 50 μg/ml DTT, in order to obtain two 1000 μg/ml solutions. Mobile phase A for plasma analysis was prepared by adding acetonitrile (70 ml), potassium dihydrogenphosphate (1.36 g) and orthophosphoric acid (1 ml), completed to 1000 ml with distilled water. Mobile phase B for urine analysis was prepared by adding acetonitrile (50 ml), tetrahydrofuran (20 ml), distilled water (950 ml) and potassium dihydrogenphosphate (1.36 g).

HPLC analysis. HPLC was performed at a flow-rate of 1 ml/min and room temperature and with UV detection at 360 nm.

Urine samples were analysed under isocratic conditions (90% B, 10% acetonitrile) and plasma samples according to the following gradient programme: 0–12 min, A–acetonitrile from 80:20 to 70:30; 12–15 min, A–acetonitrile from 70:30 to 65:35; 15–25 min, linear increase to 100% acetonitrile; 25–30 min, 100% acetonitrile; 30–32 min, linear decrease to A–acetonitrile (80:20); 32–35 min, A–acetonitrile (80:20).

Under these conditions, the retention times were thiopronine 14 min and internal standard 11 min. In urine analysis, the retention time of thiopronine was 33 min.

Preparation of calibration graphs. For the preparation of calibration graphs, to each 1 ml of blank plasma (100 μl of blank urine) 100 μl of the appropriate solution were added to achieve final thiopronine concentrations of 2, 1, 0.5, 0.2 and 0.1 μg/ml

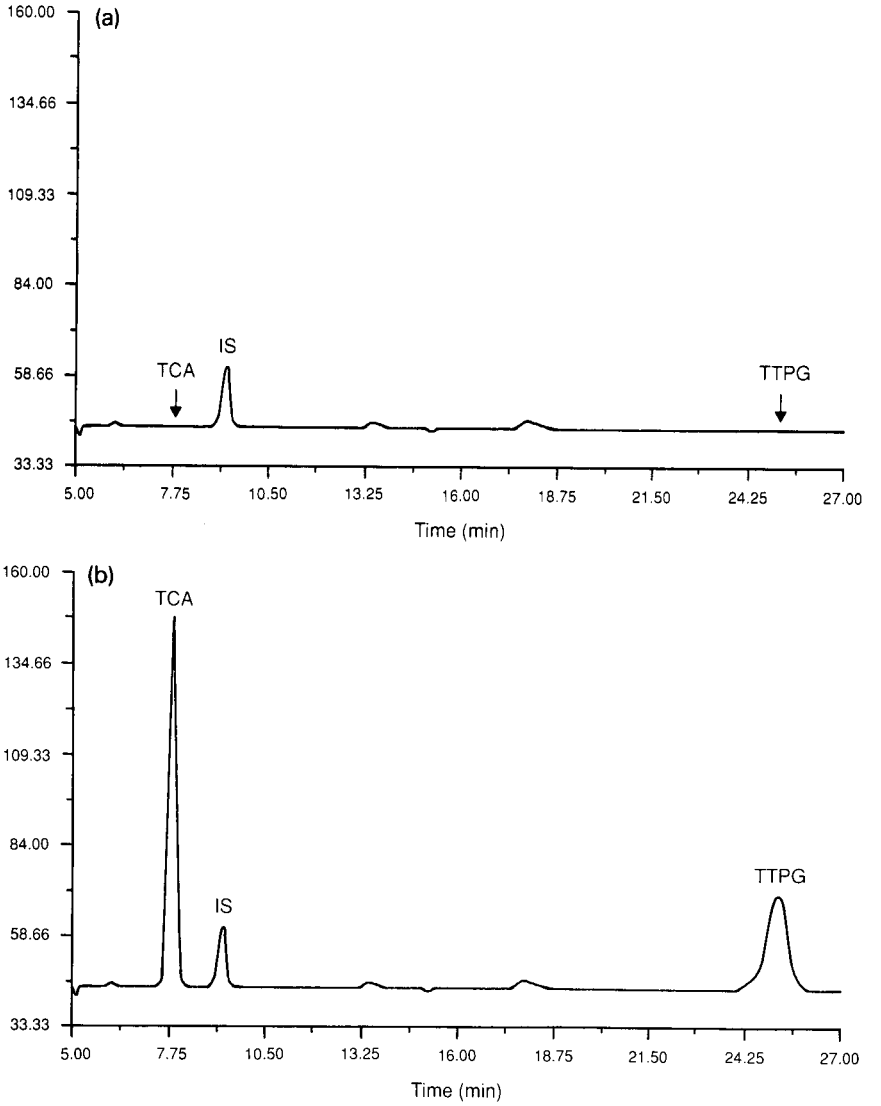

Fig. 1. Representative chromatograms obtained with (a) a blank plasma sample and (b) a blank plasma sample spiked with 2000 ng/ml of TTPG and TCA. The chromatographic column was Nucleosil C_{18}, 5 μm (125 × 4.6 mm I.D.). The eluent was 0.01 *M* potassium dihydrogenphosphate and 1 ml orthophosphoric acid in acetonitrile–water (15:85). The sample aliquot injected was 50 μl. The flow-rate was 1 ml/min. UV detection was performed at 245 nm (0.02 a.u.f.s.) from 0 to 15 min and at 295 nm (0.01 a.u.f.s.) from 5 to 25 min.

for plasma and 200, 100, 50, 20 and 10 μg/ml for urine. The blank plasma (or urine) was obtained by adding a 50 μg/ml aqueous solution of DTT (100 μl) to 1 ml of plasma (or 100 μl of urine). Reproducibility was assessed using blank plasma spiked with concentrations of the analyte of 1.5, 0.5, 0.2 and 0.1 μg/ml.

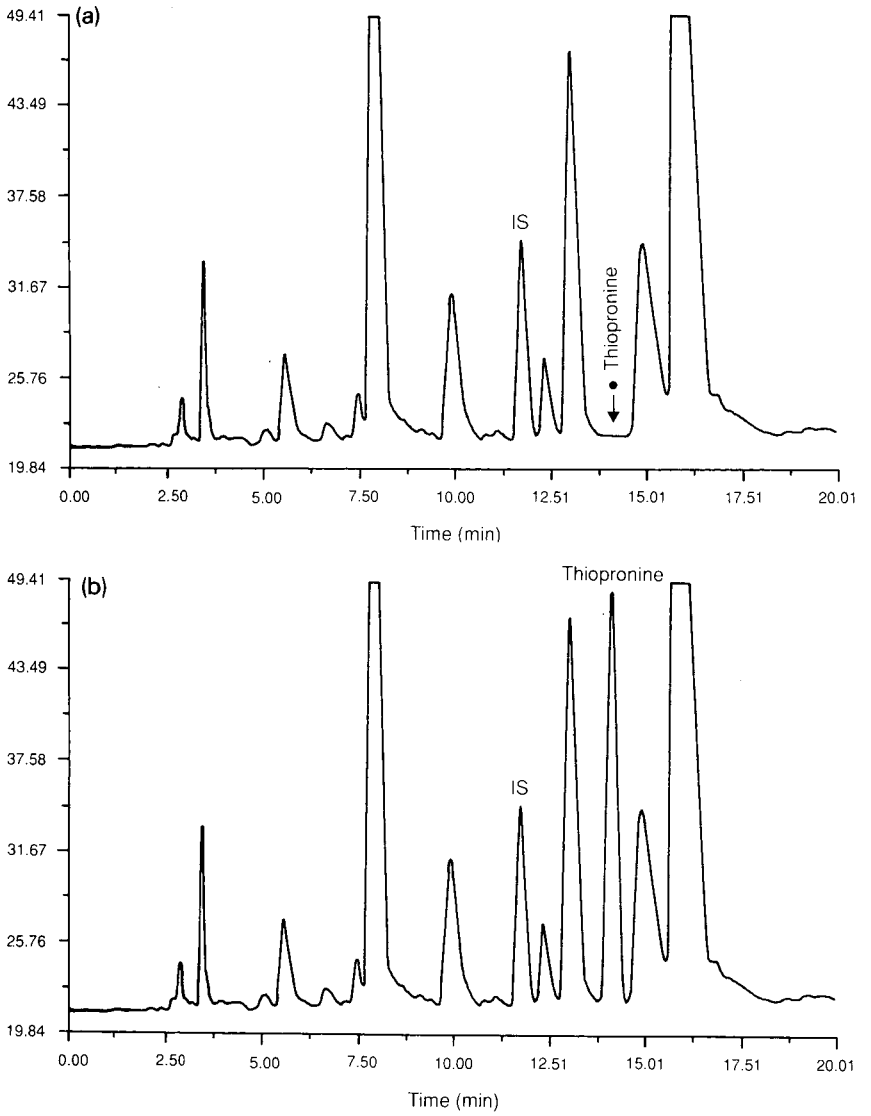

Fig. 2. Representative chromatograms obtained with (a) a blank plasma sample and (b) a blank plasma sample spiked with 2000 ng/ml of thiopronine. The chromatographic column was Hypersil ODS, 5 μm (250 × 4.6 mm I.D.). Eluent A was 0.01 *M* potassium dihydrogenphosphate and 1 ml orthophosphoric acid in acetonitrile–water (7:93). Elution was carried out according to the gradient programme given in the text. The sample aliquot injected was 20 μl. The flow-rate was 1 ml/min. UV detection was performed at 360 nm (0.01 a.u.f.s.).

Pharmacokinetic study with healthy volunteers

Twelve subjects were involved in the pharmacokinetic study; all of them received a single oral dose of 540 mg of TTPG. Blood samples were collected 10, 20, 30 and 45 min and 1, 1.25, 1.5, 2, 3, 4, 6, 8, 10 and 12 h after administration. Urine samples were collected at 0–2, 2–4, 4–6 and 6–12 h. A basal sample of blood and urine was also collected.

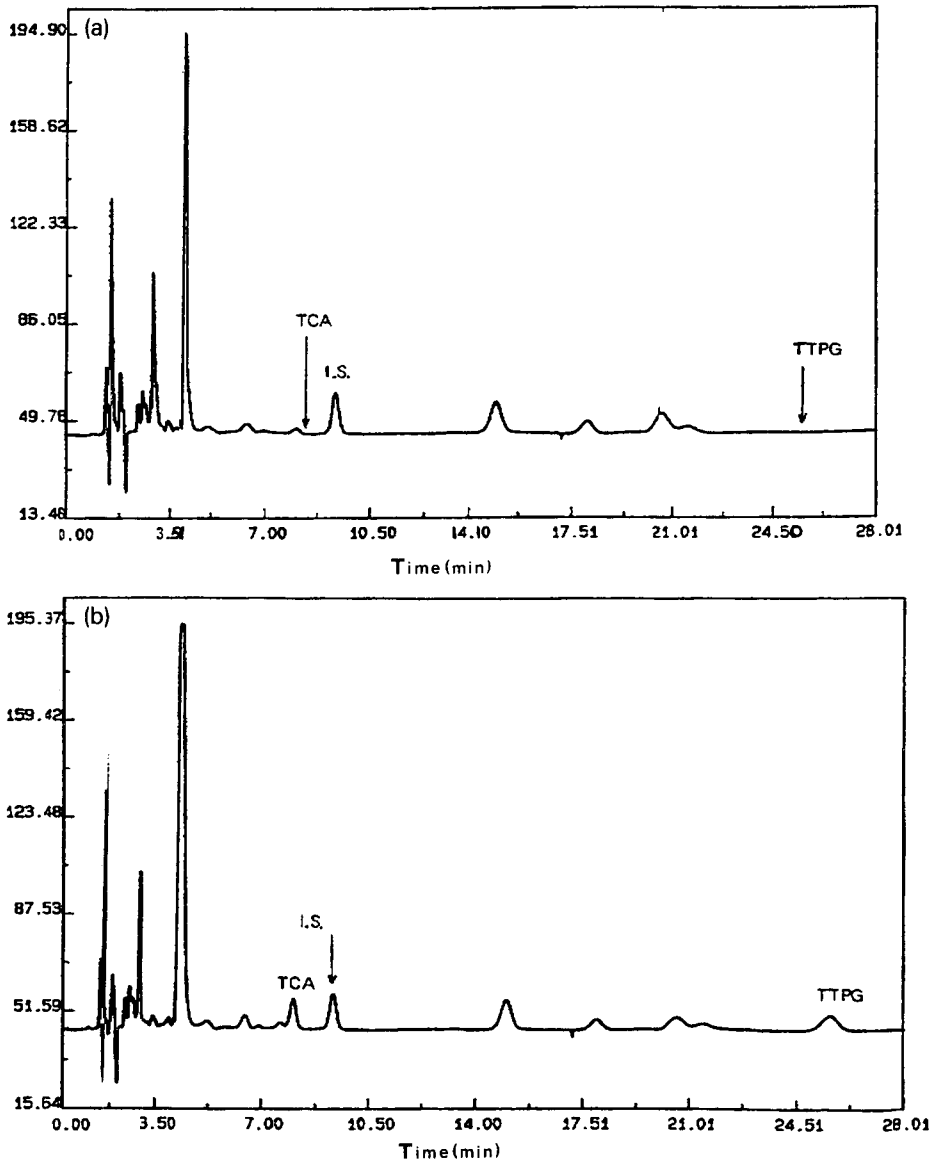

Fig. 3. Representative chromatograms obtained with (a) a blank urine sample and (b) a blank urine sample spiked with 500 ng/ml of TTPG and TCA. For chromatographic conditions, see Fig. 1.

TABLE I

RECOVERY AND LINEARITY IN THE DETERMINATION OF TTPG, TCA AND THIOPRONINE IN PLASMA AND URINE

Sample	Range studied (μg/ml)	n	Linear correlation[a]	r	Mean recovery (%)	R.S.D. (%)
TTPG in plasma	0.05–2.0	31	$y = -7.490 + 1.040x$	0.9995	100	1.72–5.26
TTPG in urine	0.2 –2.0	19	$y = 0.006 + 0.928x$	0.9996	92.7	1.03–7.73
TCA in plasma	0.05–2.0	30	$y = -4.520 + 1.059x$	0.9998	100	0.52–3.13
TCA in urine	0.2 –2.0	17	$y = -0.018 + 1.006x$	0.9937	99.1	5.27–10.88
Thiopronine in plasma	0.1 –1.5	62	$y = 10.844 + 0.9931x$	0.9941	99.3	2.01–5.40
Thiopronine in urine	10 –200	28	$y = -1.608 + 0.998x$	0.9848	97.4	7.42–13.31

[a] y = Drug recovered (μg/ml); x = drug added (μg/ml).

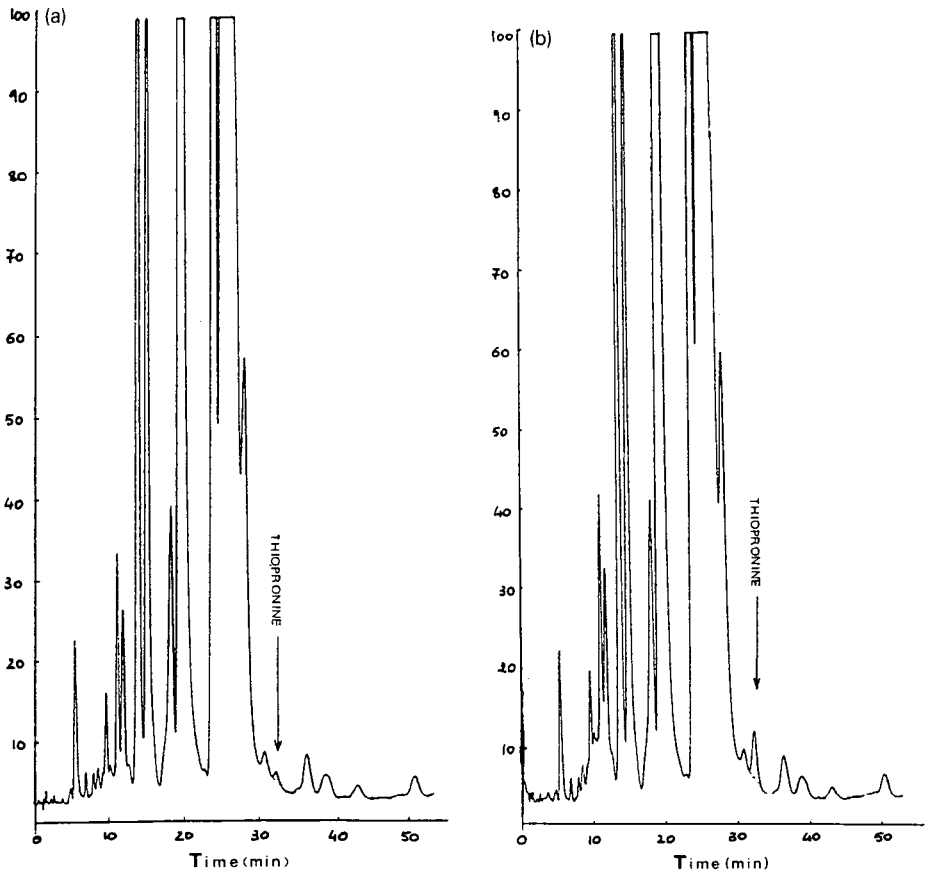

Fig. 4. Representative chromatograms obtained with (a) a blank urine sample and (b) a blank urine sample spiked with 10 μg/ml of thiopronine. The chromatographic column was Hypersil ODS, 5 μm (250 × 4.6 mm I.D.). Eluent B was 0.01 *M* potassium hydrogenphosphate in acetonitrile–tetrahydrofuran–water (5:2:93). Elution was carried out under isocratic conditions using B–acetonitrile (90:10). The sample aliquot injected was 20 μl. The flow-rate was 1 ml/min. UV detection was performed at 360 nm (0.01 a.u.f.s.).

TABLE II

MEAN VALUES ± STANDARD DEVIATION OF TTPG, TCA AND THIOPRONINE PHARMACOKINETIC PARAMETERS AFTER A SINGLE 540-mg ORAL ADMINISTRATION OF TTPG TO HEALTHY VOLUNTEERS

Parameter[a]	TTPG	TCA	Thiopronine
C_{max} ($\mu g\ ml^{-1}$)	2.49 ± 0.75	1.22 ± 0.43	8.02 ± 2.27
t_{max} (h)	0.39 ± 0.08	0.53 ± 0.32	0.71 ± 0.23
AUC_{0-t} ($\mu g\ ml^{-1}$ h)	2.04 ± 0.66	1.34 ± 0.51	23.16 ± 6.81
$AUC_{0-\infty}$ ($\mu g\ ml^{-1}$ h)	2.19 ± 0.71	1.50 ± 0.48	25.06 ± 7.20
$t_{1/2}$ (h)	0.54 ± 0.24	0.91 ± 0.36	3.51 ± 0.64
MRT (h)	0.94 ± 0.31	1.38 ± 0.47	4.04 ± 0.44
Lag time (h)	0.00 ± 0.00	0.00 ± 0.00	0.01 ± 0.05

[a] C_{max}, peak concentration; t_{max}, time to peak; AUC, area under the plasma concentration–time curve; $t_{1/2}$, dominant half-life; MRT, mean residence time.

RESULTS AND DISCUSSION

TTPG and TCA were extracted from plasma (or urine), then back-extracted into an aqueous phase and separated from endogenous compounds in a reversed-phase chromatographic mode with UV detection at 295 nm (TTPG) and 245 nm (TCA, TAA) (Figs. 1–3). The lowest detectable concentration was 50 ng/ml in plasma and 200 ng/ml in urine. The plasma and urine calibration graphs were linear for concentrations ranging from 50 to 2000 ng/ml of TCA and TTPG (Table I). The relative standard deviations (R.S.D.) were 1.72–5.26% and 1.03–7.73% for TTPG in plasma and urine, respectively, and 0.52–3.13% and 5.27–10.88% for TCA in plasma and urine (Table I).

A method able to measure thiopronine was also developed. A two-step extraction was performed, always using a reducing compound (DTT) in order to avoid the easy oxidation of thiol groups. Then a chromatographic gradient allowed the separation of both thiopronine and N-acetylcysteine from endogenous compounds to be carried out; UV detection was performed at 360 nm after derivatizing thiopronine with 2,4-dinitrofluorobenzene (Figs. 2–4). The lowest detectable concentration was 100 ng/ml. The calibration graphs were linear for concentrations ranging from 0.1 to 2.0 μg/ml of thiopronine for plasma and from 10 to 200 μg/ml of thiopronine for urine (Table I). The R.S.D.s were 2.01–5.40% for plasma and 7.42–13.31% for urine.

TABLE III

URINARY EXCRETION OF TTPG, TCA AND THIOPRONINE FOLLOWING A 540-mg SINGLE ORAL ADMINISTRATION OF TTPG TO HEALTHY VOLUNTEERS

Mean values in mg and as a percentage of the dose administered in the 0–12-h period, ± standard deviation.

Unit	TTPG	TCA	Thiopronine
mg	3.14 ± 2.42	0.125 ± 0.124	170.49 ± 49.42
%	0.58 ± 0.45	0.05 ± 0.05	52.88 ± 15.33

After a preliminary pharmacokinetic study, it was concluded that, following oral administration of a single 540-mg dose, TTPG is rapidly absorbed. As the two main metabolites, TCA and thiopronine, are rapidly detected in plasma, the metabolism of TTPG should be considered as a rapid event (Table II). Moreover considering the area under the curve and cumulative recovery for urine, thiopronine appears to be the main circulating compound (Table III).

REFERENCES

1 R. Hammer, G. Bozler, R. Jauch and F. W. Koss, *Arzneim.-Forsch.*, 28 (1978) 899.
2 R. Jauch, G. Bozler, R. Hammer and F. W. Koss, *Arzneim.-Forsch.*, 28 (1978) 904.
3 I. Duranti, G. Gagauzzi, L. Zeuli, G. Oriani, F. Lisciani and D. Nava, *Farmaco, Ed. Prat.*, 10 (1985) 347.
4 J. M. Aiache, *Dosage de l'Alpha Thenoylthiopropionylglycine (EP2) dans le Plasma par Chromatographie Liquide sous Haute Pression*, Sigma Tau, Rome, 1982.
5 W. Baeyens, G. van der Weken, B. Lin Ling and P. de Moerloose, *Anal. Lett.*, 21 (1988) 741.
6 M. Johansson and D. Westerlund, *J. Chromatogr.*, 385 (1987) 343.
7 B. Kagedal and N. Källberg, *J. Chromatogr.*, 229 (1982) 409.
8 P. A. Lewis, A. J. Woodward and J. Maddock, *J. Pharm. Sci.*, 73 (1984) 996.

Journal of Chromatography, 536 (1991) 337–341
Elsevier Science Publishers B.V., Amsterdam

CHROMSYMP. 2069

High-performance liquid chromatographic method for the determination of prolyl peptides in urine

M. CODINI*, C. A. PALMERINI and C. FINI
Dipartimento di Medicina Sperimentale e Scienze Biochimiche, Università di Perugia, Perugia (Italy)
C. LUCARELLI
Istituto Superiore di Sanità, Rome (Italy)
and
A. FLORIDI
Dipartimento di Medicina Sperimentale e Scienze Biochimiche, Università di Perugia, Perugia (Italy)

ABSTRACT

A rapid and accurate method is described for the determination of prolyl peptides in urine, with specific reference to the dipeptide prolylhydroxyproline, and free hydroxyproline and proline. Free amino acids and peptides were isolated from urine on cation-exchange minicolumns, and free imino acids and prolyl-N-terminal peptides were selectively derivatized with 4-chloro-7-nitrobenzofurazan, after reaction of amino acids and N-terminal aminoacyl peptides with *o*-phthalaldehyde. The highly fluorescent adducts of imino acids and prolyl peptides were separated on a Spherisorb ODS 2 column by isocratic elution for 12 min using as mobile phase 17.5 m*M* aqueous trifluoroacetic acid solution containing 12.5% acetonitrile (eluent A), followed by gradient elution from eluent A to 40% of 17.5 m*M* aqueous trifluoroacetic acid solution containing 80% acetonitrile in 20 min. Analytes of interest, in particular the dipeptide prolyl-hydroxyproline, can be easily quantified by fluorimetric detection (ε_{ex} = 470 nm, ε_{em} = 530 nm) without interference from primary amino-containing compounds.

INTRODUCTION

Total urinary hydroxyproline (Hyp) consists of 1–3% free Hyp and more than 95% of a peptide-bound form; the prolylhydroxyproline (Pro–Hyp) dipeptide represents about 60% of all Hyp peptides excreted [1,2]. The urinary oligo- and dipeptides containing hydroxyproline are a reflection of collagen metabolism [3,4]. A strongly increased excretion of dipeptides containing imino acids is observed in individuals suffering from diseases concerning collagen metabolism [5–7]. Thus, the determination of this dipeptide fraction in urine can be regarded as suitable for clinical biochemical studies of disorders of collagen metabolism.

The determination of urinary peptides together with free amino acids has been accomplished by ion-exchange chromatography on columns packed with sulphonated polystyrene resins [8]. The subsequent improvement of this technique has allowed the separation and identification of a large number of peptides of different molecular sizes, some of which contained Hyp [9–11].

0021-9673/91/$03.50

More recently, attention has been turned to the study of the fractionation of urinary dipeptides by gas chromatography [12–15]. Although very efficient, this method is tedious and time consuming and therefore unsuitable for routine determinations. High-performance liquid chromatography (HPLC) is simpler, but few data are available in the literature [16,17].

In this paper, we report an HPLC method for the selective determination of propyl peptides in urine, together with free imino acids.

EXPERIMENTAL

Materials

Hyp, proline (Pro), prolylleucine (Pro–Leu), prolylglycine (Pro–Gly), Pro–Hyp, prolylproline (Pro–Pro), 4-chloro-7-nitrobenzofurazan (NBD-Cl) and *o*-phthalaldehyde (OPA) were obtained from Sigma (St. Louis, MO, U.S.A.), analytical-reagent-grade trifluororacetic acid (TFA) and boric acid from Merck (Darmstadt, F.R.G.), methanol and acetonitrile (HPLC grade) from Inalco (Milan, Italy) and Dowex 50W-X8 (H^+) (100–200 mesh) from Bio-Rad Labs. (Richmond, CA, U.S.A.). Water was demineralized and glass-distilled.

A 25-m*M* NBD-Cl solution was prepared in methanol. OPA reagent was prepared at a 150 m*M* concentration in methanol.

The standard solution, prepared in 0.01 *M* hydrochloric acid, was a 2.5 m*M* mixture of each of Hyp, Pro, Pro–Hyp, Pro–Pro, Pro–Leu and Pro–Gly. This solution was stored at 4°C and freshly prepared every 2 weeks. The propyl peptides used as standards are the main dipeptides present in normal or pathological urine.

Sample preparation

Urine samples (24-h) were obtained from healthy subjects. The urine was kept at 4°C during collection. A 10-ml aliquot of the 24-h urine sample was adjusted to pH 2.0 with 6 *M* hydrochloric acid; a 5-ml aliquot of this sample was poured into a minicolumn (1 × 0.8 cm I.D.) of Dowex 50W-X8, previously washed with 5 ml of 0.01 *M* hydrochloric acid. After adsorption of the urine sample, the column was washed with 5 ml of water to remove salts, acids and neutral compounds. The adsorbed fraction of amino acids and peptides was then eluted with 5 ml of 2 *M* ammonia solution. A Rotavapor was used to remove the solvent from the collected fraction at 50°C. The dry residue was dissolved in 2.5 ml of 0.2 *M* borate buffer (pH 9.0) and derivatized according to the method described previously [18]. A 0.2-ml aliquot of this solution was poured into a screw-capped glass tube (5 × 0.5 cm I.D.) and 50 μl of OPA reagent were added. After 3 min at room temperature, 100 μl of NBD-Cl solution were added; the derivatization was carried out at 60°C for 15 min and the reaction was stopped by adding to the mixture 0.65 ml of eluent A. A 50-μl aliquot of the solution was injected into the chromatograph.

Reversed-phase chromatography

HPLC was performed by using an apparatus consisting of two Jasco 880-PU pumps (JASCO, Tokyo, Japan) and a Shimadzu (Kyoto, Japan) FC 530 spectrofluorimeter, equipped with a xenon lamp and a 12-μl quartz flow cell. The NBD derivatives were detected by setting the monochromators at 470 nm for excitation and

at 530 nm for emission. The detector was connected to a Model 3390 A integrator (Hewlett-Packard, San Diego, CA, U.S.A.). A Model 910 injection valve (Negretti, Southampton, U.K.), whose loop had been replaced with a Guard-Pak C_{18} module (Waters Assoc., Milford, MA, U.S.A.), was used as a precolumn. The separation was performed on a 15 × 0.4 cm I.D. Spherisorb ODS 2 (5 μm) column.

Chromatographic analysis was carried out by isocratic elution followed by binary gradient elution as described below. Eluent A was 17.5 m*M* aqueous TFA solution containing 12.5% acetonitrile and eluent B was 17.5 m*M* aqueous TFA solution containing 80% acetonitrile. Both mobile phases were briefly degassed under reduced pressure. Prior to analysis, the column was equilibrated with eluent A at room temperature for 20 min at a flow-rate of 1 ml/min. After sample injection, elution was first carried out under isocratic conditions with eluent A for 12 min and then by gradient elution from eluent A to 40% of eluent B in 20 min. After the analysis, the column was washed with eluent B for 5 min and then the initial conditions were re-established by passing eluent A through the analytical column for 20 min.

The concentration of the analytes was determined from peak areas in comparison with those of known standards.

A calibration graph was obtained from working standard solutions containing amounts ranging from 10 to 100 nmol/ml of analytes in 0.2 *M* borate buffer (pH 9.0); 0.2-ml aliquots of these solutions were derivatized according to the procedure described above.

RESULTS AND DISCUSSION

HPLC with precolumn derivatization

The chromatogram shown in Fig. 1 represents a typical separation of standard Hyp, Pro, Pro–Hyp, Pro–Gly, Pro–Leu and Pro–Pro (1 nmol of each). The chromatographic system allows the baseline separation of these analytes; a non-interfering peak, due to the side-product 7-nitro-4-benzofurazanol (NBD-OH), is present in the chromatogram. The optimum elution conditions were chosen after several trials, performed with different eluents with pH from 7 to 3 and with different percentages of organic modifier. The elution conditions chosen, *i.e.*, the TFA–acetonitrile system established by an isocratic step coupled with a gradient elution step, allow the baseline separation of all the components and particularly of the pair Pro–Hyp and Pro–Gly, which have similar retention times.

The reliability of the chromatographic analyses was checked from 0.01 to 1 nmol of the analytes injected in the column; the linearity of the detector response to analyte concentration was excellent for all the compounds. Calibration graphs for Hyp, Pro–Hyp, Pro, Pro–Gly, Pro–Leu and Pro–Pro showed linearity over the concentration range from 0.01 to 1 nmol. Correlation coefficients between peak areas and amounts of analytes, ranging from 0.997 to 0.999, were obtained by linear regression analysis. The precision was determined with five aliquots of a working solution, at the same concentration (1 nmol) of each standard. The within-assay relative standard deviations (R.S.D.) for Hyp (3.1%), Pro (2.8%), Pro–Hyp (3.3%), Pro–Gly (2.6%), Pro–Leu (2.5%) and Pro–Pro (3.2%) indicate good reproducibility. The between-assay R.S.D.s were less than 6.1%. Recovery experiments ($n = 5$), performed by using the same aliquot (1 ml) of a working standard solution (5 nmol/ml of 0.01 *M*

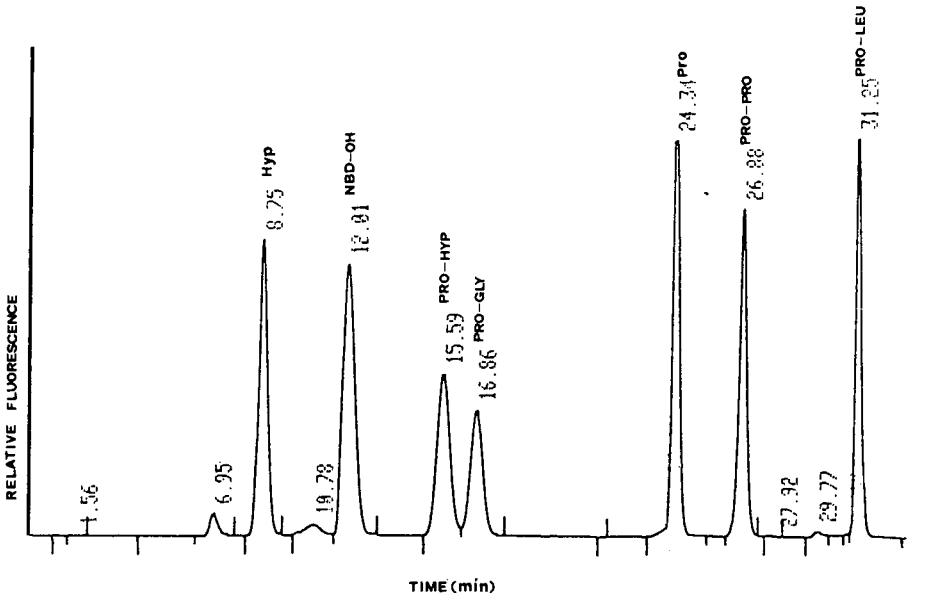

Fig. 1. Chromatogram of standard Hyp, Pro–Hyp, Pro–Gly, Pro, Pro–Pro and Pro–Leu, derivatized according to the procedure described in the text. Analyte peaks correspond to 1 nmol of each compound. Chromatographic conditions: 15 × 0.4 cm I.D. Spherisorb ODS 2 (5 μm) column; elution at a flow-rate of 1 ml/min isocratically for 12 min with 17.5 m*M* aqueous TFA solution containing 12.5% acetonitrile, then a 20-min linear gradient from this eluent to 40% of 17.5 m*M* aqueous TFA solution containing 80% acetonitrile was used. Attenuation detector sensitivity: ×8.

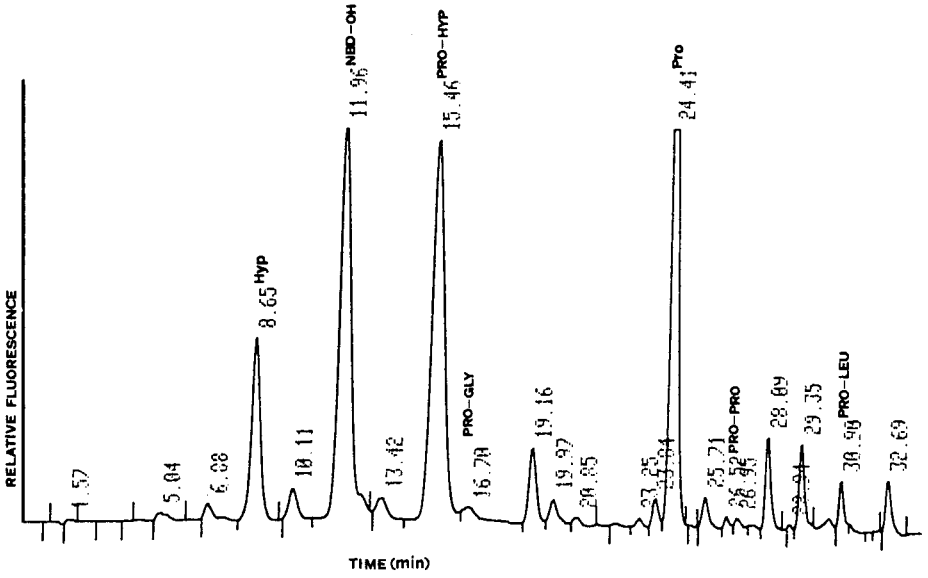

Fig. 2. Representative chromatogram of a urine sample, treated and derivatized as described in the text. Chromatographic conditions as in Fig. 1. Attenuation detector sensitivity: ×6.

hydrochloric acid) which had been treated according to the complete procedure used for the biological sample, gave recoveries above 90% for all the compounds, and the maximum R.S.D. was 8%.

Finally, the detection limit, referred to the amount of standards injected into the analytical column, was calculated to be 10 pmol for all of the compounds.

Urine analysis

Fig. 2 shows the chromatogram of a urine sample with selective separation of free amino acids and peptides having Pro as the N-terminal amino acid. Pro–Hyp and the free imino acids can be easily determined without interference from compounds containing amino groups. In this study, quantification was performed for free imino acids, Pro–Hyp and Pro–Gly, the most abundant collagen-related metabolites. The amounts (μmol/g creatinine) of free Hyp, Pro, Pro–Hyp and Pro–Gly, determined in urine of normal adult subjects, were (mean $\pm$ S.D., $n = 7$) 6.2 $\pm$ 2.3; 62.5 $\pm$ 12; 36.7 $\pm$ 8 and 1.6 $\pm$ 0.7, respectively.

As can be seen in Fig. 2, several other peaks are present in minute amounts compared with imino acids, Pro–Hyp and Pro–Gly. Two of these peaks were tentatively identified as indicated in Fig. 2, on the basis of their retention times and by standard coelution experiments.

REFERENCES

1 E. Meilman, M. M. Urivetzky and C. M. Rapoport, *J. Clin. Invest.*, 42 (1963) 40.
2 J. D. Smiley and M. Ziff, *Physiol. Rev.*, 44 (1964) 30.
3 K. I. Kivirikko, M. Koivusalo, O. Laitinen and M. Liesmaa, *Acta Physiol. Scand.*, 57 (1963) 462.
4 L. Klein and S. S. C. Yen, *Metabolism*, 19 (1970) 19.
5 S. I. Goodman, C. C. Solomons, F. Huschenheim, C. A. McIntyre, B. Miles and D. O'Brien, *Am. J. Med.*, 45 (1968) 152.
6 R. Thompson, G. Gaull, S. Horwitz and R. Schear, *Am. J. Med.*, 47 (1969) 209.
7 M.-J. Gortatowski, K. N. F. Shaw and W. A. Schroeder, *Biochem. Med.*, 5 (1971) 348.
8 S. Moore and W. H. Stein, *J. Biol. Chem.*, 192 (1951) 663.
9 P. Plaquet, G. Biserte and P. Boulanger, *Bull. Soc. Chim. Biol.*, 42 (1960) 393.
10 A. C. Kibrick, C. Q. Hashiro and L. B. Safier, *Proc. Soc. Exp. Biol. Med.*, 109 (1962) 473.
11 J. P. Borel, J. M. Caranjot and M. F. Jayle, *Clin. Chim. Acta*, 16 (1967) 409.
12 R. A. W. Johnstone, T. J. Povall, J. D. Baty, J. L. Poussete, C. Charpentier and A. Lemonnier, *Clin. Chim. Acta*, 52 (1974) 137.
13 K. F. Faull, G. M. Schier, P. Schesinger and B. Halpern, *Clin. Chim. Acta*, 70 (1976) 313.
14 C. Charpentier, R. A. W. Johnstone, A. Lemonnier, I. Nyara, M. E. Rose and D. Tuli, *Clin. Chim. Acta*, 138 (1984) 299.
15 J. Jandke and G. Spiteller, *J. Chromatogr.*, 382 (1986) 39.
16 A. Szymanowicz, P. M. Joubert, A. Garbe, A. Randaux and J. P. Borel, *Clin. Chim. Acta*, 100 (1980) 155.
17 K. Tellerova, P. Spacek and M. Adam, *J. Chromatogr.*, 273 (1983) 197.
18 C. A. Palmerini, C. Fini, A. Floridi, A. Morelli and A. Vedovelli, *J. Chromatogr.*, 339 (1985) 285.

Journal of Chromatography, 536 (1991) 343–347
Elsevier Science Publishers B.V., Amsterdam

CHROMSYMP. 2071

High-performance liquid chromatographic determination of bleomycins

H.-P. FIEDLER* and J. WACHTER
Universität Tübingen, Biologisches Institut, LB Mikrobiologie/Antibiotika, Auf der Morgenstelle 28, D-7400 Tübingen (F.R.G.)

ABSTRACT

A rapid and specific ion-pair reversed-phase high-performance liquid chromatographic method was developed for the determination of bleomycins. The use of 5-μm particles of less adsorptive reversed-phase packings and sodium perchlorate as ion-pairing reagent permitted a short analysis time and the transferability of the separations on different batches of the reversed-phase materials. The detection sensitivity and precision of the method demonstrated that the system is suitable for routine analysis.

INTRODUCTION

Commercially available bleomycin is a mixture of highly hydrophilic, cationic glycopeptide antibiotics. The complex is isolated from the fermentation broth of *Streptomyces verticillus* [1]. Bleomycins are effective against a variety of human neoplasms, sarcoma, malignant lymphoma and testicular carcinoma. Preparations used in cytostatic therapy consist of bleomycin A_2 (55–70%) and bleomycin B_2 (25–32%), the remainder being divided among the minor congeners. Bleomycin A_2 will be partially converted into demethylbleomycin A_2 during lyophilization. The structures of the main components of the bleomycin complex are shown in Fig. 1.

The most commonly used dosage has been 15 mg of bleomycin biological activity (15 units) twice weekly. The wide use of bleomycins for therapeutic purposes and pharmacokinetic studies of the individual bleomycins require a specific and sensitive assay. Several high-performance liquid chromatographic (HPLC) methods have been developed for the separation and determination of these compounds. Separations on silica gel lacked baseline resolution, showed peak tailing and required long analysis times [2,3]. Reversed-phase ion-pair HPLC using alkane sulphonic acids as lipophilic counter ions proved to be the only method to achieve baseline resolution of most bleomycins and their quantification in a sensitive detection range [4–9].

In the course of investigations on the separation behaviour of basic peptides depending on the stationary and mobile phases [10], we tested the results for the HPLC determination analysis of bleomycins. Basic compounds often show an unfavourable adsorption on the stationary phase caused by highly acidic, isolated silanol groups of

0021-9673/91/$03.50

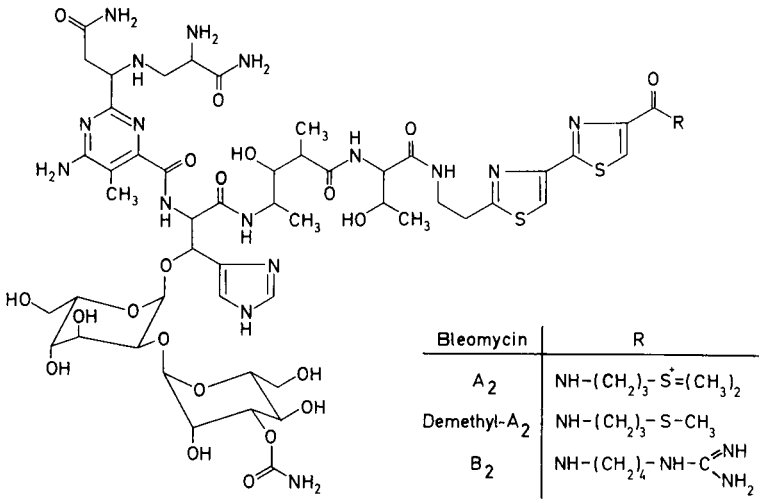

Bleomycin	R
A_2	$NH-(CH_2)_3-\overset{+}{S}=(CH_3)_2$
Demethyl-A_2	$NH-(CH_2)_3-S-CH_3$
B_2	$NH-(CH_2)_4-NH-C(=NH)-NH_2$

Fig. 1. Structure of bleomycins.

the reversed-phase packings [11–13]. We investigated the applicability of different reversed-phase materials and the addition of perchlorate as a strong ion-pairing reagent to the mobile phase to achieve selectivity in the separation of bleomycins.

EXPERIMENTAL

Chromatographic system

The chromatographic system consisted of an HP 1090M liquid chromatograph equipped with a diode-array detection system and workstation (Hewlett-Packard, Waldbronn, F.R.G.). A detection wavelength of 240 nm and a reference wavelength of 550 nm were used.

Column

The LiChrospher RP-Select B column (5 μm) (125 × 4 mm I.D.), fitted with a precolumn 4 × 4 mm I.D., was obtained from Merck (Darmstadt, F.R.G.). Columns of Nucleosil-100 C_{18} (7 μm) and Shandon Hypersil ODS (5 μm) (125 × 4.6 mm I.D.), fitted with precolumns 20 × 4.6 mm I.D., were purchased from Grom (Herrenberg, F.R.G.).

Mobile phases

Solvent A was 10 m*M* sodium perchlorate in 0.1% aqueous phosphoric acid and solvent B was acetonitrile. A linear gradient was applied from 5% to 25% solvent B in 13 min, increasing in 1 min to 100% B with a 1-min hold and followed by a post-time of 5 min under the initial conditions. The flow-rate was 1.5 ml/min for the 4-mm I.D. column and 2 ml/min for the 4.6-mm I.D. columns.

Chemicals

Acetonitrile (HPLC grade), sodium perchlorate and phosphoric acid (analytical-

reagent grade) were obtained from Merck. Water was purified by means of a Milli-Q system (Millipore, Eschborn, F.R.G.). Bleomycin sulphate (Bleomycinum) was purchased from Mack (Illertissen, F.R.G.); the composition specification was 68.6% bleomycin A_2, 0.7% demethyl-bleomycin A_2, 30.6% bleomycin B_2 and 0.1% bleomycinic acid.

Sample preparation

Bleomycin sulphate preparations in vials containing a biological activity of 15 mg of bleomycin (15 units) were dissolved in 15 ml of water and 20 μl of this bleomycin solution and of dilutions were injected onto the HPLC column.

RESULTS AND DISCUSSION

Fig. 2 shows the separation of a commercial bleomycin preparation by ion-pair reversed-phase HPLC using sodium perchlorate as ion-pairing reagent. The UV spectra of bleomycins which were recorded during the HPLC analysis by the diode-array detection system are congruent, as shown. Elution with a linear gradient of 10 m*M* sodium perchlorate dissolved in 0.1% aqueous phosphoric acid and acetonitrile resulted in a successful separation of the bleomycin mixture. The minor peaks which elute after bleomycin A_2 and B_2 are minor congeners of the bleomycin mixture because the UV spectra are identical with those of the major compounds. The retention behaviour is dependent on the concentration of the ion-pairing reagent, the gradient conditions being kept constant, as shown in Fig. 3. The same selectivity in the separation of bleomycins was reported using alkanesulphonic acids, such as pentanesulphonic acid, as the ion-pairing reagent [7–9]. However, these separations efforted elution times in the range of 45 and 75 min per analysis and problems with batch-to-batch reproducibility of the packings were observed. The use of 5-μm

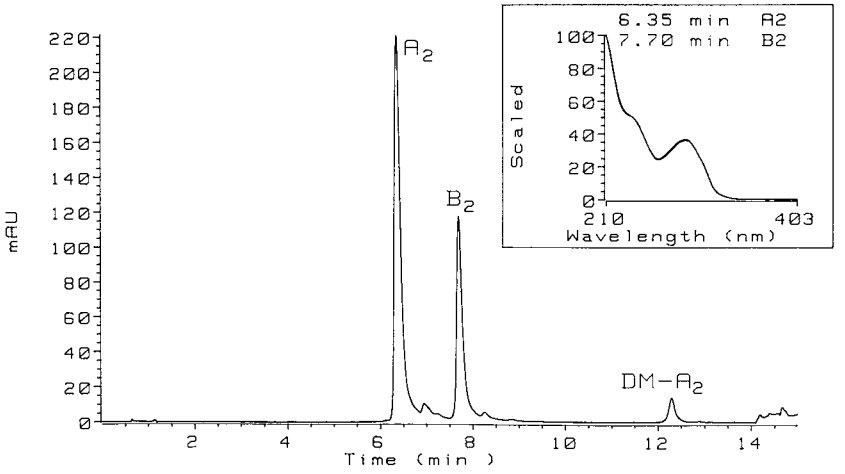

Fig. 2. HPLC separation profile of a bleomycin sulphate preparation plotted at 240 nm, and UV spectra of bleomycin A_2 and B_2 recorded during the HPLC analysis. Sample, 20 μl of Bleomycinum mixture (1 mg/ml bleomycin biological activity); column, LiChrospher RP-Select B.

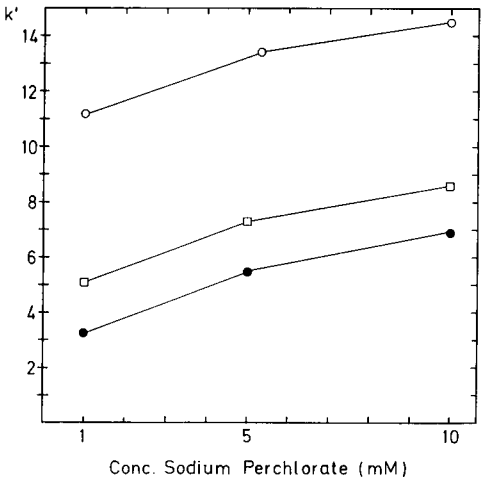

Fig. 3. Capacity factor (*k'*) *versus* concentration of the ion-pairing reagent in the mobile phase. ● = Bleomycin A_2; □ = bleomycin B_2; ○ = demethyl-bleomycin A_2.

particles and perchlorate as the ion-pairing reagent permitted a reduction in the analysis time to 13 min and the transferability of the separations from one batch to another.

Not all reversed-phase packings proved to be suitable for the separation of such basic compounds, even by ion-pair HPLC. As shown in previous investigations [10], pore size, coverage, reaction type and end-capping of the packings have no effect on selectivity and resolution in the HPLC analysis of basic compounds. Undesirable

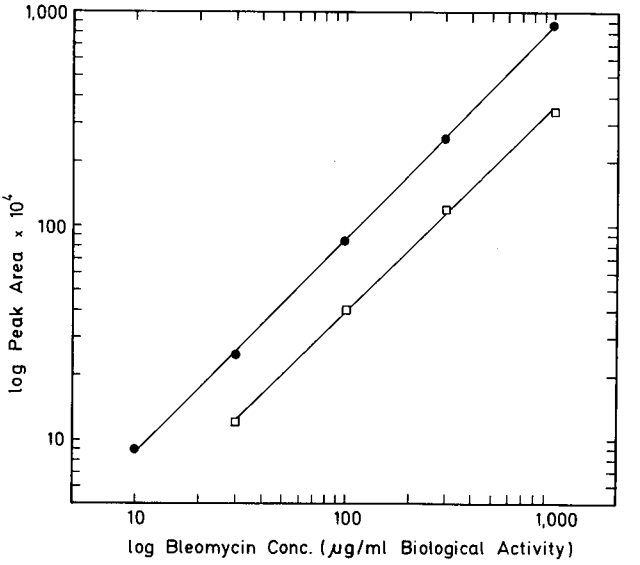

Fig. 4. Linear dynamic range of bleomycin determination. ● = Bleomycin A_2; □ = bleomycin B_2.

TABLE I

PRECISION OF RETENTION TIMES AND PEAK AREAS

Compound	Relative standard deviation (%)[a]	
	Retention time	Peak area
Bleomycin A_2	0.60	0.30
Bleomycin B_2	0.45	0.36
Demethyl-bleomycin A_2	0.20	1.37

[a] Based on 20 replicate analyses.

adsorption is caused by the presence of highly acidic, isolated silanol groups on the reversed-phase materials [11–13]. The separation of basic compounds, such as the strongly basic bleomycins, can be performed more favourably using reversed-phase materials of a less adsorptive type such as LiChrospher RP-Select B or Nucleosil C_{18}. The separation of the bleomycin mixture by ion-pair HPLC on reversed-phase packings of a strongly adsorptive type is characterized by peak tailing and incomplete baseline resolution (data not shown) and is therefore unsuitable for routine quantitative analysis.

The quantification of compounds is facilitated by a linear response in the range of analytical interest. With UV detection at 240 nm, linearity was achieved over the concentration range 10–1000 μg/ml of bleomycin biological activity (bleomycin units), as shown in Fig. 4, which corresponds to 5–500 μM bleomycin A_2 (biological activity). The detection limit for bleomycin A_2 was 100 nmol injected amount of biological activity. The detection sensitivity can be enhanced by using a fixed-wavelength UV detector instead of a relatively insensitive diode-array detector or by fluorescence detection.

The precision of the method was tested by assaying the Bleomycinum mixture 20 times (concentration 300 μg/ml biological activity), as shown in Table I. The reproducibility of both the retention times and the peak areas of bleomycin A_2 and B_2 and demethyl-bleomycin A_2 showed that the system is suitable for routine analysis.

ACKNOWLEDGEMENT

This work was supported by the Deutsche Forschungsgemeinschaft (SFB 323).

REFERENCES

1 H. Umezawa, K. Maeda, T. Takeuchi and Y. Okami, *J. Antibiot., Ser. A*, 19 (1966) 200.
2 W. J. Rzeszotarski, W. C. Eckelman and R. C. Reba, *J. Chromatogr.*, 124 (1976) 88.
3 C. R. Williams, L. A. Gifford and B. Scanlon, *Anal. Lett.*, 10 (1977) 407.
4 T. T. Sakai, *J. Chromatogr.*, 161 (1978) 389.
5 G. K. Shiu, T. J. Goehl and W. H. Pitlick, *J. Pharm. Sci.*, 68 (1979) 232.
6 G. K. Shiu and T. J. Goehl, *J. Chromatogr.*, 181 (1980) 127.
7 A. Aszalos, J. Crawford, P. Vollmer, N. Kantor and T. Alexander, *J. Pharm. Sci.*, 70 (1981) 878.
8 R. P. Klett, J. P. Chovan and I. H. R. Danse, *J. Chromatogr.*, 310 (1984) 361.
9 R. P. Klett and J. P. Chovan, *J. Chromatogr.*, 337 (1985) 182.
10 H.-P. Fiedler, T. Hörner and A. Wörn, *Chromatographia*, 24 (1987) 433.
11 J. Köhler, D. B. Chase, R. D. Farlee, A. J. Vega and J. J. Kirkland, *J. Chromatogr.*, 352 (1986) 275.
12 J. L. Glajch, J. J. Kirkland and J. Köhler, *J. Chromatogr.*, 384 (1987) 81.
13 J. Köhler and J. J. Kirkland, *J. Chromatogr.*, 385 (1987) 125.

Journal of Chromatography, 536 (1991) 349–355
Elsevier Science Publishers B.V., Amsterdam

CHROMSYMP. 2072

Isolation of 6-mercaptopurine in human plasma by aluminum ion complexation for high-performance liquid chromatographic analysis

KUN T. LIN*, FRANCE VARIN, GEORGES E. RIVARD and JEAN-MARIE LECLERC
Centre de Recherche, Hopital Ste-Justine, Montreal, Quebec H3T 1C5 (Canada)

ABSTRACT

A sample preparation technique and a high-performance liquid chromatographic method for 6-mercaptopurine (6-MP) that is simple, sensitive and without interference from its metabolites is described. 6-Thioguanine (6-TG) is added as an internal standard to the plasma sample, which is then treated with an aqueous solution of aluminum perchlorate to denature the plasma proteins and form complexes with 6-TG, 6-MP and its major metabolite, 6-thiouric acid (6-TUA). These complexes coprecipitate with proteins on centrifugation. 6-MP and its analogues are then extracted from the precipitate with perchloric acid containing sodium hydrosulfite and the extract is chromatographed on an Ultrasphere ODS column eluted with 0.1 *M* phosphoric acid and 0.001 *M* dithiothreitol in deionized water. The eluate is monitored at 340 nm. No interefering peak was encountered in over 300 clinical plasma samples. 6-TUA was separated from 6-MP and was found to be present in much higher concentration than 6-MP itself throughout the sampling time (6 h) following oral administration of the drug.

INTRODUCTION

6-Mercaptopurine (6-MP, purine-6-thiol, 6-purinethol, NSC-755, CAS 50-44-2; Fig. 1) is one of the major antineoplastic agents used in the maintenance therapy for acute lymphoblastic leukemia (ALL). As a rule, the drug is taken orally. It has been reported that there is no correlation between the prescribed dose of 6-MP and the clinical response in children with ALL [1]. Some of these unpredictable responses may be due to large individual variations in the pharmacokinetics of 6-MP [2–5]. The problem is further complicated by the fact that many pharmacokinetic data have been obtained by different analytical methods and some of these published methods might measure plasma levels of 6-MP in addition to its metabolites [6].

In this paper we describe a simple sample preparation method for isolating 6-MP and its major metabolite, 6-thiouric acid (6-TUA; Fig. 1) from either plasma or serum from patients. A high-performance liquid chromatographic (HPLC) system is used to separate 6-MP from 6-TUA. This method is shown to be reliable.

0021-9673/91/$03.50

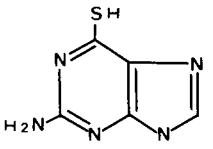

6-THIOGUANINE

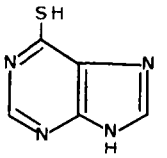

6-MERCAPTOPURINE

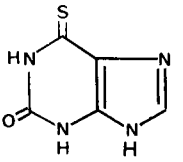

6-THIOXANTHINE

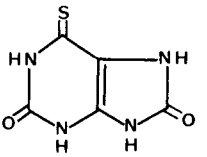

6-THIOURIC ACID

Fig. 1. Structures of 6-thioguanine, 6-mercaptopurine, 6-thioxanthine and 6-thiouric acid.

EXPERIMENTAL

Materials

6-MP, 6-thioguanine (6-TG; Fig. 1) and 6-thioxanthine (6-TX; Fig. 1) were purchased from Sigma (St. Louis, MO, U.S.A.). 6-TUA was synthesized enzymatically from 6-TX, as described previously [7]. Aluminum perchlorate was obtained from Aldrich (Milwaukee, WI, U.S.A.), dithiothreitol from Boehringer Mannheim Canada (Dorval, Quebec, Canada), sodium hydrosulfite from Fisher Scientific (Fair Lawn, NJ, U.S.A.), phosphoric acid (85.9%, analytical-reagent grade) from J. T. Baker (Phillipsburg, NJ, U.S.A.) and citrated normal human plasma from American Hospital Supply (Miami, FL, U.S.A.).

Collection of plasma sample

Venous blood (1 ml) was withdrawn with a polypropylene syringe and transferred to a polypropylene test-tube (100 × 17 mm) containing 20 units of heparin (B.P.), and chilled immediately in ice–water. For pharmacokinetic studies a blank blood sample was taken immediately before the oral administration of 6-MP (50 mg/m^2 body surface). Thereafter, samples were taken at 0.25, 0.5, 1.0, 1.5, 2.0, 4.0 and 6.0 h. The blood samples were centrifuged and the plasma samples were stored at −20°C in a polypropylene test-tube until analyzed.

Sample preparation

To 250 μl of plasma in a 1.5-ml Eppendorf polypropylene centrifuge tube were added 5 μl of 6-TG (2.5 μg/ml) as an internal standard and 25 μl of 1 *M* aluminum perchlorate (aqueous solution). The mixture was allowed to stand at room tempera-

ture for 15 min, chilled in ice–water for 15 min and then centrifuged at 15 600 *g* for 15 min. The supernatant was discarded and the precipitate was resuspended in 500 μl of a 50 m*M* aqueous solution of aluminum perchlorate by stirring to break up the precipitate. It was vortex mixed for 20 s, followed by a 15-min centrifugation (as above), after which the supernatant was thoroughly removed. The precipitate was then resuspended in 150 μl of 0.4 *M* perchloric acid, and then 5 μl of freshly prepared 0.2 *M* sodium hydrosulfite solution (in deionized water) were added. The contents of the tube were mixed and the mixture was allowed to stand at room temperature for 30 min, chilled in ice–water and centrifuged for 15 min (as above). The supernatant was then pipeted into a 1.1-ml STV glass vial (Chromacol, London, U.K.) and placed in the autosampler for injection.

HPLC system for the assay of 6-MP and 6-TUA

The Beckman System Gold for HPLC (Beckman, Berkeley, CA, U.S.A.) was used for the assay. The system consisted of an ODS (40 μm) guard column (45 × 2.0 mm I.D.), an Ultrasphere ODS (5 μm) analytical column (150 × 4.3 mm I.D.), a solvent Module 126, a Module 166 UV–VIS detector, a Model 506 autosampler, an IBM PS/2 Model 50 computer running on a Gold software Version 3.10 and an Epson FX-86e printer. The effluent was monitored at 340 nm. The sample injection volume was 50 μl and the flow-rate of the mobile phase was 1.0 ml/min. The mobile phase was prepared by mixing 6.8 ml of phosphoric acid (85.9%), 993.2 ml of deionized water and 154.3 mg of dithiothreitol and filtering through a 0.45-μm HA-type filter (Millipore, Bedford, MA, U.S.A.). The final composition of the mobile phase was 0.1 *M* phosphoric acid with 0.001 *M* dithiothreitol. It was used without further degassing. The entire HPLC operation was carried out at room temperature (21–23°C).

Quantification

The minimum quantifiable concentration of 6-MP by the detector was 3 ng/ml for a 50-μl injection volume at a peak-area ratio of sample to blank (0.4 *M* perchloric acid) of 5, and that of 6-TUA was 5 ng/ml at a peak-area ratio of 4. Normal human plasma, spiked with both 6-MP and 6-TUA at concentrations of 0, 12.5, 50, 200, 400 and 800 ng/ml, was assayed in parallel with the sample. Calibration graphs of the peak-area ratio of 6-MP to 6-TG *versus* 6-MP concentration and that of 6-TUA to 6-TG *versus* 6-TUA concentration were constructed automatically by the Gold system. The graphs were linear over the range 0–800 ng/ml for both 6-MP and 6-TUA with y (for 6-MP) = $90.2091x + 3.1073$ and y (for 6-TUA) = $340.0171x - 3.9877$. The coefficient of determination (r^2) was 0.9997 for 6-MP and 0.9997 for 6-TUA.

The percentage recovery was calculated by comparing the peak areas obtained for normal human plasma, spiked with various amounts of 6-TG, 6-MP and 6-TUA, with those observed following injection of pure compounds made up in 0.4 *M* perchloric acid containing 0.066 *M* of sodium hydrosulfite. The standard solutions were 1.613 times more concentrated than the concentrations listed in Table II, taking into account the fact that 250 μl of initial plasma sample resulted in a final volume of 155 μl of extract. The results of the recovery studies are summarized in Table I. A higher recovery for 6-MP could be obtained if the final extraction of the drug from protein with perchloric acid was performed on two successive aliquots of 0.1 ml, but for practical purpose this extra work is not justifiable.

TABLE I

RECOVERY OF 6-MERCAPTOPURINE, 6-THIOURIC ACID AND 6-THIOGUANINE FROM HUMAN PLASMA

Compound	*n*	Amount added (ng/ml)	Mean recovery (%)
6-MP	10	25	61.0
	10	50	60.3
	10	100	63.2
6-TUA	10	50	33.3
	10	200	33.3
	10	800	35.2
6-TG	30	50	51.3

Precision studies were carried out on the same group of samples by calculating the peak-area ratio of 6-MP to that of 6-TG. The relative standard deviations (R.S.D.) for 6-MP at concentrations of 25, 50 and 100 ng/ml were 3.6, 3.7 and 2.5%, respectively. The R.S.D.s for 6-TUA at 50, 200 and 800 ng/ml were 8.5, 5.1 and 5.8%, respectively.

Pharmacokinetic analysis

Standard non-compartmental pharmacokinetic analysis was carried out on the 6-MP plasma concentration–time profile according to published methods [8]. The area under the drug concentration *versus* time curve (AUC) and that under the moment curve (AUMC) were obtained by the trapezoidal method. Other parameters were derived as follows: elimination half-life (h) = $0.693/K_{el}$ (elimination rate constant), clearance ($l/h \cdot m^2$) = dose/AUC and distribution volume (l/m^2) = dose·AUMC/AUC^2.

RESULTS AND DISCUSSION

Thiols form metallic derivatives easily and rapidly in neutral solution [9]. In the sample preparation procedure described, aluminum ion was used to form a complex with 6-MP in the plasma [10]. The complex was then coprecipitated with the protein, as aluminum perchlorate is also an excellent protein precipitant. The supernatant was discarded and the precipitate was extracted with perchloric acid containing sodium hydrosulfite to obtain 6-MP and its analogues. Fig. 2 shows a typical chromatogram of a plasma sample from a leukemic patient who had taken 6-MP orally. Fig. 2A was obtained from a blood sample taken just before the administration of 6-MP. The only peak observed is that of 6-TG (t_R = 4.73 min), which was added to the sample as an internal standard. In a total of 60 blank blood samples taken from ten different patients, no peak was ever observed that might interfere with the detection of 6-TG, 6-MP or 6-TUA. In fact, peaks were virtually never detected in blank samples. Fig. 2B represents the chromatogram from the sample taken 2 h after 6-MP had been administered orally. The peaks for both 6-MP (t_R = 6.08 min) and 6-TUA (t_R = 7.57 min) are clearly visible. The presence of 6-TUA in the plasma is not surprising, as there is xanthine oxidase activity in both intestinal mucosa and liver to catalyze the oxidation of 6-MP to 6-TUA via 6-thioxanthine (6-TX; Fig. 1). 6-TX, which has

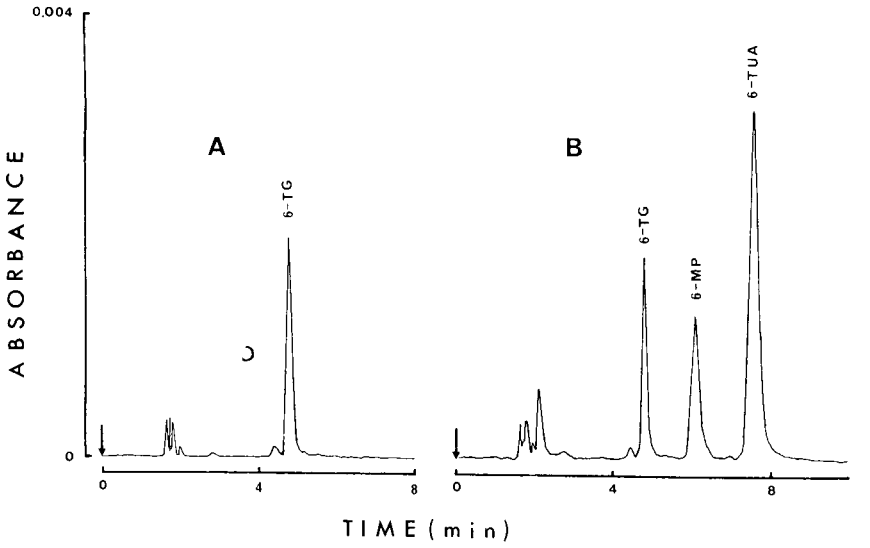

Fig. 2. Representative chromatograms obtained from plasma samples taken (A) immediately before drug administration and (B) 2 h after 6-mercaptopurine (50 mg/m^2) had been administered orally.

a longer retention time in our system (11.63 min), was virtually undetectable or showed up only as a very minor peak. 6-TX is a more effective substrate for xanthine oxidase than 6-MP and will not accumulate in the plasma [7].

Fig. 3 shows representative results of pharmacokinetic studies for 6-MP on a patient. The appearance of 6-MP in the plasma after drug administration is always accompanied by a much higher concentration of 6-TUA. This holds true for all the patients that we studied.

Table II summarizes the pharmacokinetic studies with 6-MP. The elimination half-life observed is compatible with the recently reported values [9]. However, the peak concentrations were far below those reported by others. As many workers did not discuss 6-TUA in their reports, this problem remains to be solved.

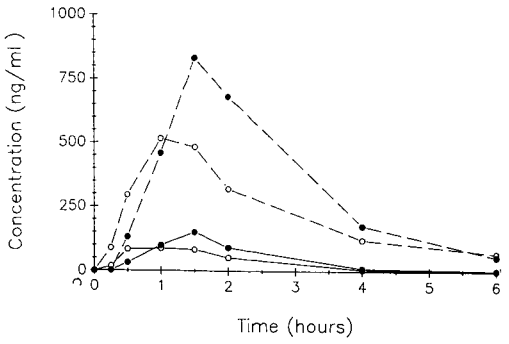

Fig. 3. Typical plasma concentration *versus* time curves for 6-mercaptopurine (solid lines) and 6-thiouric acid (broken lines) in a patient who had received 6-mercaptopurine (50 mg/m^2) orally at (●) 6 a.m. and (○) 6 p.m.

TABLE II

PHARMACOKINETICS OF 6-MERCAPTOPURINE IN EIGHT PATIENTS

The results were obtained from a total of 23 studies involving eight patients.

Parameter	Value[a]
Elimination half-life (h)	1.2 ± 0.1 (27%)
Clearance (l/h · m^2)	341 ± 36 (30%)
Distribution volume (l/m^2)	831 ± 110 (37%)
Peak concentration (ng/ml)	72 ± 9 (36%)
Peak time (h)	1.3 ± 0.1 (20%)

[a] The values are expressed as means ± standard error of the mean with the relative standard deviation in parentheses.

It has long been known that sulfhydryl compounds bind avidly to acid-denatured plasma proteins. The binding of 6-MP and 6-TG to the protein, however, is incomplete and variable. With normal plasma, freshly spiked with 6-MP and 6-TG, we found that only about 10–15% of the added 6-thiopurines bound to protein precipitate, and the binding increased with time of sample storage. As may be expected, it is also greatly affected by the hemolytic state of the blood sample, as 6-MP and 6-TG are known to bind to acid-denatured erythrocyte protein [11]. This direct binding of 6-thiopurines to the protein can be prevented by dithiothreitol and other reducing agents. By using aluminum perchlorate as a protein precipitant, all 6-thiopurines coprecipitate with the protein and thus remain in a single fraction. Although Al^{3+} is known to form only weak complexes with sulfhydryl ligands [10], with the largely excessive concentration used in our method it is safe to assume that only a very small amount of 6-thiopurines can exist in the free sulfhydryl form. It has been reported that 6-MP, 6-TG and their derivatives can undergo considerable distortion to accommodate the metal ion to form a five-membered chelate ring in which metallic ion interacts with the mercapto group at the 6-position on the purine molecule and also accepts the donation of an unshared pair of electrons on the nitrogen at the 7-position [12]. The coordination number of Al^{3+} can be 4, 5 or 6, and it is therefore possible for Al^{3+} to form complexes with 6-thiopurines, and also to bind to the protein precipitate by directing its unoccupied coordination position toward the protein. Chelate compounds are generally more hydrophobic than the parent ligands [13], thus also favoring coprecipitation with protein through hydrophobic interactions. The precipitate is then treated with perchloric acid and sodium hydrosulfite to regenerate free 6-thiopurines, as the chelates are broken down owing to protonation of the sulfur and the nitrogen atoms, and the disulfide bridges, through which 6-thiopurines may bind directly to protein, are reduced to sulfhydryl groups by the reducing agent. Sodium hydrosulfite was used in place of dithiothreitol because the latter absorbs at 340 nm and interferes with 6-TUA detection in our HPLC system.

One of the most widely used techniques for the isolation of 6-MP was described by Maddocks [14], in which phenylmercury(II) acetate was allowed to react with 6-MP in alkalinized plasma to form a complex, 6-phenylmercury(II) mercaptopurine. The complex was isolated from plasma with an organic solvent and the solvent was extracted with dilute hydrochloric acid to release free 6-MP into the aqueous medium.

Whalen *et al.* [6] used this technique for sample preparation prior to HPLC analysis of 6-MP. They noted some drawbacks of their method in that the ethyl acetate used for the extraction of 6-phenylmercury(II) mercaptopurine was carried over to the final acid extract and became an interfering peak in the chromatogram. They had to connect two analytical ODS columns from two different manufacturers in order to separate the three peaks, namely those of 6-TG, 6-MP and ethyl acetate. Further, they also reported that the 6-MP peak heights decreased after several injections owing to the interaction between the binding sites on the column and phenylmercury(II) acetate, which was also carried over from the extraction [6]. In our system, no organic solvent was used, and a single analytical column separated 6-TG, 6-MP and 6-TUA. In addition, no appreciable difference in the chromatogram was observed even after overnight automatic injection of over 60 plasma samples.

The same peak identification table, which allows the Gold systems to identify a compound by its retention time in the column, was used for the entire unattended overnight operation. Our procedure for isolating 6-MP and its metabolites from plasma was far simpler than any methods described so far. We used only one polypropylene Eppendorf centrifugation tube for each sample for the entire extraction process. No transfer of liquid was needed during the process until the last step, when the final extract must be transferred to the automatic sampler for injection.

The mobile phase for our HPLC system was also easy to prepare: it is simply dilute phosphoric acid containing dithiothreitol; no adjustment of pH is required. No undue deterioration of the analytical column has been noted, although the pH of the solution was observed to be 1.5. This low pH was necessary to obtain an optimum separation of 6-TG, 6-MP and 6-TUA. At pH values above 2, 6-MP and 6-TUA were not separated.

We are currently studing the chronopharmacokinetics of 6-MP by this method. Over 300 plasma samples have been analysed and no major technical problem has been encountered thus far.

ACKNOWLEDGEMENT

This work was supported by a grant from Leucan (Montreal, Quebec, Canada).

REFERENCES

1 S. Herber, L. Lennard, J. S. Lilleyman and J. Maddocks, *Br. J. Cancer*, 46 (1982) 138.
2 S. Zimm, J. M. Collins, R. Riccardi, D. O'Neill, P. K. Narang, B. Chabner and D. G. Poplack, *N. Engl. J. Med.*, 308 (1983) 1005.
3 D. G. Poplack, F. M. Balis and S. Zimm, *Cancer*, 58 (1986) 473.
4 P. Lafolie, S. Hayder, O. Bjork, L. Ahstrom, J. Liliemark and C. Peterson, *Acta Pediatr. Scand.*, 75 (1986) 797.
5 S. Hayder, P. Lafolie, O. Bjork, L. Ahstrom and C. Peterson, *Med. Oncol. Tumor Pharmacother.*, 5 (1988) 187.
6 C. E. Whalen, H. Tamary, M. Greenberg, A. Zipurskey and S. J. Soldin, *Ther. Drug Monit.*, 7 (1985) 315.
7 G. E. Rivard, K. T. Lin, J.-M. Leclerc and M. David, *Am. J. Pediatr. Hematol. Oncol.*, 11 (1989) 402.
8 M. Gibaldi and D. Perrier, *Pharmacokinetics*, Marcel Dekker, New York, 2nd ed., 1982, pp. 45–109.
9 F. Wild, *Estimation of Organic Compounds*, Cambridge University Press, Cambridge, 1953.
10 T. L. Macdonald and R. B. Martin, *TIBS*, 145 (1988) 15.
11 M. R. Sheen, B. K. Kim and R. E. Parks, Jr., *Mol. Pharmacol.*, 4 (1968) 293.
12 H. I. Heitner and S. J. Lippard, *Inorg. Chem.*, 13 (1974) 815.
13 R. A. Day, Jr., and A. L. Underwood, *Quantitative Analysis*, Prentice-Hall, Englewood Cliffs, NJ, 2nd ed., 1967, pp. 358–362.
14 J. L. Maddocks, *Br. J. Clin. Pharmacol.*, 8 (1979) 273.

Journal of Chromatography, 536 (1991) 357–370
Elsevier Science Publishers B.V., Amsterdam

CHROMSYMP. 2074

Reversed-phase ion-pair liquid chromatography of the angiotensins

H. B. PATEL, J. F. STOBAUGH and C. M. RILEY*
Center for BioAnalytical Research and Department of Pharmaceutical Chemistry, Malott Hall, University of Kansas, Lawrence, KS 66045-2504 (U.S.A.)

ABSTRACT

The isocratic reversed-phase liquid chromatography of the angiotensins and a number of their synthetic analogues is described. Complete separation of 10 out of 12 peptides was achieved through a solvent optimization strategy with a total analysis time of about 20 min. The retention behavior of the angiotensins studied was described in terms of the hydrophobic contribution of their amino acid residues; there was good correlation between predicted and experimental retention for those peptides that were retained by a common mechanism. However, because ion-pair chromatography was required for good peak symmetry, retention was substantially modulated by the presence of acidic and basic residues. The limit of detection of these peptides was 3–5 pmol by UV absorbance at 214 nm. For those peptides containing a primary amino group the detection limit was improved by two orders of magnitude by fluorogenic derivatization with naphthalene-2,3-dicarboxaldehyde/cyanide to the corresponding N-substituted 1-cyanobenz[*f*]isoindole (CBI) derivatives. The contribution of the CBI ring system to retention was also investigated.

INTRODUCTION

Extensive literature exists on the involvement of the peripheral and central renin/angiotensin system (RAS) in the regulation of blood pressure and aldosterone secretion [1,2]. Therefore in order to understand and investigate the RAS, the identification and quantification of the RAS components and synthetic agonists and antagonists of the angiotensins (ATs) are very important. Classical analytical approaches included radioimmunoassay or radiochemical methods [3]. Subsequently, separation techniques, such as polyacrylamide gel electrophoresis, isoelectric focusing and paper chromatography, have been employed for the analysis of native ATs and their synthetic analogues [4]. Complete resolution of closely similar title peptides, however, was not always possible.

The introduction of reversed-phase liquid chromatography initiated a renewed interest in this field, not only for the ATs but for peptides in general. Liquid chromatographic (LC) separations of the ATs have been achieved, conventionally, by linear-gradient analysis, but poor reproducibility of retention time is a common problem [5–10]. Additionally, gradient analysis can limit the choice of the reagents (salts, ion-pair reagents) that may be employed to modify peak shape and retention characteristics. Isocratic methods are generally more flexible, placing fewer restric-

0021-9673/91/$03.50

tions on the choice of the mobile phase additives and a number of such methods for the analysis of the ATs have been reported [9–14]. However, these methods either lack the desired selectivity or give very poor peak shape. Furthermore, the retention of peptides can be sensitive to very small changes in mobile phase composition and optimization of isocratic separations by the traditional trial and error method can be very tedious. Finally, polar peptides, such as ATs, exhibit non-linear relationships between the logarithm of capacity factor ($\ln k'$) and the volume fraction (φ) of the organic modifier in mobile phase (see, *e.g.*, refs. 15–17), and this has been attributed to the influence of both hydrophobic and silanophilic interactions. As well as making the optimization of separations a complex process, the interactions with residual silanol groups can give rise to assymetric peaks [15–17].

The present study was prompted by the lack of adequate isocratic methodology for the reversed-phase LC of the ATs and the objectives were firstly to investigate the factors influencing the isocratic reversed-phase LC of the ATs (Table I) and secondly to develop a strategy for the optimization of their retention.

EXPERIMENTAL

Chemicals and reagents

Synthetic angiotensin-I (AT-10, peptide content 77.6%), angiotensin-II (AT-20, 83.8%), angiotensin-III (AT-30, 96%) and the other analogues (AT-21–AT-29, Table I), were purchased from Peninsula Labs. (Belmont, CA, U.S.A.). Methanol, acetonitrile and tetrahydrofuran were obtained from Fisher Scientific (Fair Lane, NJ, U.S.A.). HPLC-grade 1-pentane-, 1-hexane-, 1-heptane- and 1-octanesulphonic acid sodium salts and 1-hexane- and 1-octanesulphate sodium salts were obtained from Eastman-Kodak (Rochester, NY, U.S.A.). High-purity water from Milli-Q water

TABLE I

AMINO ACID SEQUENCES, THEORETICAL RETENTION CONSTANTS (ΣD_j) AND CAPACITY FACTORS OF THE ANGIOTENSIN PEPTIDES AND THEIR ANALOGUES

ΣD_j values taken from Sasagawa *et al.* [25]. Capacity factor under optimized solvent conditions, mobile phase C'.

Amino acid sequence	Code	ΣD_j	k'	Name
Asp-Arg-Val-Tyr-Val-His-Pro-Phe	AT-22	4.88	1.13	
Asp-Arg-Val-Tyr-Ile-His-Pro-Phe	AT-20	5.88	1.59	Angiotensin-II
Sar-Arg-Val-Tyr-Val-His-Pro-Ala	AT-29	4.03	2.18	Saralasin
Sar-Arg-Val-Tyr-Ile-His-Pro-Gly	AT-25	5.12	2.88	
Sar-Arg-Val-Tyr-Ile-His-Pro-Thr	AT-27	5.02	2.99	
Sar-Arg-Val-Tyr-Ile-His-Pro-Ala	AT-24	5.03	3.04	
Asn-Arg-Val-Tyr-Val-His-Pro-Phe	AT-23	4.33	3.56	
Sar-Arg-Val-Tyr-Ile-His-Pro-Ile	AT-28	6.28	5.55	
Sar-Arg-Val-Tyr-Ile-His-Pro-Leu	AT-26	6.24	6.63	
Sar-Arg-Val-Tyr-Ile-His-Pro-Phe	AT-21	6.61	8.72	
Arg-Val-Tyr-Ile-His-Pro-Phe	AT-30	5.78	10.85	Angiotensin-III
Asp-Arg-Val-Tyr-Ile-His-Pro-Phe-His-Leu	AT-10	7.56	13.82	Angiotensin-I

system (Millipore, Bedford, MA, U.S.A.) was used for all solutions and mobile phase preparations. Naphthalene-2,3-dicarboxaldehyde (NDA) was obtained from Oread Labs. (Lawrence, KS, U.S.A.). Reagent-grade sodium cyanide was purchased from Matheson, Coleman and Hall (Norwood, Cincinnati, OH, U.S.A.). All other chemicals were of reagent grade.

Liquid chromatography

The chromatography was performed with a modular system which comprised a Shimadzu LC-6A liquid chromatograph (Shimadzu, Columbia, MD, U.S.A.), a SIL-6A autoinjector (Shimadzu), a SCL-6A system controller (Shimadzu), a UV-SPD6AV monitor (Shimadzu), RF-535 fluorescence monitor (Shimadzu), an Omniscribe chart recorder (Houston Instruments, Houston, TX, U.S.A.) and either an CR-6A or an CR-3A Chromatopac computing integrator (Shimadzu).

The ATs were dissolved in phosphate buffer (pH 2.5, 0.1 *M*) and injected (50 μl) into an ODS Hypersil column (5 μm, 150 × 4.6 mm I.D.) (Keystone, State College, PA, U.S.A.). The column temperature was controlled (40 ± 0.1°C) by placing it in an oven (CTO-6A, Shimadzu) and the column effluent was monitored by either UV absorbance (214 nm) or fluorescence (excitation wavelength 420 nm, emission wavelength 490 nm). The autoinjector sample tray was maintained at 6–8°C with an RM6 sample cooling unit (Brinkmann, Westbury, NY, U.S.A.). The flow-rate was varied between 1.0 and 2.0 ml/min.

The chromatographic investigations involved the establishment of the initial conditions for the isocratic separation of the ATs followed by the optimization of the separation using a modified mixture design statistical technique. The initial conditions were established by investigating the influence of the following factors on retention (k') and peak asymmetry (A_s): solvent type (methanol, acetonitrile and tetrahydrofuran) and concentration (φ = 0.2–0.6), buffer type [0.1 *M*; perchlorate, phosphate and trifluoroacetate, pH (2.5, 3.5, 4.5 and 6.0)] and ion pair reagent type (1-pentane; 1-hexane; 1-heptane- and 1-octanesulphonic acid sodium salt and 1-hexane-, 1-octane-sodium sulphate) and concentration (5, 10, 15, 20 and 30 m*M*).

From these initial experiments, three isoelutropic mobile phases were established (A, B and C) in which the peptides of interest eluted as virtually symmetrical peaks ($A_s < 1.2$) with a k' range of approximately 1–20. The aqueous component of the three mobile phases (solvent X) was a phosphate buffer (pH 6.0; 100 m*M*) containing sufficient 1-octanesulphonic acid sodium salt to give a final mobile phase concentration of 30 m*M*. The compositions of the three isoelutropic mobile phases were as follows: (A) X–acetonitrile (75:25, v/v), (B) X–methanol (51:49, v/v), and (C) X–tetrahydrofuran (81.5:18.5, v/v). The isoelutropic plane defined by the triangle A:B:C was then interrogated using a modified mixture design statistical technique to obtain the optimum conditions for the resolution of the 12 ATs of interest.

Derivatization with NDA/CN

Peptides AT-20, -22 and -23 were converted to their corresponding fluorescent N-substituted 1-cyanobenz[*f*]isoindoles (CBI-ATs) by reaction with naphthalene-2,3-dicarboxaldehyde/cyanide (NDA/CN) [18–21]. The reaction was conducted by mixing, in order, 20 μl aqueous peptide solution (25 μ*M*), 50 μl ascorbic acid (200 m*M* in water), 100 μl NaCN (10 m*M* in water), 200 μl NDA (5 m*M* in acetonitrile) and

540 μl phosphate buffer (100 m*M*, pH 7.0). The solution was mixed by inversion and stored over an ice bath (0–4°C) for 20 min. A 50-μl volume of an aqueous taurine solution (200 m*M*) was then added to quench the reaction [21].

RESULTS AND DISCUSSION

Establishment of initial conditions

To establish the initial conditions, the effects of pH, buffer salts and various anionic ion-pairing agents on the retention and peak shape of the AT were investigated in a systematic fashion using acetonitrile as the organic modifier. The objective was to obtain symmetrical peaks and retention with a k' range of 1–20. Pronounced peak tailing ($A_s > 5$) was observed for all the ATs when they were eluted with mobile phases containing various concentrations of acetonitrile in sodium perchlorate–perchloric acid, trifluoroacetic acid–sodium hydroxide and phosphoric acid–sodium hydroxide buffers (each 0.1 *M*) in the pH range of 2.5 to 3.5. A slight improvement in peak shape was achieved by adjustment of the pH of the mobile phase to a value of 6 with a phosphate buffer (0.1 *M*); however, the problem of poor peak shape was ultimately resolved by the use of ion-pair chromatography [22,23].

The addition of alkylsulphates and -sulphonates to the mobile phase increased the retention of the oppositely charged ATs and, consistent with previous observations (*e.g.*, refs. 22 and 24) retention increased with increasing concentration (5–30 m*M*) and hydrophobicity (chain length, n = 5–8) of the ion-pair reagent. More importantly the peak shape of the solutes improved dramatically with the addition of the ion-pairing agent to the mobile phase [23]. The improvement in peak shape was related to the concentration and chain length of the ion-pair reagent; and A_s values of less than 1.2 were achieved with 30 m*M* octanesulphate sodium salt in the aqueous component of the mobile phase. (Throughout these ion-pair experiments, the pH of the aqueous component of the mobile phase was maintained at a value of 6.0 with a phosphate buffer (0.1 *M*) and the volume fraction of the organic modifier, acetonitrile, was fixed at 0.25.) These initial experiments established mobile phase A as the optimum binary solvent system for the resolution of the 12 ATs, which eluted between k' = 1.47 (AT-22) and 21.6 (AT-10) with good column efficiency (N = 20 000–40 000 plates/m) and excellent symmetry ($A_s < 1.2$). The composition of mobile phase A was X–acetonitrile (75:25, v/v), where the aqueous component of the mobile phases (X) was a phosphate buffer (pH 6.0; 100 m*M*) containing sufficient 1-octanesulphonic acid sodium salt to give a final mobile phase concentration of 30 m*M*.

To reduce the consumption of the peptides, these experiments were conducted with two peptides AT-29 and AT-10, which, according to their theoretical retention constants (ΣD_j, Table I [25]), were expected to be the first and last analytes to elute, respectively. Peptide AT-30 was correctly predicted to be the last peptide to elute. However, AT-20 and -22 eluted before peptide AT-29, which was, in fact, the third peptide to elute. Nevertheless, the ΣD_j values did allow the initial conditions for the separation of the 12 peptides to be established by studying the two analytes with the largest and the smallest values of ΣD_j. An explanation for the earlier than expected elution of AT-20 and -22 is provided below, in the section *Quantitative structure–retention relationships.*

Solvent optimization

The first step in the solvent optimization was to establish that mobile phases B and C containing methanol ($\varphi = 0.49$) and tetrahydrofuran ($\varphi = 0.185$), respectively, were isoelutropic with mobile phase A (in these and subsequent experiments the composition of the aqueous solvent X was the same as in mobile phase A). The three mobile phases (A, B and C) defined an isoelutropic plane (k' for AT-10 $\approx$ 20) as shown in Fig. 1. Fig. 2 shows the isochronal chromatograms corresponding to three isoelutropic mobile phases A, B and C.

The second phase of the optimization procedure was to explore the isoelutropic plane (A:B:C) to establish the optimum quaternary mixture (acetonitrile–methanol–

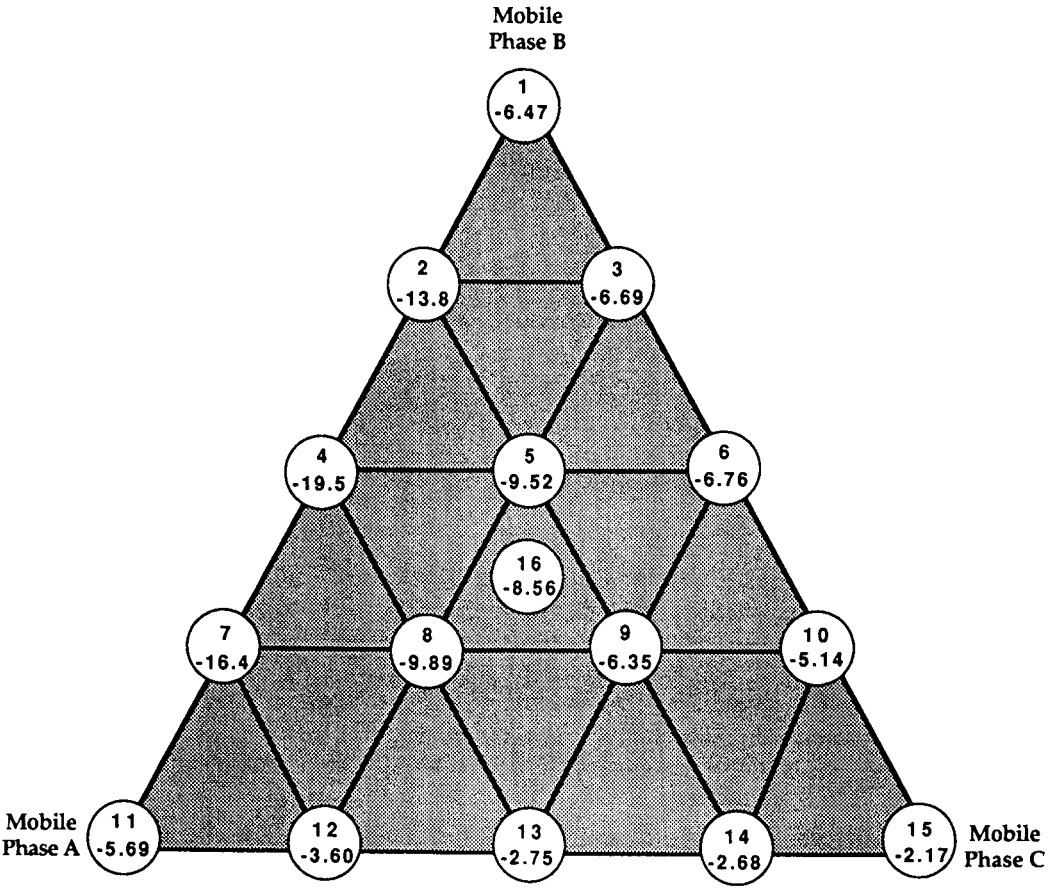

Fig. 1. Modified mixture design statistical technique. A 5-level pseudo-factorial experimental design was used in which pseudo-solvents A, B and C were combined in different proportions. Each node (1 to 16) represents a combination of these solvents. Chromatographic optimization function (COF) values corresponding to each solvent composition (nodes 1–16) are shown in the circles and in Table II. The aqueous component of the mobile phases (solvent X) was a phosphate buffer (pH 6.0; 100 mM) containing sufficient 1-octanesulphonic acid sodium salt to give a final mobile phase concentration of 30 mM. Column: ODS Hypersil (5 μm, 150 × 4.6 mm I.D.). Temperature: 40 $\pm$ 0.1°C.

tetrahydrofuran–solvent X) for the resolution of the solutes. Employing these initial conditions, a 16-point experiment (Fig. 1) was conducted so that a modified mixture design statistical technique with bi-dimensional interpolation could be employed to identify the optimum conditions [26]. The quality of each chromatogram was judged by the calculation of the chromatographic optimization function (COF) [26–29]:

$$\mathrm{COF} = \alpha \sum_{i=1}^{p-1} \ln\left(\frac{R_{s_i}}{R_{s_{di}}}\right) + \beta(t_{\max} - t_{\exp}) - \gamma(n - p) \qquad (1)$$

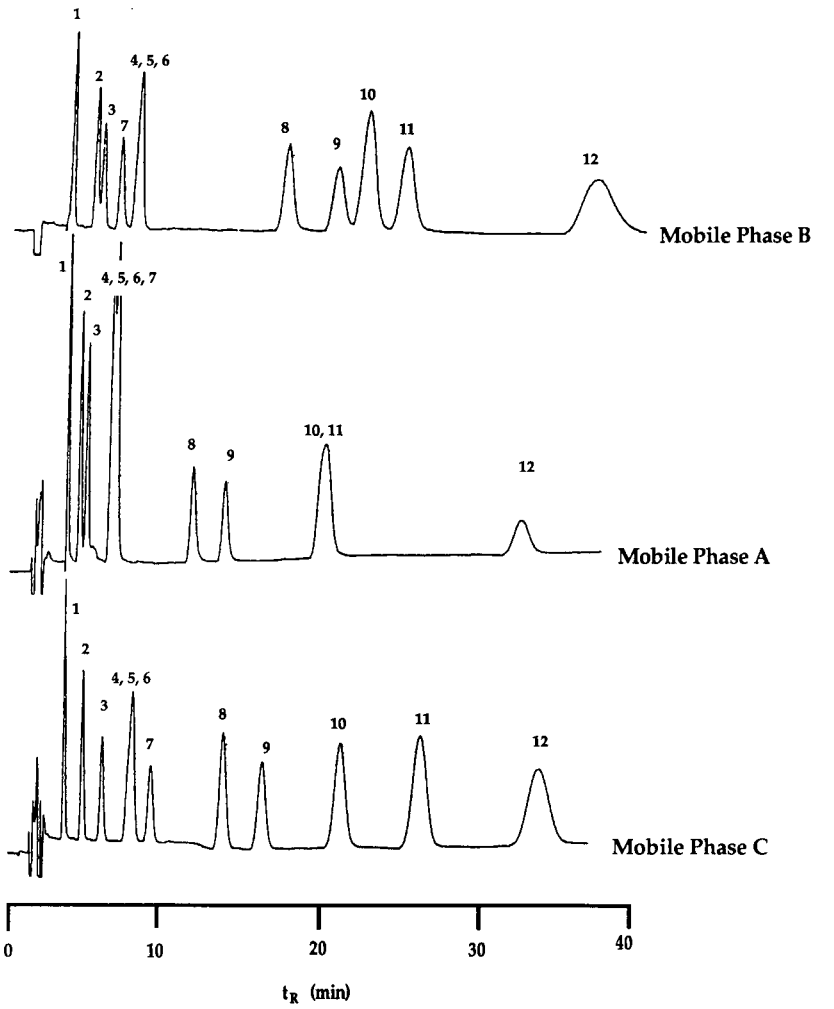

Fig. 2. Isochronal chromatograms corresponding to the three isoelutropic solvents A, B and C. Column: ODS Hypersil (5 μm, 150 × 4.6 mm I.D.). Mobile phases A, B and C as in text. Temperature: 40 ± 0.1°C. Peaks: 1 = AT-22; 2 = AT-20; 3 = AT-29; 4 = AT-24; 5 = AT-25; 6 = AT-27; 7 = AT-23; 8 = AT-28; 9 = AT-26; 10 = AT-21; 11 = AT-30; 12 = AT-10.

where R_{s_i} is the resolution factor for peak-pair i and $i + 1$, $R_{s_{di}}$ is the desired resolution for peak-pair i and $i + 1$ (in this case 1.8 for each pair), t_{exp} is the experimental analysis itime (*i.e.*, retention time, t_R, of last peak, p), t_{max} is the maximum desired analysis time (25 min), p is the actual number of peaks in the chromatogram and n is the expected number of peaks in the chromatogram (12). The weighting factors for the separation term (α), the analysis time term (β) and the total number of peaks term (γ) were arbitrarily assigned values of 1, 0.2 and 3, respectively. The COF values for the 16 chromatograms are shown in Fig. 1. The maximum COF value was obtained for node number 15, which corresponds to optimum mobile phase C.

The isochronal separations of the 12 peptides for mobile phase A, B and C are shown in Fig. 2. A further appreciation of the influence of organic modifier on the overall resolution can also be obtained from the resolution map in Fig. 3. It is clear that mobile phases containing tetrahydrofuran (C) or acetonitrile (B) were preferable to those containing methanol (A) because of the separation of AT-21 (peak 10) from AT-30 (peak 11) and the separation of AT-23 from AT-24, -25 and -27. The latter peptides (AT-24, -25 and -27, peaks 4, 5 and 6) were unresolved in all the mobile phases investigated (Fig. 2). Mobile phase C was superior to mobile phase B primarily because of the better separation that was achieved for AT-22, -20 and -29 (peaks 1–3) and the overall resolution of AT-28, -26, -21, -30 and -10 (peaks 8–12).

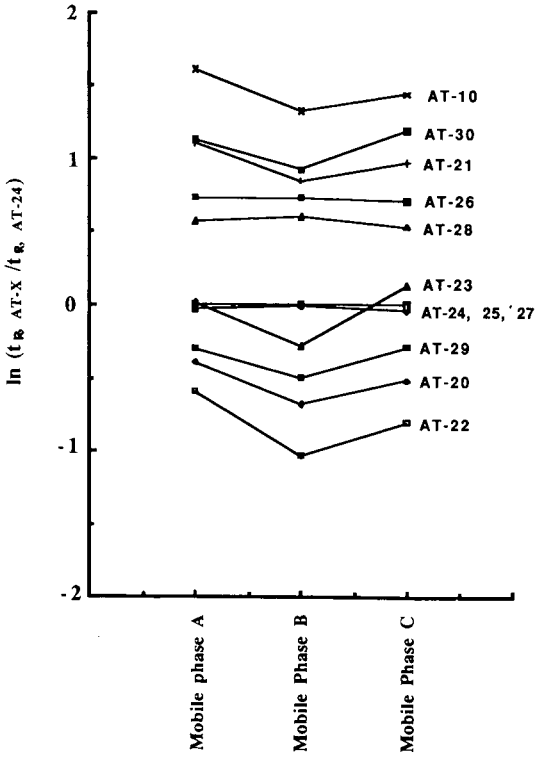

Fig. 3. Resolution map showing the retention times of the 12 ATs with the three isoelutropic solvents A, B and C (see text).

The final step in the optimization procedure was to increase the volume fraction of tetrahydrofuran from 0.185 to 0.190 (solvent C'). This decreased the overall analysis time from 30.6 to 21.2 min (Fig. 4) without altering the selectivity previously achieved. This optimization effort allowed isocratic separation of 10 of the 12 closely related AT peptides (Table I) which has not been previously reported. In addition, the peak shapes ($A_s < 1.2$) and the column efficiencies are much better than previous attempts at isocratic resolution of these peptides [5–14].

Quantitative structure–retention relationships

The optimization procedure for the isocratic separation of the 12 ATs was conducted without considering either the structure of the peptides or their retention mechanisms. After identifying the initial conditions, the only variables considered were the nature and the concentrations of the organic modifiers in the mobile phase. The ΣD_j values, which are essentially a measure of solute hydrophobicity were useful in establishing the initial conditions. However, Fig. 5 and eqn. 2 show that the overall relationship between retention and solute hydrophobicity (ΣD_j) was poor:

$$\ln k' = 0.546 \sum D_j - 1.648, \quad r^2 = 0.511 \ (r = 0.715) \tag{2}$$

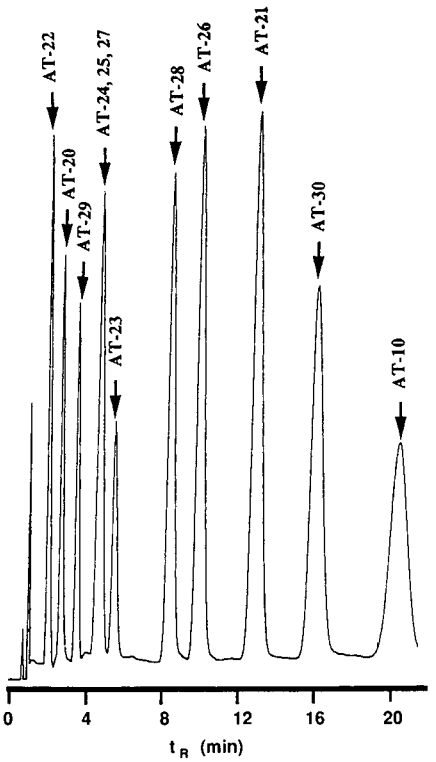

Fig. 4. Separation of ATs under optimized solvent conditions (mobile phase C'). The aqueous component of the mobile phases (solvent X) was a phosphate buffer (pH 6.0; 100 m*M*) containing sufficient 1-octanesulphonic acid sodium salt to give a final mobile phase concentration of 30 m*M*. Column: ODS Hypersil (5 μm, 150 × 4.6 mm I.D.). Temperature: 40 ± 0.1°C.

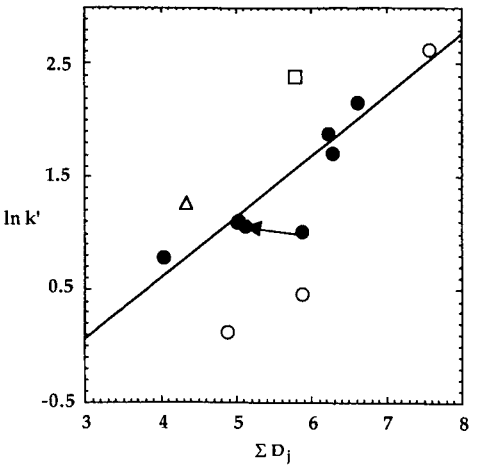

Fig. 5. Relationship between the capacity ratios of the 12 ATs studied and their theoretical retention constants (ΣD_j) (Table I). The different symbols represent peptides with the same N-terminal amino acids as follows: Sar (●, AT-21, -24, -25, -26, -27, -28, -29), Asp (○, AT-10, -20, -22), Asn (□, AT-23), Arg (△, AT-30). The aqueous component of the mobile phases (solvent X) was a phosphate buffer (pH 6.0; 100 mM) containing sufficient 1-octanesulphonic acid sodium salt to give a final mobile phase concentration of 30 mM. Column: ODS Hypersil (5 μm, 150 × 4.6 mm I.D.). Temperature: 40 ± 0.1°C.

This poor correlation (eqn. 2) was not unexpected because ion-pair chromatography was employed and several of the peptides had different charges arising mainly from differences in the N-terminal amino acid. It has been well established [23,30] that retention in reversed-phase ion-pair LC is markedly influenced by the size of the electrical charge on the solutes. Fig. 5 and eqn. 3 show that there was a very good correlation between the observed retention (ln k') and the theoretical retention constants (ΣD_j) for those peptides, which possessed a sarcosine residue at the N-terminus (AT-21, -24, -25, -26, -27, -28 and -29). It is reasonable to assume that these peptides all possessed the same electrical charge because they all have the same ionizable functional groups.

$$\ln k' = 0.541 \sum D_j - 1.562, \quad r^2 = 0.939 \ (r = 0.969) \tag{3}$$

It is interesting to note that two of the three ATs with an N-terminal aspartic acid (AT-20, -22) residue lie substantially below the regression line defined by the peptides with the N-terminal sarcosine (Fig. 5). In contrast, the data point for the other aspartic acid-containing peptide (AT-10) is very close to the regression line defined by the sarcosine-containing peptides. This observation was explained by the fact that the additional negative charge in AT-10 arising from the aspartic acid residue was cancelled by the additional positive charge from the second histidine residue, which is not present in the other two aspartic acid-containing peptides (AT-20, -22). Although the net electrical charge on the two remaining peptides (AT-23 and -30) was expected to be the same as that on the sarcosine-containing peptides, the retention of AT-23 and -30 was greater than predicted by eqn. 3. This was particularly true for AT-30, which had an N-terminal arginine residue. The retention of AT-30 was about three times

greater than would have been predicted from the regression line generated by the sarcosine-containing peptides.

One final observation worthy of comment is the poor resolution of peptides AT-24, -25 and -27, which was accurately predicted by the fragmental retention constants. These three peptides (AT-24, -25 and -27) differ only in the amino acids at the C-terminus and have only very small differences in their theoretical retention constants [25]. The ΣD_j values for Gly, Ala and Thr are 0.22, 0.13 and 0.12, respectively [25].

Fluorescent derivatives of the angiotensins

Using UV absorbance at 214 nm, the detection limit (signal-to-noise ratio 3) for the ATs studied here was 3–5 pmol injected (50 μl). This detection limit is generally inadequate for the determination of endogenous or exogenously administered ATs [30–32]. For example, the concentrations of native angiotensin-I and angiotensin-II in canine cerebrospinal fluid (CSF) are about 1.54 and 6.17 fmol/ml, respectively, as determined by radiolabelled peptides [30]. About ten-fold higher concentrations (10–50 fmol/ml) of these peptides have been reported in human plasma [31]. Recently, deMontigny *et al.* [18] and others [19–21] have described the naphthalene-2,3-dicarboxaldehyde/cyanide reagent system for the fluorogenic derivatization of primary amines. The present study has demonstrated the feasibility of using NDA/CN for the enhancement of detection of the primary amine-containing ATs, using AT-20, -22 and -23 as model compounds. The objectives of the present study were to establish the detection limit of the CBI-ATs and to investigate the contribution of the CBI-ring system to the reversed-phase retention of these peptides.

The ATs (25 μM) were converted to their fluorescent CBI-derivatives using the procedures developed previously for the derivatization of opioid peptides [21] by reaction with an excess of NDA (1 mM) and sodium cyanide (2 mM). The reaction was conducted at a pH of 7.0, which is approximately equal to the pK_a of the terminal amino group and is generally considered to be an optimum condition for the rate and yield of the reaction [18,20]. After reacting for 20 min over an ice bath (0–4°C) the reaction was quenched by the addition of excess taurine (10 mM). Quenching of the reaction was necessary to prevent accumulation of fluorescent degradation products of the NDA/CN reagents system [19–21]. With mobile phase C′ the detection limits of CBI-AT-20, -22 and -23 were 50–100 fmol (signal-to-noise ratio 3) with conventional fluorescence with excitation at 420 nm (xenon lamp) and detection of the emission at 490 nm.

Recently, it has been shown [33–35] that sub-fmol detection limits for CBIs and similar ring systems are possible with the laser-induced fluorescence (LIF) detectors based on the He–Cd laser. However, most of the previous studies [33,34] have dealt with the analysis of amino acids, biogenic amines or protein hydrolysates. Efforts in this laboratory are being devoted towards the application of LC–LIF to analysis of intact peptides in biological samples. Preliminary results on the application of LC–LIF to the analysis of opioid peptides were presented recently [35], and its application to other classes of peptides including the ATs will be presented at a later date.

The contribution of the CBI-ring system to retention was calculated by determining the capacity ratios (Fig. 6 and Table II) of AT-20, -22 and -23 and their corresponding CBI-derivatives on an ODS Hypersil column at 40°C with a mobile

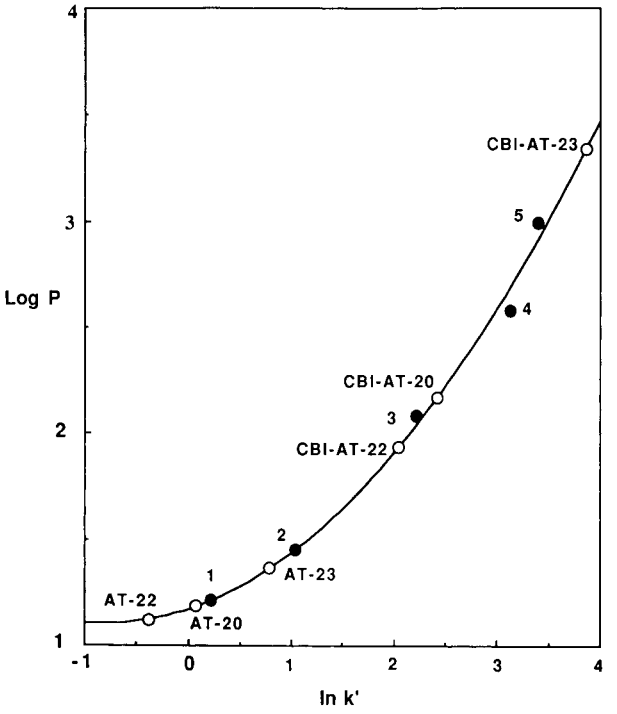

Fig. 6. Calibration plot showing the relationship between the 1-octanol–water partition coefficient (P) and chromatographic retention (k'). The data points (see also Table II) for acetanilide (1), benzaldehyde (2), anisole (3), toluene (4) and bromobenzene (5) represent experimental k' values and literature values of log P [36]. The line has been drawn according to the quadratic eqn. 4. The data points for the ATs and the CBI-ATs represent experimental k' values and values of P calculated from eqn. 5. Column: ODS Hypersil (5 μm, 150 × 4.6 mm I.D.). Mobile phase C': X–tetrahydrofuran (81:19, v/v). The aqueous component of the mobile phases (X) was a phosphate buffer (pH 6.0; 100 mM) containing sufficient 1-octanesulphonic acid sodium salt to give a final mobile phase concentration of 30 mM. Temperature: 40 ± 0.1°C.

phase of solvent X–THF (81:19, v/v). The capacity ratios (k') were converted to apparent partition coefficients (P) by calibration (Table II) of the chromatographic system with five compounds, acetanilide, benzaldehyde, anisole, toluene and bromobenzene, the partition coefficients of which are well established [35]. The experimental k' values were related to the known partition coefficients by a quadratic equation (eqn. 4) from which the apparent partition coefficients of the ATs and their CBI-derivatives were calculated.

$$\log P = 0.103 (\ln k')^2 + 0.093 \ln k' + 1.125, n = 5, r^2 = 0.992 (r = 0.996) \quad (4)$$

The contribution of the CBI-ring system to the 1-octanol–water partition coefficient (π_{CBI}) was then calculated from:

$$\pi_{CBI} = \log \left(\frac{P_{CBI\text{-}AT}}{P_{AT}} \right) \quad (5)$$

TABLE II

1-OCTANOL–WATER PARTITION COEFFICIENTS (log P) OF TEST SOLUTES AND THE CHROMATOGRAPHICALLY DERIVED log P VALUES FOR THE ANGIOTENSINS AND THEIR CYANOBENZ[*f*]ISOINDOLE DERIVATIVES

Log P (exp) = logarithm of the 1-octanol–water partition coefficient [36]; log P (calc) = logarithm of the 1-octanol–water partition coefficient calculated from eqn. 4; π_{CBI} = contribution of CBI-ring system to the 1-octanol–water partition coefficient calculated from eqn. 5.

Analyte	Log P (exp)	Log P (calc)	π_{CBI}
Acetanilide	1.21	–	–
Benzaldehyde	1.45	–	–
Anisole	2.08	–	–
Toluene	2.58	–	–
Bromobenzene	2.99	–	–
AT-22	–	1.122	–
AT-20	–	1.184	–
AT-23	–	1.364	–
CBI-AT-22	–	1.937	0.815
CBI-AT-20	–	2.166	0.982
CBI-AT-23	–	3.337	1.97

Very similar values for the contribution of the CBI-ring systems were obtained for CBI-AT-20 (π_{CBI} = 0.982) and CBI-22 (π_{CBI} = 0.815) but these values were substantially lower than the value obtained for CBI-AT-23 (π_{CBI} = 1.97). It should be noted that these values of π_{CBI} actually represent the combined effect of adding a CBI-ring system and the removal of a positively charged amino group. The values obtained here for π_{CBI} may differ from those measured in other chromatographic systems because ion-pair chromatography was used and it is expected that the positively charged amino group will be involved in the retention process via electrostatic interactions with the oppositely charged pairing ion. Nevertheless, the results indicate that the contribution of the CBI-ring system to retention is not constant, at least in ion-pair systems, and that it is influenced by the nature of the amino acid to which it is attached. The fact that the value obtained for π_{CBI} was the same for AT-20 and -22, which both have an aspartic acid residue at the N-terminus, provides some confidence that the retention contribution of the CBI-ring system is constant for a particular amino acid residue, but this needs to be substantiated in future investigations.

CONCLUSIONS

Synthetic and naturally occurring ATs were eluted from an ODS Hypersil column under isocratic conditions with excellent peak shape ($A_s < 1.2$) and good column efficiencies (N = 20 000–40 000 plates/m), provided sodium alkylsulphonates or alkylsulphates were added to the mobile phase to eliminate tailing. Once the initial isocratic conditions were determined, an optimized separation of the AT was achieved by establishing three isoelutropic mobile phases A, B and C containing acetonitrile, methanol or tetrahydrofuran, respectively. The second and final step involved the

exploration of the isoelutropic plane (A:B:C) using a modified mixture design statistical technique with bidimensional interpolation to establish the optimum quaternary mixture (acetonitrile–methanol–tetrahydrofuran–solvent X) for the resolution of the solutes. The main advantage of this approach was that it allowed the optimization of the separation to be achieved with a small number of experiments and the minimum expenditure of potentially expensive peptides. In addition, the separation was optimized in the absence of detailed knowledge of retention mechanisms or the structure of the peptides.

This study also demonstrated that the detectability of those ATs containing a primary amino group may be substantially enhanced by reaction with naphthalene-2,3-dicarboxaldehyde to the corresponding fluorescent cyanobenz[*f*]isoindole (CBI) derivatives. Finally, preliminary data were obtained to indicate that, although the addition of the hydrophobic CBI-ring system enhances the retention of peptides, its contribution to retention depends on both the chromatographic mechanism being employed and the nature of the amino acid to which it has been covalently attached.

ACKNOWLEDGEMENTS

This study was supported by grants from the Kansas Technology and Enterprise Corporation (KTEC), Oread Laboratories and the National Institute on Drug Abuse (NIDA) (DA04740).

REFERENCES

1 M. J. Peach, *Physiol. Rev.*, 57 (1977) 313.
2 D. Ganten and G. Speck, *Biochem. Pharmacol.*, 27 (1978) 2379.
3 A. E. Freedlander, A. E. Goodfriend and T. L. Goodfriend, in B. M. Jaffe and H. R. Behrman (Editors), *Methods of Hormone Radioimmunoassays*, Academic Press, New York, 1979, p. 889.
4 F. X. Galen, C. Devaux, P. Grogg, J. Menord and P. Corvol, *Biochim. Biophys. Acta*, 523 (1978) 485.
5 J. A. D. M. Tonnaer, J. Verhoff, V. M. Weigant and W. de Jong, *J. Chromatogr.*, 183 (1980) 303.
6 K. Hermann, D. Ganten, C. Bayer, T. Unger, R. E. Lang and W. Rascher, *Exp. Brain Res., Suppl.*, 4 (1982) 192.
7 P. A. Doris, *J. Chromatogr.*, 336 (1984) 392.
8 M. C. Chappel, K. B. Brosnihan, W. R. Welches and C. M. Ferrario, *Peptides*, 8 (1987) 939.
9 J. A. D. M. Tonnaer, in W. S. Hancock (Editor), *Handbook of HPLC for the Separation of Amino Acids, Peptides and Proteins*, Vol. II, CRC Press, Cleveland, OH, 1981, p. 179.
10 U. Ragnarsson, B. Fransson and O. Zetterqvist, in W. S. Hancock (Editor), *Handbook of HPLC for the Separation of Amino Acids, Peptides and Proteins*, Vol. II, CRC Press, Cleveland, OH, 1981, p. 75.
11 M. N. Guy, G. M. Robertson and L. R. Barnes, *Anal. Biochem.*, 112 (1981) 272.
12 G. R. Rhodes and V. K. Boppana, *J. Chromatogr.*, 444 (1988) 123.
13 J. Nussberger, D. B. Brunner, B. Waeber and H. R. Brunner, *Life Sci.*, 42 (1988) 1683.
14 I. Molnar and Cs. Horváth, *J. Chromatogr.*, 142 (1977) 623.
15 A. Nahum and Cs. Horváth, *J. Chromatogr.*, 203 (1981) 53.
16 K. E. Bij, Cs. Horváth, W. R. Melander and A. Nahum, *J. Chromatogr.*, 203 (1981) 65.
17 F. W. Crouch, C. M. Riley and J. F. Stobaugh, *J. Chromatogr.*, 488 (1988) 333.
18 P. deMontigny, J. F. Stobaugh, R. S. Givens, R. G. Carlson, K. Srinivasachar, L. A. Sternson and T. Higuchi, *Anal. Chem.*, 59 (1987) 1096.
19 M. Mifune, D. Krehbiel, J. F. Stobaugh and C. M. Riley, *J. Chromatogr.*, 496 (1989) 55.
20 P. deMontigny, C. M. Riley, L. A. Sternson and J. F. Stobaugh, *J. Pharm. Biomed. Anal.*, 8 (1990) 419–430.
21 L. Nicholson, H. B. Patel, F. Kristjansson, S. C. Crowley, Jr., K. Dave, J. F. Stobaugh and C. M. Riley, *J. Pharm. Biomed. Anal.*, 8 (1990) in press.

22 Cs. Horváth, W. Melander, I. Molnar and P. Molnar, *Anal. Chem.*, 49 (1977) 2295.
23 B. A. Bidlingmeyer, J. K. Del Rios and J. Korpi, *Anal. Chem.*, 54 (1982) 442.
24 R. S. Deelder, H. A. J. Linssen, A. P. Konijnendijk and J. L. M. van de Venne, *J. Chromatogr.*, 185 (1979) 241.
25 T. Sasagawa, T. Okuyama and D. C. Teller, *J. Chromatogr.*, 240 (1982) 329.
26 H. B. Patel, *Ph.D. Thesis*, University of Bath, Bath, 1987, Ch. 5.
27 P. J. Schoenmakers, *Optimization of Chromatographic Selectivity —A Guide to Method Development (Journal of Chromatography Library*, Vol. 35), Elsevier, Amsterdam, 1986, Ch. 4.
28 H. J. G. Debets, B. L. Bajema and D. A. Doornbos, *Anal. Chim. Acta*, 151 (1983) 131.
29 G. d'Agostino, L. Castagnetta, F. Mitchell and M. J. O'Hare, *J. Chromatogr.*, 338 (1983) 1.
30 C. M. Riley, E. Tomlinson and T. M. Jefferies, *J. Chromatogr.*, 185 (1979) 197.
31 M. C. Chappell, K. B. Brosnihan, W. R. Welches and C. M. Ferrario, *Peptides*, 8 (1987) 939.
32 M. D. Cain, K. J. Catt and J. P. Coghlan, *J. Clin. Endocrinol. Metab.*, 29 (1969) 1639.
33 S. C. Beale, Y.-Z. Hseih, J. C. Savage, D. Wiesler and M. Novotny, *Talanta*, 36 (1989) 321.
34 M. D. Oates, B. R. Cooper and J. W. Jorgenson, *Anal. Chem.*, 62 (1990) 1573.
35 C. Riley, J. F. Stobaugh, C. Kindberg, M. Slavik and T. Jefferies, in V. H. L. Lee (Editor), *Proc. 16th Int. Symp. on Controlled Release of Bioactive Materials*, Controlled Release Society, Lincolnshire, IL, 1989, p. 26.
36 C. Hansch and A. Leo, *Substituent Constants for Correlation Analysis in Chemistry and Biology*, Wiley-Interscience, New York, 1979.

Author Index

NEW DEXTRAN STANDARDS

Pharmacosmos introduces a complete series of 10 Dextran Standards with close to Gaussian molecular weight distribution.

Together, the Standards cover a broad molecular weight range.

Pharmacosmos' 10 Dextran Standards make molecular weight calibration much easier, much faster and much better in comparison with traditional Dextran Standards.

Like the Pullulan Standards, Pharmacosmos Dextran Standards are also very useful for universal calibration.

Pharmacosmos Dextran Standards are characterized by Low Angle Laser Light Scattering (LALLS), Gel Permeation Chromatography (GPC), Reducing End Group Titration (EGT) and Viscosity Measurements (VISC).

NEW CONCEPT FOR MOLECULAR WEIGHT CALIBRATION

Pharmacosmos has the pleasure of introducing a new concept for molecular weight calibration using the Peak Average Molecular Weight, $\bar{M}_p$. When applying the Peak Average Molecular Weight for general GPC calibration and for universal calibration it is easy to construct the correct calibration curve as described in "Pharmacosmos Dextran Standards".

Data Sheet - Pharmacosmos' 10 Dextran Standards

	GPC	GPC	LALLS	GPC	EGT	VISC
	$\bar{M}_p$	$\bar{M}_w$	$\bar{M}_w$	$\bar{M}_n$	$\bar{M}_n$	$[\eta]$ ml/g
Dextran 1	1080	1270	-	1010	1034	4.4
Dextran 5	4440	5220	5700	3260	3326	7.8
Dextran 12	9890	11600	11700	8110	8000	11.2
Dextran 25	21400	23800	22700	18300	17944	16.9
Dextran 50	43500	48600	50800	35600	36654	23.0
Dextran 80	66700	80900	79800	55500	55632	31.5
Dextran 150	123600	147600	143000	100300	98559	39.4
Dextran 270	196300	273000	262000	164200	167500	49.4
Dextran 410	276500	409800	403000	236300	239903	55.4
Dextran 670	401300	667800	676000	332800	349303	70.8

Differential Distribution - Pharmacosmos' 10 Dextran Standards

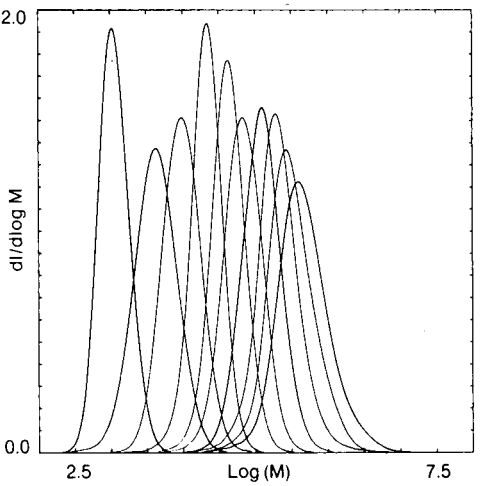

Pharmacosmos' 10 Dextran Standards are available in a 10-Kit containing 0.8 g of each Standard, at a price of DKK 4,200,-. Alternatively, each Standard is supplied separately in 5 g vials, at a price of DKK 3,000,-.
The Standards are supplied together with "Pharmacosmos Dextran Standards", which contains the complete data sheets for all Standards and instructions for molecular weight calibration.

Dextran 1, $\bar{M}_p$ = 1080
Dextran 5, $\bar{M}_p$ = 4440
Dextran 12, $\bar{M}_p$ = 9890
Dextran 25, $\bar{M}_p$ = 21400
Dextran 50, $\bar{M}_p$ = 43500
Dextran 80, $\bar{M}_p$ = 66700
Dextran 150, $\bar{M}_p$ = 123600
Dextran 270, $\bar{M}_p$ = 196300
Dextran 410, $\bar{M}_p$ = 276500
Dextran 670, $\bar{M}_p$ = 401300

PHARMACOSMOS

P.O.B. 29, DK-4130 Viby Sj., Denmark
Tel.: +45 2 39 33 62, Fax: +45 2 39 34 28, Telex: 43178 cosmos dk

PHARMACOSMOS is a large-scale producer of Dextrans and Iron Dextrans.
Pharmacosmos' production is based on methods developed from research by its own laboratories.

Scientific Computing and Automation (Europe) 1990

Proceedings of the Scientific Computing and Automation (Europe) Conference, 12-15 June, 1990, Maastricht, The Netherlands

edited by **E.J. Karjalainen,** *Helsinki, Finland*

(Data Handling in Science and Technology, 6)

This book comprises the majority of papers presented at the second **European Scientific Computing and Automation (SCA 90)** meeting which was held in June 1990 in Maastricht, The Netherlands. The increasing use of computers in data acquisition, processing, interpretation and storage makes integration of these activities possible. SCA concentrates on computer-based tools which can be applied in several disciplines.

Laboratory Information Management Systems (LIMS) are covered in depth, including LIMS design, acquisition and standards for data transfer between instruments, between LIMS and instruments and between different LIMS. Finally, scientific results are displayed as images and computer-based animations in several examples with colour illustrations.

The book should be of interest to those managing R&D projects, doing research in laboratories, acquiring or planning LIMS, designing instruments and laboratory automation systems and those involved in data analysis of scientific results.

Contents: I. Scientific Visualization and Supercomputers *(6 Papers).* II. Statistics *(6 Papers*). III. Data Analysis and Chemometrics *(8 Papers).* IV. Laboratory Robotics (*4 Papers*). V. LIMS and Validation of Computer Systems (*7 Papers*). VI. Standards Activities *(3 Papers).* VII. Databases and Documentation *(4 Papers*). VIII. Tools for Spectroscopy (*4 Papers*). Author Index. Subject Index.

1990 514 pages

Price: US$ 220.00 / Dfl. 385.00

ISBN 0-444-88949-3

Elsevier Science Publishers

P.O. Box 211, 1000 AE Amsterdam, The Netherlands
P.O. Box 882, Madison Square Station, New York, NY 10159, USA

PUBLICATION SCHEDULE FOR 1991

Journal of Chromatography and Journal of Chromatography, Biomedical Applications

MONTH	D 1990	J	F	M	
Journal of Chromatography	535/1 + 2	536/1 + 2 537/1 + 2 538/1	538/2 539/1 539/2	The publication schedule for further issues will be published later	
Cumulative Indexes, Vols. 501–550					
Bibliography Section					
Biomedical Applications		562/1 + 2 563/1	563/2	564/1	

INFORMATION FOR AUTHORS

(Detailed *Instructions to Authors* were published in Vol. 522, pp. 351–354. A free reprint can be obtained by application to the publisher, Elsevier Science Publishers B.V., P.O. Box 330, 1000 AH Amsterdam, The Netherlands.)

Types of Contributions. The following types of papers are published in the *Journal of Chromatography* and the section on *Biomedical Applications:* Regular research papers (Full-length papers), Review articles and Short Communications. Short Communications are usually descriptions of short investigations, or they can report minor technical improvements of previously published procedures; they reflect the same quality of research as Full-length papers, but should preferably not exceed six printed pages. For Review articles, see inside front cover under Submission of Papers.

Submission. Every paper must be accompanied by a letter from the senior author, stating that he/she is submitting the paper for publication in the *Journal of Chromatography*.

Manuscripts. Manuscripts should be typed in double spacing on consecutively numbered pages of uniform size. The manuscript should be preceded by a sheet of manuscript paper carrying the title of the paper and the name and full postal address of the person to whom the proofs are to be sent. As a rule, papers should be divided into sections, headed by a caption (*e.g.*, Abstract, Introduction, Experimental, Results, Discussion, etc.). All illustrations, photographs, tables, etc., should be on separate sheets.

Introduction. Every paper must have a concise introduction mentioning what has been done before on the topic described, and stating clearly what is new in the paper now submitted.

Abstract. All articles should have an abstract of 50–100 words which clearly and briefly indicates what is new, different and significant.

Illustrations. The figures should be submitted in a form suitable for reproduction, drawn in Indian ink on drawing or tracing paper. Each illustration should have a legend, all the *legends* being typed (with double spacing) together on a *separate sheet.* If structures are given in the text, the original drawings should be supplied. Coloured illustrations are reproduced at the author's expense, the cost being determined by the number of pages and by the number of colours needed. The written permission of the author and publisher must be obtained for the use of any figure already published. Its source must be indicated in the legend.

References. References should be numbered in the order in which they are cited in the text, and listed in numerical sequence on a separate sheet at the end of the article. Please check a recent issue for the layout of the reference list. Abbreviations for the titles of journals should follow the system used by *Chemical Abstracts.* Articles not yet published should be given as "in press" (journal should be specified), "submitted for publication" (journal should be specified), "in preparation" or "personal communication".

Dispatch. Before sending the manuscript to the Editor please check that the envelope contains four copies of the paper complete with references, legends and figures. One of the sets of figures must be the originals suitable for direct reproduction. Please also ensure that permission to publish has been obtained from your institute.

Proofs. One set of proofs will be sent to the author to be carefully checked for printer's errors. Corrections must be restricted to instances in which the proof is at variance with the manuscript. "Extra corrections" will be inserted at the author's expense.

Reprints. Fifty reprints of Full-length papers and Short Communications will be supplied free of charge. Additional reprints can be ordered by the authors. An order form containing price quotations will be sent to the authors together with the proofs of their article.

Advertisements. Advertisement rates are available from the publisher on request. The Editors of the journal accept no responsibility for the contents of the advertisements.

For Superior Chiral Separation From Analytical To Preparative.

The finest from DAICEL……

Why look beyond DAICEL? We have developed the finest CHIRALCEL, CHIRALPAK and CROWNPAK with up to 17 types of HPLC columns, all providing superior resolution of racemic compounds.

NEW CHIRALPAK AS

● CHIRALPAK AS

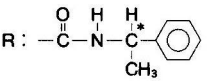

for β-Lactam antibiotics

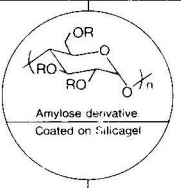

NEW CHIRALPAK AD

● CHIRALPAK AD

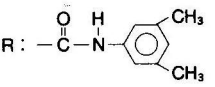

1-Acetoxy-2-azetidine

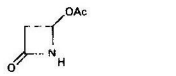

Eluent : Hexane/EtOH = 8/2
Flow rate : 1.0mℓ/min
Temperature : r.t.
Detection : UV254nm

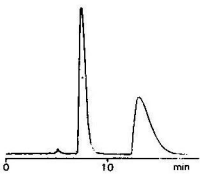

Oxyphencyclimine

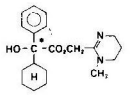

Eluent : Hexane/2-Propanol = 9/1
Flow rate : 1.0mℓ/min
Temperature : r.t.
Detection : UV254nm

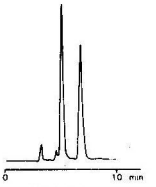

Ofloxacine methyl ester

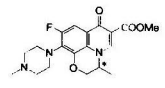

Eluent : Hexane/EtOH = 8/2
Flow rate : 1.2mℓ/min
Temperature : 40°C
Detection : UV254nm

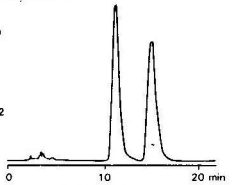

Verapamil

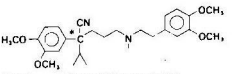

Eluent : Hexane/2-Propanol = 9/1
Flow rate : 1.0mℓ/min
Temperature : r.t.
Detection : UV254nm

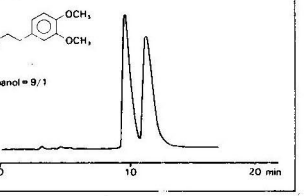

Analytical column 0.46cm × 25cm(10μm)

CHIRALCEL OA
OB
OC
OD
OJ
OF
OG
OK

CHIRALPAK AS
AD

Normal Phase

Semi-preparative column 2cm × 25cm(10μm)

You can have Pure enantiomer quickly!!

■Separation Service

- A pure enantiomer separation in the amount of 100g~10kg is now available.
- Please contact us for additional information regarding the manner of use and application of our chiral columns and how to procure our separation service.

DAICEL CHEMICAL INDUSTRIES, LTD.

chiral chemicals division.
8-1, Kasumigaseki 3-chome, Chiyoda-ku, Tokyo 100, Japan Phone: 03 (507) 3151 FAX: 03 (507) 3193

DAICEL(U.S.A.), INC.
Fort Lee Executive Park
Two Executive Drive, Fort Lee,
New Jersey 07024
Phone: (201) 461-4466
FAX: (201) 461-2776

DAICEL(U.S.A.), INC.
23456 Hawthorne Blvd.
Bldg. 5, Suit 130
Torrance, CA 90505
Phone: (213) 791-2030
FAX: (213) 791-2031

DAICEL(EUROPA)GmbH
Oststr. 22
4000 Düsseldorf 1, F.R. Germany
Phone: (211) 369848
Telex: (41) 8588042 DCEL D
FAX: (211) 364429

DAICEL CHEMICAL(ASIA)PTE. LTD.
65 Chulia Street #40-07
OCBC Centre, Singapore 0104
Phone: 5332511
FAX: 5326454